Departamento de Química
Universidad de La Laguna

PhD Thesis

Analytical strategies for sample preparation using novel materials

Estrategias analíticas de preparación de muestras utilizando novedosos materiales

Mª Idaira Pacheco Fernández

2020

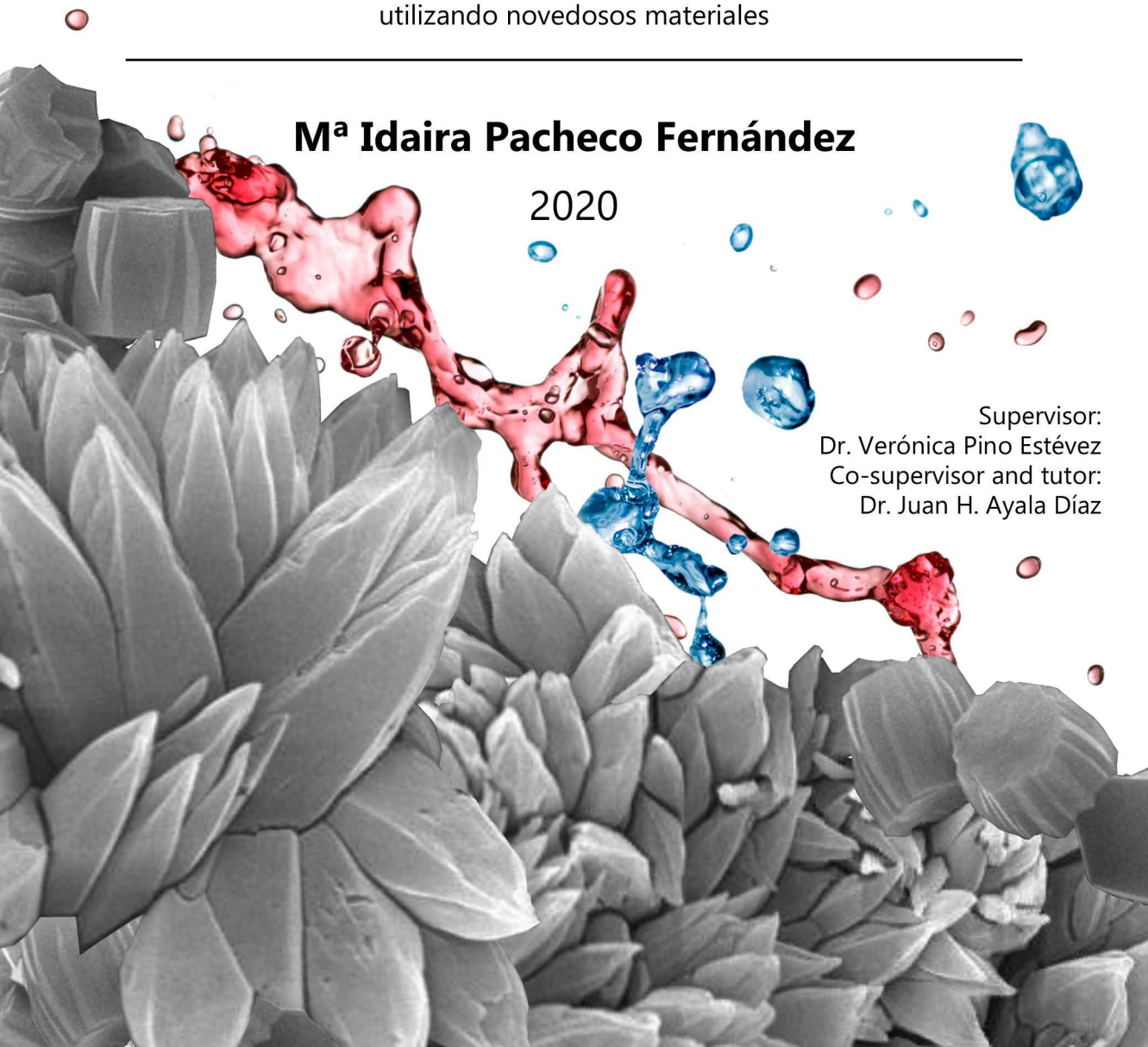

Supervisor:
Dr. Verónica Pino Estévez
Co-supervisor and tutor:
Dr. Juan H. Ayala Díaz

Departamento de Química
Universidad de La Laguna

Dra. Dña. Verónica Pino Estévez y Dr. D. Juan Heliodoro Ayala Díaz, Profesores Titulares en el Departamento de Química, Unidad Departamental de Química Analítica, de la Universidad de la Laguna,

AUTORIZAN:

La presentación de la Tesis Doctoral titulada "ESTRATEGIAS ANALÍTICAS DE PREPARACIÓN DE MUESTRAS UTILIZANDO NOVEDOSOS MATERIALES" realizada por Dña. **María Idaira Pacheco Fernández** bajo nuestra dirección para optar al Título de Doctora en Química con Mención Internacional por la Universidad de La Laguna.

Y para que conste y surta los efectos oportunos, firman la presente en La Laguna, a treinta de noviembre de dos mil veinte.

La Directora de la Tesis Doctoral

Fdo: Verónica Pino Estévez

El Co-director y Tutor de la Tesis Doctoral

Fdo: Juan Heliodoro Ayala Díaz

C/ Padre Herrera s/n
38207 La Laguna
Santa Cruz de Tenerife. España

T: 900 43 25 26

ull.es

Desde que comencé mi etapa predoctoral, mis miedos, entre otras muchas cosas, han ido evolucionando. Primero me atormentaba purgar el HPLC con la válvula cerrada, romper una fibra de SPME o tirar el táper de lentejas en el pasillo de camino al microondas. Con el paso de los años y los nuevos conocimientos y tareas, lo que no me dejaba dormir era que se acabara la botella de helio del GC-MS, romper un (otro) automuestreador, que el reviewer número 2 nos pidiera incluir más referencias y, por tanto, renumerar las 272 referencias del review, o dejar encendido el HPLC de prácticas y que se quedase sin fase móvil. Y como no, los *deadlines*, que han sido una causa de horror, fatiga e insomnio desde el primer momento. Sin embargo, lo que no ha cambiado durante estos años son las dos palabras que digo con más frecuencia al día: gracias y perdón.

Puede parecer que uso ambas palabras como una coletilla, pero nada más lejos de la realidad. El hecho de que yo haya llegado hasta aquí ha requerido que muchas personas hayan parado sus tareas y deberes para invertir parte de su tiempo en responder mis dudas, formarme, o simplemente escucharme, aunque solo fueran quejas (que han sido muchas). Por ello les he pedido perdón y me siento eternamente agradecida, porque que te presten tiempo es el más bonito y desinteresado de los regalos. Y aunque creo que nunca será suficiente, espero poder expresar con estas palabras mi más sincero agradecimiento a todas esas personas que han sido partícipes del gran proyecto de mi vida.

A mis directores de Tesis, la Dra. Verónica Pino y el Dr. Juan Ayala. Vero, eres la creadora de este pequeño "monstruo". Gracias por trasmitirme tu pasión por este trabajo, por tu profesionalidad, tu exigencia, tu compromiso y sacrificio con mi presente y mi futuro, por ser mi mentora y enseñarme que de los momentos malos se sale, y se sale aún más fuerte. Todos los días me pregunto qué habría sido de mí sin ti y espero poder llegar a ser en un futuro la mitad de lo que eres tú ahora. Gracias por compartir tantas penas y alegrías juntas. Juan, gracias por todo el apoyo desde aquel día que quise hacer el TFG en el grupo allá por el 2014 hasta ayer mismo. Siempre he admirado tu alegría y tu calma, y es lo que me has trasmitido en los momentos que más me hacía falta. Gracias por todo tu cariño, por compartir tu sabiduría inmensurable conmigo, y por enseñarme una de las virtudes más importantes que debe tener un científico y ser el mejor ejemplo de ello, la humildad. A ambos, gracias por hacer por mí algo que yo nunca habría podido hacer por mí misma, que es creer y confiar en mis capacidades, en mi criterio y, en definitiva, en mí. Siempre serán mis padres científicos y haberlos elegido para ello ha sido la mejor decisión de mi vida.

A los que han sido mis co-codirectores de Tesis, la Dra. Ana Afonso y el Dr. Jorge Pasán. Ana, gracias por enseñarme tanto sobre tantas cosas, por tu interés y ayuda en cada uno de los proyectos en lo que me embarcaba, por tu rigor y, por supuesto, por esas magníficas charlas a la hora del café. Jorge, simplemente agradecerte que me hayas hecho partícipe de tus locuras y tu espontaneidad. Gracias por animarme a ver el lado bueno de lo que parecía insalvable, por hacerme reír tanto y hacerme pensar como nunca. Trabajar con ustedes ha sido un lujo.

Al resto de integrantes del grupo de investigación, ahora MAT4LL. A la Dra. Ana I. Jiménez Abizanda, al Dr. Francisco Jiménez Moreno y al Dr. José M. Fraga, gracias por tratarme como una más de ustedes y por las lecciones tan valiosas que he aprendido durante todo el tiempo que hemos compartido docencia y pasillos. A la Dra. Ana Lago, por su interés, su alegría y su ayuda. Y por supuesto, al Dr. Venerando González, porque fue gracias a él que encontré en la Química Analítica mi pasión. Gracias por su apoyo desde el principio y por animarme a quejarme menos, siempre tengo presente sus consejos. A la Dra. Catalina Ruiz Pérez, por emprender junto con Vero esta locura de fusión de grupos. Me enorgullece haber formado parte de un grupo liderado por grandes mujeres científicas.

A los que más han sufrido el trabajar conmigo durante todos estos años, mis compañeros de laboratorio. A María José y Priscilla, mis maestras. Mari, nunca viviré lo suficiente para pagarte todo lo que has hecho por mí, profesional y personalmente. Gracias por tener tanta paciencia conmigo, ser mi profesora, ser el espejo en el que quisiera mirarme y convertirte prácticamente en una hermana. Pris, fuiste la primera en enseñarme el laboratorio, y créeme, eso nunca se olvida, y menos cuando es la locura y alegría personificada quien lo hace. Gracias por tantas risas, tantas lágrimas, tantas frustraciones y tantos detalles y meriendas juntas. A Arturo, por trasmitirme tu inagotable energía y ser un ejemplo de superación ante las adversidades. A Adri, por retroalimentar nuestras propias inseguridades como solo tú y yo sabemos hacerlo, porque es nuestra forma especial de comunicarnos y entendernos. Gracias infinitas por soportarme tanto. Gracias a Provi por ver siempre lo bueno en mí y por esos desahogos nocturnos que tanta falta nos hacían. A Raúl e Iván, gracias por ser mis vasallos particulares. Me siento un poco responsable de que hoy estén aquí, pero también muy orgullosa. A los más nuevos, Patri y Diego, con los que he compartido poco tiempo, pero el suficiente para pasar grandes momentos juntos. A los cuatro, gracias por hacerme todo más fácil durante esta última etapa y por darme tanto cariño. Gracias a todos y cada uno de ustedes por vivir conmigo esta maravillosa experiencia, una gran parte del resultado es gracias a todo su apoyo.

A todos los estudiantes que han pasado por el grupo de investigación y con los que he tenido el placer de coincidir, especialmente aquellos que he tutorizado: Judith, Alejandro, Gabriel, Diana y Mariela. De todos ellos he aprendido mucho más de lo que ellos se podrían imaginar. Gracias a los estudiantes internacionales que han pasado por el laboratorio y con los que he compartido no solo proyectos profesionales, sino también muchos momentos personales: Giulia, Meriem, Kristyna, Jakub y Tita. Trabajar con ustedes ha sido una de las cosas más bonitas de esta etapa. Estoy súper orgullosa de todos ustedes y siempre los llevaré en mi corazón.

Asimismo, también quisiera dar las gracias a todos los miembros de la Unidad Departamental de Química Analítica, tanto profesores como técnicos, que me han ayudado siempre que lo he necesitado y me han enseñado los entresijos de las prácticas. En especial, quisiera agradecer al grupo de investigación AChem, y más concretamente, al Dr. Javier Hernández Borges y al Dr. Javier González Sálamo. Gracias a Javi (padre) por confiar en mí y tener siempre palabras de ánimo. A Javi (hijo), que has sido prácticamente un compañero más de laboratorio, gracias por escucharme y compartir tantas risas y frustraciones.

Al Dr. Jared L. Anderson, por su hospitalidad durante mi estancia predoctoral en su laboratorio en Iowa State University. Gracias por la oportunidad de aprender mucho más que de líquidos iónicos. Todo el mundo sabe lo que significa Ames para mí, pero no habría sido una etapa tan importante en mi vida si no hubiera sido por toda esa gente que se cruzó en mi camino hacia el (intento de) sueño americano. Gracias a todos mis amigos *iowenses*, en especial a Israel, Miranda, Jakub, Ester, Ashley, Arianna y Fahad.

Uno de los aspectos que más valoro de esta etapa es la oportunidad que me han brindado mis directores de colaborar con grandes científicos de distintas áreas. Así, quisiera agradecer al Dr. Jacob Lorenzo Morales y a su grupo de investigación de parasitología del Instituto de Enfermedades Tropicales y Salud Pública de Canarias, y en especial a Ines, Atteneri y María. Gracias por dedicarme tanto tiempo para enseñarme sus "bichitos y aplastarlos con mis piedras". Al Dr. Francisco J. Conde, por prestarme tu ayuda desinteresada siempre que lo he necesitado y siempre con tu particular sentido del humor. Al Dr. David Díaz Díaz, por arrastrarnos de nuevo al mundo de la síntesis y por tus valiosos consejos. A la Dra. Cecilia Cagliero, la Dra. Mara G. Freire, la Dra. Francisca e Silva, al Dr. Enrique Carrasco y al Dr. José Manuel Herrero Martínez, que me han enseñado mucho a pesar de haber colaborado en la distancia.

Al Servicio de Medio Ambiente de la Universidad de La Laguna (SEMALL), y en especial a Cely y Sara, que me han prestado su ayuda y facilitado el trabajo siempre con una sonrisa. Al Instituto Canario de

Investigaciones Agrarias (ICIA) que siempre me han recibido con los brazos abiertos. A los Servicios Generales de Apoyo a la Investigación (SEGAI) de la Universidad de La Laguna y a todos sus técnicos y becarios, por tantas solicitudes y servicios prestados.

A las instituciones que han participado en la financiación para que esta Tesis se llevara a cabo:

- Mis padres, que, aunque no son una institución, costearon mi manutención durante los primeros años de Tesis.
- El Cabildo de Tenerife, por la ayuda de matrícula en el primer año.
- Caja Siete, que me permitió disfrutar de una beca de especialización en los SEGAI de la Universidad de La Laguna (2016–2017).
- La Caixa y la Universidad de la Laguna, gracias a las cuales disfruté de un contrato predoctoral en el período 2017–2018.
- La Agencia Canaria de Investigación, Innovación y Sociedad de la Información, por el contrato predoctoral cofinanciado por el Fondo Social Europeo disfrutado desde el año 2018 hasta la actualidad.
- El Cabildo de Tenerife y el Programa Fostering Grads, que financiaron mi estancia predoctoral en Estados Unidos en 2018.
- Los proyectos AGUA05 de la Fundación CajaCanarias, MAT2013-43101-R, MAT2014-57465-R y MAT2017-89207-R, que han financiado esta investigación.
- La Universidad de La Laguna y su Programa de Formación para el Personal Investigador, que ha financiado parte de mi estancia predoctoral, así como mi asistencia y participación en congresos internacionales.

A mis amigos, que han tenido una paciencia inmensa conmigo. A Paula, Pri, Carmen, Juanfra y Manu, los compañeros de carrera que aún siguen ahí y me han mostrado siempre su cariño y apoyo. A Miri, Eric, y Dani, que siempre se han interesado y preocupado por mí y mi trabajo. Soy muy afortunada de tenerlos. A mis almas gemelas, Rita y Adrián. Ustedes son los que más me entienden, con los que nunca me ha dado miedo ser yo misma, con los que me río a carcajadas y con los que he compartido mis peores y mejores momentos. Gracias de todo corazón por existir en mi vida.

Sin lugar a duda, a quien más tengo que agradecer es a mi familia. A mis padres, José y Toya, gracias por darme la libertad de elegir quién y qué quería ser. Gracias por hacerme el camino más sencillo, por darme mi espacio y mi tiempo todas esas veces que no entendían mis frustraciones y agobios, y por respetar y apoyar todas mis decisiones y sueños. Les debo mi vida y nunca podré recompensarlos. Gracias a mis hermanos, Sirenia y José David, simplemente por estar ahí y compartir tantos momentos juntos. Gracias al resto de mi familia, en especial a mi abuela Catalina, mi prima Alba y mis tíos. Gracias a todos por sentirse orgullosos de mí, porque yo sí que estoy orgullosa y soy muy feliz de estar rodeada de una familia tan especial.

Sé que se me queda mucha gente en el tintero, porque han sido muchas las personas con las que me he cruzado y he tenido el placer de coincidir durante estos cinco años, y que han sido una parte fundamental para mi crecimiento profesional y personal. A todos ustedes,

¡Gracias (y perdón)!

A José y María Victoria,

mis padres

ABSTRACT

Sample preparation is the stage of the analytical procedure that deals with the extraction of the target compounds from a sample and includes the elimination of the interferences coming from the sample matrix, thus ensuring the compatibility with the analytical instrument while improving the selectivity and sensitivity of the entire method. Given the complexity of the samples, the trace concentrations at which analytes are present in the samples, and the importance of incorporating the Green Chemistry principles in the analytical process, the development of microextraction techniques and the incorporation of new materials have been demanding research lines within analytical sample preparation to address these challenges.

Among the outstanding materials described that can meet green requirements and exhibit successful analytical performance in sample preparation, ionic liquids (ILs) and metal-organic frameworks (MOFs) must be highlighted.

ILs are molten salts formed by the combination of bulky organic cations and organic or inorganic anions. They present melting points lower than 100 °C and, depending on the moieties selected and the incorporation of specific functional groups in their structure, they can exhibit specific characteristics. Therefore, it is possible to prepare several interesting derivatives, such as polymeric ionic liquids (PILs) and IL-based surfactants.

MOFs are crystalline materials composed of metallic clusters and organic linkers connected by coordination bonds. They are mainly characterized by their high surface area and tunability, which allows designing MOFs with specific topologies by selecting the adequate components and synthetic conditions. These characteristics make MOFs potential materials to host target compounds.

In this Doctoral Thesis, ILs and MOFs were designed, synthesized and incorporated in a wide variety of challenging analytical applications using microextraction techniques. Among the existing techniques, dispersive liquid-liquid microextraction (DLLME) and solid-phase microextraction (SPME) were selected due to their simplicity, fastness, and high preconcentration ability.

ILs of low cytotoxicity formed by the combination of monoalkylguanidinium cation and chloride anion were synthesized with different alkyl chain lengths. Their cytotoxicity was evaluated, and the surface-active properties of the ILs with the longer alkyl substituents were also studied. These hydrophilic ILs were used in different DLLME approaches in which a low amount of the ionic liquids is added to the aqueous sample and then insolubilized using different reagents. The use of water-soluble solvents as extraction media improves the dispersion and the efficiency of the extraction. In the first strategies, a metathesis reaction of the IL was used to exchange the anion and obtain the hydrophobic IL droplet containing the target compounds. With the aim of improving the greenness of the method (given the toxicity of the fluorine-containing anion-exchange reagent), the non-harmful $NaClO_4$ salt was used to promote the metathesis reaction and

carry out the extraction. The guanidinium-based IL with the lowest cytotoxicity was also used in a microextraction method but based on the aqueous biphasic system formed by water, the IL and K_3PO_4, with the insolubilization of the IL accomplished due to the salting-out effect exerted by the salt.

With respect to SPME applications, functionalized PILs and MOFs were synthesized and used to prepare stable and selective coated-fibers and coated-capillaries to analyze complex samples. Thus, different crosslinked PILs-based coatings were prepared by using functionalized ILs as monomers and dicationic ILs as crosslinker agents to improve the mechanical stability of the resulting polymer. Fibers coated with PILs containing aromatic groups, long alkyl chains, and anions with higher hydrogen bond basicity, exhibited better extraction efficiency towards polar analytes. The use of zwitterionic ILs with high dipole moments as monomers to prepare coated fibers led to enhanced extraction without significant matrix effects in comparison with commercial coatings. Furthermore, PILs composed of IL monomers functionalized with carboxylic groups were evaluated for the selective extraction of DNA using in-tube SPME devices taking advantage of the anion-exchange extraction mechanism of the PIL towards this biomolecule.

Regarding the use of crystalline materials in SPME, the MOF CIM-80(Al), formed by mesaconic acid as organic linker and Al (III) as metal, was used to prepare an on-fiber SPME coating. The MOF is synthesized following a simple and green procedure directly on the surface of nitinol wires, thus ensuring the preparation of a neat MOF coating. It also exhibits low cytotoxicity, high thermal stability, surface area, and stability in several matrices, which allowed the use of the device for the analysis of complex aqueous-based samples, including brewed coffee and urine. The reusable device presented adequate precision, efficiency and stability, with comparable results in comparison with commercial coatings.

The proposed materials and microextraction methods in combination with chromatographic and spectroscopic techniques were optimized and validated, thus demonstrating to be useful for the analysis of environmental, food and biological samples with satisfactory analytical performance, which allowed the determination of the target analytes at trace concentration levels.

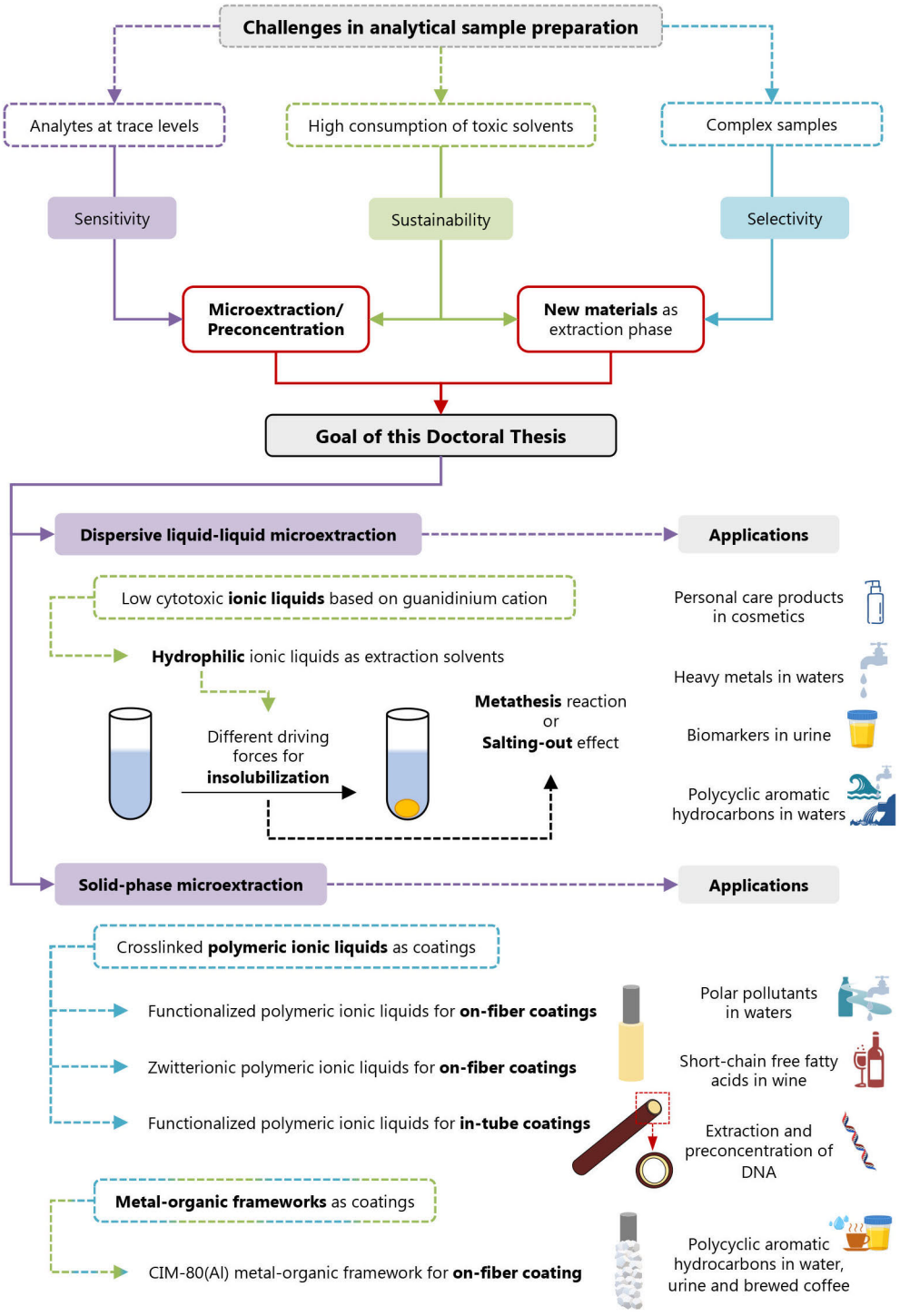
Challenges in analytical sample preparation
Analytes at trace levels
High consumption of toxic solvents
Complex samples
Sensitivity
Sustainability
Selectivity
Microextraction/ Preconcentration
New materials as extraction phase
Goal of this Doctoral Thesis
Dispersive liquid-liquid microextraction
Applications
Low cytotoxic ionic liquids based on guanidinium cation
Hydrophilic ionic liquids as extraction solvents
Different driving forces for insolubilization
Metathesis reaction or Salting-out effect
Personal care products in cosmetics
Heavy metals in waters
Biomarkers in urine
Polycyclic aromatic hydrocarbons in waters
Solid-phase microextraction
Applications
Crosslinked polymeric ionic liquids as coatings
Functionalized polymeric ionic liquids for on-fiber coatings
Zwitterionic polymeric ionic liquids for on-fiber coatings
Functionalized polymeric ionic liquids for in-tube coatings
Polar pollutants in waters
Short-chain free fatty acids in wine
Extraction and preconcentration of DNA
Metal-organic frameworks as coatings
CIM-80(Al) metal-organic framework for on-fiber coating
Polycyclic aromatic hydrocarbons in water, urine and brewed coffee

TABLE OF CONTENTS

CHAPTER I
Introduction

Chapter I

Novel materials in microextraction: ionic liquids and metal-organic frameworks in dispersive liquid-liquid microextraction and solid-phase microextraction

Own publications used in the preparation of Chapter I

Review articles

Analytica Chimica Acta 939 (2016) 26–41

Current Opinion in Green and Sustainable Chemistry 18 (2019) 42–50

Separations 6 (2019) 47

Separations 7 (2020) 37

Trends in Analytical Chemistry 125 (2020) 115839

Journal of Chromatography A 1634 (2020) 461670

Analytica Chimica Acta (2020) in press (doi: 10.1016/j.aca.2020.08.022)

Book chapters

Ionic Liquid Devices, The Royal Society of Chemistry (2018) 53–78

Advanced Ceramic and Metallic Coating and Thin Film Materials for Energy and Environmental Applications, Springer, Cham (2018) 217–243

Handbook of Smart Materials in Analytical Chemistry, John Wiley & Sons Ltd. (2019) 463–502

Handbooks in Separation Science: Liquid-Phase Extraction, Elsevier (2020) 499–537

Analytical Sample Preparation with Nano- and other High-Performance Materials, Elsevier (2021) in press (chapter 14)

I.1. Challenges in Analytical Chemistry: sample preparation

The development of novel strategies to deal with the analysis of complex samples is one of the most demanding areas within Analytical Chemistry. Despite the advances in the separation and detection techniques and instrumentation, it is still required the incorporation of a previous sample preparation step to make a complex sample suitable for its introduction in the analytical system [1]. Thus, typically, the analytical procedure involves several steps: sampling, sample preparation, separation, detection, and data analysis.

Sample preparation aims to extract and preconcentrate the target analytes and to eliminate the interferences from the matrix. Therefore, this stage of the analytical procedure is an essential step to reach the sensitivity levels required for the specific application. However, the sample processing is also the most time-consuming and labor-intensive step, and the main source of errors and wastes in the analytical procedure [2]. Moreover, conventional extraction methods, such as liquid-liquid extraction (LLE) and Soxhlet extraction, are characterized by the use of large amounts of harmful organic solvents as well as by automation impediments.

In this sense, the sample preparation stage faces different challenges (Figure I.1): (i) it must succeed with the trace levels at which the analytes are present in the samples, which is directly related to the sensitivity; (ii) it must overcome the complexity of the samples, which mostly affects the selectivity; (iii) it must decrease the high consumption of toxic solvents and reagents, which has a great impact on the sustainability; and (iv) it must ensure the simplicity and possible automation of its operational to allow the implementation in routine analysis with the aim of developing high throughput methods.

Most of the strategies proposed to overcome all these issues emerged almost at the same time as the requirements of the Green Chemistry started to be considered in the analytical procedure, leading to the development of the Green Analytical Chemistry (GAC) [3]. Despite the concept of GAC mainly focus on the sustainability of the analytical laboratories, the recommended guidelines not only aim to improve the environmental friendliness of the analytical methods, but also to increase the quality and reliability of the results.

In this sense, the solutions given to improve the characteristics of conventional sample preparation methods follow three main strategies (Figure I.1). One of them is the miniaturization of the analytical method by developing microextraction techniques, to achieve preconcentration and to reduce the consumption of both reagents and sample. The second strategy involves the design and incorporation of new solvents and sorbents to reduce, replace and even eliminate the use of toxic organic solvents, as well as to enhance both the selectivity and extraction efficiency of the analytical sample preparation step. The third trend is the development of on-site, on-line and automated methods to simplify the procedure and to reduce the errors, while guaranteeing the safety of the operator [2–4].

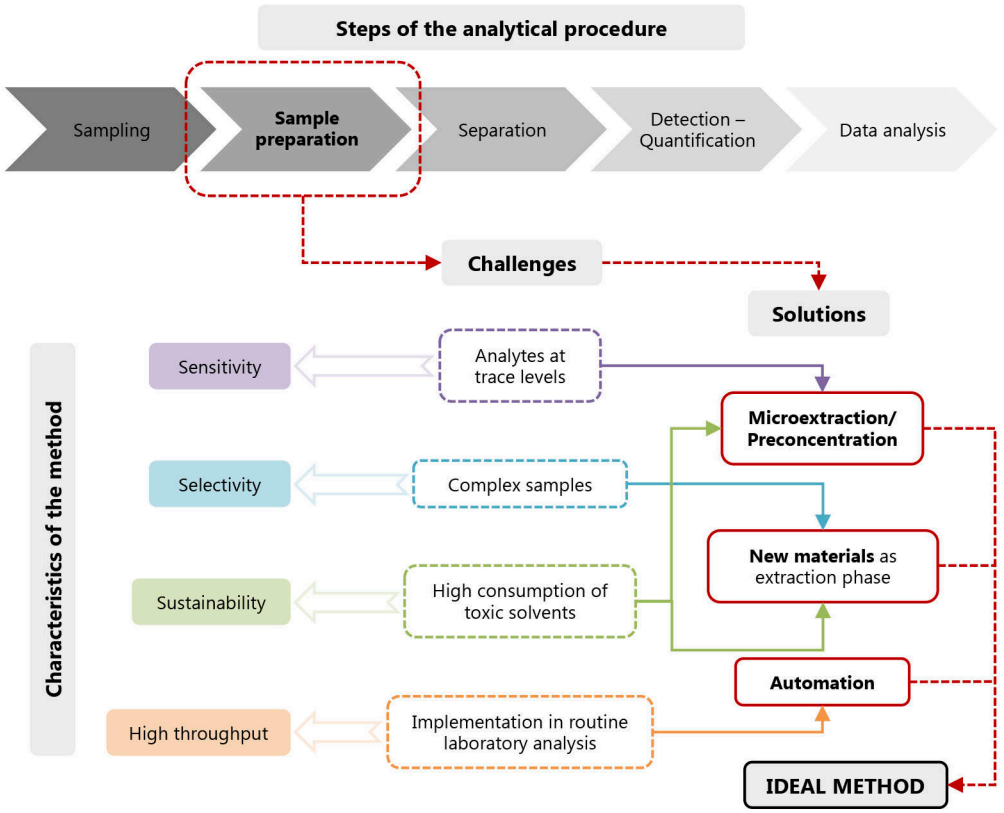

Figure I.1. Summary of the main challenges and solutions within the sample preparation stage of the analytical procedure.

This Doctoral Thesis focus on two of these approaches: the development of microextraction schemes and the use of new materials as extraction phases.

1.1. Microextraction techniques

According to the IUPAC recommendations, a microextraction is an extraction technique in which the extraction phase is significantly smaller than the sample volume [5]. Thus, microextraction techniques are generally characterized by volumes of extraction phase lower than 100 µL or amounts of sorbent lower than 10 mg. In general, these conditions make difficult to achieve exhaustive extractions and the amount of analyte extracted at equilibrium is low [1]. Far from being a disadvantage, the non-exhaustivity character of microextraction techniques provides high flexibility and versatility to these approaches, with a wide variety of configurations described

[1,6]. Moreover, the preconcentration attained with these techniques is enough to reach the concentration levels required [6].

Microextraction techniques can be classified in several categories depending on different criteria. Despite the classification based on the fundamental extraction principle has been already established (i.e., flow-through, batch and steady state) [1], the simplest classification considers the nature of the extraction phase and leads to two groups: liquid-phase microextraction (LPME) and sorbent-based microextraction [6]. In LPME, the extraction phase is a liquid, while a solid material is used as sorbent in the second case. Both techniques base on the partition of the analytes from the matrix sample to the extraction phase.

Given the versatility of LPME and sorbent-based microextraction, a high number of versions and modes have been developed in the last years. This has also led to a wide variety of names for the different modes, which creates a complex terminology and hinders the correct identification of the microextraction technique employed. Thus, this Doctoral Thesis proposes a classification of the different modes considering the operational set-up to carry out the microextraction approach, as well as the geometry of the sorbent in the case of the sorbent-based microextraction. Figure I.2 includes a scheme of this classification.

1.1.1. Overview on liquid-phase microextraction

LPME emerged as a miniaturized version of the conventional LLE, and it is based on the isolation of analytes from the sample matrix to an extracting phase of a few microliters (≤ 100 µL) [7]. As mentioned above, the use of such low volumes of extraction solvent together with the large sample volumes leads to high preconcentration factors, which allow the determination of trace amounts of analytes. Other interesting characteristics of LPME include low consumption of extraction solvents, simplicity, low generation of laboratory wastes, low cost, low energy consumption, while making possible (in most cases) the direct injection of the solvent containing the extracted and preconcentrated target compounds in the analytical system. All of these features are the key aspects justifying the success of all techniques included within LPME, which also comply with the GAC guidelines.

With the aim of simplifying the overview on LPME, the existing formats can be classified in three main modes: single-drop microextraction (SDME), membrane-based LPME, and dispersive liquid-liquid microextraction (DLLME), as shown in Figure I.2.

SDME

SDME resulted from the first attempt to miniaturize the conventional LLE. It consists in the use of a small volume of a solvent suspended from a syringe as extraction phase [8]. After a certain time, in which the solvent is in contact with the sample, the droplet is withdrawn with the syringe and injected in the analytical system for the determination of the compounds extracted.

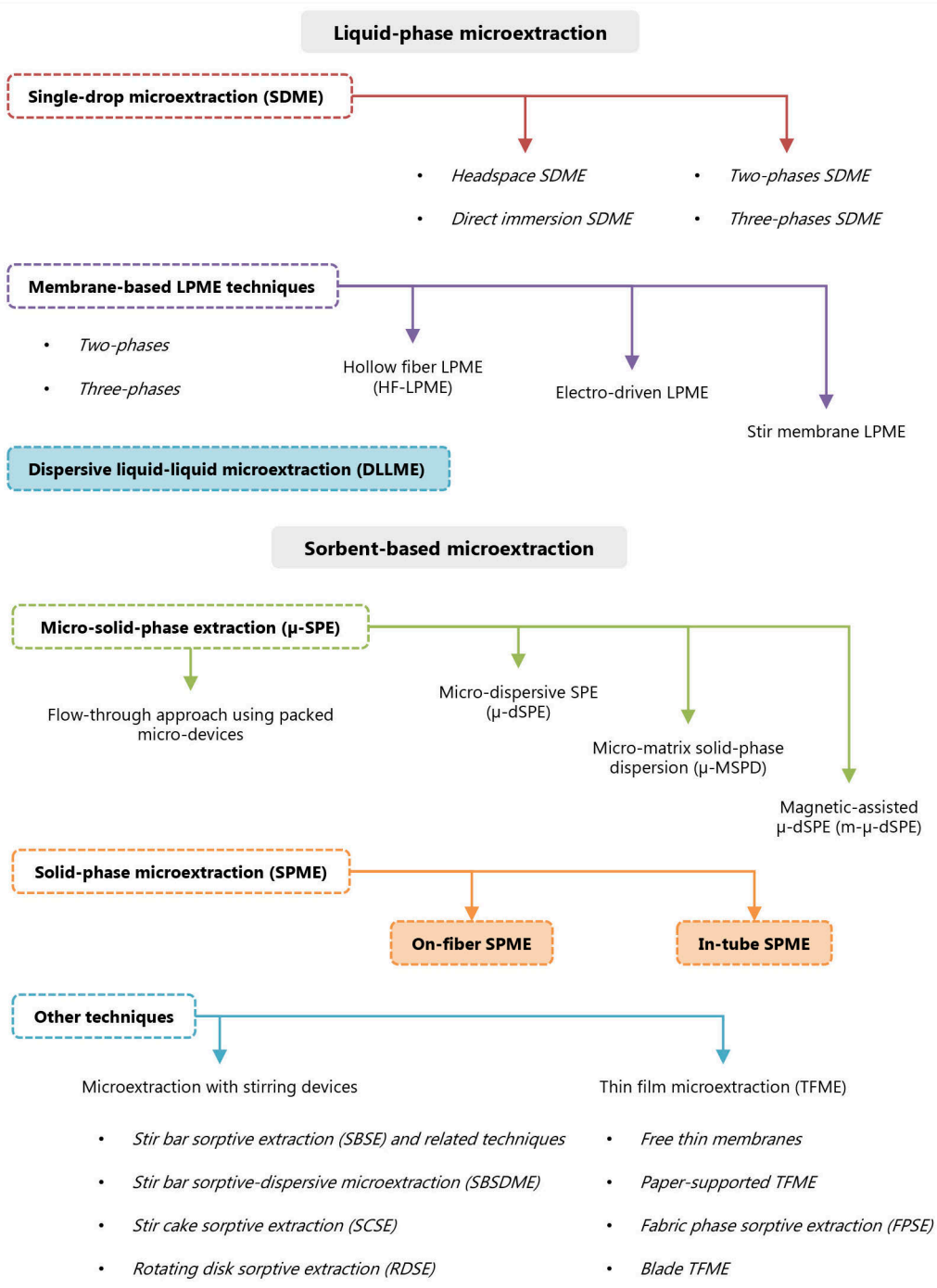

Figure I.2. Classification of main microextraction techniques using liquid or solid extraction phases. Highlighted techniques with a colored background in the text will be described in detail in other sections.

Depending on the type of contact between the droplet and the sample, there are different sub-modes of SDME: headspace mode (HS-SDME), in which the solvent droplet is exposed to the headspace over the sample; and direct immersion mode (DI-SDME), where the drop is directly introduced in the aqueous sample. Moreover, if the number of phases involved in the system during the extraction is considered, two-phases (sample and solvent droplet) and three-phases SDME can be performed [7]. Thus, in case of the three-phases SDME mode, the analytes are first extracted from the sample to an organic solvent, and then back-extracted to a droplet of an immiscible solvent or aqueous solution (acceptor phase), which is suspended in the organic phase (Figure I.3 A)). Other modifications of the experimental set-up have been proposed, such as the bubble-in-drop SDME and the continuous-flow SDME [8].

SDME has become quite popular due to its simplicity, the possibility of determining non-volatile and volatile compounds, and the low volumes of solvent employed, being around 1–15 µL However, the stability of the droplet is one of the main drawbacks on this technique. Moreover, the traditional organic solvents volatilize at high temperatures or low pressures leading to losses of the extraction solvent during the extraction process [7,8].

Membrane-based LPME

The membrane-based LPME mainly covers hollow fiber LPME (HF-LPME), electro-driven or electromembrane LPME, and stir membrane LPME. These techniques require an inert membrane to stabilize the extraction solvent, thus overcoming the main limitation of SDME.

In HF-LPME, a hollow fiber containing the extraction solvent is used as extraction device [9]. This fiber, typically of polypropylene, is introduced in the aqueous sample to carry out the extraction. This way, the extraction solvent is stabilized and protected from the large particles present in the aqueous sample (donor phase) while applying high stirring ratios. Furthermore, the contact area between the extraction solvent and the sample increases in HF-LPME in comparison with SDME. The HF with both ends sealed can be freely placed inside the vessel containing the aqueous sample while stirring. However, in general, the HF is introduced in the sample with the aid of a syringe [7]. In the three-phases mode, the pores of the hollow fiber are impregnated with a few microliters of the extraction solvent, while an acceptor phase (immiscible with the extraction phase) is placed in the lumen of the hollow fiber (Figure I.3 B)). When the acceptor phase is the same as the extraction solvent, the method is termed two-phases HF-LPME. After the optimum extraction time, the acceptor phase is injected in the analytical system (diluted or not) to accomplish the analytical determination.

In the case of electromembrane LPME, the extraction solvent is also supported in the pores of a polymeric support (hollow fiber or flat membrane), but the ionized analytes migrate from the sample to the extraction sample with the aid of an electric potential [10,11]. In general, this mode of LPME is performed at direct current electric potential, thus the anode and cathode are directly placed in the sample and the acceptor phase. The position of each electrode depends on the charge of the target analytes. Moreover, it can be carried out in the two-phases or three-phases

mode (Figure I.3 C)). This technique presents the same advantages as HF-LPME regarding the stability of the extraction phase, enrichment and clean-up capability, but with the added benefit of faster extraction rates, which can be modulated with the electric potential [10].

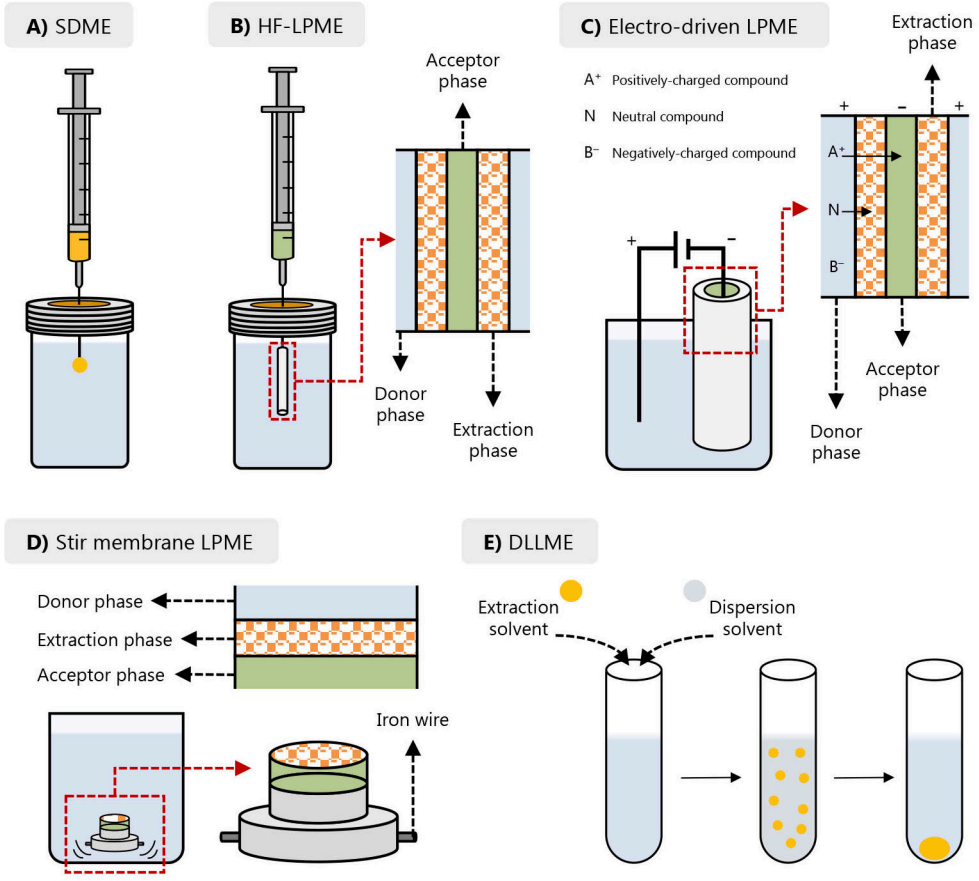

Figure I.3. General schemes for representative sub-modes of the different techniques included within LPME: **A)** DI-SDME in two-phases mode, **B)** HF-LPME in three-phases mode, **C)** electro-driven LPME in three-phases mode, **D)** stir membrane LPME in three-phases mode, and **E)** DLLME.

Stir membrane LPME requires the use of a specific disk-shaped device that contains a protected iron wire, the membrane, and a small area in which the extraction or acceptor phase is placed depending if two-phases or three-phases mode is used (Figure I.3 D)). The main advantage of this mode is the integration of the stirring element (iron wire) within the extraction device together with the high surface-to-volume ratio of the flat membrane in comparison with HF-LPME.

All these characteristics increase the diffusion of the analytes without requiring the application of an electric potential as it happens in electro-driven LPME techniques [12].

Despite membrane-based LPME techniques exhibit a set of attractive properties in comparison with SDME, passive diffusion is the main extraction mechanism in HF-LPME and stir membrane LPME, which makes the extraction process slow [5,7]. Electro-driven LPME overcomes this drawback but it requires the use of more instrumentation that makes the extraction system more complex. These limitations have made DLLME the most widely utilized LPME approach among all these strategies due to its simplicity, efficiency, and fastness [7,13]

DLLME

DLLME, which was introduced by Rezaee *et al.* in 2006 [14], bases on the dispersion of the extraction solvent in the sample with the aid of a dispersive solvent (Figure I.3 E)). The operational mode of this method involves the use of a mixture of the extraction solvent, immiscible with the sample, and the dispersion solvent, miscible with both the extraction solvent and the sample. The latter allows the formation of small microdroplets of extraction solvent through the sample, which increases the mass transfer of the analytes and therefore improves the extraction efficiency. After centrifugation, the formed microdroplet containing the enriched analytes is collected for its further analysis [14].

In this Doctoral Thesis, DLLME is one of the microextraction techniques under study and, therefore, a detailed description of this LPME mode is included in Section I.2.

1.1.2. Overview on sorbent-based microextraction

Despite the success of the different LPME modes, they still require the use of solvents and their automation is complex in some cases. In this sense, sorbent-based microextraction presents additional advantages from both operational and analytical points of view [15]. These techniques came out as the miniaturization version of solid-phase extraction (SPE), which uses a cartridge packed with the extraction phase, but using small amounts of the solid extraction material (≤ 10 mg). In general, they are easily automated, they allow the recovery and reuse of the sorbent material, and they facilitate the minimization or even the complete elimination of organic solvents in the entire procedure. Furthermore, these techniques take advantage of the material science technologies to prepare smart and task-specific solid materials, thus tuning the selectivity of the sorbent. All these features not only solve the main challenges within the analytical process (Figure I.1), but also meet many requirements established by GAC [16].

In comparison with LPME, a wider variety of sorbent-based microextraction techniques have been developed over the last decades, likely due to the versatility of the sorbent materials. Thus, they can be (i) packed in a small device, (ii) dispersed through the sample matrix, or (iii) coated on a solid support. Furthermore, the sorbent phases can be used either via a flow-through method or in DI and HS modes [15]. This has hampered their classification given the different

criteria than can be applied for this purpose. In this Doctoral Thesis, they will be categorized considering both the operational set-up and the geometry of the sorbent when assembled in a device. Therefore, as shown in Figure I.2, three groups can be distinguished: micro-solid-phase extraction (μ-SPE), solid-phase microextraction (SPME), and other techniques that present characteristics of both categories.

μ-SPE

The miniaturized sorbent-based method most similar to conventional SPE is μ-SPE. The same principles can be applied, with the main difference related to the use of lower sorbent amounts and the non-exhaustivity of the extraction process in most applications. The main route to accomplish the miniaturization is by reducing the device size by placing or packing the sorbent in a small cartridge/syringe, microcolumn, disk, pipette tip, or needle syringe, among others, as shown in Figure I.4 A) [17]. With respect to the experimental procedure, μ-SPE consists in a static flow-through method and may require one or several steps of sorbent conditioning, sample loading, sorbent washing and/or drying, and analyte elution [15].

Despite the benefits of μ-SPE, the activation of the sorbent involves the consumption of organic solvents, it requires relatively long extraction times due to the slow flow rates, and the blocking of the extraction device is a common problem. In this sense, micro-dispersive SPE (μ-dSPE) arises as an alternative to overcome all these problems [18]. In this case, the solid sorbent is dispersed in the liquid sample, thus increasing the mass transfer of the analytes towards the sorbent and avoiding the clogging issues (Figure I.4 B)). Then, the sorbent is separated and subjected to desorption using an adequate solvent or even thermal desorption using specific instrumentation coupled to the gas chromatography (GC) system.

In general, an external energy source is applied during the process to achieve adequate dispersion, typically vortex or ultrasounds [18]. Other approaches have been proposed to enhance the dispersion of the sorbent and improve the extraction efficiency, such as effervescence-assisted μ-dSPE [19], air-assisted μ-dSPE [20], and spin column μ-dSPE [21]. Despite the sorbent in packed in a plastic column in the spin column method (as in μ-SPE), the device is subjected to centrifugation after each step of the extraction procedure as a form of dispersion to facilitate and enhance the passing of the sample or solvent through the sorbent.

A limiting step during the μ-dSPE procedure is the requirement of centrifugation to separate the sorbent containing the trapped analytes from the sample matrix, followed by the need of a desorption step to free the trapped analytes from the sorbent using the proper desorption solvent. Different strategies have been described with the aim of avoiding this separation step. Thus, in the porous membrane-protected μ-dSPE, a small amount of the sorbent is placed inside a polymeric membrane forming a device [22]. The device is stirred into the liquid sample to perform extraction and then collected using a pair of tweezers, thus eliminating the centrifugation step. Moreover, the membrane acts as barrier for larger molecules when dealing with complex samples, thus reducing matrix effects. Other strategies involve performing the μ-

dSPE procedure in a syringe, where filtration by connecting a filter to the syringe is used as convenient alternative to centrifugation [15,23]. Furthermore, taking advantage of the versatility of polymeric materials, several sorbents in different shapes (as monoliths) have been designed and used to facilitate both sorbent addition and separation from the sample, with shapes that include foams, beads and tablets, among others [15].

Undoubtedly, the magnetic-assisted μ-dSPE (m-μ-dSPE) has been the most widely used sub-mode among all μ-SPE techniques to avoid centrifugation [24]. This approach requires a sorbent with paramagnetic properties to ensure a magnetic-based separation, requiring an external magnet to separate (i) the sorbent from the sample after the extraction step and (ii) the sorbent from the desorption solvent after the desorption step (Figure I.4 C)). Most applications use magnetic particles (MPs) as the paramagnetic element, which can be incorporated in the sorbent in different formats: mixing the MPs and the extraction material forming a heterogeneous sorbent, embedding the MPs in the polymeric extraction material, functionalizing the surface of the MPs with chemical groups with affinity towards the analytes, or coating the surface of the MPs with the extraction sorbent forming a core-shell structure [24,25].

The μ-dSPE strategy has also been applied for the analysis of solid samples, leading to the micro-matrix solid-phase dispersion (μ-MSPD) approach [26]. In this case, both the solid sorbent and the solid sample are strongly mixed during the microextraction stage, and then packed into a column to perform the desorption step (as in μ-SPE). Figure I.4 D) schematizes this sub-mode.

SPME

The term SPME was first introduced by Pawliszyn *et al.* in 1990 [27]. The original SPME device consisted of a small amount of a sorbent material immobilized on the surface of a small fiber, forming a coating of 1 cm of length with thicknesses up to 100 μm (Figure I.4 E)). In this technique (on-fiber SPME), the fiber is hanged in the sample or in the HS to perform the extraction of the analytes for a fixed time. Then, the analytes are desorbed from the sorbent either by thermal desorption (in the inlet port of a GC) or by using a desorption solvent. Thus, only two steps are initially involved in the procedure: extraction and desorption. A different SPME design was later proposed to improve the coupling with liquid chromatography (LC) and the analytical performance of the original on-fiber configuration. Thus, in the in-tube SPME mode, the device can be prepared by coating the inner walls of a capillary with a thin layer of the sorbent material, by packing the capillary with the sorbent material, or by placing a monolith inside the capillary [28]. The operating steps in this case resembles that of μ-SPE, following a flow-through procedure (Figure I.4 E)).

The size and amount of the sorbent material in these SPME devices are generally lower in comparison with μ-SPE, which confers high enrichment capacity to the SPME techniques due to the high phase volume ratio between the sample and the extraction phase. Moreover, the small dimensions of these SPME devices allow inserting them in the analytical system to carry out the desorption or to couple them with instruments for direct analysis, in a higher extent than μ-SPE devices. Besides, SPME devices are usually reused up to hundreds of times in comparison with the

single-use commonly recommended for µ-SPE devices. A detailed description of the SPME technique is included in Section I.3 since it is the sorbent-based microextraction technique studied in this Doctoral Thesis.

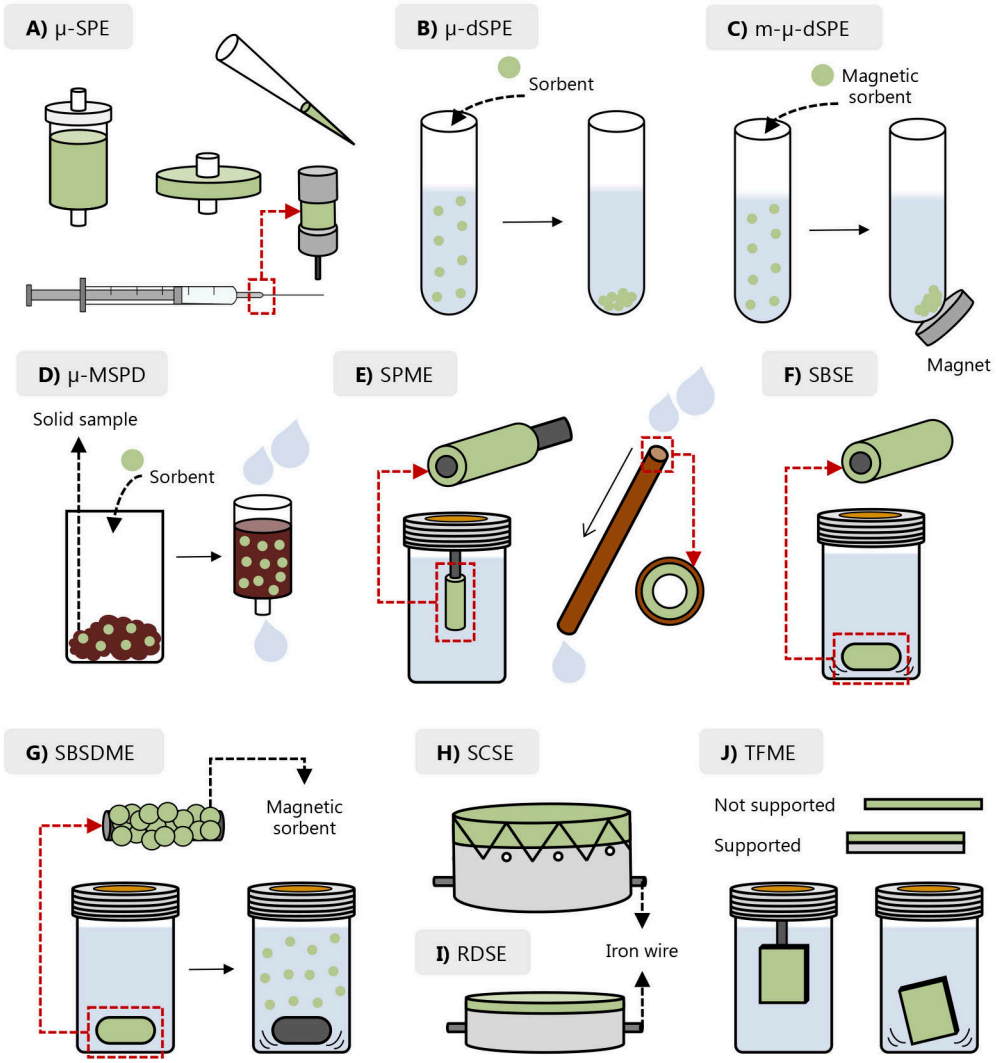

Figure I.4. General schemes for representative sorbent-based microextraction techniques and devices: **A)** microcolumn, disk, pipette tip and packed needle syringe for µ-SPE, **B)** µ-dSPE , **C)** µ-MSPD, **D)** m-µ-dSPE, **E)** on-fiber SPME in DI mode and in-tube SPME coated device, **F)** conventional SBSE, **G)** SBSDME, **H)** SCSE device, **I)** RDSE device, and **J**) not supported and supported TFME in hanged and freely dispersed modes.

Others

There are other sorbent-based microextraction techniques that exhibit distinctive characteristics of both main categories, which complicates their firmly inclusion in any of the two groups. This is particularly important for those techniques based on stirring devices and thin films. They use similar devices to SPME, but in an operational set-up that resembles more a µ-dSPE procedure [15].

With respect to stirring devices, stir bar sorptive extraction (SBSE) is a technique that can be understood as a solution to the small amount of sorbent used in the previous configurations of SPME (on-fiber and in-tube) [29]. In this design, a magnetic stir bar is coated with a thicker layer of the sorbent material as shown in Figure I.4 F). This device can be used in both HS or DI mode during the extraction step, while both solvent or thermal desorption (with a suitable thermo desorption unit, TDU) are also possible. Several modifications of the procedure have led to the development of different sub-modes of SBSE to enhance the extraction efficiency, such as the ice concentration linked with extractive stirrer (ICECLES) method [30] and the solvent-assisted SBSE (SA-SBSE) method [31]. In the first case, the sample is frozen during the extraction step to concentrate the analytes, whereas a polymeric coating is swollen with an organic solvent in SA-SBSE.

In general, the sorbent coatings in SBSE are composed of polymers. When the stir bar is coated with a porous material with adsorption properties to enhance the extraction towards more polar compounds, the technique is termed bar adsorptive micro-extraction (BAµE) [32]. In the case of stir bar sorptive-dispersive microextraction (SBSDME), the stir bar (or rod magnet) is physically coated with a hydrophobic magnetic sorbent [33]. In the extraction step, the sorbent material initially coats the magnet and, when low stirring rates are applied, the coated device rotates as in SBSE. When a high stirring rate is applied, enough to surpass the magnetic field, the sorbent phase is dispersed into the sample solution and the extraction takes place as in µ-dSPE. When the extraction ends, the stirring is stopped, and the strong magnetic field of the rod magnet is able to retain the dispersed sorbent material (Figure I.4 G)). Then, the rod magnet can be easily collected and subjected to the further desorption step.

The stir cake sorptive extraction (SCSE) approach uses an extraction device based on a labmade holder where the monolithic extraction phase and the stir bar/stirring element are placed (Figure I.4 H)) [12]. With this system, stirring could be promoted during extraction with no damage of the sorbent phase due to contact with the extraction vial walls. This is an important advantage of the technique that allows increasing the lifespan and reusability of the device in comparison to SBSE and related techniques. In the case of the rotating disk sorptive extraction (RDSE), the extraction device is similar to that of SCSE but using a thin film of the extraction phase or SPE disks to improve the surface area available for extraction, as it is illustrated in Figure I.4 I).

Besides the improvement in the extraction capacity with these stirring techniques due to the higher amounts of sorbent and better dispersion, they are also accompanied by long extraction

times to reach the equilibrium. Thin film microextraction (TFME) was proposed to address this issue due to the high surface-to-volume ratio of the sorbent in this technique [34]. TFME was initially considered a different geometry for SPME [35]. It bases on the use of a flat surface coated with a thin film of extraction phase or a free membrane with a reduced thickness and without any support. The surface area to volume ratio of the resultant TFME device is enhanced, what turns into higher sensitivity without increasing the extraction times, which was a problem in SBSE and some applications of SPME [34].

When using these TFME devices, they can be freely dispersed in the sample in a similar procedure as in μ-dSPE. However, it is more common to expose the membrane to the sample with the aid of a hanger tool as in SPME, such as a thin stainless steel wire in the shape of a flag, a cotter pin, or a mesh holder. Thus, TFME can be performed in DI o HS mode, while liquid desorption is generally carried out. However, there are some studies where thermal desorption in the GC system is performed using a large volume TDU [34].

First applications of TFME consisted of a polymeric thin membrane [36]. Due to the limited extraction capability of these devices, mixed matrix membranes (MMM), which involves the incorporation of solid particles in the polymeric membrane without any support, have been also used for TFME [15,37]. With respect to TFME using supported thin films, there are different sub-modes depending on the type of support: paper-supported TFME using paper as substrate [38]; fabric phase sorptive extraction (FPSE), which involves the use of a thin fabric substrate coated with a sorbent prepared using the sol-gel technique [39]; and blade TFME, in which a metallic flat surface coated with a thin film of extraction phase is used [40]. Figure I.4 J) includes a scheme of TFME.

1.2. New materials as extraction phases

Harmful solvents usage in the sample preparation stage is widely extended for the determination of a wide variety of compounds and, in fact, these solvents are usually (and paradoxically) recommended in official analytical methods devoted to environmental monitoring [41]. Among the proposed petroleum-based and halogenated solvents, benzene, chloroform, carbon tetrachloride, diethyl ether, cyclohexane, dichloromethane and triethylamine have been classified as hazardous or highly hazardous, with a great impact in both the environment and human health [42,43].

The substitution of traditional organic solvents by less toxic alternatives is of particular importance when designing new sustainable analytical methods according to the GAC guidelines [41,44]. Indeed, the development of different microextraction methods has been closely accompanied by the seeking of novel solvents with environmental-friendly characteristics as well as tunable properties to improve the performance of the methods [43,45,46]. Moreover, the incorporation of sorbent-based microextraction within the analytical procedure reduces the

consumption of solvents (still required in the desorption step), and even leads to the development of solventless methods in the cases where thermal desorption is carried out [47].

Regarding the improvements of the selectivity of sample preparation methods, the design and incorporation of new materials as sorbents in microextraction techniques has been one of the most important research lines in the recent years [4]. Traditional sorbent phases are based on silica materials or conventional polymers (e.g., PDMS). The selection of the adequate available sorbent for a certain application is based on the characteristics of the sample, and the target analytes, such as polarity, possible extraction mechanism justifying the interaction sorbent-analyte, or molecular weight. The main drawback of traditional sorbents is their lack of selectivity, low thermal stability, and poor matrix-compatibility [48]. Therefore, the preparation of sorbents able to selectively interact with the target analytes, and their incorporation in the analytical extraction procedure, may lead to the key to solve challenging applications while enhancing the extraction efficiency of analytical methods [49].

Several solvents and sorbents with outstanding properties and safer toxicological profiles have been proposed to replace conventional organic solvents and to perform selective single target or multi-target analysis from complex matrixes. Given their impact in the field, this section overviews the composition and characteristics of the main new liquid and solid materials that have been explored as new extraction phases in microextraction techniques. Table I.1 lists these materials according to their liquid or solid nature, while some of their properties are also included.

1.2.1. Solvents and liquid materials

The most successful liquid materials or solvents proposed to replace organic solvents as extraction phase in microextraction include supramolecular solvents (SUPRASs), deep eutectic solvents (DESs), switchable solvents (SwSs), and ionic liquids (ILs).

SUPRASs refer to amphiphilic compounds able to self-assemble under a proper environment due to the coacervation phenomenon, forming a nanostructured liquid in colloidal solutions [50]. Despite these amphiphilic compounds are initially soluble, the coacervation generates a new phase rich in colloids (supramolecular aggregates) that can be separated from the liquid dispersion. In general, amphiphilic compounds are composed of a hydrophobic tail, usually a hydrocarbon chain, and a hydrophilic head, which can be a polar uncharged group or an ionic group.

Among the wide variety of amphiphilic compounds, surfactants have been the most successful and widely used solvents in Analytical Chemistry, since they constitute the first low toxic option to replace conventional organic solvents [51]. When surfactants are added to water in a concentration higher than their critical micelle concentration (CMC), they self-assemble to form normal micelle aggregates with strong solvation properties, which allows them to interact with compounds of different polarity. Solutions of non-ionic, zwitterionic and ionic surfactants have

been widely used in different microextraction approaches, with Triton X-114, Triton X-100, sodium dodecyl sulfate, and dodecyltrimethylammonium bromide being the most commonly used [52].

Apart from surfactants, Rubio *et al.* demonstrated that other amphiphilic compounds were able to form supramolecular aggregates: alkanols and alkanoic acids with long chains [53,54]. These compounds form a colloid dispersion of reverse micelles in protic and aprotic solvents (e.g., tetrahydrofuran or acetonitrile) at concentrations higher than their respective critical aggregation concentration (CAC). The coacervation and subsequent formation of the hydrophobic supramolecular solvent is induced with the addition of water. Decanoic acid, 1-octanol, and 1-decanol, together with tetrahydrofuran, have been the most used among this type of supramolecular solvents [44,55].

More recently, Bogdanova *et al.* [56] also demonstrated the formation of supramolecular aggregates of primary amines with long hydrocarbon chains when using monoterpenoids as coacervation-inducing agent. The amines form positively charged amphiphiles when dissolved in water due to their hydration and dissociation. Terpenoids, negatively charged once added to these amine aqueous solutions, interact with the amphiphiles and induce the coacervation phenomenon. Thus, 1-decylamine is able to form a coacervate in water when adding thymol to the solution.

DESs are a group of relatively new solvents formed by the combination of a hydrogen bond donor (HBD) and a hydrogen bond acceptor (HBA) at different ratios [57]. These mixtures do not follow an ideal solid-liquid phase behavior and present melting points significantly lower than the melting temperature of the individual initial components. The resulting DES from such mixtures does not require any additional purification step. Main features of these solvents, if properly designed, may include low toxicity and high biodegradability. DESs are commonly classified depending on their composition, with type III being the most frequently exploited because of their low cost and ease of synthesis. In this group of DESs, quaternary ammonium or phosphonium salts are the most common HBAs, while alcohols, carboxylic acids or amines are used as HBDs [58]. These solvents are also versatile, because some of their physicochemical properties can be tuned by selecting the adequate combination of HBD and HBA species [44,59].

Despite most DESs are hydrophilic, given their outstanding characteristics, they have been also exploited in the different LPME techniques [52,58], particularly those composed of cholinium chloride as HBA and phenol or urea as HBD. However, in those approaches in which the hydrophilic DES is directly added to the sample (i.e., DLLME and DI-SDME), it is important to take into account that the decomposition of the DES takes place when it interacts with water due to the destruction of the hydrogen bonds between its components [60]. Therefore, when an aprotic solvent is added to promote the insolubilization of the DES, the final water-insoluble phase containing the extracted analytes is indeed mainly composed of the HBD and the aprotic solvent.

The description of new hydrophobic DESs have led to a significant increase in the use of DES in LPME [57–59]. For the preparation of these water-insoluble solvents, DL-menthol and tetraoctylammonium bromide are commonly used as HBA, while decanoic acid is selected as HBD

[59]. Moreover, a high variety of natural products has been used for the preparation of natural DESs (NADESs), such as sugars or organic acids [61]. In this case, lactic acid and citric acid have been commonly used as HBDs in combination with different sugars, DL-menthol, betaine or other common HBAs [44,61]. NADESs present safer toxicological profiles and higher biodegradability, which makes them one of the greenest options as an alternative to conventional organic solvents up to date [44].

Other novel solvents include SwSs, which are water-insoluble media that can be easily and reversibly transformed to a water-miscible solvent by a simple change in the system (mild conditions) [62]. The first description of these solvents involved the use of a water-insoluble mixture of 1,8-diazabicyclo-[5.4.0]-undec-7-ene (DBU) and 1-hexanol [63]. After the exposure to gaseous CO_2 at room temperature and atmospheric pressure, the mixture rapidly changed its polarity and a homogeneous solution was obtained. This change in miscibility was due to an acid-base reaction in which the DBU was protonated and the hydrophilic carbonate salt of the alcohol was obtained. The reaction could be easily reversed by evacuation of CO_2 from the mixture, leading to insolubilization. Since then, different compounds have been identified as SwSs, including amidine and ternary amines of low polarity [62,64], and alkanoic acids with long chains [65].

In the case of amines (insoluble in aqueous solutions), the hydrophilic carbonate protonated form of the amine is obtained when CO_2 is added. This change in the polarity can be easily reversed by increasing the pH, which leads to deprotonation of the amine. Alkanoic acids (initially water-insoluble) generate the hydrophilic form when ionized (as salt, or as the carbonate when CO_2 is used) at high pH values. Thus, acidic pH values solubilize amines and basic pH values solubilize alkanoic acids [52]. Carbonate protonated amines have been the most explored SwSs, with *N,N*-dimethylbenzylamine and triethylamine being the most commonly used, together with a concentrated NaOH solution to obtain the water-insoluble phase [52,66]. With respect to the use of long chain alkanoic acids, hexanoic acid, nonanoic acid, and decanoic acid, have been the most explored [52,66], while H_2SO_4 solution are added to obtain the hydrophobic form.

ILs are a group of non-molecular solvents with low melting points (around 100 °C) prepared by the combination of bulky organic cations and organic or inorganic cations [67,68]. These molten salts exhibit a unique set of properties, such as high thermal and chemical stability, and low vapor pressure at room temperature, which confers them lower toxicity in comparison with volatile organic solvents. The most attractive feature of ILs is their impressive synthetic versatility and tuneability, which leads to drastic changes in their physicochemical properties by small modifications in their structure and composition. Thus, viscosity, solubility, and solvation properties of ILs can be easily tuned by properly selecting the nature of the cation and the anion [69]. Moreover, this versatility also allows the preparation of task-specific ILs and interesting derivatives, such as polymeric ILs (PILs), IL-based surfactants, and magnetic ILs [44,69]. All these characteristics make ILs the most popular candidates to substitute conventional organic solvents, being the most explored option in the recent years in comparison with the abovementioned solvents [70,71].

Table I.1. Composition and main characteristics of new materials explored in microextraction techniques.

Material	Composition	Examples	Characteristics
Liquids			
Supramolecular solvents (SUPRAs)	surfactants alkanols & alkanoic acids with long chains primary amines with long chains	triton-X114, sodium dodecyl sulfate decanoic acid, 1-octanol 1-decylamine	– Form supramolecular aggregates when added above a certain concentration – Impressive solvation properties – Low toxicity
Deep eutectic solvents (DESs)	hydrogen bond donor (HBD) + hydrogen bond acceptor (HBA)	HBD: phenol, decanoic acid, lactic acid HBA: cholinium chloride, DL-menthol, betaine	– Biodegradability – Low toxicity – Simple synthesis without purification – Low cost – Synthetic versatility
Switchable solvents (SwSs)	amidine and ternary amines of low polarity alkanoic acids with long chains	*N,N*-dimethylbenzylamine, triethylamine hexanoic acid, decanoic acid	– Modulable hydrophilicity by changing the pH
Ionic liquids (ILs)	organic cation + organic/inorganic anion	hexadecylpyridinium bromide, 1-octyl-3-methylimidazolium hexafluorophopshate	– Low vapor pressure – Impressive tunable properties – Thermal stability

Table I.1 (continued).

Material	Composition	Examples	Characteristics
Solids			
Silica-based materials	polymers mesoporous silica silica particles	polymerization of silicon alkoxides by sol-gel method SBA-15 SiO_2 microspheres	– Low cost – Easy functionalization – Controllable morphology – Low toxicity
Biopolymers	polysaccharides, proteins and lipids	chitosan, alginate, cellulose	– Renewable – Biodegradable – Non-toxicity – Easy functionalization – Flexibility
Natural sorbents	plant by-products	cork, plant leaves, cotton	– Renewable – Biodegradable – Nontoxicity – Easy functionalization
Polymeric ionic liquids (PILs)	ILs monomers: organic cation + organic/inorganic anion	poly(1-vinly-3-butylimidazolium bromide), poly(diallyldimethylammonium) chloride	– Impressive tunable properties – Thermal stability – Mechanical stability
Conducting polymers	organic polymers that conduct electricity	polypyrrole, polyaniline	– Electrical properties – Thermal stability

Table I.1 (continued).

Material	Composition	Examples	Characteristics
Molecularly imprinted polymers (MIPs)	crosslinked polymers prepared in presence of a template molecule (target analyte)	methacrylic acid as monomer, ethylene glycol dimethacrylate as crosslinker, and an organic molecule as template	– Molecular recognition properties – Robustness – Chemical stability
Metallic particles	pure metal particles	Ag nanoparticles, Au nanoparticles	– Chemical stability – Mechanical stability – Thermal stability – Easy functionalization – Porosity (metal oxides)
	metal oxide particles	TiO_2 particles, ZrO_2 particles	
Magnetic particles	oxides and sulfides of transition metals	magnetite, cobalt ferrite	– Magnetic properties – Easy functionalization
Carbon-based materials	allotropic forms of carbon	graphene, carbon nanotubes	– Large surface area – Porosity – Versatility – Easy functionalization
Reticular materials	crystalline frameworks formed by the assembly of rigid building blocks	MOFs: MIL-53(Al), HKUST-1(Cu) COFs: COF-5, COF-320	– Large surface area – Porosity – Impressive tunable structure – Thermal stability

Table I.1 (continued).

Material	Composition	Examples	Characteristics
Immunosorbents	antibodies	synthetic antibodies specific for the target analyte: proteins	– Molecular recognition properties
Aptamers	oligonucleotides	biotinylated DNA, thiol-modified DNA,	– Molecular recognition properties – Low cost – Non-toxicity
Supramolecules	big molecules with host-guest chemistry characteristics	cyclodextrines, calixarenes	– Molecular recognition properties – Low cost
Restricted access materials (RAMs)	solid materials modified with hydrophobic or hydrophilic groups, supramolecules or amino acids	silica-materials modified with phenol and diol groups; graphene modified with cyclodextrines	– Size/chemical exclusion ability – Impressive tunability

In this Doctoral Thesis, ILs and IL-based surfactants were explored in different DLLME applications. Therefore, a detailed description of these materials and their incorporation in this LPME strategy is included in Section I.2.

All the novel liquids materials and solvents described meet many GAC requirements and present other interesting features for microextraction. However, the ideal solvent has not been found yet. Thus, all of them usually present high viscosity, which hinders their manipulation in LPME, and some of them are decomposed once added to the aqueous sample. Moreover, despite they do not generate volatile organic compounds in comparison with conventional organic solvents, there are still some toxicity issues that have not been addressed, particularly those towards the aquatic environment. Furthermore, the use of some of them still requires the addition of an organic solvent. (i.e., to form SUPRASs with alcohols and alkanoic acids), or extreme conditions, such as the pH change when using SSs.

1.2.2. Solid materials

The fast development of new materials within material science have triggered the incorporation of a broad spectrum of solid materials in microextraction. Among all the materials described, the most successful in microextraction include a wide variety of polymers (i.e., silica-based polymers, biopolymers, PILs, and polymers with specific functionality), metallic materials (i.e., nanoparticles and magnetic particles), carbon-based materials, silica-based materials, reticular materials, and the use of supramolecules and specific groups with recognition ability to functionalize other solid materials.

Polymers are very versatile materials, and therefore a great variety of polymeric sorbents with different properties can be prepared depending on the composition, and also on the synthetic conditions and routes followed for their preparation [49]. Moreover, the possibility of fabricating monolithic structures using polymers facilitates the preparation of sorbent-based microextraction devices [72]. Silica-based polymers are the most common polymers explored as sorbents taking advantage of the sol-gel technology to prepare materials with controllable morphology. Moreover, they are relatively cheap and the presence of functional groups in their surface allows functionalization to enhance selectivity [4,49,72].

Biopolymers are polymers obtained from natural sources and constitute a renewable and biodegradable resource of materials [73]. This group includes polysaccharides, proteins, and lipids, derived from animals and plants, being the polysaccharides chitosan, cellulose, alginate, and agarose, the most common ones. Their success in microextraction mainly lies in the versatility of their physicochemical properties, and their flexibility of design and adaptation, which allow their use in numerous formats and configurations [74]. However, they have been mainly used in combination with other functional materials to prepare composites.

Other materials derived from natural sources have been recently evaluated in analytical microextraction, with the aim of promoting recycling natural products besides using renewable materials [75]. In this trend, cork, cotton, and agricultural by-products (e.g., leaves and peels) [75,76], are starting to be considered as new green sorbents. However, in most applications, the material is chemically modified to improve its characteristics and analytical performance [76].

PILS are polyelectrolytes obtained through the polymerization of IL monomers. PILs not only retain the main characteristics of ILs, but also present the inherent properties of polymers with enhanced mechanical stability and conductivity properties [77]. Thus, they are the best option to exploit the outstanding properties of ILs in sorbent-based microextraction strategies [78]. A detailed description of PILs is included in Section I.3 since these materials were used as SPME coatings in this Doctoral Thesis.

Among polymers with specific functionality, conducting polymers characterize by their electrical properties, high thermal stability, and easily controllable synthesis. The most common conducting polymers employed as sorbents in microextraction are polypyrrole, polythiophene, polyaniline, and their derivatives [79]. Stimuli-responsive polymers have also attracted attention in the field because of their ability to alter their physical and/or chemical properties upon a change in the environment, such as pH, temperature, electric or magnetic fields, and the presence of certain substances [80].

Molecularly imprinted polymers (MIPs) are a particular group of synthetic polymers characterized by presenting molecular recognition properties similar to those exhibited by natural binding proteins [81]. These crosslinked polymers are highly selective since the target molecule for which they have specific affinity directly participates in the synthetic procedure. MIPs present an interesting set of remarkable properties for microextraction: adequate chemical and mechanical stability, high selectivity, moderate thermal stability, robustness, and reusability [82]. Furthermore, their synthesis is quite simple, and low-cost reagents are required to prepare them.

Metallic materials have also found numerous applications in microextraction. In fact, metallic nanoparticles have been widely used because of their high thermal, mechanical and chemical stability, and feasible functionalization. Among these nanoparticles, Au, Ag and Cu nanoparticles have been mainly explored [83,84]. Moreover, metal oxide particles have also been useful for the preparation of porous and highly stable sorbents, particularly those of Ti and Zr [72,84]. MPs should be included within this group, since, in general, they present a metallic nature [4]. Thus, they are mostly made from transition metals (Fe, Co and Ni) or from their oxides and sulfides, such as cobalt ferrite ($CoFe_2O_4$), magnetite (Fe_3O_4) and greigite (Fe_3S_4). Besides, they can be obtained with different particle size, which can be either nano or micrometrical [85]. Given their superparamagnetic properties, which permit their easy and quick isolation when applying an external magnetic field, they emerged as useful tools to develop m-μ-dSPE methods. Moreover, these MPs are commonly modified to obtain composite materials that present improved stability and extraction capability than the isolated sorbent [4,86].

Carbon-based materials also present exceptional physical and chemical properties, such as versatility, large surface area with delocalized π-electrons, and easily modifiable surface [87]. They constitute a group of different hexagonal structures of sp^2 hybridized carbon atoms. A single layer of these materials is called graphene. This carbon allotrope, together with graphene oxide (GO), and reduced graphene oxide (rGO), are the most representative two-dimensional forms. The difference between them lies in the presence of oxygen functional groups on their surface and their water solubility. Graphene and rGO are non-polar and hydrophobic materials with high affinity towards carbon ring structures, while it is possible to prepare hydrophilic GO [48]. The three-dimensional forms of graphene are single or multiple wall carbon nanotubes (CNTs). Both of them share the same exceptional properties as graphene and its derivatives, but with a few differences because the inner walls of these materials are blocked by the steric hindrance. The overall group of carbonaceous materials have been extensively used as sorbents due to their high surface area and high affinity towards both organic compounds and metal ions [4,48].

Apart from polymers, other silica-based materials have been widely applied in microextraction, including mesoporous silica, SiO_2 particles, and porous silicon particles [83,88. The easily formation of silanol groups in their surfaces makes them highly tunable materials and allows the attachment of other materials and specific chemical groups to improve their performance [49]. Moreover, mesoporous silica presents a high surface-to-volume ratio, well-defined pore volume, low toxicity and low cost [88].

Another important group of novel solid sorbents is formed by the reticular materials. They are large crystalline frameworks constituted by the assembly of building blocks (BBs) linked by covalent or strong coordination bonds, depending on the type of reticular material [89]. One of the main features of these materials is that the rigid BBs keep their integrity through the synthetic process [90]. They are also characterized by their impressive porosity, adequate chemical and thermal stability, and possibility of post-synthetic modification, which makes them adequate sorbents in microextraction [91,92]. Considering the huge abundance and variety of BBs, it is possible to prepare countless reticular materials with targeted structures [93]. The most common types of reticular materials are metal-organic frameworks (MOFs) and covalent-organic frameworks (COFs), which mainly differentiate by the organic or inorganic nature of their BBs. Thus, MOFs are composed of metal ions or metallic clusters and organic linkers as BBs connected by strong coordination bonds [89,90]. As MOFs were used in SPME application in this Doctoral Thesis, more information regarding their characteristics and properties is included in Section I.3. The rigid units of COFs comprise only organic molecules with non-metallic light elements (C, H, O, N, B and Si), which are then linked by covalent bonds ordered in two- or three-dimensional networks, depending on the geometry of the organic molecules [94].

The modification of the surface characteristics of all the above-mentioned solid materials may lead to the preparation of interesting materials with both impressive selective characteristics and clean-up features [4,48,49]. In general, the structures and molecules used for the functionalization give the sorbent affinity towards specific compounds [72]. Restricted access

materials (RAMs) can be included within this category. RAMs are materials with exclusion ability due to their dual surface configuration [95]. Thus, they present small pores that only allow the extraction of small and low-molecular weight compounds, while the surface is functionalized with specific groups to prevent the retention of big molecules that can interfere in the analytical determination. They can be simply prepared by the surface modification of other sorbents materials (i.e., as silica, MIPs, CNTs and graphene) with hydrophobic or hydrophilic groups, supramolecules, or amino acids [4,95].

In this context of preparing selective sorbents, antibodies have been used as binding agents to prepare immunosorbents, which are particularly useful in clinical analysis [96]. However, their use is limited due to their low stability, high cost, and labor intensive obtaining procedure. In this sense, aptamers have found more applications [97]. Aptamers are oligonucleotides (short DNA and RNA molecules) with specific binding capacity through a wide variety of interactions. Moreover, they exhibit high stability, nontoxicity, ease of synthesis and low cost. Supramolecules, including cyclodextrins, calixarenes, and crown ethers, are host molecules with the capacity of forming host-guest interactions with the target analytes [4]. Given their selectivity and low cost, they have also been explored in sorbent-based microextraction methods [4,72].

1.3. Automation of microextraction techniques

Apart from the incorporation of microextraction techniques and greener alternatives to conventional organic solvents, to address the sustainability issues of conventional analytical sample preparation methods, automation is also encouraged when upgrading these approaches to foster their implementation in routine analysis laboratories [2]. Indeed, automation is one of the requirements covered by GAC guidelines since it reduces the risks for the operator and positively affects the precision, accuracy, and total analysis time [3].

In general, two main strategies have been followed for the automation of microextraction techniques: (i) using robotics systems that require expensive and specific instrumentation but allow the processing of samples in parallel, and (ii) using flow techniques, which exhibit high sample throughput capabilities and enable sequential and continuous operation, but this way avoiding the possibility of simultaneous extractions [98,99]. Despite the success of flow techniques due to their versatility and low cost, current advances in artificial intelligence make autosamplers and robotic systems big competitors because of their huge potential to replace human operators in all the steps of the analytical procedure [99]. In any case, depending on the LPME or sorbent-based microextraction technique, both approaches permit the development of semi-automatic or fully automated sample preparation methods, as well as the hyphenation with the subsequent technique used for the analytical determination.

The automation of LPME techniques comprises a series of challenges given the difficulties associated to the manipulation of really low volumes of extraction solvent and the centrifugation

steps required in DLLME [7,100]. Most of the approaches followed for their automation are flow systems composed of multi-port valves and programable pump syringes [100,101]. Thus, they are mainly based on sequential injection analysis (SIA), leading to the development of lab-in-syringe (LIS) and lab-on-valve (LOV) methods, by changing the configuration of the valves and syringe pumps involved in the system [99].

All the LPME techniques (i.e., SDME, membrane-based LPME, and DLLME) have exploited the different SIA variations for their automation [100,101]. Moreover, DLLME allows more versatility in this aspect and automated DLLME methods have been described using a vial as extraction vessel and a robotic system equipped with syringes to perform all the steps [102]. In this case, the centrifugation is avoided and the separation of the final microdroplet can be accomplished by different modes: (i) using a demulsification agent and a labmade vial with a specific design (i.e., narrow neck or conical bottom) to facilitate the collection, or (ii) passing the emulsion (sample, extraction solvent and desorption solvent) through a filter connected to a syringe to retain the droplets of extraction solvent, followed by elution using an organic solvent [102]. Figure I.5 A) includes a scheme of a representative set-up for an automated DLLME method based on the LIS approach [103].

With respect to sorbent-based microextraction, a high level of automation is possible. This may be due to the easily handling of the sorbent, which commonly forms part of a device. In this sense, flow techniques have been widely implemented for the development of automated and on-line μ-SPE methods, in which the overall analytical method is automated [104]. These strategies, commonly based on SIA systems, are hyphenated with LC by replacing the injection loop by the packed μ-SPE device. Given the backpressure problems commonly associated to flow-injection formats, fully automated μ-SPE methods have also been described using robotic syringe systems, as well as microfluidic platforms and microchips, which are easily prepared taking advantage of the 3D printing technology [15].

In the case of μ-SPE and m-μ-SPE techniques, the automation has been mainly accomplished in a similar manner as DLLME methods [15]. Thus, robotic systems have been used to perform all the steps, while the separation of the sorbent is carried out by connecting a disk filter to one of the syringes in μ-SPE or by integrating a magnet in the system in m-μ-SPE [18].

The design of the on-fiber SPME device similar to a syringe facilitates the automation of the overall SPME procedure using a robotic arm when coupled to GC (Professional Analytical System Technology, PAS). In the case of in-tube SPME, the configuration of the extraction device (thin capillary containing the sorbent phase) allowed carrying out the method using on-line and automated approaches [15]. Thus, the in-tube SPME capillary can be easily coupled to a LC autosampler or integrated in a system based on flow techniques [28].

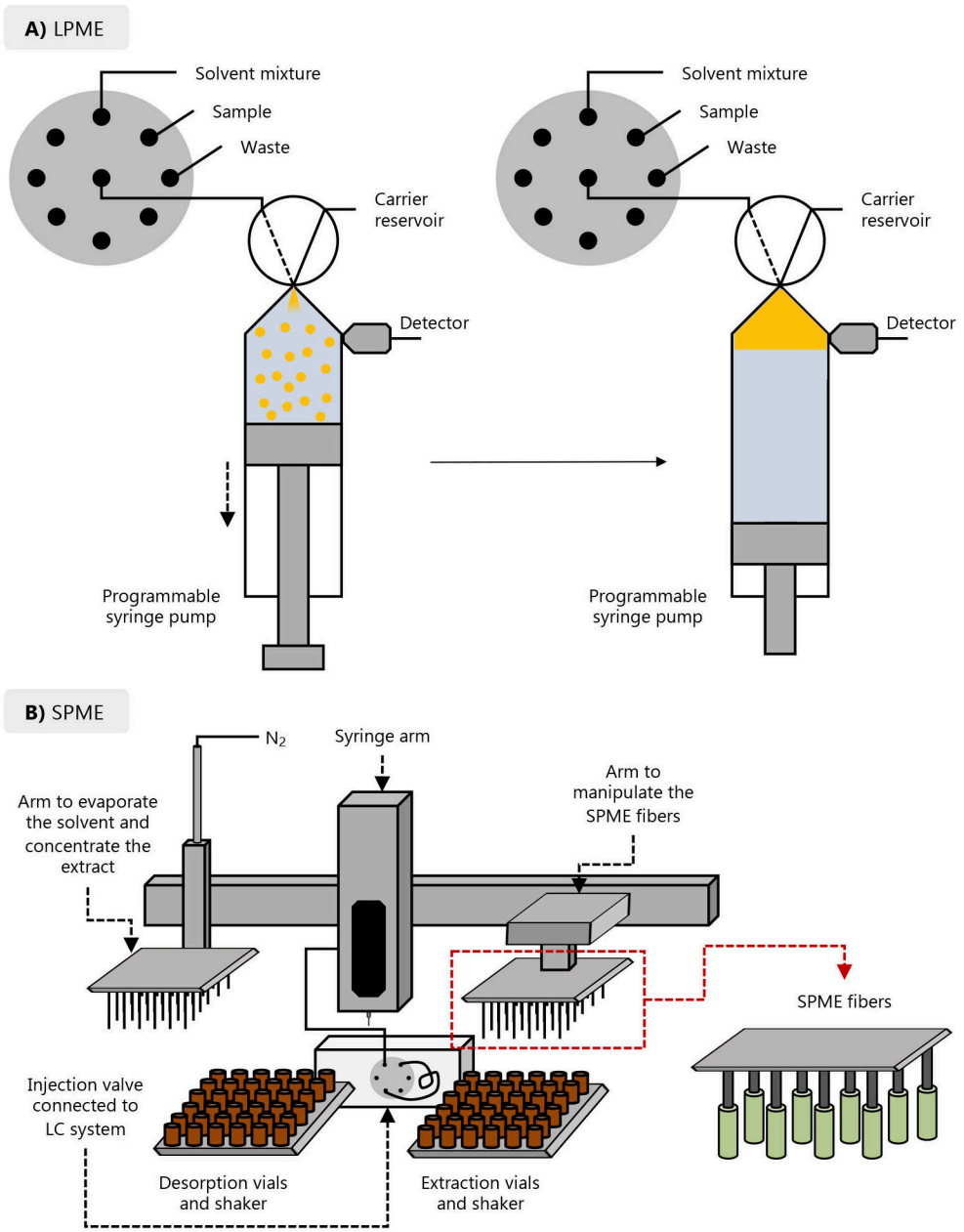

Figure I.5. Representative examples of automated systems to perform microextraction techniques: **A)** set-up for automated DLLME based on a LIS approach and directly connected to the spectrophotometric detector, **B)** set-up for automated and multi-extraction on-fiber SPME coupled to LC based on the PAS technology.

Most recent advances focus on evaluating the feasibility of developing high-throughput methods using on-fiber SPME technology and liquid desorption. This has been achieved by adapting the 96-well format to the use of SPME fibers with PAS technology, allowing not only multiple parallel extractions but also the fully automation of the procedure by using several robotics arms [15]. Figure I.5 B) shows a schematic representation of this system set-up [105].

Considering that the geometry of the blade TFME devices is similar to that of the on-fiber SPME, the automation of this technique has been also possible following the same strategy [106]. In the same manner, simultaneous and fully automated SBSE extractions can be performed when it is coupled with GC using a specific hardware composed of robotic arms and a TDU [29].

I.2. Dispersive liquid-liquid microextraction

Since the introduction of DLLME by Rezaee *et al.* in 2006 [14], an increasing number of analytical methods have included it for different applications, becoming the most popular microextraction method within all LPME methods developed up to date.

As it was described in Section I.1.1.1, DLLME consists in the addition of a mixture of a hydrophobic extraction solvent and a dispersive solvent to the aqueous sample containing the analytes. The dispersive solvent helps in the formation of an emulsion, which enlarges the contact area between the sample and the extraction solvent. Thus, the equilibrium is achieved very fast and the extraction efficiency is also enhanced. After the emulsion is broken, usually by centrifugation, a droplet of the extraction solvent is formed at the top or at the bottom of the vessel (this depending on the density of the extraction solvent). The droplet is then collected with the aid of a syringe and injected in the analytical system to carry out the detection and/or quantification of the analytes [107].

DLLME is characterized for being simple, fast, low cost, and for providing high enrichment factors due to the huge difference between the initial sample volume and the extraction solvent volume. Moreover, it is possible to obtain high extraction efficiencies (exhaustive extraction) in comparison with other LPME modes, mainly due to the improved contact area between the sample and the extraction solvent [108]. In any case, an adequate dispersion is required to achieve the maximum extraction performance in DLLME. In this sense, the type and amount of dispersive solvent have to be carefully optimized. This solvent may increase the solubility of the extraction solvent and can also participate in the partition of the analyte between the sample and extraction phase, thus leading to losses of recoveries in both the extraction solvent and the analytes. Moreover, despite its popularity, DLLME is not recommended for the analysis of matrices with high complexity due to the direct contact between the sample and extraction solvent [108].

2.1. Extraction fundamentals in DLLME

The fundamental principle of DLLME is not significantly different to that of all extraction techniques: it involves the distribution of the analyte between the sample and the extraction phase. [1,109]. Thus, the distribution constant (K_{es}) is defined as:

$$K_{es} = \frac{C_e}{C_s} \qquad \text{Equation I.1}$$

where C_e is the analyte concentration in the extraction phase at equilibrium, C_s is the analyte concentration in the sample matrix at equilibrium, and K_{es} is a constant (instead of a coefficient) since the solute-solute interactions are not considered given the low concentrations of analyte commonly found in microextraction applications (preconcentration to determine trace levels). Moreover, in this system, the mass balance is described by the following equation:

$$C_s^0 \cdot V_s = C_s \cdot V_s + C_e \cdot V_e \qquad \text{Equation I.2}$$

where C_s^0 is the initial concentration of the analyte in the sample, and V_s and V_e are the volumes of the sample and the extraction phase, respectively. If both equations are combined, it is possible to determine the amount of analyte extracted at equilibrium (n_e):

$$n_e = C_e \cdot V_e = \frac{C_s^0 \cdot V_s \cdot K_{es} \cdot V_e}{K_{es} \cdot V_e + V_s} \qquad \text{Equation I.3}$$

Therefore, the volumes of the sample and of the extraction phase have an important impact on the amount of analyte extracted, and consequently, on the sensitivity achieved. Moreover, the K_{es} determines both the selectivity and sensitivity of the method, while depending on different parameters, including temperature and pressure conditions, as well as the characteristics of the sample: pH, ionic strength, and organic solvent content [1]. It is important to point out that Equation I.3 is applied when there is a significant depletion of the analyte concentration in the sample, which is not the case in microextraction due to the huge difference between V_s and V_e. However, in practice, kinetic factors determine the amount of analyte extracted and, therefore, an intermediate situation is observed in microextraction: it is not an exhaustive extraction approach, but a significant amount can be extracted if the experimental conditions are optimized to improve the extraction efficiency [1,109]

With respect to the kinetic aspects, the extraction rate in an extraction process is governed by the diffusion of the analytes from the sample (high concentration) to the extraction phase (low concentration), which can be described by Fick's laws of diffusion [109]. The concentration profile with the time can be obtained by solving the Fick's second law differential equation:

$$\frac{dC}{dt} = D \cdot \frac{d^2C}{dx^2} \qquad \text{Equation I.4}$$

where D is the diffusion coefficient of the analyte. Figure I.6 shows a representation of the concentration profile in the extraction phase at different times and in a non-linear concentration gradient according to the Fick's second law differential equation [109].

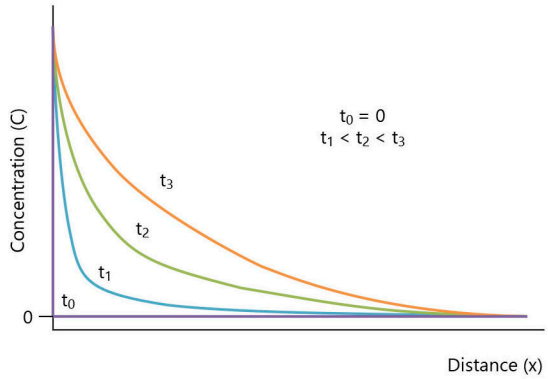

Figure I.6. Schematic concentration profile at the interface between the sample and the extraction phase according to the Fick's second law differential equation.

It is observed that a decrease in the boundary layer thickness between the sample and the extraction phase (shorter x) significantly increases the extraction rate, while the concentration gradient decreases as a function of time [1]. Therefore, the incorporation of any type of mechanical agitation during the extraction procedure, and the enhancement of the dispersion in the particular case of DLLME, will dramatically increase the mass transfer of the analytes. Indeed, if considering the nanoliter-scale droplets formed during the DLLME procedure, and consequently, the large interfacial area, the equilibrium can be reached rapidly in this LPME mode, thus demonstrating its superiority over other approaches [109].

2.2. Advances within the operational in DLLME

Despite DLLME already exhibits a set of characteristics that makes it a simple, efficient and fast sample preparation method, different sub-modes of DLLME have been developed: (i) to improve the dispersion of the extraction solvent, (ii) to avoid the tedious centrifugation step, and (iii) to facilitate the collection of the final extraction phase (the droplet) [108]. Figure I.7 includes a summary of the main variations in the operational mode of DLLME.

Enhancements in the dispersion mode

The use of external factors (e.g., heat, microwaves (MW), and ultrasounds (US)) has been the strategy most used in DLLME to enhance the dispersion, thus improving the extraction efficiency and the kinetics of the process [110]. The temperature-assisted DLLME involves heating the mixture to force the solubilization of the extraction solvent, ensuring this way an increase of the contact with the sample. Then, the extraction vessel is cooled (in general, using an ice bath) to promote the insolubilization and to obtain the emulsion. In a similar manner, the MW energy has been applied during the DLLME procedure to modulate the heating step. The ultrasound-assisted DLLME takes advantage of the cavitation phenomenon to improve the dispersion and to form more tiny droplets of extraction solvent during the procedure. In this case, the cavitation is also accompanied by increments of temperature, which also favors the dispersion of the extraction solvent. However, all these techniques with a thermal effect have to be applied with caution because it may also lead to the degradation of thermolabile compounds or to the evaporation of the organic solvents (used as extraction solvents).

DLLME has also been assisted by vortex stirring to facilitate the dispersion after the addition of both extraction and dispersive solvent, while avoiding the increase of temperature associated with the previously described strategies [110]. Furthermore, the vortex-assisted DLLME mode requires a low-cost and simpler apparatus, which may be the main reasons behind its success in the field. The combination of vortex stirring with several of the other assistance techniques has also been reported, since there is a synergetic effect that speeds up the diffusion of the analytes and leads to a more efficient DLLME method. However, it involves the incorporation of more steps within the procedure, making it more labor-intensive.

The assistance of DLLME with these strategies reduces the consumption of both extraction and dispersive solvent in comparison with non-assisted DLLME methods. Indeed, in some cases, the dispersive solvent can be totally replaced if the energy provided by these techniques is enough to distribute the extraction phase all over the aqueous sample [110]. This is also the case of the surfactant-assisted DLLME mode, in which the organic solvent commonly used to emulsify the mixture is replaced by a surfactant, and there is no need of additional stirring steps [111]. However, the surfactants participate in the distribution of the analytes to the extraction solvent, and may improve their solubilization in the aqueous sample, thus reducing the extraction efficiency.

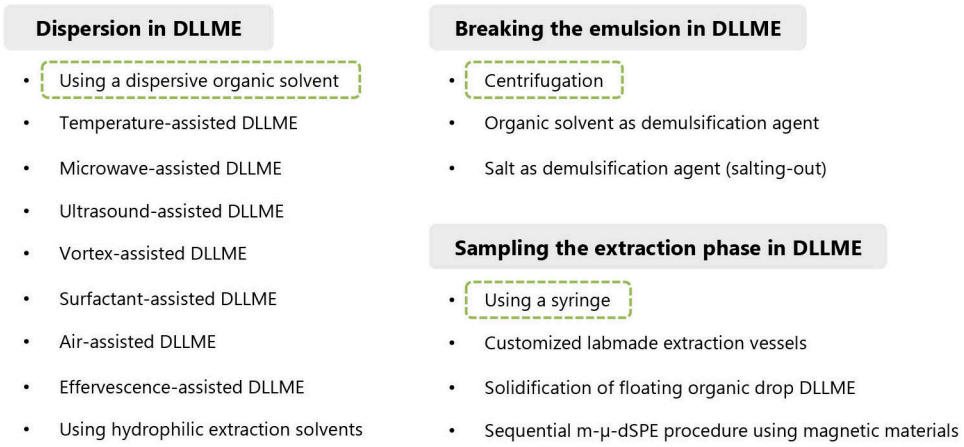

Figure I.7. Main variations of the DLLME technique to improve the different steps of the procedure. The strategies followed in the most conventional DLLME procedure are highlighted with green boxes.

With the aim of avoiding the need of a dispersive solvent and the issues associated to the solubilization of the analytes, the air-assisted DLLME mode was described in 2012 [112]. In this approach, the extraction solvent is added to the sample and then dispersed by performing draw/eject cycles of the mixture several times with the aid of a syringe. The vigorous turbulence formed in the solution increases the mass transfer of the analytes to the extraction solvent [113]. A simpler approach, termed effervescence-assisted DLLME, was reported by Lasarte-Aragonés *et al.* [114]. In this case, the effervescence reaction, which is produced by the addition of sodium carbonate and acetic acid to the sample as effervescence precursors, generates CO_2 bubbles that promote the dispersion of the extraction solvent without requiring an additional dispersive solvent. The effervescence agent can be added as a powder, but its formulation as a tablet enormously facilitates its introduction in the sample, as well as its mass production due to its easy portability [115].

Another strategy followed to upgrade the dispersion and to improve the extraction performance of DLLME is the use of a water-soluble extraction solvent [52]. The hydrophilicity of the solvent/material increase the mass transfer and extraction efficiency of the target compounds, thanks to the enhanced dispersion of the extraction medium. Despite of the water-miscibility of the extraction solvent, which goes against the definition of DLLME, the procedure resembles DLLME but including an additional insolubilization step to separate the final phase with the extracted/preconcentrated analytes from the remaining sample and non-extracted components. Depending on the type of extraction solvent used (see Section I.1.2.1) and the driving force used for the phase separation, the method exhibits a different separation mechanism and can be

classified in different categories, including coacervation phenomena-based methods and aqueous biphasic systems (ABSs) [52].

Enhancements in the separation mode

With respect to the separation stage in DLLME, centrifugation is commonly used to break the emulsion, being the most time-consuming step in the process. Several attempts to avoid this step based on the addition of a demulsification agent to the mixture [108]. The disruption of a stable emulsion can be carried out by adding a salt (i.e., NaCl) due to the salting-out effect, or by a second addition of a specific volume of dispersive solvent. These strategies have been scarcely used since the addition of salt is quite cumbersome and the increase of dispersive solvent amount affects both the greenness and the extraction efficiency of the method.

Enhancements in the sampling of the extraction phase

The sampling of the small volume (the droplet) of extraction solvent after the dispersion and separation is still the trickiest step within DLLME. Indeed, numerous efforts have been done to facilitate this step. The design of customized labmade vessels with conical bottoms for high-density extraction solvents, and narrow necks for low-density extraction solvents, has been a matter of interest in this field [111]. In any case, the best alternative to facilitate the sampling has been the solidification of the floating organic drop (SFO-DLLME method), which uses a low-density solvent with a melting point close to room temperature as extraction solvent [108,111]. In this mode, after centrifugation, the extraction vessel is cooled to solidify the droplet located at the top of the solution, which is then collected with the aid of a spatula or tweezers. Finally, the drop is melted and analyzed to carry out the detection of the analytes. Despite the advantages of this sub-mode of DLLME, the variety of solvents suitable for this approach, with compatible melting and freezing temperatures, is very limited.

One of the most successful alternatives to facilitate both the separation and the retrieving of the extraction phase is the use of magnetic materials in the process [116]. In this approach, the DLLME is assisted by a sequential m-μ-dSPE procedure, in which MPs are added after the dispersion of the extraction solvent in the sample, and then separated with the aid of an external magnet. Thus, the procedure involves the *in situ* generation of a sorbent that consists of the surface modification of the MPs with the extraction solvent [116]. This method has also benefited from other assistance approaches, such as vortex stirring [111] and effervescence [114]. The main drawback of this approach is the need of an additional step for the desorption of the analytes from the magnetic material. This desorption step requires a low volume of an organic solvent.

2.3. Ionic liquids in DLLME

The solvents used as extraction phase in DLLME in the original studies were high-density halogenated organic solvents, such as chloroform, dichloromethane and tetrachloroethylene [108]. Given the toxicity issues associated with these solvents, different alternatives have been evaluated

as extraction solvents, as it was described in Section I.1.2.1. Among all the candidates, ILs have been particularly successful in DLLME, being the LPME mode in which ILs have found the highest number of applications, as shown in Figure I.8. Considering that many strategies of DLLME with different operational modes have been described using exclusively ILs, they will be overviewed in this section, with particular attention to the main properties of these materials [117–119] (which closely relate to the different IL-DLLME modes).

2.3.1. Structure and properties of ILs

ILs are molten salts formed by bulky organic cations in combination with inorganic or organic anions [67], as it was described in Section I.1.2.1. Figure I.9 includes some representative examples of the cations and anions used for the synthesis of those ILs mostly used in DLLME methods. The most common cation used for the preparation of ILs is imidazolium, due to their ease of functionalization. Other cations include ammonium, phosphonium, pyridinium, pyrrolidinium, morpholinium and guanidinium, among others. With respect to the anionic moiety, a wide variety of anions are used, including chloride, bromide, tetrafluoroborate, hexafluorophosphate, and more complex structures, such as bis[(trifluoromethyl)sulfonyl]imide ($[NTf_2^-]$) and metal complexes.

Table I.2 includes the nomenclature that will be used in this Doctoral Thesis to identify ILs, which is based on their structure and composition.

Due to the large number of possible combinations of cations and anions and the ease of tailoring ILs, a huge number of ILs can be designed. This synthetic versatility allows the preparation of ILs with specific properties and physicochemical characteristics, with the nature and structure of the cation and anion moieties playing a key role [69,120]. For example, the thermal stability depends on both parts (cations and anions forming the IL): ILs with $[P_{n1,n2,n3,n4}^+]$ cations and anions coordinated with fluorine atoms (e.g., $[NTf_2^-]$) present higher decomposition temperatures [121]. Furthermore, the viscosity and water-solubility of the ILs can be controlled by selecting the adequate anion. Specifically, longer alkyl chains increase the viscosity of the resulting IL [120], halides and $[BF_4^-]$ generate mostly water-soluble ILs, while other bulky anions containing fluorine atoms generally yield hydrophobic ILs. Figure I.10 shows the structure of several examples for hydrophobic and hydrophilic ILs.

This versatility also permits the incorporation of other attractive features to ILs through simple changes in their structures, which leads to the preparation of a number of IL derivatives, including IL-based surfactants and magnetic ILs. These derivatives present the inherent characteristics of ILs together with those specific properties provided by their specific composition.

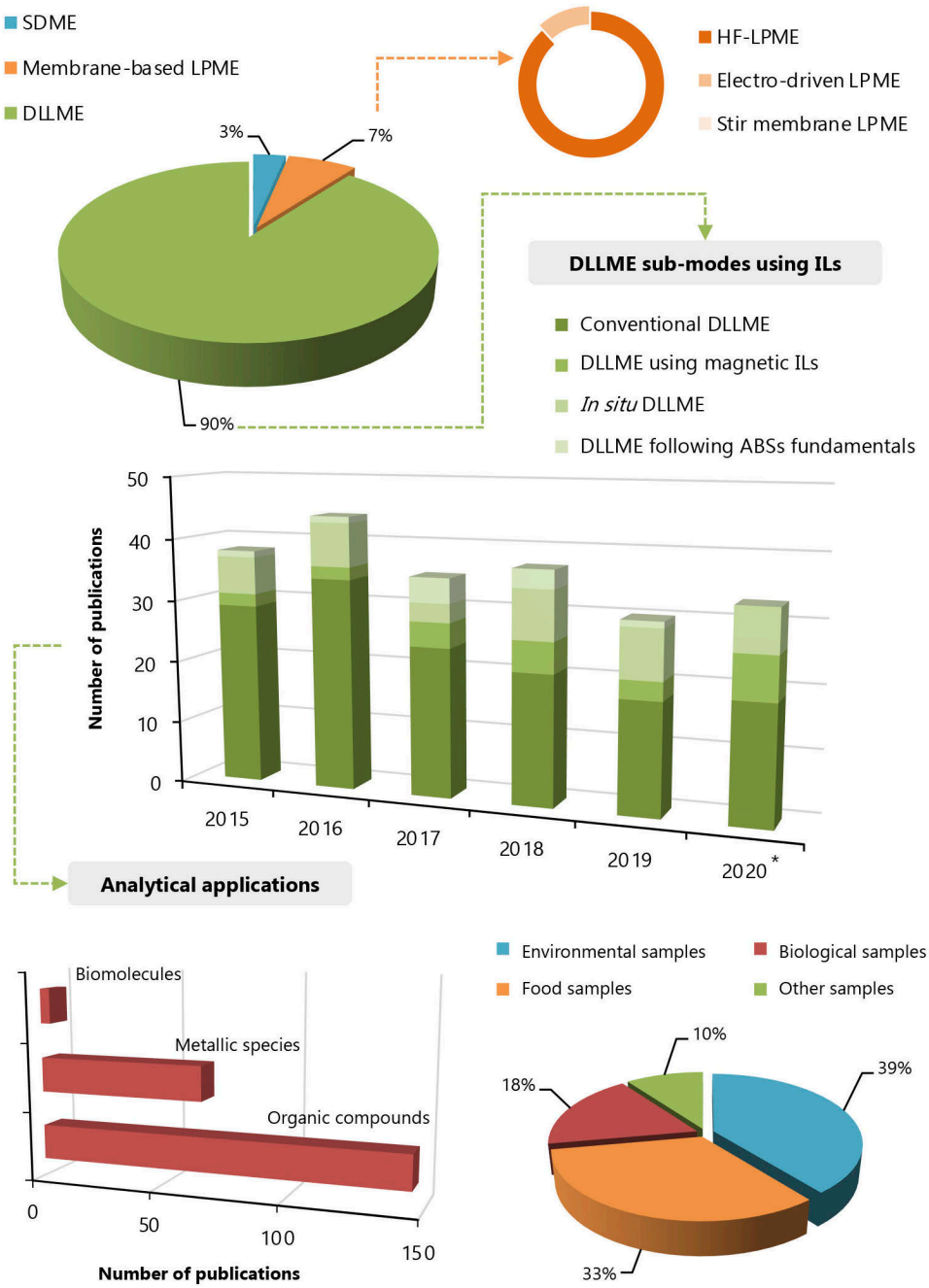

Figure I.8. Statistics showing the number of publications in the period 2015–2020 on the use of ILs as extraction solvents in LPME techniques, and particularly within the different sub-modes of DLLME and their analytical applications (*until November 2020).

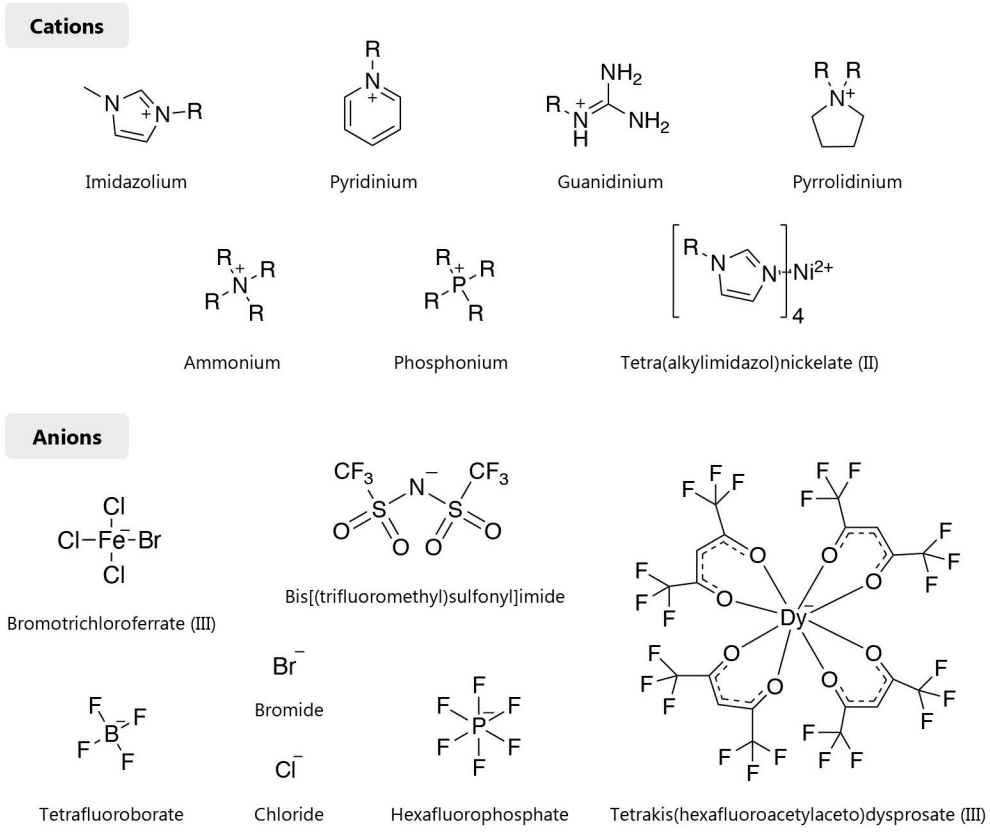

Figure I.9. Representative cations and anions used for the preparation of ILs in DLLME strategies.

ILs with active surface properties can be prepared by incorporating long alkyl chains in the cation or in the anion [122]. It is important to highlight that the majority of the authors consider more appropriate the terms IL-based surfactants or surface active ILs rather than IL surfactants, since many IL-based surfactants present melting points above 100 °C [123]. Thus, IL-based surfactants are capable of forming micellar aggregates when dissolved in water above a certain concentration (CMC). Interestingly, IL-based surfactants exhibit lower CMC values than conventional surfactants with similar structures [122], and, as conventional surfactants, an increase in the length of the alkyl chain is generally accompanied by a decrease of the CMC values [122].

Table I.2. Nomenclature used in this Doctoral Thesis to identify the most common ILs.

Name / composition	Abbreviation
Cations[a]	
Imidazolium	$[C_{n1}C_{n2}Im^+]$
Pyridinium	$[C_{n1}Py^+]$
Guanidinium	$[C_{n1}Gu^+]$
Pyrrolidinium	$[C_{n1}C_{n2}Pyrr^+]$
Cholinium	$[Cho^+]$
Morpholinium	$[Mor^+]$
Ammonium	$[N_{n1,n2,n3,n4}{}^+]$
Phosphonium	$[P_{n1,n2,n3,n4}{}^+]$
Tetra(alkylimidazol)nickelate (II)[b]	$[Ni(C_{n1}Im)_4{}^{2+}]$
Anions	
Bromide	$[Br^-]$
Chloride	$[Cl^-]$
Tetrafluoroborate	$[BF_4^-]$
Saccharinate	$[Sac^-]$
Salycilate	$[Sal^-]$
Tosylate	$[TsO^-]$
Hexafluorophosphate	$[PF_6^-]$
Bis[(trifluoromethyl)sulfonyl]imide	$[NTf_2^-]$
Tris(perfluoroethyl)trifluorophosphate	$[FAP^-]$
Dicyanamide	$[N(CN)_2^-]$
4-Styrenesulfonate	$[SS^-]$
2-naphthalenesulfonate	$[NapSO_3^-]$
Bromotrichloroferrate (III)	$[FeCl_3Br^-]$
Tetrachloromanganate (II)	$[MnCl_4{}^{2-}]$
Tetrakis(hexafluoroacetylaceto)dysprosate (III)[b]	$[Dy(hfacac)_4^-]$
Multicationic ILs[a]	
Di(alkylimidazolium)alkane	$[(C_{n1}Im)_2C_{n2}{}^{2+}]$
Tris(alkylimidazolium)alkane	$[(C_{n1}Im)_3C_{n2}{}^{3+}]$
Zwitterionic ILs[a]	
(Alkylimidazolium)alkanesulfonate	$[C_{n1}Im^+C_{n2}SO_3^-]$
(Alkylimidazolium)alkanecarboxylate	$[C_{n1}Im^+C_{n2}COO^-]$

[a] n = number of carbon atoms in the different alkyl chains. Several substituents have a specific abbreviation: A for allyl, B for benzyl, M for methyl, and V for vinyl

[b] Specific examples, different metal elements can be used.

Figure I.10 includes two representative examples of IL-based surfactants: a cationic surfactant with a long hydrophobic tail in the cation moiety, and a catanionic or biamphiphilic IL-based surfactant, which is composed of a cation with short substituents and an anion with a longer alkyl chain [124]. Given the inherent hydrophilic nature of surfactants, cationic IL-based surfactants are composed of halide or [BF_4^-] anions, while the nature of the cation is not relevant as long as it contains a long alkyl chain, in general, with more than 6 carbon atoms [122]. The knowledge of the aggregation behavior of IL-based surfactants is crucial to develop and improve their applications. Thus, the main parameter used in colloid science to characterize surfactants is the CMC, which can be experimentally determined using different techniques: surface tension, fluorescence, and/or conductivity measurements. Other parameters include the aggregation number, the maximum surface excess concentration, and the adsorption efficiency [122].

It is also possible the synthesis of magnetic ILs by including a paramagnetic component in any of the IL moieties, leading to the fabrication of ILs that can be manipulated by the application of an external magnetic field [125]. First generation of magnetic ILs were synthesized using the most common [$C_{n1}C_{n2}Im^+$], [$P_{n1,n2,n3,n4}^+$], and [$N_{n1,n2,n3,n4}^+$] cations; in combination with metal complexes, such as [$FeCl_4^-$] or complexes based on rare earth elements and fluorinated ligands, such as the complex composed of a dysprosium metal center coordinated with several tris(hexafluoroacetylaceto) (hfacac) ligands (Figure I.9) [125,126]. Thus, the metal-containing anions were the moiety responsible of the paramagnetic properties of the ILs. More recently, magnetic ILs with cations containing the metal component that provide the paramagnetic behavior have been described [127]. They were mainly composed of cations with Ni (II) or Co (II) centers coordinated with four ligands of alkylimidazole and halide anions. Figure I.10 shows the structures of some examples of these different classes of magnetic ILs. As it happens with more conventional ILs, the hydrophobicity and viscosity of magnetic ILs can be modulated by the proper selection of the cation and anion. Moreover, in this case, the nature of the metal element strongly affects the magnetic susceptibility of the resulting IL [125].

Despite most applications use monocationic structures to generate ILs, multicationic ILs can be prepared by linking two or more cations using a spacer, such as an alkane or other specific groups (e.g., benzene ring or amines). Thus, depending on the number of cation heads in the IL structure, dicationic and tricationic ILs have been synthesized, as shown in Figure I.10 [128,129]. Zwitterionic ILs have also been described, in which the cation and anion are covalently tethered to form a unique and neutral structure [130]. Essentially, they are zwitterions with chemical structures containing the same ions as conventional ILs. They present the same characteristics as ILs but higher melting points and lower ionic conductivity. Besides, they can be tailored to ensure proper modulation of its dipole moment. Figure I.10 also includes two examples for this type of ILs.

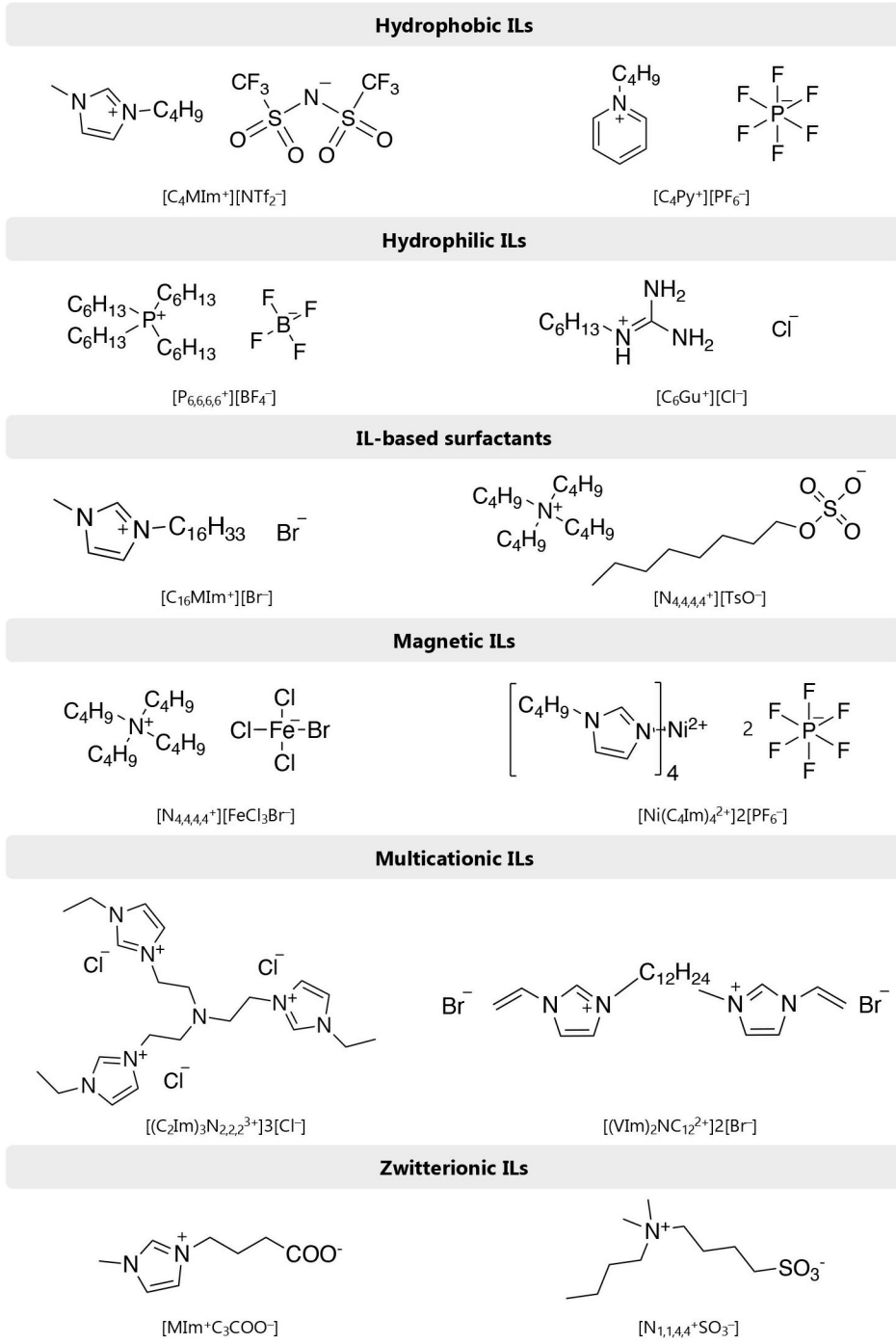

Figure I.10. Two representative examples for each type of ILs, showing the chemical composition (nature of cation and anion).

With respect to the synthesis of ILs, it normally requires an initial nucleophilic substitution reaction (S_N) followed by a metathesis reaction [131]. The S_N reaction is accomplished to functionalize the cation moiety of the IL, while the metathesis reaction allows the introduction of more complex anions in the IL structure. This approach is valid for many ILs containing cations of different nature and using imidazole, alkylimidazole, pyrrolidine, alkylpyrrolidine, pyridine, triphenylphosphine, or trialkylamine, as starting material. However, there are several ILs with specific cations that require a more specific synthetic route, such as the preparation of acyclic guanidinium-based ILs [132]. In the case of zwitterionic ILs, in general, the synthetic procedure includes the neutralization of the halogenated salt formed after the S_N reaction using a strong base to obtain the neutral compound [133]. Despite the complexity of multicationic ILs, their synthesis is quite simple and it only involves two consecutive S_N reactions followed by the metathesis reaction [134,135]. The first reaction creates the multicationic structure by the incorporation of the spacer between the cations, while the second S_N step adds the free side chains to the IL.

The success of ILs in microextraction, and particularly in DLLME, mainly lies in the abovementioned outstanding tunability, which allows developing new and exclusive DLLME sub-modes by exploiting different and specific properties of ILs [119]. Moreover, these materials present a wide liquid range, and impressive solvation properties, being able to interact with a wide variety of substances by different co-existing interactions within the same IL [69,136].

2.3.2. Toxicity of ILs

ILs present negligible vapor pressure at room temperature. Therefore, they do not generate volatile organic compounds in comparison with conventional organic solvents [67]. This has been the main reason supporting their claimed non-toxicity. However, there is an increasing concern on the real grade of greenness and the toxicological impact of ILs, particularly towards the aquatic environment due to the formation of harmful by-products after their degradation during waste treatment [137]. Indeed, diverse studies have pointed out the toxicity of several ILs [137,138].

In general, studies agree that the cation moiety plays the major role in the toxicity of the resulting IL, being [Mor^+] [139], [Gu^+] [140,141], and [Cho^+] [140] cations those providing lower toxicity in comparison with the commonly used [Im^+], [Py^+], [N^+], and [P^+]-based ILs. This effect may be due to the planarity of the cation ring and the more hydrophobic character of the heads of the most common ILs, which leads to an increase in their lipophilicity [137]. Moreover, an increase in the side chain length attached to the IL cation can also lead to a significant increase in the IL toxicity [140–142], whereas the functionalization of the substituent linked to the IL cation incorporating ether groups may reduce the toxicity of the resulting IL [142]. With respect to the most commonly used anions, despite their effects are controversial, it has been demonstrated that those belonging to the polyfluorinated group present significant toxicity, which may be due to the formation of toxic fluorides after hydrolysis [143].

Therefore, it is important to design the IL structure with enhanced biodegradability and better toxicological characteristics to guarantee the sustainability of these new solvents [69]. In this sense, the synthesis of ILs with moieties coming from natural sources have become the most promising research line to improve the greenness of ILs, such as ions derived from amino acids and sugars [137].

2.3.3. Hydrophobic ILs in DLLME

The DLLME procedure requires a water-insoluble solvent as extraction solvent, which is dispersed in the aqueous sample. Given the hydrophobicity of several ILs, which can be modulated by the proper selection of cation and anion, DLLME has also benefited from the incorporation of ILs to substitute the halogenated solvents initially used in this LPME technique [119].

2.3.3.1. Conventional DLLME

In the most classical DLLME using ILs, a water-insoluble IL is added to the aqueous sample along with a dispersive solvent to form fine droplets of IL that are dispersed through the sample. After centrifugation, the microdroplet of the IL containing the analytes settles at the bottom of the tube, being then collected for injection in the analytical system. Figure I.11 A) shows a scheme of the procedure. This conventional DLLME sub-mode can be assisted by any of the different strategies described in Section 2.2 to ensure the adequate dispersion of the IL and to facilitate the sampling of the final IL-phase.

As it can be observed in Figure I.8, this is the sub-mode of DLLME in which ILs have found the largest number of applications, representing more than 50 % of the studies reported in the last 6 years. Most applications used ILs prepared with [$C_{n1}C_{n2}Im^+$] cations paired with [PF_6^-], [NTf_2^-] and [FAP^-] anions. In general, the cations contain short alkyl chains, being [C_4MIm^+], [C_6MIm^+], and [C_8MIm^+] the most commonly used [44,119]. Due to the use of fluorinated anions, which yield high-density ILs, the final IL-phase obtained after breaking the emulsion is formed at the bottom of the extraction vessel.

The assistance of the DLLME method with a sequential m-μ-dSPE procedure to collect the hydrophobic IL has been particularly successful in recent years [118,144]. Thus, ILs easily interact with the negatively charged surface of the MPs, which are added to facilitate and speed up the separation step [118]. As disadvantages, MPs usually lack stability and tend to aggregate, and, therefore, the entire method with MPs requires an additional back-extraction step [118,144]. The use of vortex stirring to enhance the dispersion and the sampling of the microdroplet with the aid of a syringe is still the most commonly used approach. Among the peculiarities described with ILs in comparison with DLLME using traditional solvents, it is interesting to mention the use of an additional hydrophilic IL in the procedure as dispersive solvent (thus minimizing the solubilization of the hydrophobic IL used as extraction solvent, as it happens with conventional dispersive

solvents). This leads to the formation of larger volumes of final microdroplet due to the aggregation of both extraction and dispersive ILs by electrostatic interactions after the centrifugation step [119].

2.3.3.2. DLLME using magnetic ILs

Magnetic ILs have attracted much attention in microextraction techniques, and most specifically in DLLME [145]. The paramagnetic behavior of the IL itself allows the magnetic retrieval of the IL microdroplet without the use of any additional magnetic material. The experimental procedure of the DLLME using magnetic ILs resembles that of the conventional DLLME, as shown in Figure I.11 B). The hydrophobic magnetic IL is added to the aqueous sample, which is then stirred to disperse the magnetic IL in fine microdroplets, thus interacting (and extracting) the analytes. Then, the droplets of magnetic IL are collected and separated from the sample with the aid of an external magnet and, finally, subjected to analysis.

The magnetic ILs used in this DLLME sub-mode have been prepared using [$N_{n1,n2,n3,n4}^{+}$] or [$P_{n1,n2,n3,n4}^{+}$] cations paired with different types of metal-containing anions. In the first studies, [$MnCl_4^{2-}$] and [$FeCl_3Br^{-}$] anions were used to provide the IL with paramagnetic properties. However, the high viscosity of these ILs hampered their application in this LPME technique due to the difficulties associated to both their manipulation and dispersion [145]. Thus, a group of less viscous magnetic ILs containing the hfacac ligand with different metal centers in the anion moiety have been used in DLLME to overcome these issues. Indeed, since the first study reporting this new generation of magnetic ILs [146], the number of applications of this DLLME sub-mode has increased all over the years, as shown in Figure I.8. Nevertheless, the developed methods still require the use of a small amount of an organic dispersive solvent or any of the strategies described in Section I.2.2, to correctly disperse the magnetic IL [119].

It is interesting to mention the stir bar-assisted DLLME method using magnetic ILs reported by Chisvert *et al.* [146], that combines the advantages of DLLME with those of SBSE. In this approach, the magnetic IL coats a magnetic stir bar that is also added to the sample. When high stirring rates are applied, the IL disperses into the aqueous sample, while the IL keeps covering the surface of the magnetic stir bar when low speeds are used (or when the stirring stops). This procedure resembles that of SBSDME, in which a magnetic sorbent coats a stir bar (see Section I.1.1.2). After the extraction, the magnetic IL-coated magnetic bar is placed in a thermal desorption unit to desorb the analytes. This way, the method does not require organic solvents neither in the sample preparation process nor in the separation and determination step, which is noticeable particularly if compared with other DLLME methods using magnetic ILs that are combined with LC.

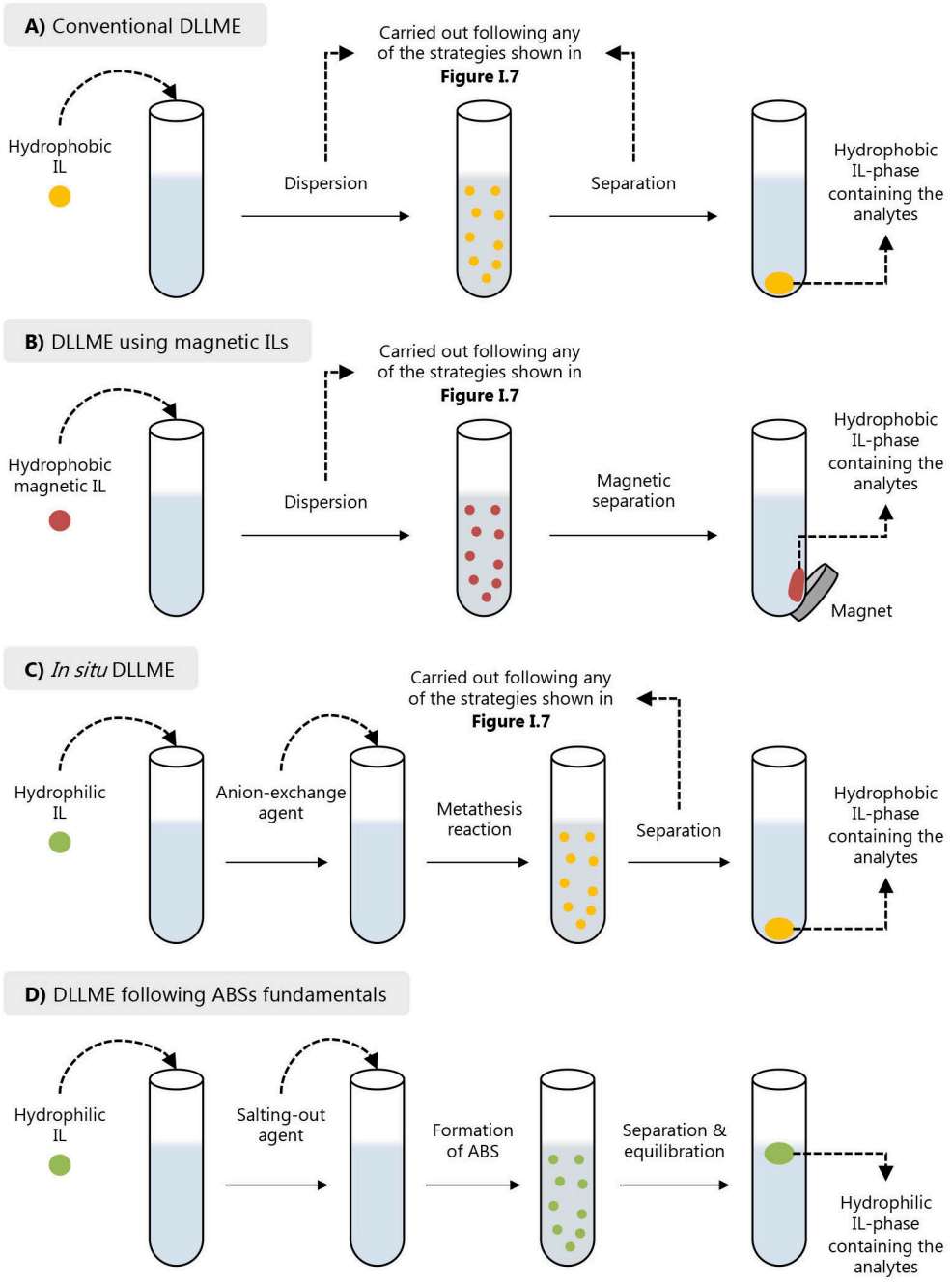

Figure I.11. Scheme of the operational procedure of the different DLLME modes using ILs as extraction solvents.

2.3.4. Hydrophilic ILs in DLLME

The versatility of ILs allows controlling their solubility by means of minor changes in their composition. Furthermore, due to the ease of synthesis of ILs, some of these changes can be easily carried out directly in solution (i.e., a simple change in the anion nature). This has led to the development of a DLLME sub-mode exclusively applicable when ILs are used as extraction solvent: *in situ* DLLME, although the generic DLLME definition involves the use a water-insoluble solvent as extraction medium. Moreover, hydrophilic ILs have found an interesting scope of application in ABSs, which can be used as a microextraction technique under certain experimental conditions and with the IL acting as the extraction solvent [52].

2.3.4.1. *In situ* DLLME

In 2009, Baghdadi and Shemirani [147] developed this new sub-mode, termed *in situ* DLLME. In this approach, unlike the conventional technique, a hydrophilic IL is initially used as extraction solvent. Then, an anion-exchange reagent is added to the aqueous sample containing the water-soluble IL. This reagent promotes a metathesis reaction in which the anion moiety of the IL is exchanged to obtain a hydrophobic IL, as it is schematically shown in Figure I.11 C). Due to the miscibility of the initial IL with water, the generated water-insoluble IL is dispersed all over the sample, leading to the formation of an emulsion. Finally, as in the conventional DLLME strategy, the mixture is centrifuged to obtain a microdroplet of the hydrophobic IL containing the analytes. In the study reported by Yao and Anderson, also in 2009, [148], the superiority of the *in situ* DLLME approach in comparison with conventional DLLME and SDME using hydrophobic ILs was demonstrated. Thus, in the *in situ* DLLME, the method is simplified, the extraction time is shortened, and the extraction efficiencies are increased due to the enhanced dispersion of the IL in the aqueous sample.

The most common ILs used as extraction solvents in *in situ* DLLME contain [$C_{n1}C_{n2}Im^+$] cations in combination with [Br^-], [Cl^-], and [BF_4^-] anions. With respect to the anion-exchange reagent, salts with [NTf_2^-] and [PF_6^-] anions are the most common, but the anion [$N(CN)_2^-$] has also been used [52]. In general, the procedure does not require a dispersive solvent in contrast to conventional DLLME, due to the initial miscibility of the IL with the aqueous sample. However, it is necessary to apply any stirring method after the addition of the anion-exchange reagent to improve the kinetics of the reaction, and/or to cool the solution for guaranteeing the further insolubilization of the IL. Moreover, this sub-mode has also benefited from the addition of magnetic sorbents to assist the separation step by a m-μ-dSPE procedure [52,144]. Thus, MPs can be added before or after the metathesis reaction.

The incorporation of magnetic ILs in the *in situ* DLLME procedure is the most recent improvement within this method [52,145]. The magnetic ILs initially synthesized were not suitable for *in situ* DLLME approach since they were prepared using paramagnetic anions, which would be exchanged during the metathesis reaction, thus losing the magnetic character. Trujillo-Rodríguez

et al. [149,150] proposed a new generation of hydrophilic magnetic ILs prepared using paramagnetic cations (e.g., $[Ni(C_{n1}Im)_4^{2+}][Cl^-]$), which can undergo insolubilization by exchanging the anion moiety using $[NTf_2^-]$ salts. In this case, after the addition of the metathesis reagent, the solution was vortexed to speed up the reaction and the hydrophobic magnetic IL was collected using a magnet. The water-insoluble magnetic IL formed by this method was also collected using a rod magnet previously inserted in the sample, which resembled SBSDME [150]. In this case, the magnet also served as stirring device to assist the metathesis reaction. Once the stirring was stopped, the *in situ* formed magnetic IL was settled in the rod magnet. This advance within the *in situ* DLLME, together with the improved dispersion obtained, are the main reasons behind the success of this sub-mode in the last years, as shown in Figure I.8.

2.3.4.2. DLLME following ABSs fundamentals

ABSs are well-known ternary systems formed by mixing two soluble solutes in water, which separate into two coexisting phases at a certain concentration, each phase being rich in a different solute [151]. Conventional ABSs comprise two polymers, or a mixture of a polymer and a salting-out inducing salt. The low differences in polarity between these two components and the high viscosity of polymers hinder the applications of ABSs in sample preparation. Thus, hydrophilic ILs has been proposed to substitute polymers in ABSs while using different types of organic and inorganic salts as salting-out agents [151,152]. These systems not only exploit the tunability and lower viscosity of ILs to improve the characteristics of ABSs, but also take advantage of the high extraction capacity of ABSs and the absence of organic solvents in the procedure for the development of sustainable and efficient extraction methods [119].

Obtaining the phase diagram of an ABS is essential prior to its application, since it allows identifying the mixture compositions that form two-phases, and knowing the partition behavior among the phases. Figure I.12 includes a ternary and orthogonal representation for a hypothetical phase diagram. The orthogonal representation, in which the amount of water corresponds to that required to reach 100 % (w/w) for a given mixture, is preferred due to its simplicity. These diagrams are characterized by a binodal curve that corresponds to the boundary between the monophasic and biphasic regimes (solid lines). The tie-lines (dotted orange lines) indicate the composition of each phase (at the endpoints that intersect the binodal curve, orange circles) for a specific biphasic mixture composition at any point of the line (orange diamonds). Thus, any mixture composition lying on the same tie-line has the same phases' composition, whereas the mass (or volume) ratios between the coexisting phases are different [151].

Once the biphasic zone is defined, a point with a specific mixture composition in the lowest region of the phase diagram can be selected to reach the desired enrichment factor, thus leading to the development of a microextraction technique based on an ABS (μ-ABS) [52]. In these methods, the mixture is prepared, stirred to solubilize the components, and left to equilibrate to achieve the separation of the phases, which can be accelerated by centrifugation. Thus, the

operational procedure resembles that of DLLME, as it is shown in Figure Figure I.11 D). It is important to highlight that the final IL-rich phase obtained with this method still contains the hydrophilic IL, thus ensuring the compatibility with the mobile phase of the LC technique commonly employed for the separation and detection of the analytes.

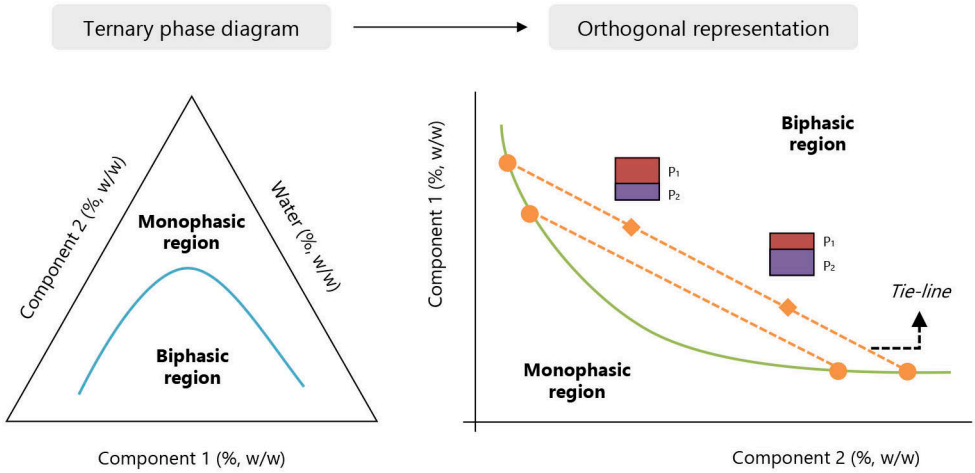

Figure I.12. Phase diagram for a hypothetical ABS in both ternary (left) and orthogonal (right) representations. Solid lines correspond to the binodal curves, dotted lines are the tie-lines, orange circles indicate the composition of each phase, and orange diamonds represent specific mixture composition in the biphasic region. P_1: phase rich in component 1, P_2: phase rich in component 2.

Despite the attractive features of ABSs composed of ILs and their broad use as extraction platform, the amount of ILs commonly used in these methods are relatively high, and particularly higher in comparison with the volumes of initial aqueous phase, being around 50 % (w/w) out of the total mass of the system [119]. Therefore, in most applications, the ABSs do no exhibit the characteristics of a microextraction method, and only a few studies have been reported meeting these requirements, as shown in Figure I.8.

The amounts of ILs used in μ-ABSs range between 1.2 and 5 % (w/w), which may theoretically lead to preconcentration factors as high as 20000 if the adequate mixture composition is selected [52]. Several cation-anion combinations have been covered to exploit the role of the IL structure on the partition of the target analytes in μ-ABSs. Thus, $[C_{n1}C_{n2}Im^+]$, $[Cho^+]$ and $[N_{n1,n2,n3,n4}^+]$ cations have been paired with the most common anions (i.e., halide and $[BF_4^-]$) and those derived from natural sources, including $[Sal^-]$ and $[Sac^-]$ [52,119]. More recently, magnetic ILs have also been explored in μ-ABSs to shorten the time required to achieve equilibrium

and dismiss the need for a centrifugation step. In this case, an IL composed of a [Gu^+] cation and an anion containing 2,2,6,6-tetra methylpiperidine-1-oxyl (TEMPO), which provided the IL with paramagnetic properties, was used as extraction phase [153]. With respect to the salting-out species, high-charge density inorganic salts have been commonly used, such as K_3PO_4, $C_6H_5K_3O_7$, K_2HPO_4, and Na_2CO_3 [52,119].

2.3.5. Analytical applications of ILs in DLLME

Figure I.8 shows a summary of the nature of the analytes determined and the type of samples analyzed by DLLME methods using ILs as extraction solvents. Moreover, Table I.3 includes some representatives examples of the analytical applications reported within the different DLLME sub-modes using ILs [142,146,154–173].

Most applications have been intended for the determination of organic compounds, mainly pesticides, dyes, and endocrine disrupting compounds (EDCs), covering polycyclic aromatic hydrocarbons (PAHs), personal care products (PCPs), drugs and pharmaceuticals, phthalates, and phenols [119]. Different metallic species have also been extracted by these microextraction strategies, particularly Cd (II), Cr (III & VI), As (III & V), Cu (II), Hg (II), Co (II), and Fe (II & III) [174]. Moreover, it is interesting to mention the recent interest on using ILs for the extraction and preconcentration of DNA, particularly magnetic ILs, coupling the approach with polymerase chain reaction (PCR) techniques. These methods take advantage of the lysis capability of ILs and their compatibility with the buffers required for PCR [166,172].

Depending on the nature and characteristics of the analytes, the DLLME methods have been coupled with different separation/detection techniques. Given the low vapor pressure of ILs, the IL-phase containing the preconcentrated analytes cannot be directly injected in a GC system. However, several studies have reported the combination of these methods with GC by using a TDU or HS sampler taking advantage of the thermal stability of ILs [119]. In any case, most applications use LC with different detectors to carry out the separation and detection of the organic analytes. However, attention should be paid to the compatibility of the IL with the mobile phase, since most of the ILs used are hydrophobic and require dilution prior injection. In the case of metal ions, atomic absorption spectroscopy (AAS) techniques with different atomization methods are used. As it occurs with LC, the final IL-phase is commonly diluted with an organic solvent or acidic solution to reduce the viscosity of the extract and to facilitate its manipulation and injection in the instrument.

With respect to the type of samples, 39 % of the applications in the period 2015–2020 are included within environmental analysis, closely followed by food analysis, representing 33 % of the total applications.

Table I.3. Representative applications described in the literature on the use of ILs as extraction phase in the different DLLME sub-modes.

IL	Amount of IL	Assistance	Analytes (number)	Sample (amount, pretreatment)	Analytical technique	LOD ($\mu g \cdot L^{-1}$)	E_F	Ref.
Conventional DLLME								
$[C_2MIm^+][NTf_2^-]$	100 µL	US, acetone as dispersive solvent & m-µdSPE	Co (II)	tap, mineral and bottled waters (10 mL)	FAAS	0.05	–	[154]
$[C_4MIm^+][PF_6^-]$	100 µL	MW & methanol as dispersive solvent	phthalates (5)	bottled waters (3 mL)	LC-UV-Vis	0.71–1.94	–	[155]
$[C_4MIm^+][PF_6^-]$	100 µL	ethanol as dispersive solvent	Fe (II)	serum (10 mL, MW digestion)	FAAS	1.29	59	[156]
$[C_6MIm^+][PF_6^-]$	45 µL	in-syringe (LIS automated)	As (V)	rice (5 mL, MW digestion)	GFAAS	0.005	–	[157]
$[C_6MIm^+][NTf_2^-]$	60 mg	vortex stirring	Hg (II)	urine (10 mL)	VA	0.5–1.5	31	[158]
$[C_6MIm^+][NTf_2^-]$	50 µL	methanol as dispersive solvent	parabens (5)	pool waters (10 mL)	TD-GC-MS	0.004–0.008	–	[159]
$[C_6MIm^+][PF_6^-]$	60 µL	MW & US	herbicides (7)	milk (4 mL)	LC-UV-Vis	0.46–1.96	–	[160]

Table I.3 (continued).

IL	Amount of IL	Assistance	Analytes (number)	Sample (amount, pretreatment)	Analytical technique	LOD ($\mu g \cdot L^{-1}$)	E_F	Ref.
$[C_8MIm^+][PF_6^-]$	85 mg	US & acetonitrile as dispersive solvent	drugs (9)	wastewaters (10 mL)	LC-MS/MS	0.0002–0.06	340	[161]
$[C_8MIm^+][PF_6^-]$	35 µL	temperature-assisted	phenols (2)	tap, lake & river waters (10 mL)	LC-UV-Vis	0.58–0.86	186	[162]
$[C_8MIm^+][PF_6^-]$	50 µL	hydrophilic IL as dispersive solvent	drugs (2)	lake, tap, snow & river waters (5 mL)	LC-UV-Vis	0.23–0.35	–	[163]
DLLME using magnetic ILs								
$[P_{6,6,6,14}^+]_2[MnCl_4^{2-}]$	30 mg	acetonitrile as dispersive solvent	organic pollutants (13)	lake and river waters (5 mL)	LC-UV-Vis	0.25–1	–	[164]
$[P_{6,6,6,14}^+][FeCl_4^-]$	100 µL	acetonitrile as dispersive solvent and vortex stirring	Cd (II)	honey (30 mL, dilution)	ETAAS	0.0004	112	[165]
$[P_{6,6,6,14}^+][Ni(hfacac)_3^-]$	25 µL	magnetic stir bar	UV filters (8)	pool and seawaters (25 mL)	TD-GC-MS	9.9–26.7	791	[146]
$[N_{8,8,8,B}^+][Ni(hfacac)_3^-]$	2 µL	vortex stirring	DNA	blood (50 µL)	qPCR	–	–	[166]

Table I.3 (continued).

IL	Amount of IL	Assistance	Analytes (number)	Sample (amount, pretreatment)	Analytical technique	LOD ($\mu g \cdot L^{-1}$)	E_F	Ref.
In situ DLLME								
$[C_4MIm^+][Cl^-]$	38 mg	Li-NTf_2 as anion-exchange agent	phenols (6)	seawaters & wastewaters (10 mL)	LC-UV-Vis	10–87	989	[167]
$[C_4MIm^+][Br^-]$	80 mg	Li-NTf_2 as anion-exchange agent	UV filters (6)	pool and lake waters (9.4 mL)	HS-GC-MS	0.5–10	400	[168]
$[BMIm^+][Cl^-]$	56 mg	NH_4PF_6 as anion-exchange reagent	antibiotics (4)	milk, eggs & honey (5 mL, deproteinization of milk and eggs)	LC-UV-Vis	0.12–0.45	98	[169]
$[C_6MIm^+][Cl^-]$	60 mg	KPF_6 as anion-exchange reagent	Cr (III) & Cr (VI)	tap & mineral waters (10 mL)	WCAES	3	233	[170]
$[Ni(C_4Im)_4^{2+}]2[Cl^-]$	20 mg	magnetic IL and Li-NTf_2 as anion-exchange agent	EDCs (10)	tap, lake and pool water (5 mL)	LC-UV-Vis	0.13–5.2	44.3	[171]
$[Ni(BIm)_4^{2+}]2[Cl^-]$	24 µmol	magnetic IL and Li-NTf_2 as anion-exchange agent	DNA	stock solutions (2 mL)	LC-UV-Vis	–	–	[172]

Table I.3 (continued).

IL	Amount of IL	Assistance	Analytes (number)	Sample (amount, pretreatment)	Analytical technique	LOD ($\mu g \cdot L^{-1}$)	E_F	Ref.
DLLME following ABSs fundamentals								
$[C_4MIm^+][Sal^-]$	2.5 % (w/w)	K_3PO_4 as salting-out agent	Cu (II)	tap and wastewaters (2 mL)	DPASV	0.008	54	[142]
$[Cho^+][Sac^-]$	1.4 % (w/w)	Na_2CO_3 as salting-out agent	alkaloids (3)	urine (9 g)	LC-UV-Vis	200–500	46	[173]

For the definition of the abbreviations, refer to the list of abbreviations.

Among environmental samples, water from different sources is the main matrix analyzed. In the case of food samples, the applications are devoted to challenging applications within food quality control. Thus, mainly vegetables, milk, and honey, are the target matrices for the determination of pesticides, antibiotics, and metals, respectively. Biological samples represent a lower number of studies, mainly due to the complexity of these samples and the strong matrix effects commonly observed when using LPME techniques. Urine is the most common sample within this category, but also plasma and whole blood have been analyzed. The group of other samples mostly includes food packaging and cosmetics, in which it is important the monitoring of plasticizers and PCPs to evaluate the human exposure to these EDCs [119,174].

In general, the samples are diluted with ultrapure water prior to the DLLME method, while previous extraction or digestion steps are required when analyzing food and biological samples. It is important to highlight that there is not a rationale between the nature of the target analytes and the characteristics and properties of the selected IL as extraction phase. Indeed, the same ILs have been successfully used for the extraction of totally different analytes: metal ions, polar analytes, and highly hydrophobic organic compounds. Therefore, despite the tunable properties of ILs, in general, the most common [$C_{n1}C_{n2}Im^+$] ILs with simple alkyl chains have been applied in the different applications. Moreover, it is important to point out the low number of applications using mass spectrometry (MS) as detection technique, which may be due to the low compatibility of the final extraction-phase with the MS system in the ionization interface. Those methods reporting the use of this detection technique do not directly inject the IL-phase in the instrument but perform thermal desorption or a previous back-extraction step.

I.3. Solid-phase microextraction

SPME was introduced in 1990 by Pawliszyn *et al.* with the aim of developing a simple, fast, and on-site sample preparation method [27]. As it was described in Section I.1.1.2, SPME is an equilibrium (non-exhaustive) technique that uses a device containing a small amount of a solid extraction phase. It is important to mention that there are cases in which the extraction phase is technically considered a liquid, as it occurs with several polymers, while other solids are appraised as porous sorbents [175]. In SPME, the extraction phase, with the aid of the device, is exposed to the sample for a specific time and then, once analytes are trapped by the extraction phase, it is subjected to desorption for attaining the detection and quantification of analytes. Thus, it allows performing several processes in a single step: sampling, extraction, and preconcentration, while permitting the reuse of the device.

Different SPME configurations have been proposed over the years to improve the diffusion of the analytes towards the surface of the extraction phase. The most conventional SPME device consists of a fiber (core) coated with the extraction phase (Figure I.4 E)), which is inserted in a stainless-steel body resembling a syringe, this way facilitating the exposure and further retraction of the sorbent phase. The on-fiber SPME coating size is normally 1 cm of length and up to 100 μm

of thicknesses, which provides a geometry suitable for the direct introduction of the device in different analytical instruments (GC injection port or LC interface) as well as ensuring the easy automation of the technique. These features are probably those justifying that the on-fiber SPME configuration is the most widely used [15,175].

The on-fiber SPME technique can be mainly performed in two modes: HS-SPME, by exposing the fiber to the HS over the sample, and DI-SPME, by directly immersing the fiber in the sample for a fixed period of time. Then, the analytes can be desorbed from the fiber either by subjecting the fiber to high temperatures in the GC injection port (thermal desorption) or by its immersion in a low volume of solvent (solvent desorption, which can take place in a LC interface).

In 1997, Eisert and Pawliszyn developed the in-tube SPME technique with the aim of overcoming the limitations of the on-fiber SPME when combined with LC: the difficulty on achieving on-line hyphenation, the fragility of the fiber coatings, and the carry-over effects (which are particularly significant when solvent desorption is used) [176]. The in-tube SPME device involved a fused silica capillary (length of 60 cm and internal diameter of 0.25 mm), which was internally coated with the sorbent phase, with thicknesses from 0.25 to 1 μm (Figure I.4 E)). In this case, instead of exposing the extraction device to the sample, the sample is passed through the extraction device to accomplish the extraction, while a solvent is used for the desorption of the analytes [15].

Given the simplicity, high enrichment capacity, versatility, and high automation feasibility of SPME techniques, they have been widely incorporated in different analytical applications [177–179]. Indeed, the huge trade expansion of on-fiber SPME in the analysis field has led to the development of standard methods using this technique [180,181]. Moreover, they have demonstrated to have improved features in terms of the greenness in comparison with other extraction methods [182]. Thus, SPME has been one of the most successful techniques among all the sorbent-based microextraction methods, and many efforts have been devoted to improving its extraction efficiency and fastness [183]. The main strategies to accomplish these goals include: (i) designing of new geometries for the SPME devices, (ii) using external factors (e.g., temperature and reduced pressure conditions) to improve the mass transfer and extraction rate of the process, and (iii) evaluating new extraction phases to enhance the extraction efficiency and selectivity.

3.1. Extraction fundamentals in SPME

SPME is based on the partition of the analytes from the sample to the extraction phase. Thus, considering the extraction phase as a "liquid" despite being a solid (i.e., polymers), the analyte diffuses from the sample to the bulk of the extraction phase in an absorption-type mechanism. In this case, it is considered that the process is completed once the equilibrium is reached [27]. If two phases are involved in the process (the sample and the extraction phase) as it occurs in on-fiber

DI-SPME and in-tube SPME applications, the amount of analyte extracted at equilibrium (n_e) can be calculated using Equation I.3, as it was described for DLLME (Section I.2.1).

However, in the case of on-fiber HS-SPME, the system is more complex and there are more equilibria involved in the extraction procedure. Thus, there are two distribution constants: between the sample and the HS (K_{hs}), and between the HS and the extraction phase (K_{eh}). They can be defined as follows:

$$K_{hs} = \frac{C_h}{C_s} \qquad \text{Equation I.5}$$

$$K_{eh} = \frac{C_e}{C_h} \qquad \text{Equation I.6}$$

where C_h is the analyte concentration in the HS at equilibrium, C_s is the analyte concentration in the sample matrix at equilibrium, and C_e is the analyte concentration in the extraction phase at equilibrium. Therefore, the equilibrium constant between the sample and the extraction phase is:

$$K_{es} = K_{hs} \cdot K_{eh} \qquad \text{Equation I.7}$$

In this system, where three phases are considered, the mass balance is described by the following equation:

$$C_s^0 \cdot V_s = C_s \cdot V_s + C_e \cdot V_e + C_h \cdot V_h \qquad \text{Equation I.8}$$

where C_s^0 is the initial concentration of the analyte in the sample, and V_s, V_e and V_h are the volumes of the sample, the extraction phase, and the HS, respectively. If Equations. I.5, I.6, I.7 and I.8 are combined, the amount of extracted analyte at equilibrium can be calculated as:

$$n_e = \frac{C_s^0 \cdot V_s \cdot K_{es} \cdot V_e}{K_{es} \cdot V_e + V_s + K_{hs} \cdot V_h} \qquad \text{Equation I.9}$$

In all SPME techniques, the volume of the extraction phase is significantly low in comparison with the volume of sample. Therefore, Equations I.3 (for DI on-fiber SPME and in-tube SPME) and I.9 (for HS on-fiber SPME) transform into:

$$n_e = C_S^0 \cdot K_{es} \cdot V_e \qquad \text{Equation I.10}$$

This Equation I.10 indicates that the amount of extracted analyte is directly proportional to its concentration in the sample matrix, and it does not depend on the sample volume, which is not a relevant factor. Therefore, as long as the volume of the extraction phase, the volume of the headspace, and the volume of sample, are constant, it does not matter whether the extraction is performed by HS- or DI-mode. This is the basis of calibration for SPME methods based on equilibrium extraction [27].

With respect to the kinetics theory in on-fiber SPME, the extraction rate is dominated by diffusion and the system is described by Fick's law of diffusion, as it occurs in DLLME (see Section I.2.1). Therefore, the boundary layer controls the kinetics and extraction rate in on-fiber SPME applications (Figure I.6) [1,27]. As the time required to reach equilibrium is infinite, in practice, the equilibration time corresponds to the time required to reach 95 % of equilibrium. At this equilibration time, the exposure of the extraction phase to the sample for longer times does not imply a significant difference in the extracted amounts of analyte. Considering these aspects, the equilibration time can be estimated as:

$$t_{eq} \approx t_{95\,\%} = \frac{3 \cdot \delta_s \cdot K_{es} \cdot (b - a)}{D_s} \qquad \text{Equation I.11}$$

where δ_s is the thickness of the boundary layer, (b – a) corresponds to the extraction phase thickness, and D_s is the diffusion coefficient. Moreover, the extraction rate can be expressed as:

$$\frac{dn}{dt} = \left(\frac{D_s \cdot A}{\delta_s}\right) C_s \qquad \text{Equation I.12}$$

where n is the amount of analyte extracted over the extraction time t, and A is the surface area of the extraction phase. The thickness of the boundary layer depends on many factors, including the geometry of the SPME device, the flow director, the temperature, and even the agitation speed. Thus, increasing the agitation speed decreases the thicknesses of the boundary layer and results in shorter equilibration times. Considering these expressions (Equations I.11 and I.12), increasing the surface area and decreasing the thickness of the extraction phase enhance the extraction rate and improve the mass transfer [27]. Moreover, a decrease of the diameter of the SPME device increases the extraction rate due to the radial diffusion [183]. Figure I.13 shows a representation

of the times profiles (extracted amount *versus* extraction time) obtained when the stirring conditions and device characteristics are modified [27].

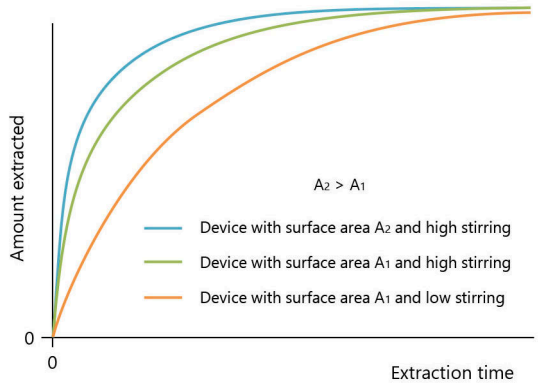

Figure I.13. Extraction time profiles obtained in SPME applications under different conditions with respect to the stirring rate and the extraction device geometry.

In in-tube SPME, a different scenario is observed due to the different geometry of the device and the flow-through extraction mechanism. In this case, the concentration profile along the tube (or capillary) as a function of time is described by the dispersion of the concentration front [27]. Thus, the speed at which the front of the analyte migrates through the tube is proportional to the linear velocity (u) of the sample and inversely related to the partition ratio (k_p), which is defined as:

$$k_p = K_{es} \cdot \frac{V_e}{V_v} \qquad \text{Equation I.12}$$

where V_v corresponds to the void volume of the extraction tube. Then, the extraction time (t_e) can be estimated by the following expression:

$$t_e = \frac{L \cdot (1 + K_{es} \cdot (V_e/V_v))}{u} \qquad \text{Equation I.12}$$

where L is the length of the extraction tube and u is the linear velocity of the sample. Therefore, the extraction time decreases when using shorter extraction devices and higher linear flows. Moreover, the extraction time increases with increasing volumes of the extraction phase but

decreases when the void volume is lower. If the flow rate used is fast enough to produce a turbulent behavior, the equilibration time can be estimated using Equation I.11 [1,27].

All these assumptions also apply for solid sorbents (porous sorbent, adsorption-type mechanism) since the total surface area available for adsorption is proportional to the volume of the extraction phase, as long as the porosity of the sorbent is constant. However, the main limitation of porous coatings is the competitive extraction mechanism. Therefore, the equilibrium amounts extracted can vary with the concentrations of the analyte and other components of the sample. The main solution to this problem is working in pre-equilibrium conditions to avoid saturation of the porous coating. The amount of extracted analyte can be still estimated by the previous equations as long as the convention conditions remain constant and the extraction time is carefully controlled [27].

3.2. SPME devices geometry and configuration

According to the theoretical kinetic model in SPME, the extraction rate is mainly limited by the thickness of the boundary layer. Considering that the need of long equilibration times is the main drawback of SPME techniques, main efforts have been shifted to accelerate the extraction rate [15]. As it was concluded in Section I.3.1, the geometry of the SPME device is the most important feature to take into account to accomplish this goal [40]. Particularly, the best strategy is to maximize the surface area to volume ratio of the coating and, indeed, different approaches have been adopted to improve this feature in SPME, and more particularly in the on-fiber SPME configuration.

On-fiber SPME

Figure I.14 includes the different geometries developed for the on-fiber SPME. The classical device requires a solid substrate with the extraction material immobilized onto its surface. The original silica substrates used to prepare the fibers suffer from certain fragility. In this sense, one of the most important advances within this conventional rod fiber configuration is the replacement of the fused silica core by a metal alloy, which improves the mechanical stability of the device [183].

Decreasing the diameter of the rod fiber was achieved by preparing a microscale conventional rod fiber by coating an acupuncture needle, which resulted in faster extraction rate, as it was achieved [184]. The device was called coated-tip SPME, and presented lengths around 150–500 µm, coating thicknesses of 5 µm, and total diameters between 20–50 µm. Moreover, they had a conical shape tip that offered better stability and even faster extractions due to the radial diffusion and thinner coatings.

The already commercially available arrow SPME fibers were firstly proposed in 2014 [185]. This configuration is based on a stainless-steel rod fiber but with an arrow tip, which helps in improving the device robustness and avoids background contamination. The arrow also allows the use of larger amounts of sorbent phase (lengths of 2 cm and thicknesses up to 250 µm), leading

to higher sensitivity in comparison with conventional rod fibers. However, this also implies longer extraction times to reach the equilibrium. As main drawbacks, the large diameter of the fibers implies a modification of the GC injection port, thus requiring the acquisition of specific liners and manual holders.

Despite monolithic fibers do not involve the coating of a solid support, the resultant monolith can be considered an on-fiber SPME device taking into account its shape and size (1 cm of length and 0.3–0.5 mm of diameter). Monolithic SPME fibers are easy to be mass-produced, and they are very flexible, which overcomes the fragility of conventional fibers [186,187]. Moreover, higher volumes of extraction phase can be used with these devices, which leads to enhance the resulting extraction efficiency [15].

It is interesting to mention the helical fiber proposed to enhance the extraction rate of SPME [188]. *A priori*, this geometry should lead to shorter times, because it presents higher surface area coating, and a reduced thickness of the boundary layer as a result of the rotational flow on the surface of the sorbent. However, it was demonstrated that the shielding effect in the interface of the helical geometry finally led to a less efficient convection, thus limiting the efficiency of the sorbent [189]. In the case of the double-braid and triple-braid SPME fibers, the configuration provides higher surface area and coating volume and, therefore, higher extraction efficiencies in comparison with a single fiber [190].

In an attempt to increase the volume of the extraction phase, multiple fibers assembled in a unique device have also been used [40]. The first strategy involved a multi-fiber brush composed of several coated fibers [191]. However, the extraction rate was not improved due to the small distance between the fibers, which was smaller than the thickness of the boundary layer. As an alternative configuration, a device consisting of 4 monolithic fibers, with a measured gap between them, was proposed [192]. The extraction efficiency with the multiple fibers increased with respect to a single fiber prepared with the same area. In this case, the extraction rate was upgraded by keeping agitation high enough, thus ensuring that the thickness of the boundary layer was smaller than the gap between fibers.

In-tube SPME

The classical configuration for in-stube SPME involved a long open tubular coated capillary, which presents a much higher surface area than the on-fiber SPME device. Therefore, according to the proposed theoretical model (Section I.3.1), this increase in the surface area of the extraction phase would lead to shorter extraction times. Indeed, this was demonstrated by Cháfer-Pericás *et al.*, who compared the performance of in-tube SPME and SPME fibers under the same experimental conditions [193]. Thus, the automated draw/eject in-tube SPME method allowed the analysis of 3 samples per hour with lower limits of detection, while only 1 sample could be analyzed with the on-fiber approach.

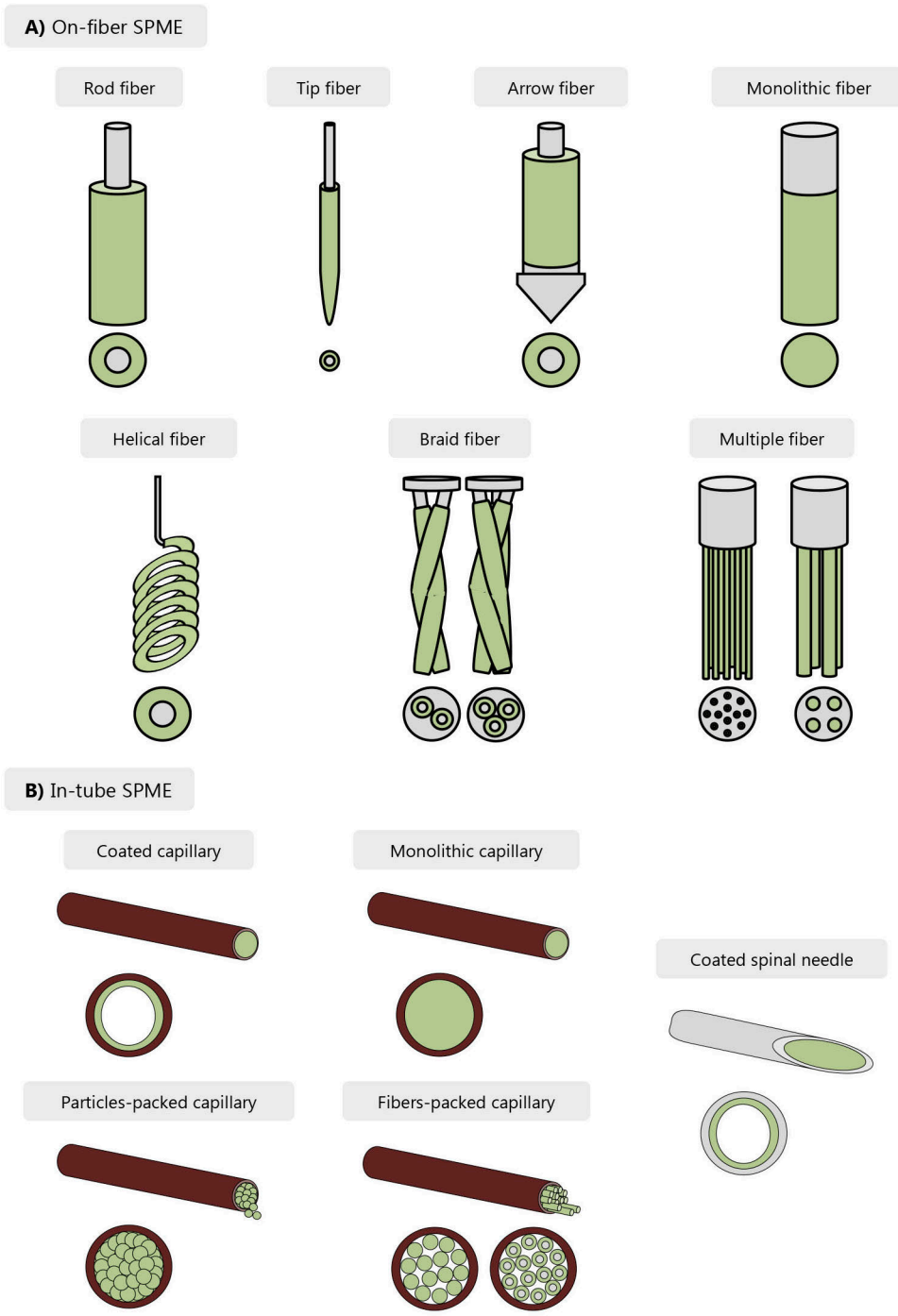

Figure I.14. Different geometries described for the preparation of **A)** on-fiber SPME and **B)** in-tube SPME devices.

Given the superior characteristics of the open-tubular extraction capillary for in-tube SPME, there has been a lower degree of innovation with respect to the geometry of this extraction device, while the evaluation of different phases to prepare new coatings has been the main research line [194,195]. Nevertheless, the amount of extraction phase that can be used to coat the internal walls of the capillary is limited, thus restricting the extraction capacity of the device. In this sense, capillaries packed with solid particles, polymeric fibers or a bundle of coated fibers, and monolithic capillaries, have been also described for in-tube SPME applications, as shown in Figure I.14 [40,194]. Despite the theory of in-tube SPME (Section I.3.1) also applies for this type of packed devices, it is important to take certain precautions during the extraction process due to back-pressure and clogging/blocking issues, which are more common than with the open-tubular device.

The miniaturization of the in-tube device has also been proposed [196]. In this case, a thin layer of the extraction phase was immobilized inside a medical grade spinal needle. Both extraction and desorption steps were carried out off-line using a syringe. Thus, the static extraction procedure involved loading the sample in the device using a plunger while stopping the sample flow for a specific time to increase contact with the extraction phase. The small size of the device allowed the analysis of sample volumes lower than 2 µL, but still achieving the sensitivity required due to the enrichment capacity of the in-tube SPME technique.

3.3. Operational modes of SPME

According to the theoretical model for SPME applications, decreasing the thickness of the boundary layer is also essential to improve the extraction rate and the mass transfer of the analytes from the sample to the extraction coating. Considering this thickness depends on several experimental conditions, including temperature and agitation rate, both on-fiber and in-tube SPME have been assisted by different strategies to improve the extraction performance and decrease the extraction time. Figure I.15 includes a scheme of the main modes of operation for on-fiber and in-tube SPME, together with a summary of the main assistance methods developed for improving the analytical performance of both techniques.

On-fiber SPME

As it was described in Section I.3, the extraction step in on-fiber SPME can be carried out either by HS- or DI-SPME, while thermal or solvent desorption can be performed. Each extraction mode present certain peculiarities and limitations that should be considered to develop the adequate strategy to improve the mass transfer and the extraction rate.

In the case of HS-SPME, there are two equilibria: (i) the transfer of the analytes from the sample to the HS and (ii) the transfer from the HS to the sorbent (see Section I.3.1). For some compounds, the first is the rate limiting step, which makes the extraction of more volatile analytes faster. In these cases, solutions to speed up the procedure include heating and/or stirring the

sample. However, higher temperatures may also lead to lower extraction efficiencies due to the exothermic nature of the sorption process [27].

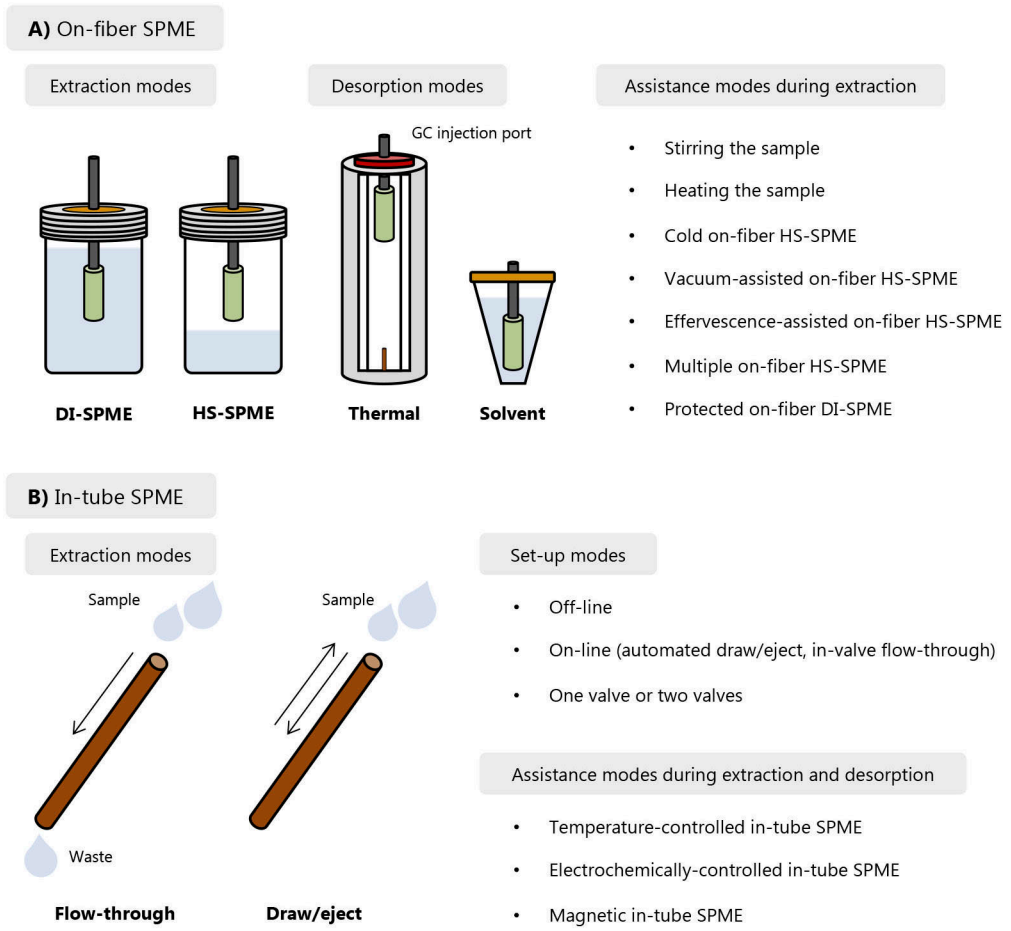

Figure I.15. Main modes of operation for **A)** on-fiber and **B)** in-tube SPME, including the variations developed to improve the procedure.

The cold HS-SPME mode was proposed to overcome this issue. In this approach, the sample is heated at high temperatures to increase the mass transfer to the HS, but the fiber is kept at low temperatures to avoid loses of analyte [197]. Indeed, the temperature gradient increases the partition coefficient and may even lead to exhaustive extractions [198]. CO_2 is used to internally cool the fiber using a manual or automated system [15]. However, a sharp increase of the pressure

in the sample vial when heating the sample is possible in cold fiber HS-SPME, leading to safety problems.

An alternative method to increase mass transfer to the HS consisted in applying reduced pressure conditions during the extraction step, which was proposed by Psillakis *et al.* [199]. This method, termed vacuum-assisted HS-SPME, add an extra step of air evacuation of the extraction vessel prior extraction. After that, the liquid sample is introduced using a gas-tight syringe and HS-SPME extraction is performed as usual by exposing the fiber to the evacuated HS. It has been demonstrated that the amount of analyte extracted at equilibrium is the same either using regular HS-SPME or vacuum-assisted HS-SPME. However, low pressures during the sampling step led to an increase of the diffusion and mass transfer coefficients for those analytes for which the transfer to the HS is the rate-limiting step [199]. Thus, vacuum-assisted HS-SPME allows reaching the equilibrium in shorter times, higher extraction efficiencies are obtained under pre-equilibrium conditions, and the use of reduced pressure conditions also involves milder temperature conditions than in regular HS-SPME methods. Moreover, this vacuum-assisted strategy has been also applied in combination with the cold HS-SPME mode to overcome the safety issues associated to high pressures [200].

More recently, the use of the tablet-induced effervescent approach, as a new and simple strategy to transfer the volatile and semivolatile compounds from the sample to the HS, has been proposed [201]. In this approach, the CO_2 bubbles generated in the solution facilitate the diffusion of the analytes to the HS. Such CO_2 bubbles appear in the neutralization reaction produced once a tablet containing the effervescence precursors is added to the sample.

Another drawback of HS-SPME is the attaining of important matrix effects when analyzing solid samples, which hinders the use of internal standards and even the standard addition method, thus making difficult the calibration. This problem can be solved by following an approach similar to multiple HS extraction, termed multiple HS-SPME [202]. In this strategy, consecutive HS-SPME extractions are carried out in the same sample. The quantification is performed by external calibration (using standards) and using the total peak area, which is estimated considering the peak area obtained in the repeated HS-SPME extractions.

In the case of the DI-SPME mode, the fiber is directly immersed in the sample to accomplish the extraction, and there is only one equilibrium involved in the procedure. In this mode, the stirring rate is one of the most important experimental factors that affects the extraction efficiency and rate of the procedure, since it helps in reducing the thickness of the boundary layer. Stirring the sample with the aid of a magnetic stir bar is the preferred method since this vortex-type of agitation enables the equalization of the mass transfer rate from any direction [183]. Moreover, increasing the sample temperature also may help in increasing the diffusion, but it is not a common strategy in DI-SPME due to the exothermicity of the sorption process.

The main problem of DI-SPME is the co-extraction of undesired compounds and the attachment of matrix components on the coating that may damage the extraction phase and

hamper the analysis [183]. In an attempt to avoid these issues when analyzing complex samples, the fiber coating has been protected with hollow fiber membranes (cellulose or polypropylene) during the extraction step in DI-SPME [203,204]. The use of this membrane protection prevents the extraction of substances with high molecular weight and allows direct analysis of high complex samples. However, the membrane-protected DI-SPME has some limitations, including slower mass transfer, likely due to the diffusion of the analytes through the membrane. In this sense, many efforts have been focused on the development of matrix-compatible coatings [205]. These fibers have enormously expanded the applications of SPME in clinical research for *in vitro*, *ex vivo*, and *in vivo* analysis [183,206]. Given the importance of developing new extraction phases for SPME, a detailed description on this topic is included in Section I.3.4.

In-tube SPME

The in-tube SPME was developed as an alternative to on-fiber SPME to accomplish the on-line coupling and/or automation of the extraction method with LC systems. Indeed, in the first study reporting the in-tube SPME technique, the extraction capillary was placed between the needle and the loop of a LC autosampler to carry out the extraction and desorption steps [176]. A specific volume of sample was repeatedly passed through the capillary in draw/eject cycles for the extraction with the aid of the metering pump of the autosampler. The mobile phase (or a solvent) was passed through for the desorption of the analytes, followed by the on-line injection in the LC injector. This first approach was termed the draw/eject in-tube SPME mode and has been particularly successful in bioclinical analysis, due to the low volumes of sample required [207].

Later, the flow-through mode was proposed, in which a specific volume of sample is continuously passed through the capillary in one direction just once. In this case, the extraction device replaces the loop of a LC injector and the analytes are extracted during the loading step. Then, the analytes can be desorbed and transferred to the analytical LC column by changing the injection valve to the inject position [207]. This mode has found a higher number of applications in the environmental analysis field due to the large volume of samples that can be processed in comparison with the draw/eject mode.

Despite a wide variety of different set-ups have been developed for each mode, all of them require the use of pumps (syringe pumps or the metering pumps of the LC autosampler in the case of automated draw/eject in-tube SPME) and can be performed using either one or two valves to control the different extraction and desorption steps. The use of the second valve emerged as a solution to: minimize contamination, improve precision, minimize peak broadening, and decrease plugging problems commonly observed, particularly with the automated method using LC autosampler [194]. Despite on-line and automated in-tube SPME have been the modes most commonly used, off-line approaches have also been described for both draw/eject [208] and flow-through modes [209]. In this case, the extraction capillary is directly connected to a syringe or

syringe pump, and it avoids the use of valves during the extraction step, while the desorption is accomplished by passing a small volume of organic solvent through the capillary.

In-tube SPME has also benefited from the incorporation of additional factors to improve the extraction efficiency of the method. In the simplest approach, the temperature-controlled in-tube SPME was developed to control the temperature inside the capillary during the different steps [210]. The set-up included inserting the internally coated capillary inside a stainless-steel tube, which is then placed inside a temperature controller box. Better results were observed when using low extraction temperatures, particularly for compounds with high molecular weight, while high temperatures decreased the time required to reach the equilibrium during both the extraction and desorption steps.

In a different approach, it was possible to develop an electrochemically controlled in tube SPME method [211]. In this case, a conducting polymer (Section I.1.2.2) was employed as extraction phase in an internally coated capillary. The extraction device was used as working electrode, and the unions of the extraction device with the different ports of the valve were used as counter and reference electrodes. During the extraction step, a positive constant potential was applied, while a negative potential was used during the static desorption process. In comparison with the absence of a constant electric potential, the analysis time was decreased, and the sensitivity was increased.

Interestingly, diamagnetic forces have been used to tune the partition of the analytes taking advantage of their diamagnetic repulsion during the different in-tube SPME steps in the so called magnetic in-tube SPME [212]. In. this approach, a magnetic material (i.e., functionalized MPs) was immobilized on the inner surface of a silica capillary. The extraction device was then placed inside a magnetic coil and accommodated in the position of the loop of an LC injection valve. The application of the magnetic fields in this method led to quantitative recoveries of the analytes in comparison with conventional in-tube SPME. The stability and extraction efficiency of this strategy have been improved by using a monolithic capillary doped with MPs as extraction device [213].

3.4. Sorbent coatings for SPME

Apart from the geometry of the device and the experimental conditions used to carry out the extraction procedure in SPME, one of the main parameters affecting the extraction performance is the affinity of the target analyte towards the extraction phase, expressed as the partition constant (K_{es}) [27]. Thus, despite there are several coatings and extraction phases commercially available with different characteristics, they still lack selectivity and present relatively low thermal stability and poor anti-fouling characteristics [40,205]. In this sense, the seeking of new phases to prepare more selective and efficient coatings has been undoubtedly the most important and active research topic within SPME advances [40,214]. Thus, numerous materials have been evaluated as sorbents to prepare fibers and capillaries, as it was described in Section I.1.2.2. Among all the candidates, PILs and MOFs have found a higher number of applications in the field

mainly due to their impressive tunability, as well as the high surface area in the case of MOFs. Since these materials were used in this Doctoral Thesis to prepare new SPME extraction phases, their main characteristics and their use in SPME applications will be overviewed in this section, together with an overview on current commercial coatings.

3.4.1. Commercial coatings

Currently, several brands, including Supelco (Merck) [215] and PAL from CTC Analytics (Restek) [216], supply SPME fibers coated with extraction phases of different polarities and thicknesses. Table I.4 lists the different commercial coatings together with their main characteristics. All commercial phases for on-fiber SPME contain a liquid polymer, which is the main component of the coating in the case of absorbent-type fibers: polydimethylsiloxane (PDMS), polyacrylate (PA), and polyethyleneglycol (PEG). These polymers are also the liquid bulk material in which the solid sorbent is suspended in the case of adsorbent-type coatings: carboxen/PDMS (CAR/PDMS), divinylbenzene/PDMS (DVB/PDMS), and DVB/CAR/PDMS.

For the preparation of commercial on-fiber SPME devices, fused silica fibers and metal wires are used as core to support the coating material, with diameters of 100 and 128 µm, respectively [217]. Despite the fragility of fused silica, it is the preferred core for most on-fiber SPME devices since the diameter can be highly controlled and long fibers can be coated precisely with absorbent materials during the manufacturing. Stableflex cores, consisting of fused fibers coated with a thin layer of an inert polymer, and metallic wires, composed of a flexible and thermally stable non-ferrous metal alloy, were introduced to overcome this stability issue [217]. These novel substrates as cores also improve the bonding of the adsorbent-type materials during the coating process and the reproducibility between batches of the resulting device.

Regarding the size of the commercial on-fiber SPME devices, all of them have cores of 1 cm and the thicknesses of the coating are up to 100 µm depending on the composition of the sorbent material (Table I.4). These coated cores assemble in a device that resembles a syringe to facilitate its manipulation. Recently, Supelco has started to manufacture an overcoated PDMS/DVB coating that incorporates an additional protective layer of PDMS, which makes the fiber more robust and provides anti-fouling characteristic to analyze complex samples by DI-SPME [218].

CTC Analytics (Restek) also commercializes on-fiber SPME devices in the arrow configuration [219]. The available stationary phases are the same as those for conventional on-fiber SPME: polymer-based coatings with different polarities depending on their composition. However, in this case, the geometry of the device allows increasing the amount of extraction phase. Thus, the length of the coatings is 2 cm, the rods have outer diameters of 1.1 or 1.5 mm, and the thicknesses for the PDMS phase range from 100 µm to 250 µm. The main characteristics of these arrow SPME fibers are included in Table I.4.

Table I.4. Characteristics of the commercial SPME fibers.

Coating	Thicknesses	Polarity	Recommended application
Conventional SPME fibers			
CAR/PDMS	75 & 85 µm	bipolar	volatile and low molecular weight compounds
DVB/CAR/PDMS	50 µm	semipolar	volatile and semivolatile compounds at trace levels
DVB/PDMS	65 µm	semipolar	amines and aromatic semivolatile compounds
PA	85 µm	polar	polar semivolatile compounds
PEG	60 µm	polar	alcohols and polar compounds
PDMS	7, 30 & 100 µm	apolar	volatile and non-polar compounds
PDMS/DVB/PDMS*	65/10 µm	semipolar	semivolatile compounds in complex matrices
Arrow SPME fibers			
CAR/PDMS	120 µm	bipolar	highly volatile compounds
DVB/CAR/PDMS	120 µm	semipolar	volatile and semivolatile compounds
DVB/PDMS	120 µm	semipolar	amines, polar and aromatic semivolatile compounds
PA	100 µm	polar	polar and semivolatile compounds
PDMS	100 & 250 µm	apolar	volatile compounds

* Overcoated fiber, with a PDMS protective layer of 10 µm.

In the case of in-tube SPME, there are not capillaries specifically manufactured for this technique and most of the devices are labmade. However, short pieces of commercial GC capillary columns, which can be open-tubular or packed, have been used in in-tube SPME [194]. Thus, considering the wide variety of GC stationary phases that are commercially available in terms of polarity and dimensions (diameters and thicknesses), there is a broad spectrum of possible applications of in-tube SPME.

3.4.2. Coatings based on polymeric ionic liquids

PILs have been the main alternative to take advantage of the properties of ILs in SPME applications due to their solid (or highly viscous liquid) nature. Moreover, they present high thermal stability, mechanical durability, and tailorable properties and structures, which makes them promising materials to prepare extraction phases that overcome the limitations of commercial SPME coatings [78]. Indeed, since their first incorporation in this technique to develop an on-fiber SPME device in 2008 [220], an almost steady number of applications have been reported every year in both on-fiber and in-tube SPME, as it can be observed in Figure I.16.

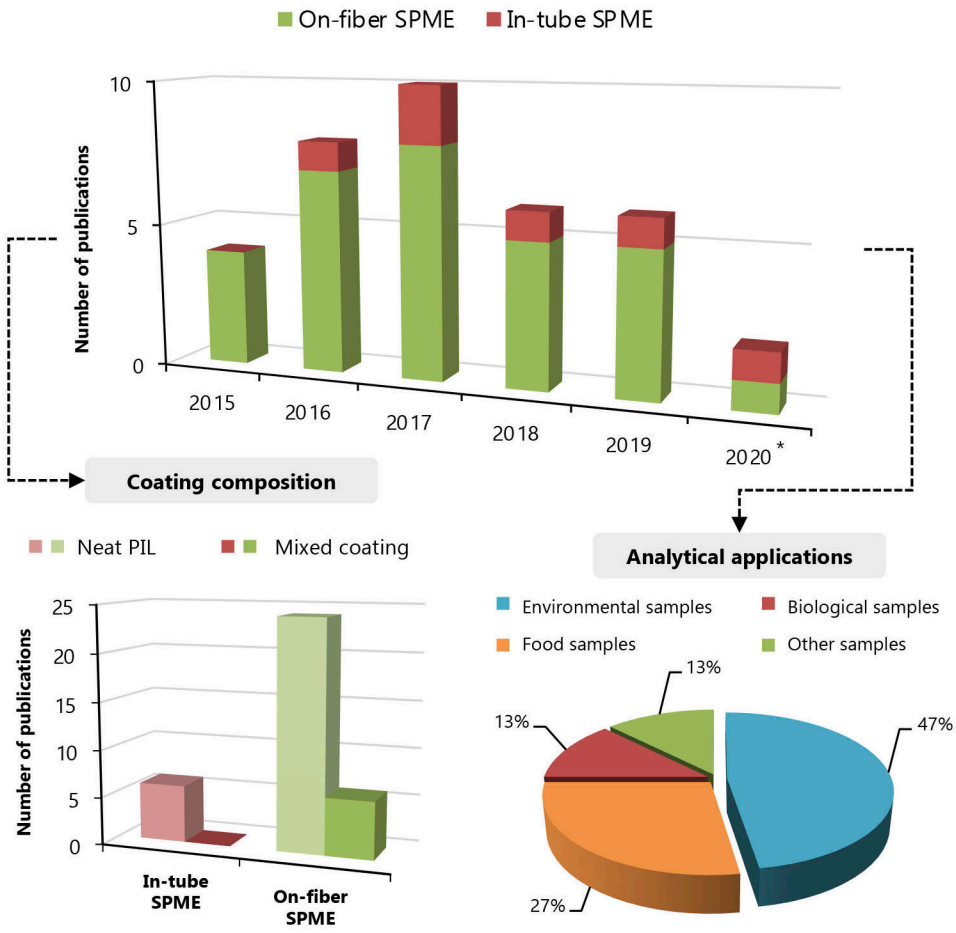

Figure I.16. Statistics showing the number of publications in the period 2015–2020 on the use of PILs as coatings in on-fiber and in-tube SPME applications, including the type of coating with respect to the composition (*until November 2020).

3.4.2.1. Structure and properties of PILs

PILs are polyelectrolytes that involve a polymeric backbone composed of ILs as monomers [77]. Thus, they are prepared by the polymerization of ILs instead of solid salt monomers, as it occurs with other polyelectrolytes [221]. The most common PILs are composed of ILs with [$C_{n1}C_{n2}Im^+$] cations with a polymerizable substituent (e.g., vinyl, allyl, and styryl), but [$C_{n1}C_{n2}Pyrr^+$], [$N_{n1,n2,n3,n4}^+$], and [$P_{n1,n2,n3,n4}^+$] cations have also been widely used [77,221]. With respect to the anionic moiety, the wide variety of exiting anions (see Section I.2.3.1) has been used to prepare PILs, in contrast with conventional polyelectrolytes, which are only composed of halide anions [221].

These polymers are classified as polycations, polyanions or polyzwitterions based on the repeating monomer unit within the PIL backbone [221]. Figure I.17 shows a representative example for each of these groups. Polycationic PILs is the largest variety of PILs, while the number of PILs described with anionic moieties and mobile cations is smaller. This may be due to the difficulties in the preparation of anionic IL monomers with the polymerizable group [221]. In the case of zwitterionic PILs, the monomers are zwitterionic salts with high melting points and a similar composition than ILs. Thus, as it occurs with ILs, technically, they are not PILs but are included within this group given their similarities in terms of composition and physicochemical properties [221,222]. Moreover, double-confined PILs can be also prepared by employing ILs monomers containing polymerizable moieties in both the cation and anion [223].

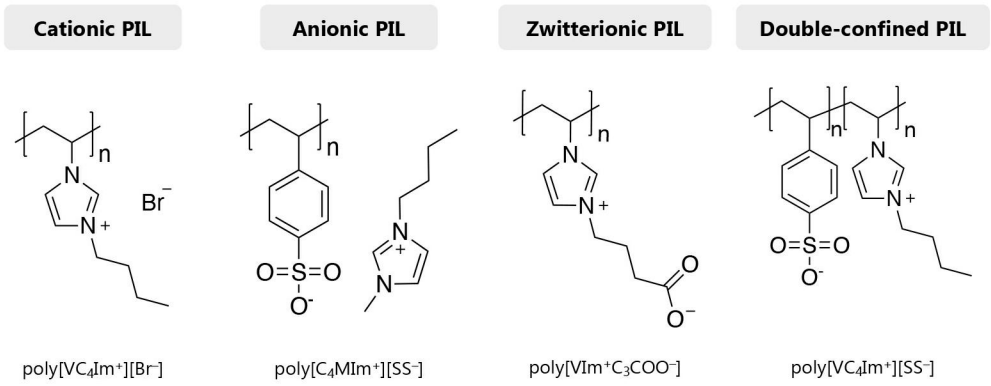

Figure I.17. Representative examples for each type of PIL, showing the chemical composition.

They present the same properties as their IL precursors: low vapor pressure at room temperature, high thermal and electrochemical stability, and outstanding synthetic versatility.

Therefore, the properties of PILs can be modulated by making slight changes in their composition. Thus, PILs are solids with low glass transition temperature, which can be decreased even more by selecting the proper anion or by the copolymerization with other components [77]. With respect to the thermal stability, it strongly depends on the composition and structure of the IL monomer [77]. Thus, PILs containing aromatic rings exhibit higher thermal stability than aliphatic backbone structures. In this sense, [$C_{n1}C_{n2}Im^+$]-based PILs have enhanced thermal stability compared to [$C_{n1}C_{n2}Pyrr^+$]-based PILs, while the temperature decomposition of PILs containing [$P_{n1,n2,n3,n4}^+$] is higher than for [$N_{n1,n2,n3,n4}^+$]-based PILs.

In general, PILs are hydrophobic but are soluble in organic solvents of different polarity [77]. However, the aqueous solubility of PILs can be adjusted through a simple anion-exchange reaction, as it occurs with ILs [224]. Moreover, in comparison with the monomeric IL unit, PILs present lower conductivity due to the depletion in the number of mobile ions after forming the polymeric backbone [225]. In the same way, the presence of small anions in the PIL provide higher conductivity in comparison with bulky counter anions.

With respect to the synthesis of these materials, most PILs are prepared by conventional radical polymerization, which can be carried out following different routes, such as thermal-initiated, UV-initiated, and atom transfer radical polymerization [77]. Moreover, the synthetic versatility of PILs allows performing an anion-exchange reaction in the polyelectrolyte and change the anion nature even after the polymerization reaction [221]. This route allows the preparation of both homopolymers and copolymers. In the first case, the PIL is composed by the same IL monomeric unit within the backbone, while copolymers consist of different IL monomers that yield branched and long polymeric structures [221]. Crosslinked PILs are included within this last group and are synthesized using a monocationic IL as monomer and a dicationic IL as crosslinker, which is used to connect the monocationic IL polymeric chains [77,221].

3.4.2.2. Preparation of PILs-coated SPME devices

Different strategies have been described for the preparation of PIL-based SPME devices depending on the type of attachment between the PIL and the support, as well as on the geometry of the device within both on-fiber and in-tube SPME. Figure I.18 includes a summary of the main strategies described.

On-fiber SPME

First applications of PILs in on-fiber SPME reported the physical immobilization of the polymer on the solid core (fused silica) taking advantage of the high viscosity of PILs [220,226]. These fiber devices were prepared by directly immersing the support in the PIL or in a solution of the polymer, followed by solvent evaporation. The fibers were able to successfully perform in both HS- and DI-SPME modes [226–228]. In a similar approach, the PILs have also been attached to the support using polyacrylonitrile as glue, which can also take part in the extraction process [229].

However, the lifespan of the fibers was very limited, and the coatings exhibited low stability in the presence of organic solvents, thus restricting their use only in GC applications with thermal desorption.

With the aim of overcoming these stability issues and improve the robustness of the PILs-based SPME coatings, different strategies have been proposed to chemically attach the PIL to the fiber support. These approaches base on the functionalization of the wire used as core with specific groups, followed by the direct polymerization of the PIL on the surface of the support. In the first studies, stainless steel was selected as support to avoid the use of fragile fused silica fibers [230,231]. In order to ensure a chemical linkage with the PIL, the modification of this support required the deposition of a silver [230,232] or gold layer [231], followed by its functionalization with thiol or silanol groups. The polymerization of the PIL was then carried out by thermal-initiated polymerization using azobisisobutyronitrile (AIBN) as radical initiator.

The most successful and most used approach to prepare chemically-attached PILs-based fibers was proposed by Ho *et al.* [233]. In this method, the UV-initiated polymerization of the IL takes place on the fiber support and inside a UV reactor, which enormously speeds up the preparation of fibers. The support, fused silica [233,234] or nitinol wires [235–237], is previously functionalized with vinyl groups to establish the chemical immobilization of the PIL. The use of nitinol alloys as core has undoubtedly led to an improvement in the mechanical stability of the PILs-based coating, being the support most widely employed in the recent years.

Other polymerization approaches have been proposed to prepare SPME fiber coatings but in a lesser extent, such as the electropolymerization of the PIL on platinum wires exploiting the conductivity properties of IL monomers [238,239]. Moreover, monolithic PILs have also been prepared to fabricate devices composed of multiple fibers (Figure I.14) [240,241]. In this case, the PILs are thermally polymerized inside a capillary with the desired diameter, and then the capillary is removed to obtain the thin monoliths that will compose the on-fiber SPME device.

With respect to the composition of all these on-fiber SPME extraction phases, the vast majority consist of neat PILs, and more specifically, composed of [$VC_{n1}Im^+$]-based IL monomers. Moreover, most of them are crosslinked PILs, in which a dicationic IL is used as crosslinking agent to improve the mechanical stability of the sorbent [78]. The IL monomers used in most PILs have also been functionalized to include specific groups in their chemical structures for tuning their selectivity. For example, the incorporation of silver ions within the IL monomer led to the preparation of coatings with unique selectivity towards alkenes and alkynes [242], while those IL monomers with vinylbenzyl groups within the cation provided better results for aromatic compounds [236,243]. Moreover, the use of double-confined PILs has improved the mechanical stability of the PILs and avoided the swelling of the coating in both aqueous solutions and organic solvents [244].

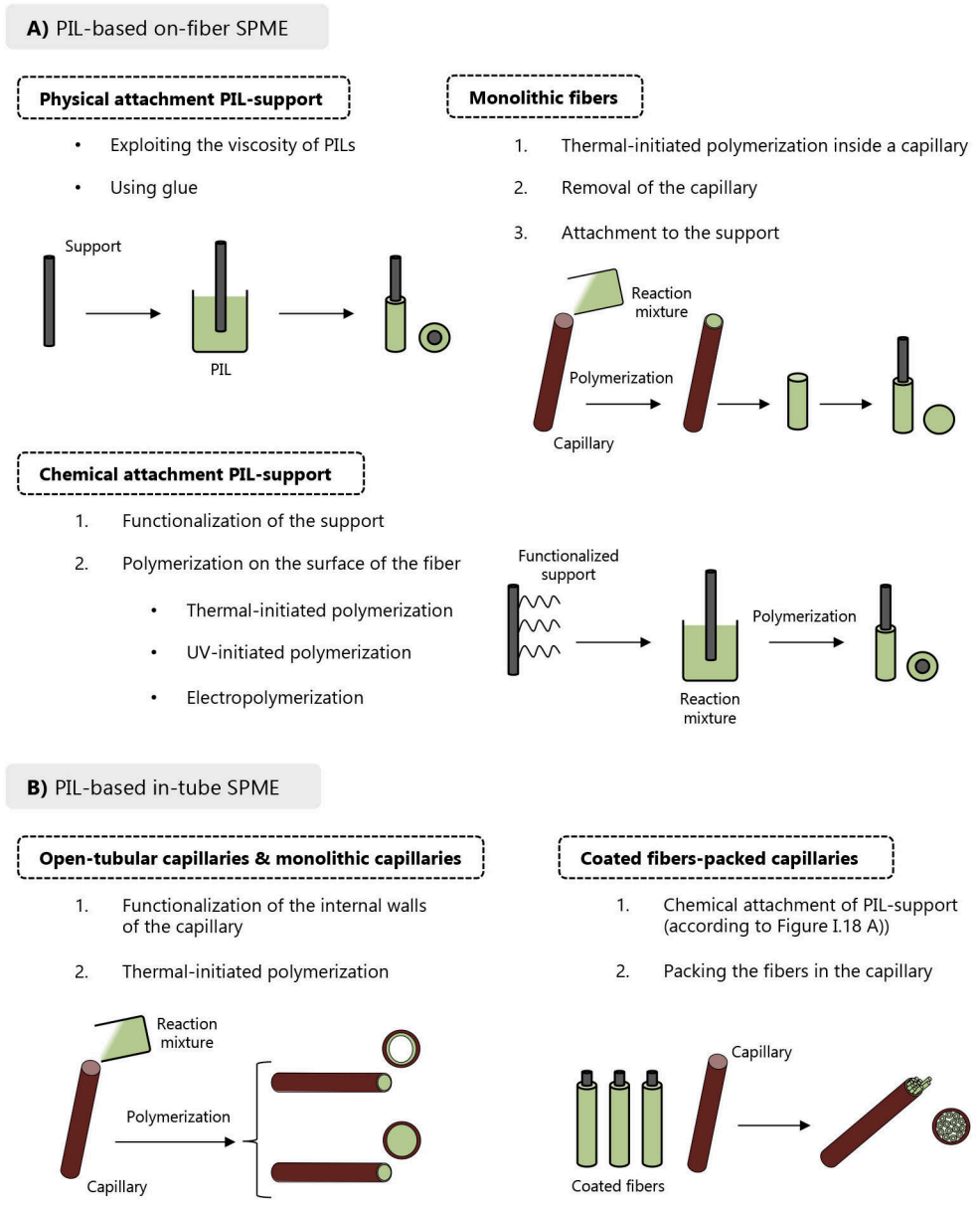

Figure I.18. Main strategies for the preparation of PIL-based **A)** on-fiber and **B)** in-tube SPME devices.

Only one study has reported the use of [$C_{n1}C_{n2}Pyrr^+$]-type PILs [245], while several studies have reported the preparation of mixed coatings in which the PIL (i) acts as matrix to disperse CNTs [239] or (ii) it is used to functionalize the surface of a fiber previously coated with the carbonaceous material (i.e., GO and CNTs) [232]. In the case of monolithic SPME fibers, they are also composed of [$VC_{n1}Im^+$] IL monomers, but the PIL is crosslinked with other components, such as ethylene dimethacrylate (ED).

In-tube SPME

In the case of PILs-based extraction phases for in-tube SPME, the number of studies reported is much lower, as it can be observed in FigureI.16. The most common types of devices prepared are coated fibers-packed capillaries (Figure I.14) [246–248]. For this type of devices, the PILs were chemically immobilized on the fiber supports by thermal polymerization following the strategies previously described for on-fiber SPME devices. Then, several fibers were inserted in the extraction tube to fabricate the in-tube device.

The preparation of monolithic capillaries has also been reported, involving a much simpler approach. It only required the thermal polymerization of the PIL inside the capillary, for which the internal surface was previously functionalized to guarantee the chemical linkage of the monolith, thus ensuring the stability of the extraction phase [249]. In general, the fabrication of open-tubular coated capillaries comprises a meticulous procedure and it faces certain difficulties in obtaining thick and uniform coatings. Indeed, only one study has reported the preparation of this type of in-tube SPME device using a crosslinked PIL, which was synthesized on the internal walls of a fused silica capillary by thermal polymerization [250].

In all cases, [$C_{n2}C_{n2}Im^+$]-type monomers were used, which were crosslinked with other imidazolium dicationic ILs, or with ED in the case of monolithic capillaries [249].

3.4.2.3. Analytical applications of PILs in SPME

FigureI.16 shows a summary of the number of studies using PILs-based coatings for both on-fiber and in-tube SPME, together with the type of samples analyzed in the analytical applications developed. Moreover, Table I.5 lists some representative examples of these applications [235–237,245,246,249–253].

In both techniques, the applications have been devoted to the determination of organic analytes, except for two particular applications in which crosslinked PIL-based on-fiber coatings, containing carboxylic groups in the cationic moiety, were used for the selective and efficient extraction of DNA and RNA [252,254].

Table I.5. Representative analytical applications described in the literature on the use of PILs as extraction phase in on-fiber and in-tube SPME.

IL monomer	Crosslinker	Type of device (additive)	SPME mode	Analytes (number)	Sample (amount, pretreatment)	Analytical technique	LOD ($\mu g \cdot L^{-1}$)	Ref.
On-fiber SPME								
$[VC_8Im^+][NapSO_3^-]$	–	coated SS rod fiber (CNTs)	HS-SPME	halogenated aromatic hydrocarbons (6)	groundwater (10 mL)	GC-FID	0.075–0.2	[232]
$[VC_6Im^+][Br^-]$	–	coated SS rod fiber	HS-SPME	PCBs (12)	river water (5 mL)	GC-ECD	0.0009–0.0058	[251]
$[VBC_{16}Im^+][NTf_2^-]$	$[(VIm)_2C_{12}^{2+}]2[NTf_2^-]$	coated NiTi rod fiber	DI-SPME	acrylamide (1)	brewed coffee (19 mL)	GC-MS	10*	[235]
$[VBC_{16}Im^+][NTf_2^-]$	$[(VIm)_2C_{12}^{2+}]2[NTf_2^-]$	coated NiTi rod fiber	HS-SPME	UV filters (9)	pool & lake water (10 mL)	GC-MS	0.0025–0.026	[236]
$[VBC_{16}Im^+][NTf_2^-]$	$[(VIm)_2C_{12}^{2+}]2[NTf_2^-]$	coated NiTi rod fiber	HS-SPME	aroma compounds	wine (4.5 mL)	GC×GC-MS	–	[237]
$[VC_{9COOH}Im^+][Br^-]$	$[(VIm)_2C_{12}^{2+}]2[Br^-]$	coated NiTi rod fiber	DI-SPME	DNA	bacterial cell lysate (10 mL)	qPCR	–	[252]
$[MC_{14}Pyrr^+][NTf_2^-]$	DVB	coated SS rod fiber	HS-SPME	alcohols, terpenes & ketones (11)	urine (4 mL)	GC-FID	0.2–200	[245]

Table I.5 (continued).

IL monomer	Crosslinker	Type of device (additive)	SPME mode	Analytes (number)	Sample (amount, pretreatment)	Analytical technique	LOD ($\mu g \cdot L^{-1}$)	Ref.
$[AMIm^+][NTf_2^-]$	ED	multiple monolith fiber	DI-SPME	hormones (7)	tap water, lake water & urine (20 mL, dilution of urine)	LC-UV-Vis	0.03–0.12	[253]
In-tube SPME								
$[VC_{12}Im^+][Br^-]$	$[(VIm)_2C_6^{2+}]2[Br^-]$	coated Cu fibers-packed capillary	flow-through (on-line, 1 valve)	estrogens (5)	bottled and sewage waters (35 mL)	LC-DAD	0.02–0.05	[246]
$[AMIm^+][NTf_2^-]$	ED	monolithic capillary (doped with MPs)	magnetic-assisted flow-through (on-line, 2 valves)	UV filters (5)	lake, river and wastewater (1.5 mL)	LC-UV-Vis	0.04–0.26	[249]
$[VC_{16}Im^+][Br^-]$	$[(VIm)_2C_{10}^{2+}]2[Br^-]$	open-tubular coated capillary	flow-through (on-line, 1 valve)	cannabinoids (2)	plasma (80 µL, deproteinization)	LC-MS/MS	0.05–0.10*	[250]

* Limits of quantification. For the definition of the abbreviations, refer to the list of abbreviations.

The type of target organic compounds is closely related to the type of sample analyzed. Thus, as shown in FigureI.16, almost half of the studies have focused on the environmental analysis field. In this sense, the group of analytes determined range from persistent pollutants (e.g., PAHs, benzene, toluene, ethylbenzene and xylene (BTEX), and aromatic amines) to EDCs of emerging concern, such as UV filters, drugs and pharmaceuticals. In the case of food samples, only the on-fiber SPME technique has been used, mainly for the determination of hormones and drugs in milk samples, acrylamide in coffee [235], and the aromatic profile of different food products [237]. The use of these extraction phases within clinical analysis is lower in comparison with the other application fields, with only 13 % of the studies dealing with biological samples. In this case, mainly drugs and pharmaceuticals in urine and plasma are the target applications [245,250]. Other samples include aqueous standards of the analytes, which were used to evaluate and to compare the extraction performance of the PILs-based extraction phases with commercial fibers [239].

The frequency on the use of HS-SPME and DI-SPME for the on-fiber SPME technique is the same, thus demonstrating the suitability of PIL-based devices for the direct analysis of samples, which usually only require dilution with ultrapure water prior to the DI-SPME procedure. With respect to the analytical technique, the majority of on-fiber SPME applications have been combined with thermal desorption and GC, taking advantage of the high thermal stability of PILs. Indeed, the cases in which the solvent desorption was employed and the on-fiber SPME technique was coupled with LC were those using monolithic devices [240,241] or double-confined PILs [244]. This may be due to the swelling of the PIL-based coatings commonly observed when the fibers are immersed in organic solvents.

Furthermore, all the in-tube SPME applications have been (obviously) coupled to LC and different detectors. The flow-through mode was used by the on-line coupling of the capillary to the LC system using the one valve set-up. Thus, the automated draw/eject in-tube SPME mode has not been recently evaluated with PILs-based extraction phases.

3.4.3. Coatings based on metal-organic frameworks

Given the high sorption capacity of MOFs, they have attracted much attention in analytical sample preparation, and particularly in SPME applications. Indeed, one of the first applications of MOFs in a microextraction technique was the use of the MOF HKUST-1(Cu) as extraction phase to prepare an on-fiber SPME device in 2009 [255]. Since then, the number of studies reporting the use of these materials in SPME have increased over the years, as shown in Figure I.19, and thus becoming one of the most explored materials to solve the main drawbacks of commercial SPME sorbent phases [256,257].

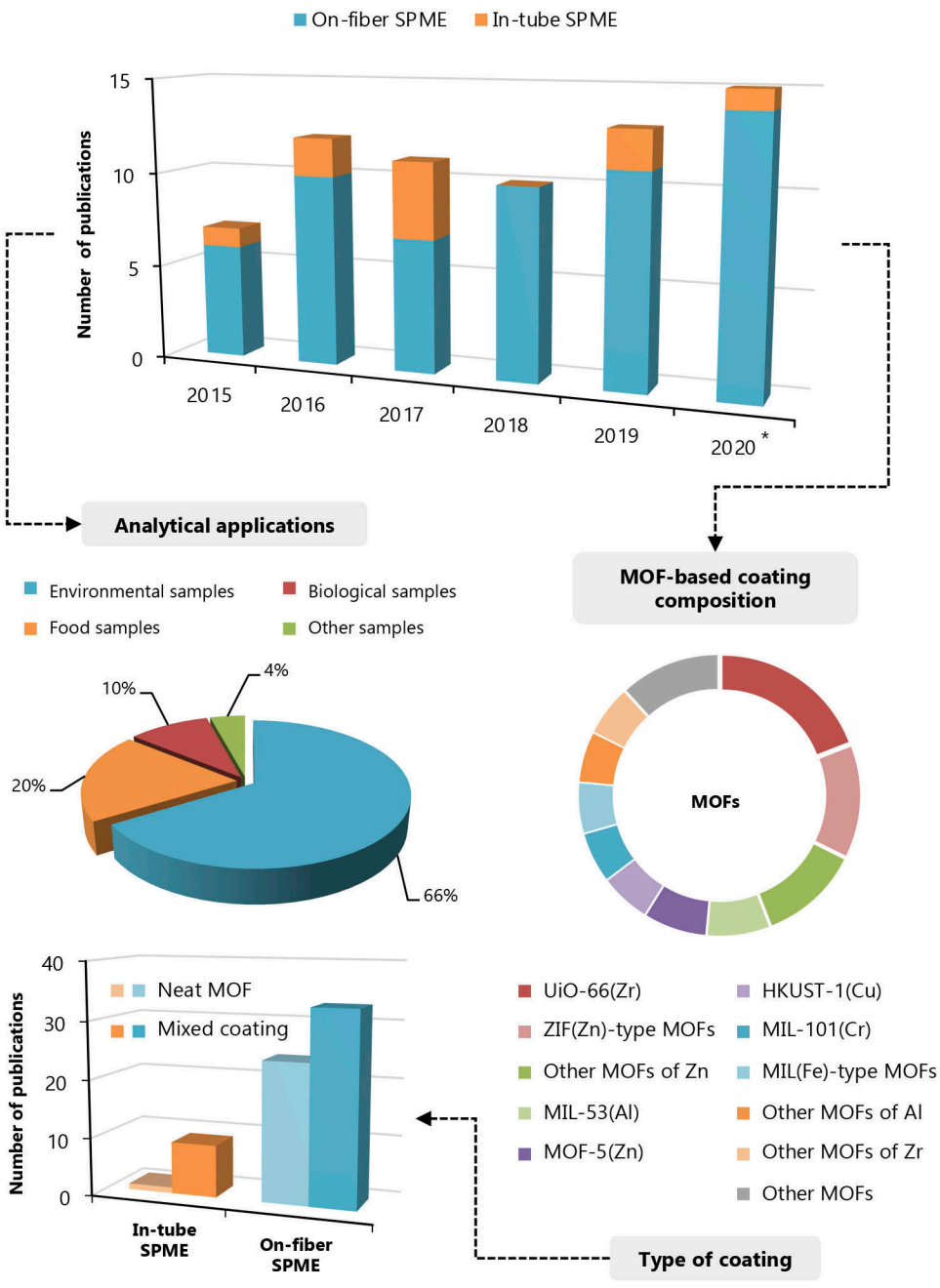

Figure I.19. Statistics showing the number of publications in the period 2015–2020 on the use of MOFs as coatings in on-fiber and in-tube SPME applications, including the type of coating with respect to the composition (*until November 2020).

3.4.3.1. Structure and properties of MOFs

MOFs are crystalline materials constructed by the combination of two BBs by strong covalent bonds: a metal ion or cluster and an organic linker [89]. They are the most widespread type of reticular materials, and indeed there are more than 80000 MOFs already registered in the Cambridge Crystallographic Data Center (CCDC) [258]. Surprisingly, there is not a unified nomenclature to name MOFs, despite the importance of specifying the composition of the BBs to correctly identify a MOF. Nevertheless, there are numerous abbreviations to designate MOFs, depending on the institution where they were first characterized or their composition, and they are well-known in the chemistry community: MIL–Materials Institute of Lavoisier, HKUST–Hong Kong University of Science and Technology, JUC–Jilin University of China, TMU– Tarbiat Modares University, UiO–University of Oslo, CIM–Canary Islands Materials, and ZIF–zeolitic imidazolate framework. These abbreviations are accompanied by a number that identifies the metal cluster and the organic linker forming the MOF [92]. Table I.6 lists the composition and name attributed to the most common MOFs, while Figure I.20 includes the structure of several representative MOFs that have been used in sorbent-based microextraction techniques.

Table I.6. Nomenclature to identify the most common MOFs.

MOF	Metal	Organic ligand
HKUST-1(Cu)	Cu (II)	benzene-1,3,5-tricarboxylate
MIL-53(Al)	Al (III)	benzene-1,4-dicarboxylate
MIL-53-NH_2(Al)	Al (III)	2-aminobenzene-1,4-dicarboxylate
MIL-53(Fe)	Fe (III)	benzene-1,4-dicarboxylate
MIL-88B(Fe)	Fe (III)	benzene-1,4-dicarboxylate
MIL-100(Fe)	Fe (III)	benzene-1,3,5-tricarboxylate
MIL-101(Cr)	Cr (III)	benzene-1,4-dicarboxylate
MIL-101(Fe)	Fe (III)	benzene-1,4-dicarboxylate
MOF-5(Zn)	Zn (II)	benzene-1,4-dicarboxylate
TMU-4(Zn)	Zn (II)	4,4′-oxydibenzoate & 1,4-bis(4-pyridyl)-2,3-diaza-1,3-butadiene
UiO-66(Zr)	Zr (IV)	benzene-1,4-dicarboxylate
UiO-66-NH_2(Al)	Zr (IV)	2-aminobenzene-1,4-dicarboxylate
UiO-67(Zr)	Zr (IV)	biphenyl-4,4′-dicarboxylate
ZIF-7(Zn)	Zn (II)	2-phenylimidazolate
ZIF-8(Zn)	Zn (II)	2-methylimidazolate

The main feature of these materials is their exceptional porosity. Indeed, MOFs stand out for presenting the highest surface areas known, with values ranging from 300 to 10000 $m^2 \cdot g^{-1}$ [90,259]. The synthetic versatility of these materials allows the preparation of MOFs with specific structures and topology, while their chemical and water stability can also be modulated by selecting the adequate BBs. Thus, large organic linkers provide MOFs with increased porosity and, therefore, with higher surface areas [259,260], while ZIFs and MOFs containing trivalent metal ions and oxygen-terminated linkers (e.g., MIL-101(Cr)), present significant water-stability, which enable their use in a wide range of applications [261].

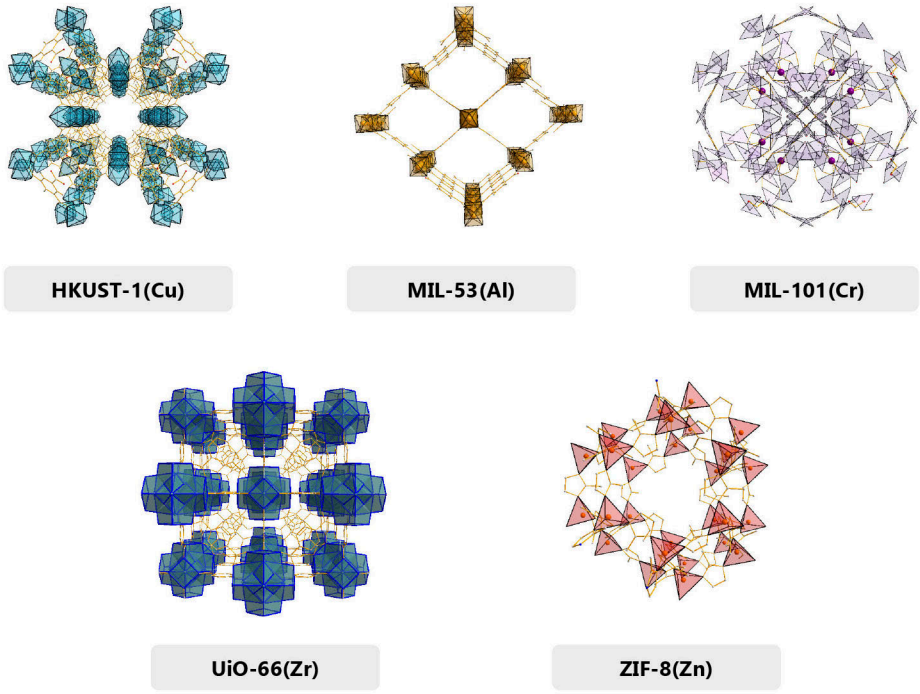

Figure I.20. Structure of representative MOFs obtained using the data from the CCDC and Diamond 4.6.2. crystallographic software.

In general, MOFs exhibit adequate thermal stability, with decomposition temperatures up to 500 °C for many of them [259]. Furthermore, the structural robustness of these frameworks permits modulating their properties by means of post-synthetic modification and functionalization of their pores and external surface [262,263].

The conventional protocols for the preparation of crystalline networks are suitable for the synthesis of MOFs, including diffusion, solvothermal, electrochemical and mechanochemical methods [264]. The solvothermal method is the most common synthetic approach, in which the BBs precursors are dissolved in an adequate solvent (sometimes requiring co-solvents and/or modulators), followed by heating at a high temperature for a certain time in a sealed container. With the aim of reducing the energy consumption of the process, microwave and ultrasound-assisted methods have also been proposed. Despite the simplicity of these strategies, the synthetic conditions must be carefully fixed and controlled since the resulting MOF structure strongly depends on several experimental conditions, such as the composition of the metal precursor, solvent, temperature, and/or modulators [90,264]. Indeed, different structures with different pore sizes and distribution can be obtained using the same BBs, as it is the case of MIL-53(Fe), MIL-88(Fe), and MIL-101(Fe), which are composed of benzene-1,4-dicarboxylate as organic linker and Fe (III) as the metallic component but exhibit different crystalline structure.

Furthermore, it is important to mention that MOFs require an activation step prior to their use as sorbents in sample preparation techniques. This step should ensure the removal of the guest solvent molecules from the pores of the MOF (by thermal treatment or washing the MOF powder with a lower boiling point solvent), to make them accessible for the sorption of target substances [264].

A proper characterization of a MOF results essential in order to understand its properties and to establish whether it is useful or not for certain applications [92,261]. Figure I.21 shows a summary of the main synthetic routes and characterization techniques used for the preparation of MOFs. X-ray diffraction is the main technique providing information regarding the crystal structure of the MOF, and consequently, it is used to identify the as-prepared MOF while determining its purity. Infrared spectroscopy can be used to determine the presence of certain bonds and groups in the crystal structure, being especially helpful to ensure the post-synthetic functionalization of the MOF. Gas adsorption measurements, using N_2 or CO_2, provides information with respect to the specific surface area, and pore size and distribution of the MOFs. The data can be analyzed using either Brunauer-Emmett-Teller (BET) or Langmuir methods, being essential to identify the type of adjustment used. Thermogravimetric analysis is the main tool to assess the thermal stability of the MOF. The thermogravimetric curve measures the weight loss of the MOF sample as the temperature is increased, and it also gives information regarding the temperature of activation (and release of solvent guest molecules) and decomposition of the MOF. Moreover, dynamic light scattering is used to determine the particle size of the synthesized MOF, which has an important effect on the properties of the material. Finally, scanning electron microscopy or transmission electron microscopy are also techniques commonly used for morphology studies.

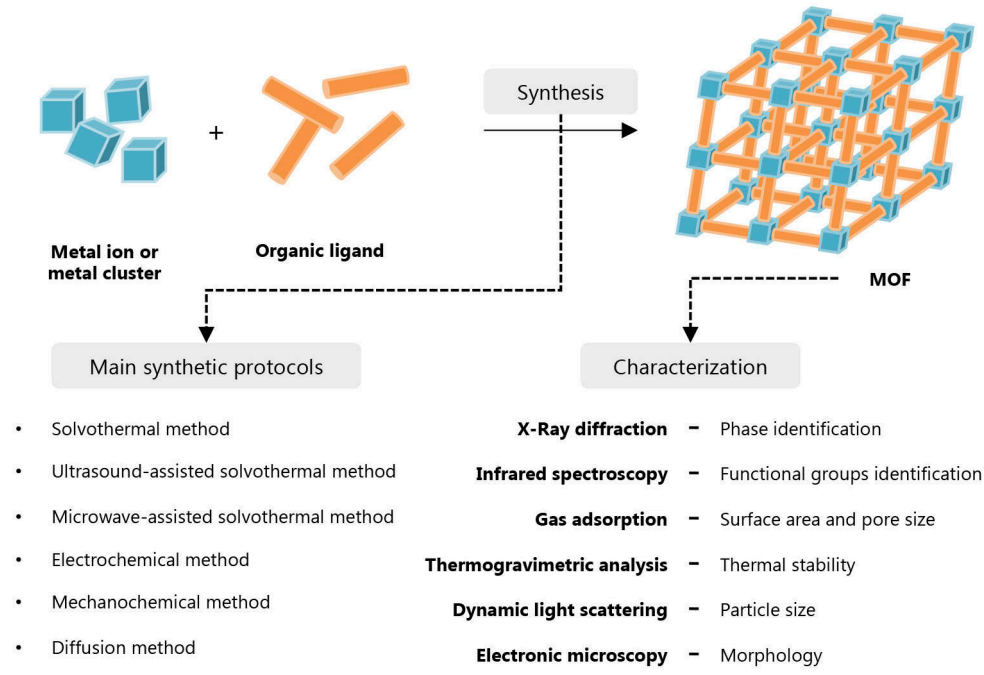

Figure I.21. Scheme of the procedure followed for the preparation of MOFs, including the main synthetic methods and characterization techniques.

3.3.4.2. Toxicity of MOFs

Despite the use of solid sorbents in sorbent-based microextraction techniques as alternative over conventional organic solvents complies with many GAC guidelines, the toxicity of the material should be taken into account to ensure the sustainability of the analytical methods [265]. Indeed, green preparation of MOFs is a hot topic of research nowadays. In this regard, particular attention should be paid to the safety of the precursors [266]. The main concern lies on the nature of the metallic BB. Thus, Fe, Cu, Mg, Ca, and Zn, together with other biologically inert cations, such as Ag, Au, Zr and Ti, are the safest candidates, while Cd is the most toxic. Nevertheless, the toxicity of a MOF is not exclusively linked to the nature of the metal, and indeed moderate to high toxic metals can form part of a MOF with low cytotoxicity [265]. Moreover, it is important to pay attention to the safety of the anions composing the metallic salt precursor. In this sense, perchlorates and nitrates should be avoided and the use of zero-valence metal precursors is highly encouraged [267]. In general, the organic BBs used for the preparation of MOFs, mainly carboxylates, imidazolates, and amines do not present important toxic issues. However, the synthetic routes followed for their preparation should fulfill with sustainable requirements and

avoid harmful reagents, multistep procedures, and the formation of intermediates and by-products [265].

Regarding the synthetic conditions for the preparation of MOFs, the main drawback consists in the nature of the solvent used in the most common solvothermal methods [266]. Polar aprotic solvents, including dimethylformamide, acetonitrile and chloroform, are still the preferred solvents, mainly due to easy solubilization of the precursors. Therefore, efforts are addressed to their substitution by greener solvents, being water and alcoholic solvents the most benign options. Furthermore, the reduction of the time and energy consumption during the synthesis reaction is another simple approach to improve the sustainability of these materials [268]. In this sense, the assistance of the synthetic procedure with microwaves or ultrasounds speeds up the synthesis and shortens times [265]. Promoting solvent-free protocols is the greenest strategy within the field and includes mechanochemical methods and chemical vapor reactions [266].

Despite the extensive information on the harmful effects of the precursors and synthetic conditions, the information regarding the toxicity of the reticular material itself is still scarce [265]. Given the interest of MOFs in biomedicine applications as biosensors and drug carriers, several studies assessing their cytotoxicity have been reported, being, for example, Fe-based MOFs the least toxic amongst those evaluated [269]. Nevertheless, this field is still in an early stage and more adequate *in vitro* and *in vivo* assays are required to confirm the safety of these materials.

3.4.3.3. Preparation of MOF-coated SPME devices

On-fiber SPME

As it can be observed in Figure I.19, most of the MOF-based extraction phases for on-fiber SPME are mixed coatings, in which the MOF is combined with other materials to obtain a stable device. This is particularly important for the classification of the strategies that have been described for the preparation of these sorbents, which strongly depends on both the type of attachment and the type of coating. Thus, they can be classified in: (i) *in situ* growth, (ii) direct immersion of the support in the sorbent powder or in the sorbent dispersion, (iii) physical attachment using adhesive materials, (iv) sol-gel approach, and (v) polymerization reactions [256,270]. Figure I.22 includes a summary of these methods.

The most common approach is the *in situ* growth of the MOF on the surface of the substrate used as core [256,257]. In this method, the support is immersed in a solution containing the reagents required to synthesize the MOF by the solvothermal method or electrodeposition [271]. In the case of electrodeposition, the electrolytic solution contains the MOFs precursors, while the working electrode is also the core of the on-fiber SPME device, and cyclic voltammetry ensures that the MOF coats its surface.

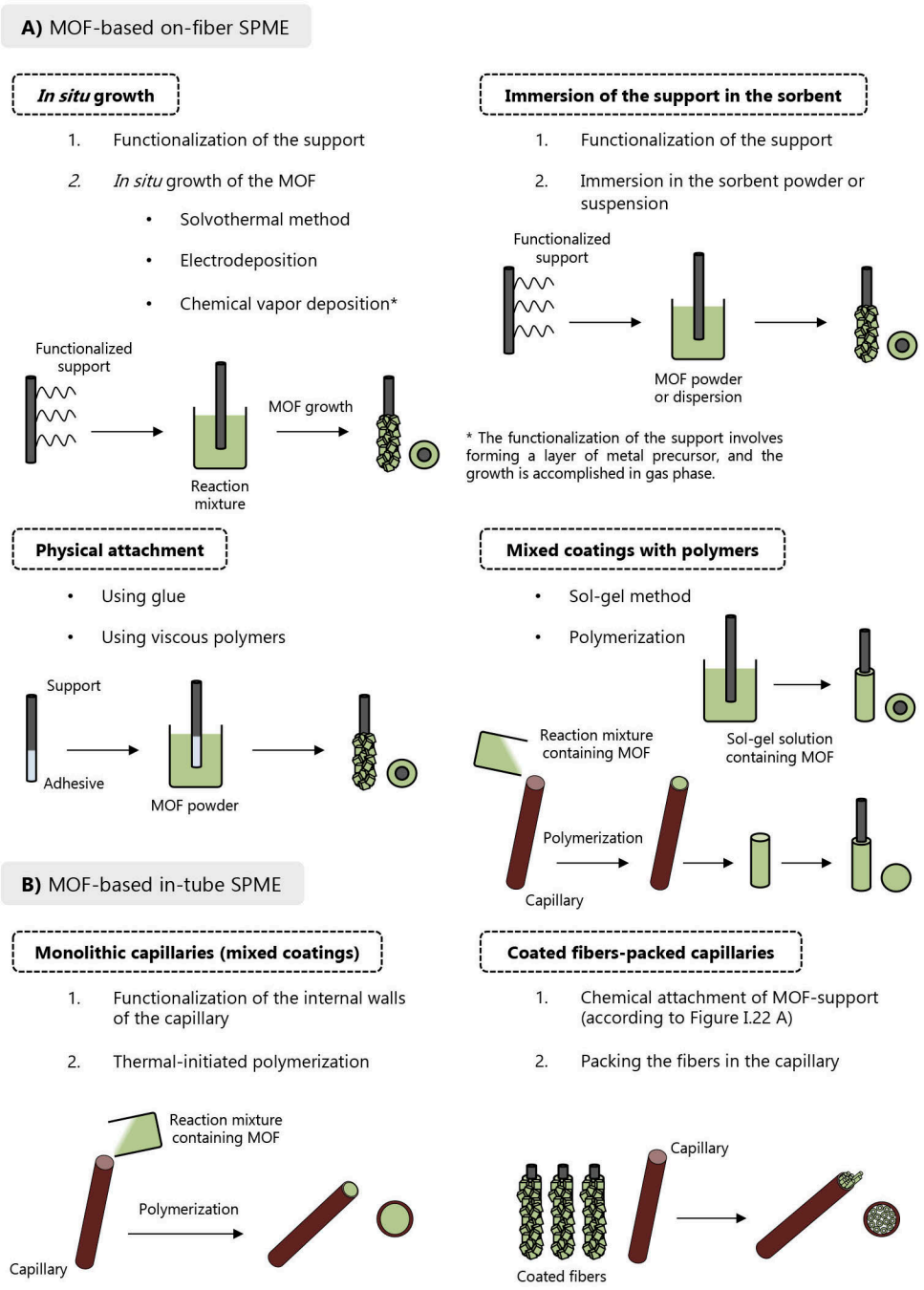

Figure I.22. Main strategies for the preparation of MOF-based **A)** on-fiber and **B)** in-tube SPME devices.

A simpler coating method involves the immersion of the support in a dispersion of the MOF or in the MOF powder [256,272,273], using always the as-synthetized MOF by any of the usual routes. This procedure needs repetition for several times with heating steps between the dipping cycles until reaching the desired thickness.

When using any of these two strategies, the core of the fiber must meet several requirements to avoid detachment of the solid coating from the support. Thus, most of these fibers have been prepared using stainless steel wires, which have been previously treated with an acidic solution to obtain a rough surface, or they have been functionalized with silanization agents to ensure a chemical linkage with the MOF. Fused silica fibers have also been commonly employed in these methods due to their ease of functionalization [256,257].

It is also interesting to mention the chemical vapor deposition strategy that has been recently described for the preparation of controllable ZIF-8(Zn)-based coatings [274,275]. The procedure involves the formation of a layer of the metal precursor on the surface of the support by atomic layer deposition methods, followed by the chemical conversion to form the MOF. This method is included within *in situ* growth approaches because the MOF is directly synthesized onto the surface of the support. In addition, one of these studies reported this method for the preparation of an arrow on-fiber SPME device [275].

With the aim of facilitating the coating procedure and allow the immobilization of any MOF, the physical attachment by using a glue or a viscous polymer layer has been one of the most common strategies [256,257,270]. In general, the support is first dipped in the sealant and then in the MOF powder to obtain the coating, while in some cases, the procedure requires repetitions to control the thickness (intending thicker coatings). Silicone and epoxy sealants are commonly used, but other glues consisting of different polymers have also been proposed, such as polyimide and polyacrylonitrile [276], and polyethersulfone [273]. It is important to point out that this method may lead to reproducibility problems between batches, and it must be also considered that the glue or the polymer used may also take part in the extraction of the resulting device.

When MOFs are incorporated in polymeric mixed coatings, in which the MOF is dispersed in the polymeric matrix, the sol-gel method is commonly used [277,278]. Thus, the MOF particles are dispersed in the sol-gel solution, where the support is then dipped to obtain the coating after letting it dry at room or high temperatures. Mixed extraction phases have also been described for the preparation of monolithic devices based on MOFs [270,279]. In this case, the powder of the previously synthesized MOF is dispersed in the polymeric mixture, which is then used to fill the capillary with the desired diameter for the monolithic fiber. These preparation methods yield extraction phases with a homogenous distribution of the MOF through the coating, thus providing a high inter-batch reproducibility.

With respect to the composition of the MOFs, the majority of on-fiber SPME devices have been prepared using already well-known MOFs. Thus, as shown in Figure I.19, UiO-66(Zr), ZIF(Zn)-type MOFs, MIL-53(Al), MOF-5(Zn), HKUST-1(Cu), and MIL-101(Cr), have been the most commonly

used [257,270]. The selection of these MOFs over others (particularly considering the vast list of possible MOFs) lies in their easy preparation, together with the fact that their characterization and properties have been already established in the literature. Moreover, MOFs containing Zn, Zr, and trivalent metals in their structures, normally present higher water and thermal stability [261,262], which makes them adequate candidates for SPME applications.

Apart from the mixed coatings composed of MOFs particles embedded in a polymeric matrix, MOF have been combined with other materials, mainly carbon-based materials [272,279–281]. The incorporation of GO, CNTs and hydrophobic graphitic carbon nitride improve the hydrophobicity and stability of the coating and enhance the extraction efficiency towards aromatic compounds. In general, these composite coatings have been prepared by immersing the support in a mixture of both solid materials, and in combination with polymers.

In-tube SPME

MOFs have also been explored to develop in-tube SPME devices, but in a lesser extent in comparison with fibers, as it can be observed in Figure I.19. This may be due to the difficulties in the preparation of stable capillaries with solid particles, since they are prone to bleed under the high pressures used during the on-line in-tube SPME procedure.

All of the in-tube SPME devices containing MOFs are monolithic capillaries [257,270], except for one study, in which a bundle of carbon fibers was coated with the MOF, and then packed in the capillary [278]. In this case, ZnO was electrodeposited on the fibers, followed by the *in situ* solvothermal growth of ZIF-8(Zn) using the layer of ZnO as metal precursor, thus leading to a homogeneous coating.

Monolithic in-tube SPME devices have been prepared by dispersing the MOF powder in the reaction mixture containing the monomers and crosslinkers, and then carrying out the thermal-initiated polymerization inside the capillary [283–285]. The internal walls of the capillaries are functionalized with different groups to ensure a chemical linkage with the polymer. MIL-53(Al) (and its amino-derivative) and UiO-66(Zr) have been the MOFs evaluated in this SPME technique, while using butyl methacrylate, ethylene dimethacrylate, DVB and *N*-vinyl carbazole as monomers or crosslinkers.

3.4.3.4. Analytical applications of MOFs in SPME

There has been an increasing interest on using MOF-based SPME extraction phases in different applications in the last 5 years, with a higher number of applications in the on-fiber SPME technique, as it is observed in Figure I.19. Several representative examples for both SPME configurations are included in Table I.7 [272,273,276,279–289].

Table I.7. Representative applications described in the literature on the use of MOFs as extraction phase in on-fiber and in-tube SPME.

MOF	Additive	Type of device	SPME mode	Analytes (number)	Sample (amount, pretreatment)	Analytical technique	LOD ($ng \cdot L^{-1}$)	Ref.
On-fiber SPME								
HKUST-1(Cu)	–	coated Cu rod fiber	HS-SPME	PAHs (8)	lake waters (10 mL)	GC-MS	0.1–9.9	[286]
MIL-88(Fe)	GO	coated SS rod fiber	DI-SPME	PAEs (8)	vegetable oils (10 mL, LLE with acetonitrile)	GC-MS	0.5–2.0*	[281]
MIL-101-NH_2(Cr)	PAN	coated quartz rod fiber	DI-SPME	antibiotics (6)	fish (*in vivo* analysis)	LC-MS/MS	0.2–4.66	[276]
MIL-101(Cr)	protective silicone layer	coated SS rod fiber	HS-SPME	PAHs (5) & BTEX (5)	river water (10 mL)	GC-MS	0.01–2.0	[287]
MOF-5(Zn)	GO	coated SS rod fiber	DI-SPME	fungicides (5)	fruit & vegetables (10mL, SLE with acetonitrile)	GC-ECD	0.05–1.58*	[272]
TMU-4(Zn)	PES	coated SS rod fiber	HS-SPME	pesticides (4)	soil, well & farm water (10 mL, SLE with methanol for soil)	GC-NPD	5–8	[273]

Table I.7 (continued).

MOF	Additive	Type of device	SPME mode	Analytes (number)	Sample (amount, pretreatment)	Analytical technique	LOD ($ng \cdot L^{-1}$)	Ref.
UiO-66(Zr)	–	coated FS rod fiber	DI-SPME	PAHs (10)	river water & soil (20 mL, SLE with hexane)	GC-MS	0.28–0.60	[288]
UiO-66(Zr)	GO	coated SS rod fiber	DI-SPME	NSAIDs (2)	river water (20 mL)	GC-FID	1–30	[280]
ZIF-8(Zn)	GO & MIP	multiple monolith fiber	DI-SPME	hormones (5)	meat, egg & vegetables (4 mL, SLE with water)	LC-MS	3–5	[279]
ZIF-8(Zn)	–	coated SS arrow fiber	HS-SPME	alkylamines (2)	wastewater, fish & mushroom (5 mL, SLE with acidic water)	GC-MS	1000	[289]
In-tube SPME								
MIL-53(Al)	Poly(BMA-EDMA) polymer and IL $[C_6MIm^+][BF_4^-]$	monolithic capillary	flow through (manual, syringe pump)	sulfonamides (7)	pond water (2 mL)	MEEKC-UV-Vis	360000 – 850000	[283]

Table I.7 (continued).

MOF	Additive	Type of device	SPME mode	Analytes (number)	Sample (amount, pretreatment)	Analytical technique	LOD ($ng \cdot L^{-1}$)	Ref.
MIL-53-NH_2(Al)	Poly(Sty-DVB-MAA)	monolithic capillary	flow through (on-line, 2 valves)	estrogens (5)	urine (6 mL)	LC-UV-Vis	2–40	[284]
UiO-66(Zr)	Poly(DVB-NVC)	monolithic capillary	flow through (manual, syringe pump)	fungicides (5)	pond water & soil (6 mL, SLE for soil samples)	LC-MS	1–15	[285]
ZIF-8(Zn)	–	coated carbon fibers-packed capillary	flow through (on-line, 1 valve)	dyes (3)	lake & tap water (20 mL)	LC-UV-Vis	2	[282]

* Limits of detection in $ng \cdot g^{-1}$. For the definition of the abbreviations, refer to the list of abbreviations.

Organic compounds belonging to different families have been the target analytes in these applications, being PAHs, BTEX, pesticides and several EDCs (e.g., pharmaceuticals and PCPs) the most commonly determined [257]. With respect to the type of samples analyzed, as it can be observed in Figure I.19, more than 50 % of the applications are included within environmental analysis. Thus, water from different sources, such as river, lake, pond and wastewater, has been the most studied matrix.

Food and biological samples have also been analyzed with these MOF-based devices, but in a lesser extent in comparison with environmental water samples. In the case of food analysis, it has been particularly successful the determination of pharmaceuticals and drugs in milk samples, and pesticides in vegetables and fruits [272,279]. It is interesting to mention the application of a MOF-based on-fiber SPME coating used for the determination of antibiotics in fish samples [276]. In this study, the biocompatibility of the polyacrylonitrile matrix, in which the MOF is dispersed, is exploited to carry out the *in vivo* SPME procedure. The bioclinical analysis is the field that has found the least number of applications of MOF-based extraction phases, with several studies devoted to the analysis of urine for the quantification of hormones and drugs [284]. In most of these cases, the samples are pretreated by an additional sample preparation step using organic solvents or by a digestion procedure prior to the SPME method.

The on-fiber SPME devices have been mainly used in HS-SPME mode, but also DI-SPME applications have been reported when analyzing water samples, and mainly using mixed coatings. As expected, taking into account the characteristics of the on-fiber SPME technique and the high thermal stability of MOFs, the vast majority of the on-fiber SPME applications were combined with thermal desorption and GC with several detectors to carry out the quantification. Only three studies were combined with LC after the DI-SPME procedure, using a low amount of an organic solvent in the desorption step, or an aqueous solution at a fixed pH value in the case of the multiple fiber device [279].

All the in-tube SPME devices with MOFs have been used in flow-through methods, and most of them using an off-line or manual approach, by coupling the labmade device to a syringe pump thus carrying out both extraction and desorption steps [283,285]. This may be due to the low stabilities of the devices to perform under high pressure conditions. These devices were combined with LC or capillary electrophoresis techniques.

REFERENCES

[1] C. Poole, Z. Mester, M. Miró, S. Pedersen-Bjergaard, J. Pawliszyn, Pure Appl. Chem. 88 (2016) 649–687.

[2] S. Armenta, S. Garrigues, F.A. Esteve-Turrillas, M. de la Guardia, Trac-Trends Anal. Chem. 116 (2019) 248–253.

[3] A. Gałuszka, Z. Migaszewski, J. Namieśnik, Trac-Trends Anal. Chem. 50 (2013) 78–84.

[4] E.V.S. Maciel, A.L. de Toffoli, E.S. Neto, C.E.D. Nazario, F.M. Lanças, Trac-Trends Anal. Chem. 119 (2019) 115633.

[5] C. Poole, Z. Mester, M. Miró, S. Pedersen-Bjergaard, J. Pawliszyn, Pure Appl. Chem. 88 (2016) 517–558.

[6] F.S. Mirnaghi, K. Goryński, A. Rodriguez-Lafuente, E. Boyacı, B. Bojko, J. Pawliszyn, J. Chromatogr. A. 1316 (2013) 37–43.

[7] Y. Yamini, M. Rezazadeh, S. Seidi, Trac-Trends Anal. Chem. 112 (2019) 264–272.

[8] S. Tang, T. Qi, P.D. Ansah, J.C.N. Fouemina, W. Shen, C. Basheer, H.K. Lee, Trac-Trends Anal. Chem. 108 (2018) 306–313.

[9] M.R. Ganjali, M. Rezapour, P. Norouzi, F. Faridbod, in: V. Pino, J.L. Anderson, A. Berthod, A.M. Stalcup, Analytical Separation Science, Wiley-VCH (2015) 1625–1658.

[10] N. Drouin, P. Kubáň, S. Rudaz, S. Pedersen-Bjergaard, J. Schappler, Trac-Trends Anal. Chem. 113 (2019) 357–363.

[11] E. Carasek, J. Merib, Anal. Chim. Acta 880 (2015) 8–25.

[12] S. Cárdenas, R. Lucena, Separations 4 (2017) 6.

[13] M. Rutkowskaa, J. Płotka-Wasylka, M. Sajid, V. Andruch, Microchem. J. 149 (2019) 103989.

[14] M. Rezaee, Y. Assadi, M.-R.M. Hosseini, E. Aghaee, F. Ahmadi, S. Berijani, J. Chromatogr. A 1116 (2006) 1–9.

[15] M.J. Trujillo-Rodríguez, I. Pacheco-Fernández, I. Taima-Mancera, J.H. Ayala, V. Pino, J. Chromatogr. A 1634 (2020) 461670.

[16] E. Boyacı, Á. Rodríguez-Lafuente, K. Gorynski, F. Mirnaghi, É.A. Souza-Silva, D. Hein, J. Pawliszyn, Anal. Chim. Acta. 873 (2015) 14–30.

[17] E.M. Thurman, K. Snavely, Trac-Trends Anal. Chem. 19 (2000) 18–26.

[18] A. Chisvert, S. Cárdenas, R. Lucena, Trac-Trends Anal. Chem. 112 (2019) 226–233.

[19] G. Lasarte-Aragonés, R. Lucena, S. Cárdenas, M. Valcárcel, J. Chromatogr. A. 1218 (2011) 9128–9134.

[20] L. Adlnasab, M. Ezoddin, M. Shabanian, B. Mahjoob, Microchem. J. 146 (2019) 1–11.

[21] S. Seidi, M. Tajik, M. Baharfar, M. Rezazadeh, Trac-Trends Anal. Chem. 118 (2019) 810–827.

[22] M. Sajid, Anal. Chim. Acta. 965 (2017) 36–53.

[23] M.T. García-Valverde, R. Lucena, S. Cárdenas, M. Valcárcel, J. Chromatogr. A. 1464 (2016) 42–49.

[24] A.L. Capriotti, C. Cavaliere, G. La Barbera, C.M. Montone, S. Piovesana, A. Laganà, Chromatographia 82 (2019) 1251–1274.

[25] A. Ríos, M. Zougagh, Trac-Trends Anal. Chem. 84 (2016) 72–83.

[26] D. Wianowska, M. Gil, Trac-Trends Anal. Chem. 112 (2019) 29–51.

[27] J. Pawliszyn, in: J. Pawliszyn, Handbook of Solid Phase Microextraction, Elsevier (2012) 13–59.

[28] M.E. Costa Queiroz, I.D. de Souza, C. Marchioni, Trac-Trends Anal. Chem. 111 (2019) 261–278

[29] F. David, N. Ochiai, P. Sandra, Trac-Trends Anal. Chem. 112 (2019) 102–111.

[30] C.S. Skaggs, A.H. Alluhayb, B.A. Logue, J. Chromatogr. A. 1622 (2020) 461102.

[31] N. Ochiai, K. Sasamoto, F. David, P. Sandra, J. Chromatogr. A. 1455 (2016) 45–56.

[32] J.M.F. Nogueira, Anal. Chim. Acta 757 (2012) 1–10.

[33] J.L. Benedé, A. Chisvert, D.L. Giokas, A. Salvador, J. Chromatogr. A. 1362 (2014) 25–33.

[34] Y.A. Olcer, M. Tascon, A.E. Eroglu, E. Boyacı, Trac-Trends Anal. Chem. 113 (2019) 93–101.

[35] R. Jiang, J. Pawliszyn, Trac-Trends Anal. Chem. 39 (2012) 245–253.

[36] J. Ríos-Gómez, R. Lucena, S. Cárdenas, Microchem. J. 133 (2017) 90–95.

[37] S. Kamaruzaman, P.C. Hauser, M.M. Sanagi, W.A.W. Ibrahim, S. Endud, H.H. See, Anal. Chim. Acta 783 (2013) 23–30.

[38] M.C. Díaz-Liñán, M.T. García-Valverde, R. Lucena, S. Cárdenas, A.I. López-Lorente, Anal. Methods 12 (2020) 3074–3091.

[39] V. Kazantzi, A. Anthemidis, Separations 4 (2017) 20.

[40] H. Piri-Moghadam, M.N. Alam, J. Pawliszyn, Anal. Chim. Acta. 984 (2017) 42–65.

[41] F. Pena-Pereira, A. Kloskowski, J. Namieśnik, Green Chem. 17 (2015) 3687–3705.

[42] C.J. Clarke, W.-C. Tu, O. Levers, A. Bröhl, J.P. Hallett, Chem. Rev. 118 (2018) 747–800.

[43] J.M. Kokosa, Trac-Trends Anal. Chem. 118 (2019) 238–247.

[44] I. Pacheco-Fernández, V. Pino, Curr. Opin. Green Sustain. Chem. 18 (2019) 42–50.

[45] J. Płotka-Wasylka, M. Rutkowska, K. Owczarek, M. Tobiszewski, J. Namieśnik, Trac-Trends Anal Chem 91 (2017) 12–25.

[46] M. Vian, C. Breil, L. Vernes, E. Chaabani, F. Chemat, Curr. Opin. Green Sustain. Chem. 5 (2017) 44–48.

[47] N. Lorenzo-Parodi, W. Kaziur, N. Stojanović, M.A. Joochmann, T.C. Schmidt, Trac-Trends Anal. Chem. 113 (2019) 321–331.

[48] Y. Chen, L. Xia, R. Liang, Z. Lu, L. Li, B. Huo, G. Li, Y. Hu, Trac-Trends Anal. Chem. 120 (2019) 115652.

[49] T. Zhou, G. Che, L. Ding, D. Sun, Y. Li, Trac-Trends Anal. Chem. 121 (2019) 115678.

[50] C. Caballo, M.D. Sicilia, S. Rubio, in: F. Pena-Pereira, M. Tobiszewski, The Application of Green Solvents in Separation Processes, Elsevier (2017) 111–137.

[51] A. Melnyk, J. Namieśnik, L. Wolska, Trac-Trends Anal Chem 71 (2015) 282–292.

[52] ACAreview2020 I. Pacheco-Fernández, R. González-Martín, F.A. e Silva, M.G. Freire, V. Pino, Anal. Chim. Acta (2020) in press (doi: 10.1016/j.aca.2020.08.022).

[53] A. Ballesteros-Gómez, S. Rubio, Anal Chem. 84 (2012) 342–349.

[54] F.-J. Ruiz, S. Rubio, D. Pérez-Bendito, Anal. Chem. 79 (2007) 7473–7484.

[55] A. Ballesteros-Gómez, M.D. Sicilia, S. Rubio, Anal. Chim. Acta 677 (2010) 108–130.

[56] P. Bogdanova, A. Pochivalov, C. Vakh, A. Bulatov, Talanta 216 (2020) 120992.

[57] A. Shishov, A. Pochivalov, L. Nugbienyo, V. Andruch, A. Bulatov, Trac-Trends Anal. Chem. 129 (2020) 115956.

[58] G. Li, K.H. Row, Trac-Trends Anal. Chem. 120 (2019) 115651.

[59] A.K. Dwamena, Separations 6 (2019) 9.

[60] A. Shishov, A. Gorbunov, L. Moskvin, A. Bulatov, J. Mol. Liq. 301 (2020) 112380.

[61] M.A. Fernández, J. Boiteux, M. Espino, F.J.V. Gomez, M.F. Silva, Anal. Chim. Acta 1038 (2018) 1–10.

[62] J.R. Vanderveen, J. Durelle, P.G. Jessop, Green Chem. 16 (2014) 1187–1197.

[63] P.G. Jessop, D.J. Heldebrant, X. Li, C.A. Eckert, C.L. Liotta, Nature 436 (2005) 1102.

[64] P.G. Jessop, L. Phan, A. Carrier, S. Robinson, C.J. Dürr, J.R. Harjani, Green Chem. 12 (2010) 809–814.

[65] H.-K. Shih, T.-Y. Shu, V.K. Ponnusamy, J.-F. Jen, Anal. Chim. Acta 854 (2015) 70–77.

[66] U. Alshana, M. Hassan, M. Al-Nidawi, E. Yilmaz, M. Soylak, Trac-Trends Anal. Chem. 131 (2020) 116025.

[67] Z. Lei, B. Chen, Y.-M. Koo, D.R. MacFarlane, Chem. Rev. 117 (2017) 6633–6635.

[68] T. Welton, Biophys. Rev. 10 (2018) 691–706.

[69] K. Yavir, K. Konieczna, Ł. Marcinkowski, A. Kloskowski, Trac-Trends Anal. Chem. 130 (2020) 115994.

[70] M.J. Trujillo-Rodríguez, H. Nan, M. Varona, M.N. Emaus, I.D. Souza, J.L. Anderson Anal. Chem. 91 (2019) 505–531.

[71] R. Marcinkowska, K. Konieczna, Ł. Marcinkowski, J. Namieśnik, A. Kloslowski, Trac-Trends Anal. Chem. 119 (2019) 115614.

[72] M. Vergara-Barberán, E.J. Carrasco-Correa, M.J. Lerma-García, E.F. Simó-Alfonso, J.M. Herrer-Marínez, Anal. Chim. Acta 1084 (2019) 1–20.

[73] M. Rinaudo, Polym. Int. 57 (2008) 397–430.

[74] I. Pacheco-Fernández, D.W. Allgaier-Díaz, G. Masellone, C. Cagliero, D. Díaz Díaz, V. Pino, Trac-Trends Anal. Chem. 125 (2020) 115839.

[75] N.H. Godage, E. Grionfriddo, Anal. Chim. Acta 1125 (2020) 187–200.

[76] G. Mafra, M.T. García-Valverde, J. Millán-Santiago, E. Carasek, R. Lucena, S. Cárdenas, Separations 7 (2020) 2.

[77] W. Qian, J. Texter, F. Yan, Chem. Soc. Rev. 46 (2017) 1124–1159.

[78] M. Mei, X. Huang, L. Chen, Trac-Trends Anal. Chem. 112 (2019) 123–134.

[79] H. Bagheri, Z. Ayazi, M. Naderi, Anal. Chim. Acta 767 (2013) 1–13.

[80] J. González-Sálamo, C. Ortega-Zamora, R. Carrillo, J. Hernández-Borges, J. Chromatogr. A (2020) in press (doi: 10.1016/j.chroma.2020.461764).

[81] L. Chen, X. Wang, W. Lu, X. Wu, J. Li, Chem. Soc. Rev. 45 (2016) 2137–2211.

[82] E. Turiel, A. Martín-Esteban, Trac-Trends Anal. Chem. 118 (2019) 574–586.

[83] A. Azzouz, S.K. Kailsa, S.S. Lee, A.J. Rascón, E. Ballesteros, M. Zhang, K.-H. Kim, Trac-Trends Anal. Chem. 108 (2018) 347–369.

[84] I. Pacheco-Fernández, A. Gutiérrez-Serpa, A.M. Afonso, V. Pino, in: J. Zhang, Y.-G. Jung, Advanced Ceramic and Metallic Coating and Thin Film Materials for Energy and Environmental Applications, Springer, Cham (2018) 217–243.

[85] D. Xiao, T. Lu, R. Zeng, Y. Bi, Microchim. Acta 183 (2016) 2655–2675.

[86] P. Rocío-Bautisa, V. Pino, in: V. Pino, J.L. Anderson, A. Berthod, A.M. Stalcup, Analytical Separation Science, Wiley-VCH (2015) 1681–1724.

[87] Y. Zhu, S. Murali, W. Cai, X. Li, J.W. Suk, J.R. Potts, R.S. Ruoff, Adv. Mater. 22 (2010) 3906–3924.

[88] L. Zhao, H. Qin, R. Wu, H. Zou, J. Chromatogr. A 1228 (2012) 193–204.

[89] O.M. Yaghi, ACS Cent. Sci. 5 (2019) 1295–1300.

[90] M.J. Kalmutzki, N. Hanikel, O.M. Yaghi, Sci. Adv. 4 (2018) eaat9180.

[91] L. Chen, Q. Wu, J. Gao, H. Li, S. Dong, X. Shi, L. Zhao, TrAC-Trends Anal. Chem. 113 (2019) 182–193.

[92] I. Pacheco-Fernández, P. González-Hernández, J. Pasán, J.H. Ayala, V. Pino, in: M. de la Guardia, F.A. Esteve-Turrillas, Handbook of Smart Materials in Analytical Chemistry, John Wiley & Sons Ltd. (2019) 463–502.

[93] Z. Wang, S. Zhang, Y. Chen, Z. Zhang, S. Ma, Chem. Soc. Rev. 49 (2020) 708–735.

[94] K. Geng, T. He, R. Liu, S. Dalapati, K.T. Tan, Z. Li, S. Tao, Y. Gong, Q. Jiang, D. Jiang, Chem. Rev. 120 (2020) 8814–8933.

[95] H.D. de Faria, L.C. de Carvalho Abrão, M.G. Santos, A.F. Barbosa, E.C. Figueiredo, Anal. Chim. Acta 959 (2017) 43–65.

[96] V. Pichon, A. Combès, N. Delaunay, Trac-Trends Anal. Chem. 113 (2019) 246–255.

[97] F. Du, L. Guo, Q. Qin, X. Zheng, G. Ruan, J. Li, G. Li, Trac-Trends Anal. Chem. 67 (2015) 134–146.

[98] M. Alexovic, Y. Dotsikas, P. Bober, J. Sabo, J. Chromatogr. B 1092 (2018) 402–421.

[99] B. Horstkotte, M. Miró, P. Solich, Anal. Bioanal. Chem. 410 (2018) 6361–6370.

[100] M. Alexovic, B. Horstkotte, P. Solich, J. Sabo, Anal. Chim. Acta 906 (2016) 22–40.

[101] M. Alexovic, B. Horstkotte, P. Solich, J. Sabo, Anal. Chim. Acta 907 (2016) 18–30.

[102] M. Alexovic, B. Horstkotte, I. Šrámková, P. Solich, J. Sabo, Trac-Trends Anal. Chem. 86 (2017) 39–55.

[103] F. Maya, B. Horstkotte, J.M. Estela, V. Cerdà, Anal. Bioanal. Chem. 404 (2012) 909–917.

[104] C. Calderilla, F. Maya, L.O. Leal, V. Cerdà, Trac-Trends Anal. Chem. 108 (2018) 370–380.

[105] D. Vuckovic, E. Cudjoe, D. Hein, J. Pawliszyn, Anal. Chem. 80 (2008) 6870–6880.

[106] E. Cudjoe, D. Vuckovic, D. Hein, J. Pawliszyn, Anal. Chem. 81 (2009) 4226–4232.

[107] J.M. Kokosa, A. Przyjazny, M.A. Jeannot, in: J.M. Kokosa, A. Przyjazny, M.A. Jeannot, Solvent Microextraction: Theory and Practice, John Wiley & Sons, Inc. (2019) 19–36.

[108] J.M. Kokosa, in: C.F. Poole, Handbooks in Separation Science: Liquid-Phase Extraction, Elsevier (2020) 473–497.

[109] J.M. Kokosa, A. Przyjazny, M.A. Jeannot, in: J.M. Kokosa, A. Przyjazny, M.A. Jeannot, Solvent Microextraction: Theory and Practice, John Wiley & Sons, Inc. (2019) 37–65.

[110] M Rutkowska, K. Owczarek, M. de la Guardia, J. Płotka–Wasylka, J. Namieśnik, Trac-Trends Anal. Chem. 97 (2017) 104–119.

[111] M. Saraji, M.K. Boroujeni, Anal. Bioanal. Chem. 406 (2014) 2027–2066.

[112] M.A. Farajzadeh, M.R.A. Mogaddam, Anal. Chim. Acta 728 (2012) 31–38.

[113] M.A. Farajzadeh, A. Mohebbi, A. Pazhohan, M. Nemati, M.R.A. Mogaddam, Trac-Trends Anal. Chem. 112 (2020) 115734.

[114] G. Lasarte-Aragonés, R. Lucena, S. Cárdenas, M. Valcárcel, Anal. Chim. Acta 897 (2014) 61–66.

[115] W. Jiang, X. Chen, F. Liu, X. You, J. Xue, J. Sep. Sci. 37 (2014) 3157–3163.

[116] C. Bendicho, I. Costas-Mora, V. Romero, I. Lavilla, Trac-Trends Anal. Chem. 68 (2015) 78–87.

[117] M.J. Trujillo-Rodríguez, P. Rocío-Bautista, V. Pino, A.M. Afonso, Trac-Trends Anal. Chem. 51 (2013) 87–106.

[118] I. Rykowska, J. Ziemblińska, I. Nowak, J. Mol. Liq. 259 (2018) 319–339.

[119] I. Pacheco-Fernández, V. Pino, in: C.F. Poole, Handbooks in Separation Science: Liquid-Phase Extraction, Elsevier (2020) 499–537.

[120] S.K. Singh, A.W. Savoy, J. Mol. Liq. 297 (2020) 112038.

[121] C. Maton, N. de Vos, C.V. Stevens, Chem. Soc. Rev. 42 (2013) 5963–5977.

[122] I. Pacheco-Fernández, P. González-Hernández, V. Pino, J.H. Ayala, A.M. Afonso, in: A. Eftekhari, Ionic Liquid Devices, The Royal Society of Chemistry (2018) 53–78.

[123] V. Pino, M. Germán-Hernández, A. Martín-Pérez and J.L. Anderson, Sep. Sci. Technol. 47 (2012) 264.

[124] P. Brown, C.P. Butts, J. Eastoe, D. Fermin, I. Grillo, H.C. Lee, D. Parker, D. Plana, R.M. Richardson, Langmuir, 28 (2012) 2502–2509.

[125] E. Santos, J. Albo, A. Irabien, RSC Adv. 4 (2014) 40008–40018.

[126] S.A. Pierson, O. Nacham, K.D. Clark, H. Nan, Y. Mudryk, J.L. Anderson, New J. Chem. 41 (2017) 5498–5505.

[127] D. Chand, M.Q. Farooq, A.K. Pathak, J. Li, E.A. Smith, J.L. Anderson, New J. Chem. 43 (2019) 20–23.

[128] M. Javaherian, S.J. Saghanezhad, Mini Rev. Org. Chem. 17 (2020) 450–464.

[129] O. Nacham, A. Martín-Pérez, D.J. Steyer, M.J. Trujillo-Rodríguez, J.L. Anderson, V. Pino, A.M. Afonso, Colloid. Surf. A Physicochem. Eng. Asp. 469 (2015) 224–234.

[130] H. Ohno, M. Yoshizawa-Fujita, Y. Kohno, Phys. Chem. Chem. Phys. 20 (2018) 10978–10991.

[131] B. Clare, A. Sirwardana, D.R. MacFarlane, in: B. Kirchneer, Ionic Liquids. Topics in Current Chemistry 290, Springer (2009) 1–40.

[132] Y. gaoo, S.W. Arritt, B. Twamley, J.M. Shreeve, Inorg. Chem. 44 (2005) 1704–1712.

[133] X.F. Liu, L.L. Dong, Y. Fang, J. Surfact. Deterg. 14 (2011) 497–504.

[134] Q.Q. Baltazar, J. Chandawalla, K. Sawyerand, J.L. Anderson, Colloid. Surf. A Physicochem. Eng. Asp. 302 (2007) 150–156.

[135] J.L. Anderson, R. Ding, A. Ellern, D.W. Armstrong, J. Am. Chem. Soc. 127 (2005) 593–604.

[136] J. Feng, H.M. Loussala, S. Han, X. Ji, C. Li, M. Sun, Trac-Trends Anal. Chem. 125 (2020) 115833.

[137] M. Sivapragasam, M. Moniruzzaman, M. Goto, Biotechnol. J. 15 (2020) 1900073.

[138] P. Kumari, V.V.S. Pillai, A. Benedetto, Biophys. Rev. 12 (2020) 1187–1215.

[139] T.B.V. Dinis, H. Passos, D.L.D. Lima, A.C.A. Sousa, J.A.P. Coutinho, V.I. Esteves, M.G. Freire, J. Chromatogr. A 1559 (2017) 69–77.

[140] T.B.V. Dinis, H. Passos, D.L.D. Lima, V.I. Esteves, J.A.P. Coutinho, M.G. Freire, Green Chem. 17 (2015) 2570–2579.

[141] H. Passos, A.C.S. Sousa, M.R. Pastorinho, A.J.A. Nogueira, L.P.N. Rebelo, J.A.P. Coutinho, M.G. Freire, Anal. Methods 4 (2012) 2664–2667.

[142] T. Trtic-Petrovic, A. Dimitrijevic, N. Zdolsek, J. Dordevic, A. Tot, M. Vranes, S. Gadzuric, Anal. Bioanal. Chem. 410 (2018) 155–166.

[143] J. Flieger, M. Flieger, Int. J. Mol. Sci. 21 (2020) 6267.

[144] A. Gutiérrez-Serpa, P.I. Napolitano-Tabares, J. Šulc, I. Pacheco-Fernández, V. Pino, Separations 7 (2020) 37.

[145] M. Sajid, Trac-Trends Anal. Chem. 113 (2019) 210–223.

[146] A. Chisvert, J.L. Benedé, J.L. Anderson, S.A. Pierson, A. Salvador, Anal. Chim. Acta 983 (2017) 130–140.

[147] M. Baghdadi, F. Shemirani, Anal. Chim. Acta 634 (2009) 186–191.

[148] C. Yao, J.L. Anderson, Anal. Bioanal. Chem. 395 (2009) 1491–1502.

[149] M.J. Trujillo-Rodríguez, J.L. Anderson, J. Chromatogr. A 1588 (2019) 8–16.

[150] M.J. Trujillo-Rodríguez, J.L. Anderson, Talanta 196 (2019) 420–428.

[151] M.G. Freire, A.F.M. Cláudio, J.M.M. Araújo, J.A.P. Coutinho, I.M. Marrucho, J.N. Canongia Lopes, L.P.N. Rebelo, Chem. Soc. Rev. 41 (2012) 4966–4995.

[152] M.G. Freire, in: M.G. Freire, Ionic-Liquid-Based Aqueous Biphasic Systems: Fundamentals and Applications, Springer (2016) 1–25.

[153] T. Yao, S. Yao, J. Chromatogr. A 1481 (2017) 12–22.

[154] H. Filik, A.A. Avan, Curr. Anal. Chem. 13 (2017) 456–463.

[155] R. Wang, P. Su, Y. Yang, Anal Methods5 (2013) 1033–1039.

[156] S.A. Arain, T.G. Kazl, H.I. Afridi, A.R. Abbasi, N. Ullah, A.H. Panhwar, S. Siraj, Anal. Methods 7 (2015) 9211–9217.

[157] X. Wang, G. Xu, P. Chen, Y. Sun, X. Yao, Y. Lv, W. Guo, G. Wang, RSC Adv. 8 (2018) 16858–16865.

[158] E. Fernández, L. Vidal, A. Costa-García, A. Canals, Anal. Chim. Acta 915 (2016) 49–55.

[159] J.I. Cacho, N. Campillo, P. Viñas, M. Hernández-Córdoba, Talanta 146 (2016) 568–574.

[160] S. Gao, J. You, X. Zheng, Y. Wang, R. Ren, R. Zhang, Y. Bai, H. Zhang . Talanta 83 (2010) 1371–1377.

[161] M.M. Parrilla Vázquez, P. Parrilla Vázquez, M. Martínez Galera, M.D. Gil García, A. Uclés, J. Chromatogr. A 129 (2013) 19–26.

[162] X. Jiang, H. Zhang, X. Chen, Microchim. Acta175 (2011) 341–346.

[163] R.-S. Zhao, X. Wang, J. Sun, C. Hu, X.-K. Wang, Microchim. Acta 174 (2011) 145–151.

[164] H. Yu, J. Merib, J.L. Anderson, J. Chromatogr. A 1463 (2016) 11–19.

[165] E.F. Florentini, L.B. Escudero, R.G. Wuilloud, Anal. Bioanal. Chem. 410 (2018) 4715–4723.

[166] M.N. Emaus, J.L. Anderson, Anal. Bioanal. Chem. 412 (2020) 8039–8049.

[167] J. López-Darias, V. Pino, J.H. Ayala, A.M. Afonso, Microchim. Acta 174 (2011) 213–222.

[168] S.A. Pierson, M.J. Trujillo-Rodríguez, J.L. Anderson, J. Sep. Sci. 41 (2018) 3081–3088.

[169] M. Kaynaker, M. Antep, M. Merdivan, J. Anal. Chem. 73 (2018) 23–29.

[170] L. Vidal, S.G. Silva, A. Canals, J.A. Nóbrega, Talanta 148 (2016) 602–608.

[171] M.J. Trujillo-Rodríguez, J.L. Anderson, J. Chromatogr. A 1588 (2019) 8–16.

[172] A.N. Bowers, M.J, Trujillo-Rodríguez, M.Q. Farooq, J.L. Anderson, Anal. Bioanal. Chem. 411 (2019) 7375–7385.

[173] M.G. Bogdanov, I. Svinyarov, J. Chromatogr. A 1559 (2017) 62–68.

[174] M.L. Dietz, C.A. Hawkins, in: C.F. Poole, Handbooks in Separation Science: Liquid-Phase Extraction, Elsevier (2020) 539–564.

[175] J. Pawliszyn, in: J. Pawliszyn, Handbook of Solid Phase Microextraction, Elsevier (2012) 1–12.

[176] R. Eisert, J. Pawliszyn, Anal. Chem. 69 (1997) 3140–3147.

[177] É.A. Souza-Silva, E, Gionfriddo, J. Pawliszyn, Trac-Trends Anal. Chem. 71 (2015) 224–235.

[178] É.A. Souza-Silva, E, Gionfriddo, J. Pawliszyn, Trac-Trends Anal. Chem. 71 (2015) 236–248.

[179] É.A. Souza-Silva, N. Reyes-Garcés, G.A. Gómez-Ríos, E. Boyacı, B. Bojko, J, Pawliszyn, Trac-Trends Anal. Chem. 71 (2015) 249–264.

[180] United States Environmental Protection Agency (USEPA), Method 8272 (2007).

[181] American Society for Testing and Matetrials, D 6438 (2005).

[182] K.M. Billiard, A.R. Dershem, E. Gionfriddo, Molecules 25 (2020) 5297.

[183] N. Reyes-Garcés, E. Gionfriddo, G.A. Gómez-Ríos, M.N. Alam, E. Boyacı, B. Bojko, V. Singh, J. Grandy, J. Pawliszyn, Anal. Chem. 90 (2018) 302–360.

[184] H. Piri-Moghadam, F. Ahmadi, G.A. Gómez-Ríos, E. Boyacı, N. Reyes-Garcés, A. Aghakhani, B. Bojko, J. Pawliszyn, Angew. Chem.-Int. Edit. 55 (2016) 7510–7514.

[185] J.S. Herrington, G.A. Gómez-Ríos, C. Myers, G. Stidsen, D.S. Bell, Separations. 7 (2020) 12.

[186] E. Turiel, J.L. Tadeo, A. Martin-Esteban, Anal. Chem. 79 (2007) 3099–3104.

[187] D. Djozan, T. Baheri, J. Chromatogr. A. 1166 (2007) 16–23.

[188] I. Ciucanu, Anal. Chem. 74 (2002) 5501–5506.

[189] I. Bruheim, H. Lord, J. Pawliszyn, Anal. Chem. 75 (2003) 3946–3951.

[190] A. Gutiérrez-Serpa, D. Schorn-García, F. Jiménez-Moreno, A.I. Jiménez-Abizanda, V. Pino, Microchim. Acta. 186 (2019) 311.

[191] X.R. Xia, R.B. Leidy, Anal. Chem. 73 (2001) 2041–2047.

[192] M. Mei, X. Huang, D. Yuan, J. Chromatogr. A. 1345 (2014) 29–36.

[193] C. Cháfer-Pericás, R. Herráez-Hernández, P. Campíns-Falcó, J. Chromatogr. A. 1125 (2006) 159–171.

[194] M.E. Costa Queiroz, I. Donizeti de Souza, C. Marchioni, Trac-Trends Anal. Chem. 111 (2019) 261–278.

[195] P. Serra-Mora, P. García-Narbona, J. Verdú-Andrés, R. Herráez-Hernández, P. Campíns-Falcó, Separations 6 (2019) 12.

[196] H. Piri-Moghadam, S. Lendor, J. Pawliszyn, Anal. Chem. 88 (2016) 12188–12195.

[197] Z. Zhang, J. Pawliszyn, Anal. Chem. 67 (1995) 34–43

[198] A.R. Ghiasvand, S. Hosseinzadeh, J. Pawliszyn, J. Chromatogr. A. 1124 (2006) 35–42.

[199] E. Psillakis, Anal. Chim. Acta. 986 (2017) 12–24.

[200] S. Xu, Q. Shuai, J. Pawliszyn, Anal. Chem. 88 (2016) 8936–8941.

[201] D.P. Elpa, S.P. Wu, P.L. Urban, Anal. Chem. 92 (2020) 2756–2763.

[202] M.T. Tena, J.D. Carrillo, Trac-Trends Anal. Chem. 26 (2007) 206–214.

[203] C. Basheer, H.K. Lee, J. Chromatogr. A. 1047 (2004) 189–194.

[204] Z. Zhang, J. Poerschmann, J. Pawliszyn, Anal. Commun. 33 (1996) 219–221.

[205] N.H. Godage, E. Gionfriddo, Trac-Trends Anal. Chem. 111 (2019) 220–228.

[206] W. Filipiak, B. Bojko, Trac-Trends Anal. Chem. 115 (2019) 203–213.

[207] Y. Moliner-Martinez, R. Herráez-Hernández, J. Verdú-Andrés, C. Molins-Legua, P. Campíns-Falcó, Trac-Trends Anal. Chem. 71 (2015) 205–213.

[208] I.D. Souza, L.P. Melo, I.C.S.F. Jardim, J.C.S. Monteiro, A.M.S. Nakano, M.E.C. Queiroz, Anal. Chim. Acta. 932 (2016) 49–59.

[209] M. Zarejousheghani, M. Möder, H. Borsdorf, Anal. Chim. Acta. 798 (2013) 48–55.

[210] Y. Yang, A. Rodriguez-Lafuente, J. Pawliszyn, J. Sep. Sci. 37 (2014) 1617–1621.

[211] S.H. Ahmadi, A. Manbohi, K.T. Heydar, Anal. Chim. Acta. 853 (2015) 335–341.

[212] Y. Moliner-Martínez, H. Prima-Garcia, A. Ribera, E. Coronado, P. Campíns-Falcó, Anal. Chem. 84 (2012) 7233–7240.

[213] M. Mei, X. Huang, X. Yang, Q. Luo, Anal. Chim. Acta. 937 (2016) 69–79.

[214] M. Lashgari, Y. Yamini, Talanta. 191 (2019) 283–306.

[215] Merck Group SPME Fiber Assemblies. https://www.sigmaaldrich.com/analytical-chromatography/analytical-products.html?TablePage=9645337 (Accessed: 26th November 2020).

[216] Restek PAL SPME Fibers. Product details. https://www.restek.com/catalog/view/47352 (Accessed: 26th November 2020).

[217] R.E. Shirey, in: J. Pawliszyn, Handbook of Solid Phase Microextraction, Elsevier (2012) 99–133.

[218] Merck Group SPME Overcoaetd Fiber, https://www.sigmaaldrich.com/technical-documents/articles/analytical/fouling-resistant-spme-overcoated-fiber.html (Accessed: 26th November 2020).

[219] PAL SYSTEM: PAL Smart SPME Arrows. https://www.palsystem.com/index.php?id=822 (Accessed: 26th November 2020).

[220] F. Zhao, Y. Meng, J. L. Anderson, J. Chromatogr. A 1208 (2008) 1–9.

[221] D. Mecerreyes, Prog. Polym. Sci. 36 (2011) 1629–1648.

[222] M. Yoshizawa, M. Hirao, K. Ito-Akita, H. Ohno, J. Mat. Chem. 11 (2001) 1057–1062.

[223] H. Qiu, A.K. Mallik, T. Sawada, M. Takafuji, H. Ihara, Chem. Commun. 48 (2012) 1299–1302.

[224] R. Marcilla, J. Alberto Blazquez, J. Rodriguez, J. A. Pomposo, D. Mecerreyes, J. Polym. Sci., Part A: Polym. Chem. 42 (2004) 208–212.

[225] M. Döbbelin, I. Azcune, M. L. Bedu, A. Ruiz de Luzuriaga, A. Genua, V. Jovanovski, G. N. Cabañero, I. Odriozola, Chem. Mater. 24 (2012) 1583–1590.

[226] M. Wasielewska, B. Zygmunt, J.L. Anderson, Chromatographia 77 (2014) 151–158.

[227] Y. Meng, V. Pino, J.L. Anderson, Anal. Chim. Acta 687 (2011) 141–149.

[228] J. López-Darias, Y. Meng, J.L. Anderson, V. Pino, A.M. Afonso, J. Chromatogr. A 1217 (2010) 7189–7197.

[229] Y. Zhang, Y. Duan, Anal. Bioanal. Chem. 411 (2019) 2209–2221.

[230] J. Feng, M. Sun, J. Li, X. Liu, S. Jiang, J. Chromatogr. A 1227 (2012) 54–59.

[231] L. Pang, J. Liu, J. Chromatogr. A 1230 (2012) 8–14.

[232] J. Feng, M. Sun, Y. Bu, C. Luo, J. Chromatogr. A 1393 (2015) 8–17.

[233] T.D. Ho, H. Yu, W.T.S. Cole, J.L. Anderson, Anal. Chem. 84 (2012) 9520–9528.

[234] M.J. Trujillo-Rodríguez, H. Yu, W.T.S. Cole, T.D. Ho, V. Pino, J.L. Anderson, A.M. Afonso, Talanta 121 (2014) 153–162.

[235] C. Cagliero, T.D. Ho, C. Zhang, C. Bicchi, J.L. Anderson, J. Chromatogr. A 1449 (2016) 2–7.

[236] M.J. Trujillo-Rodríguez, H. Nan, J.L. Anderson, J. Chromatogr. A 1540 (2018) 11–20.

[237] J. Crucello, L.F.O. Miron, V.H.C. Ferreira, H. Nan, M.O.M. Marques, M.C. Zanus, J.L. Anderson, R.J. Poppi, L.W. Hantao, Anal. Bioanal. Chem. 410 (2018) 4749–4762.

[238] J.A. Young, C. Zhang, A.M. Devasurendra, L.M. Viranga Tillekeratne, J.L. Anderson, J.R. Kirchhoff, Anal. Chim. Acta 910 (2016) 45–52.

[239] A.M. Devasurendra, C. Zhang, J.A. Young, L.M. Viranga Tillekeratne, J.L. Anderson, J.R. Kirchhoff, ACS Appl. Mater. Interfaces 9 (2017) 24955–24963.

[240] K. Liao, M. Mei, H. Li, X. Huang, C. Wu, J. Sep. Sci. 39 (2016) 566–575.

[241] L. Chen, X. Huang, Analyst 142 (2017) 4039–4047.

[242] M.J. Trujillo-Rodríguez, J.L. Anderson, Anal. Chim. Acta 1047 (2019) 52–61.

[243] E. Gionfriddo, E.A. Souza-Silva, T.D. Ho, J.L. Anderson, J. Pawslizyn, Talanta 188 (2018) 522–530.

[244] J. An, J.L. Anderson, Talantta 182 (2018) 74–82.

[245] D.J.S. Patinha, L.C. Tomé, M. Isik, D. Mecerreyes, A.J.D. Silvestrte, I.M. Marrucho, Materials 10 (2017) 1094.

[246] M. Sun, J. Feng, Y. Bu, C. Luo, J. Chromatogr. A 1458 (2026) 1–8.

[247] J. Feng, X. Wang, Y. Tian, C. Luo, M. Sun, J. Sep. Sci. 40 (2017) 4773–4779.

[248] J. Feng, X. Wang, Y. Tian, C. Luo, M. Sun, J. Sep. Sci. 41 (2018) 3267–3274.

[249] M. Mei, X. Huang, J, Chromatogr. A 1525 (2017) 1–9.

[250] I.D. Souza, L.W. Hantao, M.E.C. Queiroz, Anal. Chim. Acta 1045 (2019) 106–116.

[251] J. Li, F. Wang, J.-F. Wu, G. Zhao, Microchim. Acta 184 (2017) 2628.

[252] O. Nacham, K.D. Clark, J.L. Anderson, Anal. Chem. 88 (2016) 7813–7820.

[253] K. Liao, M. Mei, H. Li, X. Huang, C. Wu, J. Sep. Sci. 39 (2016) 566–575.

[254] O. Nacham, K.D. Clark, M. Varona, J.L. Anderson, Anal. Chem. 89 (2017) 10661–10666.

[255] X.Y. Cui, Z.Y. Gu, D.Q. Jiang, Y. Li, H.F. Wang, X.P. Yan, Anal. Chem. 81 (2009) 9771–9777.

[256] P. Rocío-Bautista, I. Pacheco-Fernández, J. Pasán, V. Pino, Anal. Chim. Acta 939 (2016) 26–41.

[257] A. Gutiérrez-Serpa, I. Pacheco-Fernández, J. Pasán, V. Pino, Separations 6 (2019) 47.

[258] Cambridge Crystallographic Data Center (CCDC), FIZ Karlsruhe, https://www.ccdc.cam.ac.uk/structures/ (Accessed: 26th November 2020).

[259] H. Furukawa, K.E. Cordova, M. O'Keeffe, O.M. Yaghi, Science 341 (2013) 1230444

[260] C. Pettinari, F. Marchetti, N. Mosca, G. Tosia, A. Drozdovc, Polym. Int., 66 (2017) 731–744.

[261] A.J. Howarth, Y. Liu, P. Li, Z. Li, T.C. Wang, J.T. Hupp, O.K. Farha Nat. Rev. Mater. 1 (2016) 15018.

[262] N.C. Burtch, H. Jasuja, K.S. Walton, Chem. Rev. 114 (2014) 10575–10612.

[263] A. Alshammari, Z. Jiang, K.E. Cordova, in: W. Cao, Semiconductor Photocatalysis: Materials, Mechanisms and Applications, InTech Open (2016) 301–341.

[264] M. Safaei, M.M. Foroughi, N. Ebrahimpoor, S. Jahani, A. Omidi, M. Khatami, Trac-Trends Anal. Chem. 118 (2019) 401–425.

[265] P. Rocío-Bautista, I. Taima-Mancera, J. Pasán, V. Pino, Separations 6(3) (2019) 33.

[266] S.B. Peh, Y. Wang, D. Zhao, ACS Sustain. Chem. Eng. 7 (2019) 3647–3670.

[267] J. Kim, S. Lee, J. Kim, D. Lee, Adv. Funct. Mater. 29 (2019) 1808466.

[268] P. Rocío-Bautista, V. Pino, J.H. Ayala, C. Ruiz-Pérez, O. Vallcorba, A.M. Afonso, J. Pasán, RSC Adv. 8 (2018) 31304–31310.

[269] A. Pandey, N. Dhas, P. Deshmukh, C. Caro, P. Patil, M. Luisa García-Martín, B. Padya, A. Nikam, T. Mehta, S. Mutalik, Coord. Chem. Rev. 409 (2020) 213212.

[270] E.J. Carrasco-Correa, I. Pacheco-Fernández, J.M. Herrero-Martínez, V. Pino, in: R. Lucena, S. Cárdenas, Analytical Sample Preparation with Nano- and other High-Performance Materials, Elsevier (2021) in press.

[271] H. Lan, D. Pan, Y. Sun, Y. Guo, Z. Wu, Anal. Chim. Acta 937 (2016) 53–60.

[272] S. Zhang, Q. Yang, W. Wang, C. Wang, Z. Wang, J. Agric. Food Chem. 64 (2016) 2792–2801.

[273] H. Bagheri, H. Amanzadeh, Y. Yamini, M.Y. Massomi, A. Morsali, J. Salarr-Amoli, J. Hassan, Microchim. Acta 185 (2018) 62.

[274] P. Rocío-Bautista, A. Gutiérrez-Serpa, A.J. Cruz, R. Ameloot, J.H. Ayala, A.M. Afonso, J. Pasán, S. Rodríguez-Hermida, V. Pino, Talanta. 215 (2020) 120910.

[275] H. Lan, L.D. Salmi, T. Rönkkö, J. Parshintsev, M. Jussila, K. Hartonen, M. Kemell, M.L. Riekkola, Anal. Chim. Acta. 1024 (2018) 93–100.

[276] S. Mondal, J. Xu, G. Chen, S. Huang, C. Huang, L. Yin, G. Ouyang, Anal. Chim. Acta. 1047 (2019) 62–70

[277] X. Zang, X. Zhang, Q. Chang, S. Li, C. Wang, Z. Wang, J. Sep. Sci. 39 (2016) 2770–2776.

[278] J. Kong, F. Zhu, W. Huang, H. He, J. Hu, C. Sun, Q. Xian, S. Yang, J. Chromatogr. A 1603 (2019) 92–101.

[279] R. Mirzajani, F. Kardani, Z Ramezani, Microchim. Acta 186 (2019) 129.

[280] H. Liu, H. Fan, S. Dang, M. Li, G. A, H. Yu, Chromatographia 83 (2020) 1065–1073.

[281] S. Zhang, Q. Yang, Z. Li, W. Wang, X. Zang, C. Wang, Z. Wang, Food Chem. 263 (2018) 258–264.

[282] X. Ling, Z. Chen, Talanta 192 (2019) 142–146.

[283] Y.-H. Shih, K.-Y. Wang, B. Singco, C.-H. Lin, H.-Y. Huang, Langmuir 32 (2016) 11466–11473.

[284] X. Luo, G. Li, Y. Hu, Talanta. 165 (2017) 377–383.

[285] W. Yao, Z. Fan, S. Zhang, J. Sep. Sci. 42 (2019) 2679–2686.

[286] S. Sun, L. Huang, H. Xiao, Q. Shuai, S. Hu, Talanta. 202 (2019) 145–151.

[287] L. Xie, S. Liu, Z. Han, R. Jiang, H. Liu, F. Zhu, F. Zeng, C. Su, G. Ouyang, Anal. Chim. Acta. 853 (2015) 303–310.

[288] J. Gao, C. Huang, Y. Lin, P. Tong, L. Zhang, J. Chromatogr. A 1436 (2016) 1–8.

[289] H. Lan, T. Rönkkö, J. Parshintsev, K. Hartonen, N. Gan, M. Sakeye, J. Sarfraz, M.L. Riekkola, J. Chromatogr. A 1486 (2017) 76–85.

CHAPTER II
Objectives

Nowadays, sample preparation is still the bottleneck of any analytical procedure. This stage of the analytical method is carried out to ensure extraction and separation of the target compounds from the sample matrix while ensuring elimination of (most) interferences. When dealing with high complex samples (the most frequent situation), sample preparation faces several issues that have a significant impact on the sensitivity and selectivity of the resulting analytical method. Moreover, the recent incorporation of the Green Chemistry principles in the analytical process also demands the development of sustainable sample preparation methods with low consumption of toxic reagents and energy, and with low generation of wastes.

The development of microextraction techniques and the incorporation of new materials as extraction phases can be cited among the most successful strategies described to address these challenges. The combination of these two approaches may lead to the development of analytical methods with improved characteristics: (i) in terms of sensitivity, due to the preconcentration ability of microextraction techniques; and (ii) in terms of selectivity, by taking advantage of the advances within Material Science research. Moreover, both strategies contribute to improving the greenness of the resulting method given the low amounts of extraction phase required in microextraction, and the replacement of those toxic organic solvents traditionally used in these applications.

A wide variety of solvents and solid sorbents have been designed, synthesized, and used in microextraction techniques. Among all of them, ILs and MOFs present a series of outstanding properties that make them adequate candidates to overcome the drawbacks of conventional extraction phases. Thus, both materials exhibit impressive tunability, while ILs characterize by excellent solvation properties, and MOFs present permanent porosity and high surface areas.

Given these considerations, the main goal of this Doctoral Thesis is the incorporation of new extraction phases based on ILs and MOFs in microextraction techniques to develop analytical methods with improved performance in terms of efficiency, selectivity and sustainability.

Among the existing microextraction techniques, DLLME and SPME have been selected due to their simplicity, high enrichment capacity, and environmentally friendly features under specific conditions in comparison with other strategies. Thus, given their liquid nature, ILs have been explored in DLLME applications, while PILs (as IL derivatives) and MOFs have been evaluated in SPME methods.

To achieve this main goal, the following specific objectives have been established:

- **Synthesis and characterization of ILs and derivatives, and MOFs-based materials, and their incorporation in extraction devices**

Considering the recent concern on the toxicity of ILs, it is intended the synthesis and use of ILs with safer toxicological profiles. Thus, ILs containing guanidinium cations with different substituents and chloride anions will be synthesized. Their main characteristics regarding

cytotoxicity and surface-active properties will be determined with the aim of demonstrating their improved attributes in comparison with the ILs most commonly used in microextraction techniques.

Considering the versatility of PILs, it is intended the utilization of IL monomers containing specific functional groups to exploit their tunability for the development of more selective extraction phases. Thus, PILs with different structural characteristics will be synthesized on different surfaces to fabricate SPME devices.

Moreover, the preparation of a stable neat MOF-based coating onto the surface of a wire for the preparation of an on-fiber SPME device is also sought.

- **Selection of the target application, including analytes and type of samples**

Different challenging applications will be selected with the aim of evaluating the feasibility of the prepared extraction phases / microextraction devices to perform in the analysis of complex samples. Thus, applications within the environmental, food, and bioclicinal fields will be studied, which include the determination or organic compounds, metal ions, and biomolecules. The detection and quantification of the target analytes will be carried out using chromatographic techniques coupled with different detectors, except for the metal species, which will require the use of atomic absorption spectroscopy.

- **Proper optimization of the experimental parameters affecting the performance of the materials in the microextraction procedure**

Once the target analytes and samples are selected, the instrumental conditions for the analytical determination will be optimized, and the different extraction phases based on ILs and MOFs will be evaluated in DLLME or SPME techniques. The main variables influencing the microextraction procedures will be studied with the aim of obtaining the maximum response and best precision, while ensuring the shortest analysis time. Moreover, the type of sample will be an important factor considered during the optimization to avoid the incorporation of additional pretreatment steps in the analytical procedure. In the case of DLLME, experimental designs will be used to facilitate and upgrade the optimization step.

- **Validation of the analytical methods**

The optimized methods will be validated through proper quality analytical parameters, and by conducting precision and accuracy studies that will also allow the assessment of the enrichment capacity and extraction efficiency of the method. When possible, synthetic matrices of the target samples will be used to evaluate the matrix effects of the developed method. Moreover, the obtained parameters will be compared with other methods reported in the literature.

- **Application of the developed methods for the analysis of complex samples**

Finally, the methods will be applied for the analysis of samples to carry out the detection and quantification of the target analytes, and as a first approximation to demonstrate their usefulness in real-life applications.

Considering these objectives, the achievements within this Doctoral Thesis are divided in several chapters:

Chapter III: Experimental, in which the reagents, materials, instrumentation, and samples required for the synthesis of the materials and the development of the analytical methods are listed. Moreover, the procedures followed for the synthesis and characterization of the materials are also detailed. This chapter also describes the optimum conditions established for the analytical methods developed in this Doctoral Thesis, including both the microextraction procedure and the detection technique.

Chapter IV: Results and discussion, in which the main results obtained during the development of the analytical methods are discussed and compared with other studies reported in the literature. This chapter includes two main sections depending on the microextraction technique employed:

- **Section IV.1: DLLME using ILs.** This section includes a preliminary subsection describing the synthesis and characterization of the guanidinium-based ILs synthesized in this Doctoral Thesis. The following subsections cover the different analytical applications developed using these hydrophilic ILs as extraction solvent, which are organized depending on the DLLME strategy used, the target analyte, and the type of sample. All sections include the results with respect to the optimization and validation studies, as well as the analysis of samples.
- **Section IV.2: SPME using PILs and MOFs.** This section is divided in two main subsections based on the material used for the preparation of the SPME extraction phase: PILs (Section IV.2.1) and MOFs (Section IV.2.2). In turn, each subsection contains a subsection describing the preparation of the SPME devices and their characterization, and several subsections dealing with the analytical applications developed and including optimization, validation, analysis of samples, and comparison with commercial coatings.

Chapter V: Conclusions, in which the most relevant conclusions obtained from this Doctoral Thesis are summarized, paying special attention to the significance of the results obtained in each one of the analytical applications developed.

CHAPTER III
Experimental

III.1. Analytes

The analytes studied in this Doctoral Thesis include a variety of organic compounds, metal species, and a biomolecule, specifically DNA. Table III.1 lists the main physicochemical characteristics of the organic analytes studied, together with their chemical structures. The Table also classifies the studied analytes in different families depending on their use and/or structure.

The group of personal care products (PCPs) covers preservatives: methylparaben (MePa), ethylparaben (EtPa), propylparaben (PPa), and isopropylparaben (iPPa); UV-filers: benzophenone (BP) and benzophenone-3 (BP3); and a disinfectant: triclosan (Trc). MePa (99.5 %), EtPa (99.5 %), and PPa (99.5 %) were purchased from Dr. Ehrenstorfer GmbH (Augsburg, Germany); BP (99.5 %), BP3 (99.5 %) and Trc (> 97 %) were supplied by Sigma-Aldrich (Steinheim, Germany); and iPPa was acquired from Alfa Aesar (Karlsrube, Germany). Individual standard solutions were prepared in acetonitrile at concentrations ranging from 1000 to 3000 $mg \cdot L^{-1}$, except for Trc, for which the concentration of the standard solution was 10 $mg \cdot L^{-1}$.

The pharmaceuticals carbamazepine (Cmz, 99 %) and gemfibrozil (Gfz, > 99 %) were acquired from Sigma-Aldrich (St. Louis, MO, USA) and the standard solutions were prepared at 10 $mg \cdot L^{-1}$ in acetonitrile.

The studied phenols include bisphenol A (BPA, 99 %), 4-cumylphenol (CuP, 99 %), 3-*tert*-butylphenol (*t*BP, 99 %), 4-*tert*-octylphenol (*t*OP, 97 %), 4-octylphenol (OP, 99 %), 4-*n*-nonylphenol (*n*NP, 98 %), and 2-nitrophenol (NP, 98 %). They were all purchased from Sigma-Aldrich (Steinheim, Germany), except for *t*BP and NP, which were supplied by Sigma-Aldrich (St. Louis, MO, USA). Standards solutions of the alkylphenols were prepared in acetonitrile at 1000 $mg \cdot L^{-1}$, while the concentration for *t*BP and NP was 10 $mg \cdot L^{-1}$.

The polycyclic aromatic hydrocarbons (PAHs) studied in this Doctoral Thesis were naphthalene (Nap, 99 %), which was supplied by Merck KGaA (Darmstadt, Germany); acenaphthylene (Acy, 85 %), acenaphthene (Ace, 99 %), fluorene (Flu, 98 %), phenanthrene (Phe, 99.5 %), anthracene (Ant, 99.9%), fluoranthene (Flt, 98 %), pyrene (Py,99 %), benzo[a]anthracene (BaAnt, 99 %), chrysene (Chry, 98 %), benz[b]fluoranthene (BbFlt, 99 %), benzo[k]fluoranthene (BkFlt, 99 %), benzo[a]pyrene (BaPy, 98 %), and indeno[1,2,3-c,d]pyrene (Ind, 99.9 %), which were all purchased from Sigma-Aldrich (Steinheim, Germany). Individual standard solutions were prepared in acetonitrile at different concentrations ranging from 340 to 3445 $mg \cdot L^{-1}$ depending on the PAH. Moreover, a solution at 161.8 $mg \cdot L^{-1}$ of Py in acetonitrile was prepared and used as fluorescence probe molecule for the determination of the critical micelle concentration (CMC) of the IL-based surfactants.

Several monohydroxylated metabolites of PAHs (OH-PAHs) were also studied, including 2-hydroxyfluorene (2OHflu), 2-hydroxyphenanthrene (2OHphe), 4-hydroxyphenanthrene (4OHphe), and 1-hydroxypyrene (1OHpy). They were all purchased from Dr. Ehrenstorfer. 2OHphe, 4OHphe

and 1OHpy were acquired as a 10 $mg \cdot L^{-1}$ standard solution in acetonitrile, 2OHflu was acquired as solid with a purity of 98 % and a solution of this analyte at 500 $mg \cdot L^{-1}$ in acetonitrile was prepared.

The short-chain free fatty acids (SCFFAs) certified reference material (CRM) CRM46975 was purchased from Supelco (Bellefonte, PA, USA). This multi-component aqueous solution was used as standard mix of this group of analytes, and contained: propionic acid (C_3), *iso*-butyric acid (*i*-C_4), *n*-butyric acid (*n*-C_4), *iso*-valeric acid (*i*-C_5), *n*-valeric acid (*n*-C_5), *iso*-hexanoic acid (*i*-C_6), *n*-hexanoic acid (*n*-C_6), and *n*-heptanoic acid (*n*-C_7), at 10 mM (range: 502–1328 $mg \cdot L^{-1}$).

Other organic compounds were also studied, including benzaldehyde (Bnzal, ≥ 99 %), ethyl benzoate (EB, ≥ 99 %), and α,α,α,6-tetrafluoro-*m*-toluidine (tfTol, 97 %). They were supplied by Sigma-Aldrich (St. Louis, MO, USA), and their individual standard solutions were prepared in acetonitrile at 10 $mg \cdot L^{-1}$.

With respect to the target metal species, certified standard solutions of 1000 $mg \cdot L^{-1}$ of $Cu(NO_3)_2 \cdot 3H_2O$ and $Cd(NO_3)_2 \cdot 3H_2O$ in HNO_3 (0.5 N) from Panreac (Barcelona, Spain) were used. In the case of the study with foreign metal ions, certified standard solutions at 1000 $mg \cdot L^{-1}$ of $Cr(NO_3)_3 \cdot 9H_2O$, $Ba(NO_3)_2$, $Pb(NO_3)_2$, $Co(NO_3)_2 \cdot 6H_2O$, $Mn(NO_3)_2$, $Zn(NO_3)_2 \cdot 6H_2O$, and $Ni(NO_3)_2 \cdot 6H_2O$, all in HNO_3 (0.5 N), were purchased from Panreac, whereas $CaCO_3$ and $Mg(NO_3)_2 \cdot 6H_2O$ certified standard solutions at 1000 $mg \cdot L^{-1}$ in HNO_3 (2 N) were supplied by VWR International (Leuven, Belgium).

Finally, DNA sodium salt from salmon testes (approximately 20 kbp) was acquired from Sigma-Aldrich (St. Louis, MO, USA). A stock solution of 2000 $mg \cdot L^{-1}$ was prepared in 1X TE buffer, composed of 10 mM of tris(hydroxymethyl)aminomethane (Tris-base) and 1 mM of ethylenediaminetetraacetic acid (EDTA) at pH 8.

Intermediate solutions containing the target group of analytes depending on the analytical application were prepared by dilution of the individual standard solutions using the same solvent as that of the individual solutions. All these solutions were kept refrigerated at 4 °C and protected from light, except for the SCFFAs mix and DNA stock solution, which were stored at -20 °C. In the case of the metal species, the solutions were stored at room temperature. The working solutions were then prepared by dilution of the intermediate solutions in ultrapure water or by spiking the corresponding samples with the intermediate solutions containing the analytes.

III.2. Solvents and reagents

Ultrapure water (18.2 MΩ·cm) was obtained from a Milli-Q water purification system (Watford, UK). Acetonitrile HiPerSolv Chromanorm® LC-MS grade was purchased from VWR (Llinars del Vallés, Spain) and used for the preparation of standard solutions, while acetonitrile HiPerSolv Chromasolv™ from Honeywell Riedel-de Haën™ (Seetze, Germany) was used as mobile phase. Methanol (≥ 99 %) and acetone (≥ 99.8 %) HPLC Plus grade from Sigma-Aldrich (Steinheim, Germany) were used for the microextraction procedures.

Table III.1. Main physicochemical characteristics of the organic analytes studied in this Doctoral Thesis (SciFinder® Database 2020).

Analyte (abbreviation)	Structure	MW ($g \cdot mol^{-1}$)	pK_a	Log K_{ow}	Vapor pressure (Pa)
PCPs					
Methylparaben (MePa)	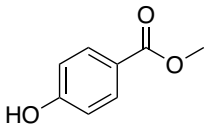	152.15	8.31	1.882	$7.39 \cdot 10^{-1}$
Ethylparaben (EtPa)	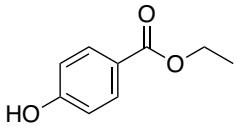	166.17	8.31	2.391	$1.01 \cdot 10^{-1}$
Propylparaben (PPa)	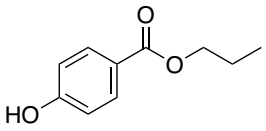	180.20	8.23	2.901	$1.24 \cdot 10^{-1}$
Isopropylparaben (iPPa)	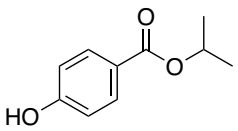	180.20	8.40	2.745	$1.87 \cdot 10^{-1}$
Benzophenone (BP)	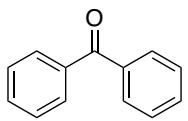	182.22	–	3.214	$1.09 \cdot 10^{-1}$
Benzophenone-3 (BP3)	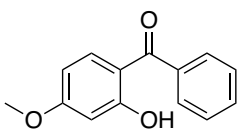	228.24	7.56	3.995	$6.99 \cdot 10^{-4}$

Table III.1 (continued).

Analyte (abbreviation)	Structure	MW (g·mol^{-1})	pK_a	Log K_{ow}	Vapor pressure (Pa)
Triclosan (Trc)	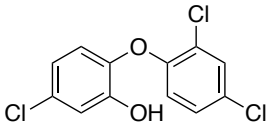	289.54	7.80	5.343	$4.35 \cdot 10^{-3}$
Pharmaceuticals					
Carbamazepine (Cmz)	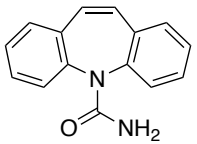	236.27	13.94	1.895	$7.71 \cdot 10^{-5}$
Gemfibrozil (Gfz)	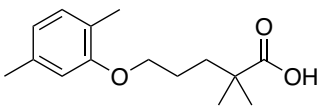	250.33	4.75	4.302	$8.17 \cdot 10^{-5}$
Phenols					
Bisphenol A (BPA)	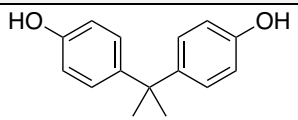	228.29	10.29	3.641	$7.12 \cdot 10^{-5}$
4-Cumylphenol (CuP)	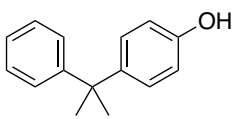	212.29	10.62	4.238	$6.64 \cdot 10^{-3}$
3-*tert*-butylphenol (*t*BP)	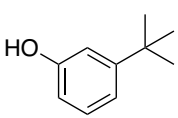	150.22	10.08	3.262	3.35

Table III.1 (continued).

Analyte (abbreviation)	Structure	MW (g·mol^{-1})	pK_a	Log K_{ow}	Vapor pressure (Pa)
4-*tert*-Octylphenol (*t*OP)	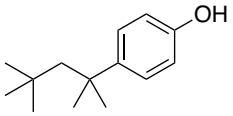	206.32	10.15	5.180	$2.64 \cdot 10^{-1}$
4-Octylphenol (OP)	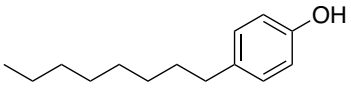	206.32	10.15	5.633	$3.33 \cdot 10^{-2}$
4-*n*-Nonylphenol (*n*NP)	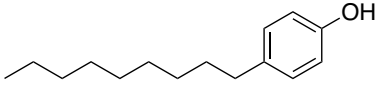	220.35	10.15	6.142	$1.14 \cdot 10^{-2}$
2-Nitrophenol (NP)	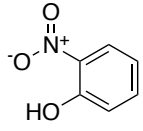	139.11	7.14	1.671	$1.32 \cdot 10^{1}$
PAHs					
Naphthalene (Nap)	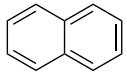	128.17	–	3.361	$2.12 \cdot 10^{1}$
Acenaphthylene (Acy)	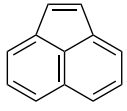	152.19	–	3.266	$2.93 \cdot 10^{-1}$
Acenaphthene (Ace)	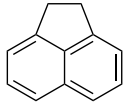	152.21	–	3.728	$9.31 \cdot 10^{-1}$

Table III.1 (continued).

Analyte (abbreviation)	Structure	MW (g·mol^{-1})	pK_a	Log K_{ow}	Vapor pressure (Pa)
Fluorene (Flu)	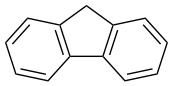	166.22	–	4.323	$4.00 \cdot 10^{-1}$
Phenanthrene (Phe)	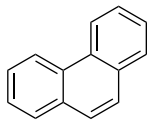	178.23	–	4.545	$2.75 \cdot 10^{-2}$
Anthracene (Ant)	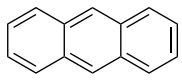	178.23	–	4.545	$2.74 \cdot 10^{-2}$
Fluoranthene (Flt)	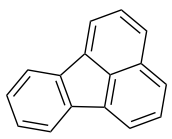	202.25	–	5.004	$2.31 \cdot 10^{-3}$
Pyrene (Py)	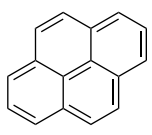	202.25	–	5.004	$3.75 \cdot 10^{-4}$
Benz[a]anthracene (BaAnt)	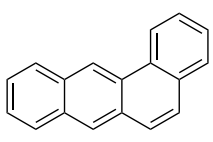	228.29	–	5.729	$2.69 \cdot 10^{-5}$
Chrysene (Chry)	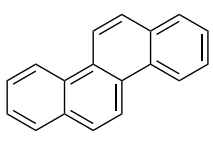	228.29	–	5.729	$1.13 \cdot 10^{-5}$

Table III.1 (continued).

Analyte (abbreviation)	Structure	MW (g·mol^{-1})	pK_a	Log K_{ow}	Vapor pressure (Pa)
Benzo[b]fluoranthene (BbFlt)	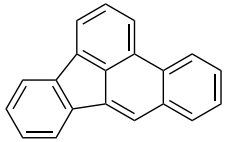	252.31	–	6.188	$2.41 \cdot 10^{-6}$
Benzo[k]fluoranthene (BkFlt)	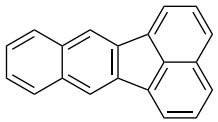	252.31	–	6.188	$8.73 \cdot 10^{-7}$
Benzo[a]pyrene (BaPy)	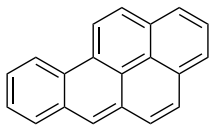	252.31	–	6.188	$2.49 \cdot 10^{-7}$
Indeno[1,2,3-c,d]pyrene (Ind)	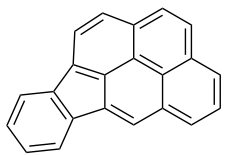	276.33	–	6.646	$2.08 \cdot 10^{-7}$
OH-PAHs					
2-Hydroxyfluorene (2OHflu)	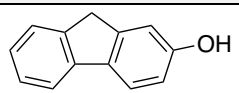	182.22	9.94	3.646	$6.15 \cdot 10^{-4}$

Table III.1 (continued).

Analyte (abbreviation)	Structure	MW (g·mol^{-1})	pK_a	Log K_{ow}	Vapor pressure (Pa)
2-Hydroxyphenanthrene (2OHphe)	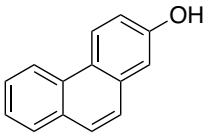	194.23	9.57	3.909	$5.36 \cdot 10^{-5}$
4-Hydroxypenanthrene (4OHphe)	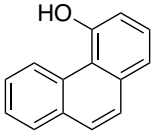	194.23	9.40	3.909	$5.36 \cdot 10^{-5}$
1-Hydroxypyrene (1OHpy)	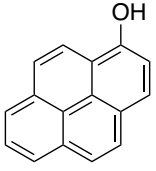	218.25	9.40	4.367	$3.89 \cdot 10^{-6}$
SCFFAs					
Propionic acid (C_3)	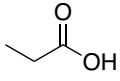	74.08	4.79	0.188	$5.64 \cdot 10^{2}$
iso-Butyric acid (*i*-C_4)	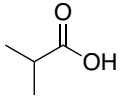	88.11	4.85	0.541	$2.17 \cdot 10^{2}$
n-Butyric acid (*n*-C_4)	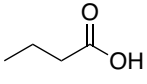	88.11	4.76	0.697	$1.80 \cdot 10^{2}$

Table III.1 (continued).

Analyte (abbreviation)	Structure	MW (g·mol^{-1})	pK_a	Log K_{ow}	Vapor pressure (Pa)
iso-Valeric acid (*i*-C_5)	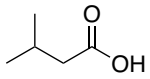	102.13	4.78	1.051	$7.39 \cdot 10^1$
n-Valeric acid (*n*-C_5)	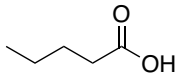	102.13	4.78	1.011	$6.03 \cdot 10^1$
iso-Hexanoic acid (*i*-C_6)	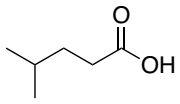	116.16	4.78	1.560	$1.75 \cdot 10^1$
n-Hexanoic acid (*n*-C_6)	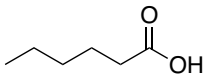	116.16	4.78	1.716	$2.11 \cdot 10^1$
n-Heptanoic acid (*n*-C_7)	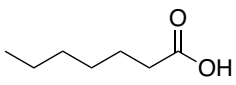	130.18	4.78	2.226	7.71
Other organic compounds					
Benzaldehyde (Bnzal)	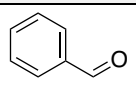	106.12	–	1.452	$1.30 \cdot 10^2$
Ethyl benzoate (EB)	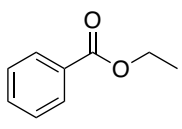	150.17	–	2.634	$2.40 \cdot 10^1$
α,α,α,6-Tetrafluoro-*m*-toluidine (tfTol)	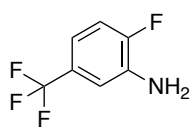	179.11	1.98	2.636	$1.80 \cdot 10^2$

The solvents used for the synthesis of the ILs and derivatives were: ethanol LiChrosolv® grade LC supplied by Merck KGaA, and isopropanol Chromasolv™, chloroform ACS grade, methanol Chromasolv™ LC-MS grade, acetonitrile ACS grade, tetrahydrofuran HPLC grade, and ethyl acetate ACS grade, all of them purchased from Fisher Scientific (Fair Lawn, NJ, USA).

NaCl (≥ 99 %), HCl (36.5–38 %), NaOH (> 99 %), K_3PO_4 (98 %), sodium acetate trihydrate (99.5 %), and acetic acid (99 %), were supplied by Sigma-Aldrich (Steinheim, Germany), while sodium perchlorate monohydrate (analytical reagent grade) was obtained from Merck KGaA. Tris(hidroxymethyl)aminomethane hydrochloride (Tris-HCl), Tris-base and EDTA, which were used to prepare the TE buffer, were acquired from Sigma-Aldrich (St. Louis, MO, USA). Thiocarbohydrazide (98 %) and salicylaldehyde (≥ 98 %) were employed to synthesize the metal complexing reagent, and were provided by Sigma-Aldrich (Steinheim, Germany).

The reagents to prepare the synthetic urine matrices were urea (99 %) and creatinine (≥ 98 %), provided by Sigma-Aldrich (Steinheim, Germany), and potassium dihydrogen phosphate, sodium hydrogen phosphate dihydrate, and KCl, all of them of analytical reagent grade and purchased from Merck KGaA. For the preparation of the synthetic wine, (+)-tartaric acid from Sigma-Aldrich (St. Louis, MO, USA), and ethanol (LiChrosolv® grade LC) supplied by Merck KGaA, were used. The enzyme β-Glucuronidase/arylsulfatase from *Helix pomatia* was supplied by Roche Diagnostics GmbH (Mannheim, Germany).

The guanilating agent 1*H*-pyrazole-1-carboxamidinehydrochloride (99 %), butylamine (99 %), hexylamine (99 %), octylamine (99.5 %), and decylamine (≥ 99 %), used for the synthesis of guanidinium-based ILs, were supplied by Sigma-Aldrich (Steinheim, Germany).

For the preparation of the imidazolium ILs, the following reagents were needed: 1-butylimidazole (98 %), 1-methylimidazole (≥ 99 %), 1-vinylimidazole (≥ 99 %), imidazole (≥ 99 %), 1-chlorohexane (99 %), 1-chlorodecane (98 %), 1-bromohexadecane (99 %), 10-bromodecanoic acid (95 %), 1,12-dibromodecane (98 %), acrylonitrile (≥ 99 %), and 4-vinylbenzyl chloride (90 %), all purchased from Sigma-Aldrich (St. Louis, MO, USA). In the case of the zwitterionic ILs, the reagents were: 1,3-propanesultone (98 %), 1,4-butanesultone (≥ 99 %), and Amberlite IRN78 (hydroxide form), also from Sigma-Aldrich.

Lithium bis[(trifluoromethyl)sulfonyl]imide (Li-NTf_2), used for the synthesis of the ILs, was obtained from SynQuest Laboratories (Alachua, FL, USA), while the Li-NTf_2 used for the LPME methods (Section IV.1.1) was supplied by Sigma-Aldrich (Steinheim, Germany). The radical initiator 2-hydroxy-2-methylpropiophenone (DAROCUR 1173, > 96 %) and the thermal initiator 2,2'-azobis(2-methylpropionitrile) (AIBN, ≥ 98 %) were supplied by Sigma-Aldrich (St. Louis, MO, USA) and used for the copolymerization of the ILs.

The commercial ILs butylmethylimidazolium chloride ($[C_4MIm^+][Cl^-]$, ≥ 98 %), 1-octyl-3-methylimidazolium chloride ($[C_8MIm^+][Cl^-]$, ≥ 97 %), and hexadecylpyridinium chloride monohydrate ($[C_{16}Py^+][Cl^-]$, > 99 %) were supplied by Sigma-Aldrich (Steinheim, Germany), and

used in the studies of cytotoxicity. The conventional nonionic surfactant Triton X-100, the conventional cationic surfactant cetyltrimethylammonium bromide (CTAB), and the conventional anionic surfactant sodium dodecyl sulfate (SDS), were also purchased from Sigma-Aldrich and employed in the cytotoxicity studies (Section IV.1.1.1).

For the synthesis of the MOF CIM-80(Al), aluminum nitrate nonahydrate (98 %), mesaconic acid (99 %), and urea (99 %), were supplied by Sigma-Aldrich (Steinheim, Germany), while ethanol LiChrosolv® grade LC from Merck KGaA was used during the washing steps. The functionalization of the wires to prepare SPME fibers required hydrogen peroxide (30 %, w/w), vinyltrimethoxysilane (VTMS, 98 %), and 3-amino-propyltriethoxysilane (APTES, ≥ 98 %), all obtained from Sigma-Aldrich (Steinheim, Germany).

The cytotoxicity of the ILs and conventional surfactants was evaluated against the J774.1 murine macrophage cell line (ATCCTIB-67, American Type Culture Collection LG Promochem, Spain), which was cultured in (Roswell Park Memorial Institute) RPMI medium. The Alamar Blue® reagent was provided by Biosource (Nivelles, Belgium), and the Roche Applied Science cytotoxicity detection kit based on lactate dehydrogenase (LDH) was acquired from Sigma-Aldrich (Steinheim, Germany).

III.3. Samples

Different samples were analyzed depending on the target analytes and the analytical methodology developed in this Doctoral Thesis, including environmental, cosmetic, food, and biological samples.

Water was the most common matrix used to demonstrate the applicability of the developed analytical methods, using water samples from different sources. With respect to drinking waters, tap water 1 was collected in San Cristóbal de La Laguna (Tenerife, Spain), tap water 2 was from Santa Úrsula (Tenerife, Spain), and tap water 3 was collected in Toledo (OH, USA). Tap water 1 was also subjected to heating (100 °C), and then used to fill empty plastic bottles (water bottles) obtained from local markets (Tenerife, Spain). These plastic bottles had the resin identification code number 7, which refers to polycarbonate, polylactic acid, and acrylic plastics, among others. The purpose was to assess if migration of the analytes from the plastic bottle occurred. They were denoted as bottled water 1 and bottled water 2. A mineral bottled water sample acquired from a local market (Tenerife, Spain) was also analyzed, and designated as bottled water 3. The drinking water CRM coming from an inter-laboratory exercise, which had a Cu (II) concentration of 138 ± 2 $\mu g \cdot L^{-1}$ and a Cd (II) concentration of 7.7 ± 0.1 $\mu g \cdot L^{-1}$, was purchased from Gabinete de Servicios para la Calidad (Madrid, Spain)

River water was collected from the Maumee River in Maumee (OH, USA), while the wastewaters and seawater samples (from different areas of Tenerife, Spain) were supplied by an environmental monitoring laboratory. In all cases, they were sampled using amber glass recipients

properly cleaned, avoiding the formation of air bubbles during sampling, and filtered through 0.45 µm filters before analysis.

Three commercial facial tonics were purchased in a local store and analyzed for the determination of PCPs. Facial tonic 1 was labelled as paraben-free, while MePa was tagged in facial tonic 2 and facial tonic 3, and PPa was also tagged in facial tonic 2.

Synthetic wine was prepared according to previously published methods [1,2] using an aqueous solution of 3.5 $g \cdot L^{-1}$ of (+)-tartaric acid containing 13 % (v/v) of ethanol, and adjusting the pH to 3.5 with NaOH 1 M. A red wine Pinot Noir 2014 (ethanol content of 13 %, v/v) was purchased from a local store in Ames, IA, USA.

Ground coffee, whole milk, red and white table wines (ethanol content of 11–12 %, v/v), and apple juice samples, were acquired from a local store in Tenerife, Spain. The brewed coffee sample was prepared with 35 g of ground coffee and 500 mL of tap water 1 and using a moka pot coffee maker.

The synthetic urine was prepared following a previously reported protocol [3], thus containing: 0.33 M of urea, 0.12 M of sodium chloride, 0.016 M of potassium dihydrogen phosphate, 0.004 M of sodium hydrogen phosphate dehydrate, and 0.015 M of creatinine (for mimicking urine with medium content of creatinine).

Four healthy volunteers supplied urine collected in the early morning: a non-smoker female, a smoker female, a non-smoker male, and a smoker male, all belonging to the same family. The urine sample from the non-smoker female was used for the validation of the analytical methods in which this type of matrix was used (Section IV.1.2.1 and IV.2.2.2). For the determination of urinary metabolites, enzymatic hydrolysis was performed according to the enzyme manufacturer and a previously reported procedure [4]: 2 mL of acetic acid/sodium acetate buffer solution (pH 5) were added to 15 mL of urine, and the pH was verified to be around 5–5.5. Then, 50 µL of β-glucuronidase/arylsulfatase enzyme were added and the samples were incubated at 37 °C overnight. In all cases, the volunteers signed an individual informed consent before providing the samples.

III.4. Materials

All the LPME procedures and conductivity measurements were performed in 15 mL (9.5 cm × 2 cm O.D.) Pyrex® glass tubes (Scilabware, UK), while tubes of 25 mL (10 cm × 2.6 cm O.D.) were used to obtain the phase diagrams of the µ-ABS and to accomplish the hydrolysis of real urine samples (Section IV.1). Hamilton syringes (Reno, NV, USA) of 25 and 50 µL were used to collect the IL-rich phase obtained in the LPME methods and to perform the manual injection in the high-performance liquid chromatograph (HPLC). All the mobile phases and water samples were filtered through Durapore filters (0.45 µm) from Millipore (Sigma-Aldrich, Steinheim, Germany).

On-fiber SPME procedures were performed in 20 mL amber glass vials with screw caps and polytetrafluoroethylene (PTFE)/silicon septa from Agilent Technologies (Santa Clara, CA, USA) and using magnetic stir bars of 10 mm × 4.5 mm from Sigma-Aldrich (Steinheim, Germany) (Section IV.2). 2 mL glass vials with PTFE/silicon septa were also purchased from Agilent Technologies, glass inserts of 0.25 mL were acquired from Supelco, and 2 mL Eppendorf tubes were supplied by Sigma-Aldrich (Steinheim, Germany).

SPME fibers (Section IV.2) were prepared using nitinol wires with average diameter of 127 µm from Nitinol Devices & Components (Fermont, CA, USA), while blank SPME assemblies (24 Ga) were supplied by Supelco. Solvothermal reactors of Teflon (15 mL) and stainless steel autoclaves from Parr Instrument Company (Moline, IL, USA), were used for the synthesis of the MOF powder as well as its synthesis on the fibers. The commercial SPME fibers polyacrylate (PA, 85 µm), polydimethylsiloxane (PDMS, 100 µm), carboxen/polydimethylsiloxane (CAR/PDMS, 75 µm and 85 µm), polydimethylsiloxane/divinylbenzene (PDMS/DVB, 60 µm), and divinylbenzene/carboxen/polydimethylsiloxane (DVB/CAR/PDMS, 50/30 µm) were also acquired from Supelco.

In the case of in-tube SPME (Section IV.2.1.4), untreated fused silica capillaries (2 m × 0.25 mm I.D.) were required for the preparation of the devices. Polyether ether ketone (PEEK) tubing (1.6 mm O.D. × 0.5 mm I.D.) from Sigma-Aldrich (St. Louis, MO, USA), stainless steel nuts, ferrules, and connectors (Agilent Technologies), were also used for setting-up the device. The manual method required a 500 µL gas tight syringe from Trajan Scientific and Medical (Ringwood, Victoria, Australia) and GlasSeal™ fused silica capillary column connectors (0.10–0.53 mm I.D.) supplied by Supelco.

III.5. Instrumentation and equipment

5.1. Instrumentation for the characterization of materials

One-dimensional proton nuclear magnetic resonance spectroscopy (^{1}H-NMR) using an AVANCE™ (500 MHz) from Bruker (Massachusetts, USA) was used for the characterization of the ILs and of the metal complexing reagent.

The fluorescence measurements (Section IV.1.1.1) were carried out using a Cary Eclipse Varian spectrofluorimeter (Mulgrave, Victoria, Australia) and a quartz cell (1 cm × 1 cm).

For the cytotoxicity assessment (Section IV.1.1.1), a Tali® image cytometer from Thermo Fisher Scientific was used to estimate cell density, and plates were analyzed on a microplate reader model 680 from Bio-Rad (Hercules, CA, USA) for LDH assays, and an EnSpire® Multimode Plate Reader from Perkin Elmer (Madrid, Spain) for the Alamar Blue® tests.

For the characterization of the MOF, the phase identification was carried out by X-ray powder diffraction (PXRD) using an Empyrean diffractometer (PANalytical, Netherlands) operating with Bragg-Brentano geometry in continuous mode. Cu-Kα radiation (λ = 1.5418 Å) at 45 KV over the angular range from 5.01° to 80.00° in 0.0263° steps with a total 10 min scan was used to collect the data. The thermogravimetric analysis (TGA) was performed using a Perkin Elmer Pyris Diamond TGA/DTA equipment (Waltham, MA, USA), while the nitrogen adsorption measurements were carried out with a Gemini Surface Area Analyzer model V2365 from Micromeritics (Norcross, GA, USA) at 77 K in the range of $0.02 \leq P/P_0 \leq 1.00$.

Scanning electron microscopy (SEM) analysis of the coated fibers and capillaries was performed using an EVO 15 microscope (ZEISS, Germany) equipped with a 50 mm^2 silicon drift X-MAX detector (Oxford Instruments, Abingdon, UK) to evaluate the morphology of the coatings and to estimate the thickness.

5.2. Analytical instrumentation

All the LPME methods in combination with HPLC were developed using a HPLC system equipped with a solvent-delivery Varian ProStar 230 Solvent Delivery module (Palo Alto, CA, USA) and different detectors depending on the application: a Varian ProStar 330 diode-array detector (DAD) for PCPs (Section IV.1.1.2); a Waters 474 fluorescence detection system (FD) (Milford, MA, USA) connected through a Varian Star 800 module interface for OH-PAHs (Section IV.1.2.1); and a 1260 Infinity multichannel FD from Agilent Technologies in the case of PAHs (Section IV.1.2.2). The manual injection was performed using a Rheodyne 7725i injection valve with a loop of 20 µL obtained from Supelco. The separation of these groups of analytes in each application was achieved using an ACE UltraCore 5 SuperC18 column (150 mm × 4.6 mm × 5 µm) supplied by Symta (Madrid, Spain), which was protected by a Pelliguard LC-18 guard column from Supelco.

In the case of SPME applications coupled with HPLC (Section IV.2.1.2), the determination of a mix of different organic compounds was carried out using a Shimadzu LC-20A HPLC (Kyoto, Japan) coupled to a SPD-20A UV-Vis detector and equipped with a Raptor C18 column (250 mm × 4.6 mm × 5 µm) from Restek (Bellefonte, PA, USA) and a Kromasil® C18 guard column (5 µm) from Supelco. A 1260 Infinity HPLC with DAD from Agilent Technologies, which was equipped with an ACE UltraCore 5 SuperC18 column (150 mm × 4.6 mm × 5 µm), was employed for the determination of alkylphenols also using SPME. Both instruments were also provided with a Rheodyne 7725i injection valve with a 20 µL loop for manual injection.

The determination of DNA was performed using two different 1290 Infinity HPLC with UV-Vis from Agilent Technologies (Section IV.2.1.4) depending on whether it was the manual or automatic method. Both instruments were equipped with a TSKgel DEAE-NPR anion-exchange column (35 mm × 4.6 mm × 2.5 µm) from Tosoh Bioscience (Griesheim, Germany). The manual

injection was carried out using a Rheodyne 7725i valve with a loop of 20 µL, while a 1290 Infinity II Vialsampler with a loop of 100 µL from Agilent Technologies was used for automated injection.

A SpectrAA 50B flame atomic absorption spectroscopy instrument (FAAS) from Varian (Palo Alto, CA, USA), which was equipped with an air/acetylene MK7 burner, was used for Cu (II) and Cd (II) determination (Section IV.1.1.3). Hollow cathode lamps of copper and cadmium were also supplied by Varian.

An Agilent Technologies model 7890B gas chromatography (GC) system coupled to a 5977A mass spectrometer (MS) detector (single quadrupole) and equipped with a HP-FFAP capillary column (30 m × 0.25 mm I.D. × 25 µm film thickness) from Agilent Technologies was used for the separation and detection of the SCFFAs (Section IV.2.1.3). A straight splitless ultra-inert liner (0.75 mm I.D.) from Agilent Technologies was also used.

For the GC applications dealing with PAHs (Section IV.2.2.2), a Varian 450 GC model CP-3800 equipped with a flame ionization detector (FID) and a FactorFour™ capillary column VF-5ms (30 m × 0.25 mm I.D. × 0.25 µm film thickness) purchased from Agilent Technologies was employed during the optimization studies. The validation of the methods was carried out using an Agilent Technologies 7820A GC equipped with a 5977B MS detector (single quadrupole) and a HP-5ms capillary column (30 m × 0.25 mm I.D. × 0.25 µm film thickness) from Agilent Technologies. Both GC systems were equipped with a straight splitless ultra-inert liner (0.75 mm I.D.) from Agilent Technologies.

5.3. Apparatus and other instrumentation

A Sartorius (Madrid, Spain) and a Mettler Toledo (Columbus, OH, USA) analytical balances with a minimum readability of 0.1 mg were used for the mass measurements, while Eppendorf micropipettes with different volume ranges were used for the measurement and dispensation of liquids. The pH-meter model GLP21, and the CM35 conductimeter equipped with a temperature sensor, were supplied by Crison Instruments (Barcelona, Spain).

The ultrasonic bath used for the degasification of the mobile phases and the thermostat employed to obtain the phase diagram of the µ-ABS and perform the conductivity measurements were purchased from Raypa® (Barcelona, Spain). A RV 10 digital evaporator with temperature control from IKA® Instruments Werke GmbH & Co. (Staufen, Germany) was used in the synthesis of the ILs. The evaporator was also equipped with a VP 2 Autovac pumping unit with vacuum and speed control from Vacuubrand (Wertheim, Germany). A Thermo Lab-Line vacuum oven from Thermo Fisher Scientific (Waltham, MA, USA) was used to dry the ILs. A hot-plate magnetic stirrer from IKA® was employed during all the procedures requiring constant agitation and/or heating.

A vortex from Reax-Control Heidolph GmbH & Co. (Schwabach, Germany) and a centrifuge model 5720 from Eppendorf (Hamburg, Germany) were used during the LPME procedures (Section

IV.1). The on-fiber SPME extractions (Section IV.2) were carried out using a metallic block placed on a magnetic stirring hotplate from IKA® or JP Selecta® (Barcelona, Spain).

The PILs were synthesized by UV polymerization using in an RPR-100 reactor provided with a spinning carrousel, which was obtained from Southern New England Ultraviolet Company (Bradford, CT, USA). The lab-made spin-coating device was fabricated using a 1.5–3 VDC high-speed motor and a 1.5 VC battery. The PILs-based coatings prepared by thermal polymerization required the use of 10 mL crimp vials and caps from Restek and an oven from Thermo Fisher Scientific, while a furnace from Nabertherm GmbH (Lilienthal, Germany) was used for the synthesis and activation of the MOF.

III.6. Software

ChemOffice Professional (version 15.0) was used to predict and analyze the ^{1}H-NMR data. The PXRD data were analyzed using the FullProf Suite Program (version September 2019), while the Mercury software (version 2020.0) from the Cambridge Structural Database System, together with the Diamond software (version 4.6.4) were employed to obtain the theoretical PXRD pattern for the MOF and to draw the structure of the crystal.

Data acquisition and analysis with the HPLC and GC instruments from Varian were carried out using the Varian Chromatography Workstation software (version 6.41). In the case of the instrumentation from Agilent Technologies, the HPLC systems were controlled using the OpenLab ChemStation software (versions C.01.04 or C.01.05 depending on the instrument), while the Mass Hunter software (version B.07.04.2260) was used with the GC-MS instruments.

The Statgraphics Centurion XV software (version 15.1) was employed for the design and analysis of the experimental designs, while the mathematical software SigmaPlot® (version 14.0) was used for the graphical analysis and the regression analysis of the phase diagrams of the μ-ABS. Microsoft Office Excel (version 2016) was used for the remaining calculations: regression analysis, statistical analysis, and analysis of the data generated from both characterization and analytical experiments.

III.7. Procedures

7.1. Synthesis of ILs, IL derivatives and PILs-based coatings

7.1.1. Synthesis of guanidinium and imidazolium ILs for LPME applications

Several ILs with cationic moieties of different nature were used as extraction solvents in the LPME methods, and their cytotoxicity was also assessed. Those that were not commercially

available were synthesized following procedures previously reported in the literature and are schematically shown in Figure III.1.

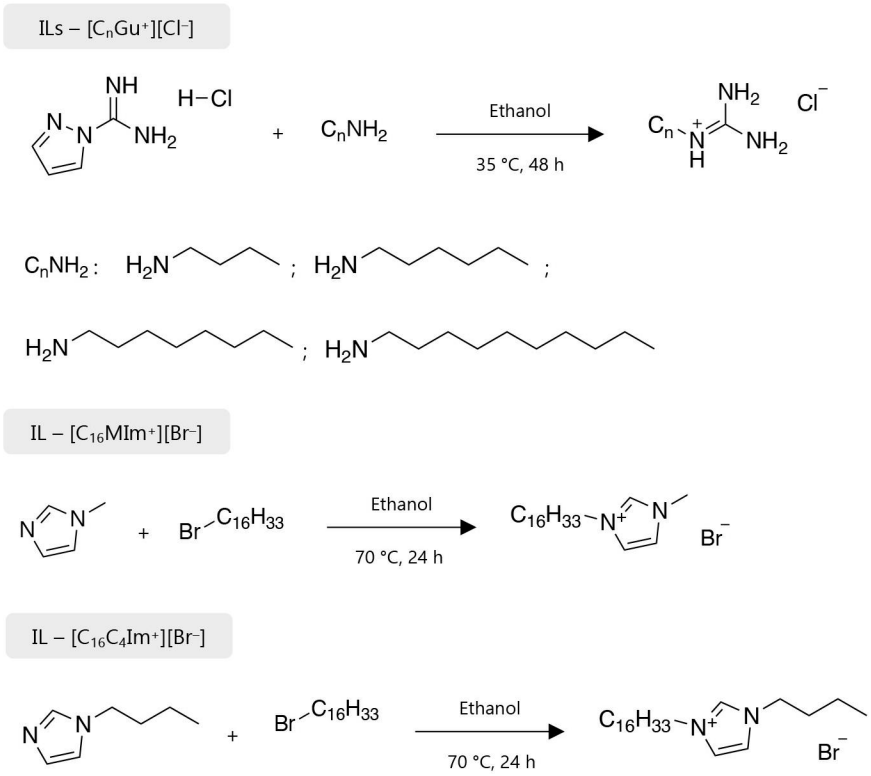

Figure III.1. Schemes of the synthetic procedures followed to prepare the ILs used in all LPME methods developed in this Doctoral Thesis.

The guanidinium ILs were synthesized according to the procedure described by Hankari and Hesemann [5]. Briefly, 1*H*-pyrazole-1-carboxamidine hydrochloride and the corresponding alkylamine (1:1 molar ratio) were refluxed in ethanol at 35 °C for 48 h. Then, the ILs were washed 3 times with ethanol, followed by solvent evaporation at 50 °C and $1.5 \cdot 10^4$ $N \cdot m^{-2}$. Thus, butylguanidinium chloride ($[C_4Gu^+][Cl^-]$), hexylguanidinium chloride ($[C_6Gu^+][Cl^-]$), octylguanidinium chloride ($[C_8Gu^+][Cl^-]$), and decylguanidinium chloride ($[C_{10}Gu^+][Cl^-]$) were prepared.

In the case of the IL-based surfactants 1-hexadecyl-3-methylimidazolium bromide ($[C_{16}MIm^+][Br^-]$) and 1-hexadecyl-3-butylimidazolium bromide ($[C_{16}C_4Im^+][Br^-]$), the protocol reported by Baltazar *et al.* was followed [6]. Briefly, 1-methylimidazole or 1-butylimidazole were

mixed with 1-bromohexadecane (1:1 molar ratio) and then refluxed in isopropanol at 70 °C during 24 h. The solvent was removed under vacuum (60 °C, $1.4 \cdot 10^4$ N·m^{-2}) and the product was dissolved in water. Then it was extracted 5 times with ethyl acetate. Finally, the solvent was evaporated under vacuum at 80 °C and $7 \cdot 10^3$ N·m^{-2}.

7.1.2. Synthesis of imidazolium IL monomers and crosslinkers for SPME applications

The PILs-based SPME phases used in this Doctoral Thesis were prepared using different imidazolium ILs as monomers, and dicationic imidazolium ILs as crosslinkers. Table III.2 includes the composition and size of the different PILs-based devices. In all cases, the excess of heat or light during the synthesis and manipulation of these ILs was minimized to prevent the free radical polymerization.

Table III.2. Composition and size of PILs-based coatings used in this Doctoral Thesis for SPME applications.

Coating	IL monomer	IL crosslinker	Mass ratio (w/w)	Size (length × thickness)
Fibers				
PIL-1a	$[VBC_{16}Im^+][NTf_2^-]$	$[(VBIm)_2C_{12}^{2+}]2[NTf_2^-]$	1:0.5	1 cm × ≈ 14 µm
PIL-1b	$[VBC_{16}Im^+][NTf_2^-]$	$[(VBIm)_2C_{12}^{2+}]2[NTf_2^-]$	1:0.5	1 cm × ≈ 35 µm
PIL-2	$[VC_{16}Im^+][NTf_2^-]$	$[(VIm)_2C_{12}^{2+}]2[NTf_2^-]$	1:0.5	1 cm × ≈ 13 µm
PIL-3	$[VC_{16}Im^+][Br^-]$	$[(VIm)_2C_{12}^{2+}]2[Br^-]$	1:0.5	1 cm × ≈ 14 µm
PIL-4	$[VC_6Im^+][Cl^-]$	$[(VIm)_2C_{12}^{2+}]2[Br^-]$	1:0.5	1 cm × ≈ 35 µm
PZIL-1	$[VIm^+C_3SO_3^-]$	$[(VIm)_2C_{12}^{2+}]2[Br^-]$	1:1	1 cm × ≈ 18 µm
PZIL-2	$[VIm^+C_3SO_3^-]$	$[(VIm)_2C_{12}^{2+}]2[NTf_2^-]$	1:1	1 cm × ≈ 20 µm
PZIL-3	$[VIm^+C_4SO_3^-]$	$[(VIm)_2C_{12}^{2+}]2[Br^-]$	1:1	1 cm × ≈ 20 µm
PZIL-4	$[VIm^+C_9COO^-]$	$[(VIm)_2C_{12}^{2+}]2[Br^-]$	1:1	1 cm × ≈ 18 µm
PZIL-5	$[VIm^+C_9COO^-]$	$[(VIm)_2C_{12}^{2+}]2[NTf_2^-]$	1:1	1 cm × ≈ 25 µm
Capillaries				
CAP-1	$[VC_{10}Im^+][Cl^-]$	$[(VIm)_2C_{12}^{2+}]2[Br^-]$	1:0.5	15 cm × ≈ 0.5 µm
CAP-2	$[VC_{9COOH}Im^+][Br^-]$	$[(VIm)_2C_{12}^{2+}]2[Br^-]$	1:0.5	15/55 cm × ≈ 0.5 µm

Imidazolium ILs with vinyl functionality were prepared following different procedures depending on the side chains, as it is shown in Figure III.2. 1-vinyl-3-alkylimidazolium-type ILs were synthesized according to a previously reported procedure [1], including 1-vinyl-3-hexylimidazolium chloride ($[VC_6Im^+][Cl^-]$), 1-vinyl-3-decylimidazolium chloride ($[VC_{10}Im^+][Cl^-]$), 1-vinyl-3-hexadecylimidazolium bromide ($[VC_{16}Im^+][Br^-]$), and 1-vinyl-3-hexadecylimidazolium bis[(trifluoromethyl)sulfonyl]imide ($[VC_{16}Im^+][NTf_2^-]$). Briefly, 1-vinylimidazole and the corresponding alkyl halide were mixed (1:1 molar ratio) in isopropanol at 60 °C during 16 h and under constant stirring. Then, the solvent was removed under vacuum, and the product was dissolved in water, and extracted with ethyl acetate 5 times. Finally, the solvent was evaporated, and the halide IL was dried in a vacuum oven at 70 °C for 48 h. In the case of $[VC_{16}Im^+][NTf_2^-]$, an additional step was required to accomplish the metathesis exchange reaction. Thus, the IL was mixed with Li-NTf_2 (1:1 molar ratio) in water and kept under constant stirring at room temperature for 8 h. Finally, the $[VC_{16}Im^+][NTf_2^-]$ was collected and dried at 70 °C for 24 h under reduced pressure conditions.

The functionalized IL 1-vinyl-3-(9-carboxynonyl)imidazolium bromide ($[VC_{9COOH}Im^+][Br^-]$) was also synthesized following an already reported procedure [7]. In this case,1-vinylimidazole was reacted with an excess of 10-bromodecanoic acid (approximately 1:2 molar ratio) in acetonitrile at room temperature for 72 h. The solvent was then evaporated using reduced pressure conditions and the product was washed 3 times with ethyl acetate. The IL was dried under vacuum at 50 °C for 12 h.

In the case of 1-vinylbenzyl-3-hexadecylimidazolium bis[(trifluoromethyl)sulfonyl]imide ($[VBC_{16}Im^+][NTf_2^-]$), the protocol described by Meng and Anderson was followed [8]. Briefly, imidazole and acrylonitrile were reacted (1:1 molar ratio) in methanol at 45 °C for 5 h and under a nitrogen atmosphere. The excess of solvent was removed using vacuum and the resulting compound was dissolved in chloroform, mixed with 1-bromohexadecane (1:1 molar ratio), and refluxed overnight (16 h) at room temperature. Then, a NaOH solution (15 %, w/v) was added to the mixture and stirred overnight (16 h) at room temperature. The chloroform layer was separated and washed with water 5 times, followed by evaporation of the chloroform to obtain 1-hexadecylimidazole. This product was then dissolved in chloroform, mixed with 4-vinylbenzyl chloride (1:1 molar ratio) and refluxed overnight (16 h) at room temperature. The obtained IL was dissolved in water, washed with ethyl acetate 5 times, and the metathesis reaction to exchange the halide counterion was performed as described above using Li-NTf_2 as anion-exchange reagent. Finally, the $[VBC_{16}Im^+][NTf_2^-]$ was separated from water and dried at 70 °C for 24 in a vacuum oven.

For the SPME fibers PZIL-1, PZIL-2, PZIL-3, PZIL-4 and PZIL-5, zwitterionic ILs were used as IL monomers. In this case, they were synthesized according to previously described methods [6,9–11], which are schematically shown in Figure III.3.

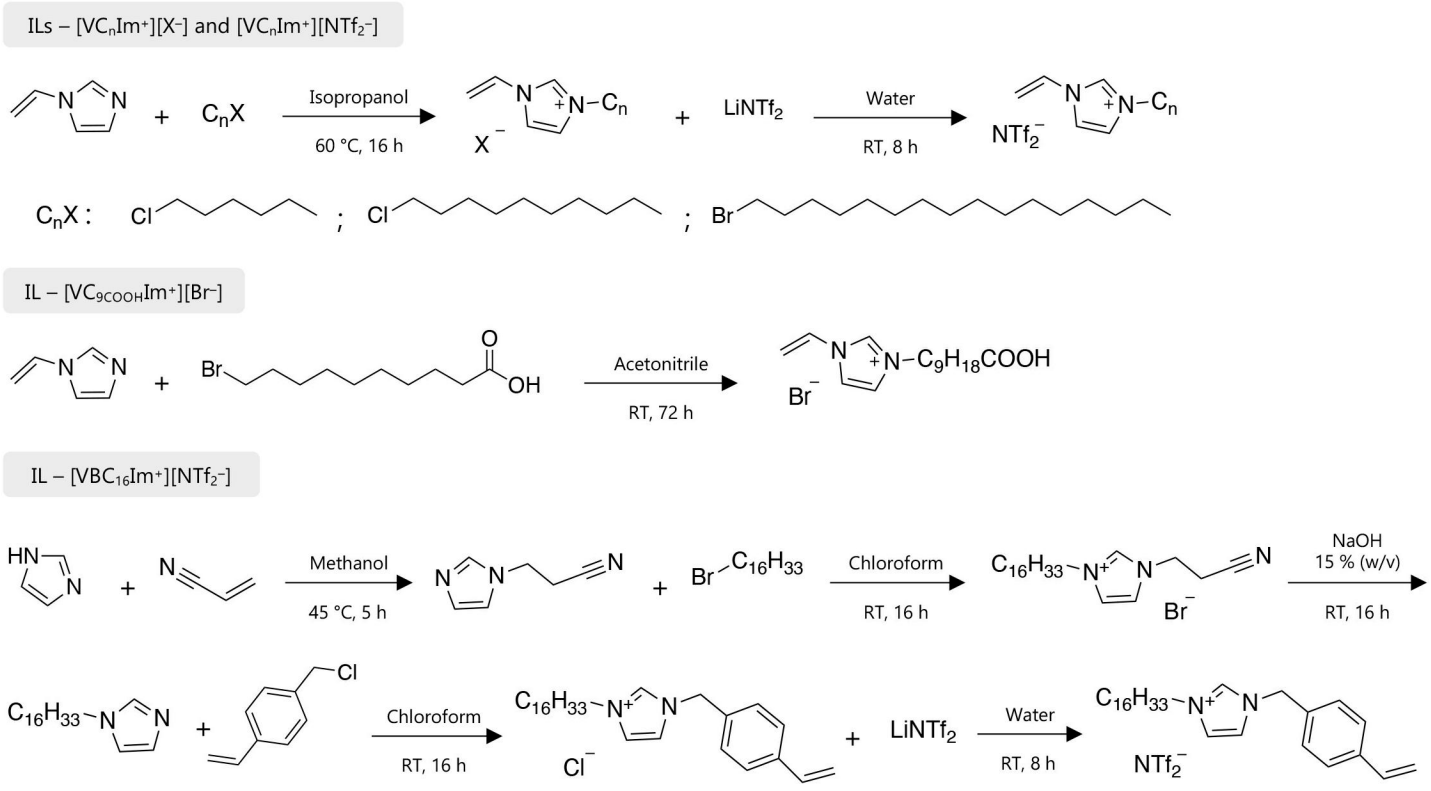

Figure III.2. Schemes of the procedures for the synthesis of the ILs monomers used in the preparation of all SPME PILs-based coatings (excluding zwitterionic-based) in this Doctoral Thesis.

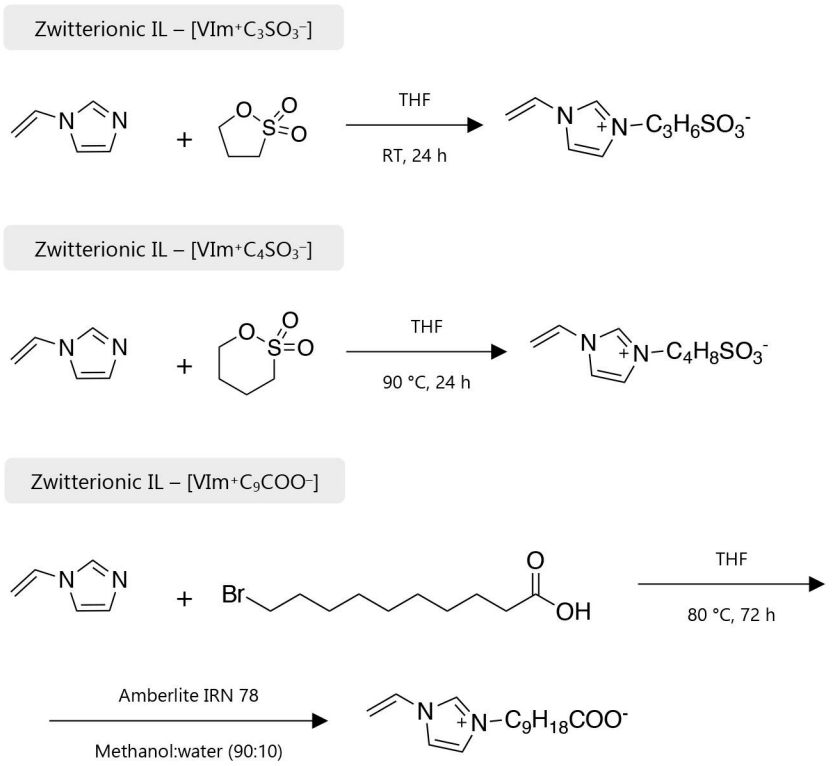

Figure III.3. Schemes of the synthetic procedures followed in the preparation of the zwitterionic ILs used for the development of SPME PILs-based coatings in this Doctoral Thesis.

The zwitterionic monomers (vinylimidazolium)propanesulfonate ([$VIm^+C_3SO_3^-$]) and (vinylimidazolium)butanesulfonate ([$VIm^+C_4SO_3^-$]) were prepared by reacting 1-vinylimidazole and 1,3-propanesultone or 1,4-butanesultone (1:1 molar ratio) in purified tetrahydrofuran under constant stirring for 24 h. In the case of ([$VIm^+C_3SO_3^-$], the synthesis was carried out at room temperature, while the temperature for the preparation of [$VIm^+C_4SO_3^-$] was 90 °C. Then, the white solid product was filtered and washed 3 times with diethyl ether, and finally dried in a vacuum oven at 40 °C for 24 h in both cases.

For the (vinylimidazolium)nonanocarboxylate ([$VIm^+C_9COO^-$]) zwitterionic IL, 1-vinylimidazole and 10-bromodecanoic acid were mixed (1:1 molar ratio) in purified tetrahydrofuran at 80 °C during 72 h. The solvent was removed under vacuum at 60 °C, the product was washed 4 times with diethyl ether and dried in a vacuum oven at 40 °C for 24 h. Then, it was dissolved in 10 mL of a mixture of methanol and water (90:10, v/v) and loaded into an Amberlite IRN 78 column (in the hydroxide form). After that, 200 mL of a methanol and water mixture (90:10, v/v) were

passed through the column until no precipitation was observed using the silver nitrate test. The solvents were removed under low vacuum at 60 °C and the obtained [$VIm^+C_9COO^-$] was finally dried in a vacuum oven at 40 °C for 24 h.

The dicationic ILs used as crosslinker agents were: 1,12-di(3-vinylimidazolium)dodecane bromide ([$(VIm)_2C_{12}^{2+}$]2[Br^-]), 1,12-di(3-vinylimidazolium)dodecane bis[(trifluoromethyl)sulfonyl]imide ([$(VIm)_2C_{12}^{2+}$]2[NTf_2^-]), and 1,12-di(3-vinylbenzylimidazolium)dodecane bis[(trifluoromethyl)sulfonyl]imide ([$(VBIm)_2C_{12}^{2+}$]2[NTf_2^-]). The synthesis was carried out following reported procedures [12,13], and are illustrated in Figure III.4.

The IL [$(VIm)_2C_{12}^{2+}$]2[Br^-] was synthesized by reacting 1-vinylimidazole and 1,12-dibromododecane (2:1 molar ratio) in isopropanol at 70 °C for 24 h. The solvent was removed under vacuum at 60 °C, the product was then dissolved in water and extracted 5 times using ethyl acetate. The solvent was evaporated under vacuum at 80 °C and the final product was dried at 70 °C for 24 h using reduced pressure conditions. The [$(VIm)_2C_{12}^{2+}$]2[NTf_2^-] IL was obtained by a metathesis exchange reaction using the previously prepared bromide dicationic IL and following the same procedure as for the IL monomers. Finally, the [$(VIm)_2C_{12}^{2+}$]2[NTf_2^-] IL was filtered and dried in a vacuum oven at 70 °C for 24 h.

In the case of ([$(VBIm)_2C_{12}^{2+}$]2[NTf_2^-]), imidazole was mixed with acrylonitrile (1:1 molar ratio) in methanol at 45 °C for 5 h and under nitrogen atmosphere. The methanol was removed under vacuum and the product was then reacted with 1,12-dibromododecane (2:1 molar ratio) in isopropanol at 70 °C for 24 h. The solvent was evaporated under reduced pressure conditions, and the solid was dissolved in water followed by washing with ethyl acetate 5 times and chloroform 6 times. Water was removed and the dicationic IL with acrylonitrile functionality was reacted with a NaOH solution (15 %, w/v) overnight (16 h) at room temperature. Chloroform was used to extract the product, which was then washed with water until neutral pH. Next, chloroform was removed under vacuum, and the resulting compound was mixed with 4-vinylbenzyl chloride in chloroform at room temperature overnight (16 h) to obtain 1,12-di(3-vinylbenzylimidazolium)dodecane bromide ([$(VBIm)_2C_{12}^{2+}$]2[Br^-]). This IL was dissolved in water and washed with ethyl acetate 5 times and then the metathesis exchange reaction was carried out as described above for the previous dicationic ILs. Finally, the [$(VBIm)_2C_{12}^{2+}$]2[NTf_2^-] IL was collected and dried at 70 °C for 24 in a vacuum oven.

Dicationic IL – $[(VIm)_2C_{12}^{2+}]2[Br^-]$

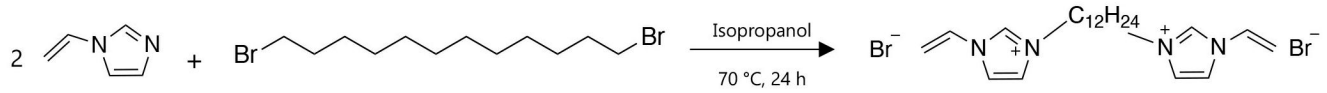

Dicationic IL – $[(VIm)_2C_{12}^{2+}]2[NTf_2^-]$

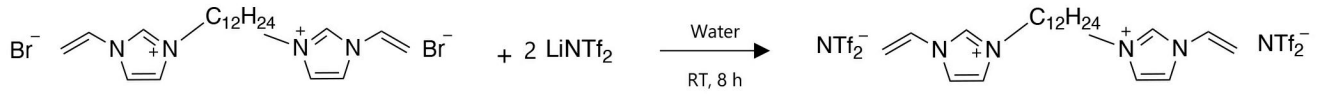

Dicationic IL – $[(VBIm)_2C_{12}^{2+}]2[NTf_2^-]$

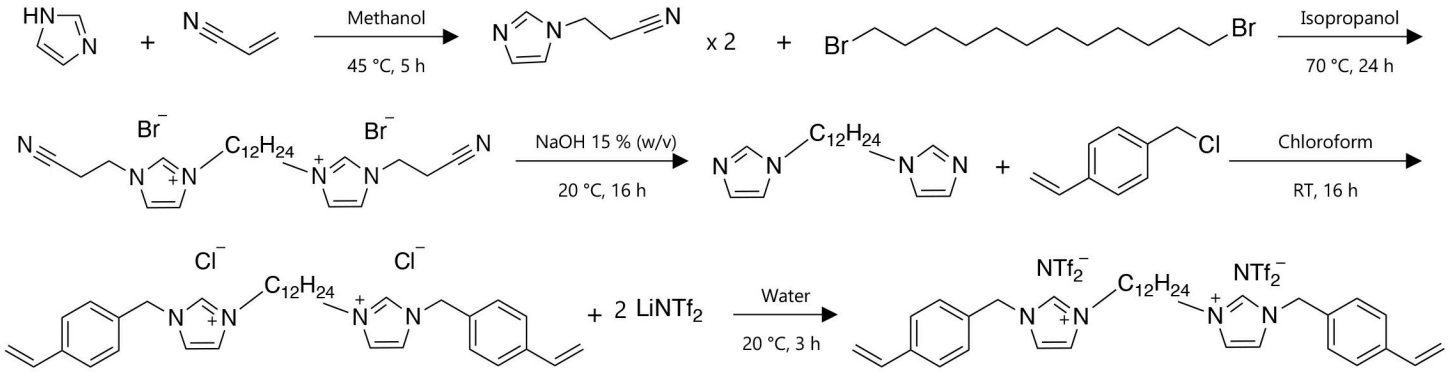

Figure III.4. Schemes of the synthetic procedures followed in the preparation of dicationic ILs, used as crosslinkers in all SPME PILs-based coatings developed in this Doctoral Thesis.

7.1.3. Synthesis and preparation of PILs-based coatings

The PILs-based SPME fibers, used in this Doctoral Thesis, were prepared following the on-fiber UV copolymerization method published by Ho *et al.* [14], which is shown in Figure III.5. The composition and sizes (length × thickness of the coating) of the prepared fibers are listed in Table III.2. Prior to copolymerization, the surface of the nitinol wire used as core was modified to ensure a chemical linkage between the support and the PIL. First, the wire was immersed in a solution of hydrogen peroxide (30 %, w/w) for 2 h at 72 °C to oxidize the surface and to create active hydroxyl groups. Then, the fiber was reacted with VTMS for 2 h at 85 °C to functionalize the support with free vinyl groups. The derivatized nitinol wires were glued in a commercial blank SPME assembly (gluing the top part of the nitinol wire to the blank support) and afterwards 1 cm (free of glue) was exposed for its coating.

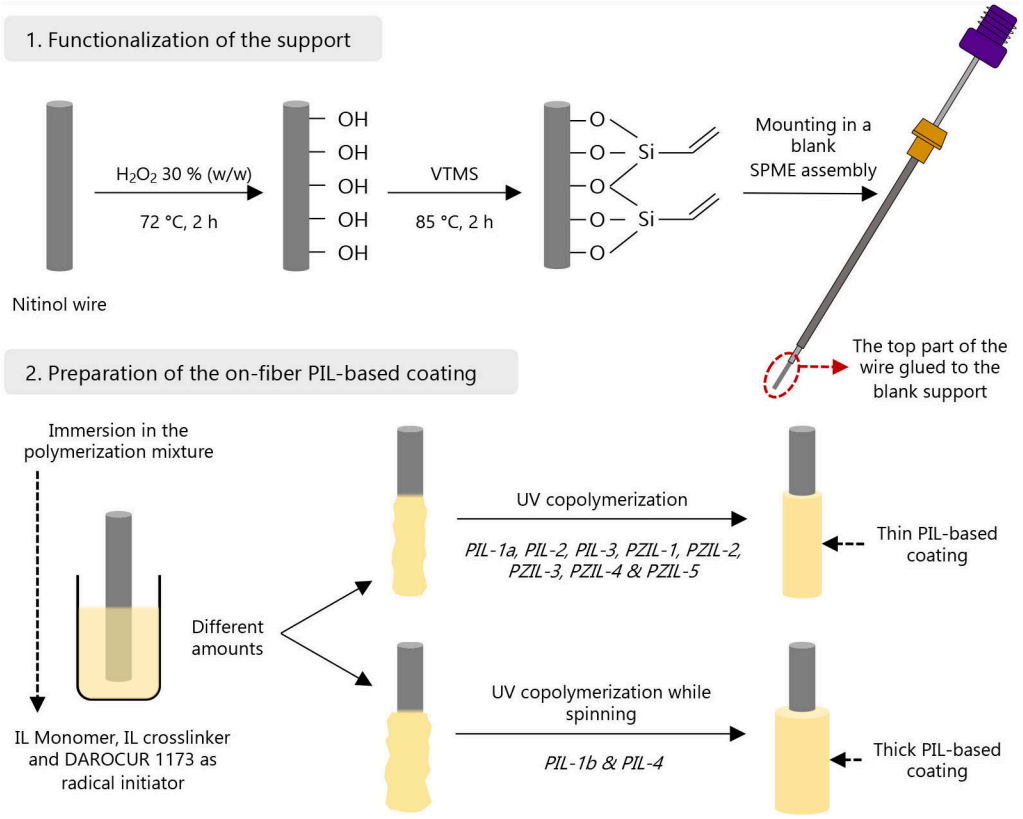

Figure III.5. General scheme of the procedures followed in the preparation of all on-fiber PILs-based SPME coatings used in this Doctoral Thesis.

The copolymerization process was directly carried out on the modified support. First, the IL monomer and the IL crosslinker were mixed at different mass ratios (w/w) depending on the composition of the fiber (see Table III.2). Thus, the mass ratio was 1:0.5 for PIL-1a, PIL-1b, PIL-2, PIL-3 and PIL-4, while a 1:1 mass ratio was used for PZIL-1, PZIL-2, PZIL-3, PZIL-4 and PZIL-5. The free radical initiator DAROCUR 1173 was added to the mixture at 3 % (w/w) respect to the IL monomer for the first batch of SPME fibers, and at 5 % (w/w) when using zwitterionic ILs as monomers (from PZIL-1 to PZIL-5). Then, the nitinol wires were dip-coated using this mixture and subjected to UV radiation for 2 h in the reactor at different wavelengths depending on the anion of the ILs: 254 nm for halide-based PILs and 360 nm for [NTf_2^-]-based PILs. In the case of PIL-1b and PIL-4, the fibers were spin-coated using a high-speed motor at 1200 min^{-1} during the UV copolymerization to obtain thicker coatings. Finally, the PILs-based fibers were conditioned using different approaches depending on the type of desorption used for each fiber. Thus, PIL-1a, PIL-1b, PIL-2, PIL-3 and PIL-4 were immersed in 50 µL of methanol for 30 min, whereas the PILs with zwitterionic monomers were placed in the GC inlet under a nitrogen flow for 30 min at 175 °C for PZIL-1, PZIL-3 and PZIL-4 and 200 °C for PZIL-2 and PZIL-5.

The preparation of the PILs-coated in-tube SPME devices CAP-1 and CAP-2 (see Table III.2) comprised two steps, as it is depicted in Figure III.6. First, the lumen of the silica capillaries (2 m) was treated with NaOH 1 M (10 mL) to expose the hydroxyl groups by passing the solution through the capillaries using a plastic syringe. The capillaries were then washed with water, treated with HCl 1 M (3 mL) to remove the excess of base, followed by additional washing steps with water and acetonitrile to remove the HCl solution. Then, the inside of the capillaries was dried with air for 30 min and one of the ends was sealed with silicon rubber, while the opposite end was used to fill the capillary with VTMS using a plastic syringe. Then, this end was also sealed, and the capillary was placed inside an oven at 80 °C for 3 h to functionalize the internal walls with free vinyl groups. Afterwards, the excess of VTMS was removed by passing 5 mL of methanol through the capillary.

In the second step, the PILs-based coatings were prepared by thermal copolymerization. The reaction solution was prepared by dissolving the IL monomer and IL crosslinker (1:0.5 mass ratio) in methanol, followed by the addition of an AIBN solution to get a concentration of the thermal radical initiator of 1 % (mol/mol) respect to the sum of monomer and crosslinker. The vial containing the solution was closed using a crimp cap and it was bubbled with nitrogen for 30 min to remove the air. One end of the capillary was inserted in the polymerization solution by piercing the PTFE/silicone septum of the cap, while the opposite end was inserted in an empty vial for which the air was previously evacuated. The system was placed in the oven at 60 °C for 48 h to accomplish the reaction. The reduced pressure conditions in the vial and high temperature allowed the polymerization solution flowing through the capillary from one vial to the other. Finally, the capillary was washed with methanol to remove the excess of reaction solution and dried at room temperature. The capillaries were cut in several pieces with the desired length, as shown in Table III.2.

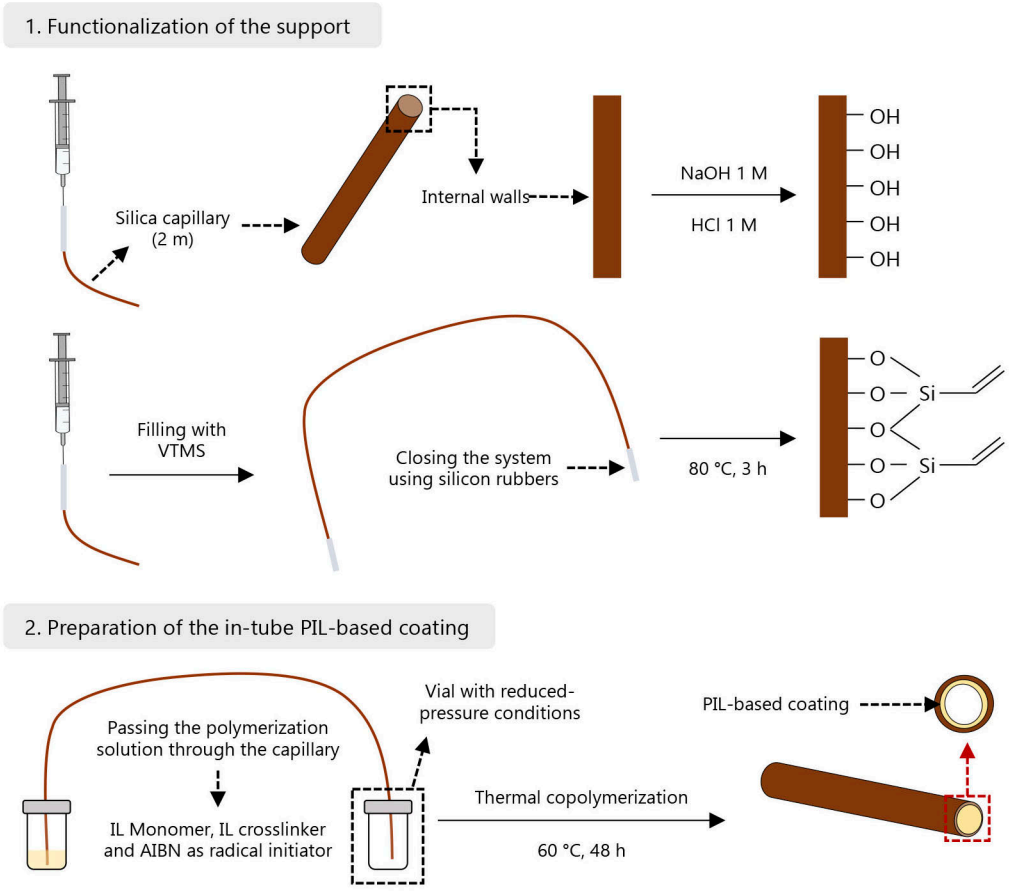

Figure III.6. General scheme of the procedures followed for the preparation of the in-tube PILs-based SPME coatings used in this Doctoral Thesis.

7.2. Synthesis of MOFs and MOF-based coatings

The MOF CIM-80(Al) was synthesized following a protocol previously described in the literature [15]. Briefly, 1 mmol of $Al(NO_3)_3 \cdot 9H_2O$, 1 mmol of mesaconic acid, and 0.5 mmol of urea were mixed in 15 mL of ultrapure water and heated at 150 °C for 3 h in the solvothermal reactor. Then, the white powder was filtered, washed with water several times, and activated at 150 °C overnight in an oven to remove the water molecules from the pores of the MOF.

7.2.1. Preparation of MOF-based fibers

The SPME fiber with the MOF-based coating was fabricated following an *in situ* solvothermal growth approach [16], which is illustrated in Figure III.7. First, the nitinol wires (≈ 3 cm length) used as core were functionalized following a similar approach as for the PILs-based SPME fibers. Briefly, they were immersed in hydrogen peroxide (30%, w/w) for 2 h at 72 °C to oxidize the surface of the alloy and to expose the hydroxyl groups. Then, the wires were immersed in pure APTES at 90 °C for 24 h to functionalize their surface with amino groups. The derivatized nitinol fibers were placed in a solution containing the MOF precursors to accomplish the *in situ* growth of CIM-80(Al) following the protocol described above (see Section III.7.2). Once the MOF was directly synthesized on the surface of the wires, the fibers were washed with water and ethanol several times to remove the excess of the initial reagents. Finally, 1 cm of the already coated fibers were mounted in blank SPME assemblies and conditioned in the GC inlet under nitrogen flow at 280 °C for 30 min.

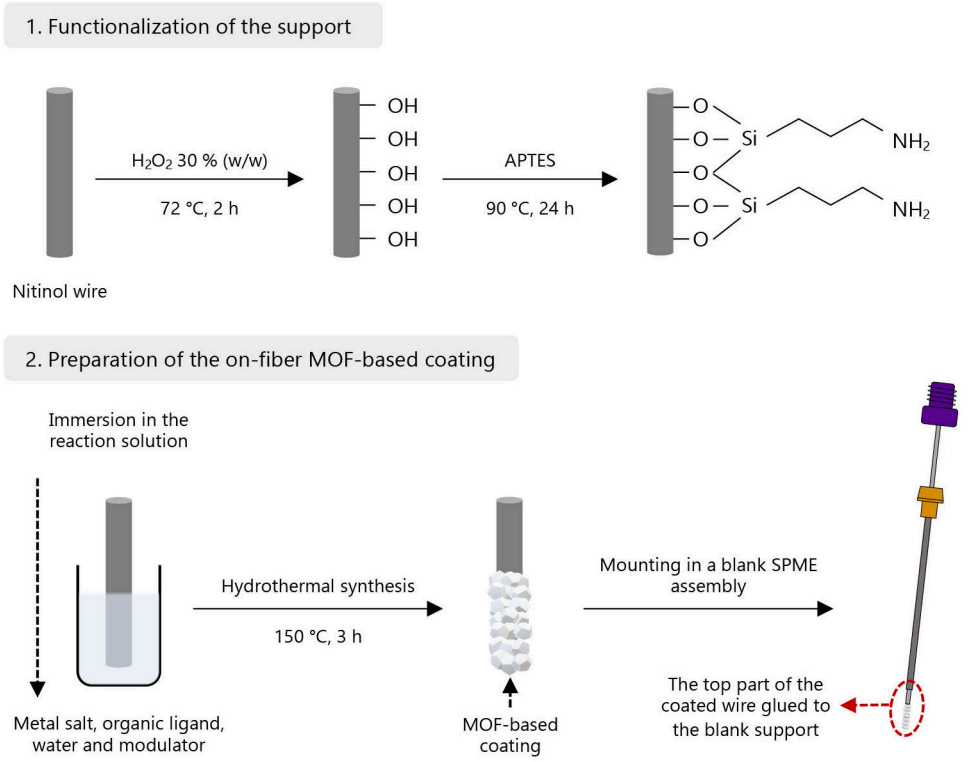

Figure III.7. General scheme of the procedures followed for the preparation of the on-fiber MOF-based SPME coating used in this Doctoral Thesis.

7.3. Synthesis of the complexing agent for the extraction of metal ions

The Schiff base *N,N*-bis(salicylidene)thiocarbohydrazide (BSTC) was prepared following a previous method reported in the literature [17]. Briefly, 2 mmol of thiocarbohydrazide were dissolved in 10 mL of ethanol. Then, the mixture was added dropwise to 20 mL solution of ethanol containing 4.4 mmol salicylaldehyde. The mixture was refluxed under constant stirring at 70 °C for 3 h. Finally, the product was purified by recrystallization in ethanol, resulting in light yellow crystals. The ^{1}H-NMR spectrum matched with the signals previously reported in the literature [17].

7.4. Characterization of the materials and SPME coatings

All the synthesized ILs and the complexing reagent were characterized by ^{1}H-NMR, while the adequate synthesis of the MOF CIM-80(Al) was evaluated by PXRD. Furthermore, the decomposition temperature and the adsorption characteristics of the MOF were determined by TGA and nitrogen adsorption measurements. In the last case, the specific surface area was calculated using the Brunauer, Emmett and Teller (BET) method with a single point reference. Other specific properties of the individual materials and the SPME devices were also determined and are described in the following subsections.

7.4.1. Determination of CMC of IL-based surfactants

The CMCs of the guanidinium ILs $[C_8Gu^+][Cl^-]$ and $[C_{10}Gu^+][Cl^-]$ were determined by fluorescence measurements following the procedure reported in a previous study [18]. Pyrene was used as fluorescent probe at a constant concentration of 161.8 mg·L^{-1}. 5 mL aqueous solutions containing pyrene and increasing concentrations of the IL-based surfactant were prepared. Concentrations ranging from 0.05 to 80 mM were used for $[C_8Gu^+][Cl^-]$ and from 0.03 to 58 mM for $[C_{10}Gu^+][Cl^-]$. The emission spectrum was registered in the range of 350–450 nm for each solution using 335 nm as excitation wavelength, and 2.5 nm as excitation and emission slit widths. The intensities of I1 and I3 bands of pyrene spectrum were measured at 373 nm and 383 nm, respectively. The effect of the ionic strength on the micellar behavior was also evaluated for each IL-based surfactant. Thus, the abovementioned IL solutions were prepared but containing different amounts of NaCl (from 5 to 25 %, w/v) and the fluorescence measurements were performed.

The CMC of the $[C_8Gu^+][Cl^-]$ was also determined by conductivity studies. 10 mL of IL-based surfactant aqueous solutions in ultrapure water were prepared at concentrations ranging from 5 to 100 mM. The solutions were properly shaken to ensure homogeneity and immersed in the thermostatic bath at 25 ± 1 °C before each measurement. The conductivity cell was calibrated using KCl standard conductivity solutions of 147 μS·cm^{-1} and 1413 μS·cm^{-1}, and then immersed in the IL-based surfactant solution. The measurements were performed in duplicate and the average conductivity value was calculated.

7.4.2. Cytotoxicity studies of ILs

The cytotoxicity of several ILs was evaluated using the macrophage J774A.1 murine macrophage cell line. Two different tests were performed with the cultured cells at a density of ≈ 10^5 cells·mL^{-1}. The estimation of the cell density was carried out with an image cytometer.

For the Alamar Blue® cell viability assay, the procedure described in the literature was followed [19]. Briefly, 50 µL of the stock solution of the cells were incubated with 50 µL of aqueous solutions of the ILs at different concentrations in 96-well plates. Subsequently, the AlamarBlue® reagent was added to the wells at 10 % (v/v) respect to the total volume of the well, and the plates were incubated for 24 h at 37 °C. Negative controls were also prepared by adding 50 µL of RPMI media instead of the IL solution. Then, the plates were analyzed with the microplate reader at 570 nm and using 630 nm as reference wavelength. Dose-response curves were plotted, and the 50 % cytotoxic concentration (CC_{50}) was determined by linear regression analysis with a 95 % confidence level. All experiments were performed in triplicate and the mean values were calculated.

Additionally, the LDH cytotoxicity test was used to evaluate the cytotoxicity of several IL-based surfactants and conventional surfactants. It was performed according to the manufacturer's instructions. In this case, 250 µL of the cells culture were transferred in a 24-well plate and appropriate volumes of concentrated aqueous solutions of the surfactants and the culture medium (final volume of 500 µL in each well) were added to obtain the desired concentration: half of the CMC value for each surfactant. After 24 h of incubation at 36 °C, 100 µL of each well supernatant were transferred to a 96-well plate and the kit reagents (iodotetrazolium chloride (INT) and catalyst) were added. The plate was then incubated for 30 min at 20 °C and protected from light. The absorbance was measured at 490 nm using the microplate reader and with a reference wavelength of 630 nm. The measurements of the supernatant were made in duplicate, while the overall experiments were performed in triplicate in 3 non-consecutive days. The cytotoxicity percentage was determined using the following equation:

$$\text{Cytotoxicity (\%)} = \frac{\text{target substance} - \text{negative control}}{\text{positive control} - \text{negative control}} \cdot 100 \qquad \text{Equation III.1}$$

where the values are the absorbance at 490 nm minus the absorbance at 630 nm, with the target substance referring to the experiments with each surfactant concentration, the positive control being the values using a solution of Triton X-100 at 2 % (v/v), and the negative control corresponding to experiments using the culture medium without any additive. Therefore, the cytotoxicity values obtained with this test are relative values considering the positive control as 100 % of cytotoxicity, and the negative control as 0 % of cytotoxicity. The results were classified based on parameters previously established: percentages of cytotoxicity between 0 and 10 % are not cytotoxic, values between 10 and 25 % correspond to low cytotoxicity, values between 25 and

40 % are equivalent to moderate cytotoxicity, and values of at least 40 % indicate high cytotoxicity [20].

7.4.3. Phase diagrams of IL-based µ-ABSs

Phase diagrams of the $[C_4Gu^+][Cl^-]$ and $[C_6Gu^+][Cl^-]$ IL-based µ-ABSs were determined following the volumetric procedure described in the literature [21]. Briefly, 65.0 µL of the IL were dissolved in 1 mL of ultrapure water in a centrifuge tube. A solution of K_3PO_4 (42.9 %, w/w) was added dropwise from a burette until turbidity was observed, which corresponds to the formation of two phases. Then, ultrapure water was added until the turbidity disappeared. The addition of the K_3PO_4 solution and subsequent addition of water were carried out successively to obtain all the points of the phase diagram. During all the procedure, the system was in constant stirring using a stir bar, while the temperature was kept at 25 °C using a thermostatic water bath.

7.4.4. Stability of MOFs in complex matrices

The stability of the MOF CIM-80(Al) was evaluated in different matrices (Section IV.2.2.1). In these experiments, 100 mg of the activated MOF powder were immersed in 100 mL of deionized water, hot deionized water (100 °C, under reflux), tap water, diluted urine (1:10 with ultrapure water), diluted coffee (1:10 with ultrapure water), white and red wine, whole milk, and apple juice. The dispersions were kept at room temperature for 24 h and for 10 days, except for hot deionized water, which was only assessed for 24 h. After this time, the MOF powder was filtered, dried at 50 °C and analyzed by PXRD.

7.4.5. Characterization of SPME coatings

SPME fibers and capillaries were characterized by SEM to evaluate their morphology, uniformity, and to estimate the thickness of the coating (Sections IV.2.1.1 and IV.2.2.1). The thicknesses were calculated by averaging the values measured for different sections of the devices after cutting them in several pieces. Moreover, in the case of the MOF-based coating, the SPME fiber was also characterized by PXRD to verify the adequate synthesis of the MOF on the surface of the coating.

7.5. Analytical methods

Different analytical methods were developed in this Doctoral Thesis depending on the material used as extraction phase, the target analytes, and the samples analyzed. Table III.3 and Table III.4 summarize the methodologies and applications developed based on LPME and SPME techniques, respectively. This section includes the optimized conditions for each of those analytical

methods, while the different conditions evaluated during the optimization studies are detailed in the corresponding section of Chapter IV.

7.5.1. *In situ* IL-DLLME in combination with HPLC-DAD for the determination of PCPs

This method was developed using the IL-based surfactant $[C_8Gu^+][Cl^-]$ for the determination of PCPs in cosmetic samples, while using ultrapure water during the optimization and validation studies (Section IV.1.1.2).

Prior to the microextraction method, an aliquot of the IL was heated at 50 °C for 30 s to reduce its viscosity and to facilitate its handling. Then, under optimum conditions, 30 µL of $[C_8Gu^+][Cl^-]$ were added to 10 mL of aqueous standard containing 8 % (w/v) of NaCl at pH 5, adjusted using a sodium acetate/acetic acid buffer solution. The tube was manually shaken for 15 s to disperse the IL, which was at a concentration close to its CMC (≈ 14.8 mM) at that ionic strength. Next, 45 µL of Li-NTf_2 aqueous solution (1 $g \cdot mL^{-1}$) were added to the sample as anion exchange reagent, and a turbid solution was observed due to the metathesis reaction. The solution was shaken using vortex for 3 min and then centrifuged for 5 min at 1921 × g to obtain a microdroplet (21 ± 1 µL, n = 20) of water-insoluble IL containing the preconcentrated analytes. The microdroplet was collected with a syringe and diluted up to 60 µL with acetonitrile in a 2 mL glass vial before its injection in the HPLC-DAD system.

With respect to the assessment of matrix effect, matrix-matched calibrations were obtained using diluted aqueous solutions of facial tonic 1 (free of PCPs), which were prepared by diluting 50 µL of the sample to 10 mL with ultrapure water. For the analysis of cosmetic samples, appropriate volumes of the facial tonics (labelled in the commercial brands as containing PCPs) were diluted up to 100 mL with ultrapure water under the optimum conditions (at pH 5 and containing 8 % (w/v) of NaCl). Then, 10 mL of the diluted sample were subjected to the procedure described above.

The analytical separation of the studied PCPs by HPLC-DAD was carried out using acetonitrile and ultrapure water as mobile phases at a flow rate of 1 $mL \cdot min^{-1}$. The separation gradient started at 30 % (v/v) of acetonitrile, which was held for 11 min and then increased to 50 % (v/v) for 2 min, being held for 6 min. Then it was increased to 100 % (v/v) in 5 min, and finally kept at this value for 3 additional min. The quantification wavelength was 254 nm for MePa, EtPa, PPa, iPPa and BP, and 289 nm for BP3.

Table III.3. General characteristics of the analytical methods developed in this Doctoral Thesis based on LPME with ILs as extraction solvent.

Microextraction method	IL as extraction solvent	Insolubilization agent	Analytical technique	Analytes	Sample	Section
In situ IL-DLLME	$[C_8Gu^+][Cl^-]$	Li-NTf_2 as anion exchange agent	HPLC-DAD	PCPs	Facial tonic	IV.1.1.2
In situ IL DLLME	$[C_{10}Gu^+][Cl^-]$	Li-NTf_2 as anion exchange agent	FAAS	Cu (II) and Cd (II)	CRM and Tap water	IV.1.1.3
	$[C_{16}C_4Im^+][Br^-]$	Li-NTf_2 as anion exchange agent	FAAS	Cu (II)	Ultrapure water (comparison purposes)	IV.1.1.3
In situ IL-DLLME	$[C_{10}Gu^+][Cl^-]$	$NaClO_4$ as anion exchange agent	HPLC-FD	OH-PAHs	Urine	IV.1.2.1
µ-ABS	$[C_4Gu^+][Cl^-]$	K_3PO_4 as salting-out agent	HPLC-FD	PAHs	Tap water, seawater and wastewater	IV.1.2.2

Table III.4. General characteristics of the analytical methods developed in this Doctoral Thesis based on SPME with PILs and MOFs as extraction phase.

Microextraction method	New extraction phase	Commercial extraction phase	Analytical technique	Analytes	Sample	Section
On-fiber DI-SPME	PIL-1a PIL-2 PIL-3	PA & PDMS/DVB	HPLC-UV-Vis	mix of organic compounds	River and tap water	IV.2.1.2
On-fiber DI-SPME	PIL-1b PIL-4	PA	HPLC-DAD	alkylphenols	Tap water	IV.2.1.2
On-fiber HS-SPME	PZIL-1 PZIL-2 PZIL-3 PZIL-4 PZIL-5	CAR/PDMS & PA	GC-MS	SCFFAs	Wine	IV.2.1.3
In-tube SPME	CAP-1 CAP-2	–	HPLC-UV-Vis	DNA	Standard solution	IV.2.1.4
On fiber HS-SPME & DI-SPME	CIM-80(Al)	PDMS	GC-MS	PAHs	Water, urine and brewed coffee	IV.2.2.2

7.5.2. *In situ* IL-DLLME in combination with FAAS for the determination of metal ions

The analytical method was developed using the IL-based surfactants $[C_{10}Gu^+][Cl^-]$ and $[C_{16}C_4Im^+][Cl^-]$ for the determination of metal ions in water samples and using ultrapure water during the optimization and validation studies (Section IV.1.1.3).

Under optimum conditions, the method required 10 mL of aqueous standard or sample containing 30 $g \cdot L^{-1}$ or 28 $g \cdot L^{-1}$ of NaCl when $[C_{10}Gu^+][Cl^-]$ or $[C_{16}C_4Im^+][Cl^-]$ were used, respectively. 500 µL of acetone containing 200 $mg \cdot L^{-1}$ of the complexing agent BSTC were added, which resulted in a final BSTC concentration in solution of 10 $mg \cdot L^{-1}$. Then, the tube was manually shaken for 3 s to ensure the formation of the metal complex. In the case of $[C_{10}Gu^+][Cl^-]$, 25 µL of the IL (resulting concentration of 11 mM in the sample) were added followed by a pH adjustment to 8.2, and the addition of 65 µL of Li-NTf_2 aqueous solution (0.5 $g \cdot mL^{-1}$) to accomplish the metathesis reaction. For the $[C_{16}C_4Im^+][Cl^-]$, the pH of 10 mL of water containing the IL-based surfactant at 10 mM was fixed to 6.8, and 60 µL of Li-NTf_2 aqueous solution (0.5 g mL^{-1}) were added. After that, the tubes were shaken by vortex stirring for 2 min to facilitate the metathesis reaction, and then centrifuged at 1921 × g for 2 min to obtain a microdroplet that contains the preconcentrated metal ions. The volumes of the microdroplets were 21 ± 2 µL (n = 20) for $[C_{10}Gu^+][NTf_2^-]$ and 39 ± 1 µL (n = 20) for $[C_{16}C_4Im^+][NTf_2^-]$. The microdroplet was collected from the bottom of the tube using a syringe and diluted with acetonitrile up to 120 µL in an Eppendorf tube. Finally, two aliquots of 50 µL of this diluted microdroplet were transferred to different Eppendorf tubes for the individually determination of Cu (II) and Cd (II) by FAAS.

Each fraction of the diluted microdroplet were introduced in the FAAS system by direct aspiration during 8 s using a propylene microtube. The area of the peak obtained in the transitional measurement was used for the quantification instead of the average absorbance. Both Cu (II) and Cd (II) were determined under a stoichiometric flame using a high purity acetylene flow of 1.5 $L \cdot min^{-1}$ and an air flow of 3.5 $L \cdot min^{-1}$. Premix burner was used with standard length of 10 cm. The lamp current was fixed at 4.0 mA and the gain varied between 27 and 30 %. The wavelengths used to measure the absorbance were 324.8 and 228.8 nm for Cu (II) and Cd (II), respectively.

7.5.3. Salt-induced IL-DLLME in combination with HPLC-FD for the determination of OH-PAHs

The method was developed using the IL-based surfactant $[C_{10}Gu^+][Cl^-]$ for the determination of OH-PAHs in urine samples using synthetic urine during the optimization, while both synthetic and real urine were used for the validation studies (Section IV.1.2.1).

The microextraction method under optimum conditions required the dilution of 1 mL of synthetic or real urine to 10 mL with ultrapure water, which was then spiked or not with the OH-PAHs depending on the experiment. For the analysis of real urine samples, they were previously subjected to the hydrolysis procedure described in Section III.3. Next, 20 µL of the $[C_{10}Gu^+][Cl^-]$ IL-

based surfactant were added to the sample and the tube was manually shaken to dissolve the IL, requiring few seconds. Subsequently, 500 µL of an aqueous solution of $NaClO_4$ at 100 % (w/v) were added, which resulted in a final concentration in the tube of 5 % (w/v) and the formation of a turbidity due to the insolubilization of the IL. The tube was stirred using vortex for 4 min, followed by centrifugation for 8 min at 2504 × g to obtain a microdroplet of 12.3 ± 0.9 µL (n = 20) of the IL containing the preconcentrated OH-PAHs. The microdroplet was collected using a syringe and diluted up to 60 µL in a 2 mL glass vial using the initial mobile phase composition of the HPLC method before its injection in the HPLC-FD system.

The HPLC separation of the analytes was carried out using acetonitrile and ultrapure water as mobile phase at a flow rate of 1 $mL \cdot min^{-1}$. The elution gradient started at 30 % of acetonitrile (v/v), which was increased up to 65 % (v/v) in 15 min, and finally increased to 100 % in 5 min and kept at this value for few additional min to ensure proper washing. The fluorescence detection conditions were fixed considering the maximum excitation (λ_{ex}) and emission (λ_{em}) wavelengths of each analyte and setting the widths slits at 18 nm.

7.5.4. µ-ABS using ILs in combination with HPLC-FD for the determination of PAHs

The µ-ABS-HPLC-FD method was developed with the $[C_4Gu^+][Cl^-]$ IL as extraction phase for the determination of 5 PAHs (Ant, BaAnt, Chry, BaPy, and Ind) in water samples, using ultrapure water for the optimization and validation studies (Section IV.1.2.2) The microextraction procedure using the ILs-based µ-ABS was performed by selecting a point of the biphasic region of the phase diagram, corresponding to a mixture with the following composition: 0.75 % (w/w) of the IL $[C_4Gu^+][Cl^-]$, 37.7 % (w/w) of K_3PO_4 and 61.55 % (w/w) of ultrapure water.

In the method, performed under optimum conditions, 6 mL of aqueous standards of PAHs at different concentrations or 6 mL of water samples were placed in a centrifuge tube. Then, 73.1 µL of the IL were added and the tube was vigorously stirred to ensure complete solubilization. Subsequently, 3.68 g of K_3PO_4 were added and dissolved, and a new IL-rich phase on the top of the aqueous phase was formed. Vortex was applied for 1 min to achieve the adequate dispersion of all the components and then the mixture was subjected to centrifugation for 2 min at 1921 × g to improve the separation among the phases. Then, the system was left for 30 min in order to ensure the equilibrium of the components between both phases. The IL-rich phase on the top of the tube was separated as a microdroplet containing all the analytes. The microdroplet was diluted with 50 µL of the mobile phase in a 2 mL glass vial and directly injected in HPLC.

The chromatographic separation of the analytes was achieved using a mobile phase composed of acetonitrile and ultrapure water at a constant flow of 0.5 $mL \cdot min^{-1}$. The elution gradient started at 85 % (v/v) of acetonitrile and it was increased to 89 % (v/v) in 5 min. Then, the percentage of acetonitrile was increased to 91 % (v/v) in 3 min and then up to 100 % (v/v) in 12 min. Finally, this value was kept for 4 additional min to ensure proper washing. The fluorescence

program used for the detection of analytes was chosen after recording each PAH at their optimal λ_{ex} and λ_{em} to guarantee the maximum sensitivity, while the widths of the emission and excitation slits were kept at 18 nm.

7.5.5. DI-SPME in combination with HPLC-DAD using commercial and PILs-based fibers for the determination of organic pollutants

This method was applied in two different studies: (i) for the determination of a mix of organic compounds as model analytes in waters to evaluate the selectivity of the PILs-based coatings, and (ii) for the determination of alkylphenols in water samples (Section IV.2.1.2). In both cases, the DI-SPME method was manually performed ensuring the same immersion depth, while the desorption was carried out in off-line mode using different amounts of desorption solvents. Then, 20 µL of desorption solvent was injected in the HPLC system. Moreover, after every extraction/desorption cycle, a single cleaning step was carried out in 1.5 mL of methanol for 15 min to avoid carry-over effects. Different PILs-based and commercial SPME fibers were used in this study as it is shown in Table III.4.

In the first application, the fiber was immersed in 10 mL of the aqueous solution containing the mix of organic compounds or in 10 mL of river and tap water samples, for which the pH was adjusted to a value of 2. Then, the extraction was carried out at room temperature for 45 min under a constant agitation rate of 500 min^{-1}. The off-line desorption step was accomplished by immersing the fiber in 50 µL of desorption solvent in a pipet tip. Methanol was the desorption solvent when using all the fibers, except for the commercial PDMS fiber, for which acetonitrile was used.

The HPLC-UV-Vis separation of the mix of organic compounds was accomplished using acetonitrile and water containing 0.1 % (v/v) of acetic acid at a flow rate of 1 $mL{\cdot}min^{-1}$. The separation gradient began at 50 % (v/v) of acetonitrile and was increased to 90 % (v/v) in 25 min. The UV detection was accomplished at 254 nm for the entire group of analytes.

With respect to the determination of alklyphenols, 18 mL of aqueous standards or tap water samples at pH 2 were required. The DI-SPME method was also performed at room temperature and under magnetic stirring at 500 min^{-1} during 45 min for the PIL-4 and PA fibers, and 60 min for PIL-1b. The fiber was then immersed in 250 µL of methanol using glass inserts placed inside 2 mL vials during 5 min for PIL-4 and PA fibers, and 15 min for PIL-1b coating.

For the determination of alkylphenols, acetonitrile, and ultrapure water containing 0.4 % (v/v) of acetic acid, were used as mobile phase at a flow rate of 1 $mL{\cdot}min^{-1}$. The separation gradient employed started at 50 % (v/v) of acetonitrile and was then increased to 100 % (v/v) for 5 min, being finally held for 3 additional min. The quantification wavelength was 280 nm.

7.5.6. HS-SPME in combination with GC-MS using commercial and PILs-based fibers for the determination of SCFFAs

A HS-SPME method was developed for the quantification of SCFFAs in a red wine sample and using different SPME coatings (Section IV.2.1.3). Several PILs-based and commercial SPME fibers were evaluated in this study, as listed in Table III.4. The method was optimized using ultrapure water, the validation was carried out using both ultrapure water and synthetic wine, and the analysis of red wine was performed by the standard addition method.

HS-SPME extractions were manually performed using 10 mL of aqueous standards of SCFFAs containing 30 % (w/v) of NaCl. For evaluating the effect of the organic solvent on the extraction efficiency, 1.3 % (v/v) of ethanol was also added to the solution. In the case of synthetic and real wine, 1 mL was diluted up to 10 mL with ultrapure water and the pH was adjusted to a value of 3. The fiber was exposed to the headspace of the solution (always at the same depth inside the HS of the vial) at 65 °C for 20 min when using PZIL-1, 40 min with PA, and 60 min for PZIL-4 and CAR/PDMS fibers. The stirring rate was fixed at 600 min^{-1}. After extraction, the SCFFAs were thermally desorbed in the GC inlet under different conditions depending on the fiber: 4 min at 175 °C for PZIL-1, 2 min at 175 °C for PZIL-4, 2 min at 290 °C for CAR/PDMS, and 4 min at 280 °C for PA. The desorption temperature used for the remaining PZIL fibers (Table III.2) during the screening study was fixed depending on the anion of the IL crosslinker: 175 °C for fibers containing [Br^-] anions, and 200 °C for the coatings composed of [NTf_2^-] anions. All the fibers were conditioned at their corresponding temperature in the GC injector for 15 min every day prior use. Blank extractions using ultrapure water were performed between samples during the analysis of red wine to avoid carry-over.

The extraction mechanism of PZIL-1 and PZIL-4 fibers in the HS-SPME method was evaluated according to previously reported methods [22,23]. The SCFFAs *i*-C_4 and *n*-C_7 were selected as the target and the interfering compounds, respectively. In this case, 1 mL of synthetic wine was diluted to 10 mL using ultrapure water and HS-SPME experiments were performed under the optimum conditions described above. Calibration curves of *i*-C_4 were constructed in the presence of two relative concentrations of *n*-C_7 with respect to *i*-C_4 (1:1 and 10:1 ratio).

The GC-MS determination was carried out using ultrapure helium as carrier gas at a flow rate of 1 $mL \cdot min^{-1}$. The inlet was operated in splitless mode at different temperatures depending on the SPME fiber. The following temperature oven program was employed: 2 min at 80 °C, then the temperature was increased to 100 °C at 25 $°C \cdot min^{-1}$, followed by an increase at 10 $°C \cdot min^{-1}$ up to 240 °C, and finally held for 2 min. The MS employed electron ionization (EI) at 70 eV and was used in gain factor mode. The transfer line temperature was set at 250 °C, while the source and quadrupole temperatures were fixed at 230 °C and 150 °C, respectively. Data was acquired in selected ion monitoring (SIM) mode, and the identification of the SCFFAs was accomplished considering the retention time, the presence of quantifier and qualifier ions for each analyte, and

the ratio between those ions. The peak area of the quantifier ion was used for the quantification of the compounds.

7.5.7. In-tube SPME in combination with HPLC-UV using PILs-based coatings for the extraction of DNA

The in-tube SPME method for the extraction of DNA was performed by the draw/eject mode and using two different approaches: (i) manual operation and (ii) fully automated operation (Section 2.1.4). CAP-1 and CAP-2 PILs-coated capillaries were used in the manual approach (Table III.2), while only CAP-2 was evaluated in the fully automated method. The different steps of the procedure (extraction, washing, desorption and regeneration) were optimized for both methods using a DNA standard solution at 5 $mg \cdot L^{-1}$ as working solution.

In the manual set-up, 15 cm of the capillaries were coupled to a gas tight syringe using a GlasSeal™ connector and the DNA and desorption solutions were kept in Eppendorf tubes. The flow during the draw and eject steps was manually controlled, being approximately 600 $\mu L \cdot min^{-1}$. First, 350 µL of sample were drawn and ejected 4 times to the same Eppendorf tube, followed by 1 draw/eject cycle of 100 µL of 1X TE buffer for the washing step. The desorption was carried out using 50 µL of NaCl 1 M and 10 and 15 draw/eject cycles for CAP-1 and CAP-2, respectively. Finally, 2 cycles of 250 µL of NaCl 1 M and 2 cycles of 250 µL of ultrapure water were required between extractions to avoid carry-over. 20 µL of the desorption solution were injected in the HPLC-UV system for the DNA determination.

For the automated method, a portion of 55 cm of the CAP-2 capillary was placed between the loop and sampling needle of a HPLC autosampler using stainless steel connections and PEEK tubing to avoid leaks. This set-up allows performing all the steps of the procedure using the autosampler by designing the injection sequence in the software. Therefore, the DNA and washing solutions were placed in 2 mL glass vials. In this case, a total sample volume of 1 mL was required but only 100 µL of sample were drawn and ejected to the same vial for 20 cycles at a controlled flow of 200 $\mu L \cdot min^{-1}$. The washing step was set as 1 cycle with 100 µL of 1X TE buffer, followed by the desorption step, which was carried out on-line by passing the initial mobile phase through the capillary for 5 min. After this time, 2 cycles of 100 µL of NaCl 1 M and 2 cycles of 100 µL of ultrapure water were used to avoid carry-over.

The DNA determination was carried out by HPLC-UV using an anion-exchange column and two buffers as mobile phase: buffer A containing 20 mM of Tris-HCl at pH 8, and buffer B containing 20 mM of Tris-HCl and 1 M of NaCl at pH 8. The elution program started at 50 % (v/v) of Buffer B, which was increased to 100 % (v/v) in 10 min at a flow rate of 1 $mL \cdot min^{-1}$. The detection wavelength was fixed at 260 nm.

7.5.8. HS- and DI-SPME in combination with GC-FID and GC-MS using commercial and MOF-based fibers for the determination of PAHs

The commercial PDMS and MOF-based SPME fibers were used for the development of both HS- and DI-SPME methods for the determination of 13 PAHs in water, urine and brewed coffee (Section IV.2.2.2). The methods were optimized with each fiber using ultrapure water standards with 8 representative PAHs (Nap, Acy, Ace, Flu, Phe, Ant, Flt, and Py) and in combination with GC-FID. The validation studies in combination with GC-MS were performed in ultrapure water as well as in the real matrices by matrix-matched calibrations and for 13 PAHs (Nap, Acy, Ace, Flu, Phe, Ant, Flt, Py, BaAnt, Chry, BbFlt, BkFlt, and BaPy).

HS-SPME extractions were carried out using 10 mL of aqueous standards, spiked urine or spiked brewed coffee at a fixed stirring rate of 300 min^{-1}, while the ionic strength was adjusted to 20 % (w/v) using NaCl. The fiber was exposed to the headspace for 60 min at 55 °C when using PDMS, and at 75 °C for the MOF-based coating. The thermal desorption was accomplished by placing the fiber in the GC inlet at 280 °C during 4 min for the MOF-based fiber and 6 min in the case of the PDMS coating. In the screening study using several commercial fibers, the desorption temperatures were 270 °C for DVB/CAR/PDMS and 310 °C for CAR/PDMS fibers.

For the DI-SPME procedure under optimum conditions, 19 mL of aqueous standards, spiked diluted urine or spiked diluted brewed coffee (1:1 with ultrapure water) were required. The fiber was immersed in the solution for 60 min at 50 °C and with a stirring rate of 300 or 700 min^{-1} for the MOF-based and PDMS fibers, respectively. The PAHs were desorbed in the GC inlet at 280 °C for 4 min using the CIM-80(Al) coating, and for 2 min with the PDMS fiber.

In all cases, the organic solvent content of the working solutions was fixed at 0.5 % (v/v) using acetonitrile. All the fibers were conditioned at their corresponding temperature in the GC inlet for 15 min every day prior use. After every desorption step, the fibers were reconditioned for 5 min at their desorption temperature to avoid carry over. Moreover, in the DI-SPME experiments with real samples, the MOF-based fiber was immersed in 19 mL of ultrapure water for 2 min followed by a thermal conditioning at 280 °C for 5 min after each desorption step to clean and recondition the coating.

During the optimization studies using GC-FID as determination technique, nitrogen at a flow rate of 1 $mL{\cdot}min^{-1}$ was used as carrier gas together with the following temperature program: 60 °C for 2 min, then increased up to 165 °C at 25 $°C{\cdot}min^{-1}$, then to 280 °C at 5 $°C{\cdot}min^{-1}$, holding this temperature for 2 min, and finally increased at 25 $°C{\cdot}min^{-1}$ to 320 °C and kept isothermal for 2 additional min. The GC injection was performed in splitless mode, while the temperature of the injector was fixed at 280 °C for the desorption of the analytes. The temperature of the detector was set at 280 °C, using an air flow of 300 $mL{\cdot}min^{-1}$, hydrogen flow of 30 $mL{\cdot}min^{-1}$, and a nitrogen as make-up gas at 30 $mL{\cdot}min^{-1}$.

The determination of the 13 PAHs during the validation of the methods was accomplished in a GC-MS system with ultrapure helium at 1 mL·min^{-1} as carrier gas. The temperature oven program was the following: 60 °C for 1 min, then increased to 140 °C at 20. °C·min^{-1} and holding this temperature for 8 min, then increased up to 180 °C at 7 °C·min^{-1} and held for 5 min, then increased at 10 °C·min^{-1} to 240 °C and isothermal for 9 min, and finally rose up to 320 °C at 12 °C ·min^{-1}, holding this temperature for 8 additional min. The transfer line was kept at 280 °C, while the source and quadrupole temperatures were fixed at 250 °C and 150 °C, respectively. The MS operated in EI mode at 70 eV under gain factor mode. Data was acquired in SIM mode and the identification of the analytes was performed using the retention time, the presence of quantifier and qualifier ions, and the ratio between those ions, while the quantification of the analytes was accomplished using the peak area of the quantifier ion.

REFERENCES

[1] F. Zhao, Y. Meng, J.L. Anderson, J. Chromatogr. A 1208 (2008) 1–9.

[2] A.C. Pereira, M.S. Reis, J.M. Leça, P.M. Rodrigues, J.C. Marques, Chemom. Intell. Lab. Syst. 179 (2018) 73–81.

[3] C.J. Haglock-Adler, A. Hurley, F.G. Strathmann, Clin. Biochem. 47 (2014) 80–82.

[4] L. Zhou, Y. Hu, G. Li, Anal. Chem. 88 (2016) 6930–6938.

[5] S.E. Hankari, P. Hesemann, Eur. J. Inorg. Chem. (2012) 5288–5298.

[6] Q.Q. Baltazar, J. Chandawalla, K. Sawyer, J.L. Anderson, Colloid Surf. A-Physicochem. Eng. Asp. 302 (2007) 150–156.

[7] C. Cagliero, H. Nan, C. Bicchi, J.L. Anderson, J. Chromatogr. A 1459 (2016) 17–23.

[8] Y. Meng, J.L. Anderson, J. Chromatogr. A 1217 (2010) 6143–6152.

[9] B. Wu, K. Kuroda, K. Takahashi, E.W. Castner, J. Chem. Phys. 148 (2018) 193807.

[10] A.C. Cole, J.L. Jensen, I. Ntai, K.L.T. Tran, K.J. Weaver, D.C. Forbes, J.H. Davis, J. Am. Chem. Soc. 124 (2002) 5962–5963.

[11] H. Satria, K. Kuroda, T. Endo, K. Takada, K. Ninomiya, K. Takahashi, ACS Sustain. Chem. Eng. 5 (2017) 708–713.

[12] M.D. Joshi, T.D. Ho, W.T.S. Cole, J.L. Anderson, Talanta 118 (2014) 172–179.

[13] J.L. Anderson, D.W. Armstrong, Anal. Chem. 77 (2005) 6453–6462.

[14] T.D. Ho, B.R. Toledo, L.W. Hantao, J.L. Anderson, Anal. Chim. Acta 843 (2014) 18–26.

[15] P. Rocío-Bautista, V. Pino, J.H. Ayala, C. Ruiz-Pérez, O. Vallcorba, A.M. Afonso, J. Pasán, RSC Adv. 8 (2018) 31304–31310.

[16] I. Pacheco Fernández, J. Pasán García, V. Pino Estévez, P. Rocío Bautista, A.M. Afonso Perera, J.H. Ayala Díaz, C. Ruiz Pérez, Spain Patent Application No. P201900092 (2019).

[17] Y. Li, B. Yan, J.-L. Liu, Nanoscale Res. Lett. 5 (2010), 797–804.

[18] O. Nacham, A. Martín-Pérez, D.J. Steyer, M.J. Trujillo-Rodríguez, J.L. Anderson, V. Pino, A.M. Afonso, Colloid Surf. A-Physicochem. Eng. Asp. 469 (2015) 224–234.

[19] I. Sifaoui, A. López-Arencibia, C.M. Martín-Navarro, M. Reyes-Batlle, C. Wagner, O. Chiboub, M. Mejri, B. Valladares, M. Abderrabba, J.E. Piñero, J. Lorenzo-Morales, PLoS One 12(8) (2017) e0183795.

[20] J. Lorenzo-Morales, C.M. Martín-Navarro, A. López-Arencibia, M.A. Santana-Morales, R.N. Afonso-Lehmann, S.K. Maciver, B. Valladares, E. Martínez-Carretero, Antimicrob. Agents Chemother. 54 (2010) 5151–5155.

[21] M.G. Freire, A.F. M. Cláudio, J.M.M. Araújo, J.A.P. Coutinho, I.M. Marrucho, J.N. Canongia Lopes, L.P.N. Rebelo, Chem. Soc. Rev. 41 (2012) 4966–4995.

[22] T.D. Ho, W.T.S. Cole, F. Augusto, J.L. Anderson, J. Chromatogr. A 1298 (2013) 146–151.

[23] M.J. Trujillo-Rodríguez, J.L. Anderson, Anal. Chim. Acta 1047 (2019) 52–61.

CHAPTER IV
Results and discussion

Section IV.1.

Liquid-phase microextraction applications with ionic liquids

Section IV.1.1

Exploring the use of low cytotoxic ionic liquids in liquid-phase microextraction

ILs have found an impressive number of applications as promising alternatives to conventional organic solvents in LPME techniques, particularly in DLLME. This success mainly lies in their adequate solvation ability, tuneability, and their claimed non-toxicity. Nevertheless, diverse studies have pointed out the toxicity of several ILs, including the most commonly used ILs of imidazolium. These studies have demonstrated that the toxicity is mainly associated to the composition and structure of the IL cation moiety. In this sense, cations derived from natural sources, such as cholinium, morpholinium, or guanidinium, are clearly desirable when designing ILs with safer toxicological profiles.

Apart from the recent concerns regarding the toxicity and low biodegradability of several ILs, it is also important to highlight the scarce attention paid to the design of IL structures with improved physicochemical properties (i.e., improved solvation features and affinity towards a specific group of compounds). Thus, the wide majority of analytical applications with ILs as extraction solvents use imidazolium-based ILs with non-functionalized butyl and hexyl chains.

The aim of the studies included in this section is to propose a new generation of guanidinium-based ILs with low cytotoxicity as extraction solvents. Thus, monoalkylguanidinium chloride ILs were synthesized with different substituent lengths. Their cytotoxicity was also evaluated in comparison with other ILs containing the imidazolium cation, and the surface-active properties of those presenting long alkyl chains were studied by different techniques. Furthermore, the IL-based surfactants from this group of ILs were incorporated in *in situ* DLLME approaches to take advantage of their micellar properties to enhance the extraction performance of the method. Thus, they were used to develop analytical methodologies for the determination of PCPs in cosmetic samples and in the multi-determination of copper and cadmium ions in water samples.

Section IV.1.1.1

Determination of surface-active properties and cytotoxicity of monoalkylguanidinium chloride ionic liquids

Journal of Chromatography A 1559 (2018) 102–111

Analytical and Bioanalytical Chemistry 410 (2018) 4701–4713

Talanta 203 (2019) 305–313

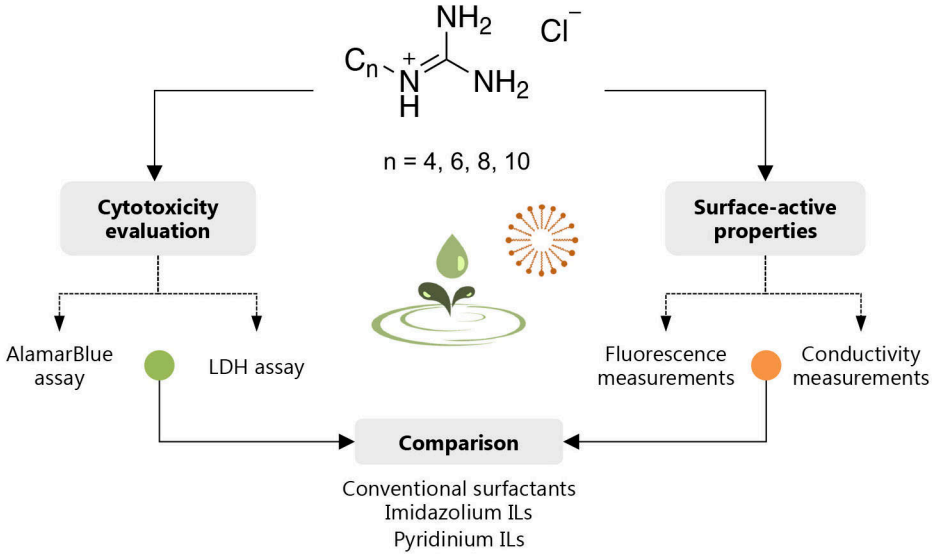

1. Synthesis of monoalkylguanidinium chloride ILs

Different ILs containing the monosubstituted guanidinium cation core and the chloride anion were synthesized following the procedure described in Section III.7.1.1. The length of the alkyl chain was varied between 4 and 10 carbon atoms to evaluate this structural feature. It was expected that ILs with carbon chains longer than 6 carbon atoms present interesting surface-active properties [1]. However, an increase in the side chain length attached to the IL cation can also lead to a significant increase of the IL toxicity [2–5].

The adequate synthesis of this group of ILs, for which the chemical structure is shown in Figure III.1, was confirmed by obtaining the ^{1}H-NMR spectrum. Figure IV.1 includes the ^{1}H-NMR spectra for $[C_4Gu^+][Cl^-]$, $[C_6Gu^+][Cl^-]$, $[C_8Gu^+][Cl^-]$, and $[C_{10}Gu^+][Cl^-]$, together with the signal assignments, which match with the values reported in the literature for these ILs.

2. Determination of the critical micelle concentration

Monoalkylguanidinium chloride ILs with alkyl chains containing from 8 to 16 carbon atoms have been reported as IL-based surfactants [6,7]. This means they can form aqueous aggregates in solution once they are added above a certain concentration, known as the CMC. The value of this concentration is strongly affected by the presence of different species in solution, such as organic solvents or inorganic salts, leading to higher and lower values, respectively [1]. Among the techniques employed for the determination of the CMC, conductivity, surface tension and fluorescence measurements are the most commonly used [1,8]. Indeed, the former two have been used to obtain the CMCs for several of the ILs synthesized in this Doctoral Thesis: $[C_8Gu^+][Cl^-]$ and $[C_{10}Gu^+][Cl^-]$. However, the fluorescence method has not been reported to estimate the CMC for this family of ILs and the effect of the presence of NaCl on the resulting CMC has neither been evaluated.

Fluorescence probes are commonly used to study micellar systems since they exhibit different fluorescence behavior depending on the solubilizing media. Pyrene is the most common fluorescent hydrophobic compound used in these studies. The intensities of bands I1 (≈ 373 nm) and I3 (≈ 383 nm) of the emission spectrum of pyrene are affected by the interactions with the solvent [8]. Thus, at concentrations above the CMC of a certain surfactant, pyrene is dissolved in the inner region of the micelles due to its hydrophobicity, which leads to a decrease on the I1 to I3 ratio. The plot I1/I3 *versus* the logarithm of surfactant concentration gives a sigmoid curve, and the inflection point of the curve determines the CMC of the surfactant.

The CMC of $[C_8Gu^+][Cl^-]$ and $[C_{10}Gu^+][Cl^-]$ ILs synthesized in this Doctoral Thesis were determined using fluorescence measurements and following the procedure described in Section III.7.4.1, also considering the influence of the ionic strength (with NaCl) in the micellar behavior.

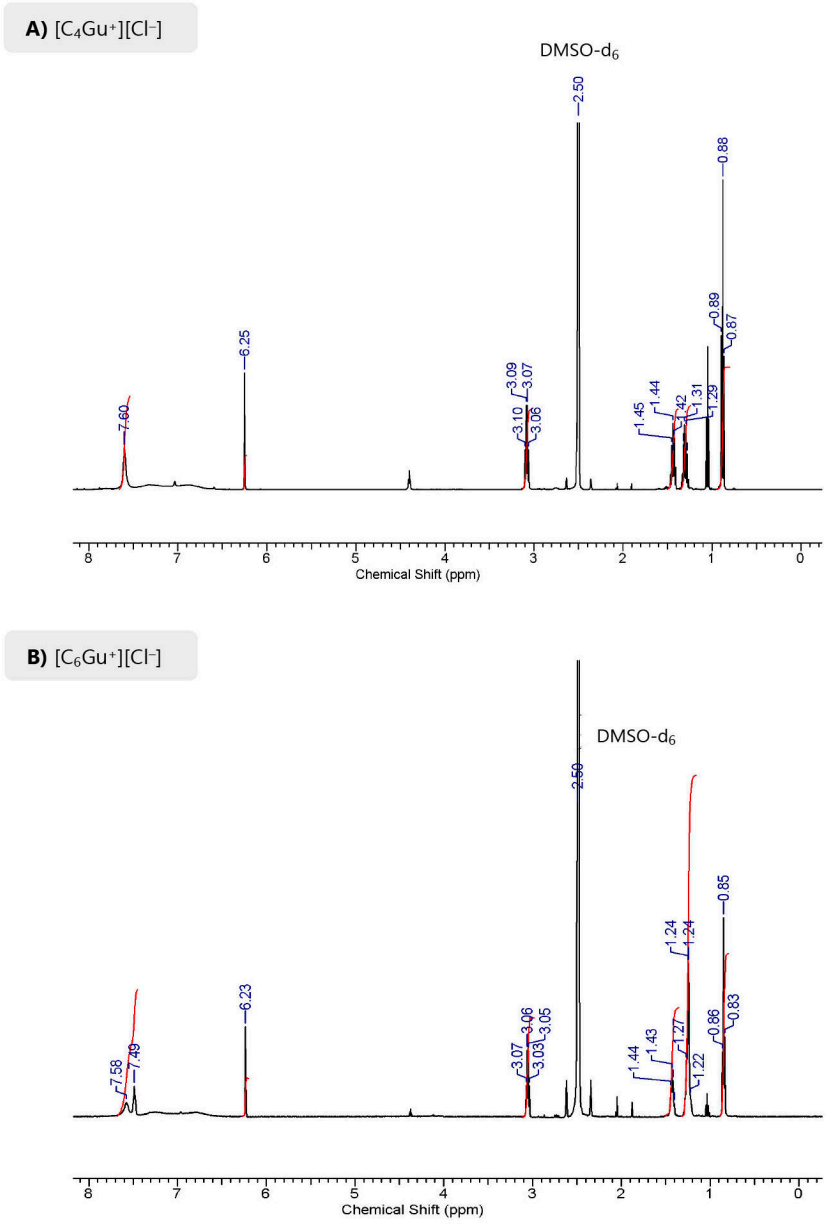

Figure IV.1. ^{1}H-NMR spectra of the synthesized guanidinium-based ILs: **A)** [C_4Gu^+][Cl^-] (δ ppm, 500 MHz, DMSO-d_6): 0.88 (t, J = 7.33 Hz, 3 H), 1.25–1.35 (m, 2 H), 1.40–1.49 (m, 2 H), 3.04–3.15 (m, 2 H), 6.25 (s, 1 H) 7.60 (br. s, 2 H). **B)** [C_6Gu^+][Cl^-] (δ ppm, 500 MHz, DMSO-d_6): 0.78–0.92 (t, J = 7.1 Hz, 3 H), 1.17–1.34 (m, 6 H), 1.36–1.52 (m, 2 H), 2.99–3.13 (m, 2 H), 6.23 (s, 1 H), 7.45–7.71 (br. m, 2 H).

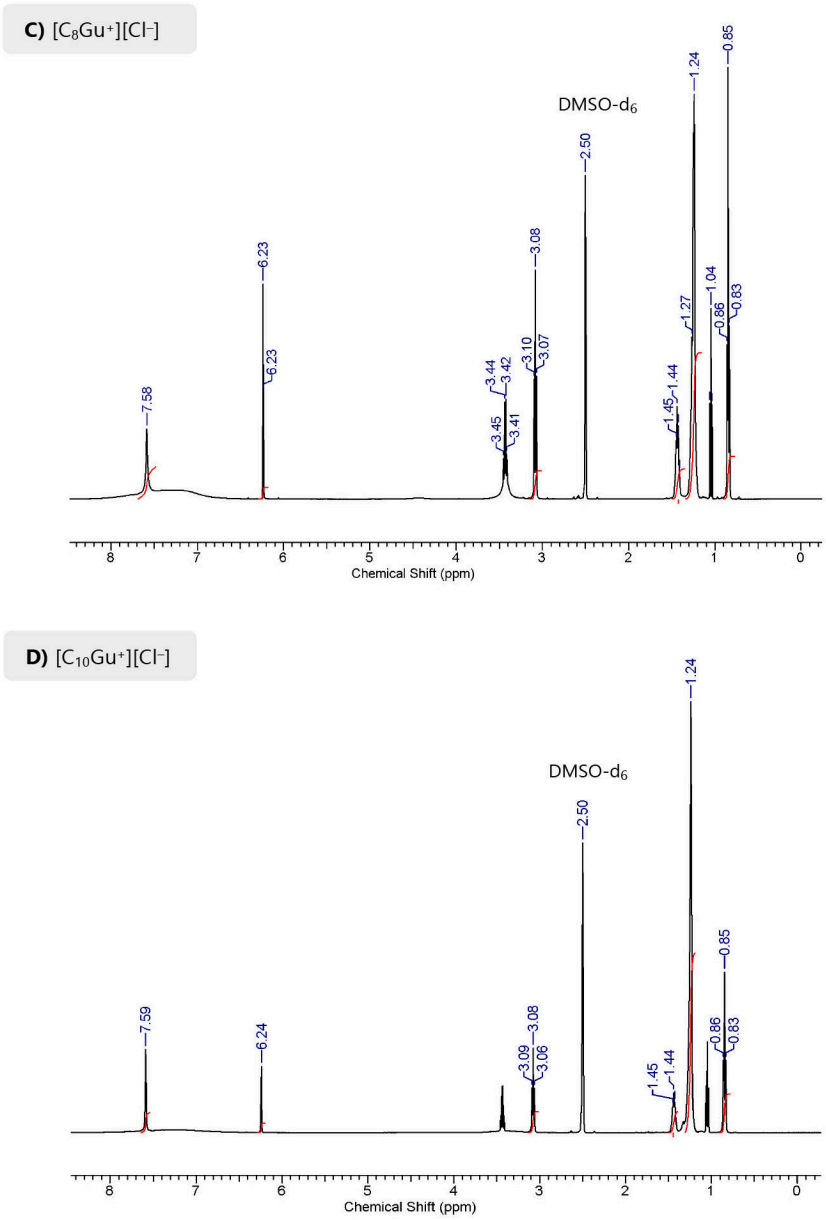

Figure IV.1 (continued). ^{1}H-NMR spectra of the synthesized guanidinium-based ILs: **C)** [C_8Gu^+][Cl^-] (δ ppm, 500 MHz, DMSO-d_6): 0.77–0.90 (t, 3 H), 1.16–1.33 (sa, 10 H), 1.36–1.52 (m, 2 H), 3.08 (t, *J* = 7.03 Hz, 2 H), 6.23 (t, J = 1.96 Hz, 1 H), 7.58 (br. s, 2 H). **D)** [$C_{10}Gu^+$][Cl^-] (δ ppm, 500 MHz, DMSO-d_6): 0.85 (t, *J* = 6.76 Hz, 3 H), 1.24 (sa, 12 H), 1.37–1.50 (m, 2 H), 3.08 (t, *J* = 6.99 Hz, 2 H), 6.20–6.29 (m, 1 H), 7.59 (br. s, 2 H).

Figure IV.2 A) shows the variation of the I1/I3 ratio with the $[C_8Gu^+][Cl^-]$ IL concentration in aqueous solutions (without NaCl in this case), as a representative example, while Table IV.1 includes the estimated polynomial equation of the curve, together with the obtained CMC values for both ILs at different NaCl contents. These CMC values were calculated through the second derivative method. In absence of salts, the obtained values of the CMC were 44.6 mM for $[C_8Gu^+][Cl^-]$ and 18.6 mM for $[C_{10}Gu^+][Cl^-]$.

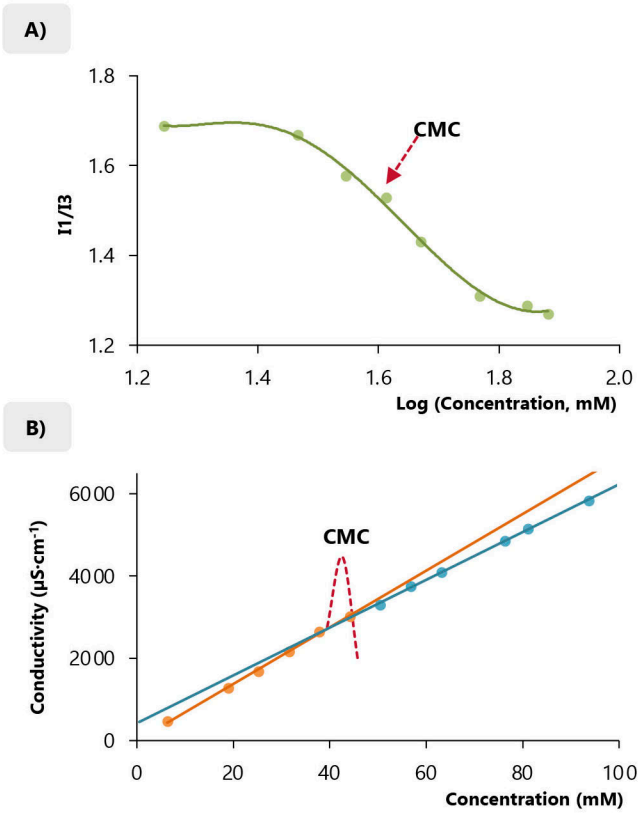

Figure IV.2. CMC determination for $[C_8Gu^+][Cl^-]$ using **A)** Plot of the variation of the ratio of band intensities I1 (373 nm) and I3 (383 nm) of the fluorescence emission spectrum of pyrene with respect to the logarithm of the IL-based surfactant concentration; and **B)** Plot of the variation of the specific conductivity with the IL-based surfactant concentration (solid lines), altogether with the change in the gradient of the conductivity *versus* concentration (dotted line).

Table IV.1. CMC values and the corresponding polynomial equations obtained by fluorescence measurements for the guanidinium IL-based surfactants.

% NaCl (w/v)	Polynomial equation[a]	R[b]	CMC (mM)
[C_8Gu^+][Cl^-]			
0	$I1/I3 = -8.02\times\log^4 c - 45.01\times\log^3 c + 91.78\times\log^2 c - 80.72\times\log c + 27.51$	0.996	44.6
5	$I1/I3 = 1.27\times\log^4 c - 4.43\times\log^3 c + 4.62\times\log^2 c - 1.91\times\log c + 2.04$	0.991	19.3
15	$I1/I3 = 0.01\times\log^4 c + 0.11\times\log^3 c - 0.34\times\log^2 c - 0.26\times\log c + 1.77$	0.996	7.66
25	$I1/I3 = 0.04\times\log^4 c + 0.19\times\log^3 c - 0.09\times\log^2 c - 0.59\times\log c + 1.50$	0.970	1.38
[$C_{10}Gu^+$][Cl^-]			
0	$I1/I3 = 1.12\times\log^4 c - 3.99\times\log^3 c + 4.33\times\log^2 c - 1.98\times\log c + 2.07$	0.998	18.6
5	$I1/I3 = -0.79\times\log^4 c + 1.89\times\log^3 c - 0.73\times\log^2 c - 0.95\times\log c + 1.68$	0.993	1.40
15	$I1/I3 = 1.31\times\log^4 c + 3.94\times\log^3 c + 3.07\times\log^2 c - 0.39\times\log c + 0.98$	0.991	0.46
25	$I1/I3 = 3.17\times\log^4 c + 15.27\times\log^3 c + 25.96\times\log^2 c + 17.60\times\log c + 5.10$	0.989	0.12

[a] I1 (373 nm)/I3 (383 nm) *versus* log of IL concentration (*c*, in mM).
[b] Correlation coefficient.

The CMC values obtained for these IL-based surfactants go in line with those reported for other guanidinium IL-based surfactants with dodecyl and tetradecyl alkyl chains: increasing the length of the alkyl group leads to a decrease of the CMC. Thus, Bouchal *et al.* reported CMC values of 6.2 mM and 1.8 mM for $[C_{12}Gu^+][Cl^-]$ and $[C_{14}Gu^+][Cl^-]$, respectively [7]. The influence of the NaCl content on the CMC values were also estimated by this technique, as it is shown in Table IV.1. It can be observed that the CMC decreases from 44.6 mM to 1.38 mM as the NaCl content increases from 0 % to 25 % (w/v) for $[C_8Gu^+][Cl^-]$. In the case of $[C_{10}Gu^+][Cl^-]$, it sharply decreases from 18.6 mM in absence of salt to 0.12 mM with a NaCl content of 25 % (w/v).

With respect to the CMC previously reported for these IL-based surfactants, the value obtained for $[C_{10}Gu^+][Cl^-]$ (18.6 mM) agrees with the values described by Song *et al.* [6] and Bouchal *et al.* [7] using conductivity and surface tension measurements. In the case of the IL $[C_8Gu^+][Cl^-]$, values between 68 and 75 mM [6] have been estimated by conductivity and surface tension studies, respectively, which are higher than those calculated in this Doctoral Thesis (44.6 mM). Despite this dissimilarity, it is important to highlight that the CMC is not a concentration itself but a narrow range of concentrations [1]. Therefore, it is very common to find a range of concentrations for the CMC depending on the method used for its determination.

In comparison with the imidazolium IL-based surfactant analogues (comparing the alkyl chain side), the guanidinium ILs present much lower CMC values. Thus, it has been reported a CMC varying between 90 and 100 mM for $[C_8MIm^+][Cl^-]$ [9], and a value around 40 mM for IL-based surfactant $[C_{10}MIm^+][Cl^-]$ [10]. Consequently, lower amounts of the IL-based surfactants synthesized in this Doctoral Thesis are required to take advantage of their aggregation properties in comparison with the most conventional imidazolium IL-based surfactants.

Additionally to the fluorescence determination, and given the disagreement with other values reported in the literature [6], the CMC of the $[C_8Gu^+][Cl^-]$ IL-based surfactant was also estimated by conductivity studies and following the procedure described in Section III.7.4.1. In this case, the specific conductivity of a solution containing the surfactant is monitored *versus* the surfactant concentration, observing that the conductivity increases with the ionic surfactant concentration. At a certain concentration value there is a change in the slope due to the formation of micelles [11]. The concentration associated to this breakpoint corresponds to the CMC. Figure IV.2 B) shows the variation of conductivity with the $[C_8Gu^+][Cl^-]$ concentration. The change in the gradient of this plot is also included as a red dotted curve to facilitate its interpretation, since the change in the slopes was not abrupt. Below and above the CMC, the correlation coefficients for the relationship between the conductivity and the $[C_8Gu^+][Cl^-]$ IL-based surfactant concentration were 0.997 and 0.999, respectively. The CMC value was estimated by the breakpoint of the two slopes, giving a value of 42 ± 6 mM (the error was calculated from mathematical propagation of the error in the prediction of the CMC concentration). Thus, there is a good agreement between the CMC values estimated by fluorescence measurements (44.6 mM) and the value obtained by conductivity studies in this Doctoral Thesis.

3. Cytotoxicity assessment

The rationale for synthesizing this family of ILs is their presumed low toxicity considering they are composed of guanidinium cations, which have been identified as less harmful and more biodegradable in comparison with other cores commonly used to prepare ILs [2,5]. However, the toxicity of this specific group has not been evaluated. In an attempt to verify their better cytotoxic character, two different cell viability tests were carried out following the procedures described in Section III.7.4.2. These assays were selected due to their simplicity, fastness, reliability, and common use when evaluating the possible *in vitro* cytotoxic effects of new compounds [12,13]. Moreover, other ILs with similar structures but different cation cores, as well as several common surfactants, were evaluated together with the guanidinium ILs to compare the results and provide conscientious results.

The AlamarBlue® cell viability assay was used as the preliminary study in the IL cytotoxicity assessment. The active ingredient of the AlamarBlue® reagent is resazurin, a non-toxic, weakly fluorescent and cell-permeable phenoxazine blue dye. Once it enters in living cells, resazurin is irreversibly reduced to the highly fluorescent and red-colored resorufin. Therefore, the change in color of the medium indicates there is no damage of the cells, while the non-reduction of the reagent and blue color in the medium implies the lysis of the cells. The main features of this cell viability test are its robustness, high sensitivity, and the possibility of obtaining quantitatively results either by absorbance or fluorescence measurements [14].

The 50 % cytotoxic concentrations (CC_{50}) of the synthesized ILs were calculated by plotting the dose-response curves, as it is shown in Figure IV.3 for $[C_4Gu^+][Cl^-]$, as a representative example. Table IV.2 includes the estimated CC_{50} values, together with that obtained for $[C_{16}MIm^+][Br^-]$, which was selected as representative imidazolium IL given its surface-active properties and wide use in analytical sample preparation approaches. It can be observed that the CC_{50} values ranged from 4490 $\mu mol \cdot L^{-1}$ for $[C_4Gu^+][Cl^-]$ to 17 $\mu mol \cdot L^{-1}$ for $[C_{10}Gu^+][Cl^-]$. Thus, there is an enhancement of the cytotoxicity of the IL when the alkyl chain length is increased as it has been suggested in previous studies [2–5]. Nevertheless, the CC_{50} for the most cytotoxic IL among the studied guanidinium ILs ($[C_{10}Gu^+][Cl^-]$) is still higher than the obtained for $[C_{16}MIm^+][Br^-]$, which presented a CC_{50} of 10 $\mu mol \cdot L^{-1}$. Therefore, use of ILs with shorter alkyl chain is advisable to develop more sustainable approaches. Moreover, regardless the alkyl chain, guanidinium-IL are still preferable considering not only their low cytotoxicity but also their lower CMC in comparison with imidazolium analogues.

The cytotoxicity of $[C_8Gu^+][Cl^-]$ was also evaluated by the LDH assay to compare the results obtained at specific concentrations with other conventional and IL-based surfactants. All surfactants were tested at concentrations approximately half of their respective CMC values in ultrapure water, taking into account that the monomeric form of the ILs will induce higher toxicity than that of the micellar aggregate (due to an expected easier introduction of the monomer though the cell membrane). In the case of $[C_8MIm^+][Cl^-]$, which exhibits a similar structure to $[C_8Gu^+][Cl^-]$ but with an imidazolium cation, its cytotoxicity was also evaluated at the same

concentration that was assessed for the guanidinium IL-based surfactant (15 mM), to also address comparison at the same concentration levels.

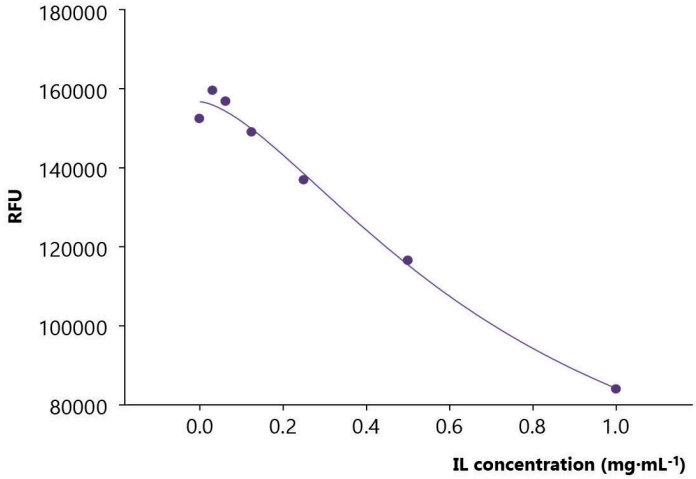

Figure IV.3. Representative dose-response curve for the $[C_4Gu^+][Cl^-]$ IL, showing the cytotoxicity of the IL towards the macrophage cells. RFU: relative fluorescence units.

Table IV.2. CC_{50} values obtained for the guanidinium-based ILs and a representative imidazolium-based IL using the Alamar Blue® cell viability assay.

IL	CC_{50}* (μmol·L^{-1})
$[C_4Gu^+][Cl^-]$	4490 ± 654
$[C_6Gu^+][Cl^-]$	752 ± 45
$[C_8Gu^+][Cl^-]$	52 ± 19
$[C_{10}Gu^+][Cl^-]$	17 ± 11
$[C_{16}MIm^+][Br^-]$	10 ± 21

* 50 % cytotoxic concentration values, which were obtained performing linear regression analysis of the dose response curves, with confidence limits at 95 %.

LDH is an enzyme found in all cells, involved in the oxidation of lactate to pyruvate, and thus it converts NAD+ (nicotinamide adenine dinucleotide) to NADH. This cytoplasmic enzyme is released quickly to the culture media once the plasma membrane is damaged. Therefore, an

increase in the number of dead cells results in an increase of the LDH activity in the culture supernatant. The LDH activity can be easily measured by adding INT to the culture media, which is reduced to red formazan dye in the presence of NADH. Hence, the intensity of the color formed (absorption maximum at about 490 nm) is proportional to the number of lysed cells [15]. The LDH release test is a simple tool used to estimate the cytotoxicity of different substances. Indeed, this test has been previously used to determine the cytotoxicity of several ILs [4,16].

Table IV.3 includes the cytotoxicity values found for the studied surfactants: $[C_8Gu^+][Cl^-]$, $[C_8MIm^+][Cl^-]$, $[C_{16}MIm^+][Br^-]$, $[C_{16}Py^+][Cl^-]$, CTAB (conventional cationic) and SDS (conventional anionic). From the results obtained, it is clear that the guanidinium IL-based surfactant exhibits lower cytotoxicity than the remaining surfactants studied. Thus, a value of 28 ± 11 % is obtained for $[C_8Gu^+][Cl^-]$ at 15 mM (half of its CMC in ultrapure water), allowing a classification of low to moderately cytotoxic, whereas a cytotoxicity value of 42 ± 6 % at 50 mM was found for its imidazolium analogue $[C_8MIm^+][Cl^-]$, and being then classified as moderate to high cytotoxic. If these IL-based surfactants are compared at the same concentration level (15 mM), it can be observed that the imidazolium IL-based surfactant is even more cytotoxic than the guanidinium IL-based surfactant, with a cytotoxicity of 95.8 ± 0.5 %.

Table IV.3. Cytotoxicity values obtained with the LDH release test for the $[C_8Gu^+][Cl^-]$ and other IL-based and conventional surfactants.

Surfactant	Concentration tested (mmol·L^{-1})	Cytotoxicity[a] (%)
$[C_8Gu^+][Cl^-]$	15	28 ± 11
$[C_8MIm^+][Cl^-]$	15	95.8 ± 0.5
	50	42 ± 6
$[C_{16}MIm^+][Br^-]$	0.3	126 ± 24
$[C_{16}Py^+][Cl^-]$	0.5	137 ± 20
CTAB	0.3	154 ± 28
SDS	3.0	n.d.[b]

[a] Relative values referred to Triton X-100 at 2 % (v/v) as 100 % of cytotoxicity, obtained using Equation III.1.
[b] Cells were lysed immediately after addition of surfactant. Thus, LDH levels were not able to be determined.

Furthermore, it is well-known that an increase in the length of the alkyl chain of a surfactant points to an intensification of its toxicity [3]. Therefore, $[C_{16}MIm^+][Br^-]$ presents a high cytotoxicity value of 126 ± 24 % at 0.3 mM while $[C_8MIm^+][Cl^-]$ exhibits lower cytotoxicity values despite it was evaluated at a much higher concentration level. With respect to conventional surfactants, CTAB and SDS are much more cytotoxic than any of the IL-based surfactants tested. In the case of SDS,

it quickly produced immediate lysis of the cells. Thus, these results demonstrate that less harmful applications can be developed if guanidinium cations are considered during the design of ILs.

REFERENCES

[1] I. Pacheco-Fernández, P. González-Hernández, V. Pino, J.H. Ayala, A.M. Afonso, in: A. Eftekhari, Ionic Liquid Devices, The Royal Society of Chemistry (2018) 53–78.

[2] R.F.M. Frade, A. Matias, L.C. Branco, C.A.M. Afonso, C.M.M. Duarte, Green Chem. 9 (2007) 873–877.

[3] R.F.M. Frade, A.A. Rosatella, C.S. Marques, L.C. Branco, P.A. Kulkarni, N.M.M. Mateus, C.A.M. Afonso, C.M.M. Duarte, Green Chem. 11 (2009) 1660–1665.

[4] X.-Y. Li, C.-Q. Jing, W.-L. Lei, J. Li, J.-J. Wang, Ecotox. Environ. Safe. 83 (2012) 102–107.

[5] J. Yu, S. Zhang, Y. Dai, X. Lu, Q. Lei, W. Fang, J. Hazard. Mater. 307 (2016) 73–81.

[6] Y. Song, Q. Li, Y. Li, Colloid Surf. A-Physicochem. Eng. Asp. 393 (2012) 11–16.

[7] R. Bouchal, A. Hamel, P. Hesemann, M. In, B. Prelot, J. Zajac, Int. J. Mol. Sci. 17 (2016) 223–238.

[8] B. Dong, X. Zhao, L. Zheng, J. Zhang, N. Li, T. Inoue, Colloid Surf. A-Physicochem. Eng. Asp. 317 (2008) 666–672.

9] J. Bowers, C.P. Butts, P.J. Martin, M.C. Vergara-Gutiérrez, Langmuir 20 (2004) 2191–2198.

[10] O.A.E. Seoud, P.A.R. Pires, T. Abdel-Moghny, E.L. Bastos, J. Colloid Interface Sci. 313 (2007) 296–304.

[11] P.C. Shanks, E.I. Franses, J. Phys. Chem. 96 (1992) 1794–1805.

[12] A. López-Arencibia, C. Martín-Navarro, I. Sifaoui, M. Reyes-Batlle, C. Wagner, J. Lorenzo-Morales, S.K. Maciver, J.E. Piñero, Antimicrob. Agents Chemother. 61 (2017) e02127-16.

[13] L. Chen, Y. Zhang, J. Liu, L. Wei, B. Song, L. Shao, J. Mater. Sci.-Mater. Med. 27 (2016) 59.

[14] AlamarBlue™ Cell Viability Reagent, ThermoFisher Scientific, https://www.thermofisher.com/order/catalog/product/DAL1025#/DAL1025 (Accessed: 2nd October 2020).

[15] Cytotoxicity Detection Kit (LDH) protocol by Roche, Sigma-Aldrich Bulletin, Version 11 (March 2016).

[16] C. Samorì, D. Malferrari, P. Valbonesi, A. Montecavalli, F. Moretti, P. Galletti, G. Sartor, E. Tagliavini, E. Fabbri, A. Pasteris, Ecotox. Environ. Safe. 73 (2010) 1456–1464.

Section IV.1.1.2

Guanidinium ionic liquid-based surfactants as low cytotoxic extractants: Analytical performance in an *in situ* dispersive liquid-liquid microextraction method for determining personal care products in cosmetic samples

Journal of Chromatography A 1559 (2018) 102–111

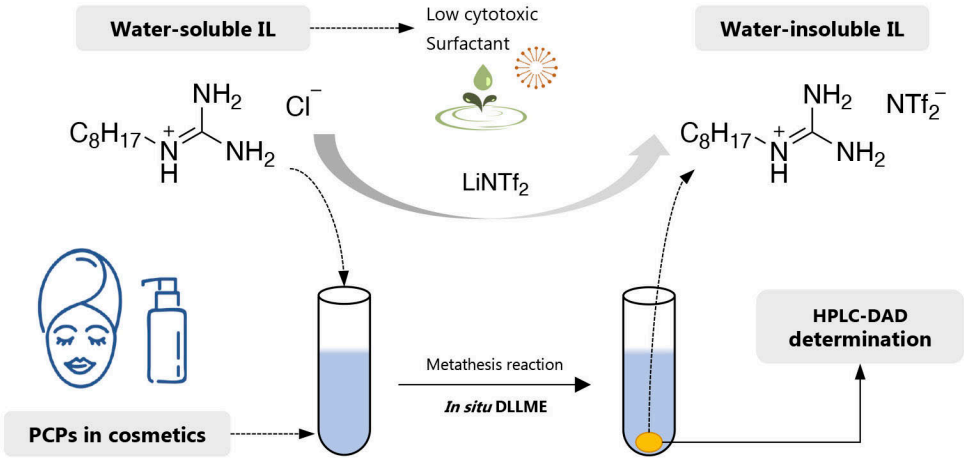

1. HPLC-DAD determination of PCPs in the presence of the IL-based surfactant

An *in situ* DLLME-HPLC-DAD method was developed for the determination of PCPs, including those most commonly used in cosmetic samples: MePa, EtPa, PPa, iPPa, BP and BP3. Parabens and benzophenones are compounds included among PCPs since they are commonly used as preservatives and UV filters in many cosmetic products. Recent studies have pointed out their toxicity due to their endocrine disrupting activity [1,2]. Indeed, the European Union has stablished a maximum concentration of 0.4 % (w/w) for single paraben (as acid) and 0.8 % (w/w) for mixtures of parabens (as acids) in cosmetic products [3]. Therefore, there is an enormous importance in developing more sensitive and selective methods for the determination of PCPs, what it is reflected in the increasing number of works in cosmetic and environmental analysis devoted to the determination of these compounds in the last years [4,5]. In this specific application, the synthesized $[C_8Gu^+][Cl^-]$ IL was selected as extraction solvent due to its surface-active properties, while being the less cytotoxic among the guanidinium IL-based surfactants evaluated (see Section IV.1.1.1).

Surfactants can present absorbance and fluorescence signals when they are used in combination with spectroscopic detectors in HPLC [6,7]. Therefore, it is necessary to determine the influence of the IL-based surfactant in the chromatographic determination of the analytes to ensure compatibility. In order to proceed this way and considering the fundamentals of the *in situ* DLLME method, it is necessary to have the PCPs dissolved in the water-insoluble IL microdroplet obtained after the metathesis reaction. Thus, 10 mL of an aqueous solution containing the selected PCPs and a $[C_8Gu^+][Cl^-]$ concentration of 14.8 mM was subjected to the *in situ* DLLME method. It was carried out under random preliminary experimental conditions: without pH and ionic strength adjustment, using 5 min of vortex stirring and 5 min of centrifugation, as well as the addition of the anionic exchange reagent in a 1:1 molar ratio. The resulting IL microdroplet was diluted up to 40, 50 or 60 µL with acetonitrile in three independent experiments. In all cases, the miscibility of the diluted IL microdroplet with the HPLC mobile phase was ensured.

The guanidinium IL provided an absorbance signal (in the range of 13.5–17.5 min using optimum separation conditions) at 254 nm, so the mobile phase was adjusted as described in Section III.7.5.1 to ensure the complete separation of the PCPs in 22 min avoiding any interference coming from the guanidinium IL. The final microdroplet was diluted up to 60 µL with acetonitrile to minimize viscosity. Figure IV.4 A) shows a representative chromatogram obtained after subjecting an aqueous solution containing the PCPs to the entire *in situ* DLLME-HPLC-DAD method, while Figure IV.4 B) shows a chromatogram obtained after the injection of a standard solution in acetonitrile containing the PCPs into the HPLC-DAD system.

Several quality analytical parameters of the HPLC-DAD method for PCPs without performing any preconcentration through DLLME are included in Table IV.4. Calibrations were obtained by direct injection of PCPs dissolved in a $[C_8Gu^+][NTf_2^-]$ solution (1:3 IL:acetonitrile v/v ratio) into the HPLC-DAD using the optimum chromatographic method, to mimic the further

solvent media in the *in situ* DLLME method. The calibration range was 0.05–7 mg·L^{-1} with determination coefficients higher than 0.993 for all the PCPs studied. The limits of detection (LODs) of the HPLC-DAD method (without *in situ* DLLME) were calculated as three times the signal-to-noise ratio (S/N), ranging from 8.0 µg·L^{-1} for BP3 to 14 µg·L^{-1} for PPa.

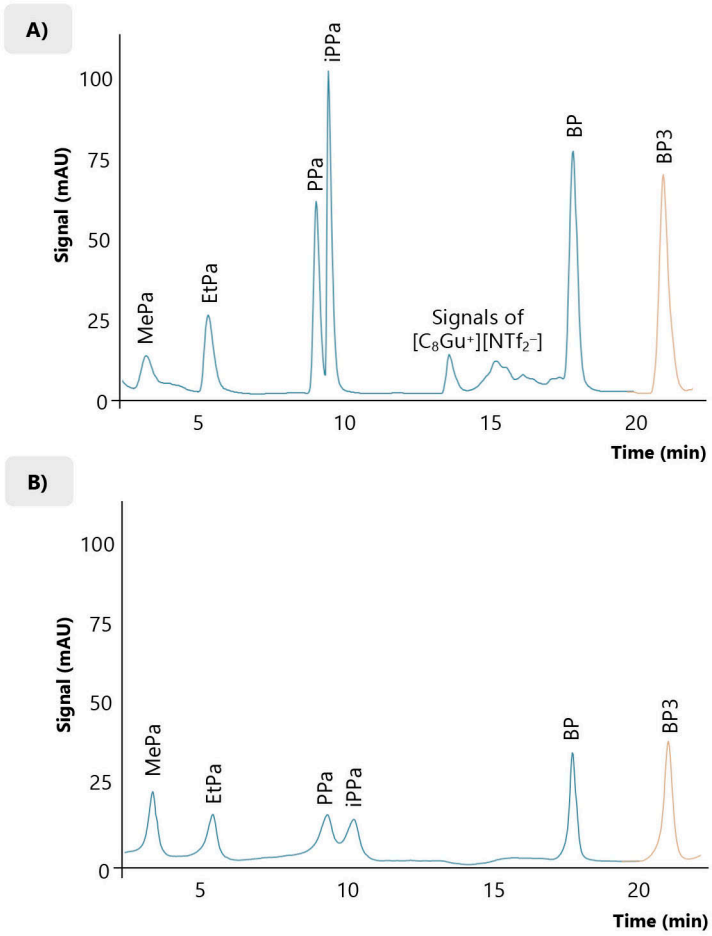

Figure IV.4. Representative chromatograms obtained after **A)** subjecting an aqueous solution containing 50 µg·L^{-1} of the PCPs to the entire *in situ* DLLME-HPLC-DAD method, and **B)** injecting a standard solution in acetonitrile containing 3.5 mg·L^{-1} of the PCPs into the HPLC-DAD system. Chromatographic conditions as described in Section III.7.5.1. Blue: 254 nm, orange: 289 nm.

Table IV.4. Several quality analytical parameters of the HPLC-DAD method, using PCPs standards in a $[C_8Gu^+][NTf_2^-]$ solution as solvent medium (1:3 IL:acetonitrile v/v ratio).

PCP	(Slope ± t·SD[a])·10^{-3}	($S_{y/x}$[b])·10^{-3}	R^2 [c]	LOD[d] (µg·L^{-1})	LOQ[e] (µg·L^{-1})
MePa	0.51 ± 0.03	78	0.999	11	37
EtPa	0.50 ± 0.01	34	0.997	11	38
PPa	0.65 ± 0.04	121	0.997	14	47
iPPa	0.57 ± 0.03	95	0.997	10	33
BP	0.84 ± 0.02	51	0.998	9.0	30
BP3	0.66 ± 0.01	45	0.993	8.0	27

[a] 95 % confidence limits for n = 7 calibration levels (5 degrees of freedom) within the calibration range: 50–7000 µg·L^{-1}.
[b] Error of the estimate (or standard deviation of the residuals).
[c] Determination coefficient.
[d] Limit of detection, calculated as 3 times the S/N ratio.
[e] Limit of quantification, calculated as 10 times the S/N ratio.

2. Optimization of the *in situ* DLLME procedure using $[C_8Gu^+][Cl^-]$

The *in situ* DLLME method is *a priori* very simple. An anionic exchange reagent is usually added to an IL aqueous solution in a 1:1 molar ratio, to ensure the formation of a water-insoluble IL. In this way, main parameters that must be optimized include the stirring strength to ensure quick formation of the microdroplet, proper separation of the formed microdroplet from the aqueous sample, ionic strength of the sample solution, and pH of the sample giving the nature of the PCPs.

Other conditions of the *in situ* DLLME procedure can be fixed to simplify the optimization process. In this case, the fixed values include: 10 mL of water sample, which is limited by the centrifuge capacity of the laboratory; and 30 µL of the neat $[C_8Gu^+][Cl^-]$ to ensure the formation of a microdroplet, and consequently to improve the enrichment factor. The resulting concentration of the IL-based surfactant in the sample solution is therefore 14.8 mM. Li-NTf_2 was selected as anion exchange reagent to obtain the water-insoluble IL microdroplet since it has been commonly used in microextraction methods for organic compounds [8]. The metathesis reaction was accomplished using an equimolar ratio (1:1). Thus, 45 µL of a solution of Li-NTf_2 with a concentration of 1 g·mL^{-1} were used. It must be noted that the final microdroplet of the $[C_8Gu^+][NTf_2^-]$ IL containing the preconcentrated analytes was diluted up to 60 µL with acetonitrile, as it was described in the previous chromatographic section, to ensure not only proper manipulation but also less interfering signals.

Therefore, the studied variables were salt concentration (as NaCl content), pH of the sample, vortex time used to speed up the metathesis reaction, and centrifugation time to speed up the microdroplet separation. The optimization was performed using an experimental design. In a first step, a screening study was used to determine which of those variables had an important effect in the method. A full two-level factorial design (2^4) was selected for the four variables. This study required 19 experiments, 3 of them involving the center point. Table IV.5 shows the design matrix of these experiments. The maximum and minimum values tested for each variable were: pH of the sample from 2 to 7, NaCl content (%, w/v) from 0 to 25 %, vortex time from 0 to 5 min, and centrifugation time from 2 to 10 min at 1921 × g. The limits selected for the pH are totally linked to the pK_a values of the PCPs studied, which range between 7.56 for BP3 and 8.40 for iPPa as shown in Table III.1. The NaCl content was tested almost up to the saturation level. Vortex times higher than 5 min were not tested to avoid the establishment of a long (and not safe for operators) procedure; and centrifugation times higher than 10 min were not tested to avoid a tedious method. In all cases, the response used in the design was the chromatographic peak area of each PCP.

Figure IV.5 includes the effect of these factors in the response and the obtained interactions among factors, for iPPa and BP as representative examples for each type of the PCPs studied: parabens-type and benzophenones-type. From the results obtained, in general, both the NaCl concentration and the centrifugation time had an important effect in the response, while the vortex time and the pH did not seem to be significant factors. From the Figure IV.5, it can also be observed that centrifugation time presents positive effects in the response, whereas the salt concentration has a different effect depending on the analyte: positive effect for the group of parabens (Figure IV.5 A)), and negative effect for benzophenones (Figure IV.5 B)).

Regarding the interaction among factors, there was not any significant trend for the PCPs. In this sense, the pH of the sample was set to a middle value of 5 (using a sodium acetate/acetic acid buffer solution) and the vortex time was fixed to an intermediate value of 3 min. Indeed, the turbidity due to the metathesis reaction visually disappeared after only 1.5 min of vortex stirring, indicating a fast kinetics for the metathesis reaction.

Once the screening design allowed fixing two of the variables, a Doehlert experimental design was performed to determine the optimum values for those main variables having an influence in the extraction method: centrifugation time (in min) and NaCl concentration (in %, w/v). In this case, the centrifugation time was studied from 2 to 10 min, and the salt concentration was studied from 0 to 15 %. Higher concentrations of NaCl were not assessed since NaCl contents over this maximum value affected the metathesis reaction and increased the turbidity of the solution, hampering the sampling of the final microdroplet.

Table IV.5. Design matrix for the screening analysis: 2^4 factorial design and 3 central points.

Experiment	pH	% NaCl (w/v)	Vortex time (min)	Centrifugation time (min)
1	2	0	5	10
2	2	25	0	10
3	2	25	5	2
4	2	0	0	2
5	7	0	5	2
6	7	25	5	10
7	7	0	0	10
8	7	25	0	2
9	2	0	5	2
10	2	0	0	10
11	2	25	5	10
12	2	25	0	2
13	7	0	0	2
14	7	25	5	2
15	7	0	5	10
16	7	25	0	10
17	4.5	12.5	2.5	6
18	4.5	12.5	2.5	6
19	4.5	12.5	2.5	6

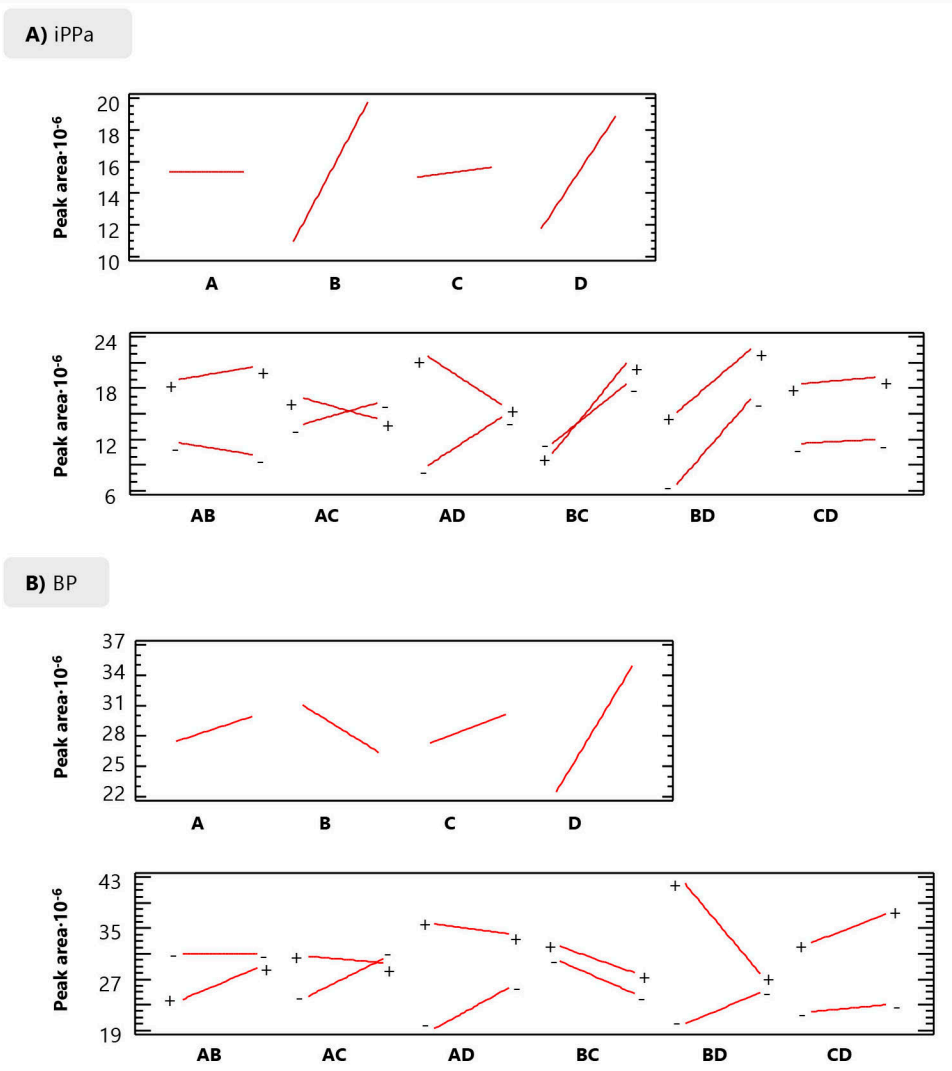

Figure IV.5. Results obtained in the preliminary screening analysis for iPPa and BP, chosen as representative examples of PCPs. The factors studied are denoted by A: pH of the sample, B: NaCl content (%, w/v), C: vortex time (min), and D: centrifugation time (min). Effects of the main factors and interactions among factors for **A)** iPPa and **B)** BP.

The Doehlert design for two variables comprises 7 experiments spatially distributed at the vertices of a hexagon with a point at the center, which is accomplished in triplicate to validate the model [9,10]. Therefore, the centrifugation time, which seems to have more influence than the NaCl concentration in the microextraction procedure, as it was shown in the screening study, was assessed at five experimental levels; and the salt content was evaluated at three experimental levels. Table IV.6 includes the coded values and the operating values of the Doehlert experimental design.

Table IV.6. Matrix of the experiments of the Doehlert design used for the optimization, including the coded values and the operating values.

Experiment	**Centrifugation time (min)**		**% NaCl (w/v)**	
	C_1	**X_1**	**C_2**	**X_2**
1	0	6	0	7.5
2	1	10	0	7.5
3	0.5	8	0.866	15
4	–1	2	0	7.5
5	–0.5	4	–0.866	0
6	0.5	8	–0.866	0
7	–0.5	4	0.866	15
8	0	6	0	7.5
9	0	6	0	7.5

C_1 and C_2 are the coded values for the levels of centrifugation time (in min) and NaCl concentration (in %, w/v), respectively.

The relationship between coded and real values is given by: $C_i = \left[\frac{X_i - X_i^o}{\Delta X_i}\right] \alpha$

where C_i is the coded value for the level of factor i, X_i is its real value in an experiment, X^o_i is the real value at the center of the experimental domain, ΔX_i is the step of variation of the real value, and α is the coded value limit for each factor.

The number of experiments required (N) is given by $N = k^2 + k + C_0$, where k is the number of variables and C_o is the number of center points.

A response surface methodology (RSM) was employed to determine the optimum experimental conditions using the results obtained in the Doehlert design. The analysis of the fitted response surface was carried out using the Lagrange's criterion [10] and the following equation:

$$R = \text{constant} + A\cdot[\text{centrifugation time}] + B\cdot[\text{NaCl concentration}] + AA\cdot[\text{centrifugation time}]^2 + AB\cdot[\text{centrifugation time}]\cdot[\text{NaCl concentration}] + BB\cdot[\text{NaCl concentration}]^2$$

Equation IV.1.

Constants and coefficients of the equation for each PCP are included in Table IV.7, while Figure IV.6 shows the three-dimensional surfaces (peak area as response × centrifugation time × NaCl concentration) for iPPa and BP, as representative examples.

Table IV.7. Constant and Doehlert coefficients values corresponding to the polynomial equation for the fitted response surface for each PCP, with A corresponding to the centrifugation time and B to the NaCl concentration.

PCP	Constant	A	B	AA	AB	BB
MePa	877316	144660	668747	3105	–32981	–3731
EtPa	909942	2617560	671119	–247051	–11613	–1768
PPa	13266500	1493440	2148490	–95088	2512	–107702
iPPa	19169000	1499880	2365710	–100754	12689	–130637
BP	37797800	3748980	1042870	–330085	51022	–140093
BP3	32339400	–560794	1610920	90701	–17583	–126439

The optimum values obtained for both variables and for each PCP are listed in Table IV.8. It can be observed that high NaCl concentrations (%, w/v) provided better results for the group of parabens, while the extraction efficiencies for BP and BP3 were higher when lower amounts of salt were used. In the case of the centrifugation time, the behavior was more complicated. Thus, MePa and EtPa presented higher responses using lower centrifugation times, but PPa, iPPa and BP3 required longer centrifugation times. Taking into account these results, a compromising solution was selected to benefit most PCPs: 5 min of centrifugation time at 1921 × g and 8 % (w/v) of NaCl content. It is important to highlight that, according to the results in Section IV.1.1.1 regarding the CMC values of $[C_8Gu^+][Cl^-]$ in presence of NaCl, the IL is added to the sample at a concentration close to the CMC (≈ 14.8 mM) under the ionic strength conditions selected.

These compromising conditions were validated by studying the relationship between the experimental values obtained under these conditions and the responses calculated under both optimum and compromising condition using Equation IV.1 for each analyte. A correlation coefficient (R) of 0.998 was obtained between the calculated peak area under optimum conditions and the experimental values under compromising conditions. Furthermore, a R value of 0.997 was obtained when correlating the calculated peak area and the experimental results obtained under compromising conditions. Besides, such correlations presented slopes close to the unity: 1.08 ± 0.02 and 1.15 ± 0.03, respectively. The variation between the theoretical peak area under optimum conditions and the experimental peak area obtained under compromising conditions was calculated for each PCP, being lower than 16 % in all cases, as it is shown in Table IV.8.

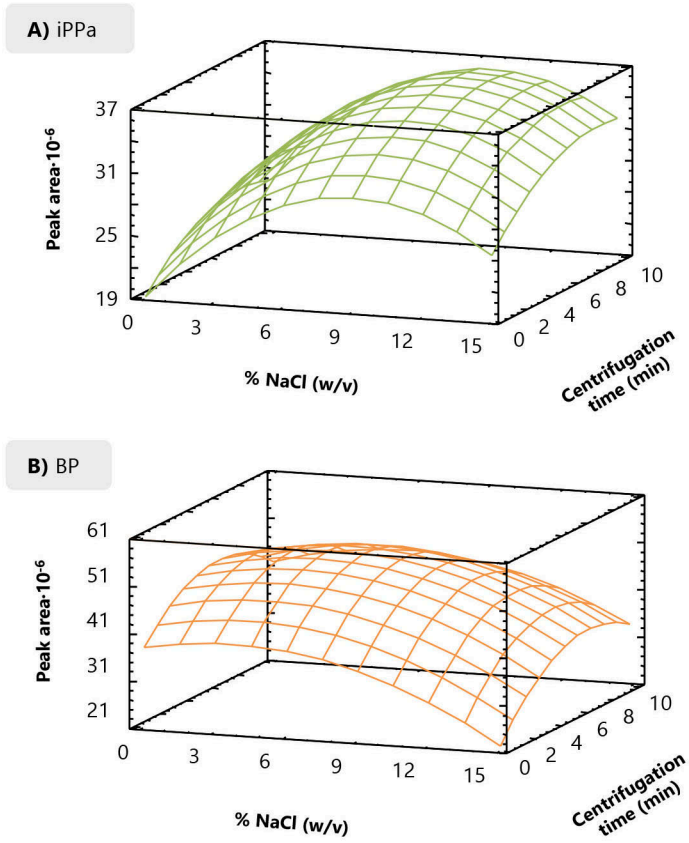

Figure IV.6. Response surfaces obtained in the final Doehlert experimental design for **A)** iPPa and **B)** BP, chosen as representative examples.

Table IV.8. Optimum values obtained for each PCP as a result of the Doehlert experimental design, together with the variation obtained between the theoretical peak area calculated under optimum conditions and the experimental peak area obtained under compromising conditions.

PCP	Centrifugation time (min)	NaCl (%, w/v)	Peak area obtained with Eq. IV.1 under optimum conditions*	Experimental peak area obtained under compromising conditions*	Variation between optimum and experimental peak areas (%)
MePa	2.0	15.0	9381406	7909611	15.7
EtPa	5.0	15.0	16620200	18194524	9.5
PPa	8.0	10.1	30044571	34047352	13.3
iPPa	8.0	9.5	36368992	42135552	15.8
BP	6.1	4.8	51656974	53835784	4.2
BP3	10	5.7	39873683	43039160	7.9

* Compromising conditions: 8 % (w/v) of NaCl and 5 min of centrifugation time.

All these results support the selection of such compromising conditions as optimum in this specific case for the entire *in situ* DLLME-HPLC-DAD method, which are schematically shown in Figure IV.7.

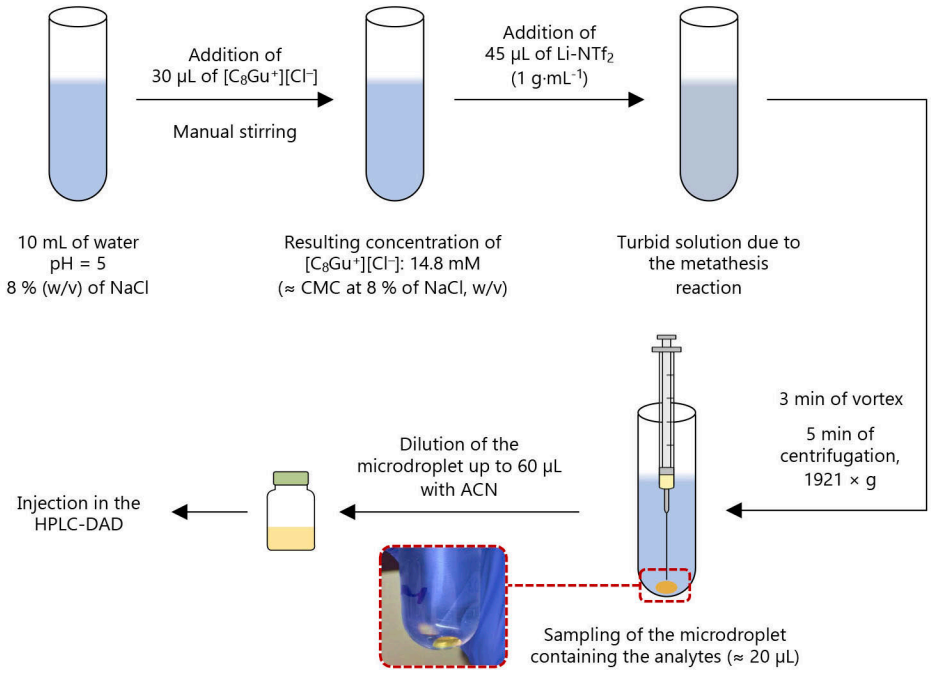

Figure IV.7. Scheme of the optimum *in situ* DLLME-HPLC-DAD method for the determination of PCPs using the $[C_8Gu^+][Cl^-]$ IL-based surfactant.

3. Analytical performance of the *in situ* DLLME-HPLC-DAD method with $[C_8Gu^+][Cl^-]$

The *in situ* DLLME-HPLC-DAD calibration curves were obtained for the group of PCPs using aqueous standards subjected to the entire method. Table IV.9 includes several quality analytical parameters, such as determination coefficients, slopes of the calibration curves, LODs, and limits of quantification (LOQs).

All calibration curves presented determination coefficients higher than 0.993 within the linear range: 5–100 µg·L^{-1}. The sensitivity of the method (evaluated as the calibration slope) was adequate for all PCPs, with MePa exhibiting the lowest sensitivity. LODs and LOQs were calculated as three and ten times the S/N, respectively, and were verified with standards prepared at these

levels and subjected to the entire method. The LODs ranged from 0.4 $\mu g \cdot L^{-1}$ for iPPa to 1.4 $\mu g \cdot L^{-1}$ for MePa. These values are satisfactory considering that the DAD was the detection system employed in this work. These LODs are ≈ 8 to 25 times lower than those obtained using HPLC-DAD (Table IV.4), showing the preconcentration achieved. Furthermore, these LODs are totally adequate compared to other values reported in the literature using other analytical methods, particularly for BP and BP3. LODs between 0.2 and 0.5 $\mu g \cdot L^{-1}$ for MePa, EtPa and PPa have been described in cosmetic samples when using a SFO-DLLME method in combination with HPLC-UV [11], and between 0.3 and 0.6 $\mu g \cdot L^{-1}$ for MePa, EtPa, PPa and iPPa in waters using vortex-assisted μ-dSPE followed by HPLC-DAD [12]. LODs ranging from 0.03 $\mu g \cdot L^{-1}$ for MePa to 1.48 $\mu g \cdot L^{-1}$ for BP3 have been reported in waters using a vortex-assisted DLLME strategy and ultra-HPLC-DAD [13]. In the case of a temperature-controlled DLLME-HPLC-UV method using an imidazolium-based IL is employed, LODs of 0.3 $\mu g \cdot L^{-1}$ for BP and 0.8 $\mu g \cdot L^{-1}$ for BP3 have been reported for environmental water samples [14].

Table IV.9. Quality analytical parameters for the entire *in situ* DLLME-HPLC-DAD method using aqueous standards subjected to the entire method.

PCP	(Slope ± t·SD[a])·10^{-3}	($S_{y/x}$[b])·10^{-3}	R^2 [c]	LOD[d] ($\mu g \cdot L^{-1}$)	LOQ[e] ($\mu g \cdot L^{-1}$)
MePa	8.5 ± 0.3	10.2	0.999	1.4	4.5
EtPa	30 ± 2	63.3	0.997	1.0	3.5
PPa	55 ± 4	118	0.997	0.6	2.0
iPPa	63 ± 4	134	0.997	0.4	1.5
BP	81 ± 4	136	0.998	0.8	2.8
BP3	54 ± 5	164	0.993	0.5	1.8

[a] 95 % confidence limits for n = 7 calibration levels (5 degrees of freedom) within the calibration range: 5–100 $\mu g \cdot L^{-1}$.
[b] Error of the estimate (or standard deviation of the residuals).
[c] Determination coefficient.
[d] Limit of detection, calculated as 3 times the S/N ratio.
[e] Limit of quantification, calculated as 10 times the S/N ratio.

The reproducibility of the entire method was evaluated by the relative standard deviation (RSD) values obtained in intra-day (n = 3) and inter-day (n = 9, in three non-consecutive days) studies, at two different concentration levels: 15 and 50 $\mu g \cdot L^{-1}$. Table IV.10 summarizes the results obtained.

Table IV.10. Analytical performance of the entire *in situ* DLLME-HPLC-DAD method, in terms of intra- and inter-day precision, relative recovery, enrichment factor, and extraction efficiency.

PCP	Concentration level: 15 µg·L^{-1}					Concentration level: 50 µg·L^{-1}				
	RR[a] (%)	Intra-day RSD[b] (%)	Inter-day RSD[c] (%)	E_F[d]	E_R[e] (%)	RR[a] (%)	Intra-day RSD[b] (%)	Inter-day RSD[c] (%)	E_F[d]	E_R[e] (%)
MePa	100	6.7	11	11.5	6.90	110	6.5	17	10.6	6.35
EtPa	114	6.1	15	61.0	36.6	109	2.0	6.5	65.5	39.3
PPa	97.2	3.4	6.8	90.3	54.2	107	1.4	5.0	91.8	55.1
iPPa	84.5	4.5	8.2	136	81.7	81.9	1.4	12	101	60.7
BP	92.4	10	16	125	74.9	99.8	1.8	8.3	101	60.5
BP3	96.3	5.0	5.2	111	66.6	88.1	4.3	9.2	91.8	55.1

[a] Relative recovery (n = 3).
[b] Intra-day precision (n = 3).
[c] Inter-day precision (n = 9, performed in 3 non-consecutive days).
[d] Enrichment factor.
[e] Extraction efficiency, E_{Fmax} = 167.

The intra-day precision varied from 3.4 % for PPa to 10 % for BP and from 1.4 % for PPa and iPPa to 6.5 % for MePa at the low and high concentration levels, respectively. For the inter-day precision, RSD values lower than 17 % were always obtained, which is totally adequate considering the low concentrations used for this study. The extraction performance of the entire method in ultrapure water (experiments in triplicate) was also evaluated by the determination of the enrichment factor (E_F), extraction efficiency (E_R, %), and relative recovery (RR, %) at the same concentration levels (15 and 50 $\mu g \cdot L^{-1}$). The results obtained in these studies are also included in Table IV.10.

RR values were calculated as the ratio of the predicted concentration obtained using the calibration curves of the entire method (Table IV.9) and the concentration of the PCPs in water. Average values of 97.4 % and 99.3 % were obtained at 15 $\mu g \cdot L^{-1}$ and at 50 $\mu g \cdot L^{-1}$ concentration levels, respectively. These RR values range from 81,9 % to 114 %, thus meeting acceptable requirements.

Regarding the E_F values of the entire method, they were estimated as the ratio between the predicted concentrations calculated using the peak area obtained with the entire *in situ* DLLME-HPLC-DAD method but using the chromatographic calibration curves (Table IV.4), and the concentration of PCPs in water. The results included in Table IV.10 show that higher E_F values were obtained for PPa, iPPa, BP and BP3, independently of the concentration level, while MePa exhibited the lowest E_F values. Thus, E_F values ranged from 11.5 for MePa to 136 for iPPa and from 10.6 for MePa to 101 for iPPa and BP at the low and high concentration level, respectively. These values can be compared with the theoretical maximum preconcentration factor (E_{Fmax}), which was estimated as the ratio of the initial volume of the sample (10 mL) and the final volume of the extract (60 µL once diluted before HPLC injection). Therefore, the E_{Fmax} for the entire *in situ* DLLME-HPLC-DAD method is ≈ 167. E_R values were calculated as the ratio E_F/E_{Fmax} (in %). MePa presented the lowest E_R values, being 6.90 % for the low concentration level and 6.35 % for the high concentration level. On the other hand, the remaining PCPs showed quite adequate E_R values for a microextraction procedure, with average values of 62.8 % for the concentration level of 15 $\mu g \cdot L^{-1}$.

4. Application of the method for the analysis of cosmetic facial tonic samples

Considering the complexity of cosmetics samples, facial tonic 1 (free of PCPs) was used to obtain matrix-matched calibrations for the optimized *in situ* DLLME-HPLC-DAD method. In this case, 50 µL of facial tonic 1 were diluted up to 10 mL with ultrapure water and spiked with PCPs prior to analysis. Table IV.11 includes several quality analytical parameters for the entire method using matrix-matched calibrations within the range: 5–100 $\mu g \cdot L^{-1}$. The obtained determination coefficients were always higher than 0.998. LODs ranged from 0.5 $\mu g \cdot L^{-1}$ for BP3 to 1.4 $\mu g \cdot L^{-1}$ for EtPa. It can be observed a slight loss of sensitivity in comparison with the calibrations in ultrapure water (Table IV.9), except for MePa for which the LOD is almost the half of that obtained with aqueous standards.

Table IV.11. Quality analytical parameters for the entire *in situ* DLLME-HPLC-DAD method using matrix-matched calibrations (facial tonic 1).

PCP	(Slope ± t·SD[a])·10^{-3}	($S_{y/x}$[b])·10^{-3}	R^2 [c]	LOD[d] (µg·L^{-1})	LOQ[e] (µg·L^{-1})
MePa	10.1 ± 0.5	16.8	0.998	0.8	2.8
EtPa	25 ± 1	30.8	0.999	1.4	4.6
PPa	48 ± 2	59.2	0.999	0.7	2.3
iPPa	52 ± 3	89.3	0.998	0.6	1.9
BP	66 ± 3	96.1	0.998	0.9	3.0
BP3	75 ± 4	127	0.998	0.5	1.5

[a] 95 % confidence limits for n = 7 calibration levels (5 degrees of freedom) within the linear range: 5–100 µg·L^{-1}.
[b] Error of the estimate (or standard deviation of the residuals).
[c] Determination coefficient.
[d] Limit of detection, calculated as 3 times the S/N ratio.
[e] Limit of quantification, calculated as 10 times the S/N ratio.

The matrix effect was evaluated by comparing the slopes obtained using standards in ultrapure water and those of matrix-matched calibrations, using the Student's *t*-test reported by Andrade and Estévez-Pérez [15]. Table IV.12 shows the statistical parameters obtained. In all cases, F_{exp} was lower than F_{crit} (α = 0.05), and therefore both calibrations are assumed to be equal according to the variance. However, the Student's *t*-test provided t_{cal} values higher than t_{crit} for all PCPs (α = 0.05). Thus, there are significant differences between the slopes, and matrix effect must be taken into account despite the *a priori* big dilution required to prepare the matrix-matched calibrations. Attending to these results, it is advisable to utilize matrix-matched calibrations to analyze cosmetic samples rather than external calibrations obtained with aqueous standards.

Facial tonic 1 (free of PCPs) was also used as matrix to perform recovery, reproducibility, and extraction efficiency studies by spiking PCPs at two concentration levels (15 and 50 µg·L^{-1}) and using the matrix-matched calibration curves previously obtained. The results of these studies (performed in triplicate) are summarized in Table IV.13. RSD values ranged from 5.6 % for iPPa to 13 % for BP at the low spiked level, and from 4.9 % for EtPa to 11 % for MePa at the high spiked level. Average RR values of 92.8 % and 103 % were obtained at 15 µg·L^{-1} and 50 µg·L^{-1} spiked levels, respectively. With respect to the extraction efficiency of the method, iPPa, BP and BP3 exhibited the higher E_F and E_R values, while MePa presented the lowest, as it was observed in ultrapure water (Table IV.10). Thus, the E_R values varied between 6.28 % for MePa and 86.5 % for iPPa at the spiked level of 15 µg·L^{-1}.

Table IV.12. Evaluation of the matrix effect for the entire *in situ* DLLME-HPLC-DAD method: comparison of the calibration slopes obtained for calibrations using PCPs standards in ultrapure water and matrix-matched calibrations (facial tonic 1) according to Andrade and Estévez-Pérez [15].

PCP	*F*-test[a]			Student's *t*-test[d]				
	F_{crit}[b]	F_{exp}[c]	Result	Variances	t_{crit}[e]	t_{cal}[f]	Result	Matrix effect
MePa	5.05	0.37	$F_{exp} < F_{crit}$	Equal	2.23	6.63	$\|t_{cal}\| > t_{crit}$	Yes
EtPa	5.05	4.24	$F_{exp} < F_{crit}$	Equal	2.23	5.68	$\|t_{cal}\| > t_{crit}$	Yes
PPa	5.05	3.95	$F_{exp} < F_{crit}$	Equal	2.23	4.40	$\|t_{cal}\| > t_{crit}$	Yes
iPPa	5.05	2.25	$F_{exp} < F_{crit}$	Equal	2.23	5.18	$\|t_{cal}\| > t_{crit}$	Yes
BP	5.05	1.99	$F_{exp} < F_{crit}$	Equal	2.23	7.44	$\|t_{cal}\| > t_{crit}$	Yes
BP3	5.05	1.67	$F_{exp} < F_{crit}$	Equal	2.23	8.35	$\|t_{cal}\| > t_{crit}$	Yes

[a] *F* statistical test to compare population variances.
[b] Critical *F* value for a significance level of 5 % and n – 2 degrees of freedom, being n the number of calibration levels.
[c] Experimental *F* value.
[d] Student's *t* test to compare the slopes.
[e] Critical *t* value for a significance level of 5 % and n – 2 degrees of freedom, being n the number of calibration levels
[f] Calculated *t* value using different approximations depending on the results of the *F*-test.

Table IV.13. Analytical performance of the optimized *in situ* DLLME-HPLC-DAD method using a cosmetic sample (facial tonic 1) spiked with PCPs, together with the concentration levels found of PCPs in facial tonic samples 2 and 3.

PCP	Facial tonic 1 (Spiked: 15 µg·L^{-1})				Facial tonic 1 (Spiked: 50 µg·L^{-1})				Facial tonic 2	Facial tonic 3
	RSD[a] (%)	E_F[b]	E_R[c] (%)	RR[d] (%)	RSD[a] (%)	E_F[b]	E_R[c] (%)	RR[d] (%)	Content[e] (µg·mL^{-1})	Content[e] (µg·mL^{-1})
MePa	13	10.5	6.28	105	11	12.8	7.67	92.6	1779 ± 14[f]	904 ± 45[f]
EtPa	5.8	35.6	31.3	79.6	4.9	61.7	37.0	110	n.d.	n.d.
PPa	7.1	83.9	50.3	96.1	7.9	87.2	52.3	116	9 ± 1[f]	n.d.
iPPa	5.6	144	86.5	90.8	7.7	122	73.1	99.2	n.d.	n.d.
BP	13	123	74.0	89.6	10	112	67.5	109	n.d.	n.d.
BP3	8.6	125	75.0	95.5	10	121	72.5	95	n.d.	n.d.

[a] Intra-day relative standard deviation (n = 3).
[b] Relative recovery (n = 3).
[c] Enrichment factor in cosmetic matrix.
[d] Extraction efficiency in cosmetic matrix, E_{Fmax} = 167.
[e] Levels of PCPs found (in µg·mL^{-1}).
[f] Standard deviation in the determination of PCPs in cosmetic samples (n = 3).
n.d.: not detected.

Two commercial facial tonics were also analyzed, both of them tagged as containing MePa, while only one of them (facial tonic 2) was also labelled as containing PPa. Considering the high concentrations of parabens reported to be found in these types of cosmetic samples [16,17], the facial tonics were highly diluted with ultrapure water prior to their analysis under optimum conditions (Section III.7.5.1) with the developed *in situ* DLLME-HPLC-DAD method. Table IV.13 shows the results obtained using matrix-matched calibrations. MePa was quantified in both samples using the current method, with contents of 1779 ± 14 $\mu g \cdot mL^{-1}$ and 904 ± 45 $\mu g \cdot mL^{-1}$ for facial tonic 2 and facial tonic 3, respectively. PPa was also quantified in facial tonic 2 sample, with a content of 9 ± 1 $\mu g \cdot mL^{-1}$. Despite the high concentrations found in both samples, they were below the maximum values established by the European Union legislation: ≈ 0.18 % (w/w) for facial tonic 2 and ≈ 0.09 % (w/w) for facial tonic 3 as total content of mixtures of parabens. Despite the high concentration found in the samples analyzed, it is important to highlight that the proposed method is also suitable for the determination of these compounds at really low concentration levels given the LOQs achieved. This may be particularly useful for the detection of false advertising and labelling of cosmetic products, which is of special interest for EU Commission and the American Food and Drug Administration.

REFERENCES

[1] J.L. Wilkinson, P.S. Hooda, J. Barker, S. Barton, J. Swinden, Crit. Rev. Environ. Sci. Technol. 46 (2016) 336–381.

[2] J.M. Brausch, G.M. Rand, Chemosphere 82 (2011) 1518–1532.

[3] Commission Regulation (EU) No 358/2014 of 9 April 2014 amending Annexes II and V to Regulation (EC) No 1223/2009 of the European Parliament and of the Council on cosmetic products, Official Journal of the European Union, L 107/5.

[4] N. Cabaleiro, I. de la Calle, C. Bendicho, I. Lavilla, Trac-Trends Anal. Chem. 57 (2014) 34–46.

[5] M. Pedrouzo, F. Borrull, R.M. Marcé, E. Pocurull, Trac-Trends Anal. Chem. 30 (2011) 749–760.

[6] V. Pino, J.L. Anderson, J.H. Ayala, V. González, A.M. Afonso, J. Chromatogr. A 1182 (2008) 145–152.

[7] M.J. Trujillo-Rodríguez, V. Pino, J.L. Anderson, J.H. Ayala, A.M. Afonso, Anal. Bioanal. Chem. 407 (2015) 8753–8764.

[8] M.J. Trujillo-Rodríguez, P. Rocío-Bautista, V. Pino, A.M. Afonso, Trac-Trends Anal. Chem. 51 (2013) 87–106.

[9] P. Araujo, S. Janagap, J. Chromatogr. B 910 (2012) 14–21.

[10] S.L.C. Ferreira, W.N.L. dos Santos, C.M. Quintella, B.B. Neto, J.M. Bosque-Sendra, Talanta 63 (2004) 1061–1067.

[11] M. Moradi, Y. Yamini, J. Chromatogr. A 1229 (2012) 30–37.

[12] P. Rocío-Bautista, C. Martínez-Benito, V. Pino, J. Pasán, J.H. Ayala, C. Ruiz-Pérez, A.M. Afonso, Talanta 139 (2015) 13–20.

[13] P. González-Hernández, V. Pino, J.H. Ayala, A.M. Afonso, Anal. Methods 7 (2015) 1825–1833.

[14] Y. Zhang, H.K. Lee, J. Chromatogr. A 1271 (2013) 56–61.

[15] J.M. Andrade, M.G. Estévez-Pérez, Anal. Chim. Acta 838 (2014) 1–12.

[16] A. Zgoła-Grześkowiak, J. Werner, M. Jeszka-Skowron, B. Czarczyńska-Goślińska, Anal. Methods 8 (2016) 3903–3909.

[17] P.G. Wang, W. Zhou, J. Sep. Sci. 36 (2013) 1781–1787.

Section IV.1.1.3

Guanidinium ionic liquid-based surfactants as low cytotoxic extractants: Analytical performance in an *in situ* dispersive liquid-liquid microextraction method for determining heavy metals in water samples

Analytical Methods 10 (2018) 1529–1537

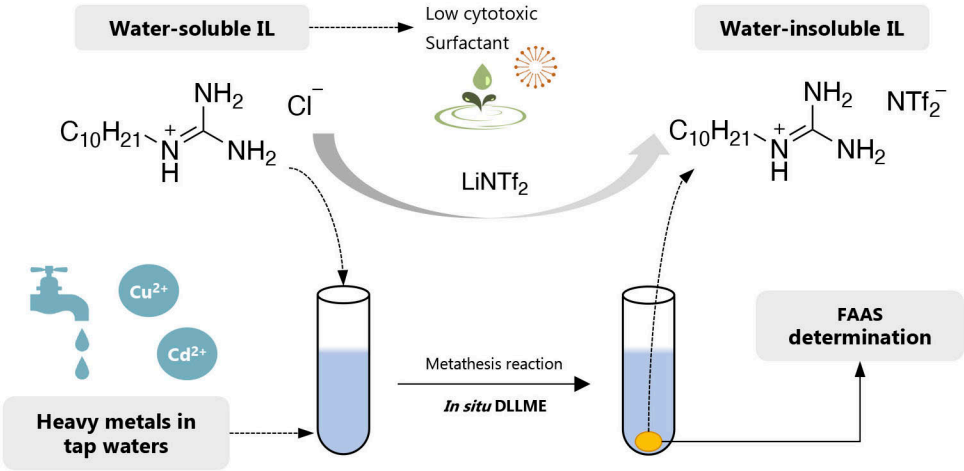

1. Optimization of the *in situ* DLLME method using IL-based surfactants

An *in situ* DLLME-FAAS method was developed for the determination of heavy metals in water samples using IL-based surfactants. The monitoring of heavy metals in environmental samples has great importance due to the high toxic potential of some of them and the continuous accumulation in the environment and living organisms [1]. Among heavy metals, cadmium is one of the most toxic due to its carcinogenic effect at low concentration and its bioaccumulation [2]. In the case of copper, despite of being an essential element in different biological process [3], an excessive exposure to copper by several environmental sources may lead to suffering different illnesses, such as hypertension [4] and neurodegenerative diseases [5]. Thus, different institutions have stablished maximum levels of these metals in drinking waters, such as the United States Environmental Protection Agency (US-EPA) which sets a maximum action value of 1.3 $mg \cdot L^{-1}$ for copper and a maximum concentration of 5 $\mu g \cdot L^{-1}$ for cadmium [6].

Considering the low concentrations of metals normally found in environmental waters, extraction and preconcentration steps prior to the analytical determination of metals are required to reach the sensitivity imposed. Indeed, *in situ* DLLME has been widely used for this purpose but using imidazolium ILs as extraction solvents [7–12]. Therefore, after demonstrating the successful performance of one of the guanidinium IL-based surfactants synthesized in this Doctoral Thesis in the previous section (Section IV.1.1.2), the remaining IL with surface-active properties (i.e., $[C_{10}Gu^+][Cl^-]$) was selected as extraction solvent in this application. Moreover, its performance was compared with that of the more common $[C_{16}C_4Im^+][Br^-]$ imidazolium IL.

1.1. Preliminary studies for optimization

The optimization of the method was performed using Cu (II). The optimum conditions were then applied to the simultaneous extraction and determination of Cu (II) and Cd (II), with the purpose of taking advantage of one single micro-droplet for multi-analyte determination. There are several experimental conditions that can directly affect the performance of the *in situ* DLLME method for the determination of metals. Among them, those having a major effect are: the pH of the sample (related to the stability of the metal-complex); the ionic strength of the solution (that promotes the salting-out effect); the amount of extractant; the concentration of complexing agent (to ensure adequate complexation of the metal); the stirring during the metathesis reaction (to ensure an adequate formation of the water-insoluble IL); and the separation of the IL-based surfactant microdroplet from the sample once formed.

Several experimental conditions were fixed with the purpose of reducing the number of variables to optimize using an experimental design. Furthermore, several preliminary studies were carried out to determine those variables that had a significant effect on the method. Thus, the sample volume was fixed to 10 mL, which ensured a satisfactory preconcentration of the analytes and facilitated the centrifugation step by using a regular centrifuge. BSTC was selected as complexing ligand since it forms stable complexes with copper and cadmium [13].

Acetone and acetonitrile were studied initially as solubilizing agent for the complexing agent, given their miscibility with the extraction solvent (the IL-based surfactants) and the aqueous sample. After several tests, acetone proved to be more adequate given the better solubility of the complexing agent in comparison with acetonitrile. An amount of 500 µL of acetone containing 200 $mg \cdot L^{-1}$ BSTC (10 mg L^{-1} in the extraction tube) was the optimum amount that guaranteed the proper formation of the metal-complex in the *in situ* DLLME method.

The amount of IL-based surfactant used in the *in situ* DLLME method should be small enough to improve the enrichment factor obtained in the entire method (by forming a microdroplet in the aqueous sample), but high enough to ensure the formation of an easy-to-handle microdroplet since volumes lower than 10 µL are normally difficult to handle and quite irreproducible. Furthermore, in order to take advantage of the micellar properties of the IL-based surfactants, concentrations higher than their CMCs were tested for both ILs. CMC value around 21 mM was obtained for $[C_{10}Gu^+][Cl^-]$ in Section IV.1.1.1. However, it was also demonstrated that slight increases in the NaCl content of the solution drastically decreases the CMC value of this guanidinium IL-based surfactant (see Table IV.1). Therefore, concentrations of $[C_{10}Gu^+][Cl^-]$ from 5 to 27 mM were studied in order to work above the CMC at different ionic strengths. It was selected as optimum a concentration of 11 mM to avoid costs and unnecessary waste of chemicals, since higher concentrations did not show better results and lower concentrations provided small microdroplets. In the case of $[C_{16}C_4Im^+][Br^-]$, a CMC of 0.1 mM has been reported [14]. Thus, concentrations between 10 and 25 mM were studied for $[C_{16}C_4Im^+][Br^-]$, selecting a final concentration of 10 mM as optimum concentration of the IL-based surfactant for the same reason as for $[C_{10}Gu^+][Cl^-]$.

For both IL-based surfactants, an equimolar ratio of IL and Li-NTf_2 was enough to promote the metathesis reaction. Therefore, 65 µL and 60 µL of 0.5 $g \cdot mL^{-1}$ solution of Li-NTf_2 were used for $[C_{10}Gu^+][Cl^-]$ and $[C_{16}C_4Im^+][Br^-]$ ILs, respectively. Furthermore, only 2 min of centrifugation at 1921 × g were necessary to obtain a good separation of the microdroplet from the aqueous sample when both IL-based surfactants were used.

Before the injection of the IL microdroplet in the FAAS system, its dilution is advisable in an adequate organic solvent to reduce its viscosity and to facilitate its aspiration. Taking into account the results obtained in studies previously reported in similar methods for the determination of metals [8], acetonitrile was chosen as dilution solvent, and the IL microdroplet was diluted up to 120 µL.

With respect to the remaining variables that can affect the entire *in situ* DLLME method (pH, NaCl concentration, and vortex time), different behaviors were observed for both IL-based surfactants. The amount of NaCl in the aqueous sample was an important variable affecting the extraction procedure as it can be observed in Figure IV.8 A). This behavior goes along with the effect of NaCl content in the CMC of the IL-based surfactants and the salting-out effect exerted by this salt.

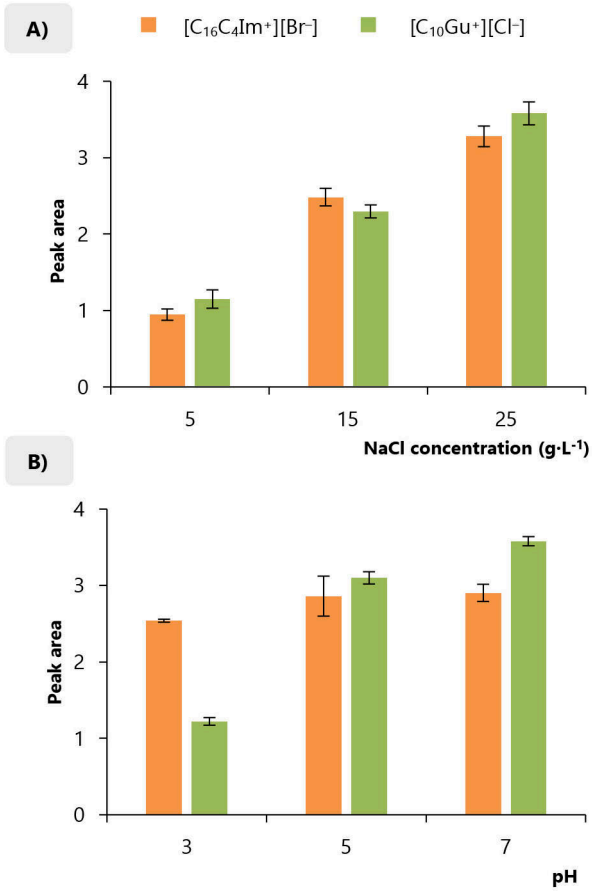

Figure IV.8. Influence of **A)** the NaCl concentration and **B)** the pH of the aqueous sample on the extraction efficiency of Cu (II) at 0.5 μg·L^{-1} with the *in situ* DLLME-FAAS method using both IL-based surfactants. Experimental conditions: 10 g·L^{-1} of NaCl in the study of the effect of the pH, without pH adjustment in the study of the ionic strength, 2 min of vortex, and 2 min of centrifugation at 1921 × g. The remaining experimental conditions were fixed as described in the text. All experiments were carried out in triplicate.

The pH of the sample seemed to play an important role in the extraction efficiency of the method when the [$C_{10}Gu^+$][Cl^-] IL-based surfactant was used, while no significant differences were observed for the imidazolium IL-based surfactant as it is shown in Figure IV.8 B). Therefore, a neutral pH value around 6.8 was selected for the entire method when the [$C_{16}C_4Im^+$][Br^-] IL was used. This pH was indeed obtained when adding all reagents to the aqueous sample, and therefore no further adjustment was carried out. In the case of the vortex time used to speed up the metathesis reaction, it had a strong influence in the results obtained for the [$C_{16}C_4Im^+$][Br^-] IL-

based surfactant. When the $[C_{10}Gu^+][Cl^-]$ IL was used, 2 min of vortex stirring were more than enough to obtain the water-insoluble IL due to the fast kinetics of the metathesis reaction. Therefore, these three variables need to be specifically studied for each IL: NaCl concentration and pH for $[C_{10}Gu^+][Cl^-]$; and NaCl concentration and vortex time for $[C_{16}C_4Im^+][Br^-]$.

1.2. Doehlert experimental design for optimization

A Doehlert experimental design was selected to determine the optimum values for each IL. This experimental design is commonly used in the optimization process in analytical chemistry due to its simplicity. It consists of seven experiments distributed at the vertices of a hexagon and in its center. The variable having a strong influence in the response is studied at five experimental levels while the other variable is assessed at three experimental levels [15]. Different points at the center of the hexagon can be included in the experimental design to cover more experiments for the main variable affecting the extraction procedure. The results obtained from these random experiments allow obtaining a three-dimensional response surface that determines the optimum experimental conditions for the extraction method. The Lagrange's criterion was selected to carry out the analysis of the response surface obtained and to determine the optimum conditions, using the peak area obtained for Cu (II) as response [15].

For the optimization of the *in situ* DLLME method using the $[C_{10}Gu^+][Cl^-]$ IL-based surfactant, the salt concentration was studied at five levels ranging from 10 to 40 $g{\cdot}L^{-1}$, while the pH was assessed at three levels varying between 3 and 8.5. When using $[C_{16}C_4Im^+][Br^-]$ as extraction solvent, the NaCl content was evaluated at five levels from 10 to 40 $g{\cdot}L^{-1}$, while the vortex time was studied at three levels ranging from 0.5 to 4 min. The Tables IV.14 and IV.15 include the coded values and the operating values of the Doehlert experimental design for $[C_{10}Gu^+][Cl^-]$ and $[C_{16}C_4Im^+][Br^-]$ IL-based surfactants, respectively.

The response surfaces included in Figure IV.9 allows predicting the optimum conditions for the variables studied when the $[C_{10}Gu^+][Cl^-]$ and $[C_{16}C_4Im^+][Br^-]$ IL-based surfactants are used. Both surface plots present a pronounced enhancement in the signal as the NaCl concentration increases. In the case of $[C_{10}Gu^+][Cl^-]$ (Figure IV.9 A)), high pH values provide better results, while higher peak areas are obtained when vortex times are around 1.5 and 3 min for the $[C_{16}C_4Im^+][Br^-]$ IL (Figure IV.9 B)).

Thus, a NaCl concentration of 30 $g{\cdot}L^{-1}$ and a pH value of 8.2 were selected as optimum values when $[C_{10}Gu^+][Cl^-]$ is the extraction solvent in the *in situ* DLLME-FAAS method. The optimum conditions for the IL $[C_{16}C_4Im^+][Br^-]$ were a NaCl concentration of 28 $g{\cdot}L^{-1}$ and 2 min of vortex stirring. Figure IV.10 shows a scheme of the procedure including the different optimum experimental conditions depending on the IL used.

Table IV.14. Matrix of the Doehlert experimental design used for the optimization of the method with $[C_{10}Gu^+][Cl^-]$ IL-based surfactant, including coded and operating values.

Experiment	NaCl concentration ($g \cdot L^{-1}$)		pH	
	C_1	X_1	C_2	X_2
1	0	25.0	0	5.75
2	1.00	40.0	0	5.75
3	0.500	32.5	0.866	8.50
4	–1.00	10.0	0	5.75
5	–0.500	17.5	–0.866	3.00
6	0.500	32.5	–0.866	3.00
7	–0.500	17.5	0.866	8.50
8	–0.500	17.5	0	5.75
9	0.500	32.5	0	5.75

C_1 and C_2 are the coded values for the levels of NaCl concentration ($g \cdot L^{-1}$) and pH, respectively.

The relationship between coded and real values is given by: $C_i = \left[\frac{X_i - X_i^o}{\Delta X_i}\right] \alpha$

where C_i is the coded value for the level of factor i, X_i is its real value in an experiment, X^o_i is the real value at the center of the experimental domain, ΔX_i is the step of variation of the real value, and α is the coded value limit for each factor.

The number of experiments required (N) is given by $N = k^2 + k + C_0$, where k is the number of variables and C_0 is the number of center points.

Table IV.15. Matrix of the Doehlert experimental design used for the optimization of the method with $[C_{16}C_4Im^+][Br^-]$ IL-based surfactant, including coded and operating values.

Experiment	NaCl concentration ($g \cdot L^{-1}$)		Vortex time (min)	
	C_1	X_1	C_2	X_2
1	0	25	0	2.25
2	1	40	0	2.25
3	0.5	32.5	0.866	4
4	–1	10	0	2.25
5	–0.5	17.5	–0.866	0.5
6	0.5	32.5	–0.866	0.5
7	–0.5	17.5	0.866	4
8	–0.5	17.5	0	2.25
9	0.5	32.5	0	2.25

C_1 and C_2 are the coded values for the levels of NaCl concentration ($g \cdot L^{-1}$) and vortex time (min), respectively. The relationship between coded and real values is given by: $C_i = \left[\frac{X_i - X_i^o}{\Delta X_i}\right] \alpha$

where C_i is the coded value for the level of factor i, X_i is its real value in an experiment, X^o_i is the real value at the center of the experimental domain, ΔX_i is the step of variation of the real value, and α is the coded value limit for each factor.

The number of experiments required (N) is given by $N = k^2 + k + C_0$, where k is the number of variables and C_o is the number of center points.

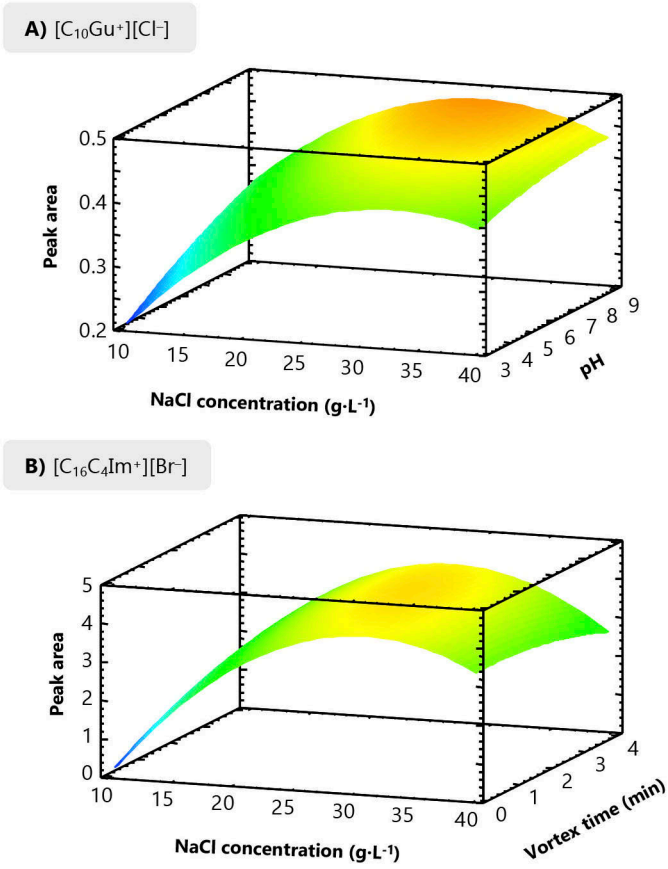

Figure IV.9. Three-dimensional response surfaces obtained with the Doehlert experimental design during the optimization of the *in situ* DLLME-FAAS method for the determination of Cu (II) using **A)** $[C_{10}Gu^+][Cl^-]$ and **B)** $[C_{16}C_4Im^+][Br^-]$ IL-based surfactants.

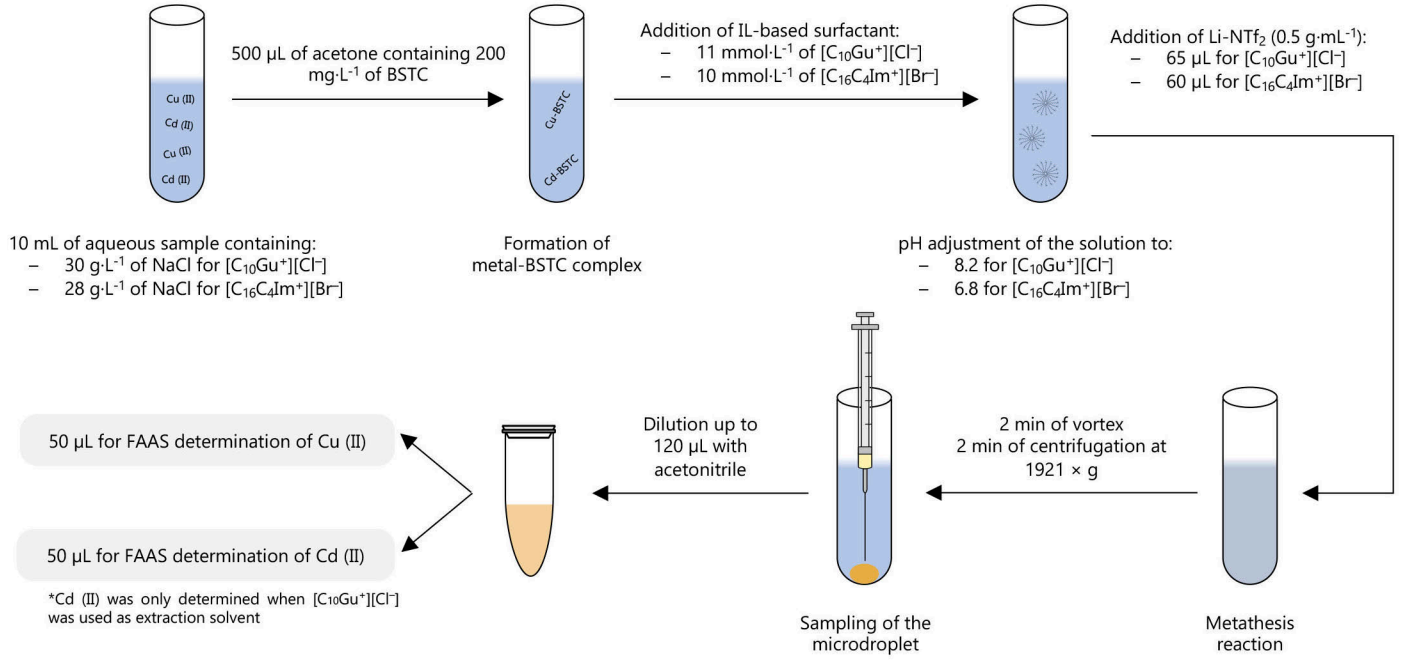

Figure IV.10. Scheme of the optimized *in situ* DLLME-FAAS method for the determination of Cu^{2+} and Cd^{2+} using the IL-based surfactants: $[C_{10}Gu^+][Cl^-]$ or $[C_{16}C_4Im^+][Br^-]$.

2. Analytical performance of the *in situ* DLLME-FAAS method using IL-based surfactants

The analytical characteristics of the *in situ* DLLME-FAAS methods using $[C_{10}Gu^+][Cl^-]$ or $[C_{16}C_4Im^+][Br^-]$ ILs as extraction solvents for the determination of Cu (II) are summarized in Table IV.16. Both methods present adequate determination coefficients (R^2) within the wide linear ranges studied, which extend from 1 to 150 $\mu g \cdot L^{-1}$ for $[C_{10}Gu^+][Cl^-]$ IL, and from 4 to 300 $\mu g \cdot L^{-1}$ for $[C_{16}C_4Im^+][Br^-]$.

The limits of detection (LODs) and limits of quantification (LOQs) were estimated as 3 and 10 times the signal-to-noise ratio (S/N), respectively. Both were experimentally verified by preparing aqueous standards at those metal concentrations and subjecting them to the entire *in situ* DLLME-FAAS method. The LOD obtained for the determination of Cu (II) using the guanidinium IL-based surfactant was 0.30 $\mu g \cdot L^{-1}$, while a LOD of 1.1 $\mu g \cdot L^{-1}$ was found for the $[C_{16}C_4Im^+][Br^-]$ IL. Therefore, the *in situ* DLLME-FAAS method developed using the $[C_{10}Gu^+][Cl^-]$ IL provides better sensitivity than the imidazolium IL-based surfactant (4 times lower LOD).

The precision of the methods was evaluated as the relative standard deviation (RSD, %) in intra- and inter-day studies in quadruplicate, and at two different spiked concentration levels: low (4 or 6 $\mu g \cdot L^{-1}$) and high (100 $\mu g \cdot L^{-1}$). Both IL-based surfactants provided adequate RSD values, being up to 11 % in intra-day studies and up to 25 % in inter-day studies. However, the $[C_{10}Gu^+][Cl^-]$ IL-based surfactant showed better reproducibility, with a RSD value of 17 % in inter-day studies at the low spiked level (4 $\mu g \cdot L^{-1}$).

The relative recovery (RR, %) of the entire method was calculated as the ratio of the concentration calculated with the obtained calibration curves and the spiked concentration of Cu (II). The RR values obtained with both IL-based surfactants at two different spiked levels were satisfactory, being 97.8 % for $[C_{10}Gu^+][Cl^-]$ and 113 % for $[C_{16}C_4Im^+][Br^-]$ at the low spiked level.

The enrichment factors (E_F) of the entire *in situ* DLLME-FAAS method were calculated as the ratio between the concentration of Cu (II) calculated using the instrumental calibration curves (without any preconcentration step) but using the peak area obtained when applying the entire method, and the spiked concentration of Cu (II). The maximum enrichment factor of the method (E_{Fmax}) was estimated as the ratio of the initial aqueous solution (10 mL) and the volume of the diluted extract (120 µL). Therefore, the theoretical E_{Fmax} for the developed *in situ* DLLME-FAAS method is ≈ 83.3. The extraction efficiency values (E_R, %) were determined as the ratio between E_F and E_{Fmax}. Enrichment factors higher than 57 were obtained when both IL-based surfactants were used as extraction solvents for Cu (II) at high and low spiked levels. Hence, adequate E_R values were found for both methods, up to 85 % for $[C_{10}Gu^+][Cl^-]$ at the low spiked level, which evidences the high preconcentration achieved when this IL is used. It is important to mention that E_R values higher than 65 % are quite adequate considering that a microextraction approach is being performed [16].

Table IV.16. Analytical performance of the *in situ* DLLME-FAAS methods developed for the determination of Cu (II) and Cd (II) in waters using the $[C_{10}Gu^+][Cl^-]$ IL-based surfactant as extraction solvent, and for the determination of Cu (II) when using $[C_{16}C_4Im^+][Br^-]$.

Parameter	**Cu (II) determination**		**Cd (II) determination**
	$[C_{16}C_4Im^+][Br^-]$	**$[C_{10}Gu^+][Cl^-]$**	**$[C_{10}Gu^+][Cl^-]$**
Determination coefficient, R^2	0.996	0.998	0.999
Standard deviation of the residuals or error of the estimate ($s_{y/x}$)	0.05	0.04	0.04
Linearity range[a] (μg L^{-1})	4–300	1–150	2–100
IL microdroplet volume (μL) / final volume after dilution (μL)	≈ 45 / ≈ 120	≈ 21 / ≈ 120	≈ 21 / ≈ 120
LOD[b] (μg L^{-1}) / LOQ[c] (μg L^{-1})	1.1 / 3.5	0.30 / 0.90	0.50 / 1.5
Intra-day RSD[d] (%) /	11 / 6	9.4 / 4	10 / 6
Concentration (μg L^{-1})	7 / 100	7 / 100	4.5 / 100
Inter-day RSD[e] (%) /	25 / 6	17 / 4	16 / 6
Concentration (μg L^{-1})	8 / 100	8.5 / 100	6.5 / 100
RR[f] (%) / Concentration (μg L^{-1})	113 / 6	97.8 / 4	102 / 6
	103 / 100	102 / 100	96.7 / 100
E_F[g] / Concentration (μg L^{-1})	62 / 6	71 / 4	78 / 6
	65 / 100	57 / 100	61 / 100
E_R[h] (%) / Concentration (μg L^{-1})	74 / 6	85 / 4	94 / 6
	78 / 100	69 / 100	73 / 100

[a] Linearity range for n = 7 calibration levels.
[b] Limit of detection, calculated as 3 times the S/N ratio.
[c] Limit of quantification, calculated as 10 times the S/N ratio
[d] Intra-day precision (n = 4) tested at two concentration levels.
[e] Inter-day precision (n = 4) tested at two concentration levels.
[f] Relative recovery (n = 4) tested at two concentration levels.
[g] Enrichment factor, tested at two concentration levels.
[h] Extraction efficiency (tested at two concentration levels), E_{Fmax} = 83.3.

The *in situ* DLLME-FAAS method using IL-based surfactants was also used for the determination of Cd (II). Given the better performance of $[C_{10}Gu^+][Cl^-]$ *versus* $[C_{16}C_4Im^+][Br^-]$, only the method with the guanidinium IL was chosen for Cd (II) determination. The final volume of the microdroplet after dilution with acetonitrile (120 µL) allows the determination of both metals using the same microdroplet, since the optimum conditions of the FAAS only required 50 µL for the measurement. In this sense, the method allowed the simultaneous extraction and preconcentration of two metals (multi-analyte determination). Thus, Table IV.16 also includes several analytical parameters for the determination of Cd (II) with $[C_{10}Gu^+][Cl^-]$ as extraction solvent. The entire method showed a R^2 value of 0.999 within the studied linear range. The obtained LOD was 0.50 $\mu g \cdot L^{-1}$, while the RSD values were lower than 10 % for intra-day studies, and lower than 17 % for inter-day studies. Regarding RR values, they were around 100 % at the low and high spiked levels, while an extraction efficiency (E_R) of 94 % was found for the determination of Cd (II) at 6 $\mu g \cdot L^{-1}$. These values demonstrate that the optimum experimental conditions obtained for the determination of Cu (II) with the proposed method are also adequate for the extraction of Cd (II). Furthermore, the analytical parameters obtained for the determination of both Cu (II) and Cd (II) indicate the outstanding applicability of the $[C_{10}Gu^+][Cl^-]$ IL-based surfactant as extractant solvent in the *in situ* DLLME-FAAS method for the environmental monitoring of these metal ions.

The precision of the calibrations for the entire *in situ* DLLME-FAAS method for the determination of Cu (II) using both $[C_{10}Gu^+][Cl^-]$ and $[C_{16}C_4Im^+][Br^-]$, and the determination of Cd (II) using $[C_{10}Gu^+][Cl^-]$ IL, were also evaluated. The tool was the ratio between the slopes of the calibration curves obtained in 3 different days. If the ratio between the slopes is in the range of 0.8–1.2, it is considered that there are no significant differences between the calibration curves, assuming a maximum variation of 20 % [17]. Table IV.17 includes the slopes and the slopes ratios calculated for the calibration curves obtained in 3 non-consecutive days. As it can be observed, the slopes ratios varied between 0.89 and 1.16 for all cases, and therefore the robustness of the developed method is also demonstrated.

Table IV.18 summarizes several experimental conditions and analytical parameters of different *in situ* DLLME methods reported in the literature for the determination of copper or cadmium, together with the characteristics of the method developed in this study using the $[C_{10}Gu^+][Cl^-]$ IL-based surfactant [8–11]. Better analytical performance in terms of LODs and preconcentration were obtained for the determination of Cu (II) using the guanidinium IL-based surfactant as extraction solvent in comparison with the *in situ* DLLME-FAAS method described using the $[C_{16}C_4Im^+][Br^-]$ [8]. In the case of the extraction of Cd (II), the preconcentration obtained in this study is comparable to that reported by Mahpishanian *et al.* using the $[C_6MIm^+][BF_4^-]$ IL [10]. Nevertheless, it is important to highlight that lower amounts of the low cytotoxic $[C_{10}Gu^+][Cl^-]$ IL are used in this study (≈ 25 mg) in comparison with the 30 mg of $[C_6MIm][BF_4^-]$ required in their method. Besides, similar E_F values are achieved in this study despite the dilution of the IL microdroplet leads to a higher final extract volume.

Table IV.17. Reproducibility of the entire *in situ* DLLME-FAAS method evaluated as the ratio between the slopes corresponding to calibration curves obtained in different non-consecutive days.

Calibration curve	Slope ± t·SD*	Dataset	Slopes ratio
Cu (II) determination using [$C_{10}Gu^+$][Cl^-]			
day 1	4.2 ± 0.3	test 1–2	0.89
day 2	4.7 ± 0.2	test 1–3	1.04
day 3	4.0 ± 0.2	test 2–3	1.16
Cu (II) determination using [$C_{16}C_4Im^+$][Br^-]			
day 1	7.00 ± 0.05	test 1–2	1.09
day 2	6.4 ± 0.2	test 1–3	1.06
day 3	6.6 ± 0.2	test 2–3	0.97
Cd (II) determination using [$C_{10}Gu^+$][Cl^-]			
day 1	9.8 ± 0.4	test 1–2	1.04
day 2	9.4 ± 0.5	test 1–3	0.96
day 3	10.2 ± 0.4	test 2–3	0.92

* 95 % confidence limits for n = 7 calibration levels (5 degrees of freedom).

Clearly, lower LODs are reported for the preconcentration of Cu (II) [9] and Cd (II) [11] when electrothermal atomic absorption spectroscopy (ETAAS) is used. This analytical technique allows the direct injection of the IL microdroplet without its dilution to reduce the viscosity and ensure the compatibility, which results in low volumes of the final extracts (30–50 µL) and thus, higher sensitivity and enrichment factors were reached. It is expected that the application of the current method with [$C_{10}Gu^+$][Cl^-] with ETAAS can also lead to much better sensitivity, while using a more environmental-friendly solvent.

Table IV.18. Comparison of several parameters of the analytical performance of the developed *in situ* DLLME method and other *in situ* DLLME methods reported in the literature for the determination of Cu (II) or Cd (II) in water samples.

Metal	Sample (mL)	Complexing agent	IL (concentration)	Anion-exchange reagent	µL of the final extract (diluted or not) / µL subjected to AAS	Detection	LOD[a] ($\mu g \cdot L^{-1}$)	E_F[b]	Ref.
Cu (II)	tap water (10 mL)	BSTC	$[C_{10}Gu^+][Cl^-]$ (11 $mmol \cdot L^{-1}$)	Li-NTf_2	120 / 50	FAAS	0.3	77	This study
Cu (II)	tap water and wastewater (10 mL)	DDTC[c]	$[C_{16}C_4Im^+][Br^-]$ (25.2 $mmol \cdot L^{-1}$)	Li-NTf_2	270 / 50	FAAS	5.1	36	[8]
Cu (II)	aqueous extract from soil and sediments (10 mL)	DDTC[c]	$[C_6MIm^+][Cl^-]$ (≈ 10 $mmol \cdot L^{-1}$)	Li-NTf_2	48 / 10	ETAAS[e]	0.004	200	[9]
Cd (II)	tap water (10 mL)	BSTC[c]	$[C_{10}Gu^+][Cl^-]$ (11 $mmol \cdot L^{-1}$)	Li-NTf_2	120 / 50	FAAS	0.5	70	This study
Cd (II)	seawater, spring and river water (5 mL)	DDTP[e]	$[C_6MIm^+][BF_4^-]$ (≈ 24 $mmol \cdot L^{-1}$)	$NaPF_6$	58 / 58	FAAS	0.07	78	[10]
Cd (II)	tap water, bottled water and seawater (10 mL)	APDC[f]	$[C_8MIm^+][Cl^-]$ (10 $mmol \cdot L^{-1}$)	Li-NTf_2	30 / 30	ETAAS[e]	0.0002	280	[11]

[a] Limit of detection.
[b] Enrichment factor.
[c] Diethyl dithiocarbamate.
[d] Electrothermal atomic absorption spectroscopy.
[e] O,O-diethyldithiophosphate.
[f] Ammonium pyrrolidine dithiocarbamate.

3. Influence of foreign ions in the *in situ* DLLME-FAAS method using IL-based surfactants

Environmental waters commonly contain other co-existing ions apart from the Cu (II) and Cd (II) cations determined in this study. Therefore, the BSTC complexing agent can react with those other ions and affect the extraction efficiency of the method developed. Thus, the influence of these interfering ions was investigated performing the optimized *in situ* DLLME-FASS method with ultrapure water containing 30 $\mu g \cdot L^{-1}$ of Cu (II) and Cd. (II), and concentrations up to 600 times higher of each foreign cation: Ca (II), Cr (III), Co (II), Pb (II), Zn (II), Ba (II), Mg (II), Ni (II), and Mn (II). The influence of the foreign ions was accomplished for both IL-based surfactants, calculating the RR values (in %) by comparing the absorbance found when the method was carried out in presence of the interfering ion and the absorbance obtained with only Cu (II) and Cd (II) in the aqueous sample. The tolerance limit of each foreign ion was estimated as the ratio between the concentration of the foreign ion and the concentration of the studied ion for which any variation of the obtained absorbance was observed. The results are shown is Table IV.19.

Table IV.19. Influence of foreign ions in the extraction performance of the entire *in situ* DLLME-FAAS method for the termination of Cu^{2+} and Cd^{2+} using $[C_{10}Gu^+][Cl^-]$, and for the determination of Cu^{2+} using $[C_{16}C_4Im^+][Br^-]$.

Foreign cation	Cu (II) determination using $[C_{10}Gu^+][Cl^-]$		Cd (II) determination using $[C_{10}Gu^+][Cl^-]$		Cu (II) determination using $[C_{16}C_4Im^+][Br^-]$	
	Tolerance limit[a]	RR[b] (%)	Tolerance limit[a]	RR[b] (%)	Tolerance limit[a]	RR[b] (%)
Ba (II)	100	107	100	91.6	100	88.1
Ca (II)	100	114	600	99.7	100	90.1
Cr (III)	100	92.2	100	86.1	100	94.3
Co (II)	100	96.7	100	101	100	102
Mg (II)	100	99.6	600	96.8	100	86.2
Mn (II)	100	92.1	80	94.0	100	91.6
Ni (II)	100	109	100	102	100	96.2
Pb (II)	100	91.9	80	103	100	81.2
Zn (II)	100	95.2	100	101	100	91.8

[a] Ratio between the concentration of the foreign ion and the concentration of studied ion (Cu (II) or Cd (II) at 30 $\mu g \cdot L^{-1}$).

[b] Relative recovery in %, calculated as the ratio between the absorbance found when the method was carried out in presence of the interfering ion and the absorbance obtained with only Cu (II) or Cd (II).

The tolerance limit for all the studied foreign ions in the determination of Cu (II) using either $[C_{10}Gu^+][Cl^-]$ or $[C_{16}C_4Im^+][Br^-]$ was 100, with average RR values of 99.7 % and 91.3 %, respectively. In the case of Cd (II) using the guanidinium IL-based surfactant as extraction solvent, tolerance limits of 80 were obtained for Mn (II) and Pb (II), 600 for Ca (II) and Mg (II), and 100 for the remaining interfering ions, with an average RR value of 97.2 %. Therefore, the determination of copper with the proposed method using $[C_{10}Gu^+][Cl^-]$ can be accomplished in presence of these foreign anions at concentrations 100 times higher than the concentration of Cu (II). Concentrations from 80 to 600 times higher of the interfering cations do not interfere in the determination of Cd (II) using the guanidinium IL as extraction solvent in the *in situ* DLLME-FAAS method.

4. Traceability and matrix effect in tap water using $[C_{10}Gu^+][Cl^-]$ as extraction solvent

Given the low cytotoxicity of the $[C_{10}Gu^+][Cl^-]$ IL-based surfactant and the better sensitivity, reproducibility, and preconcentration achieved when this IL is used in comparison with the imidazolium IL, only $[C_{10}Gu^+][Cl^-]$ was selected for further analytical performance studies. The traceability of the *in situ* DLLME-FAAS method using the guanidinium IL-based surfactant for the simultaneous determination of Cu (II) and Cd (II) was evaluated by the analysis of a drinking water certified reference material (CRM) in triplicate. The obtained concentration was statistically compared with the theoretical value established by the manufacturer [18] and the results are shown in Table IV.20.

First, the variances associated to the calculated concentration (using the obtained calibration curves included in Table IV.16) and the concentration stated by the manufacturer of the CRM were compared by a Fisher test. The experimental *F* values (F_{exp}) were lower than the critical *F* values (F_{crit}) for Cu (II) and Cd (II) cations, with a significance level $\alpha = 0.05$. Therefore, the variances were assumed equal. Then, a Student's *t* test was performed to compare the mean concentration obtained with the developed *in situ* DLLME-FAAS and the mean concentration reported by the CRM manufacturer. For both cations, the calculated *t* value (t_{cal}) was lower than the critical *t* value (t_{crit}) with $\alpha = 0.05$. Thus, no significant differences were found between the concentration values and, consequently, the accuracy of the method was demonstrated for the determination of both Cu (II) and Cd (II).

In order to validate the applicability of the *in situ* DLLME-FAAS method using $[C_{10}Gu^+][Cl^-]$ as extraction solvent, the possible matrix effect exerted by tap water was assessed by recovery studies. Tap water 1 were first analyzed with the entire method, showing to be free of Cd (II) and Cu (II) or at least with contents lower than their respective LOQs. Thus, tap water 1 and ultrapure water were spiked with both cations at 6 $\mu g \cdot L^{-1}$ and subjected to the developed microextraction method in quadruplicate. Then, the concentrations obtained in spiked tap water were statistically compared with the concentration values found in ultrapure water for both cations, using the calibration curves determined in ultrapure water in both cases (Table IV.16).

Table IV.20. Statistical parameters obtained in the evaluation of the traceability and matrix effect in tap water 1 of the *in situ* DLLME-FAAS method using $[C_{10}Gu^+][Cl^-]$ as extraction solvent.

Metal ion	Fisher test[a]			Student's *t* test[d]				
	F_{exp}[b]	F_{crit}[c]	Results	Variances	t_{cal}[e]	t_{crit}[f]	Results	Matrix effect
Comparison between the calculated concentration and the theoretical concentration in the analysis of the CRM (n = 3)								
Cu (II)	18.3	19.0	$F_{exp} < F_{crit}$	Equal	2.63	2.78	$\|t_{cal}\| < t_{crit}$	No
Cd (II)	18.2	19.0	$F_{exp} < F_{crit}$	Equal	1.97	2.78	$\|t_{cal}\| < t_{crit}$	No
Comparison between the calculated concentration in ultrapure water and tap water 1 at 6 µg·L^{-1} (n = 4)								
Cu (II)	1.15	9.28	$F_{exp} < F_{crit}$	Equal	1.43	2.45	$\|t_{cal}\| < t_{crit}$	No
Cd (II)	6.43	9.28	$F_{exp} < F_{crit}$	Equal	0.57	2.45	$\|t_{cal}\| < t_{crit}$	No

[a] Comparison between the variances of the concentration values.

[b] Calculated as the ratio between the variance (s^2) for the concentration values obtained in each case.

[c] Critical *F* value for $\alpha = 0.05$ and $n - 1$ degrees of freedom.

[d] Comparison between the concentration values obtained in each case, asuming equal variances.

[e] Calculated as $t_{cal} = (\bar{x}_1 - \bar{x}_2)/s\sqrt{(1/n_1 + 1/n_2)}$, being $\bar{x}_i$ the mean concentration value in each case, $s = \sqrt{\{(n_1 - 1)s_1^2 + (n_2 - 1)s_2^2\}/(n_1 + n_2 - 2)}$, and n_i the number of replicates in each case.

[f] Critical Student's *t* value for $\alpha = 0.05$ and $(n_1 + n_2 - 2)$ degrees of freedom.

The statistical parameters for the matrix effect assessment are included in Table IV.20. As it can be observed, the variances were assumed equal since the F_{exp} values were lower than the F_{crit} values for both Cu (II) and Cd (II) cations with $\alpha = 0.05$. In the Student's *t* test performed to compare the mean concentrations obtained in ultrapure and tap water 1, no differences ($\alpha = 0.05$) were obtained since t_{cal} was lower than t_{crit} for both cations. Therefore, tap water was considered free of matrix effect.

REFERENCES

[1] S. Bakırdere, C. Bölücek, M. Yaman, Environ. Monit. Assess. 188 (2016) 132.

[2] P. Chen, X. Duan, M. Li, C. Huang, J. Li, R. Chu, H. Ying, H. Song, X. Jia, Q. Ba, H. Wang, Toxicol. Appl. Pharmacol. 310 (2016) 150–158.

[3] L.M. Gaetke, H.S. Chow-Johnson, C.K. Chow, Arch. Toxicol. 88 (2014) 1929–1938.

[4] W. Wu, S. Jiang, Q. Zhao, K. Zhang, X. Wei, T. Zhou, D. Liu, H. Zhou, R. Zhong, Q. Zeng, L. Cheng, Z. Miao, Q. Lu, Sci. Total Environ. 622–623 (2018) 184–191.

[5] P. Zatta, A. Frank, Brain Res. Rev. 54 (2007) 19–33.

[6] The National Primary Drinking Water Regulations of The United States Environmental Protection Agency, https://www.epa.gov/ground-water-and-drinking-water/national-primary-drinking-water-regulations#seven (Accessed: 2nd October 2020).

[7] M. Baghdadi, F. Shemirani, Anal. Chim. Acta 634 (2009) 186–191.

[8] J.F. Ayala-Cabrera, M.J. Trujillo-Rodríguez, V. Pino, Ó.M. Hernández-Torres, A.M. Afonso, J. Sirieix-Plénet, Int. J. Environ. Anal. Chem. 96 (2016) 101–118.

[9] E. Stanisz, A. Zgoła-Grześkowiak, Talanta 115 (2013) 178–183.

[10] S. Mahpishanian, F. Shemirani, Talanta 82 (2010) 471–476.

[11] I. López-García, Y. Vicente-Martínez, M. Hernández-Córdoba, Talanta 110 (2013) 46–52.

[12] L. Vidal, S.G. Silva, A. Canals, J.A. Nóbrega, Talanta 148 (2016) 602–608.

[13] D. Dragancea, S. Shova, E.A. Enyedy, M. Breza, P. Rapta, L.M. Carrella, E. Rentschler, A. Dobrov, V.B. Arion, Polyhedron 80 (2014) 180–192.

[14] Q.Q. Baltazar, J. Chandawalla, K. Sawyer, J.L. Anderson, Colloid Surf. A-Physicochem. Eng. Asp. 302 (2007) 150–156.

[15] S.L.C. Ferreira, W.N.L. dos Santos, C.M. Quintella, B.B. Neto, J.M. Bosque-Sendra, Talanta 63 (2004) 1061–1067.

[16] M.J. Trujillo-Rodríguez, P. Rocío-Bautista, V. Pino, A.M. Afonso, Trac-Trends Anal. Chem. 51 (2013) 87–106.

[17] A. Pina, O. Begou, D. Kanelis, H. Gika, S. Kalogiannis, C. Tananaki, G. Theodoridis, A. Zotou, J. Chromatogr. A 1531 (2018) 53–63.

[18] J.N. Miller and J.C. Miller, Statistics and Chemometrics for Analytical Chemistry, Pearson Education Limited (2010) 37–73.

Section IV.1.2

Improving the greenness of liquid-phase microextraction methods based on low cytotoxic ionic liquids

The incorporation of ILs containing the guanidinium cation, categorized as low cytotoxic solvents, undoubtedly permits the setup of environmental-friendly *in situ* DLLME methods for different analytical applications, as those reported in Section IV.1.1. Despite their success, the strategy followed to separate the IL with the preconcentrated analytes requires the use of fluorinated salts to generate a water-insoluble IL. This anion-exchange salt, and consequently the water-insoluble IL obtained in the final step, are considered more toxic than the initial water-soluble IL, due to the ability of fluorinated anions to experience hydrolysis (thus yielding harmful products). Therefore, the environmentally friendliness of the procedure is seriously compromised when using these fluorinated salts to accomplish the metathesis reaction.

The aim of the studies included in this section is to propose new and greener strategies to promote the insolubilization of the miscible low cytotoxic IL in DLLME methods. In the first approach, the non-hazardous sodium perchlorate salt is used as alternative anion-exchange reagent for the insolubilization of a guanidinium IL-based surfactant. The method, termed salt-induced DLLME, was used for the determination of biomarkers of exposure to PAHs in urine samples. In the second strategy, the preconcentration method is based on a miniaturized ABS. The system is composed of the aqueous sample, the guanidinium IL with the shorter alkyl chain and lower cytotoxicity as extraction solvent, and non-hazardous potassium phosphate tribasic as salting-out agent. The miniaturization of the system was achieved by using small amounts of the components and a high ratio of IL and aqueous sample, which also allowed obtaining high enrichment factors. In this μ-ABS method, and as a proof of concept, the procedure was applied to develop an analytical method for the determination of PAHs in diverse water samples.

Section IV.1.2.1

Salt-induced dispersive liquid-liquid microextraction using a low cytotoxic guanidinium ionic liquid: application for the determination of monohydroxylated polycyclic aromatic hydrocarbons in urine

Analytical and Bioanalytical Chemistry 410 (2018) 4701–4713

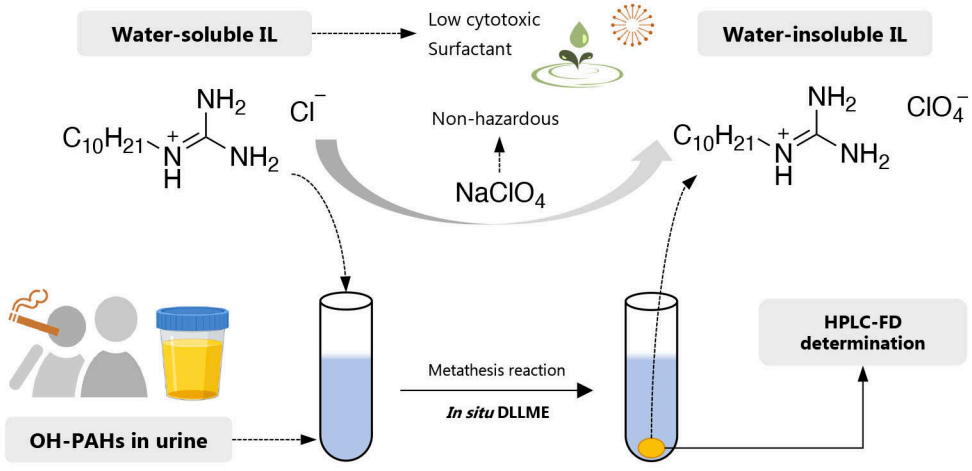

1. Selection of biomarkers of exposure to PAHs as target analytes and HPLC-FD determination

A salt-induced DLLME-HPLC-FD method was developed using the $[C_{10}Gu^+][Cl^-]$ IL-based surfactant as extraction solvent and $NaClO_4$ as anion-exchange reagent to ensure the insolubilization of the IL-containing the target analytes. The method was applied for the determination of the monohydroxylated metabolites of PAHs (OH-PAHs), which are the most common urinary biomarkers of PAHs exposure [1]. The occurrence of OH-PAHs in urine has been reported in different studies, reflecting the relation between the presence of these compounds and environmental and lifestyle factors, such as location [2], workplace [3,4], diet [2,5], and smoking habits [6]. Furthermore, higher concentrations of OH-PAHs in urine have been directly associated with greatest likelihood of suffering cardio-metabolic, kidney [7], reproductive [8] and lung dysfunctions [9].

The separation and determination of OH-PAHs have been accomplished using GC in combination with MS [10,11], normally with the isotope dilution method using ^{13}C labeled standards. However, GC needs derivatization of the polar analytes prior to injection, clearly increasing the costs and analysis time. Therefore, LC in combination with FD [12–14] or MS [15–20] has been more commonly employed for the quantification of these analytes, obtaining comparable results to those obtained by GC-MS in terms of sensitivity and accuracy.

HPLC-FD was used as determination technique in this study to take advantage of the fluorescence properties of the OH-PAHs and to avoid the use of expensive instrumentation. Among all the OH-PAHs identified as biomarkers, four of them were selected as target analytes for being the most commonly found in urine samples: 2OHflu, 2OHphe, 4OHphe, and 1OHpy. The chromatographic separation was achieved under the conditions described in Section III.7.5.3, while the fluorescence detection conditions are shown in Table IV.21, including the excitation wavelength (λ_{ex}), the emission wavelength (λ_{em}), and the chromatographic time for the wavelength change. Table IV.21 also includes the retention times and several quality analytical parameters of the calibration curves of the HPLC-FD method for the OH-PAHs studied using standards in acetonitrile. Possible interferences coming from the IL are studied in further sections.

2. Optimization of the salt-induced DLLME method for the analysis of urine

During the studies on the characterization of the micellar behavior of $[C_{10}Gu^+][Cl^-]$ in presence of different salts (Section IV.1.1.1), it was observed that the addition of bulky inorganic salts (such as $NaClO_4$) resulted in the formation of a cloudy solution. After agitation, the turbidity disappeared leading to the formation of multiple microdroplets of the insolubilized guanidinium-based IL dispersed all over the aqueous solution. These experiments suggested the possibility of developing an *in situ* DLLME approach with the $[C_{10}Gu^+][Cl^-]$ IL but using $NaClO_4$ to promote the insolubilization instead of the fluorinated salts commonly used [21] (Sections IV.1.1.2 and IV.1.1.3).

Table IV.21. Several quality analytical parameters of the HPLC-FD method (without the preconcentration step) obtained with OH-PAHs standards in acetonitrile.

Analyte	Excitation / emission wavelength[a] (nm)	Time of wavelength change (min)	Retention time ± SD[b] (min)	(Slope ± t·SD[c])·10^{-4}	R^2 [d]	LOD[e] ($\mu g \cdot L^{-1}$)	LOQ[f] ($\mu g \cdot L^{-1}$)	Intra-day RSD[g] (%)	
								Low level: 2 $\mu g \cdot L^{-1}$	High level: 40 $\mu g \cdot L^{-1}$
2OHflu	270 / 327	8.4	9.1 ± 0.1	14.7 ± 0.3	0.998	0.05	0.1	1.1	0.8
2OHphe	260 / 350	9.7	10.2 ± 0.1	7.7 ± 0.1	0.999	0.1	0.5	1.5	0.6
4OHphe	256 / 370	11.0	12.0 ± 0.1	7.0 ± 0.1	0.999	0.1	0.5	3.4	0.3
1OHpy	240 / 387	12.7	13.3 ± 0.1	12.6 ± 0.2	0.999	0.1	0.5	9.6	2.1

[a] Excitation and emission splits were fixed at 18 nm, while the gain was set at a value of 100.
[b] Standard deviation of the retention time (n = 30).
[c] 95 % confidence limits for n = 7 calibration levels (5 degrees of freedom) within the calibration range: 1–100 $\mu g \cdot L^{-1}$.
[d] Determination coefficient.
[e] Limit of detection, experimentally determined by decreasing the concentration until a signal-to-noise (S/N) ratio of 3 was obtained.
[f] Limit of quantification, estimated as 10/3 times the LOD, and verified with standards prepared at these levels.
[g] Relative standard deviation of the estimated concentration, obtained with standards not included as calibration levels (n = 3).

$NaClO_4$ concentrations ranging from 1 to 15 % (w/v) were evaluated to promote the insolubilization of the IL, fixing the vortex stirring to 3 min, and 8 min of centrifugation (2504 × g), to obtain the microdroplet. The volume of the initial aqueous solution was fixed to 10 mL, whereas the volume of the $[C_{10}Gu^+][Cl^-]$ IL-based surfactant was ≈ 20 µL to ensure a high enrichment factor. The addition of $NaClO_4$ salt to the initial aqueous solution was carried out by adding appropriate volumes of a $NaClO_4$ aqueous solution at 100 % (w/v) to obtain the desired concentration in the tube. $NaClO_4$ contents lower than 3.5 % (w/v) in the tube did not cause the turbidity of the aqueous solution, while concentrations higher than 10 % (w/v) led to the solidification of the guanidinium IL. Therefore, ≈ 5 % (w/v) of salt in the tube was selected as optimum concentration since it provided the most reproducible microdroplet. Considering the type of samples to be analyzed with the proposed method, different amounts of a urine sample (non-smoker female) were diluted up to 10 mL and the insolubilization of the IL was performed. 1 mL of urine was selected as maximum volume of sample in view of the fact that higher urine volumes caused the solidification of the IL, which remained stuck on the walls of the tube.

The centrifugation step was fixed at 8 min using 2504 × g in subsequent experiments, being the time and speed required to settle the maximum amount of IL as a microdroplet in the bottom of the tube. Once the microdroplet was obtained, it could be collected using a microsyringe. The removal of the supernatant or the incorporation of conical centrifuge tubes may also be useful to simplify the collection of the microdroplet.

The obtained microdroplet of the IL must be diluted prior to its injection in the HPLC-FD, to ensure its compatibility with the analytical system due to its viscosity, and to avoid possible interferences in the chromatographic determination. In this sense, considering the results obtained in the previous study with the $[C_8Gu^+][Cl^-]$ IL (Section IV.1.1.2), the resulting microdroplet was diluted up to 60 µL with the initial mobile phase: a mixture of acetonitrile and water (30:70, v/v). Figure IV.11 A) shows a representative chromatogram obtained when injecting in the HPLC-FD a standard solution of the analytes in acetonitrile, while Figure IV.11 B) shows a chromatogram obtained after subjecting a non-spiked synthetic urine sample to the salt-induced DLLME method. The guanidinium-IL provided several signals at ≈ 11 and 14–15 min that did not interfere in the separation of the analytes.

The remaining variables that may have an effect in the extraction efficiency of the developed method were the pH of the sample and the vortex time required to speed up the insolubilization of the IL. The optimization of these two parameters was accomplished using a simple factor by factor approach, using 1 mL of synthetic urine diluted up to 10 mL with ultrapure water as aqueous sample, with a spiking level of 0.5 $\mu g \cdot L^{-1}$ of the OH-PAHs, and keeping the remaining experimental conditions as previously described. All the experiments were performed in triplicate and using the peak area obtained after the injection of the diluted microdroplet as a measure of the extraction efficiency.

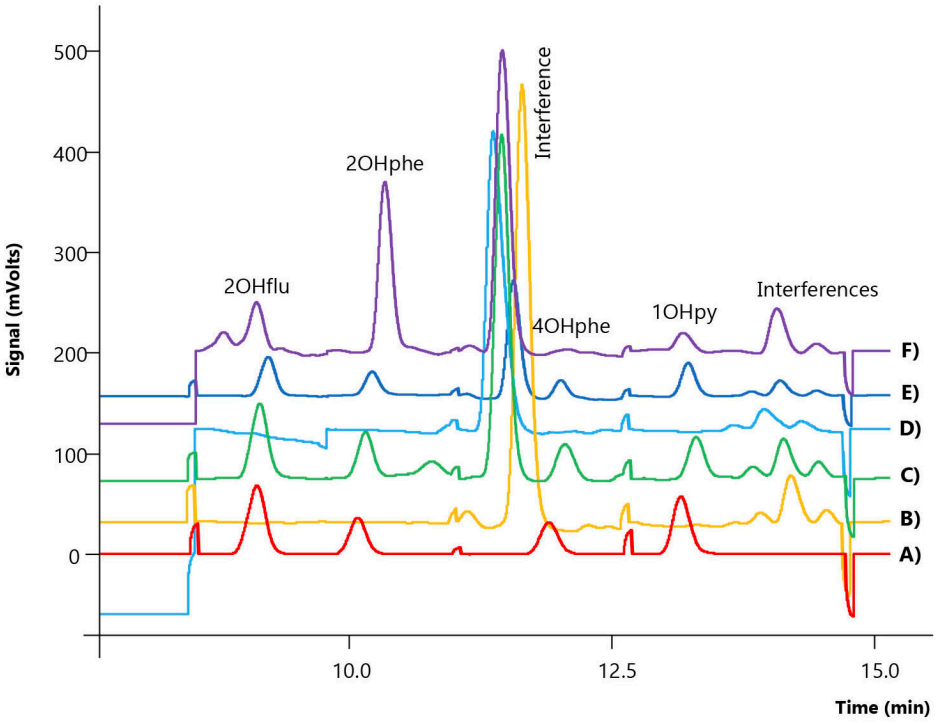

Figure IV.11. Representative chromatograms of **A)** the injection of a standard solution containing 5 $\mu g \cdot L^{-1}$ of the analytes (standards in acetonitrile) in the HPLC-FD system, **B)** the injection of an extract obtained after subjecting a non-spiked synthetic urine sample to the optimized salt-induced DLLME-HPLC-FD method, **C)** the injection of an extract after subjecting a standard prepared in synthetic urine at 0.1 $\mu g \cdot L^{-1}$ of the OH-PAHs to the optimized salt-induced DLLME-HPLC-FD method, **D)** the injection of an extract obtained after subjecting a non-spiked and non-hydrolyzed urine sample (non-smoker female) to the optimized salt-induced DLLME-HPLC-FD method, **E)** the injection of an extract obtained after subjecting a urine sample (non-smoker female) spiked with 0.1 $\mu g \cdot L^{-1}$ of the OH-PAHs to the optimized salt-induced DLLME-HPLC-FD method, **F)** the injection of an extract obtained after subjecting a non-spiked hydrolyzed urine sample (smoker female) to the optimized salt-induced DLLME-HPLC-FD method. An offset of 5 % of the signal was used in the y-axis for the overlapped representation of the chromatograms.

The pK_a values of the studied OH-PAHs range between 9.4 and 10 as shown in Table III.1. Therefore, pH values lower than 9 are advisable to obtain higher recoveries. The effect of the pH of the sample was evaluated at 2 (using a HCl/KCl buffer), 5 (using an acetic acid/sodium acetate buffer), and ≈ 6.1 (using ultrapure water without pH adjustment). Figure IV.12 A) shows the effect of the pH in the extraction of the analytes. The results obtained for the four OH-PAHs at pH 2 and 5 were similar (except for 1OHpy), but slightly lower than those obtained without pH adjustment.

Therefore, the pH of the aqueous sample was not adjusted in the next experiments to simplify the procedure.

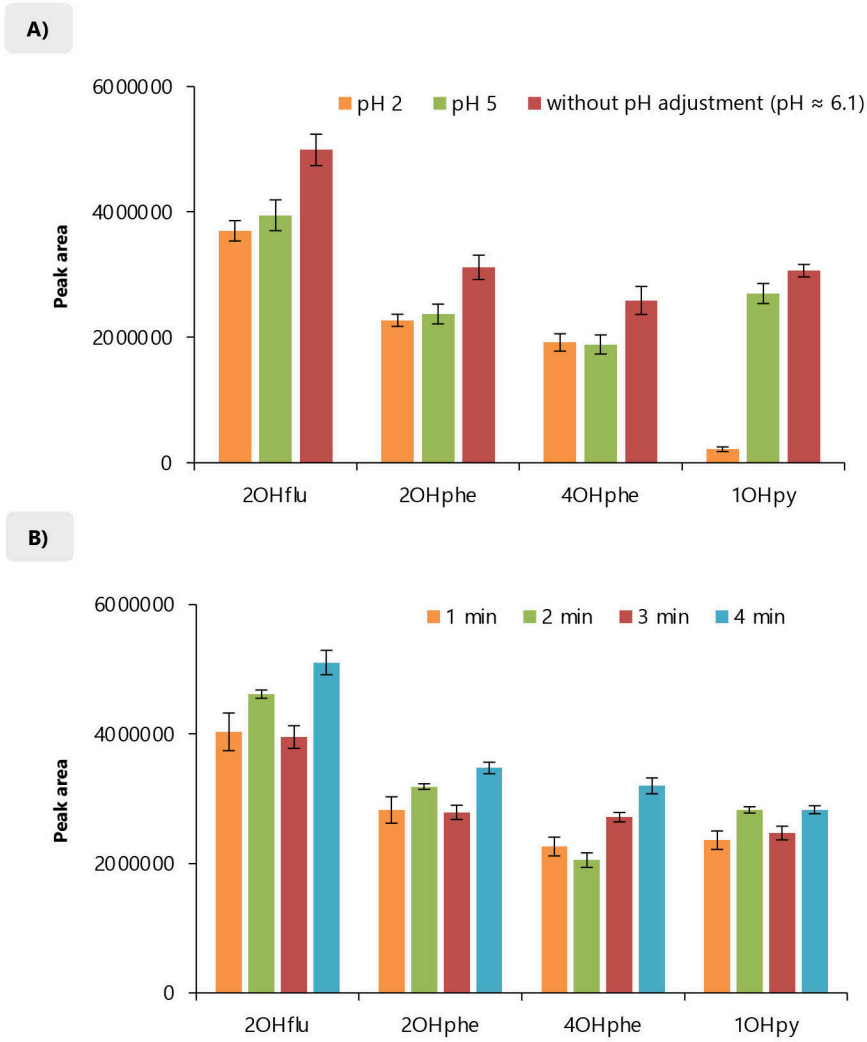

Figure IV.12. Influence of **A)** the pH of the aqueous sample and **B)** the vortex time on the extraction efficiency of the salt-induced DLLME-HPLC-FD method for the determination of OH-PAHs. Fixed experimental conditions were: 1 mL of synthetic urine diluted up to 10 mL with ultrapure water containing 0.5 $\mu g \cdot L^{-1}$ of the analytes; no pH adjustment in the study of the effect of the vortex time; 20 µL of the $[C_{10}Gu^+][Cl^-]$ IL; addition of 500 µL of $NaClO_4$ aqueous solution at 100 % (w/v) to the tube; 3 min of vortex agitation in the study of the effect of the pH; 8 min of centrifugation at 2504 × g; and dilution of the microdroplet up to 60 µL with the initial HPLC mobile phase. All experiments were carried out in triplicate.

The stirring time after the addition of $NaClO_4$ plays an important role in the extraction efficiency of the method as it ensures a quick insolubilization of the IL. Results obtained by application of different vortex times are shown in Figure IV.12 B). Significant differences were not observed among the different vortex times for all the OH-PAHs. However, 4 min provided higher peak areas, particularly for 2OHflu and 4OHphe. Therefore, 4 min were selected as optimum stirring vortex time to improve the efficiency of the method. Figure IV.13 shows the schematic procedure of the developed salt-induced DLLME method under optimum conditions for the extraction of OH-PAHs.

3. Analytical performance of the salt-induced DLLME-HPLC-FLD method using synthetic urine

Calibration curves of the entire method were firstly obtained with OH-PAHs standards in diluted synthetic urine, subjected to the entire salt-induced DLLME-HPLC-FD procedure. Synthetic urine was used with the purpose of verifying the viability of the developed method while mimicking as much as possible the matrix to be analyzed. Table IV.22 includes several quality analytical parameters of the method, including the linear range, the calibration sensitivity (evaluated as the slope), determination coefficients, limits of detection (LOD) and quantification (LOQ), precision, recoveries and extraction efficiency.

LODs were experimentally determined by decreasing the concentration of the standards in the diluted synthetic urine (subjected to the entire method) until a signal-to-noise ratio (S/N) of 3 was reached. LOQs were initially estimated as 10/3 times the LODs, and then also experimentally verified. Thus, LODs were 0.0005 $\mu g \cdot L^{-1}$ for 2OHflu, 2OHphe and 4OHphe, and 0.002 $\mu g \cdot L^{-1}$ for 1OHpy. These LODs were between 50 and 200 times lower than those of the HPLC-FLD method without the preconcentration step (see Table IV.21), which evidences the high preconcentration achieved with the developed microextraction method. The obtained LOQs were lower than 0.005 $\mu g \cdot L^{-1}$.

The reproducibility of the method was assessed by intra- and inter-day precision studies in triplicate at two different concentration levels: 0.08 $\mu g \cdot L^{-1}$ and 0.8 $\mu g \cdot L^{-1}$. The method exhibited good reproducibility as it is shown in Table IV.22. Relative standard deviation (RSD, in %) values in intra-day studies ranged from 2.4 % for 2OHflu to 6.6 % for 1OHpy at the low concentration level. RSD values lower than 15 % were found in the inter-day studies at both concentration levels.

The extraction performance achieved with the developed microextraction method was evaluated in terms of relative recovery (RR, %), enrichment factors (E_F) and extraction efficiency (E_R, %) at two levels of concentration (0.08 $\mu g \cdot L^{-1}$ and 0.8 $\mu g \cdot L^{-1}$) and in triplicate. The results obtained are summarized in Table IV.22. RR values were calculated as the ratio between the concentration predicted with the calibration curves of the entire method and the initial spiked concentration. Average RR values of 93.0 % and 105 % were obtained for the low and high concentration levels, respectively.

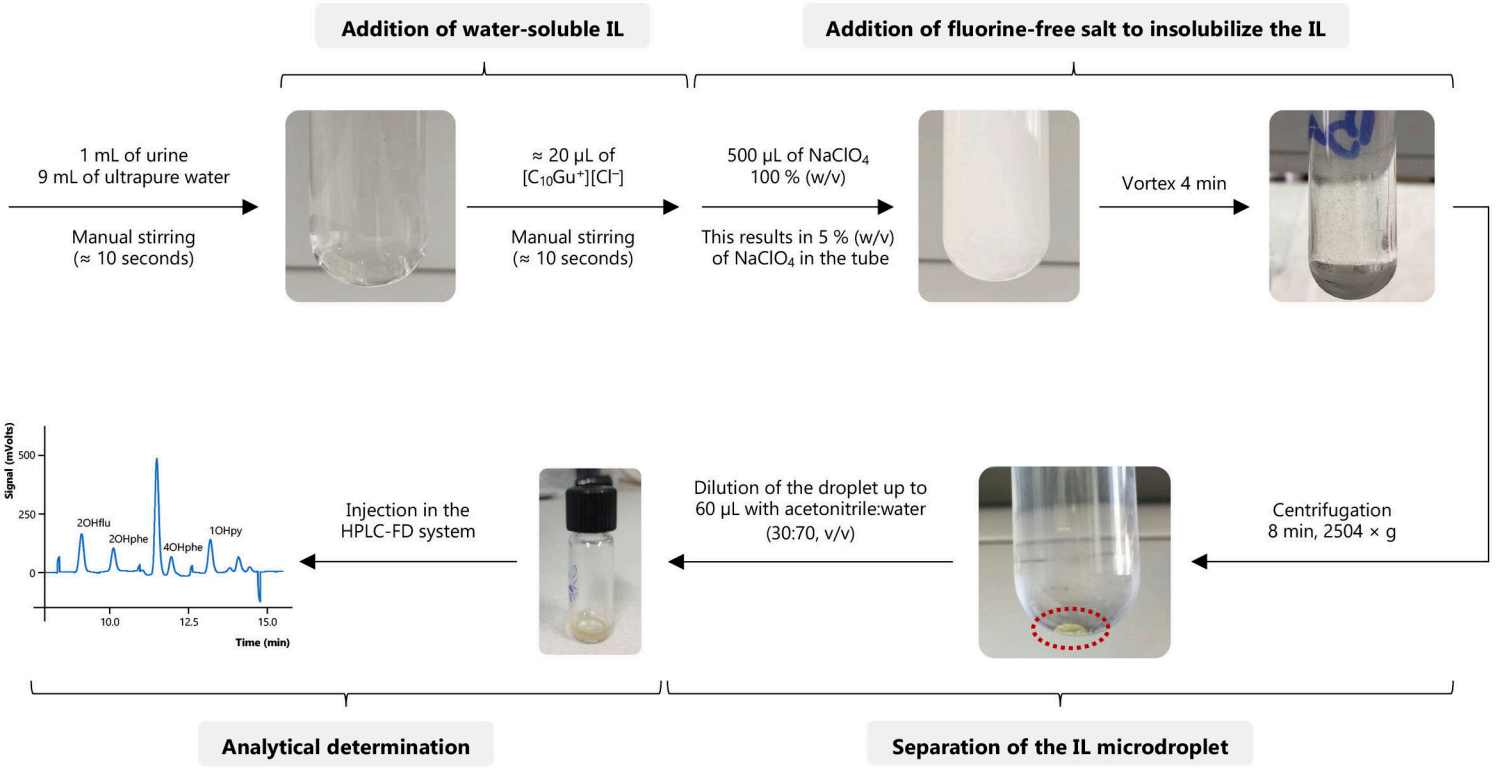

Figure IV.13. General procedure of the developed salt-induced DLLME-HPLC-FD method for the determination of OH-PAHs in urine samples.

Table IV.22. Analytical performance of the salt-induced DLLME-HPLC-FD method using synthetic urine as matrix.

Analyte	(Slope ± t·SD[a]) ·10^{-4}	R^2 [b]	LOD[c] (µg·L^{-1})	LOQ[d] (µg·L^{-1})	Concentration level: 0.08 µg·L^{-1}				Concentration level: 0.8 µg·L^{-1}			
					Intra[e]/ inter[f]-day RSD (%)	RR[g] (%)	E_F[h]	E_R[i] (%)	Intra[e]/ inter[f]-day RSD (%)	RR[g] (%)	E_F[h]	E_R[i] (%)
2OHflu	1104 ± 35	0.995	0.0005	0.002	2.4 / 14	89.5	64.4	38.6	5.7 / 8.2	101	75.5	45.3
2OHphe	632 ± 12	0.998	0.0005	0.002	4.4 / 10	89.8	76.4	45.8	7.5 / 8.9	103	85.0	51.0
4OHphe	498 ± 10	0.998	0.0005	0.002	3.5 / 9.9	87.2	83.9	50.3	8.5 / 14	99.3	72.7	43.6
1OHpy	699 ± 17	0.997	0.002	0.005	6.6 / 15	105	52.0	31.2	8.5 / 13	118	65.0	39.0

[a] 95 % confidence limits for n = 7 calibration levels (5 degrees of freedom) within the calibration range: 0.005–1.5 µg·L^{-1} for 2OHflu, 2OHphe and 4OHphe, and 0.01–1.5 µg·L^{-1} for 1OHpy.
[b] Determination coefficient.
[c] Limit of detection, experimentally determined by decreasing the concentration of the standards prepared in diluted synthetic urine (and subjected to the entire method) until a S/N ratio of 3 was obtained.
[d] Limit of quantification, estimated as 10/3 times the LOD and verified with standards prepared at these levels and subjected to the entire method.
[e] Relative standard deviation (n = 3).
[f] Relative standard deviation obtained in 3 non-consecutive days (n = 9).
[g] Relative recovery.
[h] Enrichment factor.
[i] Extraction efficiency, E_{Fmax} = 167.

With respect to the preconcentration reached, the E_F values were estimated as the ratio between the concentration associated to the peak area obtained with the overall microextraction method but calculated with the chromatographic calibration curves (Table IV.22), and the initial concentration of the OH-PAHs in the diluted synthetic urine standard. The obtained E_F values varied between 52.0 for 1OHpy at the low spiked level, and 85.0 for 2OHphe at the high spiked level. This can clearly be observed in Figure IV.11. A chromatogram obtained with the injection of a 5 $\mu g \cdot L^{-1}$ standard in the HPLC-FLD system (Figure IV.11 A)), *versus* the chromatogram obtained when injecting an extract after the application of the entire method to a standard prepared in diluted synthetic urine at 0.1 $\mu g \cdot L^{-1}$ (Figure IV.11 C)).

The overall extraction efficiency of the entire method was evaluated by means of E_R values, calculated as the ratio between the E_F values and the theoretical maximum enrichment factor (E_{Fmax}, in %). E_{Fmax} can be estimated as the ratio of the initial volume of aqueous sample (10 mL) and the volume of the resulting extract after the application of the microextraction method (60 µL after dilution of the microdroplet). Thus, the E_{Fmax} of the salt-induced DLLME method is ≈ 167. The E_R values obtained for the four analytes at both concentration levels are included in Table IV.22. All the analytes showed adequate E_R values, with average values around 43 % at both concentration levels. 2OHflue, 2OHphe and 4OHphe presented the higher E_R values, which ranged between 43.6 % for 4OHphe and 51.0 % for 2OHphe at 0.8 $\mu g \cdot L^{-1}$.

4. Analytical performance of the salt-induced DLLME-HPLC-FD method using a non-hydrolyzed urine sample

Given the complexity of the urine samples and the possible matrix effect that this type of sample can exert in the extraction of the analytes, calibration curves were also determined subjecting a diluted non-hydrolyzed urine sample to the entire salt-induced DLLME-HPLC-FD method. The urine of a non-smoker healthy female was used as blank matrix to obtain these calibration curves since theoretically, this sample may present lower contents of OH-PAHs. Furthermore, it is important to take into account that the determination of this type of analytes requires a previous enzymatic hydrolysis step of the urine. Therefore, OH-PAHs should not be detected in non-hydrolyzed urine samples and matrix-matched calibrations are obtained. Indeed, Figure IV.11 D) shows a chromatogram of an extract obtained after subjecting the non-spiked and non-hydrolyzed urine sample (non-smoker female) to the optimized salt-induced DLLME-HPLC-FD method, in which only the signals coming from the $[C_{10}Gu^+][Cl^-]$ IL are observed.

Table IV.23 includes several quality analytical parameters of this calibration performed in the non-hydrolyzed urine sample (a matrix-matched calibration), including LODs, LOQs, and the results obtained from reproducibility and extraction efficiency studies.

Table IV.23. Analytical performance of the salt-induced DLLME-HPLC-FD method using the diluted and non-hydrolyzed urine of a non-smoker female as matrix (matrix-matched calibration).

Analyte	(Slope ± t·SD[a]) ·10^{-4}	R^{2} [b]	LOD[c] (µg·L^{-1})	LOQ[d] (µg·L^{-1})	Spiked level: 0.08 µg·L^{-1}				Spiked level: 0.8 µg·L^{-1}				Spiked level: 0.5 µg·L^{-1} [j]			
					Intra[e]/ inter[f]-day RSD (%)	RR[g] (%)	E_F[h]	E_R[i] (%)	Intra[e]/ inter[f]-day RSD (%)	RR[g] (%)	E_F[h]	E_R[i] (%)	Intra[e]-day RSD (%)	RR[g] (%)	E_F[h]	E_R[i] (%)
2OHflu	454 ± 15	0.993	0.001	0.003	6.8 / 8.2	99.3	31.0	18.6	8.4 / 14	100	31.1	18.7	9.9	94.2	29.2	17.5
2OHphe	272 ± 8	0.995	0.001	0.003	6.0 / 17	109.3	44.6	26.7	7.0 / 15	110	39.6	23.7	8.6	99.5	36.2	21.7
4OHphe	231 ± 7	0.994	0.001	0.003	6.0 / 12	99.8	47.4	28.4	8.4 / 14	97.3	33.5	20.1	11.8	93.5	45.3	27.2
1OHpy	485 ± 19	0.992	0.002	0.005	5.7 / 12	98.9	39.8	23.9	11.0 / 13	95.1	36.9	22.1	7.4	116.6	46.7	28.0

[a] 95 % confidence limits for n = 7 calibration levels (5 degrees of freedom) within the calibration range: 0.003–1 µg·L^{-1} for 2OHflu, 0.003–1.5 µg·L^{-1} for 2OHphe and 4OHphe, and 0.01–1.5 µg·L^{-1} for 1OHpy.

[b] Determination coefficient.

[c] Limit of detection, experimentally determined by decreasing the concentration spiked in the diluted real urine (and subjected to the entire method) until a S/N ratio of 3 was obtained.

[d] Limit of quantification, estimated as 10/3 times the LOD and verified with standards prepared in diluted real urine at these levels and subjected to the entire method.

[e] Relative standard deviation (n = 3).

[f] Relative standard deviation obtained in 3 non-consecutive days (n = 9).

[g] Relative recovery.

[h] Enrichment factor.

[i] Extraction efficiency, E_{Fmax} = 167.

[j] Values obtained using the non-hydrolyzed smoker female urine as matrix.

With respect to the calibration sensitivity of the method, the slopes were around half of those calibration curves obtained using standard prepared in diluted synthetic urine (Table IV.22). The exception was 1OHpy, for which the calibration slopes varied in a 30 %. Therefore, a suppressing matrix effect is clearly found when urine samples are analyzed with the developed salt-induced DLLME approach. Nevertheless, the calibration slopes obtained with the urine sample as matrix are still 30 times higher than those obtained with the calibration curves of the chromatographic method (Table IV.21). Thus, high preconcentration is still achieved with the proposed microextraction method despite the existence of an important matrix effect, which can be observed comparing the representative chromatograms included in Figures IV.11 A) and E). The LODs were experimentally determined using the same approach as with synthetic urine, being 0.001 $\mu g \cdot L^{-1}$ for 2OHflu, 2OHphe and 4OHphe, and 0.002 $\mu g \cdot L^{-1}$ for 1OHpy. The experimentally obtained LOQs ranged from 0.003 $\mu g \cdot L^{-1}$ for 2OHflu, 2OHphe and 4OHphe to 0.005 $\mu g \cdot L^{-1}$ for 1OHpy.

As it is shown in Table IV.23, the intra-day precision studies with spiked diluted samples presented RSD values between 5.7 % and 11 % for 1OHpy at 0.08 $\mu g \cdot L^{-1}$ and 0.8 $\mu g \cdot L^{-1}$ spiked levels, respectively. Regarding inter-day reproducibility, RSDs lower than 17 % were obtained. With respect to RR performance using the spiked urine sample (non-hydrolyzed and non-smoker female) subjected to the entire method, RR values ranging between 95.1 % for 1OHpy at the high spiked level, and 110 % for 2OHphe at the high level were obtained.

Due to the suppressing matrix effect exerted by the urine matrix, the obtained E_F values were two times lower than those achieved with synthetic urine. Thus, average E_F values between 35 and 40 were obtained for all the tested analytes at the high and low spiked levels, respectively. Therefore, the extraction efficiency (as E_R values, %) of the entire method varied from 18.6 % for 2OHflu at 0.08 $\mu g \cdot L^{-1}$ to 28.4 % for 4OHphe at 0.08 $\mu g \cdot L^{-1}$. At this point, it is important to highlight that relatively low E_R values are acceptable for microextraction approaches as long as the reproducibility and sensitivity of the method are good enough for the analytical application for which it was developed [21].

In order to validate the applicability of the matrix-matched calibration curves obtained with the non-smoker female urine for the analysis of any urine sample, the non-hydrolyzed smoker female urine sample was diluted, spiked at 0.5 $\mu g \cdot L^{-1}$ and subjected to the method. The RR, E_F and E_R values obtained with this matrix are included in Table IV.23. Average RR values of 101 % were found with intra-day RSDs lower than 11.8 %. E_F values varied between 29.2 for 2OHflu and 46.7 for 1OHpy, and average E_R values of 23.6 % were achieved. All these values were similar to those obtained when the non-smoker female urine was used as matrix. Therefore, the quantification of the OH-PAHs in different urine samples can be accomplished using the calibration curves previously obtained.

Despite the loss of sensitivity of the method performed with the urine sample compared to synthetic urine, the preconcentration achieved is enough to carry out the determination of OH-

PAHs in urine samples at trace levels. In fact, the developed salt-induced DLLME method provided enhanced analytical performance than other methods in combination with LC reported in the literature for the determination of OH-PAHs in urine. Table IV.24 lists several characteristics of these methods [14,16,17,19]. It can be observed that the LODs obtained with the proposed method are ten times lower than those obtained using LLE [16], LLE followed by μ-dSPE [19], and m-μ-dSPE [14]. The LOQs achieved in this work are similar to those reported by Zhao *et al.* [17], in which a SBSE method in combination with LC-MS/MS was used. However, the extraction times required for the SBSE method were around 180 min, while the proposed salt-induced DLLME only takes 15 min. Furthermore, one of the main drawbacks of the majority of these methods as well as other methods coupled with GC-MS [10,11] lies in the requirements of long extraction or desorption steps, filtering, and evaporation and reconstitution steps.

5. Analysis of urine samples

The developed salt-induced DLLME-HPLC-FD method was used for the analysis of urine samples with the purpose of proving the applicability of the method. Male and female healthy volunteers (ages between 25 and 30 years old) with different smoking habits (non-smokers, and smokers: five cigarettes a day) were selected in order to tentatively assess the correlation between the PAHs exposure and the concentration of urinary OH-PAHs [6]. All urine samples were hydrolyzed to free the OH-PAHs, as it is described in Section III.3.

The results obtained for the analysis of samples are included in Table IV.25. All the studied OH-PAHs were detected in the four samples, except for 2OHphe in the non-smoker male urine sample. Indeed, the four OH-PAHs were quantified in the smoker male urine sample, with levels ranging from 0.07 ± 0.03 $\mu g \cdot L^{-1}$ for 2OHphe to 2.3 ± 0.6 $\mu g \cdot L^{-1}$ for 2OHflu. On the contrary, 4OHphe was the only analyte determined in the non-smoker male urine at 0.09 ± 0.01 $\mu g \cdot L^{-1}$. The smoker female sample was the urine that presented the highest content of OH-PAHs, with a total content of 7.4 $\mu g \cdot L^{-1}$. Figure IV.11 F) shows a chromatogram obtained after the analysis of the hydrolyzed smoker female sample with the proposed method, where it can be observed the high peak found for 2OHphe, corresponding to a final concentration of 6.0 ± 0.7 $\mu g \cdot L^{-1}$ in the urine.

It can also be observed that 2OHflu and 2OHphe are the analytes found at higher concentrations, while 4OHphe could not be quantified in female urine samples but it was determined at 0.09 ± 0.01 $\mu g \cdot L^{-1}$ and 0.103 ± 0.002 $\mu g \cdot L^{-1}$ in non-smoker and smoker male urines, respectively. All these results agree with the expected OH-PAHs concentration according to the PAH exposure of each volunteer (i.e., smoking habit, diet, and workplace) [2,5]. Clearly, a large number of samples would be required if a deep study wants to be carried out to evaluate PAHs exposure.

Table IV.24. Comparison of several parameters of the analytical performance of the developed salt-induced DLLME-HPLC-FD method with other LC-based methods reported in the literature for the determination of OH-PAHs in urine samples.

Extraction method	Extraction solvent / solid sorbent	Solvent volume / Sorbent amount	Total time[a] (min)	LOD / LOQ (μg·L^{-1})				Analytical system	Ref.
				2OHflu	2OHphe	4OHphe	1OHpy		
Salt-induced DLLME	[$C_{10}Gu^+$][Cl^-] IL	20 μL	15 + 15	0.001 / 0.003	0.001 / 0.003	0.001 / 0.003	0.002 / 0.005	LC-FD	This sutdy
LLE	pentane:toluene (80:20)	10 mL	15 + 10	0.016 / 0.040	0.002 / 0.006	0.005/ 0.006	0.005/ 0.023	LC-MS/MS	[16]
LLE-μ-dSPE	ethyl acetate & Z-sep[b]	15 mL & 180 mg	20 + 13	n.r. / 0.025	n.r. / 0.010	n.r. / 0.010	n.r. / 0.025	LC-MS/MS	[19]
SBSE	PDMS stir bar	126 μL	180 + 25	n.r. / 0.002	n.r. / 0.003	n.r. / 0.003	n.r. / 0.003	LC-MS/MS	[17]
m-μ-dSPE	magnetic polymer	10 mg	75 + 40	0.040 / n.r.	0.060 / n.r.	0.010 / n.r.	0.020 / n.r.	LC-FD	[14]

[a] Estimated extraction time + chromatographic run time.
[b] Zirconia-coated silica particles.
n.r.: not reported.

Table IV.25. Concentration levels found for the studied OH-PAHs in hydrolyzed human urine samples subjected to the entire salt-induced DLLME-HPLC-FD. Results were quantified using the calibration curves obtained in non-hydrolyzed real urine (Table IV.23).

Analyte	**Content ± SD* (μg·L^{-1})**			
	Non-smoker female	**Smoker female**	**Non-smoker male**	**Smoker male**
2OHflu	0.04 ± 0.01	1.0 ± 0.1	n.q.	2.3 ± 0.6
2OHphe	1.17 ± 0.05	6.0 ± 0.7	n.d.	0.07 ± 0.03
4OHphe	n.q.	n.q.	0.09 ± 0.01	0.103 ± 0.002
1OHpy	0.28 ± 0.03	0.40 ± 0.06	n.q.	0.21 ± 0.05

* Standard deviation in the determination of the analytes in the urine sample (n = 3).
n.d.: not detected.
n.q.: not quantified.

REFERENCES

[1] A. Seidel, A. Spickenheuer, K. Straif, H.-P. Rihs, B. Marczynski, M. Scherenberg, G. Dettbarn, J. Angerer, M. Wilhelm, T. Brüning, J. Jacob, B. Pesch, J. Toxicol. Environ. Health 71 (2008) 734–745.

[2] M. Bartolomé, J.J. Ramos, F. Cutanda, O. Huetos, M. Esteban, M. Ruiz-Moraga, E. Calvo, B. Pérez-Gómez, O. González, BIOAMBIENT.ES^2, A. Castaño, Chemosphere 135 (2015) 436–446.

[3] Z. Li, A. Sjödin, L.C. Romanoff, K. Horton, C.L. Fitzgerald, A. Eppler, M. Aguilar-Villalobos, L.P. Naeher, Environ Int. 37 (2011) 1157–1163.

[4] M. Oliveira, K. Slezakova, C.P. Magalhães, A. Fernandes, J.P. Teixeira, C. Delerue-Matos, M.C. Pereira, S. Morais, J. Hazard. Mater. 334 (2017) 10–20.

[5] Z. Li, L. Romanoff, S. Bartell, E.N. Pittman, D.A. Trinidad, M. McClean, T.F. Webster, A. Sjödin, Chem. Res. Toxicol. 25 (2012) 1452−1461.

[6] P. Suwan-ampai, A. Navas-Acien, P.T. Strickland, J. Agnew, Cancer Epidemiol. Biomarkers Prev. 18 (2009) 884–893.

[7] S.F. Farzan, Y. Chen, H. Trachtman, L. Trasande, Environ. Res. 144 (2016) 149–157.

[8] P. Yang, H. Sun, Y.-J. Gong, Y.-X. Wang, C. Liu, Y.-J. Chen, L. Sun, L.-L. Huang, S.-H. Ai, W.-Q. Lu, Q. Zeng, Int. J. Hyg. Environ. Health 220 (2017) 1340–1346.

[9] J. Hou, H. Sun, Y. Guo, Y. Zhou, W. Yin, T. Xu, J. Cheng, W. Chen, J. Yuan, Ecotoxicol. Environ. Saf. 147 (2018) 1002–1009.

[10] L.C. Romanoff, Z. Li, K.J. Young, N.C. Blakely III, D.G. Patterson Jr, C.D. Sandau, J. Chromatogr. B 835. (2006) 47–54.

[11] Z. Li, L.C. Romanoff, D.A. Trinidad, N. Hussain, R.S. Jones, E.N. Porter, D.G. Patterson Jr, A. Sjödin, Anal. Chem 78 (2006) 5744–5751.

[12] T. Chetiyanukornkul, A. Toriba, T. Kameda, N. Tang, K. Hayakawa, Anal. Bioanal. Chem. 386 (2006) 712–718.

[13] A. Chauhan, T. Bhatia, A. Singh, P.N. Saxena, C. Kesavchandran, M.K.R. Mudiam, J. Chromatogr. B 985 (2015) 110–118.

[14] L. Zhou, Y. Hu, G. Li, Anal. Chem. 88 (2016) 6930–6938.

[15] F. Onyemauwa, S.M. Rappaport, J.R. Sobus, D. Gajdošová, R. Wu, S. Waaidyanatha, J. Chromatogr. B 877 (2009) 1117–1125.

[16] R. Fan, R. Ramage, D. Wang, J. Zhou, J. Se, Talanta 93 (2012) 383–391.

[17] G. Zhao, Y. Chen, S. Wang, J. Yu, X. Wang, F. Xie, H. Liu, J. Xie, Talanta 116 (2013) 822–826.

[18] L. Zhu, H. Xu, J. Sep. Sci. 37 (2014) 2591–2598.

[19] D. Lankova, K. Urbancova, R.J. Sram, J. Hajslova, J. Pulkrabova, Anal. Bioanal. Chem. 408 (2016) 2515–2525.

[20] H. Zhang, H. Xu, J. Chromatogr. A 1521 (2017) 27–35.

[21] M.J. Trujillo-Rodríguez, P. Rocío-Bautista, V. Pino, A.M. Afonso, Trac-Trends Anal. Chem. 51 (2013) 87–106.

Section IV.1.2.2

Ionic liquid-based miniaturized aqueous biphasic system using a low cytotoxic guanidinium ionic liquid: application for the development of an analytical preconcentration method to determine polycyclic aromatic hydrocarbons in water samples

Talanta 203 (2019) 305–313

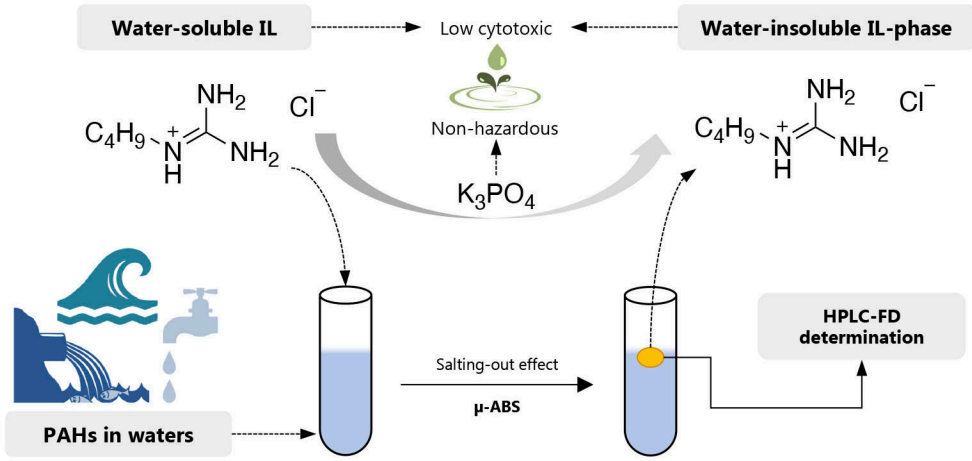

1. Selection of the ILs-based μ-ABS composition

A miniaturized IL-based ABS (μ-ABS) was used as preconcentration method for the determination of PAHs in water samples. Following the fundamentals of ABSs, it is possible to promote the insolubilization of a water-soluble IL without carrying out an anion-exchange reaction. Thus, the use of fluorinated salts is avoided (ensuring greenness). Furthermore, the final IL-rich phase obtained in the system contains the still hydrophilic IL, which facilitates the compatibility of the method with chromatographic techniques.

With the aim of improving the enrichment capacity of ABSs, several studies have shifted the composition of the optimum IL-based ABSs to those biphasic regions where the preconcentration is higher, using amounts of ILs ranging between 1.2 and 5 % (w/w) [1–6]. $[C_{n1}C_{n2}Im^+]$ ILs [1,2,4] and ILs with halogenated anions [3,4,6] are the most commonly used in the preparation of these ABSs with extraction purposes. Due to the recent concern on the toxicity of imidazolium ILs [7], the low cytotoxic guanidinium ILs synthesized in this Doctoral Thesis (Section IV.1.1.1) were used in this study to develop a more environmentally friendly ABS. Indeed, guanidinium-based ILs have not been evaluated in ABSs with extraction neither removal purposes yet.

The structure of the IL is one of the main variables that exert an influence in the formation and resulting stability of the ILs-based ABSs. Bulky cations with relatively long alkyl chains present higher hydrophobicity and, therefore, they are more adequate to promote the formation of ABSs [6]. Nevertheless, some ILs presenting alkyl chains with 8 or more carbon atoms exhibit surface active properties, which leads to the formation of micellar aggregates in water [8] and a decrease in their ability to form ABSs [9]. Concerning the anions, the more polarizable they are, the higher is their ability for hydration [10]. Therefore, the ILs $[C_4Gu^+][Cl^-]$ and $[C_6Gu^+][Cl^-]$ were selected for the preparation of the μ-ABS since they are not surfactants and present the safest toxicological profiles amongst all the guanidinium ILs synthesized in this Doctoral Thesis (Section IV.1.1.1).

The type of salting-out agent is also an important factor to take into account when designing ABSs. High-charge density inorganic salts are the most common salting-out agents employed for the preparation of ILs-based ABSs due to their ease to be hydrated [11]. Therefore, K_3PO_4 was selected as salting-out salt in this study for being one of the most popular salts within ABSs due to the high charge density of its anion [12].

As a preliminary approach, the two low cytotoxic ILs together with the most conventional $[C_4MIm^+][Cl^-]$ IL were tested in the ternary mixture composed of ultrapure water, IL, and K_3PO_4. For these studies, the following non-optimized experimental conditions were used: 5 mL of ultrapure water, 50 μL of IL, and the amount of salt required to obtain the separation of the phases. It is important to mention that those amounts were selected with the aim of evaluating the application of these ILs in a μ-ABS approach, and thus the amounts of the components should be small enough to develop a microextraction and preconcentration method.

The studies carried out with $[C_4MIm^+][Cl^-]$ showed that it is not possible to use this IL in the proposed method, since the amount of IL required to form the IL-rich phase (that could be easily sampled) would be too large for microextraction purposes. Furthermore, the $[C_4MIm^+][Cl^-]$ + K_3PO_4 + water system required a large amount of salt to form the μ-ABS despite the small amounts of IL and water involved in the system. In the case of both guanidinium-based ILs, a small droplet of IL-rich phase was formed at the surface of the salt-rich aqueous phase after the addition of the adequate amount of K_3PO_4. Therefore, both low cytotoxic guanidinium ILs were initially used for the development of the μ-ABS microextraction method.

2. Phase diagrams of guanidinium ILs-based μ-ABSs

The characterization of the guanidinium ILs-based μ-ABSs was performed from the elaboration of the corresponding phase diagrams, following the procedure described in Section III.7.4.3. It is important to highlight that small amounts of the components were used with the purpose of studying the phase diagrams in a region in which the developed method presents the characteristics of a microextraction method. Thus, an initial volume of ultrapure water of 1 mL was used in order to guarantee the dissolution of the IL. 65 μL of IL were used to provide the minimum amount of IL in the μ-ABS, allowing the formation of an IL-rich phase that could be easily manipulated.

The obtained binodal curves are shown in Figure IV.14. The percentages of salt required to generate the μ-ABS are slightly lower in the case of the system with $[C_6Gu^+][Cl^-]$ than those with the $[C_4Gu^+][Cl^-]$ IL. This behavior goes in line with the expected results, taking into account that the cation of the $[C_6Gu^+][Cl^-]$ IL presents a longer alkyl chain than the $[C_4Gu^+][Cl^-]$ IL, and consequently it is more hydrophobic and has greater tendency to form ABSs [6]. In both cases, low IL percentages were obtained, between 0.3 % and 4.4 % (w/w), which clearly favors the use of these systems for microextraction and preconcentration purposes.

The experimental data of the phase diagrams were adjusted to binodal curves according to the Equation IV.2 proposed by Merchuk *et al.* [13]. The regression parameters obtained are included in Table IV.26.

$$Y = A \cdot \exp\left[\left(B \cdot X^{0.5}\right) - \left(C \cdot X^{3}\right)\right] \qquad \text{Equation IV.2}$$

Correlation coefficients and standard deviations of residuals are satisfactory for both ILs, being slightly better the values obtained for the $[C_4Gu^+][Cl^-]$ IL. The coefficients calculated by the exponential regression of the binodal curves are similar than those previously reported in the literature for other IL + K_3PO_4 + water ABSs. Thus, values close to 100 for the A coefficient, negative

values between 0 and –1 for the B coefficient, and values around 10^{-5} for the C coefficient, are commonly obtained [1,3].

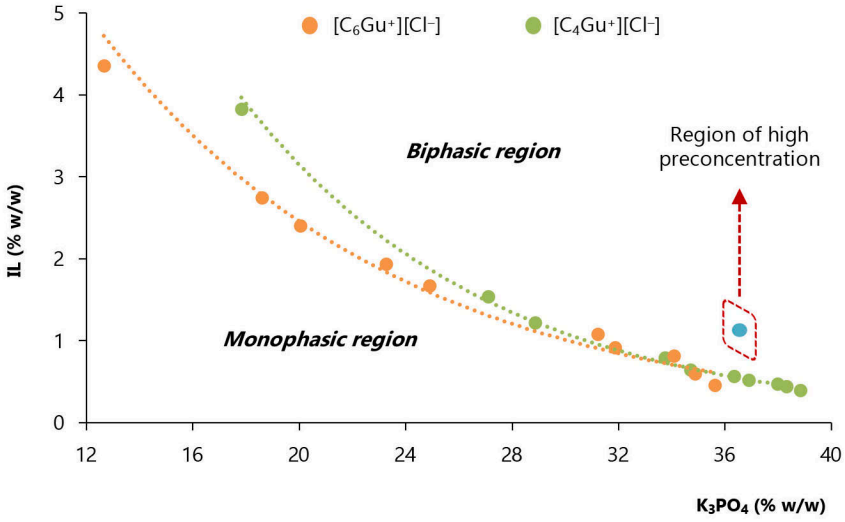

Figure IV.14. Binodal curves of the μ-ABSs $[C_4Gu^+][Cl^-]$ + K_3PO_4 + water and $[C_6Gu^+][Cl^-]$ + K_3PO_4 + water.

Table IV.26. Correlation parameters obtained by the regression according to Equation IV.2 of the guanidinium ILs-based-μ-ABSs phases diagrams.

μ-ABS	A ± SD[a]	B ± SD[a]	(C ± SD[a])·10^5	R[b]	$S_{y/x}$[c]
$[C_4Gu^+][Cl^-]$ + K_3PO_4 + water	94 ± 17	–0.74 ± 0.05	1.4 ± 0.2	0.999	0.03
$[C_6Gu^+][Cl^-]$ + K_3PO_4 + water	27 ± 5	–0.50 ± 0.05	1.7 ± 0.4	0.998	0.09

[a] Standard deviation.
[b] Correlation coefficient.
[c] Standard deviation of the residuals.

As it can be observed in Table IV.26 the three coefficients for the $[C_4Gu^+][Cl^-]$-based μ-ABS are similar to those commonly reported in the literature, while for the $[C_6Gu^+][Cl^-]$-based μ-ABS the value for the A coefficient is quite different from what it was expected. These results suggest that the μ-ABSs formed using the guanidinium ILs present a typical behavior of conventional ABSs despite the limited range of concentrations of IL used for the determination of their phase

diagrams. The limited region is dictated by the necessity of establishing a microextraction and preconcentration approach, which will be used as monitoring method.

3. Use of guanidinium ILs-based μ-ABSs for the determination of PAHs

3.1. Selection of the region of the phase diagram and the optimum IL

Once the phase diagrams for the synthesized guanidinium ILs were obtained, both μ-ABSs were evaluated as microextraction methods. A point with the following composition and included in the biphasic region was selected for the development of the method: 0.75 % (w/w) of IL, 37.70 % (w/w) of K_3PO_4, and 61.55 % (w/w) of ultrapure water. As it can be observed in Figure IV.14, this composition belongs to the lower region of the phase diagrams of both ILs. This area is characterized by high salt concentrations and low amounts of IL. These characteristics make this region of great interest to develop a microextraction method since highest preconcentration factors are obtained due to the large differences between the amount of IL and the rest of the components [3].

The difference in the amount of K_3PO_4 needed to form the μ-ABSs with both ILs is not significant, so both ILs are adequate to develop the proposed μ-ABSs method. However, the $[C_4Gu^+][Cl^-]$-rich phase obtained with the selected ABS composition forms a much more defined and easy-to-manipulate microdroplet, whereas the $[C_6Gu^+][Cl^-]$ provides a dispersed IL-rich phase that was difficult to separate from the sample. Therefore, $[C_4Gu^+][Cl^-]$ was chosen as the optimum IL to perform the microextraction method based on μ-ABSs using the above-mentioned composition. In addition to these experimental advantages, the $[C_4Gu^+][Cl^-]$ IL is less toxic due to its shorter alkyl chain [7], as it was demonstrated in Section IV.1.1.1). Therefore, $[C_4Gu^+][Cl^-]$ is the best option to meet the green requirements proposed for this environmentally friendly microextraction method.

3.2. Coupling ILs-based μ-ABS with HPLC-FD for the determination of PAHs

The proposed microextraction method based on the μ-ABS using the $[C_4Gu^+][Cl^-]$ IL was applied for the extraction and preconcentration of five PAHs as model analytes: Ant, BaA, Chry, BaPy, and Ind. This group of persistent contaminants was selected due to their carcinogenic, mutagenic and endocrine disrupting properties [14,15], and widespread environmental presence [14,16].

The selected μ-ABS microextraction method could be easily coupled with HPLC since the IL-rich phase obtained in the μ-ABS was hydrophilic and compatible with the mobile phase. The HPLC was combined with FD taking advantage of the nature fluorescence of the selected PAHs, which leads to a higher sensitivity. Despite this compatibility, the separation of the analytes in the

presence of the IL must be optimized in order to avoid the possible signals coming from the IL that may interfere in the proper detection of the analytes. In any case, the dilution of the resulting IL-rich phase with 50 µL of initial mobile phase (acetonitrile:water, 85:15 (v/v)) was required to reduce its viscosity, thus also favoring the minimization of IL interferences.

Thus, the elution gradient described in Section III.7.5.4 allowed the successful separation of the five PAHs without interferences affecting their determination. The fluorescence program was adjusted to guarantee the maximum sensitivity and selectivity for the PAHs, obtaining the optimum conditions shown in Table IV.27.

Table IV.27. Fluorescence program used for the determination of the studied PAHs.

Chromatographic time (min)	λ_{ex} (nm)	λ_{em} (nm)			Gain
		A	B	D	
0.00	248	384	406	496	10
4.00	248	–	Ant	–	12
6.80	273	BaA	–	–	12
9.70	266	Chry	–	–	12
10.60	288	–	BaPy	–	12
12.50	297	–	–	Ind	12
16.00	297	–	–	–	10

The calibration curves of the HPLC-FD method without considering the preconcentration step were obtained for the further assessment of the enrichment capacity of the µ-ABS method. Several quality analytical parameters of the HPLC-FD method are included in Table IV.28. Furthermore, Figure IV.15 includes a representative chromatogram after injecting a diluted IL-rich phase, obtained after performing the µ-ABS method to an aqueous standard containing 0.015 $\mu g \cdot L^{-1}$ of the PAHs.

Table IV.28. Several quality analytical parameters of the HPLC-FD method (without considering the μ-ABS method), using standards of PAHs in acetonitrile.

PAH	Calibration range ($ng \cdot L^{-1}$)	(Slope ± t·SD[a])·10^2	R^2 [b]	$S_{y/x}$ [c]	LOD[d] ($ng \cdot L^{-1}$)	LOQ[e] ($ng \cdot L^{-1}$)	RSD[f] (%)
Ant	100–5000	8.5 ± 0.1	0.999	2.6	3.0	10	1.5
BaA	5.0–1000	136 ± 12	0.996	34.9	0.2	0.7	2.3
Chry	100–5000	1.25 ± 0.03	0.998	0.8	2.0	5.0	3.7
BaPy	50–5000	1.86 ± 0.02	0.999	0.5	10	30	2.6
Ind	500–5000	0.224 ± 0.007	0.999	0.1	200	500	1.4

[a] 95 % confidence limits for n = 6 calibration levels (4 degrees of freedom) within the calibration range.
[b] Determination coefficient.
[c] Error of the estimate (or standard deviation of the residuals).
[d] Limit of detection, experimentally determined by decreasing the concentration of the standards until a signal-to-noise (S/N) ratio of 3 was obtained.
[e] Limit of quantification, estimated as 10/3 times the LOD and experimentally verified by the injection of standards at the predicted concentrations.
[f] Relative standard deviation (intra-day), determined by the injection of a standard of 0.7 $\mu g \cdot L^{-1}$ (n = 3).

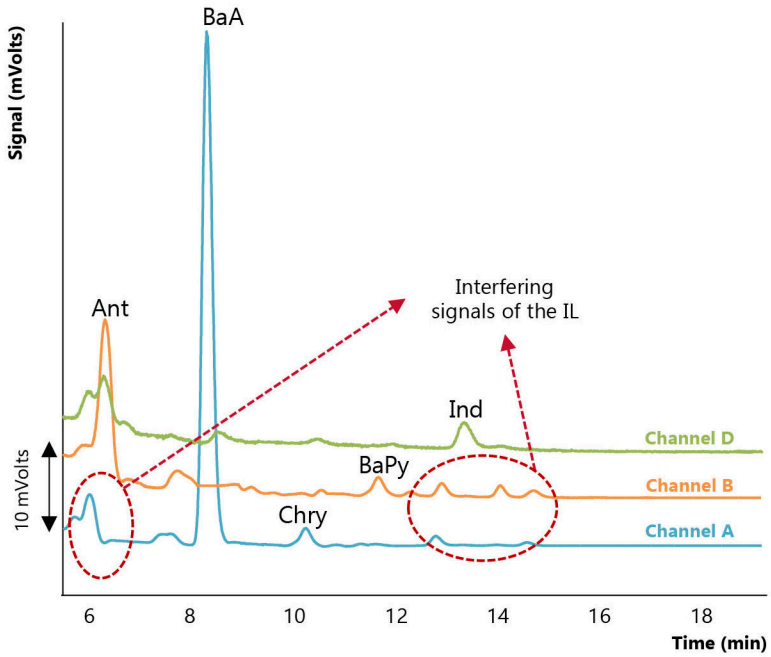

Figure IV.15. Representative HPLC-FD chromatogram for the injection of the IL-rich phase (diluted with 50 µL of acetonitrile:water (85:15, v/v)) obtained through the $[C_4Gu^+][Cl^-]$-based µ-ABS method and using an aqueous standard containing 0.015 $\mu g \cdot L^{-1}$ of the PAHs.

3.3. Optimization of the $[C_4Gu^+][Cl^-]$-based µ-ABS method

One of the main advantages of using ABSs for extraction purposes is that the elaboration of the phase diagrams directly leads to the optimization of the method. Once a point of the biphasic region is selected, it determines the concentration of the components required for the adequate formation of the two phases. For this reason, an experimental design was not considered in this optimization, because the selection of a composition of the µ-ABS in the region of the phase diagram where the difference between the amount of sample and IL is the highest, will automatically provide the highest preconcentration.

In some cases, after mixing the appropriate amounts of the three ABS components, a stirring method is applied to facilitate the mass transfer of the analytes from the aqueous phase to the IL-rich phase. However, the equilibrium time or phase separation time can be an important disadvantage in ABSs, since it usually takes between 8 min and 12 h for the complete distribution of the components between the phases [17]. Indeed, most of the ILs-based ABSs devoted to extraction and analytical determination described in the literature report equilibrium times of at

least 12 h to achieve the complete separation of the phases [1,3,18]. Therefore, it is necessary to study the equilibrium time of the developed μ-ABSs in order to minimize the total extraction time since LPME approaches are characterized by their fastness. As a green requirement, microextraction methods usually sacrifice extraction efficiency by velocity, as long as the reproducibility and sensitivity are adequate enough for the analytical application pursued.

The distribution of the analytes between the two phases during the first 12 h of equilibrium was assessed. Thus, the developed $[C_4Gu^+][Cl^-]$-based μ-ABS was applied to an aqueous standard with the PAHs at 0.09 $\mu g \cdot L^{-1}$, and the extraction efficiency was evaluated at different equilibrium times: 15 min, 30 min, 1 h, 3 h, 6 h and 12 h. The efficiency was monitored using the peak areas obtained after the injection of the diluted IL-rich phase in the HPLC-FD system. Figure IV.16 includes the results obtained for Ant and Ind as representative analytes, the lighter and the heavier of the PAHs studied, respectively.

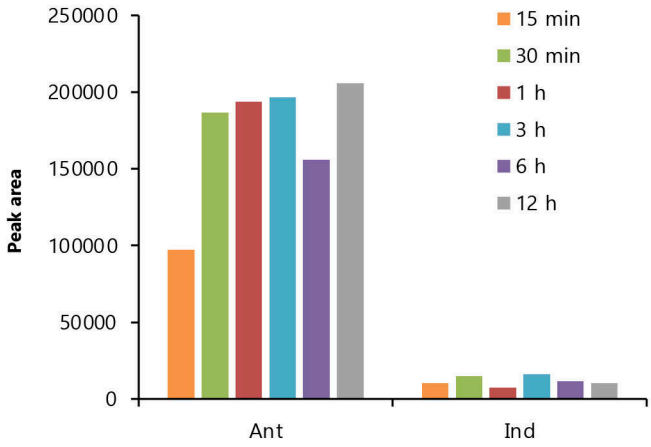

Figure IV.16. Extraction efficiency (monitored as chromatographic peak area) at different equilibrium times with the $[C_4Gu^+][Cl^-]$-based μ-ABS method, using the following composition: 0.75 % (w/w) of IL, 37.70 % (w/w) of K_3PO_4 and 61.55 % (w/w) of ultrapure water. Results are shown for two representative PAHs (aqueous standard: 0.09 $\mu g \cdot L^{-1}$).

As it can be observed, most of the distribution between the phases takes place in 30 min. Indeed, after this time of equilibrium, there are not significant differences between the peak areas obtained for both analytes. Therefore, 30 min was selected as the optimum equilibrium time in order to minimize the overall time of the microextraction method. Figure IV.17 schematically shows the procedure of the developed method. Under these optimum conditions, the IL-rich phase

obtained in the $[C_4Gu^+][Cl^-]$-based μ-ABS method was measured, obtaining an average microdroplet volume of 20 ± 1 μL (n = 4).

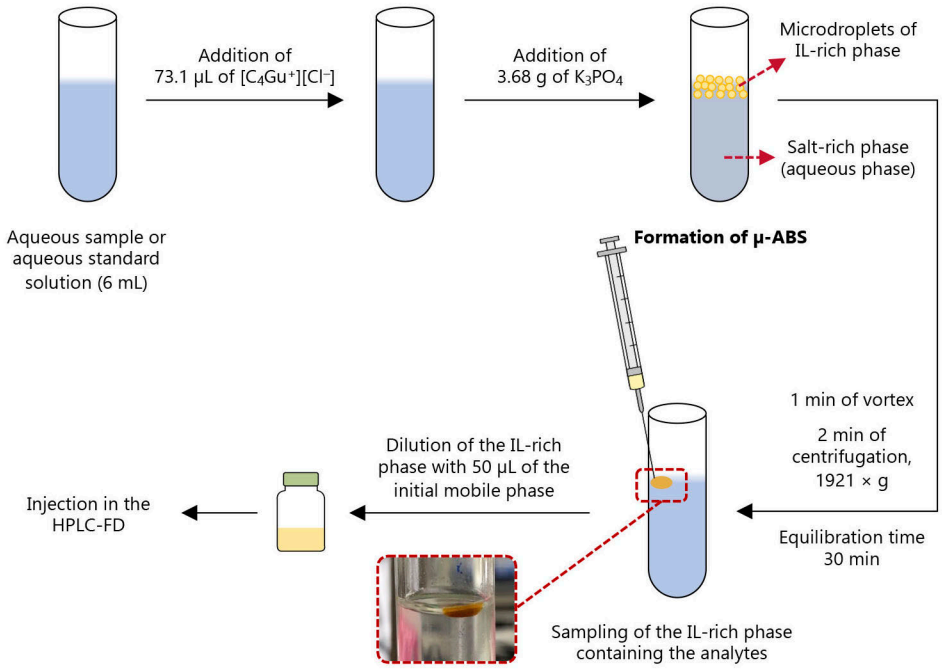

Figure IV.17. Scheme of the microextraction procedure using the $[C_4Gu^+][Cl^-]$-based μ-ABS method under optimum conditions.

3.4. Analytical performance of the $[C_4Gu^+][Cl^-]$-based μ-ABS-HPLC-FD method

Calibration curves of the optimized $[C_4Gu^+][Cl^-]$-based μ-ABS-HPLC-FD method were obtained by subjecting aqueous standards of the PAHs to the entire method. Table IV.29 includes several quality analytical parameters: calibration range, calibration slopes, determination coefficients (R^2), limits of detection (LODs) and limits of quantification (LOQs). The LODs were experimentally obtained by decreasing the concentration of the analytes in the aqueous standard until a signal-to-noise ratio (S/N) of 3 was obtained, while the LOQ were estimated as 10/3 times the LODs and experimentally verified.

Table IV.29. Several quality analytical parameters of the entire $[C_4Gu^+][Cl^-]$-based μ-ABS-HPLC-FD method for the determination of PAHs.

PAH	Calibration range ($ng \cdot L^{-1}$)	(Slope ± t·SD[a])	R^2 [b]	$S_{y/x}$ [c]	LOD[d] ($ng \cdot L^{-1}$)	LOQ[e] ($ng \cdot L^{-1}$)
Ant	10–90	4.8 ± 0.5	0.997	10	0.03	0.10
BaA	0.10–20	60 ± 4	0.998	25	0.01	0.02
Chry	10–90	0.64 ± 0.04	0.998	0.92	0.10	0.40
BaPy	10–90	1.12 ± 0.05	0.999	1.4	0.25	0.80
Ind	10–90	0.118 ± 0.005	0.999	0.14	2.0	8.0

[a] 95 % confidence limits for n = 6 calibration levels (4 degrees of freedom) within the calibration range.
[b] Determination coefficient.
[c] Error of the estimate (or standard deviation of the residuals).
[d] Limit of detection, experimentally determined by decreasing the concentration of the aqueous standards until a S/N ratio of 3 was obtained.
[e] Limit of quantification, estimated as 10/3 times the LOD and experimentally verified by preparation of aqueous standards at the predicted concentrations (standards which are subjected to the entire method).

All calibration curves presented R^2 values higher than 0.997 within the calibration range: 10–90 ng·L^{-1} for all the analytes, except for BaA, for which the calibration range was 0.10–20 ng·L^{-1} and therefore, the calibration slope was the highest. As shown in Table IV.29, LODs ranged from 0.01 ng·L^{-1} for BaA to 2.00 ng·L^{-1} for Ind. It is important to highlight the high preconcentration achieved with the [C_4Gu^+][Cl^-]-based μ-ABS system by comparing the LODs of the microextraction method with the LODs of the chromatographic method (Table IV.28), being up to 100 times lower for Ant and Ind.

Table IV.30 includes several parameters of the analytical performance of the [C_4Gu^+][Cl^-]-based μ-ABS-HPLC-FD method using an aqueous standard of the PAHs at a level of 12 ng·L^{-1}. This concentration was selected for reproducibility and relative recovery (RR, %) studies as a high concentration level for BaA and a low concentration level for the rest of the PAHs (due to the large difference of sensitivity between BaA and the remaining PAHs). The precision of the method was evaluated in intra-day and intermediate precision studies and presents adequate values considering the low concentrations studied [19]. Thus, intra-day RSD values were always lower than 12 %, while the intermediate precision RSD values ranged from 2.8 % for Ant to 17 % for BaPy in 3 consecutive days. RR were calculated as the ratio between the concentration obtained using the calibration curves of the entire method and the known spiked concentration of the analytes. RR values ranged from 75.0 % for Ind to 121 % for Ant.

Table IV.30. Analytical performance of the [C_4Gu^+][Cl^-]-based μ-ABS-HPLC-FD method in terms of precision, extraction efficiency and RR using aqueous standards of PAHs at 12 ng·L^{-1}.

PAH	Intra-day RSD range[a] (%)	Intermediate precision RSD[b] (%)	E_F[c]	E_R[d] (%)	RR[e] (%)
Ant	1.4–2.3	2.8	55.9	65.2	121
BaA	2.8–8.3	9.8	44.1	51.5	89.4
Chry	5.3–11	12	51.5	60.1	83.3
BaPy	1.9–5.0	17	60.4	70.5	115
Ind	4.5–7.0	15	52.5	61.3	75.0

[a] Range (day 1 to day 3) of relative standard deviation for intra-day precision (n = 3).
[b] Relative standard deviation for intermediate precision (n = 9; 3 consecutive different days).
[c] Enrichment factor, calculated as the ratio between the calibration slopes obtained for the μ-ABS-HPLC-FD (Table IV.29) and the HPLC-FD method (Table IV.28).
[d] Extraction efficiency, E_{Fmax} = 85.7.
[e] Relative recovery (n = 3).

Regarding the extraction performance of the developed $[C_4Gu^+][Cl^-]$-based μ-ABS-HPLC-FD method, the enrichment factors (E_F) were determined as the ratio between the calibration slopes of the entire method (Table IV.29) and the calibration slopes of the HPLC-FD method (Table IV.28). The obtained E_F values are shown in Table IV.30. They ranged from 44.1 for BaA to 60.4 for BaPy, thus supporting the high preconcentration obtained with the proposed method, which is similar for all the PAHs.

Extraction efficiencies (E_R, %) were calculated as the ratio between the E_F values and the theoretical maximum enrichment factor (E_{Fmax}) of 85.7. E_{Fmax} was estimated as the ratio between the volume of the initial aqueous sample (6 mL) and the volume of the final extract subjected to analysis (~70 μL after diluting the IL-rich phase). E_R values are also shown in Table IV.30 and ranged from 51.5 % for BaA to 70.5 % for BaPy. These values are highly adequate for a microextraction procedure considering the non-exhaustivity character of most LPME applications [20].

It should be noted the high sensitivity of the current microextraction method in comparison with other methods reported in the literature for the determination of PAHs in aqueous samples. Table IV.31 [21–26] shows that PAHs have been determined through a huge variety of extraction methods using different extraction solvents, including magnetic ILs [24], or solid sorbents like MOFs [23], in combination with HPLC [21,23,24] or GC [22,25,26] and different detectors. In all cases, LODs are at $ng \cdot L^{-1}$ level. However, it is important to highlight that the LODs achieved with the developed $[C_4Gu^+][Cl^-]$-based μ-ABS-HPLC-FD method are much lower than the LODs reported by other studies using MS [22,25] and even lower than other studies using fluorescence detection [21,23,24]. Furthermore, the proposed method requires low volumes of the IL used as extraction solvent, compared to those amounts higher than 100 μL (or 100 mg) reported in other methods. The high sensitivity achieved together with the biocompatibility and sustainability of the developed μ-ABS make the proposed method an efficient environmentally friendly preconcentration strategy.

It is also interesting to highlight the relatively low amounts of IL used in the proposed method respect to the remaining components of the system and in comparison with other μ-ABS reported in the literature, as it can be clearly observed in Table IV.32 [1–5]. Concentrations of IL ranging from 1.18 [3] to 2.7 % (w/w) [4] have been reported, while the μ-ABS developed in this study requires the lowest concentration reported up to date (lower than 1 % (w/w)), thus leading to high preconcentration factors. Two studies report E_F values without dilution around 50, which are similar to the ones obtained in our study after dilution of the IL-rich phase. The remaining studies only include theoretical enrichment factors [1,4]. Moreover, the analytical performance of the proposed method reaches adequate values in terms of sensitivity and precision with only 30 min of equilibration time, whereas most μ-ABSs intended to extraction require at least 12 h [1,3] or they do not validate the entire analytical method [1,3,4].

Table IV.31. Comparison of several parameters of the developed $[C_4Gu^+][Cl^-]$-based μ-ABS-HPLC-FD method with other microextraction methods described in the literature for the determination of PAHs in aqueous samples.

Extraction method	Extraction solvent / solid sorbent	Solvent volume / sorbent amount	Analytical system	E_R[a] (%)	LOD[b] ($ng \cdot L^{-1}$)	Ref.
μ-ABS	$[C_4Gu^+][Cl^-]$ IL	73.1 μL	HPLC-FD	51.5–70.5	0.01–2	This study
DLLME	trichloroethylene	100 μL	HPLC-FD	n.r.	18–183	[21]
MEPS[c]	C_{18} sorbent	1 g	GC-MS	n.r.	0.8–8.2	[22]
m-μ-dSPE	magnetic composite@MOF	100 mg	HPLC-FD	n.r.	0.3–4.5	[23]
DLLME	magnetic IL	20 μL	HPLC-FD	24.9–47.3	5–20	[24]
DLLME	DES	200 μL	GC-MS	n.r.	3.9–9.8	[25]
SPME	PIL	–	GC-FID	n.r.	10–40	[26]

n.r.: not reported.
[a] Extraction efficiencies.
[b] Limit of detection.
[c] Microextraction by packed sorbents, a μ-SPE technique based on packing the sorbent in a syringe needle hub.

Table IV.32. Comparison of several characteristics of the developed $[C_4Gu^+][Cl^-]$-based μ-ABS with other μ-ABSs methods described in the literature .

IL / Salt	% (w/w) IL / salt	Analytes	Sample	Equilibration time (h)	Analytical technique	Experimental E_F[a]	Ref.
$[C_4Gu^+][Cl^-]$ / K_3PO_4	0.75 / 37.70	PAHs	water	0.5	LC-FD	44.1–60.4	This study
$[C_4MIm^+][N(CN)_2^-]$ / $KNaC_4H_4O_6$	≈ 2.5 / ≈ 36	ethinylestradiol	wastewater	12	LC-UV	n.r.[b]	[1]
$[Chol^+][Sac^-]$ / Na_2CO_3	1.4 / 32.6[c]	enzyme inhibitors	urine	n.r.	LC-UV	46	[5]
$[C_2MIm^+][Cl^-]$ / K_3PO_4	2.7 / 37	bisphenol A	urine	n.r.	UV	n.r.[b]	[4]
$[N_{4444}^+][Cl^-]$ / $K_3C_6H_5O_7$	1.18 / 49.85	caffeine and carbamazepine	wastewater	12	LC-UV	50	[3]
$[C_4MIm^+][Sal^-]$ / K_3PO_4	≈ 2.5 / ≈ 21.5	Cu (II)	water	0.2	DPASV[d]	54	[2]

[a] Enrichment factor.
[b] Evaluated exclusively from a theoretical point of view.
[c] These values were calculated according to the data reported in the article.
[d] Differential pulse anodic stripping voltammetry.
n.r.: not reported.

3.5. Analysis of water samples using the [C_4Gu^+][Cl^-]-based μ-ABS-HPLC-FD method

The optimized [C_4Gu^+][Cl^-]-based μ-ABS-HPLC-FD method was initially applied for the analysis of different water samples: two tap water samples (tap water 1 and tap water 2), one seawater and two wastewater samples. None of the five PAHs studied were detected in the tap water 2, the seawater and the wastewater samples. Nevertheless, BaPy was quantified in the tap water 1 sample as shown in Table IV.33. At this point, it is important to highlight that the LOQs achieved with the current method for BaPy is 0.80 ng·L^{-1}. This value is more than 10 times lower than the parametric value established by the Spanish regulations for PAHs in drinking waters, which sets a maximum value of 10 ng·L^{-1} for BaPy [19].

In order to assess the possible matrix effect, tap water 1 and tap water 2 were used to carry out precision and RR studies of the [C_4Gu^+][Cl^-]-based μ-ABS-HPLC-FD method at a spiked level of 12 ng·L^{-1}. As shown in Table IV.33, the RSD values were lower than 15 % for both tap water samples despite the low spiked level used. Regarding the RR values, a Student's *t* test was applied to assess if the obtained RR values were quantitative [27]. The t_{crit} values for a significance level of 2 % together with the t_{cal} values are shown in Table IV.34. The RR values obtained in tap water 1 were only acceptable for Ant and BaPy, for which $|t_{cal}| < t_{crit}$. In the case of tap water 2, only Ant and Ind presented acceptable values of RR taking into account the obtained t_{cal} values. In general, the statistical study suggests there are matrix effects in both samples. Nevertheless, it is important to highlight the good results obtained for some of the PAHs taking into account the ultra-low spiked level used in this study. Regarding the extraction efficiency (E_R values), lower or higher (depending on the PAH) values than those obtained in ultrapure water (Table IV.30) were obtained in both tap water samples. Therefore, matrix-matched calibrations are recommended for the analysis of water samples with the [C_4Gu^+][Cl^-]-based μ-ABS-HPLC-FD method.

Table IV.33. Analytical performance of the $[C_4Gu^+][Cl^-]$-based μ-ABS-HPLC-FD method with tap water samples in terms of precision, extraction efficiency, and relative recovery.

Analyte	Tap water 1	Tap water 1 (spiked level: 12 ng·L^{-1})			Tap water 2 (spiked level: 12 ng·L^{-1})		
	Content ± SD[a] (ng·L^{-1})	E_R[b] (%)	RR[c] (%)	RSD[d] (%)	E_R[b] (%)	RR[c] (%)	RSD[d] (%)
Ant	n.d.	53.1	69.4	14	58.1	77.0	11
BaA	n.d.	24.1	52.5	3.6	19.9	44.3	12
Chry	n.d.	17.1	76.1	11	10.2	64.7	9.4
BaPy	4 ± 1	38.4	76.4	13	36.3	73.4	2.0
Ind	n.d.	92.9	53.0	7.9	97.3	60.3	12

[a] Standard deviation in the determination of the analytes in the tap water sample (n = 3).
[b] Extraction efficiency, E_{Fmax} = 85.7.
[c] Relative recovery.
[d] Intra-day relative standard deviation (n = 3).
n.d.: not detected.

Table IV.34. Recovery, intra-day precision, and Student's *t* statistical test for spiked tap water samples (12 ng·L^{-1} for all PAHs) using the optimum [C_4Gu^+][Cl^-]-based μ-ABS-HPLC-FD method.

PAH	Tap water 1					Tap water 2				
	RR ± SD[a] (%)	t_{crit}[b]	t_{cal}[c]	Result	Matrix effect	RR ± SD[a] (%)	t_{crit}[b]	t_{cal}[c]	Result	Matrix effect
Ant	69 ± 12	6.96	4.36	$\|t_{cal}\| < t_{crit}$	No	77 ± 8	6.96	5.26	$\|t_{cal}\| < t_{crit}$	No
BaA	52 ± 3	6.96	30.5	$\|t_{cal}\| > t_{crit}$	Yes	44 ± 4	6.96	26.8	$\|t_{cal}\| > t_{crit}$	Yes
Chry	76 ± 6	6.96	7.25	$\|t_{cal}\| > t_{crit}$	Yes	65 ± 4	6.96	16.2	$\|t_{cal}\| > t_{crit}$	Yes
BaPy	76 ± 8	6.96	5.40	$\|t_{cal}\| < t_{crit}$	No	73 ± 1	6.96	59.8	$\|t_{cal}\| > t_{crit}$	Yes
Ind	53 ± 7	6.96	11.2	$\|t_{cal}\| > t_{crit}$	Yes	60 ± 12	6.96	5.80	$\|t_{cal}\| < t_{crit}$	No

[a] Relative recovery together with its intra-day standard deviation (n = 3).
[b] Critical Student's *t* for a significance level of 2 %.
[c] Calculated Student's *t* using 100 % as true value for RR.

REFERENCES

[1] T.B.V. Dinis, H. Passos, D.L.D. Lima, V.I. Esteves, J.A.P. Coutinho, M.G. Freire, Green Chem. 17 (2015) 2570–2579.

[2] T. Trtic-Petrovic, A. Dimitrijevic, N. Zdolsek, J. Dordevic, A. Tot, M. Vranes, S. Gadzuric, Anal. Bioanal. Chem. 410 (2018) 155–166.

[3] T.B.V. Dinis, H. Passos, D.L.D. Lima, A.C.A. Sousa, J.A.P. Coutinho, V.I. Esteves, M.G. Freire, J. Chromatogr. A 1559 (2017) 69–77.

[4] H. Passos, A.C.S. Sousa, M.R. Pastorinho, A.J.A. Nogueira, L.P.N. Rebelo, J.A.P. Coutinho, M.G. Freire, Anal. Methods 4 (2012) 2664–2667.

[5] M.G. Bogdanov, I. Svinyarov, J. Chromatogr. A 1559 (2017) 62–68.

[6] W.Y. Lee, K.-S. Kim, J.K. You, Y.K. Hong, ACS Sustainable Chem. Eng. 4 (2016) 572–576.

[7] R.F.M. Frade, A.A. Rosatella, C.S. Marques, L.C. Branco, P.S. Kulkarni, N.M.M. Mateus, C.A.M. Afonso, C.M.M. Duarte, Green Chem. 11 (2009) 1660–1665.

[8] I. Pacheco-Fernández, P. González-Hernández, V. Pino, J.H. Ayala, A.M. Afonso, in: A. Eftekhari, Ionic Liquid Devices, The Royal Society of Chemistry (2018) 53–78.

[9] M.G. Freire, C.M.S.S. Neves, J.N.C. Lopes, I.M. Marrucho, J.A.P. Coutinho, L.P.N. Rebelo, J. Phys. Chem. B 116 (2012) 7660–7668.

[10] M.G. Freire, A.F.M. Cláudio, J.M.M. Araújo, J.A.P. Coutinho, I.M. Marrucho, J.N. Canongia Lopes, L.P.N. Rebelo, Chem. Soc. Rev. 41 (2012) 4966–4995.

[11] M.V. Quental, H. Passos, K.A. Kumia, J.A.P. Coutinho, M.G. Freire, J. Chem. Eng. Data 60(6) (2015) 1674–1682.

[12] S. Shahriari, C.M.S.S. Neves, M.G. Freire, J.A.P. Coutinho, J. Phys. Chem. B 116(24) (2012) 7252–7258.

[13] J.C. Merchuk, B.A. Andrews, J.A. Asenjo, J. Chromatogr. B 711 (1998) 285–293.

[14] K.H. Kim, S.A. Jahan, E. Kabir, R.J.C. Brown, Environ. Int. 60 (2013) 71–80.

[15] Y. Zhang, S. Dong, H. Wang, S. Tao, R. Kiyama, Environ. Poll. 213 (2016) 809–824.

[16] A. Nzila, Environ. Pollut. 239 (2018) 788–802.

[17] J. An, M.J. Trujillo-Rodríguez, V. Pino, J.L. Anderson, J. Chromatogr. A 1500 (2017) 1–23.

[18] H. Passos, A.R. Ferreira, A.F.M. Cláudio, J.A.P. Coutinho, M.G. Freire, Biochem. Eng. J. 67 (2012) 68–76.

[19] Spanish Royal Decree No 140/2003 of 7 February 2003, which establishes the safety criteria for drinking water quality, BOE-A-2003-3596.

[20] M.J. Trujillo-Rodríguez, P. Rocío-Bautista, V. Pino, A.M. Afonso, Trac-Trends Anal. Chem. 51 (2013) 87–106.

[21] M. Fernández, S. Clavijo, R. Forteza, V. Cerdà, Talanta 138 (2015) 190–195.

[22] S. Fu, J. Fan, Y. Hashi, Z. Chen, Talanta 94 (2012) 152–157.

[23] P. Rocío-Bautista, V. Pino, J. Pasán, J.H. Ayala, C. Ruiz-Pérez, A.M. Afonso, LC GC N. Am. 36 (2018) 464–471.

[24] M.J. Trujillo-Rodríguez, O. Nacham, K.D. Clark, V. Pino, J.L. Anderson, J.H. Ayala, A.M. Afonso, Anal. Chim. Acta 934 (2016) 106–113.

[25] P. Makos, A. Przyjazny, G. Boczkaj, J. Chromatogr. A 1570 (2018) 28–37.

[26] M. Merdivan, V. Pino, J.L. Anderson, Environ. Technol. 38(15) (2016) 1897–1904.

[27] J.N. Miller and J.C. Miller, Statistics and Chemometrics for Analytical Chemistry, Pearson Education Limited (2010) 37–73.

Section IV.2.

Solid-phase microextraction applications with new coatings

Section IV.2.1

Exploiting the tunability of polymeric ionic liquids to prepare more efficient solid-phase microextraction coatings

PILs are one of the materials most extensively studied in SPME due to their high chemical and thermal stability, adequate viscosity, and tunable selectivity through simple chemical modifications. They have been mainly used in combination with GC applications, taking advantage of their thermal stability, to carry out the thermal desorption of the analytes. Few studies describe the use of PIL–based SPME fibers or capillaries with HPLC given the swelling of most common PILs in the organic solvents required during the desorption step.

Furthermore, despite the synthetic versatility of PILs, most of the applications described in the literature still use PILs composed of 1-vinyl-3-alkylimidazolium ILs monomers without any structural singularity or functionalization within the cation or anion moieties.

The aim of the studies included in this section is to exploit the tunability of PILs to prepare new SPME coatings with enhanced physical-chemical characteristics as well as selectivity features for different analytical applications. Thus, highly robust PILs composed of functionalized or zwitterionic ILs as monomers and dicationic ILs as crosslinkers were immobilized on nitinol wires to prepare PIL-based SPME fibers. In the first case, the functionalized PILs were evaluated in DI-SPME in combination with HPLC for the determination of organic pollutants in water samples, specifically polar compounds. In the case of zwitterionic PILs, the fibers were applied in a HS-SPME method coupled with GC for the analysis of wines to obtain their SCFFAs profile. In both cases, PILs with different compositions were tested, and their performance was compared with that of the commercial SPME fibers. Furthermore, crosslinked PILs containing ILs functionalized with carboxylic groups as monomers were also used to prepare internally coated capillaries, which were then evaluated in different in-tube SPME strategies for the extraction of DNA.

Section IV.2.1.1

Selection and characterization of polymeric ionic liquids-based solid-phase microextraction coatings

Talanta 158 (2016) 125–133

Talanta 200 (2019) 415–523

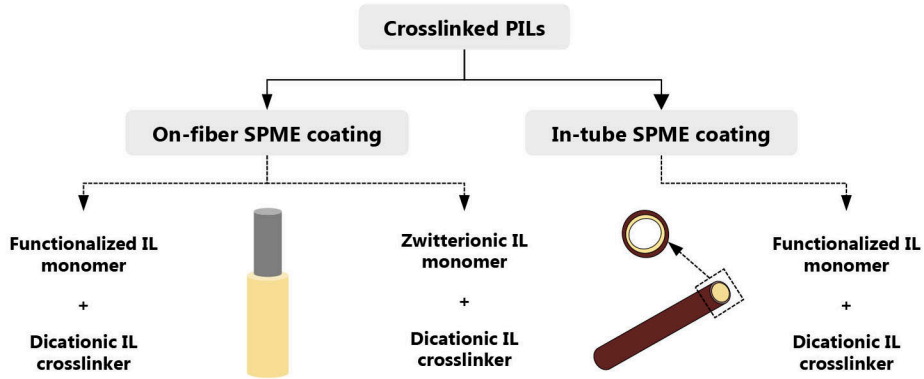

1. Selection of PILs-based coatings

It is important to select proper PILs-based SPME coatings for specific analytical applications. In this sense, the PILs and SPME devices were designed considering not only the target application but also the chromatographic technique used for the analytical determination. At the same time, new compositions for the PILs were explored to upgrade their selectivity and extraction capability. Thus, crosslinked PILs were selected with the aim of improving the mechanical stability of the PILs-based coatings while prolonging their lifetime [1,2]. To achieve this goal, the PILs were chemically immobilized on the support surface through the copolymerization of two different ILs: a monocationic IL monomer and a dicationic IL crosslinker. Prior to the polymerization, the surfaces were functionalized with vinyl groups to ensure the chemical linkage with the PIL coating.

Table III.2 shows the composition and size of the PILs-based coatings prepared in this Doctoral Thesis, which can be classified depending on the type of support: fibers for on-fiber SPME and capillaries for in-tube SPME.

1.1. PILs-coated fibers for on-fiber SPME applications

In 2012, Ho *et al.* developed an on-fiber copolymerization method assisted by UV light for the preparation of crosslinked PIL-based SPME coatings [3]. In this method, the copolymerization of the IL together with the crosslinker agent takes place on the fiber support and inside a UV reactor, which enormously speeds up the preparation of fibers. Thus, this method was selected for the preparation of the PILs-coated fibers in this Doctoral Thesis, as it was described in Section III.7.1.3. Moreover, the use of nitinol wires as core for the preparation of the crosslinked PILs-based fibers provided highly robust and flexible coatings [4].

With respect to the chemical composition, previous studies have demonstrated that PIL-based coatings containing halide anions or polar substituents in the cationic moiety are more efficient for the extraction of polar compounds [3], while those with vinylbenzyl groups within the cation provided better results for aromatic compounds [5,6]. However, these functionalized coatings have been mainly used in HS-SPME methods in combination with GC, and they have been scarcely evaluated in DI-SPME and HPLC applications.

Thus, the fibers PIL-1a, PIL-1b, PIL-2, PIL-3, and PIL-4 (see Table III.2) containing IL monomers with alkyl or benzyl substituents and different anions were prepared in this Doctoral Thesis for their application in DI-SPME-HPLC methods. Figure IV.18 A) shows a SEM micrograph of the cross-section for fiber PIL-1b as a representative example of this group of fiber coatings. The thicknesses of the coatings were estimated by measuring different sections of the same PIL-based fiber and then calculating the average value. The obtained values are included in Table III.2. Thicker coatings were obtained for PIL-1b and PIL-4 by spinning the fiber during the copolymerization process, as described in Section III.7.1.3 [7].

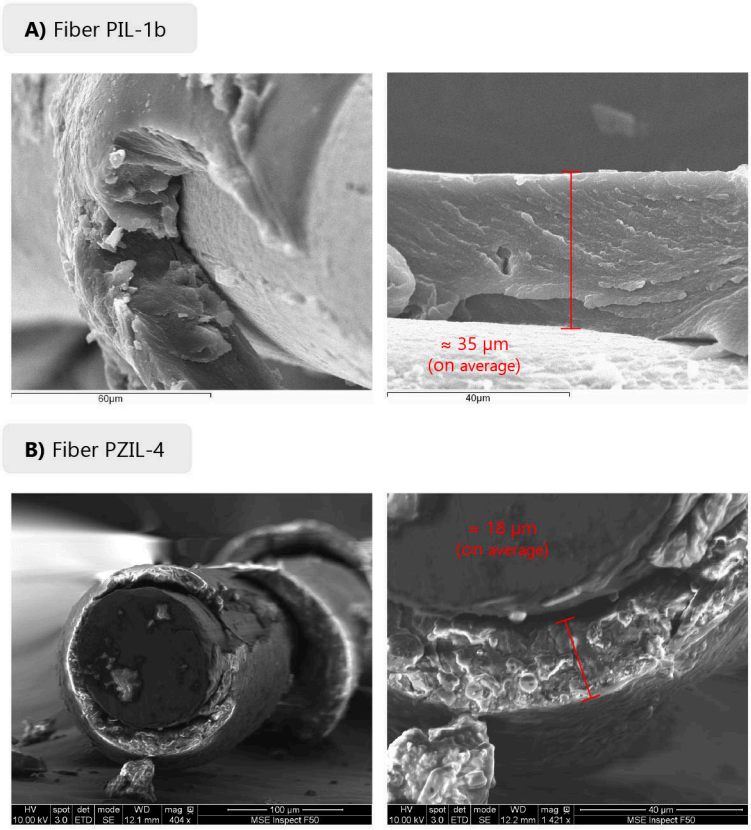

Figure IV.18. Representative SEM micrographs of the fibers cross-sections for **A)** PIL-1b and **B)** PZIL-4.

Zwitterionic PILs are also interesting materials that exhibit high dipole moments while maintaining charge neutrality [8,9]. In addition to this, they possess a wide chemical diversity due to the possibility of combining different cations and anions, and the feasibility of modulating the proximity of these positive and negative charges [8]. Despite all these features, zwitterionic PILs have never been applied in SPME.

Thus, five zwitterionic PILs were prepared using imidazolium-type ILs with sulfonate and carboxylate alkyl lengths, as shown in Table III.2. Furthermore, the anion of the dicationic IL crosslinker was also varied to adjust the thermal stability of the coatings, which will be further use in GC applications (thermal desorption). Thus, the maximum operating temperature was 175 °C for the fibers containing [Br^-] anions, and 200 °C for those prepared with [NTf_2^-] anions. Figure IV.18 B) includes a SEM micrograph for fiber PZIL-4 as a representative example of the zwitterionic PILs-

based fiber coatings. In this case, the thickness varied between ≈ 18 µm for PZIL-1 and PZIL-4 and ≈ 25 µm for PZIL-5.

1.2. PILs-coated capillaries for in-tube SPME applications

Among the high variety of PILs that have been described for specific analytical applications, it is interesting to highlight those crosslinked PILs-based fiber coatings prepared with carboxylic groups in the cationic moiety for the selective extraction of DNA [10]. In this type of PILs, electrostatic interactions as well as ion-exchange mechanism were identified as the driving forces in DNA extraction, since the cationic framework of the PIL interacts with the negatively charged phosphate backbone of the DNA.

This DI-SPME method using functionalized PILs-based fibers coupled with real-time polymerase chain reaction (PCR) exhibited many advantages over other conventional methods for the extraction and purification of small amounts of DNA. As disadvantages, the method required long extraction times together with long cleaning steps after every extraction to avoid carry-over effects. In this sense, the in-tube SPME configuration may lead to faster and more efficient methods considering the increase in the surface area of the coating [11].

Therefore, the same crosslinked PILs evaluated for the extraction of DNA by on-fiber SPME were used in this Doctoral Thesis to fabricate internally coated capillaries for the development of an in-tube SPME approach. Two coatings were prepared, as listed in Table III.2: CAP-1 containing an aklylimidazolium cation, and the functionalized CAP-2, which incorporates a carboxyl group in its structure to tune the selectivity towards DNA. In both cases, the dicationic IL crosslinkers were composed of halide anions, which have demonstrated to enhance the extraction of DNA [10].

Given the geometry of the device (i.e., a thin long capillary), the coating process was carried out by thermal copolymerization, as it was described in Section III.7.1.3. Figure IV.19 shows several representative SEM images for CAP-1 and CAP-2. The thicknesses for both coatings were estimated to be ≈ 0.5 µm. Although the coatings are much thinner in comparison with PILs-based fibers, in-tube SPME applications require capillary lengths between 15 and 60 cm. Therefore, the surface area of the coating is significantly increased with this geometry.

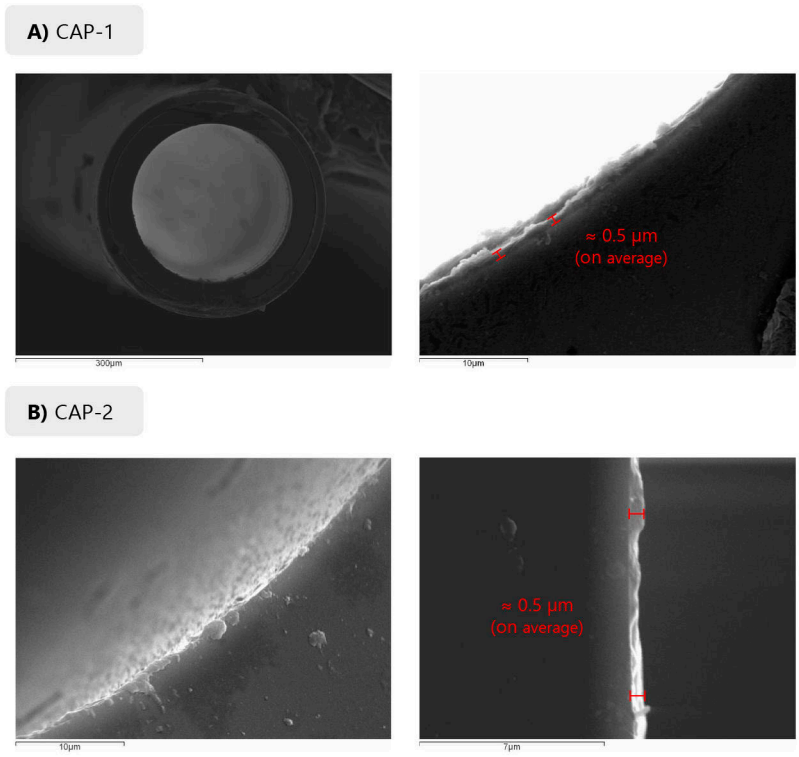

Figure IV.19. Representative SEM micrographs of the capillaries cross-sections for **A)** CAP-1 and **B)** CAP-2.

REFERENCES

[1] J. Feng, M. Sun, X. Wang, X. Liu, S. Jiang, J. Chromatogr. A 1245 (2012) 32–38

[2] H. Yu, J. Merib, J.L. Anderson, J. Chromatogr. A 1438 (2016) 10–21.

[3] T.D. Ho, H. Yu, W.T.S. Cole, J.L. Anderson, Anal. Chem. 84 (2012) 9520–9528.

[4] T.D. Ho, B.R. Toledo, L.W. Hantao, J.L. Anderson, Anal. Chim. Acta 843 (2014) 18–26.

[5] M.J. Trujillo-Rodríguez, H. Nan, J.L. Anderson, J. Chromatogr. A 1540 (2018) 11–20.

[6] E. Gionfriddo, E.A. Souza-Silva, T.D. Ho, J.L. Anderson, J. Pawslizyn, Talanta 188 (2018) 522–530.

[7] C. Cagliero, T.D. Ho, C. Zhang, C. Bicchi, J.L. Anderson, J. Chromatogr. A 1449 (2016) 2–7.

[8] L. Mi, S. Jiang, Angew. Chem. Int. Ed. 53 (2014) 1746–1754.

[9] M.E. Taylor, M.J. Panzer, J. Phys. Chem. B 122 (2018) 8469–8476.

[10] O. Nacham, K.D. Clark, J.L. Anderson, Anal. Chem. 88 (2016) 7813–7820.

[11] C. Cháfer-Pericás, R. Herráez-Hernández, P. Campíns-Falcó, J. Chromatogr. A 1125 (2006) 159–171.

Section IV.2.1.2

Crosslinked functionalized polymeric ionic liquids-based fiber coatings in direct-immersion solid-phase microextraction coupled with high-performance liquid chromatography: application for the determination of polar organic pollutants in water samples

Talanta 158 (2016) 125–133

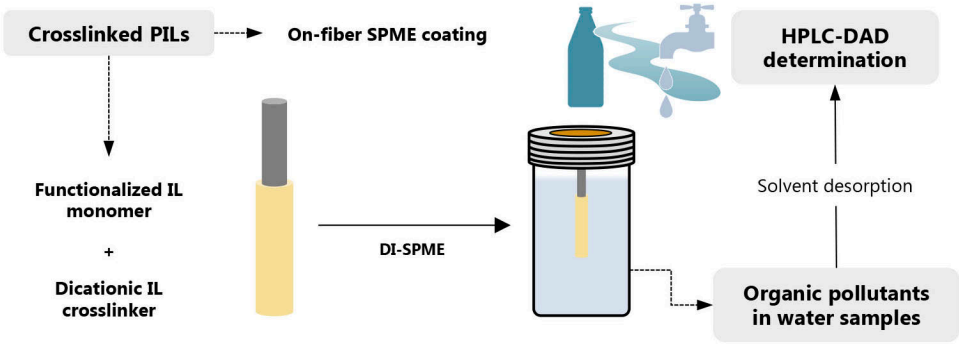

1. Performance of the PILs-based sorbent coatings with model analytes and HPLC-UV-Vis determination

In this section, crosslinked PILs-based fiber coatings were evaluated in a DI-SPME-HPLC method (off-line desorption) to expand the use of these sorbents in HPLC applications. The PILs-based fibers were first examined with a group of 10 different model analytes including polar analytes such as BPA and non-polar analytes such as Nap. The analytical determination was carried out by HPLC-UV-Vis following the conditions described in Section III.7.5.5, which allowed the baseline separation of the analytes in less than 22 min as shown in Figure IV.20.

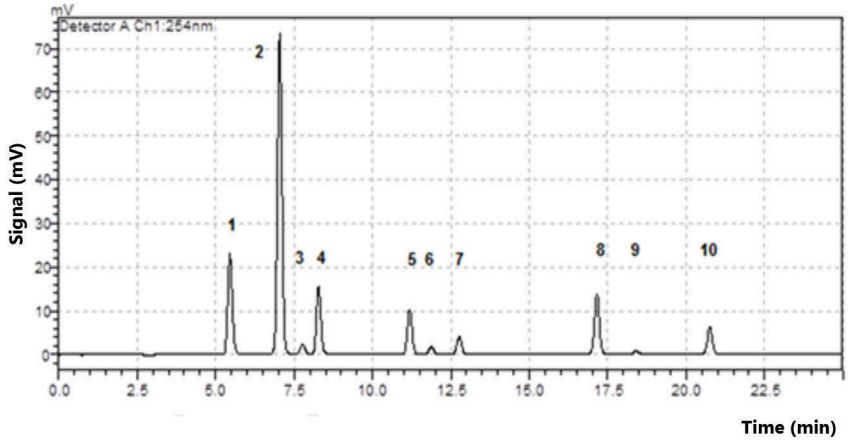

Figure IV.20. HPLC-UV separation obtained for model analytes, being (1) Cmz, (2) Bnzal, (3) BPA, (4) NP, (5) tfTol, (6) *t*BP, (7) EB, (8) Nap, (9) Gfz, and (10) Trc.

In this preliminary study, fibers PIL-1a, PIL-2 and PIL-3, with a film thickness of approximately 14 µm (Table III.2), were evaluated together with several commercial SPME fibers compatible with HPLC analysis: PA, PDMS and PDMS/DVB. The main goal at this point was to test the influence of the nature of the sorbent coating without considering differences in thicknesses. Thus, the overall DI-SPME-HPLC-UV-Vis method was optimized and validated with all the fibers. Then, a comparison among all coatings was performed to assess the possible selectivity exhibited by the PILs-based coatings.

1.1. Optimization of the DI-SPME-HPLC-UV-Vis method using all SPME fibers

Several parameters affecting the method were previously fixed to ensure high sensitivity, such as the volume of the aqueous sample (10 mL), the volume of desorption solvent in off-line

mode (50 µL, to ensure complete immersion of the fiber) and the agitation rate (500 min^{-1}, to guarantee the integrity of the fiber while stirring as well as an adequate homogenization of the sample). The nature of the desorption solvent, desorption time, extraction time, and pH of the sample were evaluated as the main parameters affecting the analytical performance. The optimization followed a simple one-factor-at-a-time approach using 10 mL of aqueous working solutions containing the analytes at different concentrations, depending on the analyte: Cmz 200 $\mu g \cdot L^{-1}$, Bnzal 400 $\mu g \cdot L^{-1}$, BPA 400 $\mu g \cdot L^{-1}$, NP 10 $\mu g \cdot L^{-1}$, tfTol 400 $\mu g \cdot L^{-1}$, *t*BP 200 $\mu g \cdot L^{-1}$, EB 200 $\mu g \cdot L^{-1}$, Nap 100 $\mu g \cdot L^{-1}$, Gfz 25 $\mu g \cdot L^{-1}$, and Trc 10 $\mu g \cdot L^{-1}$. They were subjected to the overall DI-SPME-HPLC-UV-Vis method under the tested conditions (in triplicate) and the obtained peak areas were used as the response to assess the extraction efficiency.

Figures IV.21, IV.22, IV.23, IV.24, IV.25, and IV.26, include all the results obtained during the optimization studies carried out for the model analytes and with all the fibers. According to the results observed, the optimum conditions selected were: methanol as desorption solvent for PIL-based, PA and PDMS/DVB fibers, and acetonitrile for PDMS fiber; desorption time of 30 min for commercial fibers, PIL-1a and PIL-3, and 40 min for fiber PIL-2; extraction time of 45 min for all the SPME fibers as a compromise solution with the aim of benefiting most analytes; and a pH value of 2 for all the PILs and commercial fibers.

1.2. Evaluation of analytical extraction of PILs-based and commercial sorbent coatings for model analytes

Once the DI-SPME-HPLC-UV-Vis method was optimized for each fiber for the group of model analytes, the extraction efficiency of PILs-based and commercial fibers was compared. Figure IV.27 shows the normalized peak area obtained (peak area divided by the coating thickness) [1] to focus the comparison on the fiber nature and to discard the effect exerted by the film thicknesses. The PIL-1a fiber exhibited higher selectivity for aromatic compounds such as Cmz and Nap, which may be due to the vinyl benzyl moiety within the cation that enhances π-π interactions with these analytes [2]. It can be also clearly observed that fiber PIL-3 provides higher affinity for polar compounds such as BPA and tfTol. This may be related to the anionic component of the fiber since it has been demonstrated that halide anions exhibit higher hydrogen bond basicity, which leads to stronger hydrogen bonding interactions with polar analytes [3]. Therefore, it can be concluded that PILs-based sorbent coatings offer an interesting tunable selectivity for a wide range of compounds, depending on their chemical composition.

With respect to the commercial fibers, the PDMS/DVB fiber was the best and exhibited significantly higher extraction efficiencies for model analytes in comparison with the other fibers studied. However, the PA fiber was more suitable for the extraction of highly polar analytes such as BPA. Poor extraction efficiency was shown for the PDMS fiber, which was not able to extract BPA or NP. For these reasons, only the PA and PDMS/DVB commercial fibers were selected for a further comparative study with the PILs-based sorbent coatings.

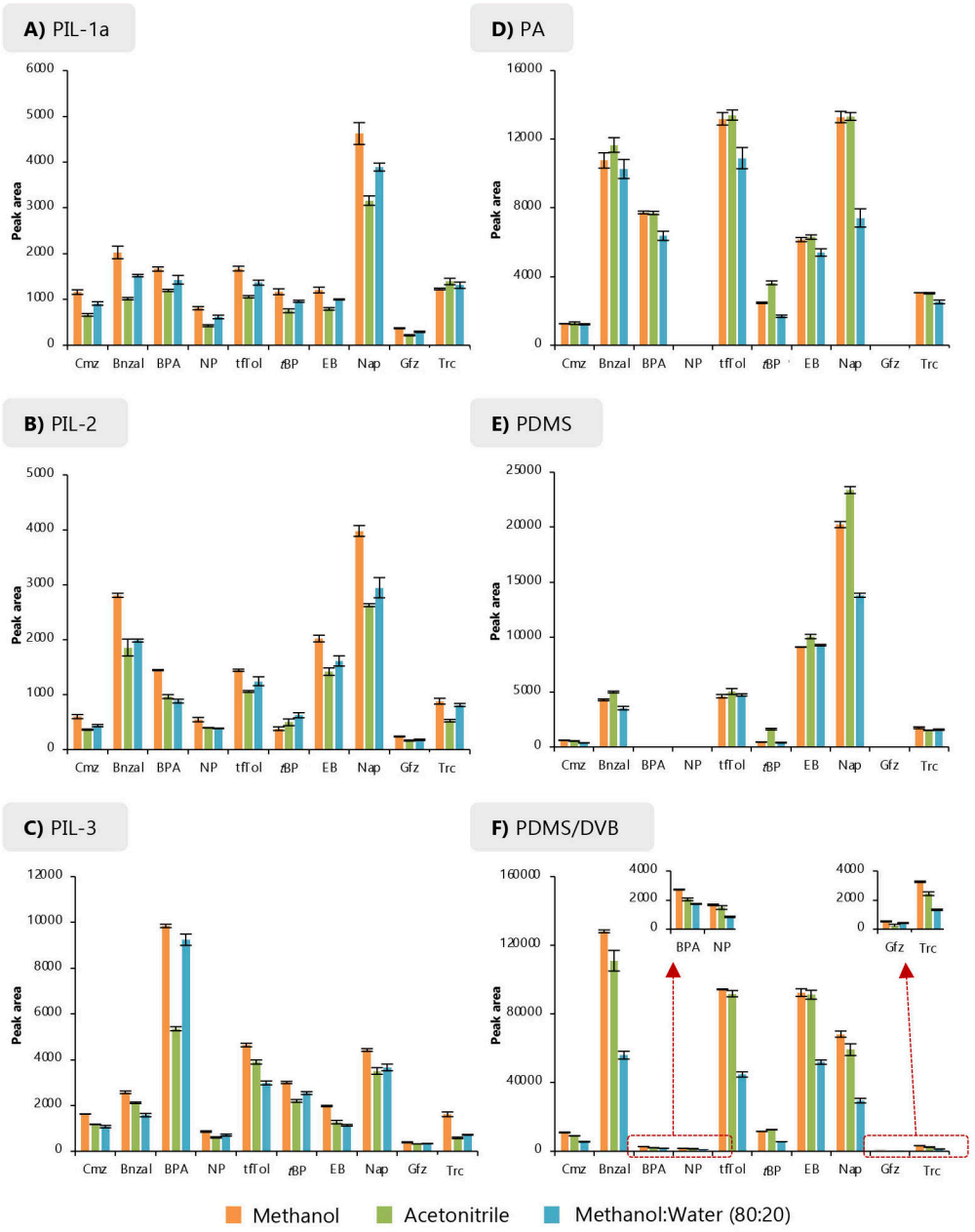

Figure IV.21. Influence of the nature of the desorption solvent on the extraction efficiency measured as peak area for the DI-SPME-HPLC-UV-Vis method using fibers **A)** PIL-1a, **B)** PIL-2, **C)** PIL-3, **D)** PA, **E)** PDMS, and **F)** PDMS/DVB. Fixed experimental conditions: 30 min of extraction time; 30 min of desorption time; and pH value of 7. The remaining experimental conditions are detailed in the text.

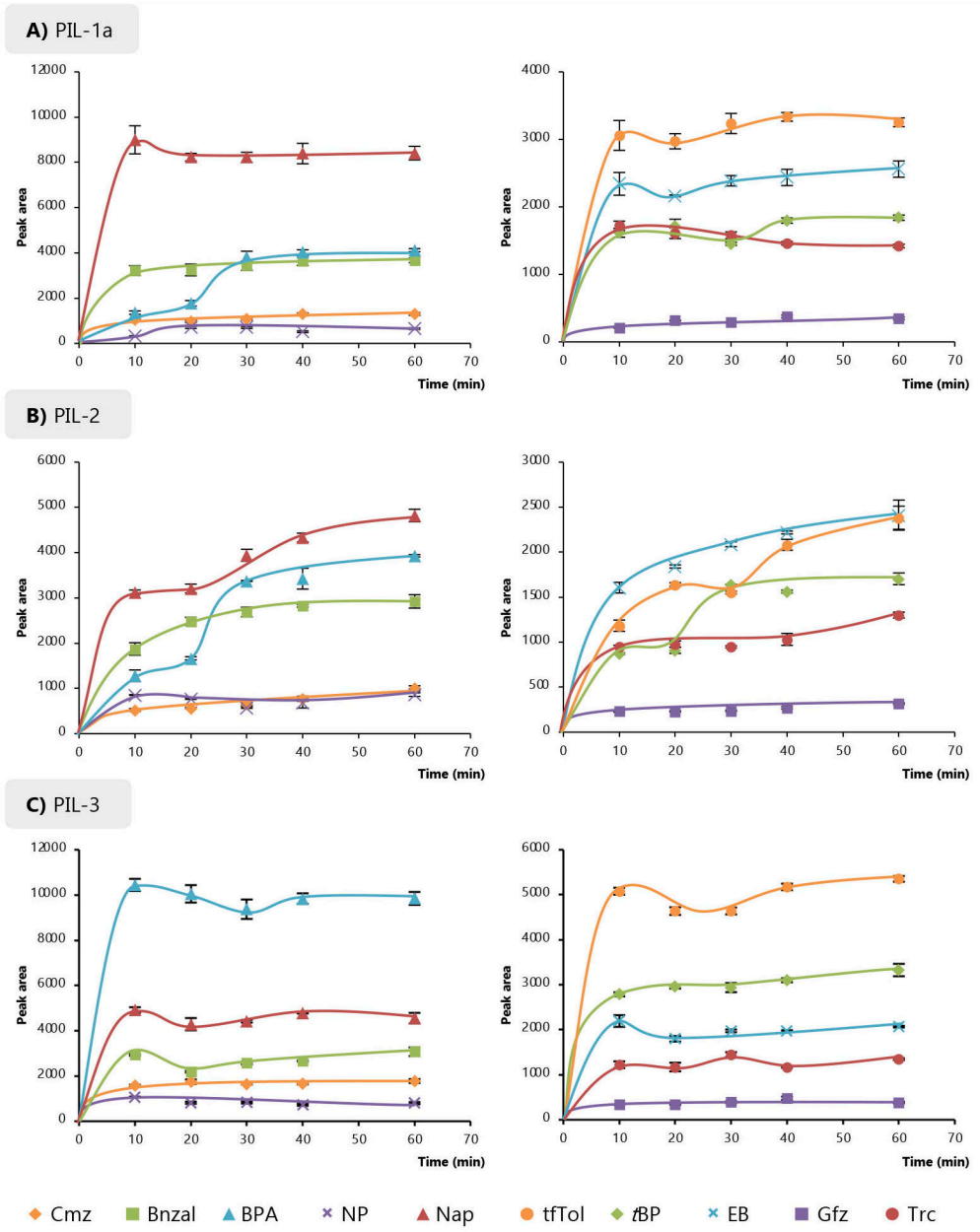

Figure IV.22. Desorption time profiles obtained for the DI-SPME-HPLC-UV-Vis method using fibers **A)** PIL-1a, **B)** PIL-2, and **C)** PIL-3. Analytes with higher sensitivities are plotted on the left side. Analytes with lower sensitivities are plotted on the right side. Non-detected analytes were not represented. Fixed experimental conditions: 30 min of extraction time; pH value of 7; and methanol as desorption solvent. The remaining experimental conditions are detailed in the text.

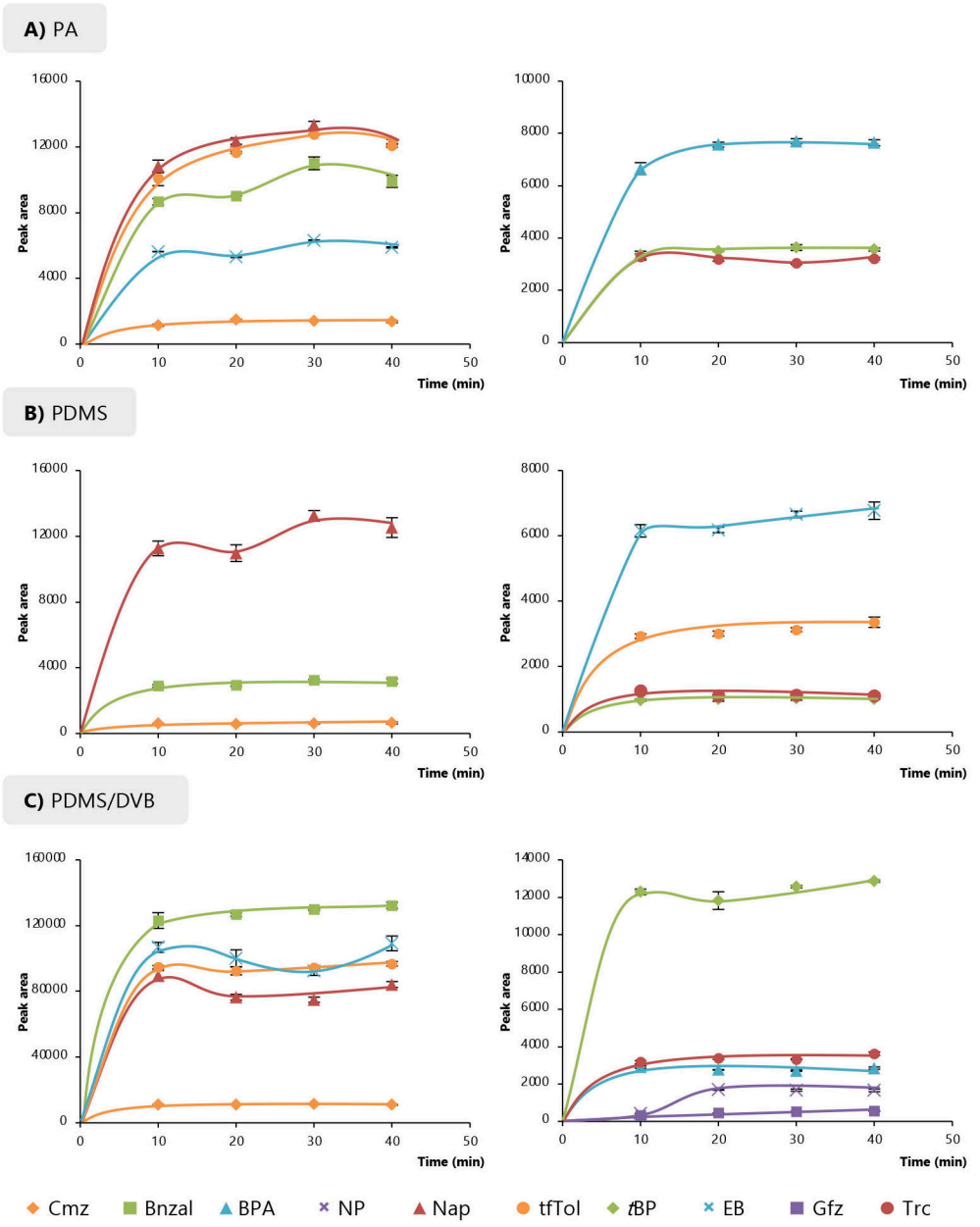

Figure IV.23. Desorption time profiles obtained for the DI-SPME-HPLC-UV-Vis method using fibers **A)** PA, **B)** PDMS, and **C)** PDMS/DVB. Analytes with higher sensitivities are plotted on the left side. Analytes with lower sensitivities are plotted on the right side. Non-detected analytes were not represented. Fixed experimental conditions: 30 min of extraction time; pH value of 7; methanol as desorption solvent for PA and PDMS/DVB fibers; and acetonitrile as desorption solvent for PDMS. The remaining experimental conditions are detailed in the text.

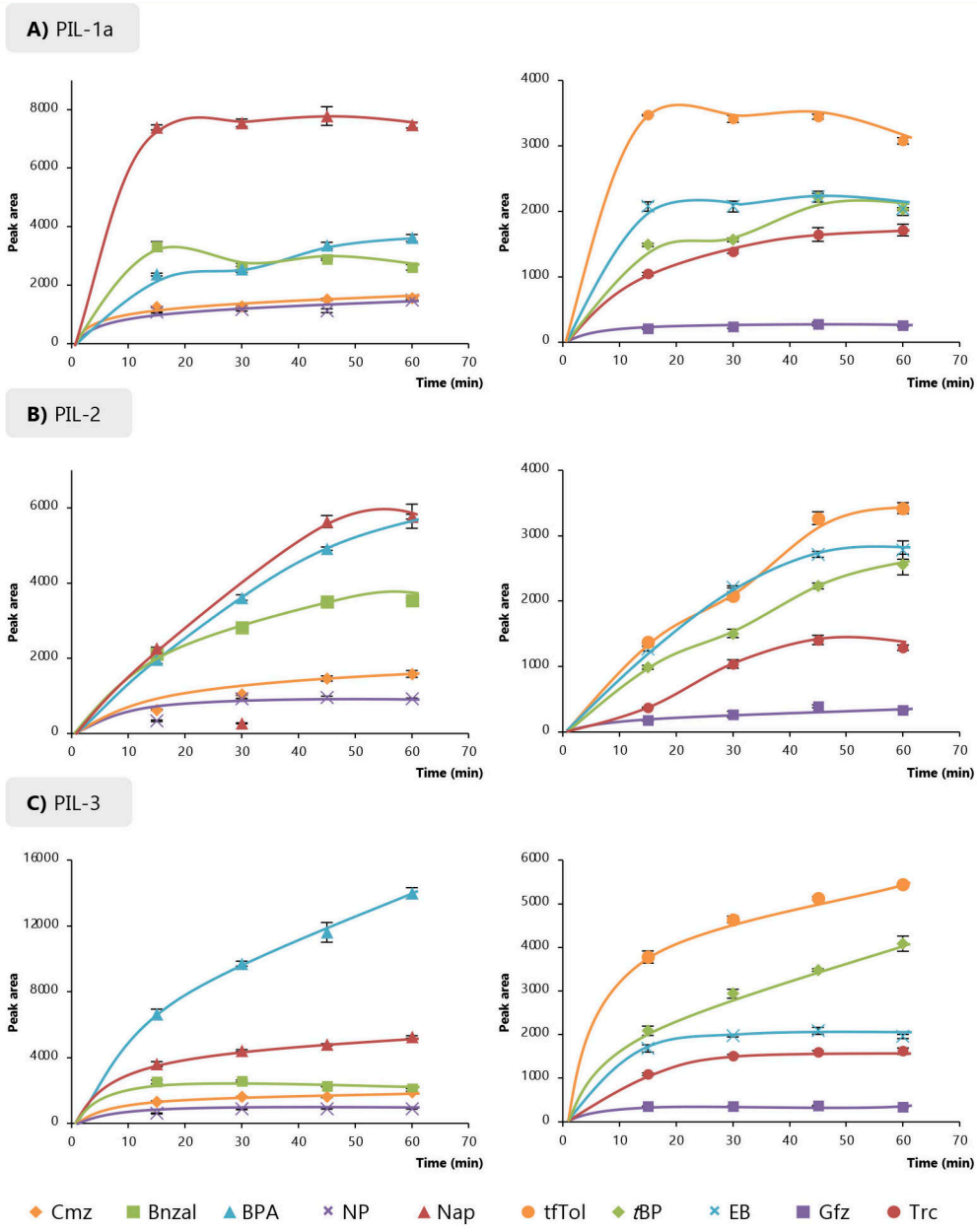

Figure IV.24 Extraction time profiles obtained for the DI-SPME-HPLC-UV-Vis method using fibers **A)** PIL-1a, **B)** PIL-2, and **C)** PIL-3. Analytes with higher sensitivities are plotted on the left side. Analytes with lower sensitivities are plotted on the right side. Non-detected analytes were not represented. Fixed experimental conditions: pH value of 7; methanol as desorption solvent; desorption time of 30 min for PIL-1a and PIL-3; and 40 min of desorption time for PIL-2. The remaining experimental conditions are detailed in the text.

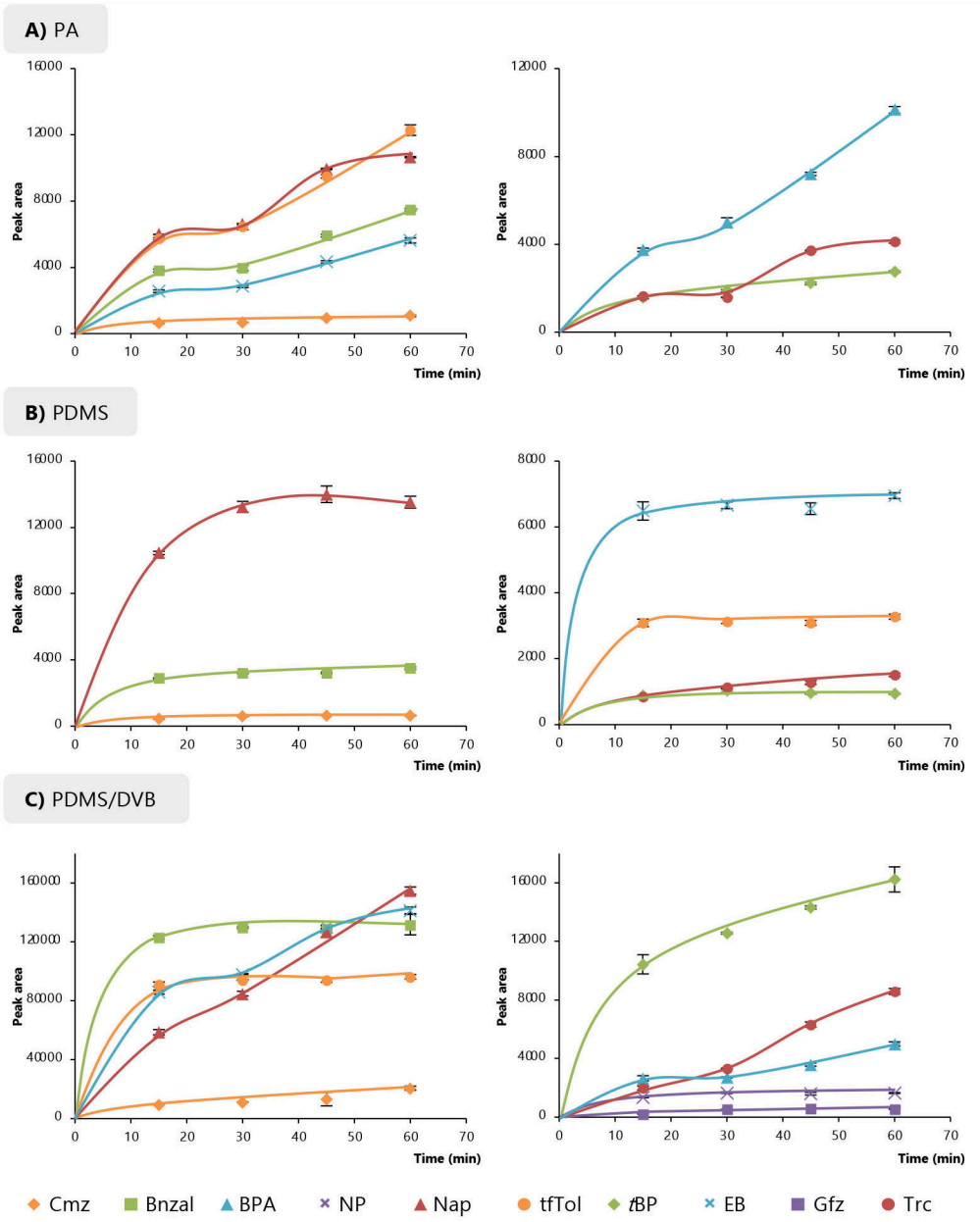

Figure IV.25. Extraction time profiles obtained for the DI-SPME-HPLC-UV-Vis method using fibers **A)** PA, **B)** PDMS, and **C)** PDMS/DVB. Analytes with higher sensitivities are plotted on the left side. Analytes with lower sensitivities are plotted on the right side. Non-detected analytes were not represented. Fixed experimental conditions: pH value of 7; methanol as desorption solvent for PA and PDMS/DVB fibers; acetonitrile as desorption solvent for PDMS fiber; and desorption time of 30 min. The remaining experimental conditions are detailed in the text.

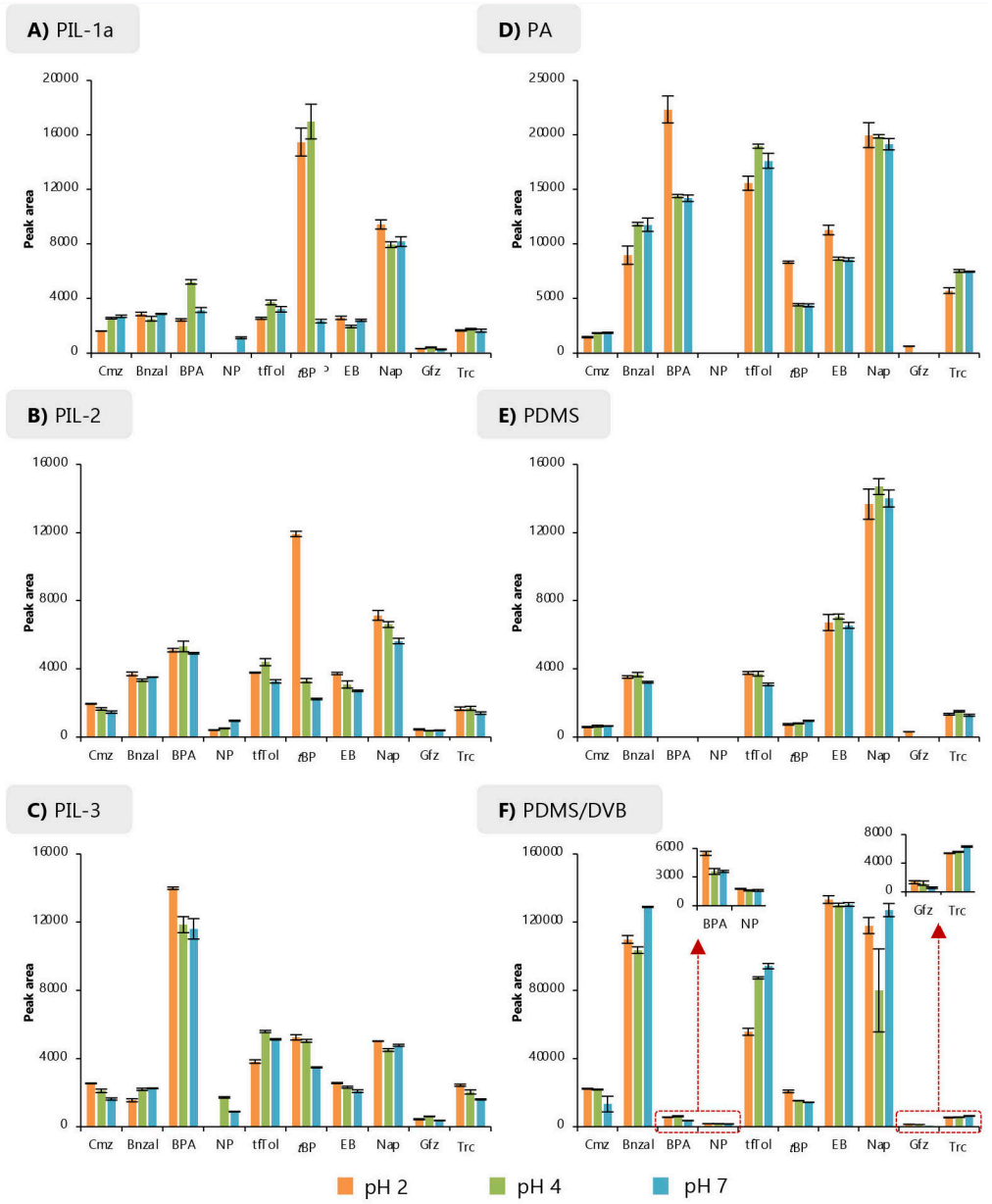

Figure IV.26. Evaluation of the effect of the pH in the extraction efficiency for the DI-SPME-HPLC-UV-Vis method using fibers **A)** PIL-1a, **B)** PIL-2, **C)** PIL-3, **D)** PA, **E)** PDMS, and **F)** PDMS/DVB. Non-detected analytes were not represented. Fixed experimental conditions: extraction time of 45 min; methanol as desorption solvent for PIL-based, PA, and PDMS/DVB fibers; acetonitrile as desorption solvent for PDMS fiber; desorption time of 30 min for commercial fibers, PIL-1a, and PIL-3; 40 min for fiber PIL-2. The remaining experimental conditions are detailed in the text.

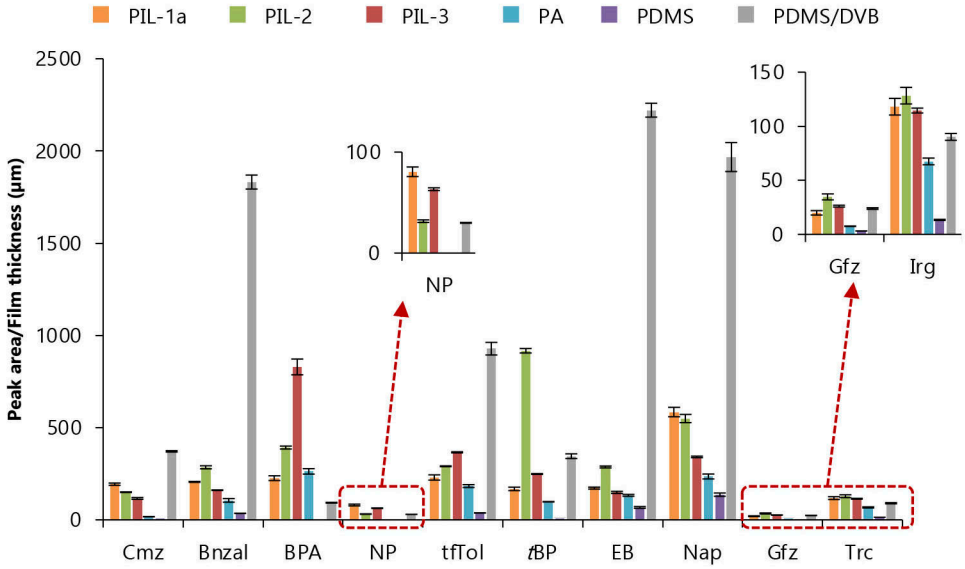

Figure IV.27. Comparison of the extraction efficiency, measured as normalized peak area, for each fiber when testing model analytes. The normalized peak area is calculated as the ratio between the peak area obtained under the optimized extraction/desorption conditions described in the text, and the film thickness of each coating. Concentrations of analytes were: Cmz 200 µg·L^{-1}, Bnzal 400 µg·L^{-1}, BPA 400 µg·L^{-1}, NP 10 µg·L^{-1}, tfTol 400 µg·L^{-1}, *t*BP 200 µg·L^{-1}, EB 200 µg·L^{-1}, Nap 100 µg·L^{-1}, Gfz 25 µg·L^{-1}, and Trc 10 µg·L^{-1}.

1.3. Analytical performance of all on-fiber SPME sorbent coatings

The validation of the optimized DI-SPME-HPLC-UV-Vis method was carried out for the PA, PDMS/DVB and PILs-based fibers with the model analytes. The analytical quality parameters for PILs-based fibers are listed in Table IV.35, including linear ranges, sensitivities (as calibration slopes), determination coefficients (R^2), and limits of detection (LODs). All calibrations provided high R^2 values varying from 0.988 to 0.998 within the linear ranges. The maximum sensitivity was found for Trc when using all the PIL-based fibers. As it was predicted in the previous comparative study, the PIL-1a fiber exhibited a better sensitivity for aromatic compounds, while the PIL-3 fiber containing the bromide anion was more suitable for polar compounds. The PIL–2 fiber showed higher slope values for Bnzal, *t*BP, Gfz and Trc in comparison with the other fibers. The LODs were calculated as three times the signal-to-noise ratio (S/N) and were verified by subjecting a standard solution prepared at the calculated concentrations to the overall method. The lowest LODs were found for Trc, with a value of 2 µg·L^{-1} using the PIL-2 fiber. The overall LODs were in a range of 2.5–20 µg·L^{-1} for PIL-1a, 2–20 µg·L^{-1} for PIL-2 and 2.5–20 µg·L^{-1} for PIL-3. It is important to point out that these LODs values are satisfactory considering that a UV-Vis detector was employed.

Table IV.35. Quality analytical parameters for the DI-SPME-HPLC-UV-Vis method using the PIL-1a, PIL-2 and PIL-3 fibers for model analytes (aqueous standards in ultrapure water subjected to the entire method).

Analyte	Fiber PIL-1a				Fiber PIL-2				Fiber PIL-3			
	Linear range ($\mu g \cdot L^{-1}$)	Slope ± t·SD[a]	R^2 [b]	LOD[c] ($\mu g \cdot L^{-1}$)	Linear range ($\mu g \cdot L^{-1}$)	Slope ± t·SD[a]	R^2 [b]	LOD[c] ($\mu g \cdot L^{-1}$)	Linear range ($\mu g \cdot L^{-1}$)	Slope ± t·SD[a]	R^2 [b]	LOD[c] ($\mu g \cdot L^{-1}$)
Cmz	40–500	14 ± 1	0.993	20	40–500	10.3 ± 0.4	0.998	20	40–500	7.2 ± 0.3	0.998	20
Bnzal	40–500	8 ± 2	0.991	20	40–500	9.5 ± 0.2	0.998	20	40–500	7.2 ± 0.9	0.988	20
BPA	20–500	14 ± 3	0.991	10	20–500	26 ± 1	0.998	10	10–500	32.2 ± 0.5	0.998	5.0
NP	5–500	93 ± 17	0.996	2.5	10–500	13.6 ± 0.2	0.998	5.0	10–500	84 ± 4	0.998	2.5
tfTol	40–500	14 ± 5	0.990	20	40–500	9.2 ± 0.3	0.998	20	40–500	15 ± 1	0.998	20
*t*BP	40–500	9 ± 2	0.996	20	10–500	24 ± 1	0.998	5.0	40–500	7.7 ± 0.3	0.998	20
EB	40–500	13± 4	0.990	20	40–500	7.51 ± 0.08	0.998	20	40–500	12.3 ± 0.5	0.998	20
Nap	5–500	168 ± 35	0.998	2.5	10–500	73 ± 1	0.998	5.0	10–500	49 ± 3	0.998	5.0
Gfz	20–500	5 ± 1	0.994	10	20–500	21.9 ± 0.7	0.998	10	20–500	11.7 ± 0.4	0.998	10
Trc	5–500	171 ± 28	0.992	2.5	10–500	225 ± 5	0.998	2.0	5–500	172 ± 10	0.996	2.5

[a] 95 % confidence limits for n = 7 calibration levels (5 degrees of freedom).

[b] Determination coefficient.

[c] Limit of detection, calculated as 3 times the S/N, and verified with aqueous standards prepared at these levels and subjected to the overall method.

Table IV.36 includes the analytical quality parameters obtained with the PA and PDMS/DVB commercial fibers. The PDMS/DVB fiber showed better sensitivities for all analytes, except for BPA in comparison with the PA and PILs-based fibers. Thus, wider ranges and lower LODs were obtained for the PDMS/DVB fiber, ranging from 0.2 to 10 $\mu g \cdot L^{-1}$. With respect to the polar PA fiber, a higher slope was found for BPA, while the LODs varied between 1 and 25 $\mu g \cdot L^{-1}$. In all cases, the R^2 values were higher than 0.992. In general, commercial fibers provide better sensitivities for model analytes than PILs-based sorbent coatings, which may be due to their higher film thickness (60–85 μm and ≈ 14 μm for commercial and PIL coatings, respectively). However, PIL-based fibers showed much better sensitivities and lower LODs for Cmz and NP in comparison with the PA fiber, and for BPA compared to the PDMS/DVB coating.

1.4. Relative recovery and precision studies with water samples

In order to prove the applicability of the DI-SPME-HPLC-UV-Vis method using PILs-based fibers for the analysis of samples, relative recovery (RR, in %) and intra-day precision (as RSD, in %) studies were carried out for the model analytes tested. This study was performed at two different spiked levels in both river and tap water samples (tap water 3) subjected to the overall method (n = 3): 40 $\mu g \cdot L^{-1}$ and 200 $\mu g \cdot L^{-1}$. Only the PIL-1a and PIL-2 fibers were tested since both of them showed satisfactory analytical performance for most analytes.

The results included in Table IV.37 show that the PIL-2 fiber exhibits better relative recovery values at both concentration levels in both water samples. It provided average values of 91.2 % at 40 $\mu g \cdot L^{-1}$ and 95.1 % at 200 $\mu g \cdot L^{-1}$ in river waters, and 85.9 % at 40 $\mu g \cdot L^{-1}$ and 93.8 % at 200 $\mu g \cdot L^{-1}$ in tap water 3. In the case of the PIL-1a fiber, poor values of relative recovery were found for NP, with average values lower than 68 % at both concentration levels in both type of water samples. However, the recovery results obtained for NP using both PIL fibers are adequate since it has been reported that commercially available SPME fibers cannot even extract this analyte from water samples when they are combined with HPLC [4].

The RSD values for the PIL-1a fiber in both samples ranged from 2.9 to 15 % at 40 $\mu g \cdot L^{-1}$, and from 3.7 to 16 % at 200 $\mu g \cdot L^{-1}$. With respect to the PIL-2 fiber, the RSD values were lower in both water samples, varying in the ranges of 0.5–18 % at 40 $\mu g \cdot L^{-1}$, and 0.7–14 % at 200 $\mu g \cdot L^{-1}$.

All of these results highlight that these PILs-based SPME fibers are suitable in SPME-HPLC applications for the determination of a broad range of compounds in real water samples with adequate analytical performance. Moreover, it is also important to point out that these fibers are able to perform with adequate reproducibility while resisting the swelling and detaching from the support when they are immersed in organic solvents or aqueous solutions at low pH values. Thus, the fibers did not show losses of the extraction efficiency even after ≈ 100 extraction-desorption steps.

Table IV.36. Quality analytical parameters for the overall DI-SPME-HPLC-UV-Vis method using the commercial fibers and aqueous standards of the model analytes.

	Fiber PA				Fiber PDMS/DVB			
Analyte	**Linear range ($\mu g \cdot L^{-1}$)**	**Slope ± t·SD[a]**	**R^2 [b]**	**LOD[c] ($\mu g \cdot L^{-1}$)**	**Linear range ($\mu g \cdot L^{-1}$)**	**Slope ± t·SD[a]**	**R^2 [b]**	**LOD[c] ($\mu g \cdot L^{-1}$)**
Cmz	50–500	8.7 ± 0.8	0.996	25	5–500	89 ± 5	0.998	2.5
Bnzal	25–500	22.1 ± 0.7	0.998	10	5–500	322 ± 13	0.998	2.5
BPA	25–500	57 ± 3	0.998	10	25–500	14.1 ± 0.5	0.998	10
NP	25–500	17.7 ± 0.8	0.998	20	2.5–200	161 ± 6	0.998	1.0
tfTol	25–500	39 ± 2	0.998	10	5–500	134 ± 12	0.994	2.5
*t*BP	25–500	20 ± 1	0.998	10	25–500	41 ± 3	0.996	2.5
EB	25–500	27 ± 3	0.994	10	5–500	267 ± 4	0.998	2.5
Nap	5–500	194 ± 15	0.996	2.5	0.5–500	1103 ± 47	0.998	0.2
Gfz	25–500	31 ± 2	0.996	20	5–500	85 ± 7	0.994	2.5
Trc	2.5–500	585 ± 34	0.996	1.0	2.5–500	518 ± 43	0.992	1.0

[a] 95 % confidence limits for n = 7 calibration levels (5 degrees of freedom).

[b] Determination coefficient.

[d] Limit of detection, calculated as 3 times the S/N, and verified with aqueous standards prepared at these levels and subjected to the overall method.

Table IV.37. Recovery and precision study with model analytes, using water samples spiked at two different levels, and fibers PIL-1a and PIL-2 in the entire DI-SPME-HPLC-UV-Vis method.

	Fiber PIL-1a								**Fiber PIL-2**							
Analyte	**River water**				**Tap water 3**				**River water**				**Tap water 3**			
	Spiked level: 40 µg·L^{-1}		**Spiked level: 200 µg·L^{-1}**		**Spiked level: 40 µg·L^{-1}**		**Spiked level: 200 µg·L^{-1}**		**Spiked level: 40 µg·L^{-1}**		**Spiked level: 200 µg·L^{-1}**		**Spiked level: 40 µg·L^{-1}**		**Spiked level: 200 µg·L^{-1}**	
	RR[a] (%)	**RSD[b] (%)**	**RR[a] (%)**	**RSD[b] (%)**	**RR[a] (%)**	**RSD[b] (%)**	**RR[a] (%)**	**RSD[b] (%)**	**RR[a] (%)**	**RSD[b] (%)**	**RR[a] (%)**	**RSD[b] (%)**	**RR[a] (%)**	**RSD[b] (%)**	**RR[a] (%)**	**RSD[b] (%)**
Cmz	127	12	119	10	121	12	110	15	93.1	7.8	77.2	8.7	85.2	12	93.6	7.9
Bnzal	81.8	8.9	65.9	11	122	6.9	104	11	76.7	11	98.5	14	67.9	1.1	96.6	6.1
BPA	95.4	3.3	108	9.0	125	15	100	6.7	99.7	4.8	90.2	2.7	98.2	14	92.2	7.4
NP	65.5	5.5	61.4	7.0	67.8	5.4	60.7	10	84.2	0.6	107	9.3	93.5	0.5	105	11
tfTol	96.8	10	73.0	12	91.5	9.5	75.2	4.6	94.2	11	122	13	83.4	2.8	90.9	5.7
*t*BP	104	3.9	88.5	6.9	95.2	8.1	85.1	12	97.1	11	84.9	8.4	81.1	1.9	92.9	7.8
EB	72.3	7.1	65.0	5.1	74.1	9.1	68.2	3.7	99.5	2.6	83.8	7.3	91.7	14	87.1	3.7
Nap	96.2	2.9	88.5	9.7	80.4	6.5	73.4	6.8	85.6	10	101	1.7	76.8	18	90.9	1.6
Gfz	74.3	5.4	67.6	16	66.8	9.1	73.7	12	78.9	5.2	85.7	6.8	91.6	1.5	90.3	10
Trc	86.6	12	78.4	4.7	88.7	8.6	79.5	6.1	103	6.4	101	0.7	89.3	17	98.1	5.0

[a] Relative recovery (n = 3).
[b] Relative standard deviation (n = 3).

2. Application of PILs-based sorbent coatings for the determination of alkylphenols

Considering the results obtained in the preliminary study, several PILs-based fibers were used for the determination of alkylphenols. Five polar disrupting endocrine alkylphenols, including BPA, CuP, *t*OP, OP and *n*NP, were chosen.

Given the polarity of these compounds as well as the presence of an aromatic ring in their structure, fibers similar to the PIL-1a and PIL-3 coatings were employed. Hence, two new fibers were developed in an attempt to obtain the desired selectivity. These fibers include PIL-1b, which is identical to PIL-1a but with a higher film thickness (≈ 35 µm); and PIL-4 (≈ 35 µm). The latter possesses a similar chemical composition as PIL-3, except for a shorter side chain in the cationic moiety of the monomer as well as the presence of chloride anion instead of bromide as anion within the monomer (see Table III.2). In this case, the anion was changed since it has been pointed out that the presence of chloride anion increases the sensitivity and selectivity for polar compounds [3]. With the aim of making a further comparison with commercial fibers not only based on the nature of the coatings but also on the film thicknesses, these PILs-based fibers were prepared with thicker coatings [5] (see Section III.7.1.3).

The commercial PA fiber was also evaluated in this study for the determination of alkylphenols to carry out an exhaustive comparative study. The selection of this commercial coating is based on its polar nature, the good results previously obtained for BPA, together with the fact it is the most common SPME fiber employed for the determination of these compounds [6].

The HPLC-DAD separation of the five analytes was attained in 7 min using the conditions described in Section III.7.5.5, as shown in Figure IV.28.

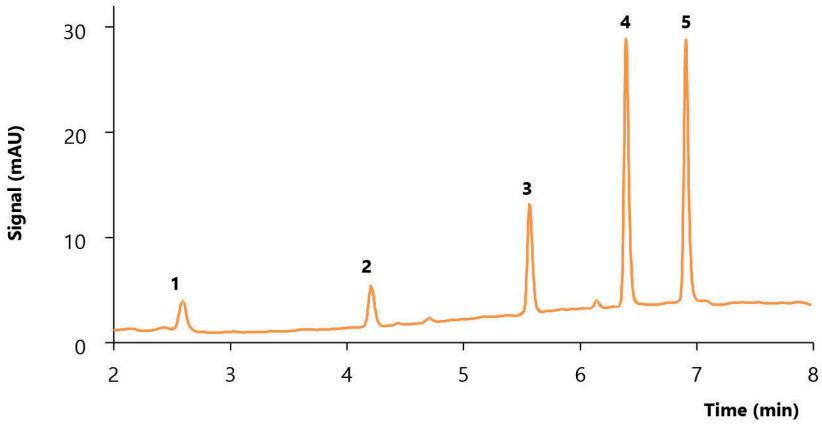

Figure IV.28. HPLC-DAD separation for alkylphenols, being (1) BPA, (2) CuP, (3) *t*OP, (4) OP, and (5) *n*NP.

The off-line desorption step was performed by immersing the fiber into 250 µL of methanol, which was the best desorption solvent for PILs-based coatings in the preliminary study with the model analytes. In this case, pH of the sample, extraction time, and desorption time were examined in order to optimize the overall method with this specific group of analytes. The experiments were performed in triplicate using 18 mL of aqueous standards at a concentration level of 200 $\mu g \cdot L^{-1}$ for all the alkylphenols.

2.1. Optimization of the DI-SPME-HPLC-DAD method

The analytes employed in this study are considered weakly acidic considering their pK_a values (see Table III.1). Thus, it is necessary to work at low pH values to guarantee they are not ionized and improve the extraction efficiency. The effect of the sample pH was examined at two pH conditions: pH 2 and pH 5. As shown in Figure IV.29, in general, the best results were obtained when the pH was adjusted at a value of 2 for all the fibers.

The extraction and desorption time profiles were obtained for all of the SPME fibers and are included in Figure IV.30. With respect to the PIL-based fibers, it is observed that most analytes reach the equilibrium after an extraction time of ≈ 60 min for PIL-1b and ≈ 45 min for PIL-4. In the case of the PA fiber, an equilibrium time of ≈ 45 min was obtained, except for OP and *n*NP, which needed extraction times longer than 60 min. Based on these results, the optimum extraction times selected were 45 min for the PIL-4 and PA fibers, and 60 min for the PIL-1b fiber.

The desorption time was evaluated between 5 and 20 min to avoid extremely long analysis times. Figure IV.30 also includes the desorption time profiles obtained for each analyte and each fiber. The best efficiencies were obtained using a desorption time of 15 min for fiber PIL-1b, while most analytes reached the equilibrium after only 5 min for the PIL-4 sorbent coating. With respect to the PA fiber, the optimum desorption time was found at 5 min for the majority of the analytes.

2.2. Analytical performance of the optimized DI-SPME-HPLC-DAD method for alkylphenols

The DI-SPME-HPLC-DAD calibration curves were obtained with each fiber: PIL-1b, PIL-4 and PA and the studied analytes. Several quality analytical parameters are included in Table IV.38. All calibration curves presented high R^2 values within the linear range studied, between 0.990 and 0.998. The sensitivity of the method (assessed as the calibration slope) was higher for OP and *n*NP, regardless the fiber employed. In all cases, the commercial PA fiber provided the higher calibration slopes. However, it must be pointed out that the PIL-1b coating provided satisfactory sensitivities for all analytes, with slope values comparable to those obtained with the PA fiber.

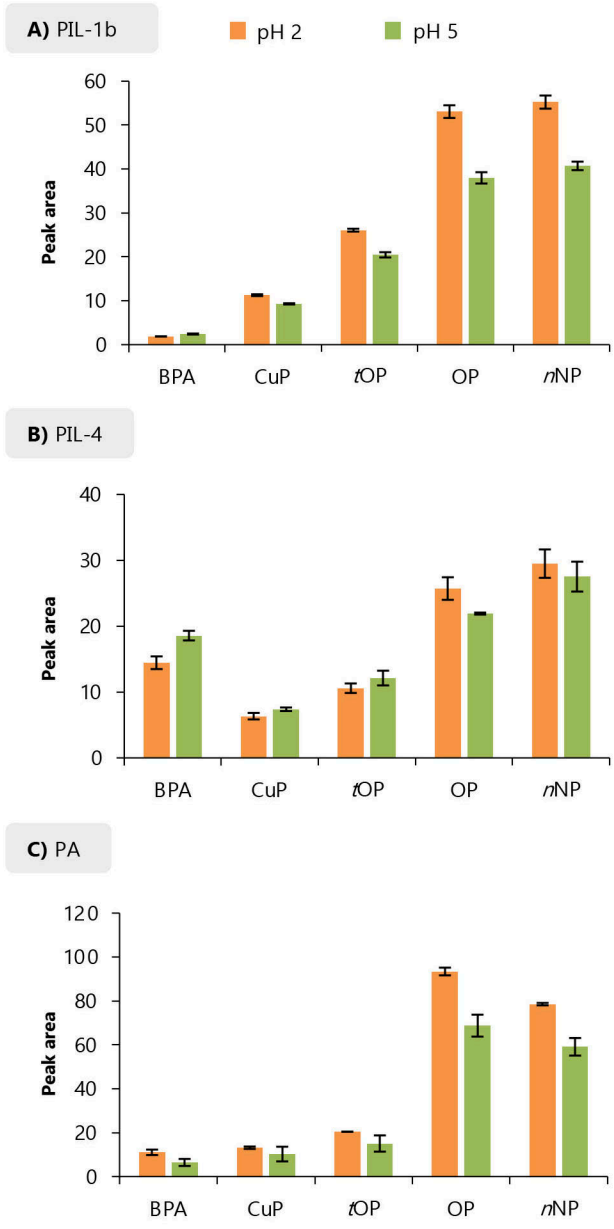

Figure IV.29. Effect of the pH in the extraction efficiency of alkylphenols for the DI-SPME-HPLC-DAD method using fibers **A)** PIL-1b, **B)** PIL-4, and **C)** PA. Fixed experimental conditions: extraction time of 45 min; methanol as desorption solvent; and 20 min of desorption time. The remaining experimental conditions are detailed in the text.

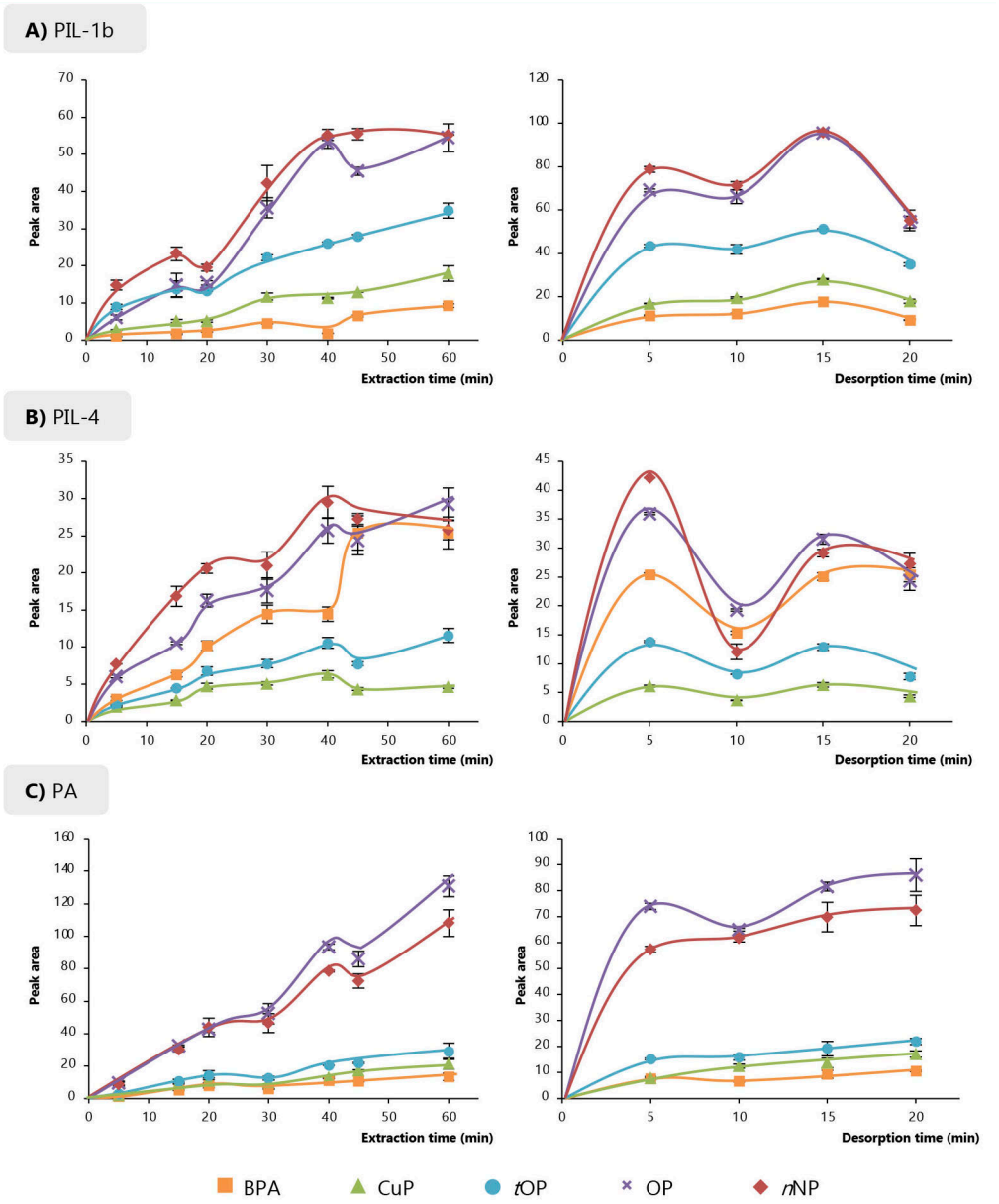

Figure IV.30. Extraction and desorption time profiles obtained for the DI-SPME-HPLC-DAD method using fibers **A)** PIL-1b, **B)** PIL-4, and **C)** PA. Extraction profiles are plotted on the left side and desorption profiles are plotted on the right side. Fixed experimental conditions: pH value of 2; desorption time of 20 min in the study of extraction time; extraction time of 45 min for PIL-4 and PA fibers, and 60 min of extraction time for PIL-1b in the study of desorption time. The remaining experimental conditions are detailed in the text.

Table IV.38. Quality analytical parameters for the overall DI-SPME-HPLC-DAD method for alkylphenols in ultrapure water using the PIL-1b, PIL-4, and commercial PA fibers.

Analyte	Fiber PIL-1b				Fiber PIL-4				Fiber PA			
	Linear range ($\mu g \cdot L^{-1}$)	Slope ± t·SD[a]	R^{2} [b]	LOD[c] ($\mu g \cdot L^{-1}$)	Linear range ($\mu g \cdot L^{-1}$)	Slope ± t·SD[a]	R^{2} [b]	LOD[c] ($\mu g \cdot L^{-1}$)	Linear range ($\mu g \cdot L^{-1}$)	Slope ± t·SD[a]	R^{2} [b]	LOD[c] ($\mu g \cdot L^{-1}$)
BPA	10–100	115 ± 13	0.998	2.0	10–90	119 ± 28	0.992	1.0	10–100	182 ± 21	0.996	2.0
CuP	5–100	127 ± 21	0.994	2.7	10–100	36 ± 2	0.998	2.9	10–100	188 ± 51	0.990	1.0
*t*OP	5–100	210 ± 23	0.998	1.7	20–90	52 ± 10	0.992	2.2	10–100	336 ±13	0.998	0.5
OP	5–100	365 ± 46	0.996	2.4	10–90	131 ± 31	0.992	3.3	10–100	597 ± 46	0.998	0.5
*m*NP	5–100	390 ± 59	0.994	2.1	10–100	124 ± 15	0.996	1.9	10–100	509 ± 103	0.990	0.6

[a] 95 % confidence limits for n = 7 calibration levels (5 degrees of freedom).

[b] Determination coefficient.

[c] Limit of detection, calculated as 3 times the S/N, and verified with aqueous standards prepared at these levels and subjected to the overall method.

LODs were calculated as three times the S/N and verified by subjecting an aqueous standard solution prepared at the calculated concentrations to the overall method. The lowest LODs were achieved using the PA fiber: 2.0 $\mu g \cdot L^{-1}$ for BPA, 1.0 $\mu g \cdot L^{-1}$ for CuP, 0.5 $\mu g \cdot L^{-1}$ for *t*OP and OP, and 0.6 $\mu g \cdot L^{-1}$ for *n*NP. However, the PIL-4 fiber presented a value of 1.0 $\mu g \cdot L^{-1}$ for BPA, demonstrating the great affinity and sensitivity previously pointed out for this PIL-based fiber toward this analyte.

In addition, intra- and inter-day RR and precision studies were accomplished with all the fibers at different concentration levels. Table IV.39 includes the average RR values and RSD ranges obtained for all the analytes.

Table IV.39. Recovery and precision studies using PIL-1b, PIL-4 and PA fibers and DI-SPME-HPLC-DAD with aqueous standards of alkylphenols.

Fiber	Concentration level ($\mu g \cdot L^{-1}$)	Average of intra-day RR[a] (%)	Range of intra-day RSD[b] (%)	Average of inter-day RR[c] (%)	Range of inter-day RSD[d] (%)
PIL-1b	10	106	11–15	108	2.5–19
	20	103	7.2–15	84.6	4.2–18
	30	89.6	5.4–16	98.4	8.2–18
PIL-4	30	82.7	6.1–18	–	–
PA	10	111	6.1–16	–	–
	30	76.7	5.7–19	–	–

[a] Relative recovery for all the analytes (n = 3).
[b] Relative standard deviation for all the analytes (n = 3).
[b] Relative recovery for all the analytes (n = 9, performed in 3 non-consecutive days)
[d] Relative standard deviation (n = 9, performed in 3 non-consecutive days).

The intra-day precision at 30 $\mu g \cdot L^{-1}$, expressed as RSD, varied from 5.4 to 16 % for PIL-1b, from 6.1 to 18 % for PIL-4, and from 5.7 to 19 % for PA. Since the PIL-1b fiber showed comparable results to PA fiber, an intra-day precision study was carried out at lower concentration levels for both fibers. Thus, PIL-1b presented RSD values from 11 to 15 % at 10 $\mu g \cdot L^{-1}$, and from 7.2 to 15 % at 20 $\mu g \cdot L^{-1}$, whereas the commercial fiber exhibited RSD values ranging from 6.1 to 16 % at 10 $\mu g \cdot L^{-1}$. With respect to the PILs-based coatings, PIL-1b exhibited the best results for most analytes. Therefore, an inter-day precision study was accomplished for this fiber at different spiked levels. The results obtained were lower or similar to the intra-day precision values achieved, with RSD

ranges of 2.5–19 % at 10 μg·L^{-1}, 4.2–18 % at 20 μg·L^{-1}, and 8.2–18 % at 30 μg·L^{-1}. It is important to point out that the found RSD values are completely adequate, especially if the low concentration levels, the manual DI-SPME procedure, and the off-line desorption step are considered. Furthermore, it should be highlighted that significant differences between PILs-based fibers and PA fiber RSD values were not found.

With respect to RR, the values obtained at the different concentration levels with each fiber were within the acceptable requirements, being higher than 70 % and lower than 120 %. PIL-1b presented average values of 106 and 108 % at 10 μg·L^{-1}, 103 and 84.6 % at 20 μg·L^{-1}, 89.6 and 98.4 % at 30 μg·L^{-1}, for the intra-day and inter-day study, respectively. In the case of PIL-4, a RR average value of 82.7 % was found at 30 μg·L^{-1}, while PA fiber showed an average RR of 111 % at 10 μg·L^{-1}, and 76.7 % at 30 μg·L^{-1}, being the lowest value reached in this study.

2.3. Comparison with a commercial SPME fiber and estimation of partition constants

The extraction efficiency of a SPME fiber depends on many different factors, including the chemical nature, film thickness, and surface area of the sorbent coating [7]. This feature for the studied fibers in the optimum DI-SPME-HPLC-DAD method was first assessed by measuring the peak area obtained for each analyte using an aqueous working solution of 30 μg·L^{-1} (n = 3). Figure IV.31 A) shows the values for the PIL-1b, PIL-4 and PA fibers. Considering the results obtained, it can be observed that the commercial PA fiber results more efficient for the extraction of alkylphenols. However, it is important to mention that PIL-1b fiber provided comparable results and better precision for *m*NP (peak area 7.9 ± 0.6) in comparison with the PA fiber (peak area 8.2 ± 1.8) despite the different thicknesses among these fibers (≈ 35 μm and 85 μm, respectively). With respect to the nature of PILs-based sorbents coatings, PIL-1b exhibited higher peak areas for the analytes in comparison with PIL-4 fiber, except for BPA, for which they were similar.

As it was pointed out in the previous sections, there is an important difference on the film thicknesses of the PILs-based fibers (≈ 35 μm) and PA coating (85 μm). In these cases, several studies have proposed the use of the normalized calibration slopes to compare the extraction efficiency of the different coatings [8,9]. This parameter is calculated as the ratio between the calibration slope obtained from the SPME method and the film thickness of the fiber. Thus, the obtained differences of the efficiencies can be only attributed to the nature of the SPME coating.

Figure IV.31 B) includes the normalized calibration slopes calculated for the PILs-based and PA fibers. The affinity of PIL-1b fiber is higher for the entire group of phenols in comparison with the other fibers studied, except for BPA, for which the PIL-4 fiber shows a slightly higher value. The results indicate that PILs-based sorbent coatings may be more sensitive for the extraction of this group of analytes if the film thickness of these fibers is increased at the same level as commercial fibers. In addition, the different behavior observed for both PILs-based fibers

demonstrate the versatility of these novel coatings for the extraction of different compounds, which can be improved by modifying the chemical structure of the polymer.

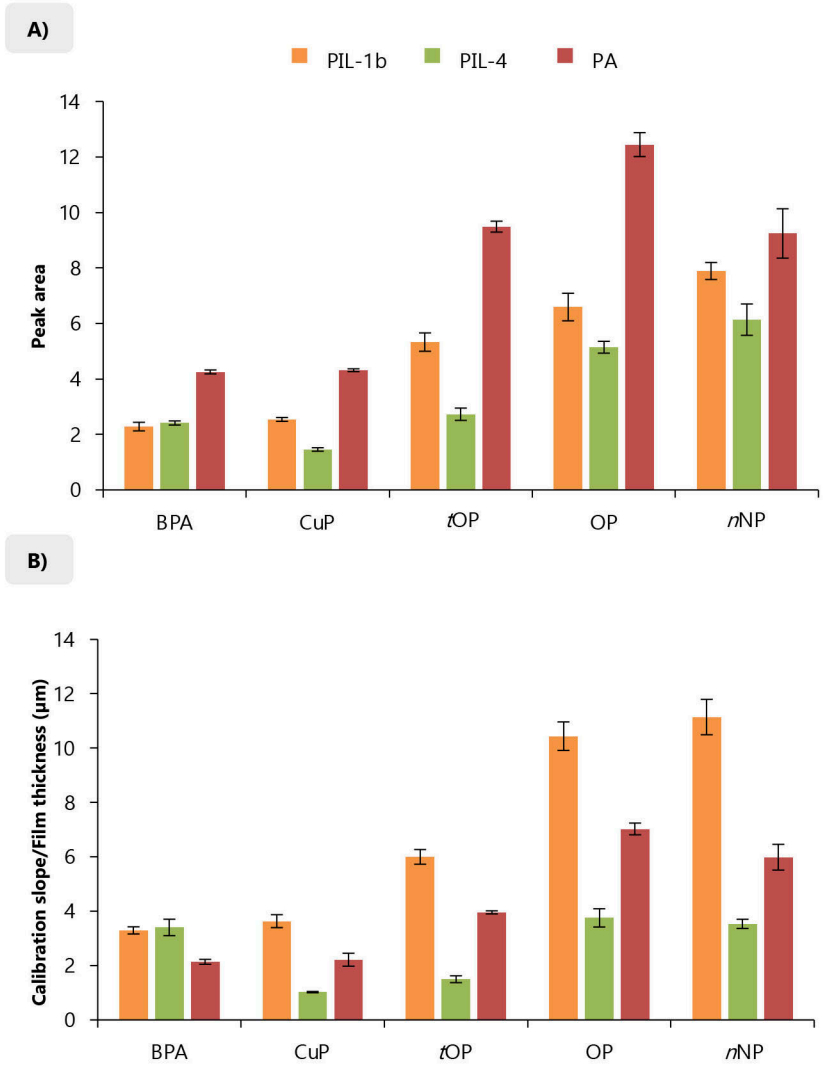

Figure IV.31. Comparison of the extraction efficiency using PIL-1b, PIL-4 and PA in the determination of alkylphenols, measured as **A)** the peak area obtained with the optimized DI-SPME-HPLC-DAD method (concentration of analytes: 30 $\mu g \cdot L^{-1}$) and **B)** normalized calibration slopes, calculated as the ratio between the calibration slope of the DI-SPME-HPLC-DAD method and the film thickness of the sorbent coating.

Despite this preliminary comparison can give interesting information about the performance of the sorbents, the obtaining of the partition constants (K_{fs}) is often the best approach to compare the extraction performance of different SPME fibers. These values refer to the equilibrium that analytes experience between the sample and the sorbent phase of the fiber. This parameter only takes into account the nature of the sorbent coating and it is independent of the fiber thickness. The partition constants for the PIL-1b, PIL-4 and PA fibers were estimated using the following Equation IV.3.

$$K_{fs} = \frac{V_s}{V_f\left(\frac{n_0}{n_f} - 1\right)} \qquad \text{Equation IV.3}$$

where n_0 is the initial amount of analyte in the sample (in mg), while n_f indicates the amount of analyte on the fiber once the equilibrium is reached. n*f* values can be calculated with the chromatographic calibrations (obtained in absence of DI-SPME experiences) but using the peak area obtained after a n_0 initial amount of analyte is subjected to the DI-SPME-HPLC-DAD method. In this equation, V_s indicates the sample volume (18 mL for alkylphenols), and V_f represents the volume of the sorbent coating, which can be calculated considering the thickness of the fiber coating and the coating length (1 cm). The V_f values obtained for the PILs-based sorbent coatings employed for the determination of alkylphenols were 0.283 µL for both PIL–1b and PIL–4, while a value of 0.520 µL was calculated for the commercial PA fiber.

The calculated partition constants for all alkylphenols and each fiber are included in Table IV.40, expressed as logarithms (log K_{fs}).

Table IV.40. Estimated partition constants, expressed as log K_{fs}, for the studied alkylphenols and the PIL-1b, PIL-4 and PA SPME fiber coatings.

Analyte	**log K_{fs} ± error[a]**		
	Fiber PIL-1b	**Fiber PIL-4**	**Fiber PA**
BPA	1.69 ± 0.06	1.73 ± 0.06	1.58 ± 0.03
CuP	2.05 ± 0.02	1.50 ± 0.08	1.83 ± 0.01
*t*OP	2.45 ± 0.01	1.85 ± 0.05	2.25 ± 0.01
OP	2.39 ± 0.01	2.36 ± 0.01	2.30 ± 0.01
*n*NP	2.44 ± 0.01	2.35 ± 0.01	2.05 ± 0.01

[a] Error in the determination of the log K_{fs}, calculated from the error in the prediction of n_f and considering the mathematical propagation of errors.

It is important to point out that the partition constants obtained are not totally quantitative values because: (i) the equilibrium conditions for each fiber are not guaranteed in the DI-SPME-HPLC-DAD method, and (ii) the coating volumes for PIL-based fibers are approximate values estimated by SEM. Despite these assumptions, the obtained partition constants correlate adequately with those results previously observed when comparing the analytical performance of the fibers using the peak area and normalized calibration slope. Furthermore, partition constants were obtained under the optimum conditions for the coatings used, and thus they are useful to establish comparisons among them.

According to the results included in Table IV.40, it should be highlighted that the K_{fs} values using the PIL-1b fiber are higher than PA and for all alkylphenols. This high affinity demonstrates that the PIL-1b fiber may be a promising sorbent coating for the extraction of these analytes, especially for *n*NP. It is clear that the benzyl group in the structure of the PIL improves the π-π interactions towards these aromatic compounds. In addition, the PIL-4 fiber presents better values for BPA, which may be related to the possible hydrogen bonding interactions that enhance its affinity for polar compounds.

2.4. Evaluation of matrix effect and analysis of water samples

The evaluation of matrix effect for the DI-SPME-HPLC-DAD method was performed using tap water 1, which was shown to be free of analytes after being subjected to the validated method. This study was only performed using the PIL-1b fiber as a representative PIL-based coating given the good results obtained with this coating. Table IV.41 includes several analytical quality parameters for the matrix-matched calibration curves. In comparison with the calibration curves obtained in ultrapure water (Table IV.38), the sensitivity (calibration slope) was higher for BPA in this sample matrix. For the remaining analytes, the slopes decreased in tap water. These values go in line with the LODs obtained, which are higher than the obtained in ultrapure water for all analytes, except for BPA, which had a value of 1 $\mu g \cdot L^{-1}$ in tap water.

In order to assess the presence of matrix effect, the slopes obtained in ultrapure water and tap water were statistically compared by the Student's *t*-test reported by Andrade and Estévez-Perez. [10]. In all cases, F_{exp} was lower than F_{crit}, thus both calibration slopes are assumed to be equals in view of the variance. Then, the Student's *t*-test provided t_{cal} values higher than t_{crit} for all analytes. This means that both slopes are significantly different and therefore, matrix effect must be considered.

Based on the previous results, the matrix-matched calibration curves were employed to carry out the RR and precision study to demonstrate the application of the method for the analysis of water samples. In this study, different samples were analyzed: tap water 1 was heated and used to fill different empty plastic bottles to evaluate the migration of the analytes from the plastic (bottled water 1 and bottled water 2), and a bottled water acquired from a local market (bottled

water 3). Bottled water 1 and 2 were spiked at 50 μg·L^{-1}, while bottled water 3 was spiked at a concentration level of 30 μg·L^{-1}. The results are included in Table IV.41. RSD (intra-day precision) values were lower than 16 % in all cases. It is worth mentioning that these RSD values are adequate if the experimental conditions of the method are considered. With respect to the RR, all the samples provided similar values. Bottled water 1 presented an average value of 83.1 %, the average RR was 89.1 % for bottled water 2, while bottled water 3 had a value of 89.5 %.

Table IV.41. Several quality analytical parameters of the DI-SPME-HPLC-DAD method for alkylphenols in tap water using the fiber PIL-1b, including the performance of the entire method in terms of recovery and precision with these water samples.

	Fiber PIL-1b[a]			Bottled water 1 (50 µg·L^{-1})		Bottled water 2 (50 µg·L^{-1})		Bottled water 3 (30 µg·L^{-1})	
Analyte	**Slope ± t·SD[b]**	**R^2 [c]**	**LOD[d] (µg·L^{-1})**	**RR[e] (%)**	**RSD[f] (%)**	**RR[e] (%)**	**RSD[f] (%)**	**RR[e] (%)**	**RSD[f] (%)**
BPA	146 ± 5	0.998	1.0	82.8	14	74.4	13	89.8	11
CuP	101 ± 3	0.996	3.4	89.6	8.9	97.1	6.8	85.7	16
*t*OP	182 ± 8	0.994	3.6	79.4	13	95.6	12	92.5	14
OP	309 ± 10	0.996	2.5	81.3	6.0	87.8	14	87.3	12
*n*NP	326 ± 13	0.996	1.6	82.6	2.3	90.9	7.1	91.5	16

[a] Linear range from 10 to 100 µg·L^{-1} for BPA, and from 5 to 100 µg·L^{-1} for the remaining analytes.
[b] 95 % confidence limits for n = 7 calibration levels (5 degrees of freedom).
[c] Determination coefficient.
[d] Limit of detection, calculated as 3 times the S/N, and verified with aqueous standards (matrix-matched) prepared at these levels and subjected to the overall method.
[e] Relative recovery (n = 3).
[f] Intra-day relative standard deviation (n = 3).

REFERENCES

[1] J. López-Darias, V. Pino, J.L. Anderson, C.M. Graham, A.M. Afonso, J. Chromatogr. A 1217 (2010) 1236–1243.

[2] C. Zhang, J.L. Anderson, J. Chromatogr. A 1344 (2014) 15–22.

[3] Y. Meng, V. Pino, J.L. Anderson, Anal. Chim. Acta 687 (2011) 141–149.

[4] E. González-Toledo, M.D. Prat, M.F. Alpendurada, J. Chromatogr. A 923 (2001) 45–52.

[5] C. Cagliero, T.D. Ho, C. Zhang, C. Bicchi, J.L. Anderson, J. Chromatogr. A 1449 (2016) 2–7.

[6] C. Chang, C. Chou, M. Lee, Anal. Chim. Acta 539 (2005) 41–47.

[7] I. Bruheim, X. Liu, J. Pawliszyn, Anal. Chem. 75 (2003) 1002–1010.

[8] J. López-Darias, V. Pino, Y. Meng, J.L. Anderson, A.M. Afonso, J. Chromatogr. A 1217 (2010) 7189–7197.

[9] M.J. Trujillo-Rodríguez, H. Yu, W.T.S. Cole, T.D. Ho, V. Pino, J.L. Anderson, A.M. Afonso, Talanta 121 (2014) 153–162.

[10] J.M. Andrade, M.G. Estévez-Pérez, Anal. Chim. Acta 838 (2014) 1–12.

Section IV.2.1.3

Crosslinked zwitterionic polymeric ionic liquids-based fiber coatings in headspace solid-phase microextraction coupled with gas chromatography: application for the determination of short-chain free fatty acids in wine

Talanta 200 (2019) 415–423

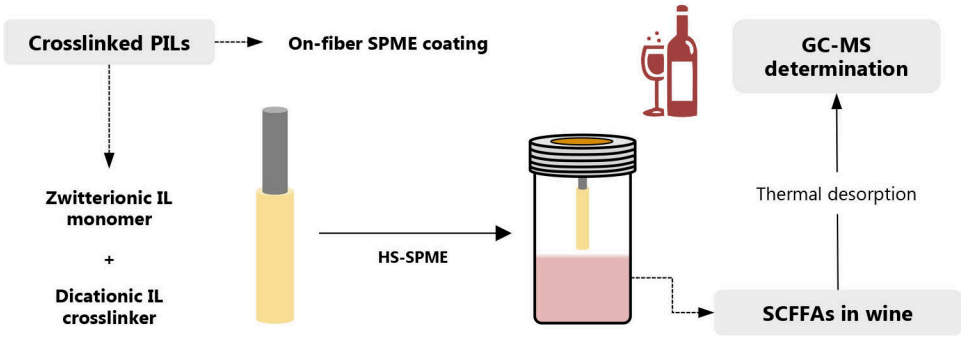

1. Screening of different zwitterionic PIL SPME fibers for the determination of SCFFAs by GC-MS

In this section, crosslinked PILs-based SPME fibers were prepared using zwitterionic ILs as monomers, with the compositions listed in Table III.2. The PILs-based SPME fibers were evaluated in a HS-SPME-GC-MS method for the determination of SCFFAs. The GC-MS conditions were described in Section III.7.5.6, while Table IV.42 includes the segment program, the retention times and the ions considered for each analyte. The determination of volatile compounds in foods and beverages is important since their concentration affects sensory properties and often determines the quality of the product [1]. Volatile SCFFAs are among the main compounds that contribute to the aroma of fermented products, while also being responsible for various characteristic flavors and off-flavors in dairy products and alcoholic fermented beverages [2–4].

HS-SPME has already been explored in these applications [2,5–7]. In general, adsorption-type commercial fibers such as CAR/PDMS and DVB/CAR/PDMS have been used over absorption-type coatings given their higher sensitivity. However, a large number of interferences are generally extracted from samples together with target analytes, which makes the analysis of real samples very challenging [7]. Therefore, the development of sorbent coatings able to selectively extract specific groups of compounds without being affected by the presence of interfering substances is of particular interest when analyzing complex matrixes with SPME. In the case of alcoholic beverage analysis, the use of sorbent coatings that are not affected by the alcohol content of the sample is of special interest [7].

As a preliminary study, the prepared zwitterionic PILs-based sorbent coatings were screened for the determination of SCFFAs together with the commercial CAR/PDMS fiber, which has been previously reported as one of the most suitable SPME fibers for these compounds [5,6]. Extractions were performed from an aqueous solution containing 20 % (w/v) of NaCl at 45 °C for 20 min, followed by thermal desorption for 6 min. The thermal desorption was fixed at the maximum operating temperature for each fiber.

Figure IV.32 shows the extraction efficiency expressed as the chromatographic peak area for each analyte and fiber. Fibers PZIL-4 and PZIL-5, containing the [$VIm^+C_9COO^-$] zwitterionic IL monomer, provided similar or better results than the commercial CAR/PDMS fiber for all analytes. When the fibers containing sulfonate-based zwitterionic IL monomers were compared, fibers PZIL-1 and PZIL-2 (containing [$VIm^+C_3SO_3^-$]) yielded slightly higher peak areas than PZIL-3 (with the [$VIm^+C_4SO_3^-$] monomer). This result seems to indicate that the length of the alkyl chain of the zwitterionic IL monomer may not have an important effect on the extraction efficiency.

Table IV.42. Segment program used in the MS during SIM acquisition for the identification and quantification of the SCFFAs, together with the retention time and characteristic ions for each analyte.

Segment	Ions	Time (min)	SCFFA	Retention time ± SD[a] (min)	Quantifier ion (m/z)	Qualifier ion (m/z)
1	41, 43, 45, 73, 74	6.5	C_3	6.93 ± 0.05	74	73
	–	–	*i*-C_4	7.19 ± 0.03	43	73
2	41, 60, 73	7.5	*n*-C_4	7.86 ± 0.02	60	73
3	43, 60, 87	8.0	*i*-C_5	8.28 ± 0.01	60	43
4	41, 60, 73	8.7	*n*-C_5	9.03 ± 0.01	60	73
5	57, 73, 74	9.4	*i*-C_6	9.71 ± 0.01	57	74
6	60, 73, 87	10.0	*n*-C_6	10.16 ± 0.01	60	73
	–	–	*n*-C_7	11.27 ± 0.02	60	73

[a] Standard deviation (n = 20).

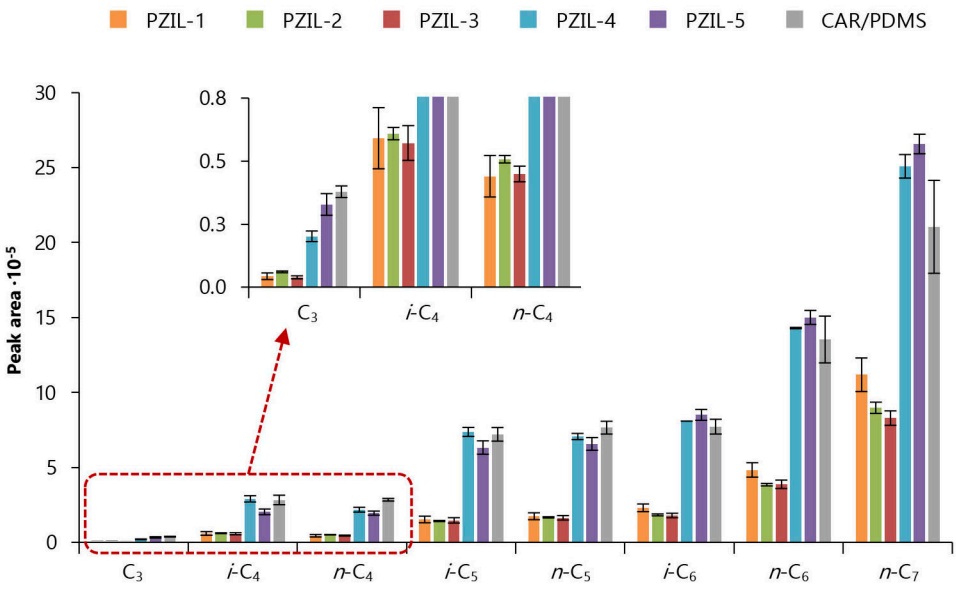

Figure IV.32. Extraction efficiency, expressed as chromatographic peak area, obtained for the SCFFAs after performing the HS-SPME-GC-MS method using zwitterionic PILs and CAR/PDMS sorbent coatings. Experimental conditions (n = 3): 10 mL of aqueous solution containing the SCFFAs at 1.00–2.66 $mg{\cdot}L^{-1}$ depending on the analyte (0.02 $mmol{\cdot}L^{-1}$); 20 % (w/v) of NaCl; 20 min of extraction at 45 °C and 600 min^{-1} of stirring rate; desorption for 6 min at 175 °C for fibers PZIL-1, PZIL-3 and PZIL-4, 200 °C for fibers PZIL-2 and PZIL-5, and 290 °C for CAR/PDMS.

With respect to the crosslinker, there were generally no significant differences observed between fibers with the same monomer and different crosslinker. However, the results obtained with fibers containing the [Br^-]-based crosslinker were slightly better for longer alkyl chain SCFFAs with the [$VIm^+C_3SO_3^-$]-based sorbent coating (fiber PZIL-1) compared to fiber PZIL-2. They were also better for smaller SCFFAs using PZIL-4 fiber rather than PZIL-5 fiber. These results may be related to the relatively higher hydrogen-bond basicity of the sorbent coatings containing bromide anions with respect to coatings containing the [NTf_2^-] anion, which can promote additional strong interactions with the analytes [8,9]. Based on the results, fibers PZIL-1 and PZIL-4 were selected for the development of the HS-SPME-GC-MS method for the determination of SCFFAs.

2. Optimization of the HS-SPME method with commercial and zwitterionic PIL-based fibers

The HS-SPME procedure was optimized following a one-factor-at-a-time approach for the zwitterionic PILs (fibers PZIL-1 and PZIL-4), together with the commercial CAR/PDMS and PA fibers. CAR/PDMS was selected as it has been previously used in the determination of SCFFAs [5,6]. Given

the polarity of the analytes, the PA fiber was also included in the study as a representative fiber with an absorptive-type extraction mechanism [10].

Several experimental parameters affecting HS-SPME were previously fixed to ensure high extraction efficiency and adequate sensitivity, such as 10 mL of aqueous standard (or sample) volume, 600 min^{-1} of stirring rate and the desorption temperature at the maximum operating temperature for each fiber: 175 °C for zwitterionic PIL-based fibers, 280 °C for PA, and 290 °C for CAR/PDMS. The main parameters influencing HS-SPME, including the ionic strength (evaluated as NaCl content), extraction temperature, extraction time and desorption time, were optimized.

2.1. Effect of NaCl content

In HS-SPME, the extraction efficiency can be improved by the addition of a salting-out agent in order to reduce the solubility of the analytes, effectively increasing the concentration of analytes in the headspace [2]. Therefore, the effect of the NaCl concentration was evaluated from 0 to 30 % (w/v) for the zwitterionic PILs sorbent coatings. Figure IV.33 includes the peak areas obtained for each SCFFA examined. Extractions were performed at 45 °C for 20 min followed by desorption for 6 min. As expected, the higher NaCl concentration resulted in higher amounts of analyte extracted with the best results using 30 % (w/v). It is interesting to mention the sharper enhancement in extraction efficiency obtained for fiber PZIL-1 in comparison with PZIL-4, which leads to similar peak areas using both zwitterionic PIL-based fibers for all the SCFFAs. Considering this general tendency, 30 % (w/v) of NaCl was selected as optimum for both PIL-based and commercial fibers [3,5,6].

2.2. Effect of temperature

The temperature plays an important role in the amount of analyte extracted in HS-SPME since higher temperatures improve the transfer of analytes from the sample to the headspace [11]. However, relatively high temperatures can be detrimental as they can reduce the partition coefficients of the analytes to the sorbent coating. In most cases using HS-, a compromise temperature needs to be chosen. The extraction temperature was evaluated between 35 and 65 °C for 20 min using 30 % (w/v) of NaCl and a desorption time of 6 min. Figure IV.34 shows similar behavior for both PZIL-1 and PZIL-4 fibers with the extraction efficiency increasing as the temperature was increased. In these cases, the relatively high temperatures did not reduce the partitioning of the analytes due to the strong interaction between the zwitterionic PILs and the SCFFAs. Given these results, 65 °C was selected for subsequent experiments using all studied fibers [3].

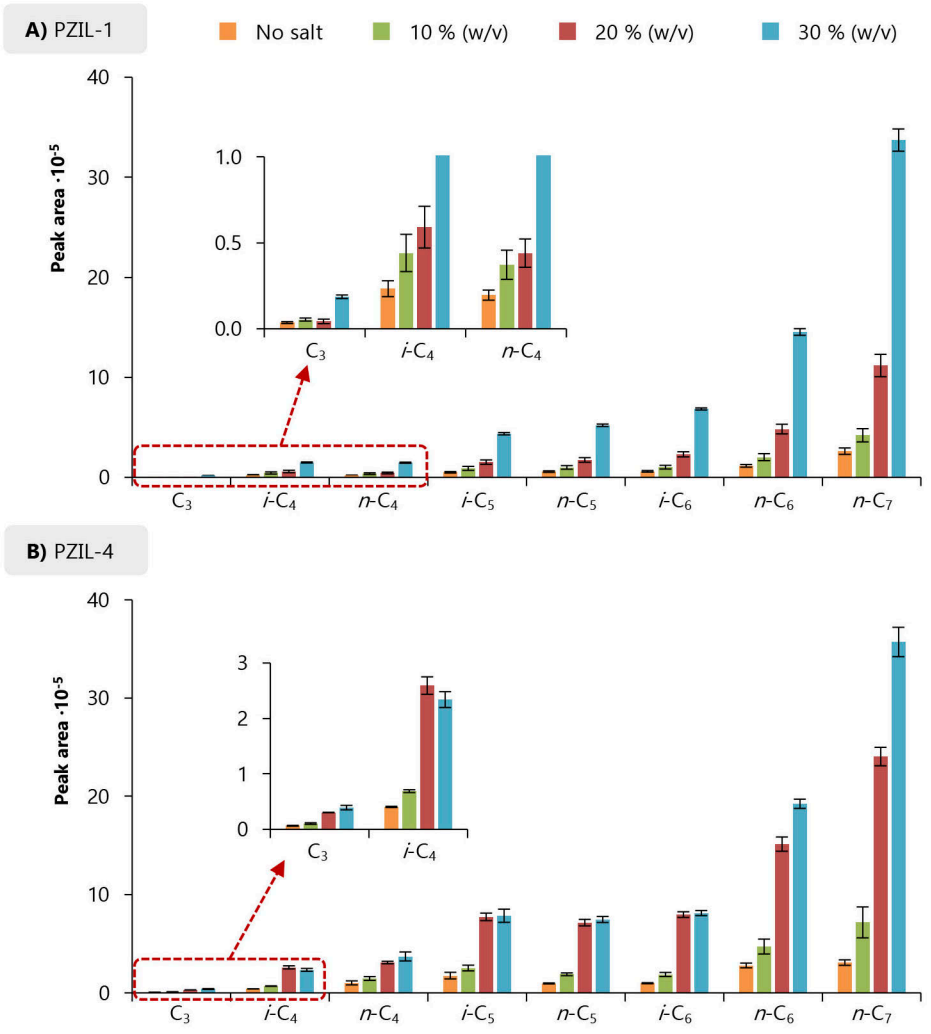

Figure IV.33. Influence of the NaCl content on the performance of the HS-SPME-GC-MS method for the determination of SCFFAs using **A)** fiber PZIL-1, and **B)** fiber PZIL-4. Experimental conditions (n = 3): 10 mL of aqueous standard solution containing the SCFFAs at 1.00–2.66 mg·L^{-1} depending on the analyte (0.02 mmol·L^{-1}); 0–30 % (w/v) of NaCl; 20 min of extraction at 45 °C and 600 min^{-1} of stirring rate; and desorption for 6 min at 175 °C.

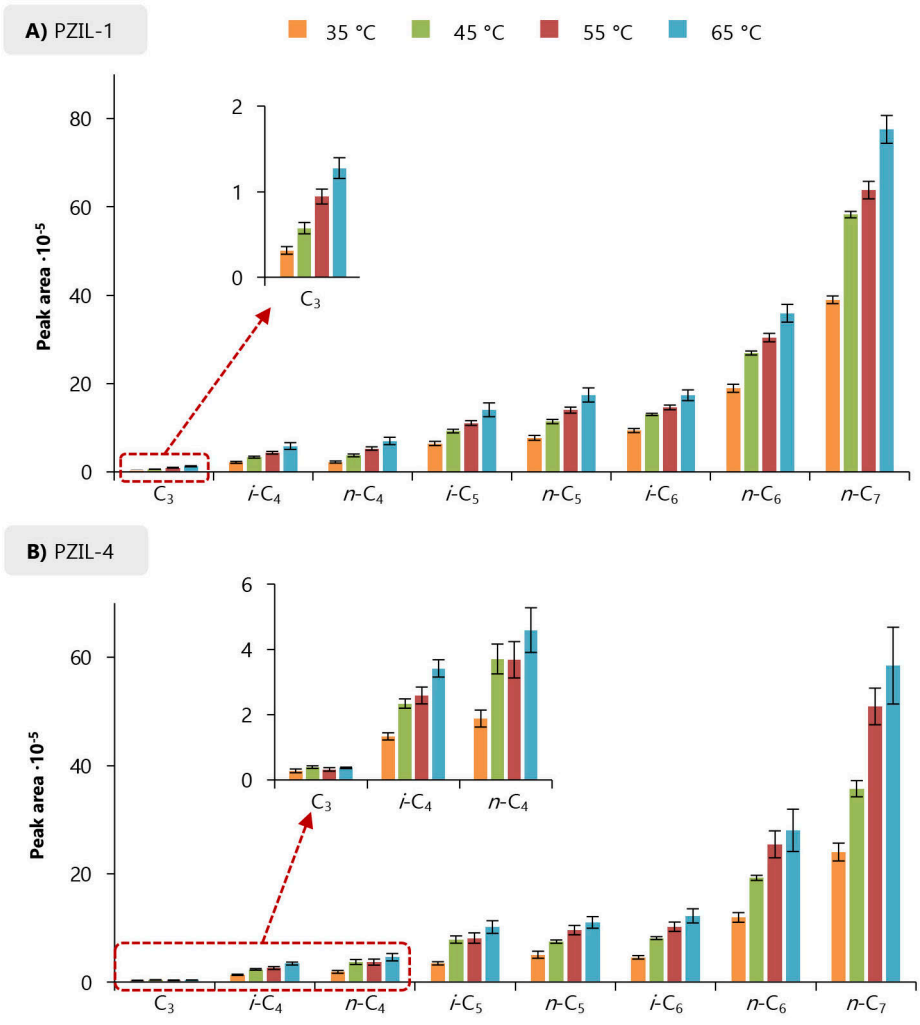

Figure IV.34. Influence of the extraction temperature on the performance of the HS-SPME-GC-MS method for the determination of SCFFAs using **A)** fiber PZIL-1, and **B)** fiber PZIL-4. Experimental conditions (n = 3): 10 mL of standard aqueous solution containing the SCFFAs at 1.00–2.66 mg·L^{-1} depending on the analyte (0.02 mmol·L^{-1}); 30 % (w/v) of NaCl; 20 min of extraction at 35–65 °C and using 600 min^{-1} of stirring rate; and desorption for 6 min at 175 °C.

2.3. Effect of extraction time

The extraction time in SPME is a key factor in the resulting performance of the method [11]. Figure IV.35 includes the extraction time profiles obtained for the zwitterionic PILs together with those of the commercial CAR/PDMS and PA fibers. The extraction time was assessed between 20

and 80 min, followed by thermal desorption for 6 min. Regarding the zwitterionic PILs sorbent coatings, the results indicated that most of the SCFFAs reached equilibrium at around 20 min when using fiber PZIL-1, while 60 min was required when using PZIL-4 coating, except for *n*-C_6 and *n*-C_7, which did not reach equilibrium in the time range studied. The peak areas obtained with PZIL-1 at 20 min were similar to those obtained using fiber PZIL-4 with longer extraction times. Therefore, reduced extraction times can be used with fiber PZIL-1 without sacrificing extraction efficiency in comparison with PZIL-4. In the case of commercial fibers, most of the smaller SCFFAs reached equilibrium at 60 min using CAR/PDMS, except for *n*-C_4. This analyte, together with *n*-C_6 and *n*-C_7, required more than 80 min to achieve maximum extraction efficiency. For PA, an equilibration time of 40 min was required for all analytes. Therefore, 20 min was selected as the optimum extraction time for fiber PZIL-1, 40 min for PA, and 60 min for fiber PZIL-4 and CAR/PDMS.

2.4. Effect of desorption time

The desorption time was optimized to guarantee quantitative desorption of the analytes from the fibers and avoid carry-over. The desorption time was studied between 2 and 10 min for both the zwitterionic PILs-based and commercial fibers at their maximum working temperatures. Figure IV.36 includes the time profiles obtained for each fiber. For fiber PZIL-1, the maximum extraction efficiency for all SCFFAs was obtained after 4 min of desorption, while PZIL-4 provided the best results after only 2 min. For CAR/PDMS, 2 min was sufficient to obtain the highest results for all analytes, except for *n*-C_7. In the case of PA, different behavior was observed depending on the analyte. Better results were obtained with a desorption time of 2 min for *n*-C_4 and *i*-C_6, 6 min for *n*-C_7, and 4 min for the remaining analytes. A desorption time of 4 min was selected as optimum for PA as well as for fiber PZIL-1 whereas 2 min was selected for the remaining fibers.

Table IV.43 lists the optimum conditions for the HS-SPME-GC-MS using all the tested fibers.

3. Effect of ethanol content in the performance of all the SPME fibers

The presence of ethanol in the sample can be detrimental for fibers such as CAR/PDMS that extract primarily via an adsorption-type mechanism. However, it should be less important for the developed zwitterionic PILs as they extract via a non-competitive pathway. In addition, fibers with CAR-based coatings can swell in the presence of a high organic solvent content. To reinforce this hypothesis, relative recovery (RR, in %) studies were performed under optimum conditions using standards prepared in ultrapure water with 1.3 % (v/v) of ethanol and without ethanol. This ethanol content was selected to mimic the conditions that will be employed when analyzing diluted wine samples (1 mL of wine diluted up to 10 mL with water). In all cases, calibration curves of the HS-SPME-GC-MS method were obtained using standards prepared in ultrapure water and were then used to estimate RR for standards with or without ethanol.

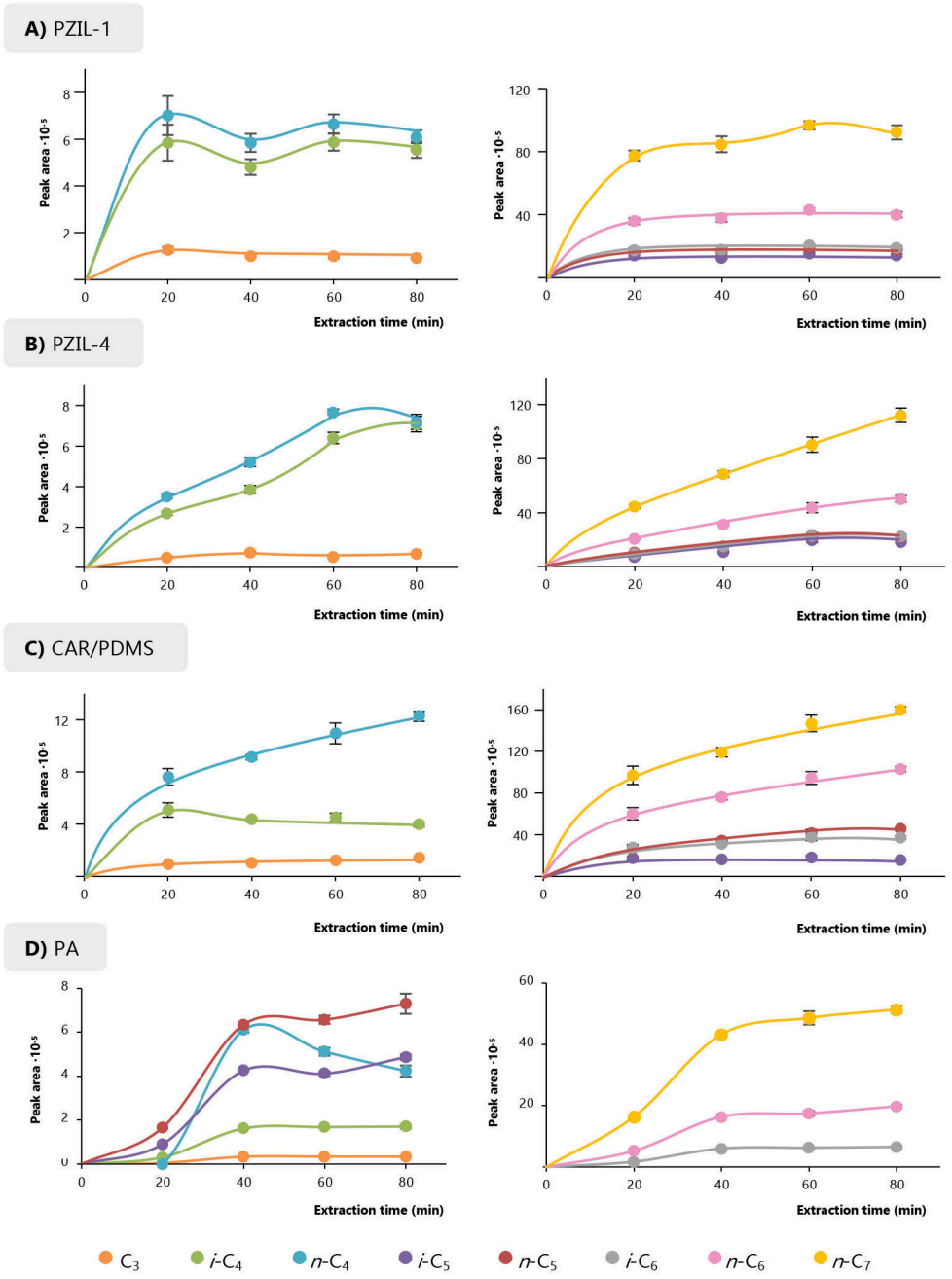

Figure IV.35. Extraction time profiles of the HS-SPME-GC-MS method for the determination of SCFFAs using **A)** Fiber PZIL-1, **B)** Fiber PZIL-4, **C)** CAR/PDMS, and **D)** PA. Experimental conditions (n = 3): 10 mL of aqueous solution containing the SCFFAs at 1.00–2.66 mg·L^{-1} depending on the analyte (0.02 mmol·L^{-1}); 30 % (w/v) of NaCl; 20–80 min of extraction at 65 °C and 600 min^{-1} of stirring rate; and desorption for 6 min at 175 °C for PILs-based fibers, 280 °C for PA, and 290 °C for CAR/PDMS.

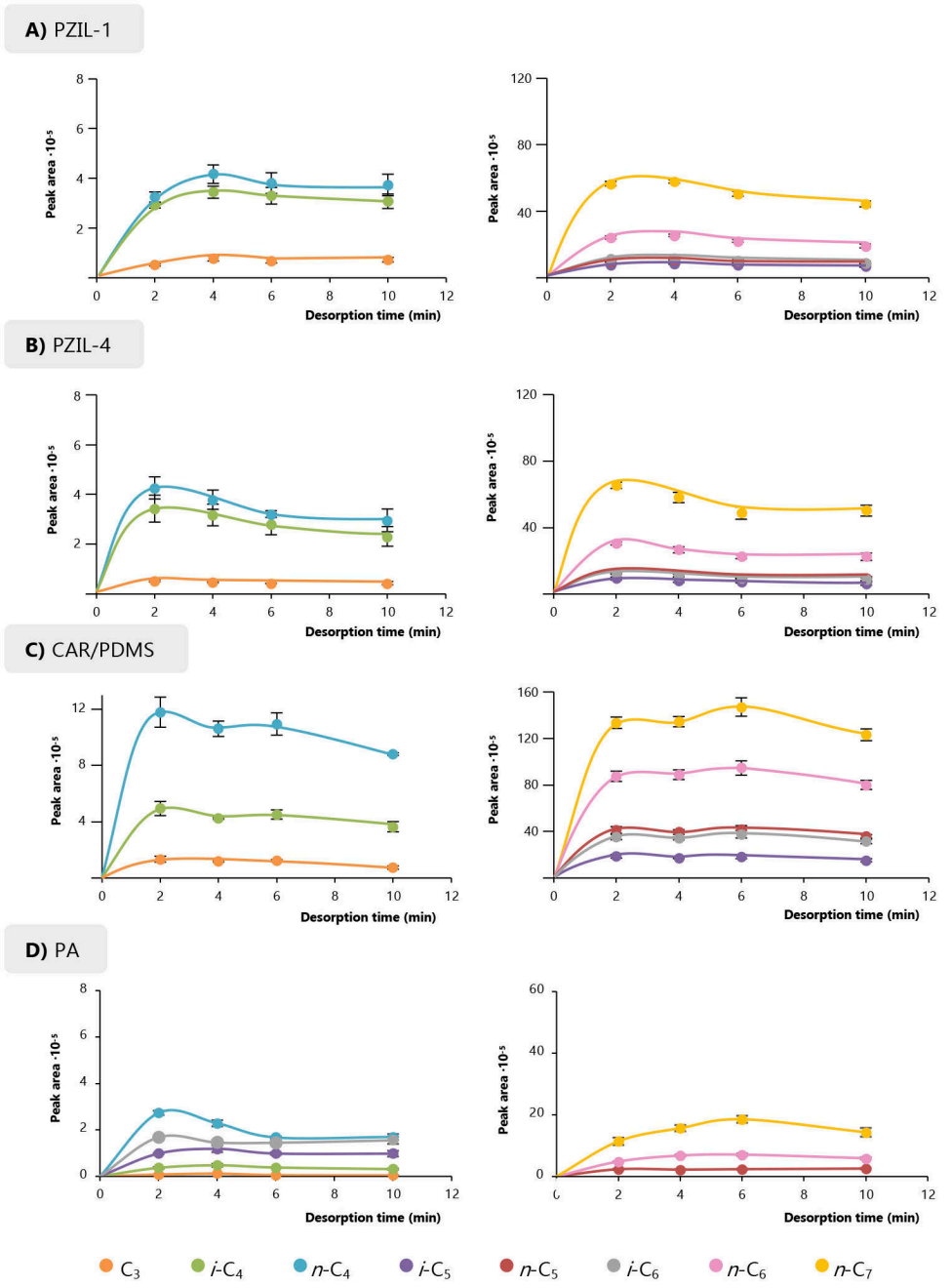

Figure IV.36. Influence of the desorption time on the HS-SPME-GC-MS method for the determination of SCFFAs using **A)** fiber PZIL-1, **B)** fiber PZIL-4, **C)** CAR/PDMS, and **D)** PA. Experimental conditions (n = 3): 10 mL of aqueous solution containing the SCFFAs at 1.00–2.66 mg·L^{-1} depending on the analyte (0.02 mmol·L^{-1}); 30 % (w/v) of NaCl; extraction at 65 °C and 600 min^{-1} of stirring rate for 20 min for fiber PZIL-1, 40 min for PA, and 60 min for fiber PZIL-4 and CAR/PDMS; and desorption for 2–10 min at 175 °C for fibers PZIL-1 and PZIL-4, 280 °C for PA, and 290 °C for CAR/PDMS.

Table IV.43. Optimum conditions for the HS-SPME-GC-MS method using different fibers.

Parameter	PZIL-1	PZIL-4	CAR/PDMS	PA
Standard solution or sample volume (mL)	10	10	10	10
NaCl content (%, w/v)	30	30	30	30
Extraction temperature (°C)	65	65	65	65
Extraction stirring rate (min^{-1})	600	600	600	600
Extraction time (min)	20	60	60	40
Desorption temperature (°C)	175	175	290	280
Desorption time (min)	4	2	2	4

Several analytical quality parameters of these calibration curves are shown in Tables IV.44, IV.45, and IV.46. If these calibration curves are compared, the results indicate that CAR/PDMS exhibited higher sensitivity for most of the analytes. The exceptions are *i*-C_4 and *i*-C_5, for which similar sensitivities were achieved using all fibers. Furthermore, the zwitterionic PILs fibers provided wider linear ranges for the longer alkyl chain SCFFAs, while the precision of the method (evaluated as the relative standard deviation, RSD, in %) was adequate for all fibers at the two different concentration levels tested.

The RR was calculated as the ratio of the predicted concentration obtained using these calibration curves and the concentration in the aqueous standard: ranging between 544 and 929 $\mu g \cdot L^{-1}$ depending on the analyte. The obtained results are shown in Figure IV.37. The amount of analyte extracted using fiber PZIL-1 was not affected by the presence of ethanol in the aqueous sample, as the same RR values were obtained in both cases for all the SCFFAs. In the case of PZIL-4 fiber, there was a 10–15 % decrease in the *i*-C_6 and *n*-C_6 RR values when ethanol was added to the sample. This may be due to the higher H-bond basicity of the carboxylate anions of the PIL in comparison with the sulfonate anions of fiber PZIL-1 [12], what could promote certain degree of competence between these analytes and the ethanol. However, similar results were obtained with fiber PZIL-4 for smaller SCFFAs. As expected, the RR values using CAR/PDMS in the presence of ethanol were lower than in absence of this organic solvent. This decrease is sharper for *iso*- and longer alkyl chain SCFFAs, especially in the case of *i*-C_4 and *i*-C_5, for which the RR dropped from 93 to 4.2 % and from 110 to 23 %, respectively. These results suggest that the zwitterionic PIL fibers may be less affected by the presence of ethanol in the sample compared with the CAR/PDMS fiber.

Table IV.44. Analytical performance of the HS-SPME-GC-MS method using the fiber PZIL-1 and aqueous standards prepared in ultrapure water.

SCFFA	Working range (µg·L^{-1})	(Slope ± t·SD[a])·10^{-4}	R^{2} [b]	$S_{y/x}$[c]·10^{-4}	LOD[d] (µg·L^{-1})	RSD[e] (%) low / high level
C_3	78–7778	2.0 ± 0.1	0.993	0.3	7.8	20 / 17
i-C_4	89–8899	9.4 ± 0.5	0.997	1.9	8.9	9.8 / 9.9
n-C_4	89–8899	12.0 ± 0.8	0.996	2.7	8.9	13 / 12
i-C_5	105–10519	24 ± 2	0.996	6.4	11	9.2 / 8.8
n-C_5	105–10519	34 ± 2	0.996	8.9	11	10 / 9.4
i-C_6	116–11616	34 ± 2	0.997	8.8	8.1	12 / 10
n-C_6	116–11616	74 ± 5	0.996	21	8.1	10 / 9.3
n-C_7	133–13278	105 ±15	0.983	75	9.3	2.2 / 8.9

[a] 95 % confidence limits for n = 7 calibration levels (5 degrees of freedom).
[b] Determination coefficient.
[c] Error of the estimate (or standard deviation of the residuals).
[d] Limit of detection, calculated as the concentration corresponding to 3 times the S/N, and verified with aqueous standards prepared at these levels and subjected to the overall method.
[e] Relative standard deviation (n = 3) for a low concentration level of 0.35–0.93 mg·L^{-1} depending on the analyte (0.007 mmol·L^{-1}) and a high concentration level of 2.5–6.6 mg·L^{-1} depending on the analyte (0.05 mmol·L^{-1}).

Table IV.45. Analytical performance of the HS-SPME-GC-MS method using the fiber PZIL-4 and aqueous standards prepared in ultrapure water

SCFFA	Working range (µg·L^{-1})	(Slope ± t·SD[a])·10^{-4}	R^{2} [b]	$S_{y/x}$[c]·10^{-4}	LOD[d] (µg·L^{-1})	RSD[e] (%) low / high level
C_3	78–7778	3.1 ± 0.6	0.987	1.3	7.8	9.8 / 7.6
i-C_4	89–8899	12 ± 1	0.992	0.5	8.9	16 / 9.6
n-C_4	89–8899	17 ± 3	0.986	7.3	8.9	18 / 20
i-C_5	105–10519	26 ± 3	0.992	9.8	11	18 / 18
n-C_5	105–10519	47 ± 8	0.985	25	11	18 / 20
i-C_6	116–11616	33 ± 6	0.984	20	8.1	19 / 20
n-C_6	116–11616	81 ± 14	0.985	48	8.1	19 / 16
n-C_7	133–13278	109 ± 14	0.991	56	9.3	13 / 11

[a] 95 % confidence limits for n = 6 calibration levels (4 degrees of freedom).
[b] Determination coefficient.
[c] Error of the estimate (or standard deviation of the residuals).
[d] Limit of detection, calculated as the concentration corresponding to 3 times the S/N, and verified with aqueous standards prepared at these levels and subjected to the overall method.
[e] Relative standard deviation (n = 3) for a low concentration level of 0.35–0.93 mg·L^{-1} depending on the analyte (0.007 mmol·L^{-1}) and a high concentration level of 2.5–6.6 mg·L^{-1} depending on the analyte (0.05 mmol·L^{-1}).

Table IV.46. Analytical performance of the HS-SPME-GC-MS method using the fiber CAR/PDMS and aqueous standards prepared in ultrapure water.

SCFFA	Working range (μg·L^{-1})	(Slope ± t·SD[a])·10^{-4}	R^{2} [b]	$S_{y/x}$[c]·10^{-4}	LOD[d] (μg·L^{-1})	RSD[e] (%) low / high level
C_3	78–7778	5 ± 1	0.980	2.6	7.8	2.3 / 8.9
i-C_4	89–8899	10.0 ± 0.8	0.995	2.7	8.9	6.3 / 11
n-C_4	89–6229	43 ± 6	0.991	11	1.8	14 / 8.1
i-C_5	105–10519	30 ± 6	0.988	16	11	13 / 1.2
n-C_5	105–7364	103 ± 28	0.982	63	1.1	15 / 7.1
i-C_6	116–8131	61 ± 17	0.997	42	1.2	16 / 3.4
n-C_6	116–8131	167 ± 56	0.982	136	0.6	19 / 4.0
n-C_7	133–9295	222 ± 61	0.993	169	0.7	5.1 / 5.3

[a] 95 % confidence limits for n = 6 calibration levels (4 degrees of freedom).
[b] Determination coefficient.
[c] Error of the estimate (or standard deviation of the residuals).
[d] Limit of detection, calculated as the concentration corresponding to 3 times the S/N, and verified with aqueous standards prepared at these levels and subjected to the overall method.
[e] Relative standard deviation (n = 3) for a low concentration level of 0.35–0.93 mg·L^{-1} depending on the analyte (0.007 mmol·L^{-1}) and a high concentration level of 2.5–6.6 mg·L^{-1} depending on the analyte (0.05 mmol·L^{-1}).

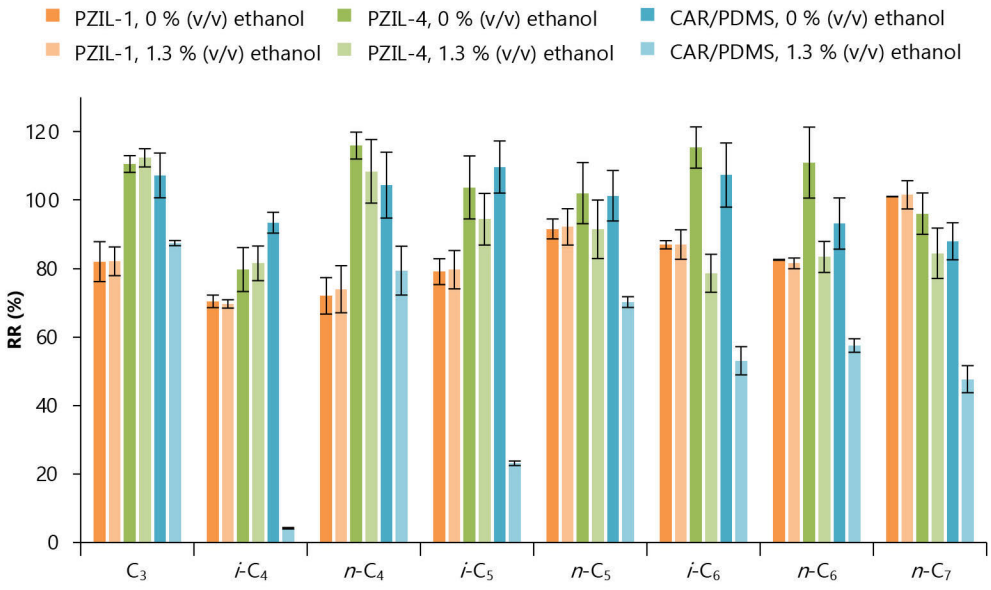

Figure IV.37. Effect of the ethanol content on the extraction efficiency of the developed HS-SPME-GC-MS method for the determination of SCFFAs, evaluated as relative recovery. The experiments were performed under optimum conditions (Table IV.43) using aqueous standard solution containing the SCFFAs at 0.35–0.93 mg·L^{-1} depending on the analyte (0.007 mmol·L^{-1}).

4. Extraction mechanism of the zwitterionic PILs-based fibers

The primary extraction mechanism (i.e., absorption or adsorption) exhibited by the zwitterionic PILs fibers PZIL-1 and PZIL-4 was evaluated by performing a previously reported approach [10,13]. The method consists of developing calibration curves of a target sorbate in the presence of an interfering compound at two different relative concentration levels. If adsorption is the primary extraction mechanism, both the sorbate and the interfering compound can compete for the limited available sorption sites of the coating. The concentration of the sorbate in this particular case can be affected under equilibrium conditions, especially for analytes with lower affinity to the sorbent coating [13,14]. Therefore, an increase in the concentration of the interfering compound can cause a change of the sensitivity of the target analyte [14].

In absorptive-type extractions, diffusion of the analytes through the sorbent coating is a dominant effect [11]. Therefore, analytes can freely partition into the sorbent, with little competition among analytes, and the concentration of each analyte at equilibrium is less affected by the presence of other analytes.

In this approach, calibration curves of *i*-C_4 (as target sorbate) were constructed in diluted synthetic wine (1 mL diluted up to 10 mL using ultrapure water) and in the presence of two relative concentrations of *n*-C_7, acting as interfering compound, as it was described in Section III.7.5.6. The two relative concentration ratios were denoted as 1:1 and 1:10 (*i*-C_4:*n*-C_7 concentration ratio). The obtained curves are shown in Figure IV.38. Both fibers exhibited similar behavior and no differences were observed for the curves of *i*-C_4 when different relative concentrations of the interfering compound, *n*-C_7, were present in the extraction vial.

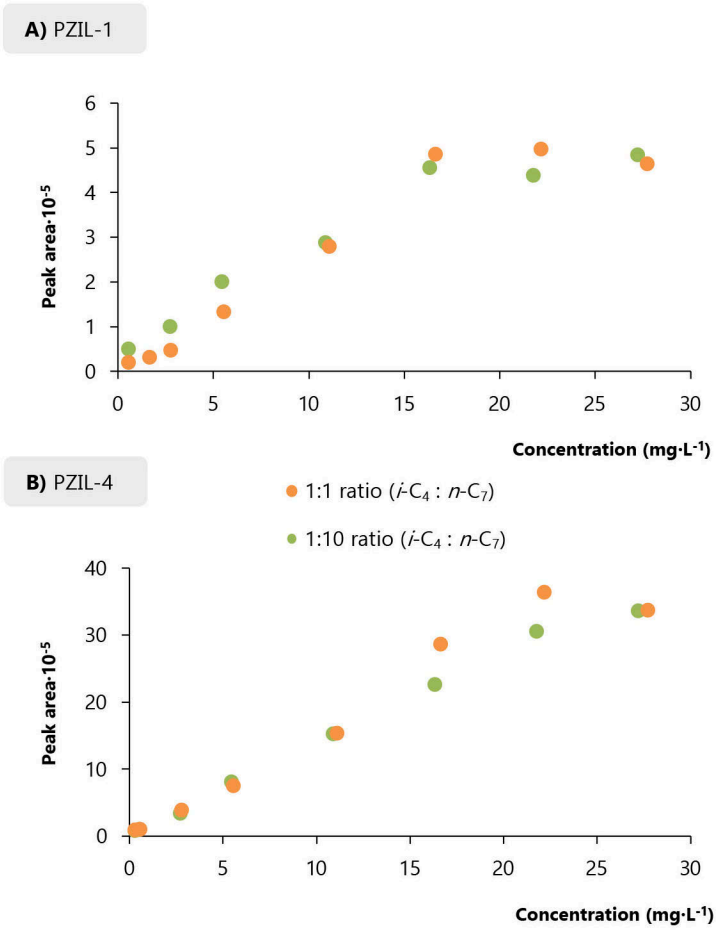

Figure IV.38. Calibration curves of *i*-C_4 in the presence of two *i*-C_4:*n*-C_7 concentration ratios (1:1 or 1:10) for fibers **A)** PZIL-1 and **B)** PZIL-4. Experiments were performed in dilute synthetic wine using optimum conditions summarized in Table IV.43.

The results were confirmed by the analysis of the corresponding linear segments of the curves, as it is shown in Table IV.47. For PZIL-1 fiber, the obtained slopes in the linear range 0.5–16 mg·L^{-1} were (2.5 ± 0.6)·10^4 and (2.9 ± 0.6)·10^4 for calibrations employing 1:1 and 1:10 ratios, respectively, and the standard deviation of the residuals was 2.1·10^4 in both cases. Statistical analysis revealed equal slope variances and no significant differences between the slopes (95 % confidential level, statistical test according to Andrade and Estévez-Pérez [15]). With respect to PZIL-4 fiber, the results indicated different slope variances but no significant differences between the slopes. The obtained data also revealed that the sensitivity of the fibers towards the extraction of *i*-C_4 was not affected by the presence of *n*-C_7. Therefore, it can be concluded that absorption is the primary extraction mechanism of the studied zwitterionic PILs-based coating. This behavior is similar to the commercially available PA and PDMS fibers, and different than that observed for CAR/PDMS, for which a competitive extraction mechanism is typical [10,11,13]. Indeed, these results support the different behavior previously observed for the performance of PILs-based and CAR/PDMS fibers when ethanol is present in the sample (or in the aqueous standard).

Table IV.47. Calibration curves of *i*-C_4 in the presence of *n*-C_7 at two relative *i*-C_4:*n*-C_7 concentration ratios (1:1 and 1:10, mg·L^{-1}). HS-SPME-GC-MS experiments were performed in diluted synthetic wine (1 mL up tp 10 mL with ultrapure water) using optimum conditions of Table IV.43, and for fibers PZIL-1 and PZIL-4.

Ratio	Linearity range (mg·L^{-1})	(Slope ± t·SD[a])·10^{-4}	R^2 [b]	($S_{y/x}$[c])·10^{-4}	n[d]
Fiber PZIL-1					
1:1	0.5–16	2.5 ± 0.6	0.987	2.1	5
1:10	0.5–16	2.9 ± 0.6	0.989	2.1	6
Fiber PZIL-4					
1:1	0.2–22	13.9 ± 0.5	0.999	3.5	7
1:10	0.2–22	16 ± 2	0.990	15	7

[a] 95 % confidence limits for n calibration levels (n – 2 degrees of freedom).
[b] Determination coefficient.
[c] Error of the estimate (or standard deviation of the residuals).
[d] Calibration levels.

This approach has been previously applied for studying the primary extraction mechanism of both linear and crosslinked PIL-based sorbent coatings [10,13]. The studies performed with sorbent coatings based on monocationic IL monomers revealed an absorption-type extraction mechanism [10]. However, sorbent coatings generated with IL monomers containing silver ions demonstrated primarily an adsorptive-type extraction mechanism [13]. Therefore, it can be

concluded that PILs can be chemically tuned to extract analytes via absorption- or adsorption-type mechanisms by simple changes on the composition of the IL monomer.

5. Analytical performance of the HS-SPME-GC-MS method using PILs and commercial fibers

Calibrations using standards prepared in diluted synthetic wine (1 mL of synthetic wine diluted up to 10 mL using ultrapure water) were carried out for fibers PZIL-1 and PZIL-4. For comparison purposes, calibrations for CAR/PDMS (adsorption) and PA (absorption) commercial fibers were also obtained. Table IV.48 lists several analytical figures of merit of the curves, whereas detailed information of the analytical performance for all fibers is included in Tables IV.49, IV.50, IV-51 and IV-52. The calibrations presented wide linear ranges, ranging from 75–13300 $\mu g \cdot L^{-1}$ depending on the analyte and fiber. It is interesting to mention that, in general, wider linear ranges were obtained for the absorptive-type fibers (fibers PZIL-1, PZIL-4 and PA) in comparison with CAR/PDMS.

The sensitivity of the method was evaluated using calibration slopes (Table IV.48) that ranged from $(1.3 \pm 0.3) \cdot 10^4$ to $(17 \pm 1) \cdot 10^4$ for fiber PZIL-1, $(1.4 \pm 0.3) \cdot 10^4$ to $(48 \pm 2) \cdot 10^4$ for fiber PZIL-4, $(1.8 \pm 0.3) \cdot 10^4$ to $(161 \pm 23) \cdot 10^4$ for CAR/PDMS, and $(0.44 \pm 0.03) \cdot 10^4$ to $(11 \pm 1) \cdot 10^4$ for PA. The sensitivity of the method was the lowest and highest for C_3 and *n*-C_7 for all fibers, respectively. In general, higher sensitivities were achieved using CAR/PDMS, with the exception of *i*-C_4, for which similar sensitivities were obtained with the zwitterionic PILs. These results are in accordance with the data obtained in previous sections, indicating the presence of ethanol significantly decreased the extraction efficiency of CAR/PDMS for the extraction of *i*-C_4 with respect to the remaining SCFFAs. The results also indicate that there are other components of the matrix aside from ethanol (i.e., (+)-tartaric acid) that were able to affect the partitioning of analytes to the HS, likely due to an increase in solubility of the analytes in the initial aqueous sample, among other reasons. In any case, the results demonstrate the suitability of the zwitterionic PILs for this application.

If the film thickness of the sorbent coatings is considered, the zwitterionic PILs are significantly thinner than the commercial fibers: 18 ± 3 µm for fiber PZIL-1 and 18 ± 6 µm for PZIL-4 *versus* 75 µm of CAR/PDMS and 85 µm of PA. Improvements in the coating process will produce sorbent coatings as thick as commercial fibers, which should significantly increase the sensitivity of the zwitterionic PILs. As an estimation, Figure IV.39 shows the normalized slopes obtained by dividing the calibration slopes in diluted synthetic wine by the film thickness. Normalized slopes 1–3 times higher were achieved for the smaller SCFFAs (C_3–*n*-C_4) and *n*-C_7 if the results of zwitterionic PILs are compared with CAR/PDMS. However, it is important to emphasize that this normalization is only an estimation of the sensitivity of the method, independent of film thickness. As the CAR/PDMS fiber extracts via an adsorptive-type mechanism, the analytes interact primarily with the surface of the sorbent coating instead of partitioning into the entire film and, therefore, the sensitivity of this fiber depends on other factors such as the surface area and porosity of the material, among others [11,16].

Table IV.48. Several analytical figures of merit of the HS-SPME-GC-MS method after performing matrix-matched calibration using standards prepared in diluted synthetic wine.

SCFFA	(Slope ± t·SD[a])·10^{-4}				LOD[b] (µg·L^{-1})				%RR[c] (%RSD[d])			
	PZIL-1	PZIL-4	CAR/ PDMS	PA	PZIL-1	PZIL-4	CAR/ PDMS	PA	PZIL-1	PZIL-4	CAR/ PDMS	PA
C_3	1.3 ± 0.3	1.4 ± 0.3	1.8 ± 0.3	0.44 ± 0.03	53	36	33	61	115 (1.9)	115 (2.6)	104 (8.4)	88.4 (14)
i-C_4	3.0 ± 0.3	5.3 ± 0.5	7 ± 3	1.7 ± 0.3	60	20	155	57	107 (3.5)	118 (3.8)	120 (5.2)	102 (10)
n-C_4	4.7 ± 0.5	7.2 ± 0.3	24 ± 5	2.1 ± 0.3	40	42	45	47	115 (5.0)	115 (10)	82.7 (6.8)	78.3 (7.5)
i-C_5	4.9 ± 0.5	11.4 ±0.8	74 ± 26	3.0 ± 0.3	19	26	38	42	112 (4.9)	116 (3.1)	81.5 (6.2)	80.5 (15)
n-C_5	7.0 ± 0.8	14.7 ± 0.8	136 ± 26	4.4 ± 0.3	15	31	8.9	47	105 (4.7)	96.3 (3.5)	98.4 (10)	74.6 (12)
i-C_6	4.3 ± 0.3	12 ± 1	103 ± 21	2.5 ± 0.3	76	48	10	52	107 (8.6)	107 (3.2)	91.0 (8.1)	115 (5.0)
n-C_6	9.7 ± 0.8	26 ± 2	202 ± 41	7.1 ± 0.6	22	23	8.4	43	103 (6.2)	98.5 (9.0)	115 (11)	71.2 (13)
n-C_7	17 ± 1	48 ± 2	161 ± 23	11 ± 1	22	12	11	27	93.4 (3.9)	106 (5.5)	112 (11)	95.1 (13)

[a] 95 % confidence limits for n = 7 calibration levels (5 degrees of freedom) for PZIL-1, PZIL4 and CAR/PDMS, n = 5 calibration levels (3 degrees of freedom for PA.

[b] Limit of detection, calculated as the concentration corresponding to 3 times the S/N.

[c] Relative recovery for a concentration level of 0.35–0.93 mg·L^{-1} depending on the analyte (0.007 mmol·L^{-1}).

[d] Intra-day precision (n = 3) for a concentration level of 0.35–0.93 mg·L^{-1} depending on the analyte (0.007 mmol·L^{-1}).

Table IV.49. Analytical performance of the HS-SPME-GC-MS method using the fiber PZIL-1 and standard solutions prepared in diluted synthetic wine.

SCFFA	Working range (μg·L^{-1})	(Slope ± t·SD[a])·10^{-4}	R^2 [b]	$S_{y/x}$[c]·10^{-4}	LOD[d] (μg·L^{-1})
C_3	78–7778	1.3 ± 0.3	0.988	0.43	53
i-C_4	89–8899	3.0 ± 0.3	0.994	0.77	60
n-C_4	89–8899	4.7 ± 0.5	0.989	1.6	40
i-C_5	105–10519	4.9 ± 0.5	0.991	1.8	19
n-C_5	105–10519	7.0 ± 0.8	0.984	3.5	15
i-C_6	116–11616	4.3 ± 0.3	0.999	0.7	76
n-C_6	116–11616	9.7 ± 0.8	0.995	3.0	22
n-C_7	133–13278	17 ± 1	0.997	4.5	22

[a] 95 % confidence limits for n = 7 calibration levels (5 degrees of freedom).
[b] Determination coefficient.
[c] Error of the estimate (or standard deviation of the residuals).
[d] Limit of detection, calculated as the concentration corresponding to 3 times the S/N.

Table IV.50. Analytical performance of the HS-SPME-GC-MS method using the fiber PZIL-4 and standard solutions prepared in diluted synthetic wine.

SCFFA	Working range (μg·L^{-1})	(Slope ± t·SD[a])·10^{-4}	R^2 [b]	$S_{y/x}$[c]·10^{-4}	LOD[d] (μg·L^{-1})
C_3	78–7778	1.4 ± 0.3	0.993	3.6	36
i-C_4	89–8899	5.3 ± 0.5	0.995	14	20
n-C_4	89–8899	7.2 ± 0.3	0.998	11	42
i-C_5	105–10519	11.4 ±0.8	0.996	31	26
n-C_5	105–10519	14.7 ± 0.8	0.998	27	31
i-C_6	116–11616	12 ± 1	0.996	39	48
n-C_6	116–11616	26 ± 2	0.997	75	23
n-C_7	133–13278	48 ± 2	0.999	77	12

[a] 95 % confidence limits for n = 7 calibration levels (5 degrees of freedom).
[b] Determination coefficient.
[c] Error of the estimate (or standard deviation of the residuals).
[d] Limit of detection, calculated as the concentration corresponding to 3 times the S/N.

Table IV.51. Analytical performance of the HS-SPME-GC-MS method using the commercial CAR/PDMS fiber and standard solutions prepared in diluted synthetic wine.

SCFFA	Working range (μg·L^{-1})	(Slope ± t·SD[a])·10^{-4}	$R^{2\,b}$	$S_{y/x}$[c]·10^{-4}	LOD[d] (μg·L^{-1})
C_3	78–5445	1.8 ± 0.3	0.980	6.39	33
i-C_4	890–6229	7 ± 3	0.963	40.3	155
n-C_4	89–6229	24 ± 5	0.981	87.8	45
i-C_5	526–4208	74 ± 26	0.982	275	38
n-C_5	105–4208	136 ± 26	0.983	335	8.9
i-C_6	116–4646	103 ± 21	0.984	273	10
n-C_6	116–4646	202 ± 41	0.982	574	8.4
n-C_7	664–9295	161 ± 23	0.990	664	11

[a] 95 % confidence limits for n = 7 calibration levels (5 degrees of freedom).
[b] Determination coefficient.
[c] Error of the estimate (or standard deviation of the residuals).
[d] Limit of detection, calculated as the concentration corresponding to 3 times the S/N.

Table IV.52. Analytical performance of the HS-SPME-GC-MS method using the commercial PA fiber and standard solutions prepared in diluted synthetic wine.

SCFFA	Working range (μg·L^{-1})	(Slope ± t·SD[a])·10^{-4}	R^{2} [b]	$S_{y/x}$[c]·10^{-4}	LOD[d] (μg·L^{-1})
C_3	78–7778	0.44 ± 0.03	0.997	0.87	61
i-C_4	89–8899	1.7 ± 0.3	0.990	6.4	57
n-C_4	89–8899	2.1 ± 0.3	0.991	7.4	47
i-C_5	105–10519	3.0 ± 0.3	0.997	7.9	42
n-C_5	105–10519	4.4 ± 0.3	0.998	8.5	47
i-C_6	116–11616	2.5 ± 0.3	0.998	5.9	52
n-C_6	116–11616	7.1 ± 0.6	0.995	24	43
n-C_7	133–13278	11 ± 1	0.996	42	27

[a] 95 % confidence limits for n = 5 calibration levels (3 degrees of freedom).
[b] Determination coefficient.
[c] Error of the estimate (or standard deviation of the residuals).
[d] Limit of detection, calculated as the concentration corresponding to 3 times the S/N.

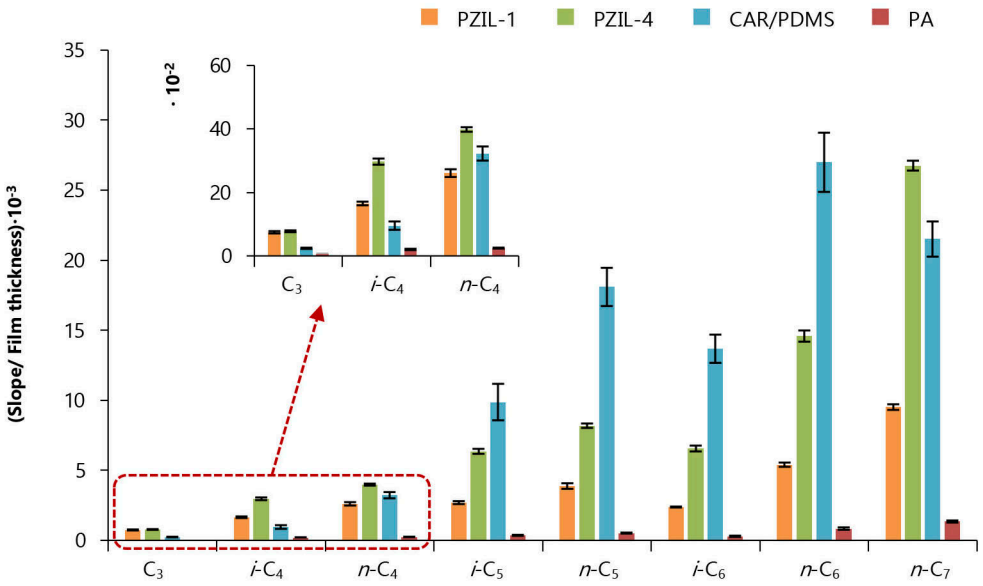

Figure IV.39. Comparison of normalized calibration slopes (calibration slope *versus* film thickness of the fiber) for the different SPME fibers. Slops were obtained after performing the HS-SPME-GC-MS calibrations using standards prepared in synthetic wine.

The limits of detection (LOD) were estimated as the concentration corresponding to three times the signal-to-noise ratio (Table IV.48). The LOD ranges were 15–76 $\mu g \cdot L^{-1}$ for fiber PZIL-1, 12–48 $\mu g \cdot L^{-1}$ for fiber PZIL-4, 8.4–155 $\mu g \cdot L^{-1}$ for CAR/PDMS, and 27–61 $\mu g \cdot L^{-1}$ for PA. These values are particularly low for the determination of SCFFAs [5,6].

The reproducibility (as RSD, in %) of the method was evaluated at a concentration level of 0.35–0.93 $mg \cdot L^{-1}$ depending on the analyte (0.007 $mmol \cdot L^{-1}$). The RSD values ranged from 1.9 to 8.6 % for PZIL-1, 2.6–10 % for PZIL-4, 5.2–11 % for CAR/PDMS, and 5.0–15 % for PA. The RR was calculated at the same concentration level as the ratio of the predicted concentration obtained using the calibrations of Table IV.48 and the concentration value at which the standards were prepared. The obtained RR values were acceptable for all fibers.

6. Evaluation of matrix effect and analysis of a real samples

The proposed method was applied for the analysis of red wine. Standard addition curves were developed with fibers PZIL-1, PZIL-4 and CAR/PDMS. PA was excluded in this comparison due to reproducibility problems in the red wine sample, likely due to the complexity of the sample

and its lower sensitivity for the determination of SCFFAs. Tables IV.53, IV.54 and IV.55 show the analytical figures of merit obtained using the standard addition method. The calibration curves for *i*-C_4 and *n*-C_5 could not be obtained using CAR/PDMS as this fiber was negatively affected by the presence of ethanol. The calibration slopes ranged from (0.75 ± 0.07)·10^4 to (83 ± 5)·10^4 for fiber PZIL-1, (1.6 ± 0.3)·10^4 to (74 ± 8)·10^4 for fiber PZIL-4, and (2.1 ± 0.3)·10^4 to (315 ± 28)·10^4 for CAR/PDMS.

The matrix effect with this sample was assessed by a statistical comparison of the calibration slopes obtained with standards in diluted synthetic wine (Table IV.48) and the standard addition method. The comparison was performed using the Student's *t*-test reported by Andrade and Estévez-Pérez [15]. The results are included in Tables IV.56, IV.57 and IV.58 and indicated a significant matrix effect for the majority of analytes and sorbent coatings. Therefore, equal slopes were found only for *i*-C_4 for fiber PZIL-1; C_3, *i*-C_4 and *n*-C_4 for fiber PZIL-4; and C_3 and *i*-C_5 for CAR/PDMS. It is interesting to note that, for the rest of the analytes (excluding the cases of *i*-C_4 and *n*-C_5 with the CAR/PDMS fiber), an enhancement of the sensitivity was observed when the standard addition method was employed. Thus, slopes between 1.3–4.8, 1.1–1.5 and 1.2–1.9 times higher were obtained using standard addition for PZIL-1, PZIL-4 and CAR/PDMS, respectively.

Considering the significant matrix effect for most of the SCFFAs, the standard addition method was selected for the quantification of the analytes in red wine. Figure IV.40 shows the predicted concentrations using the PILs-based and the commercial fibers. The concentration of the SCFFAs *i*-C_4 and *n*-C_5 could not be detected with the CAR/PDMS. In the remaining cases, no significant differences in the SCFFAs concentrations were observed for fiber PZIL-4 respect to CAR/PDMS, and in the C_3, *i*-C_6 and *n*-C_7 concentrations for fiber PZIL-1 in comparison with CAR/PDMS. These results demonstrated the potential of these zwitterionic PILs for the analysis of real samples. The SCFFA concentrations ranged from 0.18 ± 0.03 mg·L^{-1} to 4.8 ± 0.9 mg·L^{-1}, depending on the fiber. The presence of SCFFAs in wine is commonly associated with the fruity, fatty and rancid aroma of wines [17].

The proposed method was compared with other methods from the literature that used GC for the determination of SCFFAs. The proposed method provided similar analytical performance to previously reported HS-SPME methods for the determination of SCFFAs in wine [3], while it is simpler than other SPME modes employed for FFA determination, such as vacuum HS-SPME [6], and faster than multiple HS-SPME [5].

Table IV.53. Analytical performance of the HS-SPME-GC-MS method using fiber PZIL-1 and the standard addition calibration method with diluted red wine.

SCFFA	Working range ($mg \cdot L^{-1}$)	(Slope ± t·SD[a])·10^{-4}	R^{2} [b]	$S_{y/x}$[c]·10^{-5}	Calibration levels	Predicted concentration ± SD[d] ($mg \cdot L^{-1}$)
C_3	0–3112	0.75 ± 0.07	0.992	0.008	8	2.8 ± 0.5
i-C_4	0–3560	4.0 ± 0.2	0.998	0.031	8	2.9 ± 0.4
n-C_4	0–3560	4.4 ± 0.6	0.990	0.070	6	2.6 ± 0.9
i-C_5	0–4208	11.4 ± 0.5	0.998	0.081	8	0.66 ± 0.04
n-C_5	0–4208	15.3 ± 2	0.994	0.23	7	0.18 ± 0.03
i-C_6	0–4646	17 ± 1	0.994	0.23	8	0.33 ± 0.07
n-C_6	0–4646	39 ± 2	0.998	0.33	7	2.0 ± 0.2
n-C_7	0–5311	83 ± 5	0.996	1.2	8	1.5 ± 0.7

[a] 95 % confidence limits for n calibration levels (n – 2 degrees of freedom).
[b] Determination coefficient.
[c] Error of the estimate (or standard deviation of the residuals).
[d] Standard deviation in the prediction of the concentration.

Table IV.54. Analytical performance of the HS-SPME-GC-MS method using fiber PZIL-4 and the standard addition calibration method with diluted red wine.

SCFFA	Working range ($mg \cdot L^{-1}$)	(Slope ± t·SD[a])·10^{-4}	R^{2} [b]	$S_{y/x}$[c]·10^{-5}	Calibration levels	Predicted concentration ± SD[d] ($mg \cdot L^{-1}$)
C_3	0–2334	1.6 ± 0.3	0.981	0.22	6	3.1 ± 0.9
i-C_4	0–3560	5.6 ± 0.5	0.995	0.63	7	3.9 ± 0.6
n-C_4	0–3560	7.6 ± 0.3	0.999	0.42	7	2.1 ± 0.3
i-C_5	0–4208	12.8 ± 0.5	0.999	0.74	7	1.3 ± 0.3
n-C_5	0–4208	16.3 ± 0.8	0.998	1.2	7	0.57 ± 0.04
i-C_6	0–4646	15 ± 1	0.994	2.3	7	0.81 ± 0.08
n-C_6	0–4646	33 ± 2	0.997	3.7	7	3.7 ± 0.6
n-C_7	0–5311	74 ± 8	0.993	14	7	1.3 ± 0.1

[a] 95 % confidence limits for n calibration levels (n – 2 degrees of freedom).
[b] Determination coefficient.
[c] Error of the estimate (or standard deviation of the residuals).
[d] Standard deviation in the prediction of the concentration.

Table IV.55. Analytical performance of the HS-SPME-GC-MS method using the fiber CAR/PDMS and the standard addition calibration method with diluted red wine.

SCFFA	Working range ($mg \cdot L^{-1}$)	(Slope ± t·SD[a])·10^{-4}	R^{2} [b]	$S_{y/x}$[c]·10^{-5}	Calibration levels	Predicted concentration ± SD[d] ($mg \cdot L^{-1}$)
C_3	0–2334	2.1 ± 0.3	0.985	0.029	6	3.5 ± 0.9
i-C_4	–	–	–	–	–	–
n-C_4	0–3560	39 ± 2	0.998	0.27	7	2.3 ± 0.4
i-C_5	0–4208	91 ± 8	0.996	0.55	6	1.6 ± 0.4
n-C_5	–	–	–	–	–	–
i-C_6	0–4646	159 ± 18	0.996	3.2	7	1.0 ± 0.1
n-C_6	0–4646	305 ± 28	0.987	4.6	6	4.8 ± 0.9
n-C_7	0–5311	315 ± 28	0.996	5.6	6	2.3 ± 0.9

[a] 95 % confidence limits for n calibration levels (n – 2 degrees of freedom).
[b] Determination coefficient.
[c] Error of the estimate (or standard deviation of the residuals).
[d] Standard deviation in the prediction of the concentration.

Table IV.56. Comparison of the slopes obtained using the standard addition method in red wine and the calibrations with standards prepared in diluted synthetic wine, for the fiber PZIL-1.

SCFFA	*F*-test[a]			Student's *t*-test[d]				
	F_{crit}[b]	F_{exp}[c]	Result	Variances	t_{crit}[e]	t_{cal}[f]	Result	Matrix effect
C_3	4.387	5.412	$F_{exp} > F_{crit}$	Different	2.201	20.69	$\|t_{cal}\| > t_{crit}$	Yes
i-C_4	4.387	1.427	$F_{exp} < F_{crit}$	Equal	2.201	–11.09	$\|t_{cal}\| > t_{crit}$	Yes
n-C_4	6.256	1.007	$F_{exp} < F_{crit}$	Equal	2.262	1.508	$\|t_{cal}\| < t_{crit}$	**No**
i-C_5	4.284	1.061	$F_{exp} < F_{crit}$	Equal	2.179	33.91	$\|t_{cal}\| > t_{crit}$	Yes
n-C_5	4.387	2.415	$F_{exp} < F_{crit}$	Equal	2.201	15.71	$\|t_{cal}\| > t_{crit}$	Yes
i-C_6	4.950	58.85	$F_{exp} > F_{crit}$	Different	2.201	25.71	$\|t_{cal}\| > t_{crit}$	Yes
n-C_6	4.387	6.752	$F_{exp} > F_{crit}$	Different	2.201	40.37	$\|t_{cal}\| > t_{crit}$	Yes
n-C_7	4.284	36.04	$F_{exp} > F_{crit}$	Different	2.179	30.35	$\|t_{cal}\| > t_{crit}$	Yes

[a] *F* statistical test to compare population variances.
[b] Critical *F* value for a significance level of 5 % and n – 2 degrees of freedom, being n the number of calibration levels.
[c] Experimental *F* value.
[d] Student's *t* test to compare the slopes.
[e] Critical *t* value for a significance level of 5 % and n – 2 degrees of freedom, being n the number of calibration levels
[f] Calculated *t* value using different approximations depending on the results of the *F*-test.

Table IV.57. Comparison of the slopes obtained using the standard addition method in red wine and the calibrations with standards prepared in diluted synthetic wine, for the fiber PZIL-4.

SCFFA	*F*-test[a]			Student's *t*-test[d]				
	F_{crit}[b]	F_{exp}[c]	Result	Variances	t_{crit}[e]	t_{cal}[f]	Result	Matrix effect
C_3	5.192	4.645	$F_{exp} < F_{crit}$	Equal	2.262	1.188	$\|t_{cal}\| < t_{crit}$	**No**
i-C_4	5.050	1.056	$F_{exp} < F_{crit}$	Equal	2.228	0.666	$\|t_{cal}\| < t_{crit}$	**No**
n-C_4	5.050	1.188	$F_{exp} < F_{crit}$	Equal	2.228	–1.544	$\|t_{cal}\| < t_{crit}$	**No**
i-C_5	5.050	3.266	$F_{exp} < F_{crit}$	Equal	2.228	–2.350	$\|t_{cal}\| > t_{crit}$	Yes
n-C_5	5.050	1.055	$F_{exp} < F_{crit}$	Equal	2.228	2.895	$\|t_{cal}\| > t_{crit}$	Yes
i-C_6	6.256	1.768	$F_{exp} < F_{crit}$	Equal	2.262	3.892	$\|t_{cal}\| > t_{crit}$	Yes
n-C_6	6.256	1.475	$F_{exp} < F_{crit}$	Equal	2.262	4.760	$\|t_{cal}\| > t_{crit}$	Yes
n-C_7	5.050	20.22	$F_{exp} > F_{crit}$	Different	2.228	8.837	$\|t_{cal}\| > t_{crit}$	Yes

[a] *F* statistical test to compare population variances.
[b] Critical *F* value for a significance level of 5 % and n – 2 degrees of freedom, being n the number of calibration levels.
[c] Experimental *F* value.
[d] Student's *t* test to compare the slopes.
[e] Critical *t* value for a significance level of 5 % and n – 2 degrees of freedom, being n the number of calibration levels
[f] Calculated *t* value using different approximations depending on the results of the *F*-test.

Table IV.58. Comparison of the slopes obtained using the standard addition method in red wine and the calibrations with standards prepared in diluted synthetic wine, for the commercial fiber CAR/PDMS.

SCFFA	*F*-test[a]			Student's *t*-test[d]				
	F_{crit}[b]	F_{exp}[c]	Result	Variances	t_{crit}[e]	t_{cal}[f]	Result	Matrix effect
C_3	6.591	1.248	$F_{exp} < F_{crit}$	Equal	2.365	–1.417	$\|t_{cal}\| < t_{crit}$	**No**
n-C_4	5.192	4.046	$F_{exp} < F_{crit}$	Equal	2.262	–6.459	$\|t_{cal}\| > t_{crit}$	Yes
i-C_5	6.591	11.67	$F_{exp} > F_{crit}$	Different	2.365	–1.683	$\|t_{cal}\| < t_{crit}$	**No**
i-C_6	5.409	1.299	$F_{exp} < F_{crit}$	Equal	2.306	–5.397	$\|t_{cal}\| > t_{crit}$	Yes
n-C_6	6.591	2.651	$F_{exp} < F_{crit}$	Equal	2.365	–5.769	$\|t_{cal}\| > t_{crit}$	Yes
n-C_7	9.117	1.230	$F_{exp} < F_{crit}$	Equal	2.365	10.78	$\|t_{cal}\| > t_{crit}$	Yes

[a] *F* statistical test to compare population variances.
[b] Critical *F* value for a significance level of 5 % and n – 2 degrees of freedom, being n the number of calibration levels.
[c] Experimental *F* value.
[d] Student's *t* test to compare the slopes.
[e] Critical *t* value for a significance level of 5 % and n – 2 degrees of freedom, being n the number of calibration levels
[f] Calculated *t* value using different approximations depending on the results of the *F*-test.

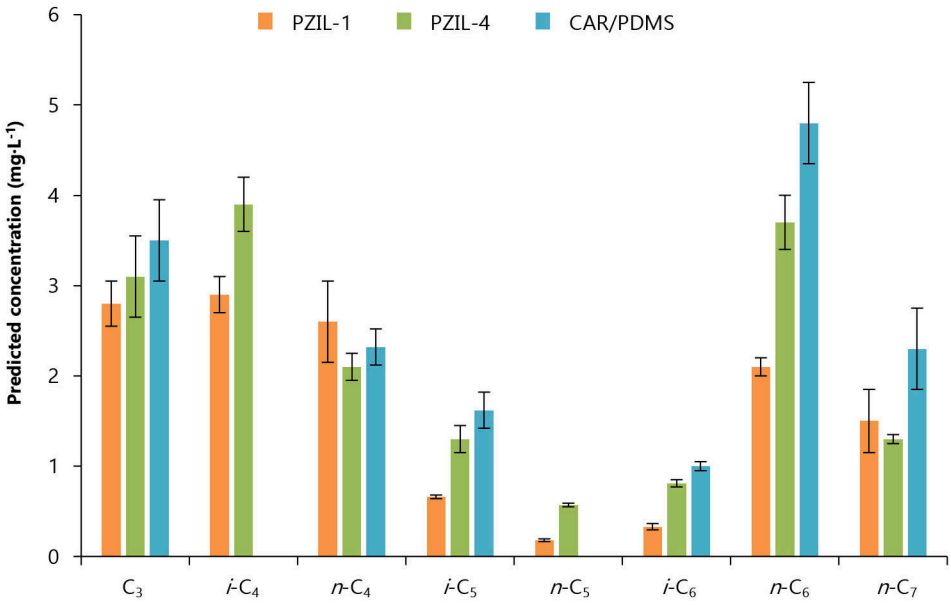

Figure IV.40. Results from the analysis of red wine using the standard addition method and different SPME fibers.

REFERENCES

[1] G. Lubes, M. Goodarzi, Chem. Rev. 117 (2017) 6399–6422.

[2] D. Fiorini, D. Pacetti, R. Gabbianelli, S. Gabrielli, R. Ballini, J. Chromatogr. A 1409 (2015) 282–287.

[3] S.G. Arcari, V. Caliari, M. Sganzerla, H.T. Godoy, Talanta 174 (2017) 752–766.

[4] D.T. Mannion, A. Furey, K.N. Kilcawley, Int. J. Dairy Technol. 69 (2016) 1–12.

[5] A.A. Rincón, V. Pino, J.H. Ayala, A.M. Afonso, Talanta 129 (2014) 183–190.

[6] M.J. Trujillo-Rodríguez, V. Pino, E. Psillakis, J.L. Anderson, J.H. Ayala, E. Yiantzi, A.M. Afonso, Anal. Chim. Acta 962 (2017) 41–51.

[7] S.J. Pérez Olivero, J.P. Pérez Trujillo, Anal. Chim. Acta 696 (2011) 59–66.

[8] A. Oehlke, K. Hofmann, S. Spange, New J. Chem. 30 (2006) 533–536.

[9] J. Palgunadi, S.Y. Hong, J.K. Lee, H. Lee, S.D. Lee, M. Cheong, H.S. Kim, J. Phys. Chem. B 115 (2011) 1067–1074.

[10] T.D. Ho, W.T.S. Cole, F. Augusto, J.L. Anderson, J. Chromatogr. A 1298 (2013) 146–151.

[11] J. Pawliszyn, Handbook of Solid Phase Microextraction, Elsevier (2012) 13–59.

[12] B. Wu, K. Kuroda, K. Takahashi, E.W. Castner, J. Chem. Phys. 148 (2018) 193807.

[13] M.J. Trujillo-Rodríguez, J.L. Anderson, Anal. Chim. Acta 1047 (2019) 52–61.

[14] T. Górecki, X. Yu, J. Pawliszyn, Analyst 124 (1999) 643–649.

[15] J.M. Andrade, M.G. Estévez-Pérez, Anal. Chim. Acta 838 (2014) 1–12.

[16] N.H. Godage, E. Gionfriddo, Trac-Trends Anal. Chem. 111 (2019) 220–228.

[17] E. Sánchez-Palomo, R. Alonso-Villegas, M.A. González Viñas, Food Chem. 173 (2015) 1195–1202.

Section IV.2.1.4

Crosslinked functionalized polymeric ionic liquids-based capillary coatings in in-tube solid-phase microextraction coupled with high-performance liquid chromatography: application for the determination of DNA

In preparation for submission to Analytical and Bioanalytical Chemistry

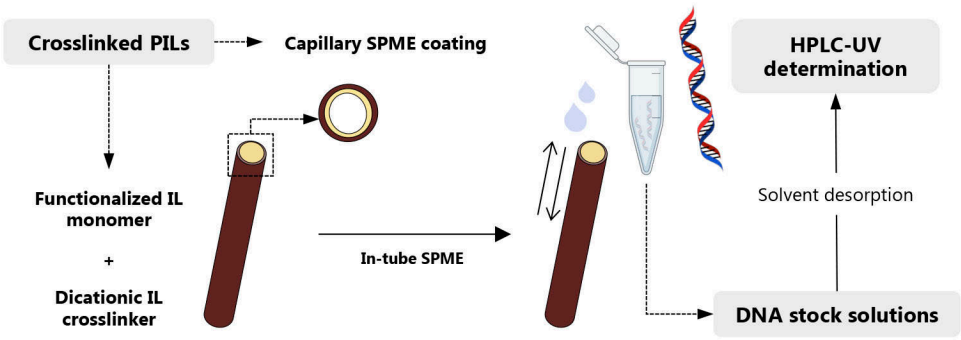

1. Determination of DNA by HPLC-UV-Vis

PILs-coated capillaries were evaluated in in-tube SPME for the extraction of DNA, as an alternative approach to the time-consuming, expensive, non-sustainable and non-reproducible conventional methods [1,2]. Among the two main modes of performing in-tube SPME, the draw/eject mode was selected considering the target application of this study, included within the clinical analysis field [3–5]. This mode can be carried out either by a manual or an automated set-up [3]. In this study, the manual approach was used to evaluate the extraction ability of the PILs-coated devices CAP-1 and CAP-2 (see Table III.2), while the automated set-up was developed to demonstrate the feasibility of using in-tube SPME as a routine method for the extraction and preconcentration of DNA.

As a proof of concept, DNA sodium salt from salmon testes was used as model DNA molecule. The amount of extracted DNA was determined by HPLC-UV-Vis following the conditions described in Section III.7.5.7 and using 260 nm as detection wavelength. Figure IV.41 shows a representative chromatogram obtained for the direct injection of the working solution, containing 5 $mg \cdot L^{-1}$ of DNA.

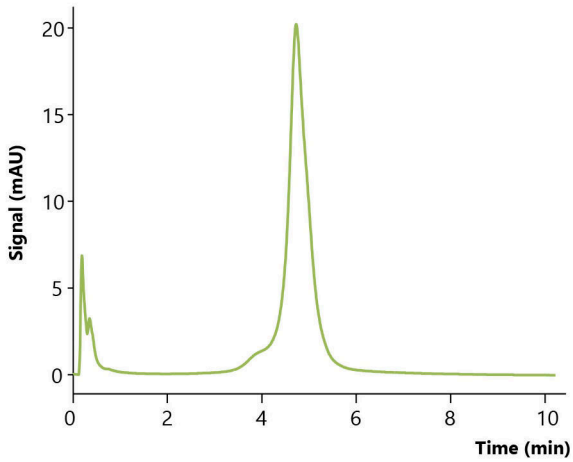

Figure IV.41. Representative chromatogram obtained injecting a 5 $mg \cdot L^{-1}$ DNA stock solution in 1X TE buffer at pH 8.

Two different HPLC systems were used depending on whether the manual (off-line) or the automated (on-line) method were used (see Section III.5.2). The chromatographic calibration curves were obtained in both instruments to quantify the extracted DNA and mainly to calculate the enrichment factor obtained with the proposed in-tube SPME methods. Table IV.59 lists several

quality analytical parameters, including linear range, calibration slope, determination coefficient (R^2) and the precision, evaluated as relative standard deviation (RSD, %).

Table IV.59. Several quality analytical parameters of the HPLC-UV-Vis method for the determination of DNA using different instruments.

HPLC mode	Linear range ($mg \cdot L^{-1}$)	(Slope ± t·SD[a])	R^2 [b]	$S_{y/x}$[c]	Intra-day RSD[d] (%) / Concentration ($mg \cdot L^{-1}$)
Manual	0.5–260	16.0 ± 0.3	0.999	32.4	6.0 / 13
Automated	1–100	6.9 ± 0.3	0.998	11.9	1.5 / 5

[a] 95 % confidence limits for n = 7 calibration levels (5 degrees of freedom).
[b] Determination coefficient.
[c] Error of the estimate (or standard deviation of the residuals).
[d] Intra-day relative standard deviation for the peak areas (n = 3).

Both calibration curves exhibited R^2 higher than 0.998 within the linear range studied: 0.5–260 $mg \cdot L^{-1}$ for the off-line mode, and 1–100 $mg \cdot L^{-1}$ using the HPLC equipped with the autosampler. With respect to the precision, it was evaluated by injecting standard solutions (prepared in 1X TE buffer at pH 8) containing the DNA at 13 $mg \cdot L^{-1}$ and 5 $mg \cdot L^{-1}$ for the off-line and on-line injection, respectively. As expected, the RSD was lower for the automated injection, with a value of 1.5 % in comparison with the RSD value of 6.0 % obtained for the manual injection.

2. Manual in-tube SPME using PILs-coated capillaries

Despite the draw/eject mode of in-tube SPME is commonly performed in an automated set-up, several studies have also used this approach in a manual configuration [6,7]. In this case, the capillary containing the sorbent material is coupled to a syringe, as it is schematically shown in Figure IV.42 A). Thus, the different steps of the extraction procedure are carried out by pulling back and pushing down the plunger of the syringe; with the flow depending on the operator, while the length of the capillary is limited since long capillaries are difficult to handle.

Therefore, 15 cm of the PILs-coated capillaries CAP-1 and CAP-2 were connected to a syringe using a borosilicate glass connection, as it can be observed in Figure IV.42 B). The glass connector is a leak-free connection usually employed to quickly couple two capillary GC columns, while a gas tight syringe was used to ensure accurate volumes as well as to avoid leaks in the system.

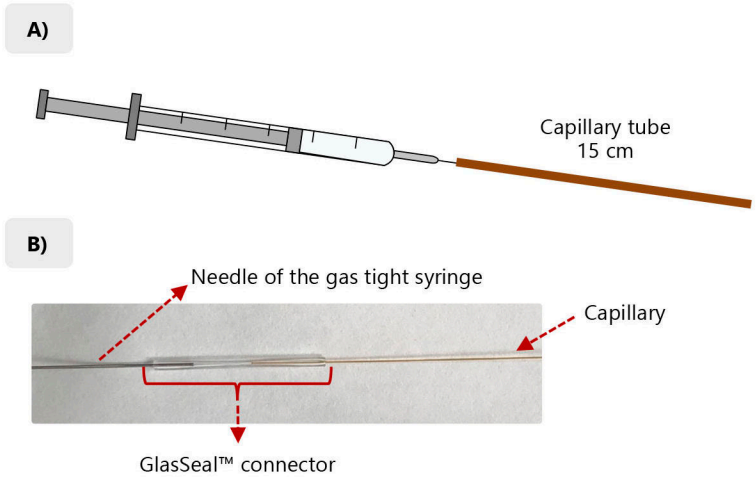

Figure IV.42. A) Schematic representation of the in-tube SPME set up in the manual draw/eject mode, and **B)** image showing the coupling of the SPME capillary to the syringe.

2.1. Optimization of extraction and desorption conditions

The in-tube SPME draw/eject mode consists of: (1) the loading step of the matrix to ensure trapping of the DNA by the coating of the in tube, (2) a washing step before the desorption to remove the interferences coming from the matrix, (3) the desorption step of the DNA, and (4) the regeneration step, to avoid carry-over effects and to ensure reusability of the coating. In this manual approach, the same volume of solution (not a fresh solution each time but the same solution) is drawn and ejected during the loading and desorption steps. Furthermore, several draw/eject cycles can be performed in each step. Each step was optimized in order to obtain the highest extraction efficiency, which was measured as the chromatographic peak area obtained for the DNA. A working solution in 1X TE buffer (pH 8) containing the DNA at 5 $mg \cdot L^{-1}$ was used during the one-factor-at-a-time optimization study, while each experiment was performed in triplicate.

The flow in the different steps was manually controlled at ≈ 600 $\mu L \cdot min^{-1}$, avoiding the formation of bubbles while being slow enough to guarantee the solutions are in contact with the PIL-based coating of the capillary during the draw/eject steps. For the washing and regeneration steps, similar conditions to those previously described with PILs-based SPME fibers for the extraction of DNA were used [8]. Thus, 1 draw/eject cycle of 100 µL of 1X TE buffer was used for the washing step. To sum up, 2 cycles of 250 µL of NaCl 1 M solution and 2 cycles of 250 µL of water (using a fresh solution in each cycle) were required in the regeneration step with the aim of avoiding carry-over.

With these fixed conditions, the composition of the desorption solution was optimized in order to ensure the complete elution of the DNA from the capillary. Previous studies using PILs-based SPME coatings have demonstrated that the addition of NaCl to the desorption solution resulted in a significant recovery of the extracted DNA [8,9]. This behavior agrees with the ion-exchange extraction mechanism reported for these coatings towards DNA [8]. Thus, in the loading step, the cationic PIL interacts with the negatively charged phosphate backbone of the DNA, while the chloride anions of the salt interact with the PIL framework and releases the DNA during the desorption step. Figure IV.43 shows a schematic representation of the mechanism that takes places during the extraction and desorption steps. Therefore, the NaCl concentration of the desorption solution (in ultrapure water) was evaluated between 0.5 and 2 M while employing 3 draw/eject cycles of working solution (100 µL) in the loading step and 5 draw/eject cycles of desorption solution (50 µL) in the desorption step. Figure IV.44 A) shows the results obtained for both capillaries. The highest peak area was obtained when using a NaCl concentration of 1 M during the desorption step. Lower concentration did not ensure the desorption of the DNA, while higher concentrations were not compatible with the HPLC column and led to poor chromatographic resolutions and determinations.

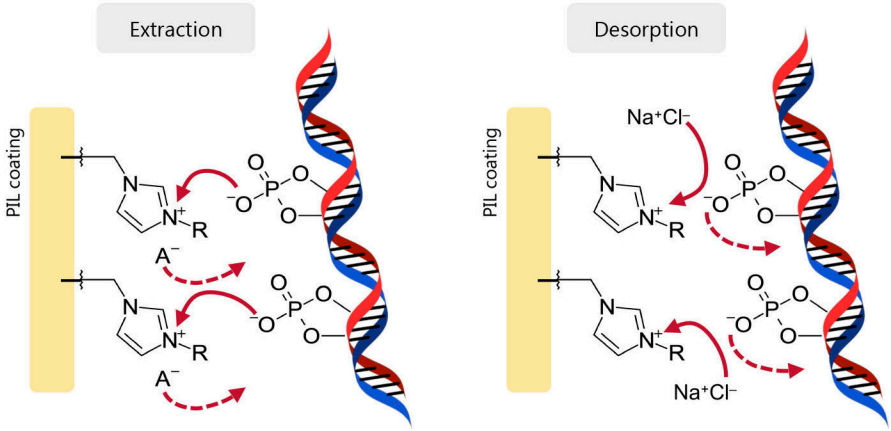

Figure IV.43. General scheme of the ion-exchange mechanism involved in the extraction and desorption of the DNA using the PIL-based coating. The solid arrows represent the interactions formed, while dotted arrows denote the release of the ionic species.

The loaded volume for the standard solution (and afterwards for the sample to be extracted), was evaluated between 150 and 500 µL. The maximum volume was limited by the total capacity of the syringe used to perform the in-tube SPME method. Higher extraction volumes lead

to higher amounts of DNA extracted, but it also increases the number of cycles required, the extraction time, and the extraction of interfering substances [4]. Figure IV.44 B) includes the results obtained for each PIL-coated capillary. In this case, the number of extraction draw/eject cycles was fixed at 1, while 5 draw/eject cycles of 50 µL of NaCl 1 M solution were used in the desorption step. As it can be observed, the equilibrium was reached when using 350 µL of loaded volume for the standard solution (sample) for both capillaries.

With respect to the number of draw/eject cycles, this parameter must be optimized since more cycles allow reaching the equilibrium while providing higher extraction efficiency [4]. Thus, the number of cycles during the loading step were increased from 1 to 10 using CAP-1 and CAP-2, while the desorption conditions were set at 5 draw/eject cycles of 50 µL of NaCl 1 M solution. Considering the results obtained, shown in Figure IV.44 C), 4 draw/eject extraction cycles using 350 µL of standard solution (sample) were selected for further experiments with both coatings.

With respect to the desorption conditions, desorption volumes lower than 350 µL were evaluated to ensure preconcentration. Despite the internal volume of the capillaries (15 cm) is ≈ 7 µL, volumes higher than 50 µL were studied since the volume of the injection loop in the HPLC system is 20 µL. In this case, the number of draw/eject desorption cycles was fixed at 5. As it can be observed in Figure IV.44 D), the highest peak area was obtained using 50 µL of desorption solution, while higher volumes significantly decreased the extraction performance, mainly due to the low preconcentration.

Finally, the number of draw/eject desorption cycles is one of the most important parameters to optimize since it ensures the total desorption of the DNA, maximizes the extraction efficiency, and minimizes the carry-over effects. Thus, it was studied between 3 and 20 cycles until the equilibrium was reached, as it is depicted in Figure IV.44 E). The best results were obtained when using 10 cycles for CAP-1 and 15 cycles for CAP-2. Increasing the number of desorption cycles provided slightly lower peak areas, maybe due to the re-extraction of the DNA by the PIL coating.

As it can be observed in all the studies performed during the optimization, the CAP-2 containing the IL monomer functionalized with the carboxylic group (see Table III.2) provided the highest peak area. Moreover, a RSD value of 8.5 % was obtained under optimum conditions, which is adequate considering the manual operating of the in-tube SPME method and the manual injection in the HPLC system.

The enrichment factor with this PIL-coated capillary was estimated as the ratio between the predicted concentration calculated using the peak area obtained with the manual in-tube SPME-HPLC-UV-Vis method but using the chromatographic calibration curve (Table IV.59). Thus, an enrichment factor of only 0.4 was obtained with CAP-2. This value can be improved by using longer capillaries [4]. Therefore, this PIL-coated capillary was used for the development of an automated in-tube SPME method, which not only will allow the use of longer extraction devices but also will upgrade the extraction efficiency, simplicity and precision of the method.

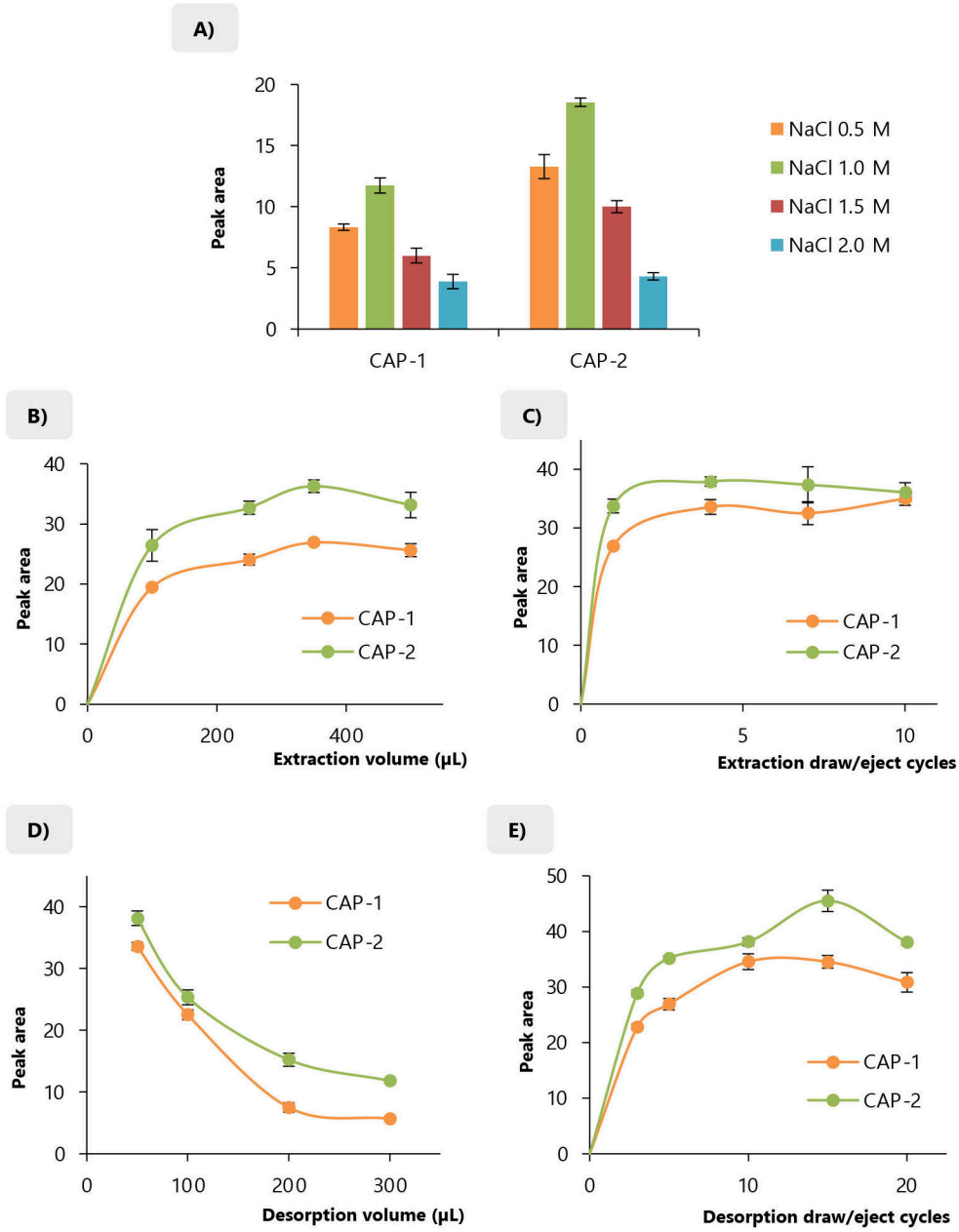

Figure IV.44. Influence of **A)** NaCl concentration of the desorption solution, **B)** loaded volume of sample/standard solution, **C)** number of extraction draw/eject cycles, **D)** desorption volume, and **E)** number of desorption draw/eject cycles in the manual in-tube SPME method using both CAP-1 and CAP-2. The experimental conditions are detailed in the text. Experiments were performed in triplicate.

3. Automated in-tube SPME using functionalized PIL-coated capillary

In the automated in-tube SPME set-up, the extraction capillary is placed between the sampling needle and the loop of a HPLC autosampler, as it is schematically shown in Figure IV.45 A) [10]. The main advantage of this approach is that it is fully automated. It only requires the design of the injection sequence including all the steps using the autosampler software. Furthermore, this mode allows controlling the draw/eject flow, which is an important parameter influencing the performance of the in-tube SPME method [4]. Moreover, the length of the capillary could be increased to 55 cm, which will also contribute to improve the extraction efficiency of the method.

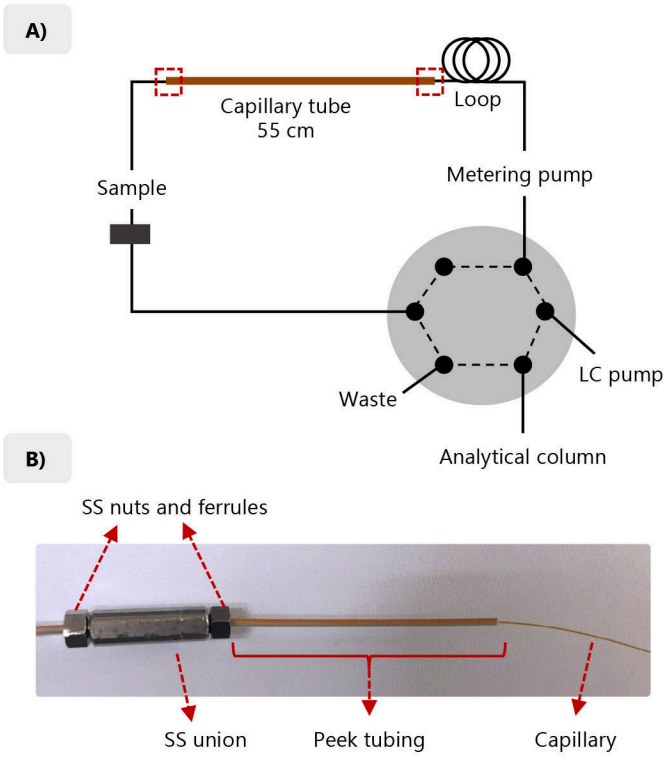

Figure IV.45. A) Schematic representation of the in-tube SPME set up in the automated draw/eject mode using the HPLC autosampler, and **B)** image showing the connections system used to couple the SPME capillary to the HPLC autosampler.

The coupling of the CAP-2 capillary in the HPLC autosampler was carried out using a stainless steel union between the sampling needle and the capillary, and another union between

the capillary and the injection loop. They were connected with the aid of stainless steel nuts and ferrules, as it is shown in Figure IV.45 B). The ends of the capillary were also placed inside a PEEK tubing to avoid the damage of the capillary and to ensure a leak-free system. The injection loop of the HPLC autosampler was kept in the system to protect the metering pump of the autosampler from contamination [4].

3.1. Optimization of extraction conditions

The steps of the automated in-tube SPME method are the same as those of the manual approach: (1) loading (extraction), (2) washing, (3) desorption, and (4) regeneration. The main difference lies in the desorption step. In this case, the DNA is desorbed by passing the mobile phase through the capillary, which is then directly injected in the analytical column [4]. Thus, the initial mobile phase composed of 20 mM of Tris-HCl at pH 8 and 20 mM of Tris-HCl and 1 M of NaCl at pH 8 (50:50, v/v) was used for the desorption during 5 min. After this time, the injection valve was changed to the bypass mode and the autosampler started the sequence for the regeneration of the PIL-based coating. This time was enough to ensure the desorption of the DNA, while longer times caused peak broadening and tailing.

With respect to the washing steps, the same conditions as in the manual mode were employed. Thus, 1 draw/eject cycle with 100 µL of 1X TE buffer was used, while 2 cycles of 100 µL of NaCl 1 M solution and 2 cycles of 250 µL of water (using fresh solution in each cycle) were enough to avoid carry-over effects and to ensure proper regeneration.

Thanks to the automation, it is possible to control the flow during the draw and eject steps. This advantage, together with the use of longer capillaries, allows the analysis of larger volumes in comparison with the manual mode. Thus, during the loading (extraction) step, a specific volume of the standard solution (or sample) is drawn and ejected several times to the same sample vial. Since the controlled ejection also acts as a form of agitation, in every draw/eject cycle, a fresh portion of working standard solution (or sample) is passed through the capillary. In this case, the volume of the working standard solution was fixed at 1 mL. Therefore, only the remaining parameters affecting the loading (extraction) step were optimized.

The extraction volume was evaluated between 40 and 100 µL, which are the internal volume of the capillary (≈ 30 µL) and the maximum volume of the loop, respectively. The flow rate was set at 100 $\mu L/min^{-1}$, while 5 draw/eject cycles were used during these experiments. As it can be observed in Figure IV.46 A), the higher the volume passed through the capillary, the higher the peak area obtained for the DNA. Thus, 100 µL was selected as extraction volume.

The draw/eject flow was also optimized, ranging between the minimum and maximum values established by the autosampler software. In these experiments, 5 draw/eject extraction cycles were used. Slow flows ensure a longer contact between the working solution and the sorbent coating. However, high flows also improve the agitation of the working solution in the ejection

step and reduce the extraction time. As it is shown in Figure IV.46 B), using flows faster than 200 $\mu L \cdot min^{-1}$ led to a decrease on the extraction efficiency, maybe due to the formation of bubbles during the draw and eject steps. Thus, this value was selected as optimum value for further experiments. Finally, the number of draw/eject cycles during the loading (extraction) step was also optimized, reaching the equilibrium after 20 cycles, as it is shown in Figure IV.46 C).

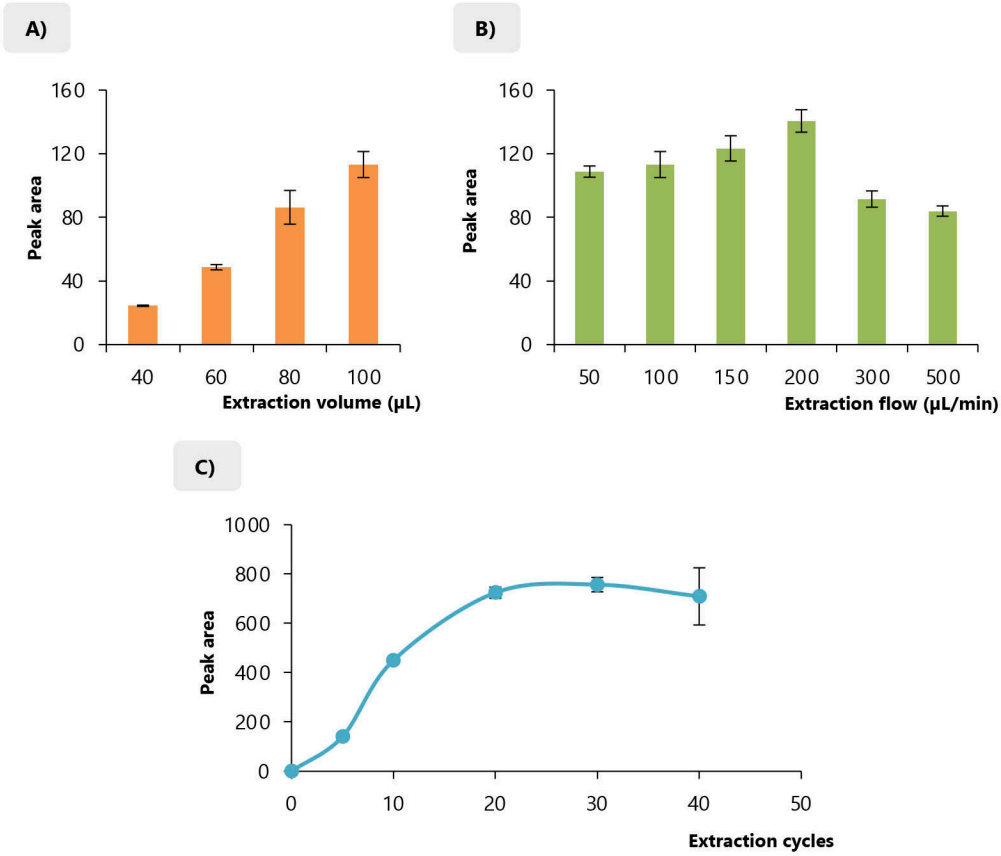

Figure IV.46. Influence of **A)** loading (extraction) volume, **B)** extraction flow, and **C)** number of extraction draw/eject cycles in the automated in-tube SPME method using CAP-2. The experimental conditions are detailed in the text. Experiments were performed in triplicate.

Under optimum conditions, the RSD value after performing the in-tube SPME method using the CAP-2 and a DNA standard solution at 5 $mg \cdot L^{-1}$ was 3.1 %, which is lower than the precision achieved with the manual mode. Furthermore, the enrichment factor was also calculated using the

chromatographic calibration curve obtained with the automated injection (Table IV.59) and the peak area obtained for the DNA with the automated in-tube SPME HPLC-UV-Vis method. Thus, the enrichment factor was 20 using the CAP-2 PIL-based coating, which is highly noticeable for a DNA extraction method.

4. Comparison amongst in-tube SPME methods and on-fiber SPME

The main characteristics of the developed manual and automated in-tube SPME methods are summarized in Table IV.60. If the performance of both methods is compared, it is clear that the automated method exhibits better results in terms of preconcentration and precision. Thus, the automated in-tube SPME approach provided much higher enrichment factors, with a value of 20. Indeed, preconcentration could not be achieved with the manual mode, since an enrichment factor of 0.4 was obtained. This is mainly due to the amount of sorbent coating or length of the capillary, which is of 15 cm and 55 cm for the automated and manual mode, respectively. The extraction time of both methods was ≈ 20 min, but the precision obtained with the automated approach was better, and a lower RSD value was obtained. Therefore, increasing the length of the capillary and automating the procedure of the in-tube SPME method leads to promising results for the extraction of DNA.

Table IV.60 also includes the characteristics of the on-fiber SPME method previously reported for the extraction of DNA [8]. In that study, the same PIL-based coating was used but in a different SPME configuration: $[VC_{9COOH}Im^+][Br^-]$ as IL monomer and $[(VIm)_2C_{12}^{2+}]2[Br^-]$ as IL crosslinker. Despite the thickness of the fiber (≈ 69 µm) is much higher than that of the PIL-coated capillary prepared in this Doctoral Thesis (≈ 0.5 µm), the length of the SPME device for the in-tube SPME method is larger (1 cm *versus* 15 or 55 cm). Thus, the surface area of the coating for the capillaries is from 14 to 50 times higher in comparison with the PIL-coated fiber. Therefore, the analysis time can be drastically reduced with the in-tube SPME strategy. Indeed, the on-fiber SPME method required 30 min for the extraction, 30 min for the desorption, and 25 min for the washing step prior to the next extraction. However, in this study, all the steps were performed in only ≈ 20 min. Moreover, the enrichment factor with the PIL-coated SPME fiber was not considered or reported [8], while in this study, an enrichment factor of 20 was obtained following a fully automated strategy.

All these results demonstrate the advantages and potential of the in-tube SPME mode over the on-fiber SPME method for the extraction and preconcentration of DNA. It is simple, fast, fully automated, efficient, it does not require the use of organic solvents, and allows the reusability of the device, since each capillary could be used for ≈ 80 extraction cycles without losing extraction capability. Ongoing work focuses on evaluating the matrix effect of the automated in-tube SPME method using CAP-2 as extraction device, applying the method for the analysis of samples and studying the possibility of coupling the proposed method with other DNA determination techniques, such as PCR.

Table IV.60. Comparison of the in-tube SPME methods using the CAP-2 in terms of size of the coating, analysis time, precision and preconcentration, together with an on-fiber SPME application using the same PIL as coating.

Characteristic	Manual in-tube SPME	Automated in-tube SPME	On-fiber SPME[a]
Coating size (length × thickness)	15 cm × ≈ 0.5 µm	55 cm × ≈ 0.5 µm	1 cm × ≈ 69 µm
Surface area of the coating	117 mm^2	430 mm^2	8.3 mm^2
Volume of sample	350 µL	1 mL	1.5 mL
Loading/Extraction volume	350 µL	100 µL	1.5 mL
Extraction cycles	4	20	–
Desorption	NaCl 1 M	Mobile phase[b]	NaCl 1 M
Desorption volume	50 µL	–	50 µL
Desorption cycles	15	–	–
Draw/eject flow – agitation	≈ 600 $\mu L \cdot min^{-1}$	350 $\mu L \cdot min^{-1}$	650 min^{-1}
Total extraction time[c]	≈ 20 min	≈ 20 min	≈ 85 min
Precision (RSD)	8.5 %	3.1 %	4.6 %
Enrichment factor	0.4	20	n.r.

[a] Application reported by Nacham *et al.* [8] using the same PIL as coating.
[b] Composed of 20 mM of Tris-HCl at pH 8 and 20 mM of Tris-HCl and 1 M of NaCl at pH 8, with an initial composition of 50:50 (v/v).
[c] Total time including extraction, desorption and washing steps
n.r.: not reported

REFERENCES

[1] M.M. Rahman, A. Elaissari, Drug Discov. Today 17 (2012) 1199–1207.

[2] M.N. Emaus, M. Varona, D.R. Eitzmann, S.-A. Hsieh, V.R. Zeger, J.L. Anderson, Trac-Trends Anal. Chem. 130 (2020) 115985.

[3] M.E.C. Queiroz, I.D. de Souza, C. Marchioni, Trac-Trends Anal. Chem. 111 (2019) 261–278.

[4] M. Fernández-Amado, M.C. Prieto-Blanco, P. López-Mahía, S. Muniategui-Lorenzo, D. Prada-Rodríguez, Anal. Chim. Actta 906 (2016) 41–57.

[5] N. Manousi, P.D. Tzanavaras, C.K. Zacharis, Molecules 25 (2020) 2096.

[6] I.D. de Souza, L.P. Melo, I.C.S.F. Jardim, J.C.S Monteiro, A.M.S. Nakano, M.E.C. Queiroz, Anal. Chim. Acta 932 (2016) 49–59.

[7] M.J. Trujillo-Rodríguez, I. Pacheco-Fernández, I. Taima-Mancera, J.H. Ayala, V. Pino, J. Chromatogr. A 1634 (2020) 461670.

[8] O. Nacham, K.D. Clark, J.L. Anderson, Anal. Chem. 88 (2016) 7813–7820.

[9] O. Nacham, K.D. Clark, J.L. Anderson, Anal. Methods 7 (2015) 7202.

[10] Y. Moliner-Martínez, R. Herráez-Hernández, J. Verdú-Andrés, C. Molins-Legua, P. Campíns-Falcó, Trac-Trends Anal. Chem. 71 (2015) 205–213.

Section IV.2.2.

Metal-organic frameworks as new porous solid-phase microextraction coatings with anti-fouling characteristics

The fouling of the sorbents caused by the matrix components is the main limitation of SPME fibers when dealing with the analysis of complex samples. Thus, the development of matrix compatible SPME coatings is an important research line to expand the applications of SPME for environmental, food and biological analyses. Despite porous coatings are more adequate for the extraction of low-molecular weight compounds at trace levels, they are susceptible to fouling and still require the incorporation of a polymer within the coating to obtain a stable sorbent phase. Therefore, the preparation of completely porous coatings with adequate stability to perform in complex samples, which is of special interest for certain SPME applications, is still a challenging task in the field.

Among the porous materials explored as SPME coatings, MOFs stand out due to their exceptional surface area, synthetic versatility, and high thermal stability. However, there are only a few studies reporting the analysis of complex samples (different from water) using MOFs coatings either in HS-SPME or DI-SPME. Indeed, most of these MOF-based phases are mixed coatings, in which the MOF is embedded in a polymeric matrix or it is combined with other hydrophobic materials. Moreover, in those studies using neat MOFs or hybrid coatings, the samples still require a pretreatment step using organic solvents.

The aim of this section is the preparation of a neat MOF-based SPME fiber coating based on the MOF CIM-80(Al) with improved stability and anti-fouling characteristics, able to successfully perform with complex samples. The analytical performance of the coating in both HS- and DI-SPME methods coupled to GC-MS was evaluated for the determination of PAHs as model compounds. Moreover, in order to prove its suitability for different SPME applications, the analytical performance was also assessed in urine and brewed coffee samples, and thoroughly compared with a commercial SPME fiber.

Section IV.2.2.1

Characterization of the CIM-80(Al) metal-organic framework-based solid-phase microextraction fiber coating

Analytica Chimica Acta 1133 (2020) 137–149

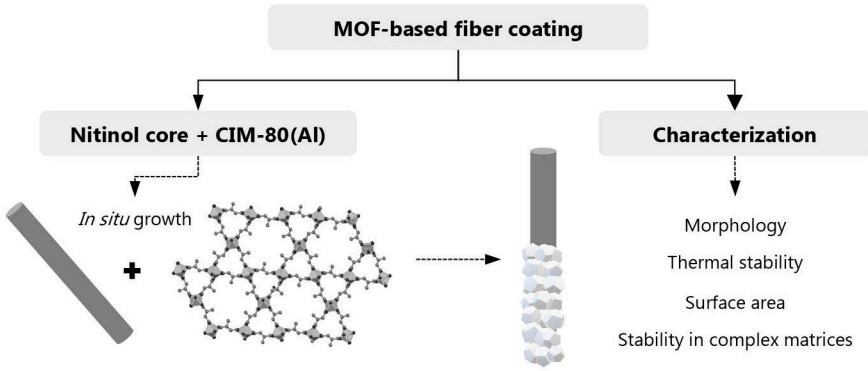

1. Characterization of the CIM-80(Al) MOF-based SPME fiber coating

A MOF-based SPME coating was evaluated in HS- and DI-SPME methods. The fiber was prepared by the immobilization of the neat MOF CIM-80(Al) on the surface of nitinol wires by the *in situ* growth method, without the need of glues or any additional material to ensure the attachment of the MOF to the support, as it was described in Section III.7.2.1 [1]. This composition was selected given the green features associated to its components: the CIM-80(Al) MOF is prepared in an aqueous media at moderate temperatures and it is characterized by a low cytotoxicity [2], while the nitinol support is labelled as biocompatible material [3].

The adequate synthesis of the CIM-80(Al) MOF on the surface of the nitinol fibers was assessed by PXRD. Figure IV.47 A) shows the theoretical PXRD pattern for the MOF [2] together with the patterns obtained after the direct measurement of the coated fiber, the coating scrapped from the fiber, and the excess of MOF in the reactor after fiber preparation. Moreover, the PXRD pattern of the MOF obtained in a regular synthesis is also included for comparison purposes.

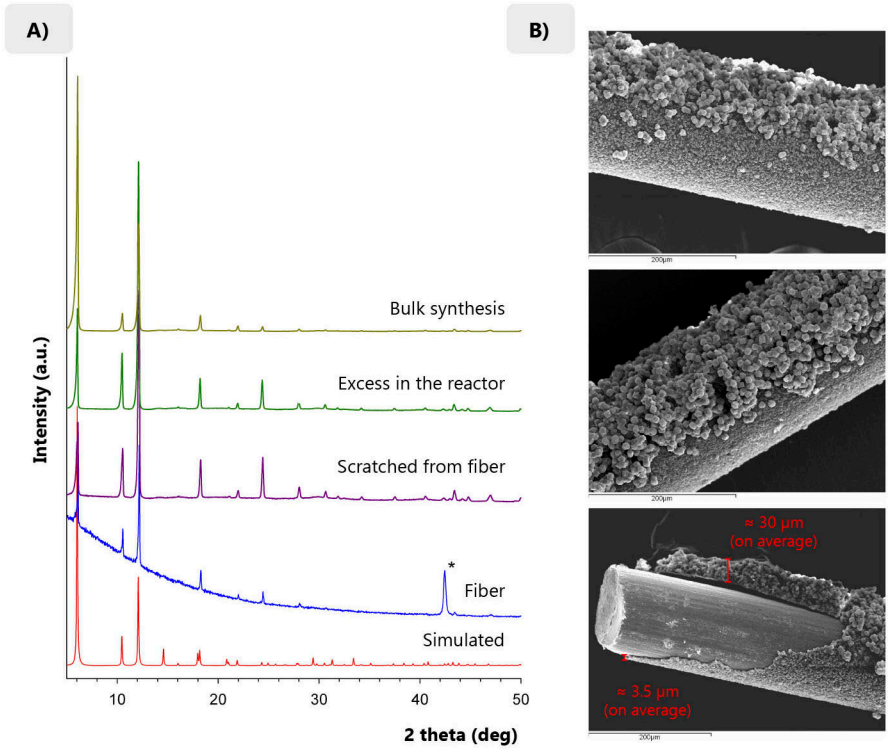

Figure IV.47. A) PXRD patterns for the MOF-coated fiber, the coating scrapped from the fibers, the excess of MOF in the reactor after the preparation of the fibers, and the MOF obtained in a regular synthesis compared with the CIM-80(Al) theoretical pattern. (*) This peak comes from the nitinol fiber **B)** SEM images of CIM-80(Al) fibers obtained from three different batches.

All the peaks corresponding to the CIM-80(Al) crystal phase are observed in the patterns associated to the *in situ* synthesis on the fiber support, which confirms the correct formation of the MOF. In addition, the pattern of the coated fiber shows a peak at around 45° that corresponds to the nitinol core of the fiber [4]. It is important to note that MOF-based SPME fibers from literature scarcely show the PXRD of the coated fiber or that of the scrapped coating material.

Regarding the surface morphology and uniformity of the CIM-80(Al) coating, it was characterized by SEM. As shown in Figure IV.47 B), the fibers were homogenously coated with a first layer of CIM-80(Al) crystals with a thickness around 3.5 μm, and half of the fiber was also coated with a thicker coating of approximately 30 μm (estimated by measuring and averaging the thicknesses of different fibers). Despite the asymmetry of the coating, this growing behavior was observed every time the fibers were prepared with the proposed method (see Section III.7.2.1). Indeed, Figure IV.47 B) includes SEM micrographs of several fibers from different synthetic batches, for which the same coating morphology was obtained. The volume of the CIM-80(Al) coating was estimated to be roughly 0.1 μL. As a comparison, the volume for commercial PDMS is 0.66 μL and for PA is 0.52 μL.

2. Stability assessment of the CIM-80(Al) MOF

Figure IV.48 A) includes the TGA profile of the synthesized MOF, where it can be observed a weight loss below 100 °C, which corresponds to the loss of crystallization water molecules. After that temperature, the MOF does not exhibit any process up to 400 °C, thus demonstrating its high thermal stability. These results agree with those reported for previous characterization data for this material [2,5]. However, it is important to point out that the thermal stability of the MOF ranges from 350 to 400 °C depending on the technique used for this determination, which is closely related to the way the heating is applied [2,5]. Considering these results, high temperatures can be used for the desorption step of the fiber in GC. Furthermore, Figure IV.48 B) shows the N_2 isotherm plot obtained for the MOF CIM-80(Al), which yields a BET surface area of 884 $m^2 \cdot g^{-1}$, a similar value to that previously reported for this MOF [2].

In order to evaluate the possibility of using the fiber coated with the CIM-80(Al) for the analysis of more complex samples and in DI-SPME applications, the stability of the MOF was assessed in different matrices. The PXRD patterns for the MOF powder after being in contact with hot deionized water (100 °C) refluxing for 24 h, diluted urine, diluted coffee deionized water, tap water, whole milk, white and red wine, and apple juice, for 24 h and 10 days, are included in Figure IV.49. It can be observed that the patterns for the MOF immersed during 24 h in the samples were the same as the pattern for the bulk synthesis of the MOF (Figure IV.49 A)), even in non-diluted complex samples, such as red wine and milk samples. Interestingly, when the experiments were performed using a longer contact time (10 days, Figure IV.49 B)), the MOF kept maintaining its crystallinity, except for the whole milk matrix. Milk presents a complex composition, including a high fat content and other nutritional components that may have a strong effect on the material,

leading to the modification of its structure after 10 days of contact. Moreover, a previous study in the literature has shown the stability of this MOF after being immersed in aqueous solutions at pH 1, 5 and 10 for 7 days [2]. These results suggest that this coating can be used (and reused) for the analysis of water and other aqueous-based complex samples in DI mode without losing its crystalline structure despite long extraction times.

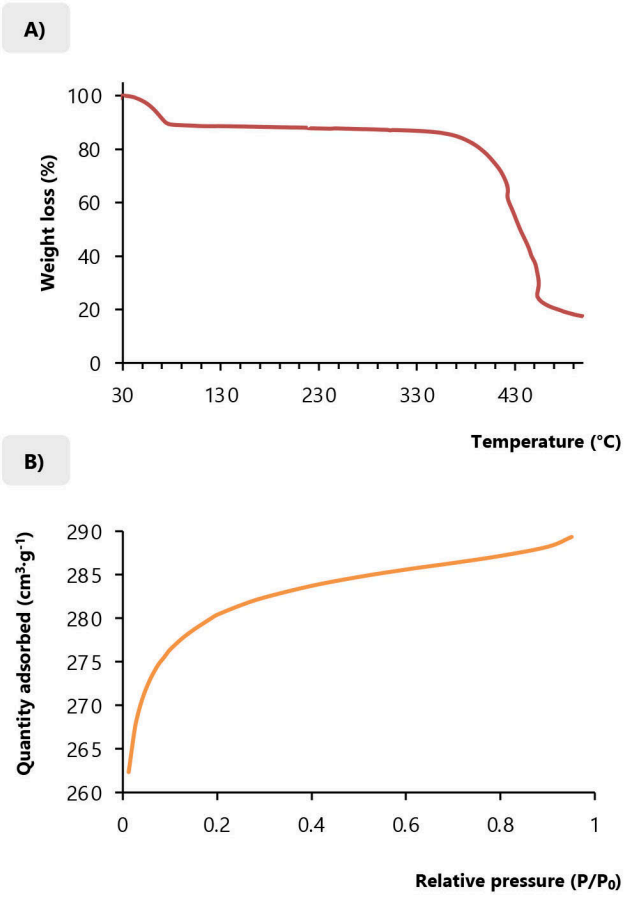

Figure IV.48. A) TGA profile and **B)** N_2 adsorption isotherm plot for the CIM-80(Al) obtained in the bulk synthesis.

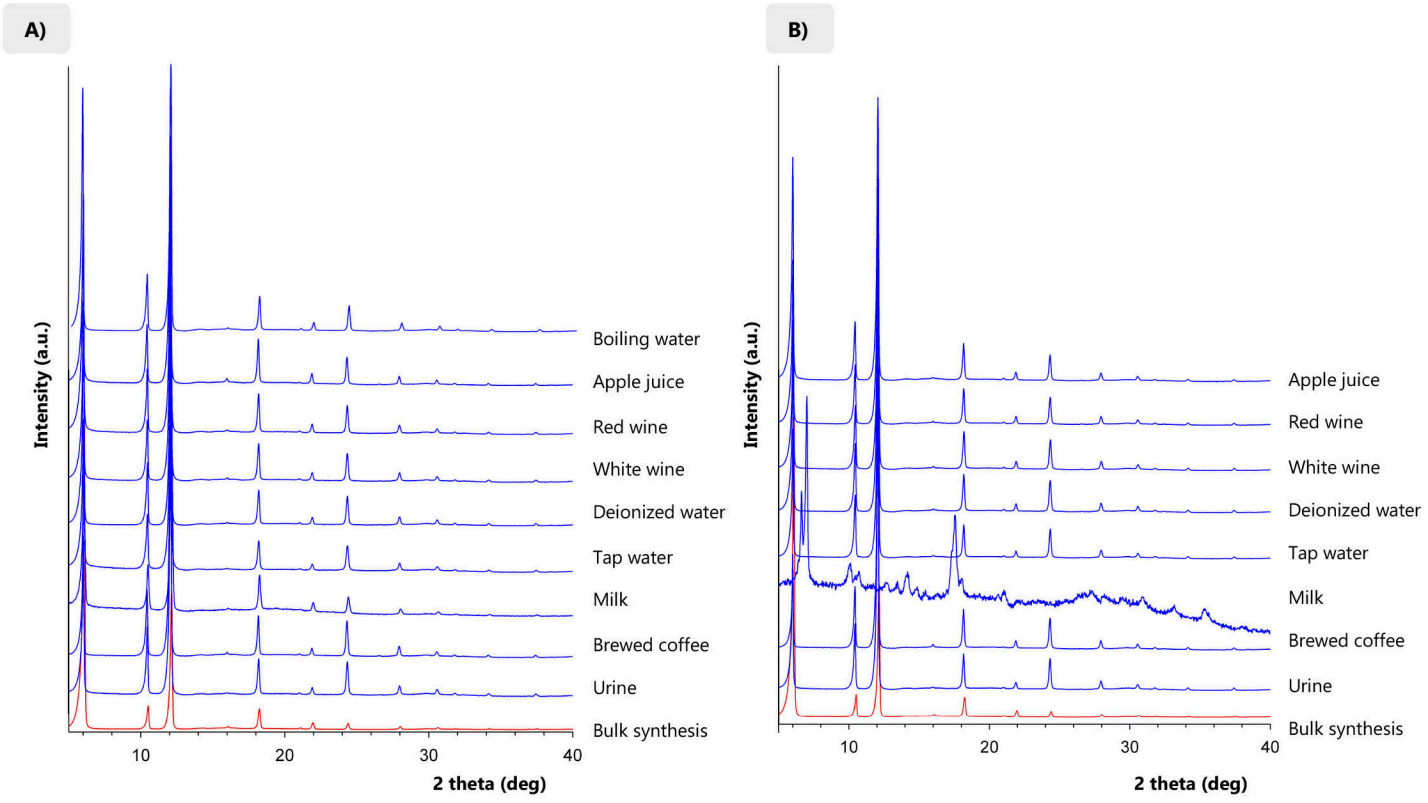

Figure IV.49. PXRD pattern for the CIM-80(Al) obtained in the bulk synthesis compared with the PXRD patterns for the MOF after being immersed in different matrices for **A)** 24 h and **B)** 10 days. Brewed coffee and urine matrices were diluted with ultrapure water (1:10).

REFERENCES

[1] I. Pacheco Fernández, J. Pasán García, V. Pino Estévez, P. Rocío Bautista, A.M. Afonso Perera, J.H. Ayala Díaz, C. Ruiz Pérez, Spain Patent Application No. P201900092 (2019).

[2] P. Rocío-Bautista, V. Pino, J.H. Ayala, C. Ruiz-Pérez, O. Vallcorba, A.M. Afonso, J. Pasán, RSC Adv. 8 (2018) 31304–31310.

[3] J. Ryhänen, Minim. Invasive Ther. Allied Technol. 9 (2000) 99–105.

[4] J.M. McNaney, V. Imbeni, Y. Jung, P. Papadopoulos, R.O. Ritchie, Mech. Mater. 35 (2003) 969–986.

[5] H. Reinsch, T. Homburg, N. Heidenreich, D. Fröhlich, S. Hennninger, M. Wark, N. Stock, Chem.-Eur. J. 24 (2018) 2173–2181.

Section IV.2.2.2

CIM-80(Al) metal-organic framework-based fiber coating in direct-immersion and headspace solid-phase microextraction coupled with gas chromatography: application for the determination of polycyclic aromatic hydrocarbons in water, urine and brewed coffee

Analytica Chimica Acta 1133 (2020) 137–149

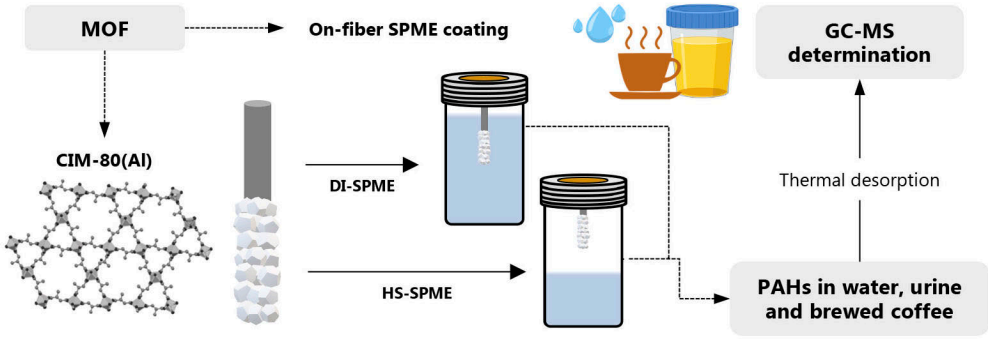

1. Screening of commercial and MOF-based SPME fibers for the extraction of PAHs

The CIM-80(Al) SPME coating was evaluated in HS- and DI-SPME applications using different aqueous samples. PAHs were used as model compounds since the main goal of this section is to demonstrate the suitability of this porous coating for the analysis of complex samples.

First, the fiber was tested in a HS-SPME-GC-MS method under random preliminary conditions together with other commercial SPME coatings to evaluate the extraction capacity of the sorbent. The extractions (in triplicate) were performed at 75 °C for 60 min with a stirring rate of 300 min^{-1} and using 10 mL of aqueous standard solution containing 20 % (w/v) of NaCl and 50 $\mu g \cdot L^{-1}$ of each of the 13 PAHs: Nap, Acy, Ace, Flu, Phe, Ant, Flt, Py, BaAnt, Chry, BbFlt, BkFlt, and BaPy. These random extraction conditions were kept the same for all fibers, whereas desorption was accomplished for 4 min at different temperatures depending on the fiber (see Section III.7.5.8). Table IV.61 includes the MS program used for the identification and quantification of the PAHs in the SIM acquisition mode, together with the retention times for each analyte.

The peak area obtained for the tested PAHs was used as a tool to compare the extraction efficiency of the different coatings, as shown in Figure IV.50. Both PDMS and MOF-based fibers are the most suitable ones, showing significant extraction capacity for the entire group of PAHs in comparison with the remaining fibers. These results turn out to be interesting considering the different nature of both coatings (liquid polymer and porous material, respectively) and the extraction mechanism involved in the extraction procedure for both materials, mainly absorption for PDMS and adsorption for the MOF sorbent [1]. Regarding the commercial CAR/PDMS and DVB/CAR/PDMS fibers, which contain porous materials in a PDMS matrix, they exhibited better extraction performance for the lighter analytes (Nap, Acy and Ace), which may be associated to the porosity and adsorption extraction mechanism of CAR sorbents [2]. However, the extraction capacity of these coatings decreased as the molecular weight and size of the analytes increased, yielding poor results for the heaviest 4-ring and 5-ring PAHs.

The different behavior between the MOF-based coating and the porous commercial fibers may be related to the ordered framework and small size of the pores of the MOF, which presents pore diameters of 2 and 6 Å, and volume of micropore of 0.46 $cm^3 \cdot g^{-1}$ [3]. These micropores are much smaller than those described for CAR or DVB, which exhibit not only micropores with a volume of 0.11 and 0.29 $cm^3 \cdot g^{-1}$, respectively, but also macro- and mesopores in their structures [1]. The small size of the ordered pores (lower than 10 Å) in the MOF coating may lead to capillary condensation, phenomenon for which the molecules condense into the pores and increase the sorption capacity of the porous sorbent [2]. Furthermore, it is also important to point out the high BET surface area of the MOF CIM-80(Al), which is similar or higher than those reported for DVB and CAR materials, which have values of 750 and 950 $m^2 \cdot g^{-1}$, respectively [1].

Table IV.61. Program used during the SIM acquisition in the GC-MS for the identification and quantification of the PAHs, together with the retention time and characteristic ions for each analyte.

Segment	Time (min)	Ions	PAH	Retention time ± SD[a] (min)	Quantifier ion (m/z)	Qualifier ion (m/z)
1	5.0	127, 128, 129	Nap	6.12 ± 0.02	128	129
2	9.0	151, 152, 153	Acy	10.8 ± 0.1	152	153
3	11.3	152, 153, 154	Ace	11.9 ± 0.1	153	154
4	14.0	165, 166, 167	Flu	15.2 ± 0.1	166	165
5	18.0	176, 178, 179	Phe	20.1 ± 0.1	178	176
			Ant	20.4 ± 0.1	178	179
6	24.0	200, 202, 203	Flt	27.49 ± 0.07	202	203
			Py	28.35 ± 0.07	202	203
7	31.0	226, 228, 229	BaAnt	33.35 ± 0.03	228	226
			Chry	33.54 ± 0.02	228	226
8	38.0	250, 252, 253	BbFlt	40.48 ± 0.02	252	253
			BkFlt	40.70 ± 0.02	252	253
			BaPy	41.96 ± 0.02	252	253

[a] Standard deviation (n = 20).

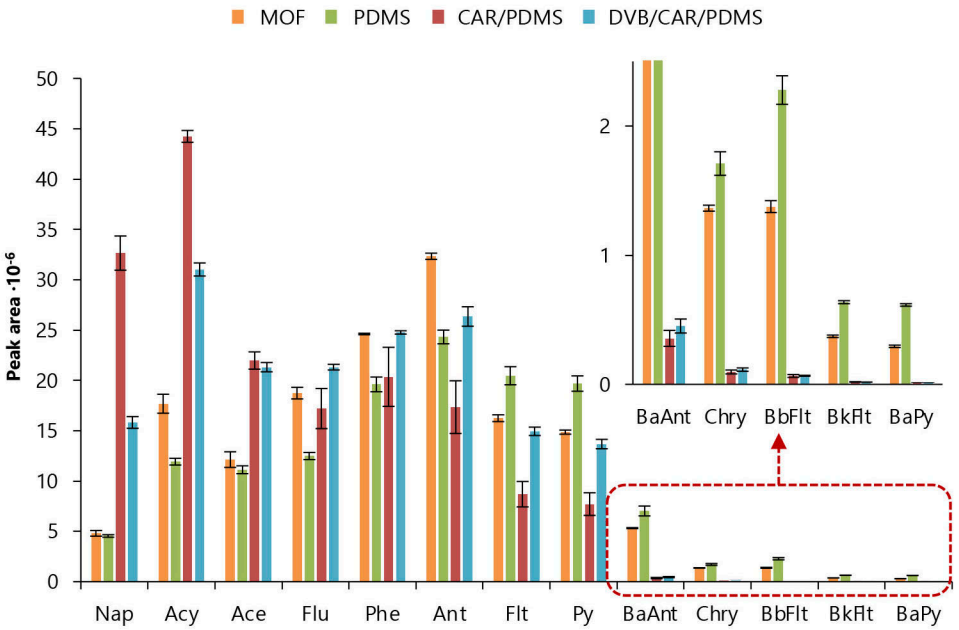

Figure IV.50. Extraction efficiency (as peak area) obtained for the studied PAHs using the MOF-based and commercial fibers in a HS-SPME-GC-MS method under preliminary random conditions: 10 mL of aqueous standard at 50 $\mu g \cdot L^{-1}$ of each PAH, containing 20 % (w/v) of NaCl, using 60 min of extraction at 75 °C and 300 min^{-1} of stirring rate, and desorption for 4 min at 270 °C for DVB/CAR/PDMS, 280 °C for PDMS and MOF-based fiber, and 310 °C for CAR/PDMS. The extractions were performed in triplicate.

Among the results obtained using the commercial polymeric PDMS (coating volume of 0.66 µL) and the lab-made porous MOF-based fiber (coating volume of ≈ 0.1 µL), it is interesting to highlight that the MOF coating exhibited better extraction performance for the 2- and 3-ring PAHs, while the peak areas obtained for the remaining analytes were slightly higher for the PDMS fiber. Based on these results, the commercial PDMS fiber was selected for a further comparative study with the prepared MOF-based fiber, in which HS- and DI-SPME methods were optimized and validated with both fibers.

2. Optimization of the SPME methods using MOF-based and PDMS fibers

Both HS- and DI-SPME methods were optimized for the prepared MOF-based and the commercial PDMS fibers by a simple one-factor-at-a-time approach. The optimization study was carried out in combination with GC-FID, using the chromatographic conditions described in

Section III.7.5.8. The carry-over effect was optimized using GC-MS to take advantage of its higher sensitivity achieved and considering that GC-MS will be used during the validation of the method. The extraction efficiency (as peak area) was evaluated for 8 representative PAHs at 100 $\mu g \cdot L^{-1}$: Nap, Acy, Ace, Flu, Phe, Ant, Flt, and Py. Different parameters were evaluated depending on the SPME mode, including ionic strength of the solution, stirring rate during extraction, extraction time and temperature, and desorption time and temperature. The pH of the sample was not assessed during the optimization study given the non-ionizable nature of the PAHs.

2.1. Optimization of the HS-SPME method

One of the most important features of a SPME coating for GC applications is the maximum operating temperature used for the desorption of the analytes. The maximum working temperature for most of the commercial SPME fibers is between 280 °C and 320 °C depending on the nature of the coating [4]. Thus, the performance of the MOF-based fiber was evaluated at these two temperature values. As shown in Figure IV.51 A), there was not significant differences between the two desorption temperatures for Nap, Acy and Ace, while higher peak areas were obtained for the heaviest PAHs when using 320 °C for the desorption. Despite 320 °C is below the maximum temperature stability range reported for the CIM-80(Al) [3,5], the strong heating at which the coating is subjected in the GC inlet may lead to the decomposition of the sorbent and the subsequent decrease of the lifetime of the fiber. Therefore, with the aim of extending the lifetime of the fiber, 280 °C was selected as desorption temperature in the next experiments, which is also the maximum operating temperature for the PDMS fiber (100 µm of thickness) used in this study. Moreover, significantly carry-over effects were not observed for any of the fibers once they were left at 280 °C for additional 5 min in the GC inlet after each extraction, as representatively shown in Figure IV.52.

In the HS-SPME mode, the salting-out effect is commonly used to reduce the solubility of the analytes in the aqueous sample, thus increasing their concentration in the HS and, therefore, improving the extraction efficiency of the method [6]. The results included in Figure IV.51 B) shows that the peak area of the analytes increased as the ionic strength of the sample solution increased up to 20 % (w/v) of NaCl. Therefore, this concentration of NaCl was used for both PDMS and MOF-based fibers in subsequent experiments.

Regarding the extraction temperature in HS-SPME applications, it is important to increase the temperature to enhance the transfer of the analytes to the HS. However, since the partitioning of the analytes from the HS to the coating is an exothermic process, high extraction temperatures may lead to the release of the analytes and consequently to low extraction efficiencies [7]. Therefore, the extraction temperature must be carefully optimized in HS-SPME applications.

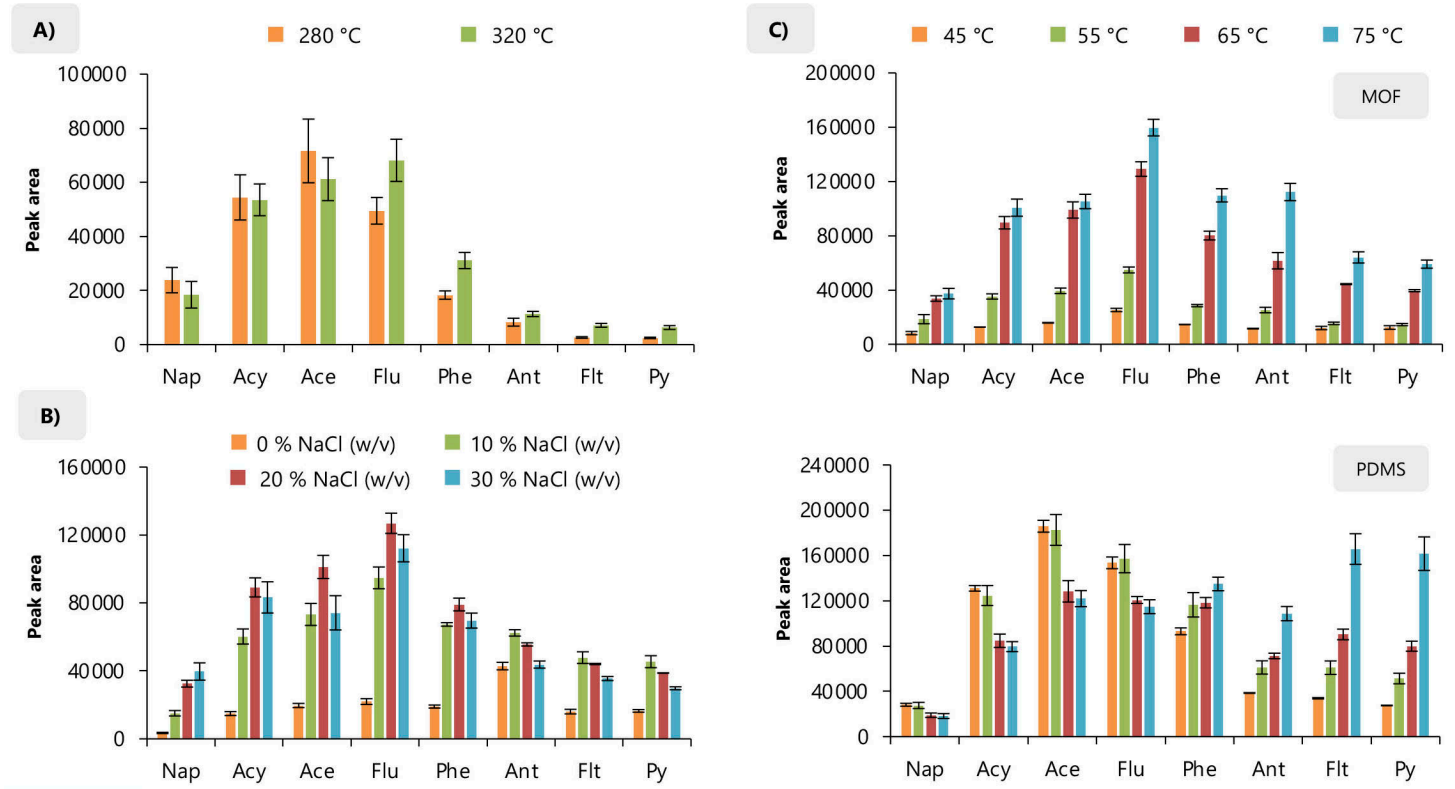

Figure IV.51. A) Study of the maximum desorption temperature for the MOF-based fiber. Experimental conditions: HS-SPME using 10 mL of aqueous standard at 100 $\mu g \cdot L^{-1}$ of the PAHs containing 30 % (w/v) of NaCl; 40 min of extraction at 65 °C stirring at 300 min^{-1}; and desorption for 4 min at different temperatures. **B)** Influence of NaCl content on the extraction efficiency (as peak area) of the HS-SPME method using MOF-based fiber. Experimental conditions: 10 mL of aqueous standard at 100 $\mu g \cdot L^{-1}$ of the PAHs; 40 min of extraction at 65 °C stirring at 300 min^{-1}; and desorption for 4 min at 280 °C. All extractions were performed in triplicate. **C)** Effect of the extraction temperature on the extraction efficiency (as peak area) of the HS-SPME method using MOF-based and commercial PDMS fibers. Experimental conditions: 10 mL of aqueous standard at 100 $\mu g \cdot L^{-1}$ of the PAHs; NaCl content of 20 % (w/v); 40 min of extraction at 300 min^{-1} of stirring rate; and desorption for 4 min at 280 °C. All extractions were performed in triplicate.

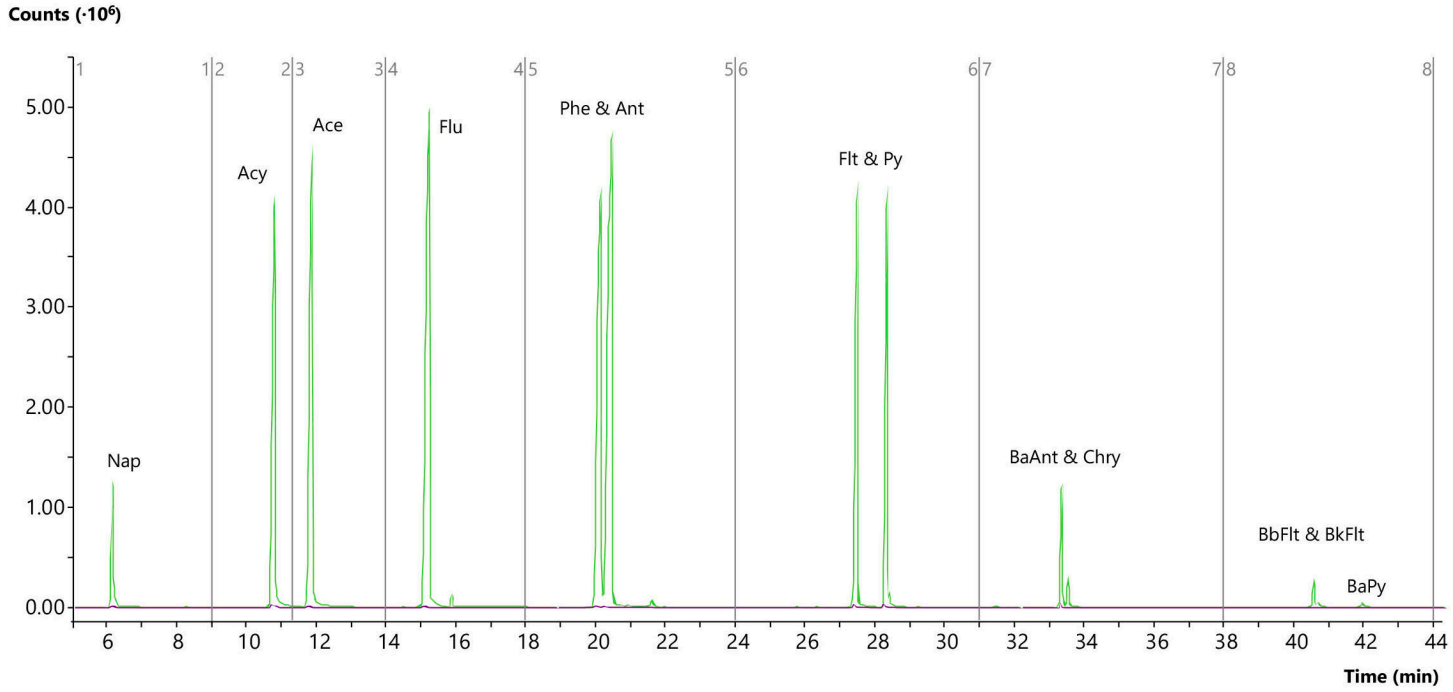

Figure IV.52. Chromatogram obtained by HS-SPME-GC-MS of an aqueous standard at a concentration level of 50 $\mu g \cdot L^{-1}$ of each PAH using the MOF-based fiber under the random preliminary conditions described in the screening study (green), and the chromatogram obtained by placing the same fiber in the GC inlet for 5 min after preforming the previous extraction (purple).

Figure IV.51 C) includes the extraction temperature profile between 45 and 75 °C obtained for the MOF-based and PDMS fibers. Both fibers exhibited completely different behavior. In the case of the CIM-80(Al) coating, the extraction efficiency increased for all the PAHs as the temperature increased, demonstrating the strong interaction between the analytes and the coating. Thus, 75 °C was selected as the optimum extraction temperature when using the MOF-based fiber. Higher temperatures were not tested to avoid water evaporation of the sample. For PDMS, better results were observed for lightest PAHs at lower extraction temperature, while higher peak areas were obtained at 75 °C for Phe, Ant, Flt and Py. Considering these results and with the aim of avoiding losses of analytes during the extraction, 55 °C was selected for HS-SPME experiments using PDMS fiber.

Figure IV.53 A) includes the time profiles obtained of the MOF-based fiber. As it can be observed, the equilibrium was reached at 60 min of extraction for all the analytes. Regarding the desorption step, better results were observed after 4 min of desorption time. In the case of the commercial PDMS fiber, different behavior was observed depending on the molecular weight of the analytes, as shown in Figure IV.53 B). For the lightest PAHs, the peak area increased from 20 to 40 min, then it decreased at 60 min to increase again at 80 min, which may be strongly related to the effect of the extraction temperature. For Ant, Flt and Py, the peak areas were higher as the extraction time increased, but without reaching the equilibrium. Therefore, with the aim of benefiting the analytes of higher molecular weight, a compromise value of 60 min was selected as optimum extraction time for PDMS fiber. For the desorption of the analytes with the commercial fiber, 6 min yielded the highest extraction efficiencies. Table IV.62 lists the optimum conditions selected for each fiber in the HS-SPME method.

2.2. Optimization of the DI-SPME method

Proper agitation of the sample during DI-SPME is a key parameter to evaluate, since it enhances the diffusion of the analytes from the sample to the coating and accelerates the process [7]. The effect of the stirring rate was evaluated for both MOF-based and PDMS fibers, as shown in Figure IV.54 A). Different profiles were observed depending on the sorbent. For the CIM-80(Al) fiber, there was no significant difference in the results obtained at different stirring rates. This may be due to the outstanding porosity of the sorbent, which results in the adsorption of the analytes on the surface of the coating. In the case of the PDMS fiber, higher speeds provided higher peak areas since the agitation facilitates the diffusion of the analytes to the bulk of the liquid polymer coating. Therefore, 300 and 700 min^{-1} were selected for the MOF-based and PDMS fibers, respectively.

Regarding the ionic strength, several studies in the literature have pointed out the negative effect of salt addition in DI-SPME for the extraction of PAHs [8–10]. Therefore, this parameter was not evaluated in the optimization of the DI-SPME method.

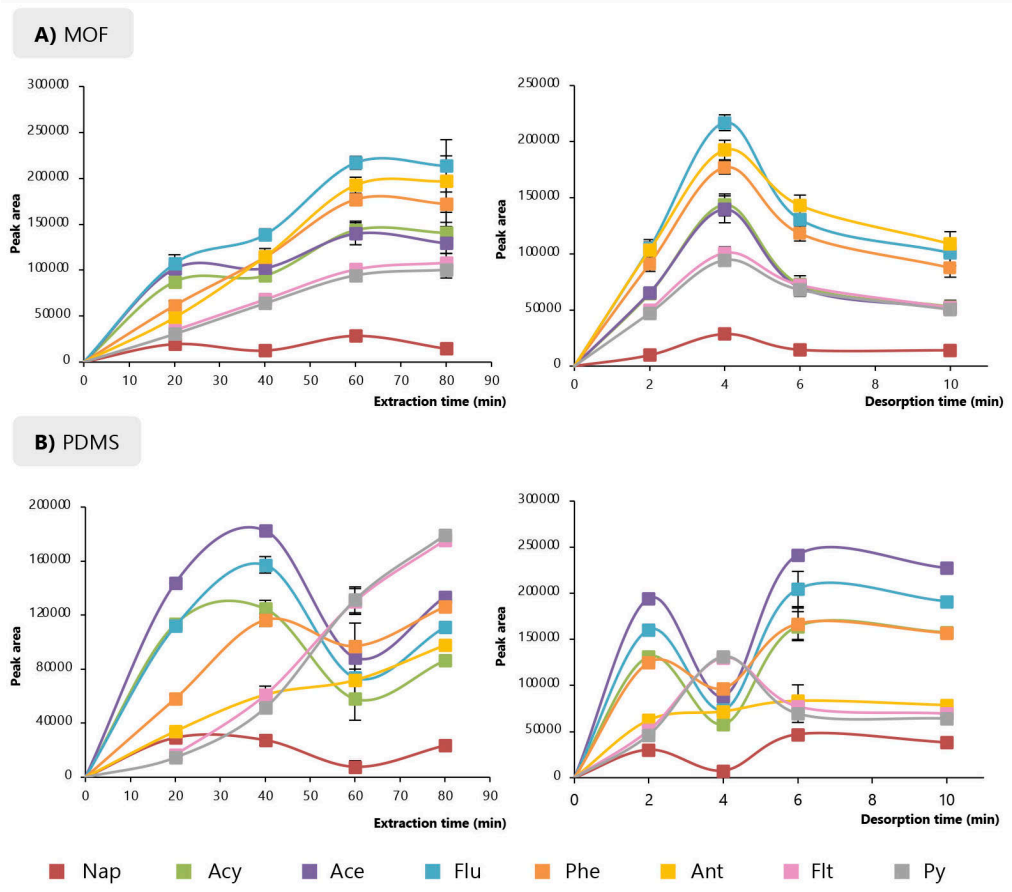

Figure IV.53. Time profiles for **A)** MOF-based fiber and **B)** commercial PDMS fiber, all obtained with the HS-SPME method. Experimental conditions: 10 mL of aqueous standard at 100 $\mu g \cdot L^{-1}$ of the PAHs containing 20 % (w/v) of NaCl; extraction at 75 °C or 55 °C for MOF-based and PDMS fibers, respectively, and using 300 min^{-1} as stirring rate. The desorption was performed at 280 °C for 4 min during the optimization of the extraction time. For the optimization of the desorption time, the extraction time was fixed at 60 min. All extractions were performed in triplicate.

Despite the extraction temperature is not a factor commonly considered in DI-SPME applications, it has been demonstrated its positive effect on the extraction of PAHs [8,9]. In this sense, the extraction temperature was evaluated at 25, 50 and 60 °C for both fibers, as shown in Figure IV.54 B). In the case of the CIM-80(Al) coating, the best results were obtained at 50 °C for all the analytes, while the PDMS showed different behavior depending on the molecular weight of the analyte. Thus, there is an increase in the extraction efficiency as the temperature increases for

the heaviest PAHs and *vice versa* for the lightest analytes. In order to benefit most of the analytes, 50 °C was also selected for next experiments with the PDMS fiber.

Table IV.62. Optimum conditions selected for the HS- and DI-SPME methods using MOF-based and PDMS fibers.

	HS-SPME		DI-SPME	
Parameter	**CIM-80(Al)**	**PDMS**	**CIM-80(Al)**	**PDMS**
Aqueous standard/sample volume (mL)	10	10	19	19
NaCl content (%, w/v)	20	20	0	0
Extraction stirring (min^{-1})	300	300	300	700
Extraction temperature (°C)	75	55	50	50
Extraction time (min)	60	60	60	60
Desorption temperature (°C)	280	280	280	280
Desorption time (min)	4	6	4	2

The extraction and desorption time profiles using both fibers are included in Figure IV.55. For the CIM-80(Al) coating, the equilibrium was reached at 80 min for most of the analytes but without higher differences on the peak areas obtained at 60 min. However, for the heavier PAHs (Phe, Ant, Flt and Py), a significant increase on the extraction efficiency was observed at 100 min, which may be due to the capillary condensation [2]. In the case of the PDMS fiber, the equilibrium was reached at around 40 min for Nap, Acy, Ace and Flu, while the remaining PAHs required 80 min. In order to avoid prolonged extractions and given the non-significant differences at long extraction times, 60 min was selected as optimum extraction time for both fibers. In this case, the extraction time was carefully controlled to guarantee reproducibility while working under non-equilibrium conditions [7]. Regarding the desorption time, best results were obtained using 4 and 2 min for the MOF-based and PDMS fibers, respectively.

The optimum conditions of the DI-SPME method for each fiber are included in Table IV.62.

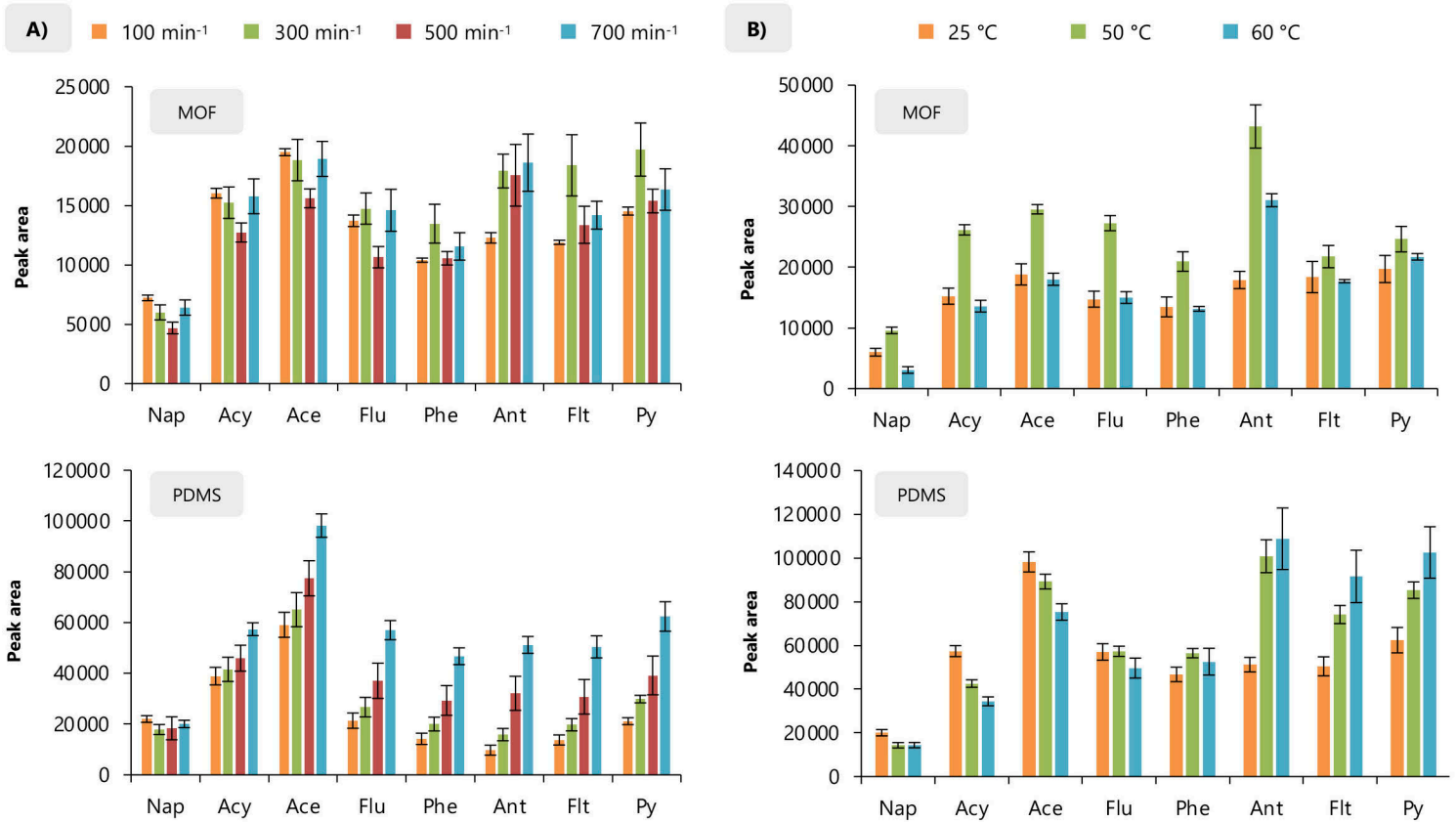

Figure IV.54. Influence of **A)** stirring rate and **B)** extraction temperature on the extraction efficiency (as peak area) of the DI-SPME method using MOF-based and commercial PDMS fibers. Experimental conditions: 19 mL of aqueous standard at 100 $\mu g \cdot L^{-1}$ of the PAHs; 40 min of extraction; and desorption for 4 min at 280 °C. The extractions were performed at 25 °C during the stirring rate optimization. The stirring rate was set at 300 min^{-1} and 700 min^{-1} during temperature optimization for MOF-based and PDMS fibers, respectively. All extractions were performed in triplicate.

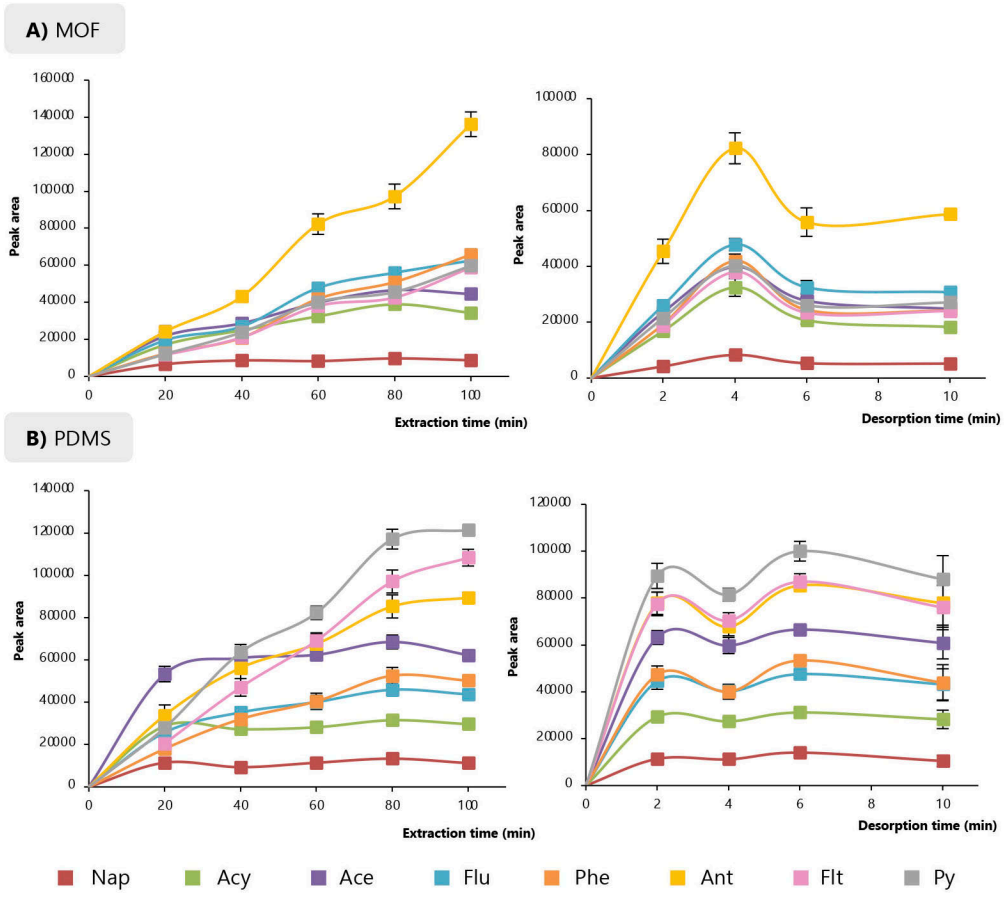

Figure IV.55. Time profiles for **A)** MOF-based fiber and **B)** commercial PDMS fiber, obtained with the DI-SPME method. Experimental conditions: 19 mL of aqueous standard at 100 $\mu g \cdot L^{-1}$ of the PAHs; extraction at 50 °C using a stirring rate of 300 min^{-1} and 700 min^{-1} for MOF-based and PDMS fibers, respectively; and desorption at 280 °C for 4 min during extraction time optimization. The extraction time was set at 60 min during the evaluation of the desorption time. All extractions were performed in triplicate.

3. Analytical performance of the developed HS- and DI-SPME methods

The analytical performance of the PDMS and MOF-based fibers in both HS- and DI-SPME methods was assessed by obtaining the calibration curves using standards in ultrapure water of the group of 13 PAHs and in combination with GC-MS. The linear range was from 5 to 500 $ng \cdot L^{-1}$ for HS-SPME and from 10 to 500 $ng \cdot L^{-1}$ for DI-SPME experiments, using 8 calibration levels in both cases. The limits of detection (LODs) were experimentally obtained by decreasing the concentration of the analytes until a signal to noise ratio (S/N) of 3 was obtained. The limits of quantification (LOQs) were estimated as 10/3 times the LODs and experimentally verified by performing SPME extractions at the predicted concentrations. Precision (evaluated using relative standard deviation, RSD, %) and relative recovery (RR) studies were also performed at 40 $ng \cdot L^{-1}$ in all cases.

For the HS-SPME-GC-MS method, Table IV.63 includes several quality analytical parameters obtained for both fibers, while Tables IV.64 and IV.65 list the detailed information of the calibration curves obtained. Determination coefficients were always higher than 0.994 for both fibers. The sensitivity achieved with each fiber was evaluated using the calibration slopes, which are included in Figure IV.56 A). The slope values ranged from 442 to 23281 using the MOF-based fiber, and between 175 and 20294 using PDMS fiber for BaPy and Ant, respectively in both cases. Thus, in comparison with the PDMS phase, the CIM-80(Al) coating provided the highest calibration slopes for most of the heaviest PAHs: Ant, Py, BaAnt, Chry, BbFlt, BkFlt and BaPy. On the contrary, the PDMS fiber exhibited higher sensitivity for the remaining analytes, except for Flu and Flt, for which the calibration slopes were similar. The LODs ranged between 0.3 and 1.5 $ng \cdot L^{-1}$ for the MOF-based fiber and from 0.5 to 1.5 $ng \cdot L^{-1}$ for the commercial fiber. Thus, the lowest LOQs were obtained with the MOF coating for most of the analytes, which ranged from 1.0 $ng \cdot L^{-1}$ for Ant to 4.0 $ng \cdot L^{-1}$ for BbFlt, BkFlt and BaPy. For the rest of the analytes, similar LOQs were obtained using both fibers, except for the values of Acy and Ace with the PDMS fiber, which were slightly lower (2.0 $ng \cdot L^{-1}$) than those obtained with the CIM-80(Al) phase (2.5 $ng \cdot L^{-1}$).

Regarding the precision of the HS-SPME method, intra-day RSD values ranged from 11 % to 18 % for the MOF-based fiber, and from 5.6 % to 16 % for the commercial PDMS fiber. The inter-fiber precision was also evaluated for the MOF coating using 3 different fibers and performing 3 consecutive extractions with each fiber. The inter-fiber RSD values were lower than 19 % in all cases (see Table IV.64). The accuracy was evaluated using RR values, which were on average 99.3 % and 95.3 % for the MOF and PDMS fibers, respectively. The lifetime of the MOF-based fiber in this mode was around 80–90 extraction cycles.

Table IV.63. Several quality analytical parameters of the HS-SPME-GC-MS method using the commercial PDMS fiber and the MOF-based fiber in different matrices.

PAH	LOQ[a] (ng·L^{-1})		RR[b] (%) / RSD[c] (%)					
	PDMS fiber	MOF-based fiber	PDMS fiber			MOF-based fiber		
	Ultrapure water	Ultrapure water	Ultrapure water	Urine	Coffee	Ultrapure water	Urine	Coffee
Nap	3.0	3.0	76.2 / 15	107 / 11	117 / 14	107 / 13	89.9 / 12	87.1 / 16
Acy	2.0	2.5	84.5/ 5.7	98.7 / 16	77.6 / 18	95.7 / 14	107 / 21	96.0 / 14
Ace	2.0	2.5	81.8 / 5.9	98.7 / 13	85.7 / 15	102 / 18	78.7 / 9.1	89.2 / 18
Flu	1.5	1.5	95.6 / 8.6	81.5 / 16	93.2 / 4.8	102 / 11	85.8 / 20	82.1 / 11
Phe	1.5	1.5	109 / 5.6	74.7 / 19	93.1 / 10	96.3 / 13	84.8 / 13	107 / 12
Ant	2.0	1.0	82.1 / 5.6	88.8 / 21	111 / 16	100 / 11	80.2 / 7.4	89.1 / 14
Flt	2.0	2.0	115 / 14	81.5 / 12	109 / 13	103 / 11	95.3 / 18	85.0 / 7.6
Py	2.0	1.5	99.8 / 12	98.0 / 17	82.1 / 11	93.0 / 12	93.2 / 12	79.2 / 12
BaAnt	3.0	3.0	113 / 16	121 / 12	92.8 / 20	99.3 / 16	80.1 / 5.0	101 / 15
Chry	3.0	3.0	113 / 8.2	118 / 16	93.2 / 15	101 / 14	85.9 / 3.5	95.8 / 16
BbFlt	5.0	4.0	102 / 15	75.1 / 19	–	102 / 14	85.0 / 10	82.7 / 13
BkFlt	5.0	4.0	91.5 / 15	80.4 / 17	–	95.8 / 13	89.1 / 7.4	74.6 / 14
BaPy	5.0	4.0	75.7 / 7.9	93.1 / 21	–	94.1 / 11	91.8 / 2.4	–

[a] Limit of quantification estimated as 10/3 times the limit of detection, and experimentally verified.
[b] Relative recovery at a concentration level of 40 ng·L^{-1} (n = 3).
[c] Relative standard deviation for intra-day precision at a concentration level of 40 ng·L^{-1} (n = 3).

Table IV.64. Several quality analytical parameters of the HS-SPME-GC-MS method in ultrapure water using the MOF-based fiber.

PAH	(Slope ± t·SD[a])	R^2 [b]	$S_{y/x}·10^{-3}$ [c]	LOD[d] ($ng·L^{-1}$)	LOQ[e] ($ng·L^{-1}$)	Intra-day RSD[f] (%)	Inter-fiber RSD[g] (%)	RR[h] (%)
Nap	2422 ± 137	0.997	27	1.0	3.0	13	13	107
Acy	7510 ± 299	0.998	59	0.8	2.5	14	14	95.7
Ace	3949 ± 132	0.999	26	0.8	2.5	18	18	102
Flu	13390 ± 800	0.996	158	0.5	1.5	11	12	102
Phe	11268 ± 614	0.997	121	0.5	1.5	13	12	96.3
Ant	23281 ± 1451	0.996	287	0.3	1.0	11	16	100
Flt	9158 ± 602	0.996	119	0.5	2.0	11	11	103
Py	13816 ± 793	0.997	156	0.5	1.5	12	13	93.0
BaAnt	4677 ± 291	0.996	58	1.0	3.0	16	15	99.3
Chry	2514 ± 110	0.998	22	1.0	3.0	14	13	101
BbFlt	1544 ± 113	0.995	22	1.5	4.0	14	19	102
BkFlt	1438 ± 73	0.997	14	1.5	4.0	13	12	95.8
BaPy	442 ± 27	0.996	5	1.5	4.0	11	15	94.1

[a] 95 % confidence limits for n = 8 calibration levels (6 degrees of freedom) within the calibration range 5–500 $ng·L^{-1}$.

[b] Determination coefficient.

[c] Error of the estimate (or standard deviation of the residuals).

[d] Limit of detection, determined by decreasing the concentration of the PAHs until a S/N ratio of 3 was obtained.

[e] Limit of quantification, estimated as 10/3 times the LOD, and experimentally verified by performing the entire method at the predicted concentrations.

[f] Average (from 3 different fibers) of relative standard deviation for intra-day precision at a concentration level of 40 $ng·L^{-1}$ (n = 3).

[g] Relative standard deviation for inter-fiber precision using different fibers at a concentration level of 40 $ng·L^{-1}$ (n = 9, 3 extractions using 3 different fibers).

[h] Relative recovery at a concentration level of 40 $ng·L^{-1}$ (n = 3).

Table IV.65. Several quality analytical parameters of the HS-SPME-GC-MS method in ultrapure water using the commercial PDMS fiber.

PAH	(Slope ± t·SD[a])	R^{2} [b]	$S_{y/x} \cdot 10^{-3}$ [c]	LOD[d] ($ng \cdot L^{-1}$)	LOQ[e] ($ng \cdot L^{-1}$)	Intra-day RSD[f] (%)	RR[g] (%)
Nap	4161 ± 269	0.996	53	1.0	3.0	15	76.2
Acy	14483 ± 893	0.996	177	0.5	2.0	5.7	84.5
Ace	12006 ± 952	0.994	188	0.5	2.0	5.9	81.8
Flu	13384 ± 844	0.996	167	0.5	1.5	8.6	95.6
Phe	14567 ± 749	0.997	148	0.5	1.5	5.6	109
Ant	20294 ± 1155	0.997	228	0.5	2.0	5.6	82.1
Flt	11000 ± 492	0.998	97	0.5	2.0	14	115
Py	10926 ± 377	0.999	74	0.5	2.0	12	99.8
BaAnt	3024 ± 135	0.998	27	1.0	3.0	16	113
Chry	1990 ± 100	0.997	20	1.0	3.0	8.2	113
BbFlt	398 ± 32	0.994	6	1.5	5.0	15	102
BkFlt	621 ± 29	0.998	6	1.5	5.0	15	91.5
BaPy	175 ± 7	0.999	1	1.5	5.0	7.9	75.7

[a] 95 % confidence limits for n = 8 calibration levels (6 degrees of freedom) within the calibration range 5–500 $ng \cdot L^{-1}$.

[b] Determination coefficient.

[c] Error of the estimate (or standard deviation of the residuals).

[d] Limit of detection, determined by decreasing the concentration of the PAHs until a S/N ratio of 3 was obtained.

[e] Limit of quantification, estimated as 10/3 times the LOD, and experimentally verified by performing the entire method at the predicted concentrations.

[f] Relative standard deviation for intra-day precision at a concentration level of 40 $ng \cdot L^{-1}$ (n = 3).

[g] Relative recovery at a concentration level of 40 $ng \cdot L^{-1}$ (n = 3).

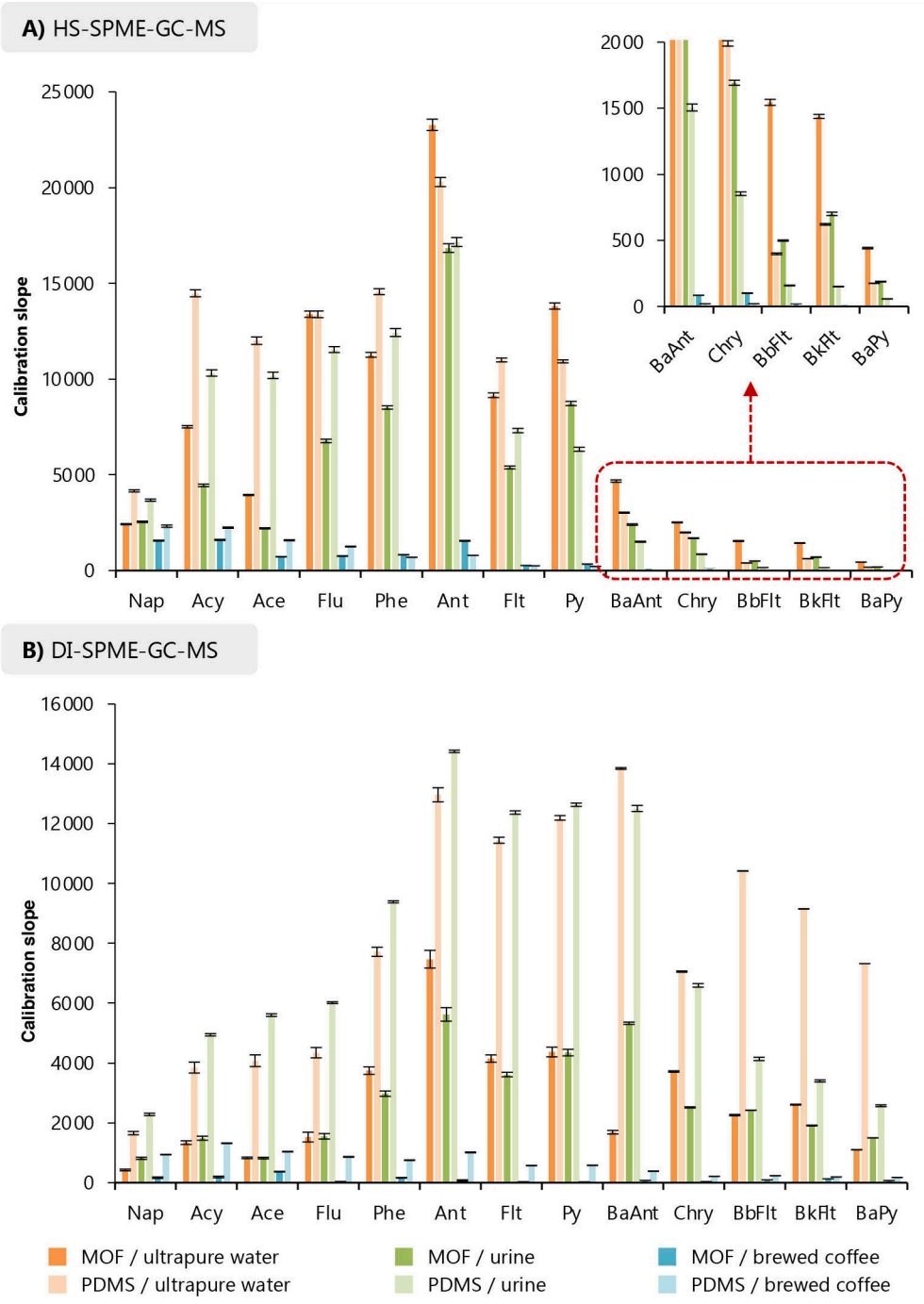

Figure IV.56. Comparison of the calibration slopes (in absence of any kind of normalization) obtained for the **A)** HS-SPME-GC-MS and **B)** DI-SPME-GC-MS methods using commercial PDMS and MOF-based fibers in different matrices, under the selected optimum conditions included in Table IV.62.

Table IV.66 includes several quality analytical parameters for the DI-SPME-GC-MS using both fibers, while the specific information of the calibration curves are shown in Tables IV.67 and IV.68. Determination coefficients higher than 0.994 were obtained for both fibers within the calibration range. Regarding the sensitivity, it was higher using the PDMS fibers for all the PAHs as it can be observed in Figure IV.56 B). The calibration slopes varied from 424 for Nap to 7469 for Ant using the MOF-based fiber, while they ranged between 1657 for Nap and 13845 for BaAnt with the PDMS coating. In general, slopes from 3 to 8 times higher were obtained using the polymeric fiber in comparison with the MOF phase, except for Phe, Ant and Chry, for which the slopes were only 2 times higher. This significant difference may be due to the porous nature of the MOF coating, which leads to the adsorption of water molecules on the pores and thus, reduces the extraction capacity of the fiber. Therefore, the LODs and LOQs were much lower for the PDMS coating, ranging from 0.5 to 1.5 $ng \cdot L^{-1}$ and from 1.5 to 5.0 $ng \cdot L^{-1}$, respectively. Nap and Acy were the least sensitive, and Py and BaAnt had the lowest LOD and LOQ values. In the case of the CIM-80(Al) coating, the LODs were between 1.5 and 3.0. $ng \cdot L^{-1}$, while the LOQs varied from 5.0 to 10 $ng \cdot L^{-1}$, with Ant and Chry having the lowest values and Nap and BaPy having the higher limits.

The precision of the DI-SPME method was similar to the HS-SPME mode. Intra-day RSD values were lower than 15 % and 19 % for the MOF-based and PDMS fibers, respectively. For the MOF coating, the inter-fiber precision showed RSD values between 9.8 % for Acy and 14 % for Flt and BaAnt (see Table IV.67). Regarding the accuracy, the fibers provided adequate RR values, which were on average around 95.5 % for both fibers, thus exhibiting reliable results. Moreover, the MOF-based fiber could be also used for 80–90 extractions without losing extraction efficiency.

Table IV.69 [10–19] includes several characteristics and analytical performance of other MOF-based fibers (not necessarily using neat MOFs but composites) reported in the literature for the determination of PAHs in waters using GC-MS. In general, stainless steel is the preferred support for the fabrication of the SPME fibers, but fused silica has also been used for fibers intended to DI-SPME applications [10,17,19]. In this study, nitinol was used as core, which improves the stability and robustness of the fiber due to its flexibility. The prepared CIM-80(Al) fiber could be used at a higher desorption temperature in comparison with most of the other MOFs, for which the maximum desorption temperature was lower than 280 °C [11,12,14,16–19]. The lifetime of the coating developed in this study was similar to those described. Higher reusability for the fibers has been reported for mixed coatings, since the presence of polymers [11,12,18] or hydrophobic graphitic carbon nitride [17] in the coating protect it from the components of the matrix. The use of mixed coatings also improves the stability of the fiber apart from playing an important role in the extraction capacity of the resulting phase. The inter-fiber RSD values are in accordance with SPME applications and are lower than 20 % for all the fibers. Regarding HS-SPME applications, the CIM-80(Al) fiber prepared in this study exhibited the lowest LODs in comparison with other MOFs.

Table IV.66. Several quality analytical parameters of the DI-SPME-GC-MS method using the commercial PDMS fiber and the MOF-based fiber in different matrices.

PAH	LOQ[a] (ng·L^{-1})		RR[b] (%) / RSD[c] (%)					
	PDMS fiber	MOF-based fiber	PDMS fiber			MOF-based fiber		
	Ultrapure water	Ultrapure water	Ultrapure water	Urine	Coffee	Ultrapure water	Urine	Coffee
Nap	5.0	10	117 / 7.0	90.0 / 7.7	104 / 8.1	106 / 11	84.7 / 7.7	76.4 / 13
Acy	5.0	8.5	100 / 17	97.4 / 5.6	101 / 11	91.9 / 7.7	96.8 / 9.1	114 / 9.0
Ace	3.0	8.5	114 / 12	97.1 / 5.7	103 / 9.5	105 / 12	91.0 / 7.1	113 / 16
Flu	3.0	7.0	102 / 19	107 / 3.2	108 / 15	114 / 11	79.3 / 17	80.7 / 12
Phe	2.5	7.0	96.6 / 11	102 / 3.0	102 / 12	104 / 11	103 / 18	99.1 / 5.2
Ant	2.0	5.0	84.8 / 8.8	97.8 / 5.1	99.7 / 11	99.0 / 10	111 / 9.4	112 / 5.6
Flt	2.0	6.0	91.8 / 9.0	99.8 / 8.4	111 / 15	110 / 14	114 / 5.9	101 / 16
Py	1.5	7.0	84.2 / 6.4	115 / 14	105 / 15	90.4 / 14	109 / 10	96.4 / 14
BaAnt	1.5	7.0	101 / 13	91.8 / 12	93.0 / 14	99.7 / 15	84.0 / 11	90.5 / 4.1
Chry	3.0	5.0	95.8 / 17	91.2 / 12	95.9 / 13	86.7 / 14	81.0 / 5.8	85.0 / 19
BbFlt	3.0	8.5	91.6 / 12	108 / 13	94.3 / 14	90.5 / 14	74.3 / 11	116 / 5.1
BkFlt	3.0	8.5	85.5 / 11	99.5 / 13	90.8 / 16	87.7 / 13	80.1 / 5.8	110 / 6.5
BaPy	3.0	10	87.0 / 7.8	113 / 11	88.6 / 12	75.9 / 11	96.6 / 11	110 / 9.3

[a] Limit of quantification estimated as 10/3 times the limit of detection, and experimentally verified.
[b] Relative recovery at a concentration level of 40 ng·L^{-1} (n = 3).
[c] Relative standard deviation for intra-day precision at a concentration level of 40 ng·L^{-1} (n = 3).

Table IV.67. Several quality analytical parameters of the DI-SPME-GC-MS method in ultrapure water using the MOF-based fiber.

PAH	(Slope ± t·SD[a])	R^2 [b]	$S_{y/x}\cdot10^{-3}$ [c]	LOD[d] ($ng\cdot L^{-1}$)	LOQ[e] ($ng\cdot L^{-1}$)	Intra-day RSD[f] (%)	Inter-fiber RSD[g] (%)	RR[h] (%)
Nap	424 ± 15	0.999	3	3.0	10	11	10	106
Acy	1338 ± 88	0.996	17	2.5	8.5	7.7	9.8	91.9
Ace	829 ± 39	0.998	8	2.5	8.5	12	12	105
Flu	1524 ± 71	0.998	14	2.0	7.0	11	10	114
Phe	3745 ± 250	0.996	49	2.0	7.0	11	12	104
Ant	7469 ± 484	0.996	96	1.5	5.0	10	11	99.0
Flt	4148 ± 267	0.996	52	2.0	6.0	14	14	110
Py	4368 ± 303	0.995	60	2.0	7.0	14	13	90.4
BaAnt	1688 ± 110	0.996	22	2.0	7.0	15	14	99.7
Chry	3716 ± 218	0.997	43	1.5	5.0	14	13	86.7
BbFlt	2258 ± 137	0.996	27	2.5	8.5	14	12	90.5
BkFlt	2608 ± 174	0.996	34	2.5	8.5	13	13	87.7
BaPy	1101 ± 66	0.996	13	3.0	10	11	12	75.9

[a] 95 % confidence limits for n = 8 calibration levels (6 degrees of freedom) within the calibration range 10–500 $ng\cdot L^{-1}$.

[b] Determination coefficient.

[c] Error of the estimate (or standard deviation of the residuals).

[d] Limit of detection, determined by decreasing the concentration of the PAHs until a S/N ratio of 3 was obtained.

[e] Limit of quantification, estimated as 10/3 times the LOD, and experimentally verified by performing the entire method at the predicted concentrations.

[f] Average (from 3 different fibers) of relative standard deviation for intra-day precision at a concentration level of 40 $ng\cdot L^{-1}$ (n = 3).

[g] Relative standard deviation for inter-fiber precision using different fibers at a concentration level of 40 $ng\cdot L^{-1}$ (n = 9, 3 extractions with each of 3 different fibers).

[h] Relative recovery at a concentration level of 40 $ng\cdot L^{-1}$ (n = 3).

Table IV.68. Several quality analytical parameters of the DI-SPME-GC-MS method in ultrapure water using the commercial PDMS fiber.

PAH	(Slope ± t·SD[a])	R^2 [b]	$S_{y/x}\cdot10^{-3}$ [c]	LOD[d] ($ng\cdot L^{-1}$)	LOQ[e] ($ng\cdot L^{-1}$)	Intra-day RSD range[f] (%)	RR[g] (%)
Nap	1657 ± 103	0.996	21	1.5	5.0	7.0	117
Acy	3847 ± 235	0.996	47	1.5	5.0	17	100
Ace	4077 ± 223	0.997	44	1.0	3.0	12	114
Flu	4345 ± 279	0.996	55	1.0	3.0	19	102
Phe	7718 ± 509	0.996	101	1.0	2.5	11	96.6
Ant	12965 ± 937	0.995	185	0.5	2.0	8.8	84.8
Flt	11446 ± 719	0.996	142	0.5	2.0	9.0	91.8
Py	12194 ± 918	0.994	181	0.5	1.5	6.4	84.2
BaAnt	13845 ± 754	0.997	149	0.5	1.5	13	101
Chry	7055 ± 257	0.999	51	1.0	3.0	17	95.8
BbFlt	10419 ± 475	0.998	94	1.0	3.0	12	91.6
BkFlt	9150 ± 609	0.996	120	1.0	3.0	11	85.5
BaPy	7322 ± 311	0.998	61	1.0	3.0	7.8	87.0

[a] 95 % confidence limits for n = 8 calibration levels (6 degrees of freedom) within the calibration range 10–500 $ng\cdot L^{-1}$.

[b] Determination coefficient.

[c] Error of the estimate (or standard deviation of the residuals).

[d] Limit of detection, determined by decreasing the concentration of the PAHs until a S/N ratio of 3 was obtained.

[e] Limit of quantification, estimated as 10/3 times the LOD, and experimentally verified by performing the entire method at the predicted concentrations.

[f] Relative standard deviation for intra-day precision at a concentration level of 40 $ng\cdot L^{-1}$ (n = 3).

[g] Relative recovery at a concentration level of 40 $ng\cdot L^{-1}$ (n = 3).

Table IV.69. Comparison of the characteristics performance of the prepared CIM-80(Al) coating with other MOF-based fibers reported in the literature for the determination of PAHs in waters using GC-MS.

Coating	Support	Coating method / Thickness (μm)	Number of PAHs	LOD ($ng \cdot L^{-1}$)	Inter-fiber RSD (%)	Temperature (ºC) / Lifetime	Ref.
HS-SPME mode							
IRMOF-3(Zn)/IL/PDMS	SS[a]	*in situ* growth, layer of IL & PDMS / 140	4	12.0–15.4	< 9.6	230 / 100	[10]
MIL-101(Cr)/PDMS	SS[a]	sol-gel approach / 70	5	1–4	< 13.8	250 / 120	[11]
MOF-177(Zn)	SS[a]	adhesion with glue / 30	7	0.69–4.42	< 9.8	280 / 100	[12]
TMU-6(Zn)	SS[a]	adhesion with glue / –	6	5–8	< 10.4	250 / 60	[13]
HKUST-1(Cu)	Cu	*in situ* growth / 2	8	0.1–9.9	< 9.1	300 / 150	[14]
CIM-80(Al)	Nitinol	*in situ* growth / 3.5–30	13	0.5–1.5	< 19	280 / 85	This study
DI-SPME mode							
UiO-66(Zr)	FS[b]	*in situ* growth / 25	10	0.3–0.6	< 8.9	290 / 90	[15]
CBDC(Cu)/Polyimide	SS[a]	immersion in composite / 2	5	0.1–2.1	< 11.7	250 / –	[16]
NZBDC(Ni/Zn)/g-C_3N_4[c]	FS[b]	*in situ* growth / 27.1	12	0.1–3	< 11.8	250 / 150	[17]
ZIF-8(Zn)/Silica polymer	SS[a]	sol-gel approach / 10	16	0.3–27	< 11.5	260 / 100	[18]
PUM-210(Zn)	FS[b]	adhesion with glue / 71.6	16	0.5–3.7	< 9	270 / –	[19]
CIM-80(Al)	Nitinol	*in situ* growth / 3.5–30	13	1.5–3.0	< 14	280 / 85	This study

[a] Stainless steel
[b] Fused silica
[c] hydrophobic graphitic carbon nitride

Moreover, this is the study in which the highest number of PAHs are determined. In the case of DI-SPME methods, the LODs obtained with the CIM-80(Al) fiber are comparable to those reported for other MOF-based coatings. Similar thicknesses were obtained in comparison with other MOF-based coatings prepared by the *in situ* growth approach.

It is important to highlight the greenness in the preparation of the fiber in comparison with other MOF coatings reported in the literature. In the present study, ethanol is the only solvent used in the entire fabrication process for cleaning the coating, and the proposed SPME methods are completely solvent-free. Furthermore, the low cytotoxicity reported for the CIM-80(Al) MOF [3] together with the biocompatibility of the nitinol core [20] makes possible its application for *in vivo* applications without requiring the incorporation of an additional polymeric material in the coating.

4. Application of HS- and DI-SPME methods in urine and brewed coffee samples

With the aim of evaluating the applicability of the prepared CIM-80(Al) fiber, the calibration curves were obtained in aqueous-based complex samples using both the MOF-based coating and commercial PDMS fiber. Given the demonstrated occurrence of PAHs in urine due to the human exposure to these compounds by dietary, working or smoking factors [8,21], and in brewed coffee samples due to the drying and roasting steps during its preparation [22], these samples were selected as complex matrices to test the performance of the MOF-based fibers. Moreover, the stability of the neat MOF in these matrices was previously demonstrated (see Figure IV.49 in Section IV.2.2.1).

Calibration curves were obtained in the range of 0–200 $ng \cdot L^{-1}$ (6 calibration levels) without any pretreatment other than the dilution of the samples for DI-SPME experiments and following the SPME procedures described in Section III.7.5.8 A Student's *t*-test was also used to determine whether if the intercepts of the calibration curves were or not zero to determine the concentration of the PAHs in the samples using both fibers (according to the standard addition method). In all cases, the results of these tests indicated that the intercepts were zero and the analytes could not be quantified, or the samples were free of PAHs (Tables IV.70, IV.71, IV.72, and IV.73). Therefore, the calibration curves were obtained using these matrices as free of analytes and considered as matrix-matched calibrations. RR and precision studies were performed at a spiked concentration level of 40 $ng \cdot L^{-1}$ to evaluate the performance in the samples. Furthermore, the matrix effects were evaluated using a statistical test previously reported by Andrade and Estévez-Pérez [23], in which the calibration slopes obtained in the samples were compared with those obtained with standards in ultrapure water.

Table IV.70. Intercepts obtained with the calibration curves performed in the urine sample using the MOF-based fiber in the different modes of the SPME-GC-MS method, and Student's *t*-test results to determine whether the intercepts are statistically zero.

Analyte	HS-SPME-GC-MS			DI-SPME-GC-MS		
	(Intercept ± SD[a])	P[b]	Intercept[c]	(Intercept ± SD[a])	P[b]	Intercept[c]
Nap	26282 ± 6882	0.07 > 0.05	= 0	3337 ± 2343	0.2 > 0.05	= 0
Acy	32309 ± 12503	0.06 > 0.05	= 0	10936 ± 2568	0.1 > 0.05	= 0
Ace	15591 ± 5033	0.1 > 0.05	= 0	3927 ± 1949	0.1 > 0.05	= 0
Flu	263140 ± 17293	0.06 > 0.05	= 0	13645 ± 4346	0.06 > 0.05	= 0
Phe	203109 ± 16546	0.07 > 0.05	= 0	8560 ± 5650	0.2 > 0.05	= 0
Ant	116044 ± 42588	0.06 > 0.05	= 0	–8015 ± 17309	0.6 > 0.05	= 0
Flt	216090 ± 14016	0.06 > 0.05	= 0	27411 ± 11074	0.07 > 0.05	= 0
Py	234558 ± 20668	0.07 > 0.05	= 0	49814 ± 9936	0.07 > 0.05	= 0
BaAnt	-8541 ± 7119	0.3 > 0.05	= 0	–39950 ± 17965	0.09 > 0.05	= 0
Chry	17566 ± 3563	0.08 > 0.05	= 0	–18601 ± 8661	0.1 > 0.05	= 0
BbFlt	21579 ± 824	0.06 > 0.05	= 0	–20407 ± 8572	0.08 > 0.05	= 0
BkFlt	11759 ± 2356	0.08 > 0.05	= 0	–16185 ± 6808	0.08 > 0.05	= 0
BaPy	–916 ± 532	0.2 > 0.05	= 0	–12572 ± 5361	0.08 > 0.05	= 0

[a] Standard deviation of the intercept (n = 6).
[b] Probability that the intercept has a value of zero.
[c] Intercept value for a significance level of 5 % (4 degrees of freedom).

Table IV.71. Intercepts obtained with the calibration curves performed in the brewed coffee sample using the MOF-based fiber in the different modes of the SPME-GC-MS method, and Student's *t*-test results to determine whether the intercepts are statistically zero.

Analyte	HS-SPME-GC-MS			DI-SPME-GC-MS		
	(Intercept ± SD[a])	P[b]	Intercept[c]	(Intercept ± SD[a])	P[b]	Intercept[c]
Nap	2779 ± 4400	0.6 > 0.05	= 0	6335 ± 2987	0.2 > 0.05	= 0
Acy	–4968 ± 4934	0.4 > 0.05	= 0	5983 ± 5351	0.6 > 0.05	= 0
Ace	–716 ± 1898	0.7 > 0.05	= 0	92186 ± 25217	0.06 > 0.05	= 0
Flu	104619 ± 2613	0.08 > 0.05	= 0	5821 ± 919	0.06 > 0.05	= 0
Phe	59666 ± 1829	0.2 > 0.05	= 0	3534 ± 5071	0.7 > 0.05	= 0
Ant	29881 ± 4113	0.2 > 0.05	= 0	1337 ± 921	0.08 > 0.05	= 0
Flt	58232 ± 535	0.06 > 0.05	= 0	526 ± 377	0.07 > 0.05	= 0
Py	93392 ± 1067	0.08 > 0.05	= 0	2074 ± 1265	0.4 > 0.05	= 0
BaAnt	4007 ± 149	0.2 > 0.05	= 0	31142 ± 3367	0.06 > 0.05	= 0
Chry	6939 ± 373	0.3 > 0.05	= 0	1247 ± 1045	0.4 > 0.05	= 0
BbFlt	3201 ± 66	0.1 > 0.05	= 0	26440 ± 9433	0.07 > 0.05	= 0
BkFlt	3409 ± 38	0.07 > 0.05	= 0	30957 ± 8582	0.06 > 0.05	= 0
BaPy	–	–	–	2471 ± 1264	0.1 > 0.05	= 0

[a] Standard deviation of the intercept (n = 6).
[b] Probability that the intercept has a value of zero.
[c] Intercept value for a significance level of 5 % (4 degrees of freedom).

Table. IV.72. Intercepts obtained with the calibration curves performed in the urine sample using the PDMS fiber in the different modes of the SPME-GC-MS method, and Student's *t*-test results to determine whether the intercepts are statistically zero.

Analyte	HS-SPME-GC-MS			DI-SPME-GC-MS		
	(Intercept ± SD[a])	P[b]	Intercept[c]	(Intercept ± SD[a])	P[b]	Intercept[c]
Nap	43848 ± 11007	0.07 > 0.05	= 0	163 ± 7531	1 > 0.05	= 0
Acy	82109 ± 31071	0.06 > 0.05	= 0	–37 ± 7139	1 > 0.05	= 0
Ace	97115 ± 31064	0.07 > 0.05	= 0	819 ± 8177	0.9 > 0.05	= 0
Flu	229145 ± 28838	0.06 > 0.05	= 0	21410 ± 5433	0.06 > 0.05	= 0
Phe	339333 ± 38857	0.07 > 0.05	= 0	28895 ± 6566	0.02 > 0.05	= 0
Ant	222107 ± 44245	0.08 > 0.05	= 0	17267 ± 7467	0.08 > 0.05	= 0
Flt	116526 ± 21057	0.08 > 0.05	= 0	32036 ± 10541	0.06 > 0.05	= 0
Py	125910 ± 19819	0.06 > 0.05	= 0	38040 ± 10364	0.07 > 0.05	= 0
BaAnt	–1887 ± 4970	0.7 > 0.05	= 0	–22117 ± 19024	0.3 > 0.05	= 0
Chry	1881 ± 2573	0.5 > 0.05	= 0	–10731 ± 11249	0.4 > 0.05	= 0
BbFlt	332 ± 508	0.6 > 0.05	= 0	22063 ± 10291	0.1 > 0.05	= 0
BkFlt	456 ± 371	0.3 > 0.05	= 0	9706 ± 6717	0.2 > 0.05	= 0
BaPy	–141 ± 235	0.6 > 0.05	= 0	5737 ± 5824	0.4 > 0.05	= 0

[a] Standard deviation of the intercept (n = 6).
[b] Probability that the intercept has a value of zero.
[c] Intercept value for a significance level of 5 % (4 degrees of freedom).

Table IV.73. Intercepts obtained with the calibration curves performed in the brewed coffee sample using the PDMS fiber in the different modes of the SPME-GC-MS method, and Student's *t*-test results to determine whether the intercepts are statistically zero.

Analyte	HS-SPME-GC-MS			DI-SPME-GC-MS		
	(Intercept ± SD[a])	P[b]	Intercept[c]	(Intercept ± SD[a])	P[b]	Intercept[c]
Nap	24291 ± 11281	0.1 > 0.05	= 0	4313 ± 1325	0.06 > 0.05	= 0
Acy	15831 ± 6317	0.07 > 0.05	= 0	3310 ± 1876	0.2 > 0.05	= 0
Ace	13715 ± 4751	0.07 > 0.05	= 0	747 ± 1572	0.7 > 0.05	= 0
Flu	37634 ± 3472	0.08 > 0.05	= 0	9772 ± 2376	0.06 > 0.05	= 0
Phe	48415 ± 1197	0.07 > 0.05	= 0	6837 ± 1798	0.07 > 0.05	= 0
Ant	35902 ± 894	0.06 > 0.05	= 0	1086 ± 2650	0.7 > 0.05	= 0
Flt	9705 ± 601	0.06 > 0.05	= 0	9138 ± 1196	0.06 > 0.05	= 0
Py	11784 ± 713	0.06 > 0.05	= 0	8781 ± 1343	0.06 > 0.05	= 0
BaAnt	711 ± 61	0.06 > 0.05	= 0	213 ± 1250	0.9 > 0.05	= 0
Chry	1087 ± 49	0.06 > 0.05	= 0	1681 ± 568	0.08 > 0.05	= 0
BbFlt	–	–	–	125 ± 543	0.8 > 0.05	= 0
BkFlt	–	–	–	–171 ± 532	0.8 > 0.05	= 0
BaPy	–	–	–	136 ± 381	0.7 > 0.05	= 0

[a] Standard deviation of the intercept (n = 6).
[b] Probability that the intercept has a value of zero.
[c] Intercept value for a significance level of 5 % (4 degrees of freedom).

Table IV.63 shows several quality analytical parameters obtained for the HS-SPME-GC-MS method in both samples using MOF-based and commercial PDMS fibers, while Tables IV.74, IV.75, IV.76 and IV.77 include detailed information for the calibration curves. In the case of the coffee sample, the calibration curve for BaPy using the MOF-based fiber, and for BbFlt, BkFlt and BaPy using the PDMS fiber could not be determined due to the low sensitivity for the analytes in the calibration range studied. For the remaining PAHs and the MOF-based coating, the determination coefficients were higher than 0.993 in the coffee sample, and higher than 0.995 in the urine sample. In the case of the PDMS fiber, the determination coefficients were higher than 0.992 in both matrices. The obtained matrix-matched calibration slopes in each matrix with both fibers are included in Figure IV.56 A) together with the calibration slopes previously obtained in ultrapure water.

In the case of urine samples with the MOF-based fiber in HS-SPME, the slopes present quite similar values or significatively lower values than those obtained in ultrapure water. Thus, the slopes for Nap were 2422 in ultrapure water and 2547 in the urine sample, while the slopes for the remaining PAHs were from 1.5 to 3 times lower in urine than those obtained with ultrapure water. As expected, the results obtained in the statistical test for the assessment of the matrix effect in urine included in Table IV.78 showed that there is matrix effect for all the PAHs except for Nap in urine. The average RR value was 88.2 %, while the RSD values ranged from 2.4 % for BaPy to 21 % for Acy.

The performance of PDMS fiber in urine samples exhibited a similar behavior. The HS-SPME calibration slopes obtained in urine were slightly lower than those obtained in ultrapure water. According to the statistical tests included in Table IV.79, there is matrix effects for all the PAHs. In comparison with the performance of the MOF-based fiber in urine, it is interesting to highlight that the calibration slopes with the CIM-80(Al) coating are significantly higher than the slopes with the PDMS fiber for the heaviest PAHs, as it is shown in Figure IV.56 A). The average RR and RSD values for PDMS in this matrix was 93.5 % and 16 %, respectively.

With respect to the analysis of coffee with the HS-SPME method, there is a sharp decrease on the calibration slope for all the PAHs with both fibers. In the case of the MOF-based coating, they were from 1.5 for Nap to 145 for BkFlt times lower in this matrix than in ultrapure water. This may be due to the wide variety of volatile constituents of coffee aroma, which may interfere the extraction ability towards PAHs. As it was observed with urine sample, the performance of the CIM-80(Al) fiber was better than PDMS for the PAHs with higher molecular weight (from Ant to BkFlt). The matrix effects in this sample were confirmed with the statistical tests performed (see Tables IV.80 and IV.81). The use of the MOF-based coating with this sample leads (in general) to lower precision, with RSD values ranging from 7.6 % for Flt to 18 % for Ace, while an average RR value of 89.1 % was obtained for all the analytes. In the case of PDMS fiber, average RR values of 95.4 % were obtained, while RSD values were lower than 20 %.

Table IV.74. Several quality analytical parameters of the HS-SPME-GC-MS calibration curves using the MOF-based fiber in urine.

PAH	(Slope ± t·SD[a])	R^{2} [b]	$S_{y/x}\cdot10^{-3}$ [c]	Intra-day RSD[d] (%)	RR[e] (%)
Nap	2547 ± 203	0.997	12	12	89.9
Acy	4452 ± 369	0.996	22	21	107
Ace	2206 ± 147	0.998	9	9.1	78.7
Flu	6770 ± 511	0.997	31	20	85.8
Phe	8517 ± 489	0.998	30	13	84.8
Ant	16845 ± 1255	0.997	76	7.4	80.2
Flt	5387 ± 414	0.997	25	18	95.3
Py	8727 ± 608	0.997	37	12	93.2
BaAnt	2402 ± 211	0.996	13	5.0	80.1
Chry	1693 ± 106	0.998	6	3.5	85.9
BbFlt	498 ± 25	0.999	1	10	85.0
BkFlt	701 ± 69	0.995	4	7.4	89.1
BaPy	188 ± 17	0.996	1	2.4	91.8

[a] 95 % confidence limits for n = 6 calibration levels (4 degrees of freedom) within the calibration range 0–200 $ng\cdot L^{-1}$.
[b] Determination coefficient.
[c] Error of the estimate (or standard deviation of the residuals).
[d] Relative standard deviation for intra-day precision at a concentration level of 40 $ng\cdot L^{-1}$ (n = 3).
[e] Relative recovery at a concentration level of 40 $ng\cdot L^{-1}$ (n = 3).

Table IV.75. Several quality analytical parameters of the HS-SPME-GC-MS calibration curves using the MOF-based fiber in brewed coffee.

PAH	(Slope ± t·SD[a])	R^{2} [b]	$S_{y/x}\cdot10^{-3}$ [c]	Intra-day RSD[d] (%)	RR[e] (%)
Nap	1563 ± 130	0.996	8	16	87.1
Acy	1602 ± 144	0.996	9	14	96.0
Ace	723 ± 56	0.997	3	18	89.2
Flu	759 ± 78	0.995	5	11	82.1
Phe	827 ± 53	0.998	3	12	107
Ant	1554 ± 122	0.997	7	14	89.1
Flt	266 ± 17	0.998	1	7.6	85.0
Py	340 ± 31	0.996	2	12	79.2
BaAnt	84 ± 6	0.999	0.3	15	101
Chry	101 ±11	0.994	0.7	16	95.8
BbFlt	17 ± 3	0.994	0.1	13	82.7
BkFlt	10 ± 1	0.993	0.1	14	74.6
BaPy	–	–	–	–	–

[a] 95 % confidence limits for n = 6 calibration levels (4 degrees of freedom) within the calibration range 0–200 $ng\cdot L^{-1}$.
[b] Determination coefficient.
[c] Error of the estimate (or standard deviation of the residuals).
[d] Relative standard deviation for intra-day precision at a concentration level of 40 $ng\cdot L^{-1}$ (n = 3).
[e] Relative recovery at a concentration level of 40 $ng\cdot L^{-1}$ (n = 3).

Table IV.76. Several quality analytical parameters of the HS-SPME-GC-MS calibration curves using the PDMS fiber in urine.

PAH	(Slope ± t·SD[a])	R^2 [b]	$S_{y/x} \cdot 10^{-3}$ [c]	Intra-day RSD[d] (%)	RR[e] (%)
Nap	3679 ± 325	0.996	20	11	107
Acy	10319 ± 916	0.996	56	16	98.7
Ace	10196 ± 916	0.996	56	13	98.7
Flu	11543 ±850	0.997	52	16	81.5
Phe	12432 ± 1147	0.996	70	19	74.7
Ant	17160 ± 1305	0.997	79	21	88.8
Flt	7312 ± 622	0.996	38	12	81.5
Py	6336 ± 583	0.996	36	17	98.0
BaAnt	1505 ± 147	0.995	9	12	121
Chry	853 ± 75	0.996	5	16	118
BbFlt	158 ± 14	0.995	0.9	19	75.1
BkFlt	150 ± 11	0.997	0.7	17	80.4
BaPy	57 ± 6	0.992	0.4	21	93.1

[a] 95 % confidence limits for n = 6 calibration levels (4 degrees of freedom) within the calibration range 0–200 $ng \cdot L^{-1}$.
[b] Determination coefficient.
[c] Error of the estimate (or standard deviation of the residuals).
[d] Relative standard deviation for intra-day precision at a concentration level of 40 $ng \cdot L^{-1}$ (n = 3).
[e] Relative recovery at a concentration level of 40 $ng \cdot L^{-1}$ (n = 3).

Table IV.77. Several quality analytical parameters of the HS-SPME-GC-MS calibration curves using the PDMS fiber in brewed coffee.

PAH	(Slope ± t·SD[a])	R^{2} [b]	$S_{y/x}\cdot10^{-3}$ [c]	Intra-day RSD[d] (%)	RR[e] (%)
Nap	2320 ± 333	0.998	20	14	117
Acy	2241 ± 186	0.996	11	18	77.6
Ace	1585 ± 139	0.996	9	15	85.7
Flu	1255 ± 103	0.997	6	4.8	93.2
Phe	693 ± 36	0.999	2	10	93.1
Ant	794 ± 25	0.999	2	16	111
Flt	248 ± 17	0.997	1	13	109
Py	218 ± 22	0.995	1	11	82.1
BaAnt	20 ± 2	0.996	0.1	20	92.8
Chry	21 ± 1	0.997	0.09	15	93.2
BbFlt	–	–	–	–	–
BkFlt	–	–	–	–	–
BaPy	–	–	–	–	–

[a] 95 % confidence limits for n = 6 calibration levels (4 degrees of freedom) within the calibration range 0–200 $ng\cdot L^{-1}$.
[b] Determination coefficient.
[c] Error of the estimate (or standard deviation of the residuals).
[d] Relative standard deviation for intra-day precision at a concentration level of 40 $ng\cdot L^{-1}$ (n = 3).
[e] Relative recovery at a concentration level of 40 $ng\cdot L^{-1}$ (n = 3).

Table IV.78. Statistical comparison of the slopes of the HS-SPME-GC-MS method using the MOF-based fiber and performed in ultrapure water and in urine to assess the matrix effect, according to Andrade and Estévez-Pérez [23].

PAH	*F*-test[a]			Student's *t*-test[d]				
	F_{crit}[b]	F_{exp}[c]	Result	Variances	t_{crit}[e]	t_{cal}[f]	Result	Matrix effect
Nap	6.16	4.78	$F_{exp} < F_{crit}$	Equal	2.23	0.88	$\|t_{cal}\| < t_{crit}$	No
Acy	6.16	6.89	$F_{exp} > F_{crit}$	Different	2.49	16.9	$\|t_{cal}\| > t_{crit}$	Yes
Ace	6.16	8.21	$F_{exp} > F_{crit}$	Different	2.48	22.9	$\|t_{cal}\| > t_{crit}$	Yes
Flu	6.16	26.0	$F_{exp} > F_{crit}$	Different	2.46	17.6	$\|t_{cal}\| > t_{crit}$	Yes
Phe	6.16	16.7	$F_{exp} > F_{crit}$	Different	2.47	8.95	$\|t_{cal}\| > t_{crit}$	Yes
Ant	6.16	14.1	$F_{exp} > F_{crit}$	Different	2.47	8.60	$\|t_{cal}\| > t_{crit}$	Yes
Flt	6.16	22.3	$F_{exp} > F_{crit}$	Different	2.46	13.1	$\|t_{cal}\| > t_{crit}$	Yes
Py	6.16	17.8	$F_{exp} > F_{crit}$	Different	2.46	13.0	$\|t_{cal}\| > t_{crit}$	Yes
BaAnt	6.16	20.4	$F_{exp} > F_{crit}$	Different	2.46	16.1	$\|t_{cal}\| > t_{crit}$	Yes
Chry	6.16	11.3	$F_{exp} > F_{crit}$	Different	2.47	14.0	$\|t_{cal}\| > t_{crit}$	Yes
BbFlt	6.16	223	$F_{exp} > F_{crit}$	Different	2.45	22.5	$\|t_{cal}\| > t_{crit}$	Yes
BkFlt	6.16	11.7	$F_{exp} > F_{crit}$	Different	2.47	18.8	$\|t_{cal}\| > t_{crit}$	Yes
BaPy	6.16	31.6	$F_{exp} > F_{crit}$	Different	2.46	20.3	$\|t_{cal}\| > t_{crit}$	Yes

[a] *F* statistical test to compare population variances.
[b] Critical *F* value for a significance level of 5 % and n – 2 degrees of freedom, being n the number of calibration levels.
[c] Experimental *F* value.
[d] Student's *t* test to compare the slopes.
[e] Critical *t* value for a significance level of 5 % and n – 2 degrees of freedom, being n the number of calibration levels
[f] Calculated *t* value using different approximations depending on the results of the *F*-test.

Table IV.79. Statistical comparison of the slopes of the HS-SPME-GC-MS method using the PDMS fiber and performed in ultrapure water and in urine to assess the matrix effect, according to Andrade and Estévez-Pérez [23].

PAH	*F*-test[a]				Student's *t*-test[d]			
	F_{crit}[b]	F_{exp}[c]	Result	Variances	t_{crit}[e]	t_{cal}[f]	Result	Matrix effect
Nap	6.16	7.31	$F_{exp} > F_{crit}$	Different	2.49	2.99	$\|t_{cal}\| > t_{crit}$	Yes
Acy	6.16	10.0	$F_{exp} > F_{crit}$	Different	2.48	8.46	$\|t_{cal}\| > t_{crit}$	Yes
Ace	6.16	11.4	$F_{exp} > F_{crit}$	Different	2.47	3.55	$\|t_{cal}\| > t_{crit}$	Yes
Flu	6.16	10.4	$F_{exp} > F_{crit}$	Different	2.48	3.99	$\|t_{cal}\| > t_{crit}$	Yes
Phe	6.16	4.49	$F_{exp} < F_{crit}$	Equal	2.23	2.78	$\|t_{cal}\| > t_{crit}$	Yes
Ant	6.16	8.27	$F_{exp} > F_{crit}$	Different	2.48	4.70	$\|t_{cal}\| > t_{crit}$	Yes
Flt	6.16	6.60	$F_{exp} > F_{crit}$	Different	2.49	12.3	$\|t_{cal}\| > t_{crit}$	Yes
Py	6.16	4.37	$F_{exp} < F_{crit}$	Equal	2.23	11.8	$\|t_{cal}\| > t_{crit}$	Yes
BaAnt	6.16	8.97	$F_{exp} > F_{crit}$	Different	2.48	19.9	$\|t_{cal}\| > t_{crit}$	Yes
Chry	6.16	18.3	$F_{exp} > F_{crit}$	Different	2.46	23.1	$\|t_{cal}\| > t_{crit}$	Yes
BbFlt	6.16	45.5	$F_{exp} > F_{crit}$	Different	2.45	17.4	$\|t_{cal}\| > t_{crit}$	Yes
BkFlt	6.16	75.4	$F_{exp} > F_{crit}$	Different	2.45	37.5	$\|t_{cal}\| > t_{crit}$	Yes
BaPy	6.16	8.29	$F_{exp} > F_{crit}$	Different	2.48	33.3	$\|t_{cal}\| > t_{crit}$	Yes

[a] *F* statistical test to compare population variances.
[b] Critical *F* value for a significance level of 5 % and n – 2 degrees of freedom, being n the number of calibration levels.
[c] Experimental *F* value.
[d] Student's *t* test to compare the slopes.
[e] Critical *t* value for a significance level of 5 % and n – 2 degrees of freedom, being n the number of calibration levels
[f] Calculated *t* value using different approximations depending on the results of the *F*-test.

Table IV.80. Statistical comparison of the slopes of the HS-SPME-GC-MS method using the MOF-based fiber and performed in ultrapure water and in brewed coffee to assess the matrix effect, according to Andrade and Estévez-Pérez [23].

PAH	*F*-test[a]			Student's *t*-test[d]				
	F_{crit}[b]	F_{exp}[c]	Result	Variances	t_{crit}[e]	t_{cal}[f]	Result	Matrix effect
Nap	6.16	11.7	$F_{exp} > F_{crit}$	Different	2.47	11.7	$\|t_{cal}\| > t_{crit}$	Yes
Acy	6.16	44.2	$F_{exp} > F_{crit}$	Different	2.45	44.5	$\|t_{cal}\| > t_{crit}$	Yes
Ace	6.16	57.7	$F_{exp} > F_{crit}$	Different	2.45	56.3	$\|t_{cal}\| > t_{crit}$	Yes
Flu	6.16	1138	$F_{exp} > F_{crit}$	Different	2.45	38.5	$\|t_{cal}\| > t_{crit}$	Yes
Phe	6.16	1367	$F_{exp} > F_{crit}$	Different	2.45	41.5	$\|t_{cal}\| > t_{crit}$	Yes
Ant	6.16	1509	$F_{exp} > F_{crit}$	Different	2.45	36.5	$\|t_{cal}\| > t_{crit}$	Yes
Flt	6.16	15316	$F_{exp} > F_{crit}$	Different	2.45	36.2	$\|t_{cal}\| > t_{crit}$	Yes
Py	6.16	6683	$F_{exp} > F_{crit}$	Different	2.45	41.6	$\|t_{cal}\| > t_{crit}$	Yes
BaAnt	6.16	46488	$F_{exp} > F_{crit}$	Different	2.45	38.5	$\|t_{cal}\| > t_{crit}$	Yes
Chry	6.16	1036	$F_{exp} > F_{crit}$	Different	2.45	54.0	$\|t_{cal}\| > t_{crit}$	Yes
BbFlt	6.16	34743	$F_{exp} > F_{crit}$	Different	2.45	33.5	$\|t_{cal}\| > t_{crit}$	Yes
BkFlt	6.16	45844	$F_{exp} > F_{crit}$	Different	2.45	47.7	$\|t_{cal}\| > t_{crit}$	Yes

[a] *F* statistical test to compare population variances.
[b] Critical *F* value for a significance level of 5 % and n – 2 degrees of freedom, being n the number of calibration levels.
[c] Experimental *F* value.
[d] Student's *t* test to compare the slopes.
[e] Critical *t* value for a significance level of 5 % and n – 2 degrees of freedom, being n the number of calibration levels
[f] Calculated *t* value using different approximations depending on the results of the *F*-test.

Table IV.81. Statistical comparison of the slopes of the HS-SPME-GC-MS method using the PDMS fiber and performed in ultrapure water and in brewed coffee to assess the matrix effect, according to Andrade and Estévez-Pérez [23].

PAH	*F*-test[a]			Student's *t*-test[d]				
	F_{crit}[b]	F_{exp}[c]	Result	Variances	t_{crit}[e]	t_{cal}[f]	Result	Matrix effect
Nap	6.16	6.96	$F_{exp} > F_{crit}$	Different	2.49	11.3	$\|t_{cal}\| > t_{crit}$	Yes
Acy	6.16	243	$F_{exp} > F_{crit}$	Different	2.45	32.9	$\|t_{cal}\| > t_{crit}$	Yes
Ace	6.16	488	$F_{exp} > F_{crit}$	Different	2.45	26.5	$\|t_{cal}\| > t_{crit}$	Yes
Flu	6.16	719	$F_{exp} > F_{crit}$	Different	2.45	34.9	$\|t_{cal}\| > t_{crit}$	Yes
Phe	6.16	4733	$F_{exp} > F_{crit}$	Different	2.45	45.4	$\|t_{cal}\| > t_{crit}$	Yes
Ant	6.16	20288	$F_{exp} > F_{crit}$	Different	2.45	41.3	$\|t_{cal}\| > t_{crit}$	Yes
Flt	6.16	8113	$F_{exp} > F_{crit}$	Different	2.45	53.5	$\|t_{cal}\| > t_{crit}$	Yes
Py	6.16	3375	$F_{exp} > F_{crit}$	Different	2.45	69.6	$\|t_{cal}\| > t_{crit}$	Yes
BaAnt	6.16	58687	$F_{exp} > F_{crit}$	Different	2.45	54.4	$\|t_{cal}\| > t_{crit}$	Yes
Chry	6.16	50380	$F_{exp} > F_{crit}$	Different	2.45	48.2	$\|t_{cal}\| > t_{crit}$	Yes

[a] *F* statistical test to compare population variances.
[b] Critical *F* value for a significance level of 5 % and n – 2 degrees of freedom, being n the number of calibration levels.
[c] Experimental *F* value.
[d] Student's *t* test to compare the slopes.
[e] Critical *t* value for a significance level of 5 % and n – 2 degrees of freedom, being n the number of calibration levels
[f] Calculated *t* value using different approximations depending on the results of the *F*-test.

For the DI-SPME-GC-MS method performed in real samples, Tables IV.82 and IV.83 list the quality analytical parameters of the matrix-matched calibration curves for the MOF-based fiber, while Tables IV.84 and IV.85 include those of the PDMS fiber. Moreover, Table IV.66 includes a summary of these figures of merit. For the MOF coating, the determination coefficients were higher than 0.994 in urine, and higher than 0.990 in coffee samples except for Ace, for which the determination coefficient was 0.979. Regarding the PDMS, the determination coefficients were higher than 0.995 in all cases. Figure IV.56 B) shows the calibration slopes in both samples in comparison with those obtained in ultrapure water.

It is important to highlight that the calibration slopes obtained in the urine sample were similar to those obtained in ultrapure water for most analytes using the MOF-based coating. Furthermore, it is interesting to note that there is an enhancement on the sensitivity for Nap and BaAnt, obtaining slopes 2 times higher than in ultrapure water. The results of the statistical test performed to compare the calibration slopes (see Table IV.86) determined there is matrix effect for all the PAHs, except for Ace, Flu, Py and BbFlt, for which the slopes were almost the same. Regarding the precision and RR in the urine matrix with the proposed fiber, the RSD values ranged from 5.9 % to 18 %, while average RR values of 92.7 % were obtained.

In the case of the performance of PDMS fiber in the DI-SPME method for the analysis of urine, the calibration slopes were also similar but higher to those obtained in ultrapure water. The exception were BbFlt, BkFlt and BaPy, for which the calibration slopes in the sample are around 3 times lower. Indeed, according to the statistical tests shown in Table IV.87, matrix effects were observed for all the analytes, except for Py. In comparison with the CIM-80(Al) fiber, the calibration slopes were higher for the commercial fiber, as it was observed during the validation in ultrapure water. However, due to the loss of sensitivity for the PAHs with the highest molecular weight, the differences between the slopes are now much lower, while matrix effects were observed for more analytes when using the commercial fiber than with the MOF-based coating. In general, better precision was observed with the PDMS fiber, with average RSD values of 8.7 %, while the RR values ranged from 90.0 to 115 %.

As it happened in the HS-mode, the performance of the DI-SPME method using both fibers in brewed coffee samples was lower, maybe due to its complex composition in comparison with urine samples. As shown in Figure IV.56 B), the calibration slopes obtained in the coffee sample are much lower than those obtained in ultrapure water, being even more than 100 times lower for Ant, Flt, Py and Chry. Therefore, matrix effects were observed for all the PAHs with both fibers in this sample according to the results of the statistical tests shown in Tables IV.88 and IV.89. In the case of the MOF-based fiber, the RR values ranged from 76.4 % for Nap to 116 % for BbFlt, while intra-day RSD values were lower than 16 % for all the analytes. In comparison, the calibration slopes with the PDMS fiber were higher, average RR values of 100 % were obtained, and the RSD values were lower than 16 %.

Table IV.82. Several quality analytical parameters for the DI-SPME-GC-MS calibration curves using the MOF-based fiber in diluted urine.

PAH	(Slope ± t·SD[a])	R^2 [b]	$S_{y/x}\cdot10^{-3}$ [c]	Intra-day RSD[d] (%)	RR[e] (%)
Nap	814 ± 69	0.996	4	7.7	84.7
Acy	1487 ± 75	0.999	5	9.1	96.8
Ace	822 ± 58	0.997	3	7.1	91.0
Flu	1550 ± 128	0.996	8	17	79.3
Phe	2976 ± 167	0.998	10	18	103
Ant	5625 ± 511	0.996	31	9.4	111
Flt	3615 ± 328	0.996	20	5.9	114
Py	4349 ± 292	0.998	18	10	109
BaAnt	5329 ± 530	0.995	32	11	84.0
Chry	2516 ± 255	0.995	16	5.8	81.0
BbFlt	2422 ± 253	0.994	15	11	74.3
BkFlt	1910 ± 200	0.994	12	5.8	80.1
BaPy	1498 ± 158	0.994	10	11	96.6

[a] 95 % confidence limits for n = 6 calibration levels (4 degrees of freedom) within the calibration range 0–200 $ng\cdot L^{-1}$.
[b] Determination coefficient.
[c] Error of the estimate (or standard deviation of the residuals).
[d] Relative standard deviation for intra-day precision at a concentration level of 40 $ng\cdot L^{-1}$ (n = 3).
[e] Relative recovery at a concentration level of 40 $ng\cdot L^{-1}$ (n = 3).

Table IV.83. Several quality analytical parameters for the DI-SPME-GC-MS calibration curves using the MOF-based fiber in diluted brewed coffee.

PAH	(Slope ± t·SD[a])	R^{2} [b]	$S_{y/x}\cdot10^{-3}$ [c]	Intra-day RSD[d] (%)	RR[e] (%)
Nap	167 ± 8	0.999	0.5	13	76.4
Acy	191 ± 17	0.996	1	9.0	114
Ace	369 ± 75	0.979	5	16	113
Flu	27 ± 3	0.995	0.2	12	80.7
Phe	163 ±14	0.996	0.9	5.2	99.1
Ant	72 ± 6	0.996	0.4	5.6	112
Flt	29 ± 2	0.997	0.1	16	101
Py	20 ± 2	0.995	0.1	14	96.4
BaAnt	76 ± 11	0.991	0.6	4.1	90.5
Chry	35 ± 6	0.992	0.3	19	85.0
BbFlt	93 ± 14	0.990	0.8	5.1	116
BkFlt	129 ± 17	0.991	1	6.5	110
BaPy	73 ± 8	0.994	0.5	9.3	110

[a] 95 % confidence limits for n = 6 calibration levels (4 degrees of freedom) within the calibration range 0–200 $ng\cdot L^{-1}$.
[b] Determination coefficient.
[c] Error of the estimate (or standard deviation of the residuals).
[d] Relative standard deviation for intra-day precision at a concentration level of 40 $ng\cdot L^{-1}$ (n = 3).
[e] Relative recovery at a concentration level of 40 $ng\cdot L^{-1}$ (n = 3).

Table IV.84. Several quality analytical parameters for the DI-SPME-GC-MS calibration curves using the PDMS fiber in diluted urine.

PAH	(Slope ± t·SD[a])	R^2 [b]	$S_{y/x} \cdot 10^{-3}$ [c]	Intra-day RSD[d] (%)	RR[e] (%)
Nap	2283 ± 222	0.995	14	7.7	90.0
Acy	4944 ± 211	0.999	13	5.6	97.4
Ace	5601 ± 242	0.999	15	5.7	97.1
Flu	6017 ± 161	0.999	10	3.2	107
Phe	9386 ± 194	0.999	12	3.0	102
Ant	14417 ± 219	0.999	13	5.1	97.8
Flt	12373 ± 311	0.999	19	8.4	99.8
Py	12632 ± 305	0.999	19	14	115
BaAnt	12509 ± 561	0.999	34	12	91.8
Chry	6595 ± 330	0.999	20	12	91.2
BbFlt	4136 ± 303	0.997	18	13	108
BkFlt	3402 ± 197	0.998	12	13	99.5
BaPy	2571 ± 172	0.998	10	11	113

[a] 95 % confidence limits for n = 6 calibration levels (4 degrees of freedom) within the calibration range 0–200 $ng \cdot L^{-1}$.
[b] Determination coefficient.
[c] Error of the estimate (or standard deviation of the residuals).
[d] Relative standard deviation for intra-day precision at a concentration level of 40 $ng \cdot L^{-1}$ (n = 3).
[e] Relative recovery at a concentration level of 40 $ng \cdot L^{-1}$ (n = 3).

Table IV.85. Several quality analytical parameters for the DI-SPME-GC-MS calibration curves using the PDMS fiber in diluted brewed coffee.

PAH	(Slope ± t·SD[a])	R^2 [b]	$S_{y/x}\cdot10^{-3}$ [c]	Intra-day RSD[d] (%)	RR[e] (%)
Nap	938 ± 39	0.999	2	8.1	104
Acy	1318 ± 56	0.999	3	11	101
Ace	1038 ± 47	0.999	3	9.5	103
Flu	863 ± 69	0.997	4	15	108
Phe	751 ± 53	0.997	3	12	102
Ant	1012 ± 78	0.997	5	11	99.7
Flt	571 ± 36	0.998	2	15	111
Py	580 ± 39	0.998	2	15	105
BaAnt	384 ± 36	0.995	2	14	93.0
Chry	210 ± 17	0.997	1	13	95.9
BbFlt	233 ± 17	0.998	1	14	94.3
BkFlt	191 ± 17	0.996	1	16	90.8
BaPy	174 ± 11	0.998	0.7	12	88.6

[a] 95 % confidence limits for n = 6 calibration levels (4 degrees of freedom) within the calibration range 0–200 $ng\cdot L^{-1}$.
[b] Determination coefficient.
[c] Error of the estimate (or standard deviation of the residuals).
[d] Relative standard deviation for intra-day precision at a concentration level of 40 $ng\cdot L^{-1}$ (n = 3).
[e] Relative recovery at a concentration level of 40 $ng\cdot L^{-1}$ (n = 3).

Table IV.86. Statistical comparison of the slopes of the DI-SPME-GC-MS method using the MOF-based fiber and performed in ultrapure water and in diluted urine to assess the matrix effect, according to Andrade and Estévez-Pérez [23].

PAH	*F*-test[a]			Student's *t*-test[d]				
	F_{crit}[b]	F_{exp}[c]	Result	Variances	t_{crit}[e]	t_{cal}[f]	Result	Matrix effect
Nap	6.16	1.82	$F_{exp} < F_{crit}$	Equal	2.23	17.2	$\|t_{cal}\| > t_{crit}$	Yes
Acy	6.16	14.2	$F_{exp} > F_{crit}$	Different	2.47	3.29	$\|t_{cal}\| > t_{crit}$	Yes
Ace	6.16	5.11	$F_{exp} < F_{crit}$	Equal	2.23	0.19	$\|t_{cal}\| < t_{crit}$	No
Flu	6.16	3.13	$F_{exp} < F_{crit}$	Equal	2.23	0.34	$\|t_{cal}\| < t_{crit}$	No
Phe	6.16	23.8	$F_{exp} > F_{crit}$	Different	2.46	6.47	$\|t_{cal}\| > t_{crit}$	Yes
Ant	6.16	9.50	$F_{exp} > F_{crit}$	Different	2.48	6.79	$\|t_{cal}\| > t_{crit}$	Yes
Flt	6.16	6.98	$F_{exp} > F_{crit}$	Different	2.49	3.31	$\|t_{cal}\| > t_{crit}$	Yes
Py	6.16	11.3	$F_{exp} > F_{crit}$	Different	2.47	0.11	$\|t_{cal}\| < t_{crit}$	No
BaAnt	6.16	2.16	$F_{exp} < F_{crit}$	Equal	2.23	21.7	$\|t_{cal}\| > t_{crit}$	Yes
Chry	6.16	7.69	$F_{exp} > F_{crit}$	Different	2.48	9.32	$\|t_{cal}\| > t_{crit}$	Yes
BbFlt	6.16	3.10	$F_{exp} < F_{crit}$	Equal	2.23	1.12	$\|t_{cal}\| < t_{crit}$	No
BkFlt	6.16	7.96	$F_{exp} > F_{crit}$	Different	2.48	6.84	$\|t_{cal}\| > t_{crit}$	Yes
BaPy	6.16	1.81	$F_{exp} < F_{crit}$	Equal	2.23	5.35	$\|t_{cal}\| > t_{crit}$	Yes

[a] *F* statistical test to compare population variances.
[b] Critical *F* value for a significance level of 5 % and n – 2 degrees of freedom, being n the number of calibration levels.
[c] Experimental *F* value.
[d] Student's *t* test to compare the slopes.
[e] Critical *t* value for a significance level of 5 % and n – 2 degrees of freedom, being n the number of calibration levels
[f] Calculated *t* value using different approximations depending on the results of the *F*-test.

Table IV.87. Statistical comparison of the slopes of the DI-SPME-GC-MS method using the PDMS fiber and performed in ultrapure water and in diluted urine to assess the matrix effect, according to Andrade and Estévez-Pérez [23].

PAH	*F*-test[a]			Student's *t*-test[d]				
	F_{crit}[b]	F_{exp}[c]	Result	Variances	t_{crit}[e]	t_{cal}[f]	Result	Matrix effect
Nap	6.16	2.31	$F_{exp} < F_{crit}$	Equal	2.23	5.53	$\|t_{cal}\| > t_{crit}$	Yes
Acy	6.16	13.2	$F_{exp} > F_{crit}$	Different	2.47	8.96	$\|t_{cal}\| > t_{crit}$	Yes
Ace	6.16	9.04	$F_{exp} > F_{crit}$	Different	2.48	12.1	$\|t_{cal}\| > t_{crit}$	Yes
Flu	6.16	32.1	$F_{exp} > F_{crit}$	Different	2.46	13.1	$\|t_{cal}\| > t_{crit}$	Yes
Phe	6.16	73.2	$F_{exp} > F_{crit}$	Different	2.45	7.59	$\|t_{cal}\| > t_{crit}$	Yes
Ant	6.16	192	$F_{exp} > F_{crit}$	Different	2.45	3.71	$\|t_{cal}\| > t_{crit}$	Yes
Flt	6.16	56.4	$F_{exp} > F_{crit}$	Different	2.45	2.95	$\|t_{cal}\| > t_{crit}$	Yes
Py	6.16	94.9	$F_{exp} > F_{crit}$	Different	2.45	1.12	$\|t_{cal}\| < t_{crit}$	No
BaAnt	6.16	19.1	$F_{exp} > F_{crit}$	Different	2.46	3.63	$\|t_{cal}\| > t_{crit}$	Yes
Chry	6.16	6.29	$F_{exp} > F_{crit}$	Different	2.49	2.90	$\|t_{cal}\| > t_{crit}$	Yes
BbFlt	6.16	25.8	$F_{exp} > F_{crit}$	Different	2.46	28.2	$\|t_{cal}\| > t_{crit}$	Yes
BkFlt	6.16	99.8	$F_{exp} > F_{crit}$	Different	2.45	22.2	$\|t_{cal}\| > t_{crit}$	Yes
BaPy	6.16	34.3	$F_{exp} > F_{crit}$	Different	2.46	33.7	$\|t_{cal}\| > t_{crit}$	Yes

[a] *F* statistical test to compare population variances.
[b] Critical *F* value for a significance level of 5 % and n – 2 degrees of freedom, being n the number of calibration levels.
[c] Experimental *F* value.
[d] Student's *t* test to compare the slopes.
[e] Critical *t* value for a significance level of 5 % and n – 2 degrees of freedom, being n the number of calibration levels
[f] Calculated *t* value using different approximations depending on the results of the *F*-test.

Table IV.88. Statistical comparison of the slopes of the DI-SPME-GC-MS method using the MOF-based fiber and performed in ultrapure water and in diluted brewed coffee to assess the matrix effect, according to Andrade and Estévez-Pérez [23].

PAH	*F*-test[a]			Student's *t*-test[d]				
	F_{crit}[b]	F_{exp}[c]	Result	Variances	t_{crit}[e]	t_{cal}[f]	Result	Matrix effect
Nap	6.16	33.9	$F_{exp} > F_{crit}$	Different	2.46	35.7	$\|t_{cal}\| > t_{crit}$	Yes
Acy	6.16	326	$F_{exp} > F_{crit}$	Different	2.45	31.6	$\|t_{cal}\| > t_{crit}$	Yes
Ace	6.16	3.05	$F_{exp} < F_{crit}$	Equal	2.23	10.8	$\|t_{cal}\| > t_{crit}$	Yes
Flu	6.16	7123	$F_{exp} > F_{crit}$	Different	2.45	52.4	$\|t_{cal}\| > t_{crit}$	Yes
Phe	6.16	2952	$F_{exp} > F_{crit}$	Different	2.45	35.0	$\|t_{cal}\| > t_{crit}$	Yes
Ant	6.16	58314	$F_{exp} > F_{crit}$	Different	2.45	37.4	$\|t_{cal}\| > t_{crit}$	Yes
Flt	6.16	144589	$F_{exp} > F_{crit}$	Different	2.45	37.9	$\|t_{cal}\| > t_{crit}$	Yes
Py	6.16	261713	$F_{exp} > F_{crit}$	Different	2.45	35.1	$\|t_{cal}\| > t_{crit}$	Yes
BaAnt	6.16	1325	$F_{exp} > F_{crit}$	Different	2.45	35.4	$\|t_{cal}\| > t_{crit}$	Yes
Chry	6.16	27556	$F_{exp} > F_{crit}$	Different	2.45	41.3	$\|t_{cal}\| > t_{crit}$	Yes
BbFlt	6.16	1212	$F_{exp} > F_{crit}$	Different	2.45	38.6	$\|t_{cal}\| > t_{crit}$	Yes
BkFlt	6.16	1089	$F_{exp} > F_{crit}$	Different	2.45	34.7	$\|t_{cal}\| > t_{crit}$	Yes

[a] *F* statistical test to compare population variances.
[b] Critical *F* value for a significance level of 5 % and n – 2 degrees of freedom, being n the number of calibration levels.
[c] Experimental *F* value.
[d] Student's *t* test to compare the slopes.
[e] Critical *t* value for a significance level of 5 % and n – 2 degrees of freedom, being n the number of calibration levels
[f] Calculated *t* value using different approximations depending on the results of the *F*-test.

Table IV.89. Statistical comparison of the slopes of the DI-SPME-GC-MS method using the PDMS fiber and performed in ultrapure water and in diluted coffee to assess the matrix effect, according to Andrade and Estévez-Pérez [23].

PAH	*F*-test[a]			Student's *t*-test[d]				
	F_{crit}[b]	F_{exp}[c]	Result	Variances	t_{crit}[e]	t_{cal}[f]	Result	Matrix effect
Nap	6.16	74.7	$F_{exp} > F_{crit}$	Different	2.45	16.1	$\|t_{cal}\| > t_{crit}$	Yes
Acy	6.16	191	$F_{exp} > F_{crit}$	Different	2.45	25.7	$\|t_{cal}\| > t_{crit}$	Yes
Ace	6.16	245	$F_{exp} > F_{crit}$	Different	2.45	32.8	$\|t_{cal}\| > t_{crit}$	Yes
Flu	6.16	168	$F_{exp} > F_{crit}$	Different	2.45	29.8	$\|t_{cal}\| > t_{crit}$	Yes
Phe	6.16	976	$F_{exp} > F_{crit}$	Different	2.45	33.3	$\|t_{cal}\| > t_{crit}$	Yes
Ant	6.16	1521	$F_{exp} > F_{crit}$	Different	2.45	31.1	$\|t_{cal}\| > t_{crit}$	Yes
Flt	6.16	4376	$F_{exp} > F_{crit}$	Different	2.45	37.0	$\|t_{cal}\| > t_{crit}$	Yes
Py	6.16	5652	$F_{exp} > F_{crit}$	Different	2.45	31.0	$\|t_{cal}\| > t_{crit}$	Yes
BaAnt	6.16	4418	$F_{exp} > F_{crit}$	Different	2.45	43.6	$\|t_{cal}\| > t_{crit}$	Yes
Chry	6.16	2463	$F_{exp} > F_{crit}$	Different	2.45	65.3	$\|t_{cal}\| > t_{crit}$	Yes
BbFlt	6.16	9269	$F_{exp} > F_{crit}$	Different	2.45	52.5	$\|t_{cal}\| > t_{crit}$	Yes
BkFlt	6.16	15911	$F_{exp} > F_{crit}$	Different	2.45	36.0	$\|t_{cal}\| > t_{crit}$	Yes

[a] *F* statistical test to compare population variances.
[b] Critical *F* value for a significance level of 5 % and n – 2 degrees of freedom, being n the number of calibration levels.
[c] Experimental *F* value.
[d] Student's *t* test to compare the slopes.
[e] Critical *t* value for a significance level of 5 % and n – 2 degrees of freedom, being n the number of calibration levels
[f] Calculated *t* value using different approximations depending on the results of the *F*-test.

SPME has been previously reported in the literature for the determination of PAHs in urine [8,21,24] and brewed coffee [22,25,26]. In the case of urine samples, commercial PDMS [21] and overcoated PDMS/DVB/PDMS fiber coatings [8] have been used in DI-SPME methods. They exhibited low to significant intra- and inter-matrix effects (suppression of the signal) for most of the tested PAHs, as it was also observed in the present study. In these studies, these effects were balanced with the use of internal standards. Regarding coffee samples, nanomaterials-based fiber coatings have been prepared and applied in HS-SPME [25,26]. Matrix effects were not observed in these cases. However, it is important to point out that the ground coffee samples were first extracted with methanol and the extracts were diluted with ultrapure water prior to the HS-SPME procedure.

According to these results, the CIM-80(Al) coating is suitable for the analysis of aqueous-based complex samples without an exhaustive pretreatment, particularly for urine samples. Despite the matrix effects observed in the coffee and urine samples, which have also been observed for commercial fibers, it is important to highlight the stability of the MOF-based coating in these matrices. Thus, it was possible to obtain the calibration curves and perform precision studies with the fiber without losing efficiency. Moreover, it is important to highlight the superiority of the MOF-based fiber in comparison with the commercial PDMS fiber in the HS-SPME mode for most of the analytes in all the matrixes evaluated. This is the first time a MOF-based SPME fiber (without any additional component in the coating) is directly used for the analysis of samples of such complexity. Furthermore, Figure IV.57 shows SEM images for the MOF-based fibers after DI-SPME experiments in the different matrices: ultrapure water, urine and coffee. As it can be observed, the fiber coating kept its uniformity and morphology even after ≈ 40 extractions in the real samples, and only a slight smoothing of the MOF coating is observed in comparison with the unused fiber.

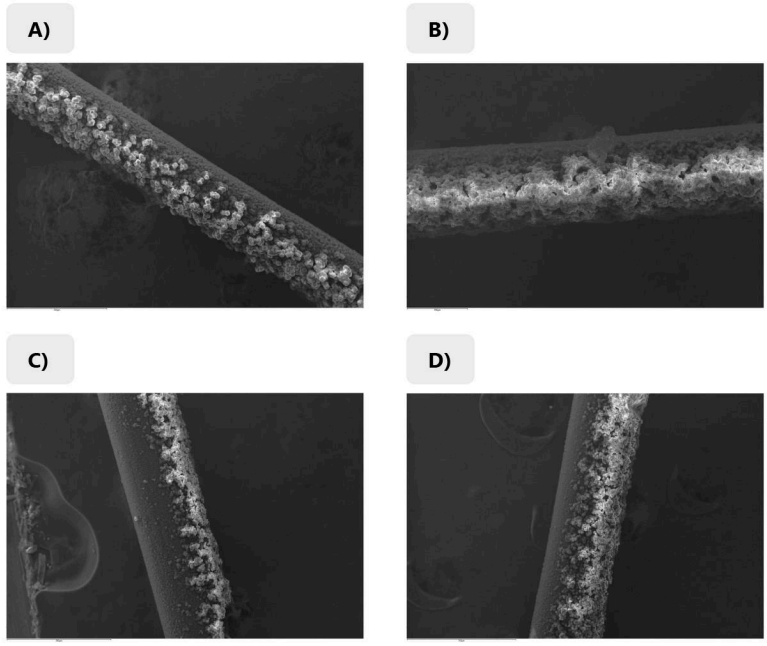

Figure IV.57. SEM micrographs of CIM-80 fibers **A)** immediately after its preparation and thermal activation, **B)** after ≈ 60 extractions in DI-SPME in ultrapure water, **C)** after ≈ 40 extractions in DI-SPME in urine, and **D)** after ≈ 40 extractions in DI-SPME in brewed coffee.

REFERENCES

[1] R.E. Shirey, in: J. Pawliszyn, Handbook of Solid Phase Microextraction, Elsevier (2012) 99–133.

[2] T. Gorecki, in: J. Pawliszyn, Applications of Solid Phase Microextraction, The Royal Society of Chemistry (1999) 92–108.

[3] P. Rocío-Bautista, V. Pino, J.H. Ayala, C. Ruiz-Pérez, O. Vallcorba, A.M. Afonso, J. Pasán, RSC Adv. 8 (2018) 31304–31310.

[4] Supelco | Sigma-Aldrich website: Solid Phase Microextraction Fiber Assemblies: Product Information. https://www.sigmaaldrich.com/content/dam/sigma-aldrich/docs/Sigma/General_Information/1/t794123.pdf (Accessed: 23rd October 2020).

[5] H. Reinsch, T. Homburg, N. Heidenreich, D. Fröhlich, S. Hennninger, M. Wark, N. Stock, Chem. - A Eur. J. 24 (2018) 2173–2181.

[6] D. Fiorini, D. Pacetti, R. Gabbianelli, S. Gabrielli, R. Ballini, J. Chromatogr. A 1409 (2015) 282–287.

[7] J. Pawliszyn, in: J. Pawliszyn, Handbook of Solid Phase Microextraction, Elsevier (2012) 13–59.

[8] A. Naccarato, E. Gionfriddo, R. Elliani, J. Pawliszyn, G. Sindona, A. Tagarelli, J. Sep. Sci. 41 (2018) 929–939.

[9] Y. Wang, J. Zhang, Y. Ding, J. Zhou, L. Ni, C. Sun, J. Sep. Sci. 32 (2009) 3951–3957.

[10] J. Zheng, S. Li, Y. Wang, L. Li, C. Su, H. Liu, F. Zhu, R. Jiang, G. Ouyang, Anal. Chim. Acta 829 (2014) 22–27.

[11] G. Zhang, X. Zang, Z. Li, C. Wang, Z. Wang, Talanta 129 (2014) 600–605.

[12] G. Wang, Y. Lei, H. Song, Talanta 144 (2015) 369–374.

[13] H. Amanzadeh, Y. Yamini, M.Y. Masoomi, A. Morsali, New J. Chem. 41 (2017) 12035–12043.

[14] S. Sun, L. Huang, H. Xiao, Q. Shuai, S. Hu, Talanta 202 (2019) 145–151.

[15] J. Gao, C. Huang, Y. Lin, P. Tong, L. Zhang, J. Chromatogr. A 1436 (2016) 1–8.

[16] S. Wei, W. Lin, J. Xu, Y. Wang, S. Liu, F. Zhu, Y. Liu, G. Ouyang, Anal. Chim. Acta 971 (2017) 48–54.

[17] N. Zhang, C. Huang, P. Tong, Z. Feng, X. Wu, L. Zhang, J. Chromatogr. A 1556 (2018) 37–46.

[18] J. Kong, F. Zhu, W. Huang, H. He, J. Hu, C. Sun, Q. Xian, S. Yang, J. Chromatogr. A 1603 (2019) 92–101.

[19] F. Bianchi, A. Pankajakshan, F. Fornari, S. Mandal, P. Pelagatti, A. Bacchi, P.P. Mazzeo, M. Careri, Microchem. J. 154 (2020) 104646.

[20] J. Ryhänen, Minim. Invasive Ther. Allied Technol. 9 (2000) 99–105.

[21] L. Campo, S. Fustinoni, P. Bertazzi, Anal. Bioanal. Chem. 401 (2011) 625–634.

[22] R.R. dos Santos, L.D. Vidotti Leal, Z. de Lourdes Cardeal, H.C. Menezes, J. Chromatogr. A 1584 (2019) 64–71.

[23] J.M. Andrade, M.G. Estévez-Pérez, Anal. Chim. Acta 838 (2014) 1–12.

[24] L. Campo, R. Mercadante, F. Rossella, S. Fustinoni, Anal. Chim. Acta 631 (2009) 196–205.

[25] H. Bagheri, G. Soofi, H. Javanmardi, M. Karimi, Microchim. Acta 185 (2018) 418.

[26] M.N. Yazdi, Y. Yamini, H. Asiabi, J. Chromatogr. A 1554 (2018) 8–15.

CHAPTER V
Conclusions

In this Doctoral Thesis, several analytical methods based on the use of ILs or MOFs as extraction phase in different microextraction techniques have been successfully developed for the determination of a wide variety of analytes in different samples, covering applications from the environmental, food and bioclininal analysis fields. The methods were characterized by their high sensitivity due to the use of preconcentration strategies, and by their improved sustainability in comparison with conventional methods given the negligible (or zero) use of organic solvents and the low amount of extraction phase required. Furthermore, the solvation properties of ILs, the high sorption capacity of MOFs, and the tunability of both types of materials, were exploited to develop methods with enhanced performance in terms of selectivity and extraction efficiency.

A detailed description of the conclusions derived from this Doctoral Thesis is presented below in different sections, depending on the microextraction technique and the material employed as extraction phase.

Section 1. Dispersive liquid-liquid microextraction using ionic liquids

Synthesis and characterization of ILs

- A series of ILs composed of monoalkylguanidinium cation and chloride anion were successfully synthesized, with lengths of the alkyl chain ranging from 4 to 10 carbon atoms.
- The CMC of the ILs containing longer alkyl chains (8 and 10 carbon atoms) was adequately determined by conductivity and fluorescence measurements. The CMC decreased with the length of the side chain and the concentration of NaCl in the aqueous solution. The obtained values agreed with other guanidinium IL-based surfactants and were lower in comparison with those reported for imidazolium IL-based surfactant analogues.
- The cytotoxicity studies showed an increase in the toxicity of the monoalkylguanidinium ILs as the length of the side alkyl chain increases. Furthermore, the lower cytotoxicity of this new generation of ILs in comparison with the most commonly used imidazolium-based ILs and conventional surfactants was also demonstrated.

Analytical applications in DLLME

- The $[C_8Gu^+][Cl^-]$ IL-based surfactant was successfully employed as extraction phase in an *in situ* DLLME approach and using Li-NTf_2 as anion-exchange reagent to accomplish the metathesis reaction and to insolubilize the IL. The method was conveniently combined with HPLC-DAD for the determination of 6 PCPs (parabens, benzophenones and a disinfectant) in cosmetic samples. After the optimization using experimental

designs, the method was characterized by being fast (≈ 30 min), requiring low volumes of extraction solvent (30 µL), and presenting: low LODs (0.4–1.4 µg·L^{-1}), inter-day RSD values lower than 16 % (at 15 µg·L^{-1}), and enrichment factors ranging from 10.6 to 136 depending on the analyte. The method was applied for the analysis of facial tonics after dilution with ultrapure water, allowing the quantification of the labelled analytes despite the matrix effects.

– A similar *in situ* DLLME method (based on the anion-exchange reaction initiated by Li-NTf_2) was developed but using the [$C_{10}Gu^+$][Cl^-] IL-based surfactant as extraction phase. The method was adequately optimized (using experimental designs) and validated in combination with FAAS for the determination of Cu^{2+} and Cd^{2+} in water samples, requiring ≈ 25 mg of the IL, and exhibiting quantitative extraction efficiencies (average E_R values of 90 %) and inter-day RSD values lower than 17 % (at 4 µg·L^{-1}) in less than 5 min. Furthermore, the most common [$C_{16}C_4Im^+$][Br^-] IL-based surfactant was also used as extraction phase in a similar *in situ* DLLME method, showing lower analytical performance in terms of sensitivity and precision. The applicability of the method was demonstrated by analyzing a CRM (drinking water) and conducting RR studies in tap water samples.

– The [$C_{10}Gu^+$][Cl^-] IL-based surfactant was also used as extraction phase in an *in situ* DLLME method in which the toxic fluorine salt (i.e., Li-NTf_2) is replaced by the non-harmful $NaClO_4$ to accomplish the metathesis reaction, thus improving the greenness of the method. The method was conveniently coupled with HPLC-FD for the determination of PAHs exposure biomarkers in urine. Matrix-matched calibrations were obtained using a non-hydrolyzed urine sample, demonstrating the presence of important suppressing matrix effects in comparison with the method performed in synthetic urine samples. However, the method exhibited enhanced analytical performance in comparison with other methods reported in the literature, including LODs down to 0.001 µg·L^{-1}, average enrichment factors of 40.7, and inter-day RSD values lower than 17 % (at 0.08 µg·L^{-1}). Finally, the method was applied for the analysis of urine samples from different individuals, showing total contents of OH-PAHs ranging from 0.09 µg·L^{-1} and 7.4 µg·L^{-1} for non-smoker male and smoker female, respectively.

– The phase diagrams for the ABSs composed of the least cytotoxic [C_4Gu^+][Cl^-] and [C_6Gu^+][Cl^-] ILs, water and K_3PO_4 were obtained in a range of concentrations suitable for microextraction and preconcentration purposes: low amounts of IL and high volumes of water. The µ-ABS of the [C_4Gu^+][Cl^-] IL was selected for the development of a microextraction method similar to DLLME but using K_3PO_4 as salting-out agent to promote the insolubilization of the IL in the sample. Thus, the method overcomes most of the sustainability issues of DLLME due to the low cytotoxicity of the IL, the low volume of IL required (73.1 µL), the non-toxicity of the salting-out salt, and the absence

of organic solvents in the extraction step. Moreover, the hydrophilicity of the final IL-rich phase obtained guaranteed the compatibility with the HPLC-FD system used for the determination PAHs. The method provided low LODs (ranging from 0.01 to 2.0 $ng \cdot L^{-1}$), high enrichment factors (up to 60.4), and inter-day RSD values lower than 17 % (at 12 $ng \cdot L^{-1}$).

Section 2. Solid-phase microextraction using new materials

PILs-based SPME coatings

- Several crosslinked PILs were chemically immobilized on the surface of nitinol wires via UV-initiated polymerization to fabricate on-fiber SPME devices. The combination of crosslinked PILs and this metal alloy as core yielded highly robust and flexible fibers. Different imidazolium ILs were used as monomers: 5 coatings were prepared with ILs containing alkyl or benzyl substituents and [Br^-] and [NTf_2^-] anions, and 5 coatings were composed of zwitterionic IL monomers with sulfonate and carboxylate chains. Adequate thicknesses for SPME coatings (around 20 μm) were obtained, depending on the fiber.
- The PILs-based on-fiber SPME coatings composed of functionalized imidazolium IL monomers were evaluated in a DI-SPME-HPLC-DAD method for the determination of wide variety of organic compounds with different structures. After the proper optimization and validation of the method, the coatings with benzyl groups showed better sensitivities towards polar analytes with aromatic rings within their structures in comparison with commercial fibers. Thus, the best PILs-based coatings, together with the commercial PA phase, were selected for the development of the DI-SPME-HPLC-DAD to determine alkylphenols in water samples. The partition constants were calculated for each coating, obtaining slightly higher values for the PILs-based fibers, particularly for BPA. Crosslinked PILs exhibited similar or better extraction performance for this specific analyte in terms of LOD (1 $\mu g \cdot L^{-1}$ *versus* 2 $\mu g \cdot L^{-1}$) and precision compared to PA, while showing high stability without swelling in organic solvents (methanol) and aqueous solutions at low pH values.
- The crosslinked PILs-based coatings containing zwitterionic ILs as monomers, together with commercial PA and CAR/PDMS fibers, were efficiently used in a HS-SPME-GC-MS method for determining the SCFFAs profile in wine. After the validation of the optimized method using standards prepared in synthetic wine, the results demonstrated that the zwitterionic PILs were more sensitive than the PA fiber (LODs of 12–76 $\mu g \cdot L^{-1}$ *versus* 27–61 $\mu g \cdot L^{-1}$) and were less affected by the ethanol sample content in comparison with CAR/PDMS, which provided similar or better analytical performance (LODs of 8.4–155 $\mu g \cdot L^{-1}$). A diluted wine sample was analyzed by the standard addition method using both PILs and CAR/PDMS fibers, demonstrating

enhancement matrix effects in most cases. Comparable SCFFAs contents were obtained with both type of fibers, except for the *i*-C_4 and *n*-C_5, which were not detected when using the commercial fiber.

- Coated open-tubular in-tube SPME devices were successfully prepared by the immobilization of crosslinked PILs on the internal surface of small and long capillaries. Two imidazolium ILs monomers with different side chains were used: a non-functionalized decyl substituent and a chain containing a carboxyl group. The thermal polymerization was directly carried out inside the capillary after the functionalization with vinyl groups, yielding adequate thicknesses of ≈ 0.5 µm.
- The two PILs-coated capillaries were evaluated in a draw/eject and off-line in-tube SPME method for the extraction and preconcentration of DNA and using HPLC-UV-Vis as detection technique. The PIL containing the carboxyl group in its structure showed better results, being selected for the development of a fully automated in-tube SPME procedure by connecting the extraction capillary in a HPLC autosampler. The optimized method was characterized by an enrichment factor of 20 and RSD values of 3.1 % (at 5 $mg \cdot L^{-1}$). The in-tube SPME method was much faster, precise and effective than an on-fiber SPME method using the same PILs-based coating.

MOFs-based SPME coatings

- The MOF CIM-80(Al), composed of Al (III) and mesaconate ligands, was successfully *in situ* growth on the surface of nitinol wires by the solvothermal method, obtaining coatings with an estimated volume of 0.1 µL. PXRD measurements demonstrated the adequate synthesis of the MOF, while TGA and gas adsorption analysis showed adequate thermal stability (up to 400 °C) and high surface area (884 $m^2 \cdot g^{-1}$). The stability of the MOF in different matrices was evaluated by PXRD after its immersion for 24 h and 10 days. The MOF kept its structure in all the matrices (e.g., boiling water, urine, and brewed coffee) even after 10 days, except for the whole milk sample when using long exposure times.
- The MOF-based on-fiber SPME device, together with the commercial PDMS fiber (thickness of 100 µm, volume of 0.6 µL), were used for the development of HS- and DI-SPME-GC-MS methods for the determination of PAHs. The methods were optimized and validated for both fibers using standards prepared in ultrapure water. The CIM-80(Al) provided enhanced results in the HS-SPME method (LODs of 0.3–1.5 $ng \cdot L^{-1}$ for MOF *versus* 0.5–1.5 $ng \cdot L^{-1}$ for PDMS), while the analytical performance of the commercial fiber was better in the DI-SPME method (LODs of 1.5–3.0 $ng \cdot L^{-1}$ for MOF *versus* 0.5–1.5 $ng \cdot L^{-1}$ for PDMS). Both fibers were also used for obtaining matrix-matched calibrations for the HS- and DI-SPME methods in urine and brewed coffee

samples without any previous pretreatment step of the sample apart from dilution. Despite the significant suppressing matrix effects, particularly in the HS-SPME method, this is the first time a neat MOF-based fiber (not a mixed-coating) could be applied for the direct analysis of complex samples, allowing the reuse of the device up to 40 extraction cycles.

In this sense, the results obtained in this Doctoral Thesis demonstrate the importance of expanding the knowledge and strategies derived from Material Science breakthrough to solve challenging analytical applications. Furthermore, it is important to take into account the greenness of the procedures involved in the sample preparation stage, as well as in the fabrication of these materials, and the toxicity of the material itself, to ensure that the overall procedure complies with the requirements established by the GAC. Given the versatility demonstrated by ILs and MOFs in the applications developed in this Doctoral Thesis, there is a still a need for a better understanding of the possible interactions between the target compounds and the materials in the different microextraction strategies with the aim of elucidating the mechanism that takes place during the extraction and desorption processes, which may help in the designing of more selective and useful materials for a wider range of applications.

ABBREVIATIONS

^{1}H-NMR	One-dimensional proton nuclear magnetic resonance spectroscopy
1OHpy	1-Hydroxypyrene
2OHflu	2-Hydroxyfluorene
2OHphe	2-Hydroxyphenanthrene
4OHphe	4-Hydroxyphenanthrene
AAS	Atomic absorption spectroscopy
ABS	Aqueous biphasic system
Ace	Acenaphthene
Acy	Acenaphthylene
AIBN	2,2′-Azobis(2-methylpropionitrile)
Ant	Anthracene
APDC	Ammonium pyrrolidine dithiocarbamate
APTES	3-Amino-propyltriethoxysilane
BaAnt	Benzo[a]anthracene
BaPy	Benzo[a]pyrene
BAµE	Bar adsorptive micro-extraction
BB	Building block
BbFlt	Benz[b]fluoranthene
BET	Brunauer–Emmett–Teller (method to determine the surface area)
BkFlt	Benzo[k]fluoranthene
BMA	Butyl methacrylate
Bnzal	Benzaldehyde
BP	Benzophenone
BP3	Benzophenone-3
BPA	Bisphenol A
BSTC	*N*,*N*′-Bis(salicylidene)thiocarbohydrazide
BTEX	Benzene, toluene, ethylbenzene and xylene
C_3	Propionic acid
CAC	Critical aggregation concentration
CAR	Carboxen
CC_{50}	50 % cytotoxic concentration
CCDC	Cambridge Crystallographic Data Center
Chry	Chrysene
CMC	Critical micelle concentration
Cmz	Carbamazepine
CNT	Carbon nanotube
COF	Covalent-organic framework
CRM	Certified reference material
CTAB	Cetyltrimethylammonium bromide

CuP	4-Cumylphenol
DAD	Diode-array detector
DAROCUR 1173	2-Hydroxy-2-methylpropiophenone
DBU	1,8-Diazabicyclo-[5.4.0]-undec-7-ene
DDTC	Diethyl dithiocarbamate
DDTP	O,O-Diethyldithiophosphate
DES	Deep eutectic solvent
DI	Direct immersion
DLLME	Dispersive liquid-liquid microextraction
DPASV	Differential pulse anodic stripping voltammetry
DVB	Divinylbenzene
ECD	Electon capture detection
ED	Ethylene dimethacrylate
EDC	Endocrine disrupting compound
EDMA	Ethylene glycol dimethacrylate
EDTA	Ethylenediaminetetraacetic acid
E_F	Enrichment factor
E_{Fmax}	Maximum enrichment factor
E_R	Extraction efficiency
ETAAS	Electrothermal atomic absorption spectroscopy
EtPa	Ethylparaben
FAAS	Flame atomic absorption spectroscopy instrument
F_{crit}	Critical *F* value
FD	Fluorescence detection system
F_{exp}	Experimental *F* value
FID	Flame ionization detection
Flt	Fluoranthene
Flu	Fluorene
FPSE	Fabric phase sorptive extraction
FS	Fused silica
g-C_3N_4	Hydrophobic graphitic carbon nitride
GAC	Green Analytical Chemistry
GC	Gas chromatography
GFAAS	Graphite furnace atomic absorption spectroscopy
Gfz	Gemfibrozil
GO	Graphene oxide
HBA	Hydrogen bond acceptor
HBD	Hydrogen bond donor
HF-LPME	Hollow fiber liquid-phase microextraction
hfacac	Tris(hexafluoroacetylaceto)

HPLC	High-performance liquid chromatography
HS	Headspace
i-C_4	*iso*-Butyric acid
i-C_5	*iso*-Valeric acid
i-C_6	*iso*-Hexanoic acid
ICECLES	Ice concentration linked with extractive stirrer
IL	Ionic liquid
Ind	Indeno[1,2,3-c,d]pyrene
INT	Iodotetrazolium chloride
iPPa	Isopropylparaben
K_{fs}	Partition constant (sample to fiber)
LC	Liquid chromatography
LDH	Lactate dehydrogenase
LIS	Lab-in-syringe
LLE	Liquid-liquid extraction
LOD	Limit of detection
LOQ	Limit of quantification
LOV	Lab-on-valve
LPME	Liquid-phase microextraction
m-µ-dSPE	Magnetic-assisted micro-dispersive solid-phase extraction
MAA	Methacrylic acid
MEEKC	Microemulsion electrokinetic chromatography
MePa	Methylparaben
MEPS	Microextraction by packed sorbents
MIP	Molecularly imprintetd polymer
MMM	Mixed matrix membranes
MOF	Metal-organic framework
MP	Magnetic particle
MS	Mass spectrometry
MW	Microwave
n-C_4	*n*-Butyric acid
n-C_5	*n*-Valeric acid
n-C_6	*n*-Hexanoic acid
n-C_7	*n*-Heptanoic acid
NADES	Natural deep eutectic solvent
Nap	Naphthalene
NiTi	Nitinol
*n*NP	4-*n*-Nonylphenol
NP	2-Nitrophenol
NPD	Nitrogen-phosphorus detector

NSAID	Nonsteroidal anti-inflammatory drug
NVC	*N*-Vinylcarbazole
OH-PAH	Monohydroxylated polycyclic aromatic hydrocarbon
OP	4-Octylphenol
PA	Polyacrylate
PAE	Phthalate acid ester
PAH	Polycyclic aromatic hydrocarbon
PAN	Polyacrylonitrile
PAS	Professional Analytical System Technology
PCB	Polychlorinated biphenyl
PCP	Personal care product
PCR	Polymerase chain reaction
PDMS	Polydimethylsiloxane
PEEK	Polyether ether ketone
PEG	Polyethyleneglycol
PES	Polyethersulfone
Phe	Phenanthrene
PIL	Polymeric ionic liquid
PPa	Propylparaben
PTFE	Polytetrafluoroethylene
PXRD	Powder X-ray diffraction
Py	Pyrene
qPCR	Quantitative polymerase chain reaction
R	Correlation coefficient
R^2	Determination coefficient
RAM	Restricted access material
RDSE	Rotating disk sorptive extraction
rGO	Reduced graphene oxide
RPMI	Roswell Park Memorial Institute
RR	Relative recovery
RSD	Relative standard deviation
RSM	Response surface methodology
S/N	Signal-to-noise ratio
SA-SBSE	Solvent-assisted stir bar sorptive extraction
SBSDME	Stir bar sorptive-dispersive microextraction
SBSE	Stir bat sorptive extraction
SCFFA	Short-chain free fatty acid
SCSE	Stir cake sorptive extraction
SD	Standard deviation
SDME	Single-drop microextraction

SDS	Sodium dodecyl sulfate
SEM	Scanning electron microscopy
SFO	Solidification of floating organic drop
SIA	Sequential injection analysis
SIM	Selected ion monitoring
S_N	Substitution reaction
SPE	Solid-phase extraction
SPME	Solid-phase microextraction
SS	Stainless steel
Sty	Styrene
SUPRAS	Supramolecular solvent
SwS	Switchable solvent
$S_{y/x}$	Error or the estimate or standard deviation of the residuals
*t*BP	3-*tert*-butylphenol
t_{cal}	Calculated *t* value
t_{crit}	Critical *t* value
TD	Thermal desorption
TDU	Thermal desorption unit
TFME	Thin film microextraction
tfTol	α,α,α,6-Tetrafluoro-*m*-toluidine
TGA	Thermogravimetric analysis
*t*OP	4-*tert*-Octylphenol
Trc	Triclosan
Tris-base	Tris(hydroxymethyl)aminomethane
Tris-HCl	Tris(hidroxymethyl)aminomethane hydrochloride
US	Ultrasound
US-EPA	United States Environmental Protection Agency
VA	Voltammetric analysis
VTMS	Vinyltrimethoxysilane
WCAES	Tungsten coil atomic emission spectrometry
λ_{em}	Emission wavelength
λ_{ex}	Excitation wavelength
μ-ABS	Micro-aqueous biphasic system
μ-dSPE	Micro-dispersive solid-phase extraction
μ-MSPD	Micro-matrix solid-phase dispersion
μ-SPE	Micro-solid-phase extraction

For the abbreviations of the ILs and MOFs, refer to Table I.2. and Table I.6 in Chapter I, respectively.

MAT4LL

Materials for Chemical Analysis
ULL Research Group